frontiers | Research Topics

Revealing neural plasticity in responding to non-invasive physical therapies via fMRI

Edited by
Yihuai Zou, Jian Kong, Aniko Bartfai, Jiliang Fang and Lijun Bai

Published in
Frontiers in Neurology

ISSN 1664-8714
ISBN 978-2-83251-187-9
DOI 10.3389/978-2-83251-187-9

About Frontiers

Frontiers is more than just an open access publisher of scholarly articles: it is a pioneering approach to the world of academia, radically improving the way scholarly research is managed. The grand vision of Frontiers is a world where all people have an equal opportunity to seek, share and generate knowledge. Frontiers provides immediate and permanent online open access to all its publications, but this alone is not enough to realize our grand goals.

Frontiers journal series

The Frontiers journal series is a multi-tier and interdisciplinary set of open-access, online journals, promising a paradigm shift from the current review, selection and dissemination processes in academic publishing. All Frontiers journals are driven by researchers for researchers; therefore, they constitute a service to the scholarly community. At the same time, the *Frontiers journal series* operates on a revolutionary invention, the tiered publishing system, initially addressing specific communities of scholars, and gradually climbing up to broader public understanding, thus serving the interests of the lay society, too.

Dedication to quality

Each Frontiers article is a landmark of the highest quality, thanks to genuinely collaborative interactions between authors and review editors, who include some of the world's best academicians. Research must be certified by peers before entering a stream of knowledge that may eventually reach the public - and shape society; therefore, Frontiers only applies the most rigorous and unbiased reviews. Frontiers revolutionizes research publishing by freely delivering the most outstanding research, evaluated with no bias from both the academic and social point of view. By applying the most advanced information technologies, Frontiers is catapulting scholarly publishing into a new generation.

What are Frontiers Research Topics?

Frontiers Research Topics are very popular trademarks of the *Frontiers journals series*: they are collections of at least ten articles, all centered on a particular subject. With their unique mix of varied contributions from Original Research to Review Articles, Frontiers Research Topics unify the most influential researchers, the latest key findings and historical advances in a hot research area.

Find out more on how to host your own Frontiers Research Topic or contribute to one as an author by contacting the Frontiers editorial office: frontiersin.org/about/contact

Revealing neural plasticity in responding to non-invasive physical therapies via fMRI

Topic editors

Yihuai Zou — Beijing University of Chinese Medicine, China
Jian Kong — Massachusetts General Hospital, Harvard Medical School, United States
Aniko Bartfai — Karolinska Institutet (KI), Sweden
Jiliang Fang — Guang'anmen Hospital, China Academy of Chinese Medical Sciences, China
Lijun Bai — Xi'an Jiaotong University, China

Citation

Zou, Y., Kong, J., Bartfai, A., Fang, J., Bai, L., eds. (2023). *Revealing neural plasticity in responding to non-invasive physical therapies via fMRI*.
Lausanne: Frontiers Media SA. doi: 10.3389/978-2-83251-187-9

Table of contents

frontiers | Frontiers in Neurology

TYPE Editorial
PUBLISHED 16 December 2022
DOI 10.3389/fneur.2022.1110063

OPEN ACCESS

EDITED AND REVIEWED BY
Jan Kassubek,
University of Ulm, Germany

*CORRESPONDENCE
Yihuai Zou
zouyihuai2004@163.com

SPECIALTY SECTION
This article was submitted to Applied Neuroimaging, a section of the journal Frontiers in Neurology

RECEIVED 28 November 2022
ACCEPTED 30 November 2022
PUBLISHED 16 December 2022

CITATION
Zou Y, Kong J, Fang J and Bai L (2022) Editorial: Revealing neural plasticity in responding to non-invasive physical therapies *via* fMRI.
Front. Neurol. 13:1110063.
doi: 10.3389/fneur.2022.1110063

Editorial: Revealing neural plasticity in responding to non-invasive physical therapies *via* fMRI

Yihuai Zou[1]*, Jian Kong[2], Jiliang Fang[3] and Lijun Bai[4]

[1]Department of Neurology, Dongzhimen Hospital Affiliated to Beijing University of Chinese Medicine, Beijing, China, [2]Department of Psychiatry, Massachusetts General Hospital, Harvard Medical School, Boston, MA, United States, [3]Lab for Functional Imaging, Department of Radiology, Guang'anmen Hospital China Academy of Chinese Medical Sciences, Beijing, China, [4]Department of Biomedical Information Engineering, School of Life Science and Technology, Xi'an Jiaotong University, Xi'an, China

KEYWORDS

neural plasticity, non-invasive physical therapy, fMRI, acupuncture, transcranial magnetic stimulation, neural pathway, neural network

Editorial on the Research Topic
Revealing neural plasticity in responding to non-invasive physical therapies *via* fMRI

Neuroplasticity, which refers to the dynamic character of the brain's neural networks, is fundamental in theories of neural rehabilitation that include changes in the structure and function of the brain. It usually takes a long time to get improved during neurological rehabilitation. Thus, non-invasive physical therapy, with its high safety and long-lasting efficacy, could be an important support in the rebuilding of neurological and psychiatric diseases. Blood oxygen level-dependent (BOLD) functional magnetic resonance imaging (fMRI) reflects changes in deoxyhemoglobin concentration resulting from task-induced or spontaneous regulation of neural metabolism. With the development of fMRI, increasing numbers of neuroimaging biomarkers have been tested. This topic contains 15 papers that investigated brain structural and functional changes in neural plasticity associated with non-invasive physical therapies.

Non-invasive physical therapies in neurological and psychiatric diseases

Transcranial magnetic stimulation (TMS) is a non-invasive treatment technique that uses a magnetic field to activate the brain cortex. An et al. used continuous theta-burst stimulation (cTBS) to induce an inhibitory aftereffect in the motor cortex in short time periods and observed the offline effect of cTBS-induced changes to the left posterior inferior frontal gyrus (pIFG) in healthy subjects. Further research will examine the therapeutic effects of cTBS on the right Broca's homolog area.

Recently, TMS has been used to treat mental disorders such depression, obsessive-compulsive disorder, schizophrenia (SCZ), and other brain-related conditions. Chen et al. conducted a randomized, double-blind, placebo-controlled study of rTMS in patients with stress-related depression. They found that 10-Hz rTMS over the left DLPFC improved the cognitive function of patients with stress-related depression. Ning et al. identified several potential TMS targets on the brain surface (with dlPFC and SMA being the most promising regions) and locations on the scalp for treating SCZ patients.

As a non-invasive peripheral neuromodulation method, non-invasive transcutaneous vagus nerve stimulation (taVNS) has drawn the attention of the investigators. Ma et al. proposed direct stimulation of the afferent nerve fibers on the ear should have a comparable impact on lowering depression symptoms as traditional invasive VNS, but without the requirement for invasive surgery. Meanwhile, He et al. observed a modulational effect of taVNS on the pre-frontal cortex in patients with chronic insomnia.

Continuous positive airway pressure (CPAP) is a conventional non-invasive physical therapy to eliminate snoring and prevent sleep apnea. Liu et al. proposed that short-term CPAP therapy may not be enough, and further longitudinal studies are warranted to explore the reversible alterations in white matter (WM) microstructure in the brain after long-term treatment.

Acupuncture, a key component of traditional Chinese medicine, has become an popular alternative method for stroke rehabilitation and has been used for overall wellness, including pain relief. It can be practiced not only in traditional forms but also in compound methods. Wang et al. conducted traditional acupuncture at acupoint (GB 34) on stroke patients and showed that acupuncture could improve the neurological motor deficit symptoms based on the group-level post-stroke neuroplasticity. Besides, traditional acupuncture was verified by Ning et al. as being able to widely modulate all brain networks and reverse the specific network functional connectivity associated with sleep deprivation. To enhance the intensity of the stimulation during acupuncture, Xu et al. attached a small electrode to the needles as they applied the electroacupuncture (EA) treatment in post-stroke aphasia. The EA procedure involved a continuous, constant-amplitude pulse wave as the stimulation waveform, with 2 mA of electric current and 150 Hz of frequency recorded. Zhan et al. proposed another option for EA parameters in the treatment of Alzheimer's disease (AD), in which acupoints (DU24 and GB12) were electrically stimulated as a pair with a disperse-dense wave of 2/50 Hz and 0.5 mA. They found that treatment with EA and donepezil in Alzheimer's disease patients could primarily increase spontaneous neural activity in specific brain regions, which was associated with improved cognitive function.

Acupuncture paired with exercise training is a type of integrated Chinese and western therapy. Ocular Acupuncture Kinesitherapy (OAKT) is a form of moving acupuncture in which exercise training is carried out while ocular acupuncture needles are embedded in the orbital tissues. Zhang D. et al. introduced a prospective functional neuroimaging and neurotic electrophysiological study with a case-control design in which they assessed the central-peripheral neural function alterations and tried to explain the central-peripheral coupling effect of OAKT on post-stroke dyskinesia. Meanwhile, the role of Tai Chi Chuan, another part of traditional Chinese medicine and often referred to as "meditation in action," in treating or preventing a range of diseases, is becoming more and more clear. Li et al. found individuals with chronic fatigue syndrome may benefit from practicing Tai Chi Chuan to enhance their quality of life.

Biomarkers represent neural plasticity as reflected by fMRI

Neural plasticity, which includes structural and functional changes through growth and reorganization, has significant implications for healthy development, learning, memory, and recovery from brain damage. Imaging biomarkers have been applied to estimate structural and functional neural plasticity in an efficient manner.

Functional plasticity refers to the brain's ability to alter and adapt the functional properties of neurons. Activation of the brain regions results in a local increase in oxygen delivery that exceeds the actual metabolic demand. An et al. reported language-related brain regions' activation. Functional connectivity (FC) is defined as the temporal coincidence of spatially distant neurophysiological events since 1994, which was analyzed in most of our reviewed studies. Functional connectivity has opened up another dimension for the analysis of fMRI data. Li et al. conducted Granger causality analysis (GCA) on FC results to show the causal relationship between specific brain networks. Xu et al. adopted independent component analysis (ICA) and general psychophysiological interaction (gPPI) to investigate static and dynamic FC changes both at the level of a region of interest (ROI) and at the large-scale network level. Zhang J. et al. conducted characteristic analysis to classify the prognosis of patients based on the Z values of regions resulting from FC analysis. Further, Ning et al. combined FC and network analysis to elucidate the large-scale brain organization and indicate that this combination might be a potentially powerful approach to understanding brain functional architecture. Wang et al. innovatively introduced intersubject functional correlation (ISFC), a new analytical method for revealing the FC of stimuli in various brain regions across subjects to seek a common activation and suppression pattern triggered by interventions. Such analyses of cross-subject studies may help optimize acupuncture regimens based on the common features of particular patients'

conditions. Amplitude of Low Frequency Fluctuations (ALFF) and fractional Amplitude of Low Frequency Fluctuations (f/ALFF) are neuroimaging methods used to find spontaneous fluctuations in the BOLD-fMRI signal intensity for a certain region in the resting brain. The regional homogeneity (ReHo) method was used to estimate regional activation patterns through indices of localized concordance. Since their effectiveness and robustness in analysis, the ALFF, fALFF, and ReHo methods have been used in five articles in this topic.

Structural plasticity is often understood as the brain's ability to change its neuronal connections. The changes in gray matter proportion and white matter fiber form are considered examples of structural neuroplasticity. Sun et al. quantitatively analyzed the cortical thickness (CT) and cortical surface area (SA) of infants with global developmental delay (GDD), draw the developmental trajectory maps, and analyze the hemispheric asymmetry to help find the brain structural changes related to the disease. The commonly used indexes of white matter fiber integrity assessment, including fractional anisotropy (FA), mean diffusion coefficient (MD), axial diffusion coefficient (AD), and radial diffusion coefficient (RD), were evaluated by Liu et al. to feature changes in WM microstructure in patients. Since multimodal neuroimaging methods may provide more information than single imaging tool alone, articles in our topic incorporate magnetic resonance spectrum imaging (MRSI) into resting-state fMRI to determine the chemical composition of specific tissue areas *in vivo* by Chen et al. and arterial spin labeling (ASL) combined with three-dimensional time-of-flight magnetic resonance angiography (3D-TOF MRA) into a DTI study to evaluate the regional cerebral blood flow (CBF) and microstructural changes in white matter by Yang et al..

Taken together, neurological rehabilitations are usually outpatient and need a considerable amount of time to develop brain plasticity. Non-invasive physical may be a promising treatment option for those who need continual intervention. There's still room for improvement to fit the various demands of patients. Regarding the evidence in this topic for both structural and functional biomarkers in regional and network-level analyses, multimodal neural imaging may represent a powerful way to conduct research on neural plasticity in the future.

Author contributions

YZ, JK, JF, and LB organized and proofread the writing of the editorial. All authors read and approved the final version of the manuscript.

Conflict of interest

The authors declare that the research was conducted in the absence of any commercial or financial relationships that could be construed as a potential conflict of interest.

Publisher's note

frontiers in Neurology

ORIGINAL RESEARCH
published: 15 December 2021
doi: 10.3389/fneur.2021.766736

Potential Locations for Non-Invasive Brain Stimulation in Treating Schizophrenia: A Resting-State Functional Connectivity Analysis

Yanzhe Ning[1,2†], *Sisi Zheng*[1,2†], *Sitong Feng*[1,2], *Binlong Zhang*[3*] and *Hongxiao Jia*[1,2*]

[1] The National Clinical Research Center for Mental Disorders & Beijing Key Laboratory of Mental Disorders, Beijing Anding Hospital, Capital Medical University, Beijing, China, [2] Advanced Innovation Center for Human Brain Protection, Capital Medical University, Beijing, China, [3] Department of Acupuncture and Moxibustion, Guang'anmen Hospital, China Academy of Chinese Medical Sciences, Beijing, China

OPEN ACCESS

Edited by:
Jian Kong,
Massachusetts General Hospital and Harvard Medical School, United States

Reviewed by:
Jordi A. Matias-Guiu,
Hospital Clínico San Carlos, Spain
Yann Quidé,
University of New South Wales, Australia

***Correspondence:**
Binlong Zhang
binlongzhang@bucm.edu.cn
Hongxiao Jia
jhxlj@ccmu.edu.cn

[†] *These authors have contributed equally to this work*

Specialty section:
This article was submitted to Applied Neuroimaging, a section of the journal Frontiers in Neurology

Received: *30 August 2021*
Accepted: *09 November 2021*
Published: *15 December 2021*

Citation:
Ning Y, Zheng S, Feng S, Zhang B and Jia H (2021) Potential Locations for Non-Invasive Brain Stimulation in Treating Schizophrenia: A Resting-State Functional Connectivity Analysis. Front. Neurol. 12:766736. doi: 10.3389/fneur.2021.766736

Introduction: Non-invasive brain stimulation (NIBS) techniques have been widely used for the purpose of improving clinical symptoms of schizophrenia. However, the ambiguous stimulation targets may limit the efficacy of NIBS for schizophrenia. Exploring effective stimulation targets may improve the clinical efficacy of NIBS in schizophrenia.

Methods: We first conducted a neurosynth-based meta-analysis of 715 functional magnetic resonance imaging studies to identify schizophrenia-related brain regions as regions of interest. Then, we performed the resting-state functional connectivity analysis in 32 patients with first-episode schizophrenia to find brain surface regions correlated with the regions of interest in three pipelines. Finally, the 10–20 system coordinates corresponding to the brain surface regions were considered as potential targets for NIBS.

Results: We identified several potential targets of NIBS, including the bilateral dorsal lateral prefrontal cortex, supplementary motor area, bilateral inferior parietal lobule, temporal pole, medial prefrontal cortex, precuneus, superior and middle temporal gyrus, and superior and middle occipital gyrus. Notably, the 10-20 system location of the bilateral dorsal lateral prefrontal cortex was posterior to F3 (F4), not F3 (F4).

Conclusion: Conclusively, our findings suggested that the stimulation locations corresponding to these potential targets might help clinicians optimize the application of NIBS therapy in individuals with schizophrenia.

Keywords: schizophrenia, non-invasive brain stimulation, functional magnetic resonance imaging, functional connectivity, DLPFC (dorsolateral prefrontal cortex)

INTRODUCTION

Schizophrenia (SCZ) is a complex psychiatric disorder associated with disturbances in social interaction and communication (1). Despite centuries of research, the pathophysiological cause of SCZ remains elusive. Around 18.8 to 20.8% of the patients with SCZ are thought to be non-responders to antipsychotic drugs (2). It is considered that the efficacious management also requires non-pharmacotherapies to treat SCZ patients in clinic.

Notably, non-invasive brain stimulation (NIBS) techniques have been widely used to improve the clinical symptoms of SCZ. The most commonly used NIBS technique is repetitive transcranial magnetic stimulation (rTMS). Low-frequency ($\leq$ 1 Hz) rTMS reduces cortical excitability, whereas high-frequency (5–20 Hz) rTMS does the opposite (3). It has been demonstrated that rTMS on the left temporo-parietal region effectively reduced auditory hallucinations than bilateral or sham stimulation (4). Another frequent NIBS application used in treating SCZ is transcranial direct current stimulation (tDCS), which produces polarity-dependent cortical excitability changes (3). The tDCS appeared to be effective not only for ambulatory and higher-functioning patients but also for patients with ultra-treatment resistant SCZ (5). Specifically, NIBS exerts a small transdiagnostic effect on working memory (6). Nonetheless, a meta-analysis indicated that NIBS was not associated with a reliable improvement in working memory for individuals with SCZ (7). A possible reason limiting the efficacy of NIBS for SCZ is the ambiguous stimulation site (8). Indeed, there are several sites reported in studies, such as dorsolateral prefrontal cortex (dlPFC) (9–11), temporoparietal cortex (TPC) (12, 13), and superior temporal gyrus (STG) (14, 15). The sites used in NIBS research were empirical. Thus, it is necessary to identify viable stimulation sites before using NIBS techniques.

Novel stimulation sites for depression (16), mild cognitive impairment (17), and autism (18) were identified by combining meta-analysis and functional connectivity (FC) analysis from three pipelines. The pipelines contain brain surfaces from (1) meta-analysis, (2) FC analysis results from disease network, and (3) FC analysis results from each disease-associated region of interest (ROI). This method combines the preponderance of meta-analysis and the FC analysis. Researchers optimized the sites of NIBS for treating neuropsychiatric disorders, suggesting the worth of a connectivity-based targeting strategy for NIBS techniques. However, there have been no studies using this method to find potential sites for SCZ. In the present study, we performed a meta-analysis and resting-state FC analysis to identify brain surface regions associated with SCZ-related ROIs to investigate potential targets of NIBS treatment in SCZ.

PATIENTS AND METHODS

Patients

A total of 32 right-handed first episode SCZ patients (13 males and 19 females) were included in the FC analysis. The age of these patients was 23.625 ± 7.404, $17 \sim 42$ (M $\pm$ SD, Min $\sim$ Max) years old. All examinations were carried out under the guidance of the Declaration of Helsinki. The present study was approved by the Ethics Committee of Beijing Anding Hospital, Capital medical university, China. All the subjects were Chinese Han people. Diagnoses were given by two trained psychiatrists using the Mini-International Neuropsychiatric Interview (M.I.N.I.) (19) under DSM-IV criteria. Psychiatric symptomatology was evaluated by using the Positive and Negative Syndrome Scale (PANSS) (20). Participants were excluded if they (a) were $<$ 16 years old, (b) had current comorbid substance-use disorder (daily consumption of substances for at least one year), (c) had a history of neurological disorders or family history of hereditary neurological disorders, (d) had gross morphological anomalies as evidenced by brain MRI scans, and (e) had any electronic or metal implants.

MRI Data Acquisition

Resting-state functional magnetic resonance imaging (RS-fMRI) data were acquired with a 3.0 Tesla MRI scanner (Prisma 3.0; Siemens, Germany) in the Beijing Anding Hospital, Capital medical university, China. RS-fMRI were acquired with a single-shot, gradient-recalled echo-planar imaging sequence with the following parameters: repetition time = 2000 ms, echo time = 30 ms, flip angle = 90°, matrix = 64 × 64, field of view = 200 mm × 200 mm, slice thickness = 3.5 mm, gap = 1 mm, 33 axial sections, and 240 volumes.

High-resolution brain structural images were acquired with a T1-weighted three-dimensional (3D) multi-echo magnetization-prepared rapid gradient-echo (MPRAGE) sequence [echo time: 3.39 ms, repetition time: 2,530 ms, slice thickness 1.3 mm, voxel size: $1.3 \times 1 \times 1$ mm^3, field of view (FOV): 256×256 mm^2, and volume number: 128].

Before scanning, all participants were asked to rest for 30 min and were instructed to stay still, keep their eyes closed, and not fall asleep during scanning. Foam head holders were immobilized to minimize head movements during scanning.

Image Processing

Firstly, the initial five volumes of the RS-fMRI data were removed. Secondly, the subjects whose head motion evaluated by the mean relative root mean square (RMS) exceeded 0.2 mm or whose maximum head motion exceeded 3 mm were excluded from the analysis. The two steps were conducted by Data Processing and Analysis for Brain Imaging (DPABI) version 5.1 (http://rfmri.org/dpabi) (21). Finally, the remaining subjects' images were preprocessed and analyzed in Conn version 18a (https://sites.google.com/view/conn/) (22) and SPM12 (using Conn's default preprocessing pipeline).

Conn's default preprocessing pipelines included both functional images' and structural images' preprocessing steps. Functional images were slice-timing corrected, realigned, normalized [$3 \times 3 \times 3$ mm^3 in Montreal Neurological Institute (MNI) space], and smoothed ($6 \times 6 \times 6$ mm^3). The outliers ($>$3 SD and $>$0.5 mm) for subsequent scrubbing regression were detected by the Artifact Detection Tool (www.nitrc.org/projects/artifact_detect/). The structural images were segmented into gray matter, white matter (WM), and cerebral spinal fluid (CSF) and normalized ($3 \times 3 \times 3$ mm^3) to MNI space. Then, linear regression using WM and CSF signals (CompCor; 10 components for WM and five components for CSF), linear trend, subject motion (six rotation/translation motion parameters and six first-order temporal derivatives), and outliers (scrubbing) was conducted to remove confounding effects. After that, the residual blood oxygen level dependent (BOLD) time series was band-pass filtered (0.01–0.1 Hz).

Identifying SCZ-Associated ROIs From Meta-Analysis

In order to identify SCZ-associated ROIs, we conducted a meta-analysis including 715 fMRI studies under the "schizophrenia" term *via* Neurosynth platform (https://neurosynth.org/;accessed 13 August 2020) (23). The complete list of studies can be found in **Supplementary Table S1**. Neurosynth platform provides two types of meta-analysis results: the uniformity test maps and association test maps. The uniformity test map was used to identify the SCZ-associated brain regions since the uniformity test maps provide information about the consistency of activation for a given process. Association test maps provided information

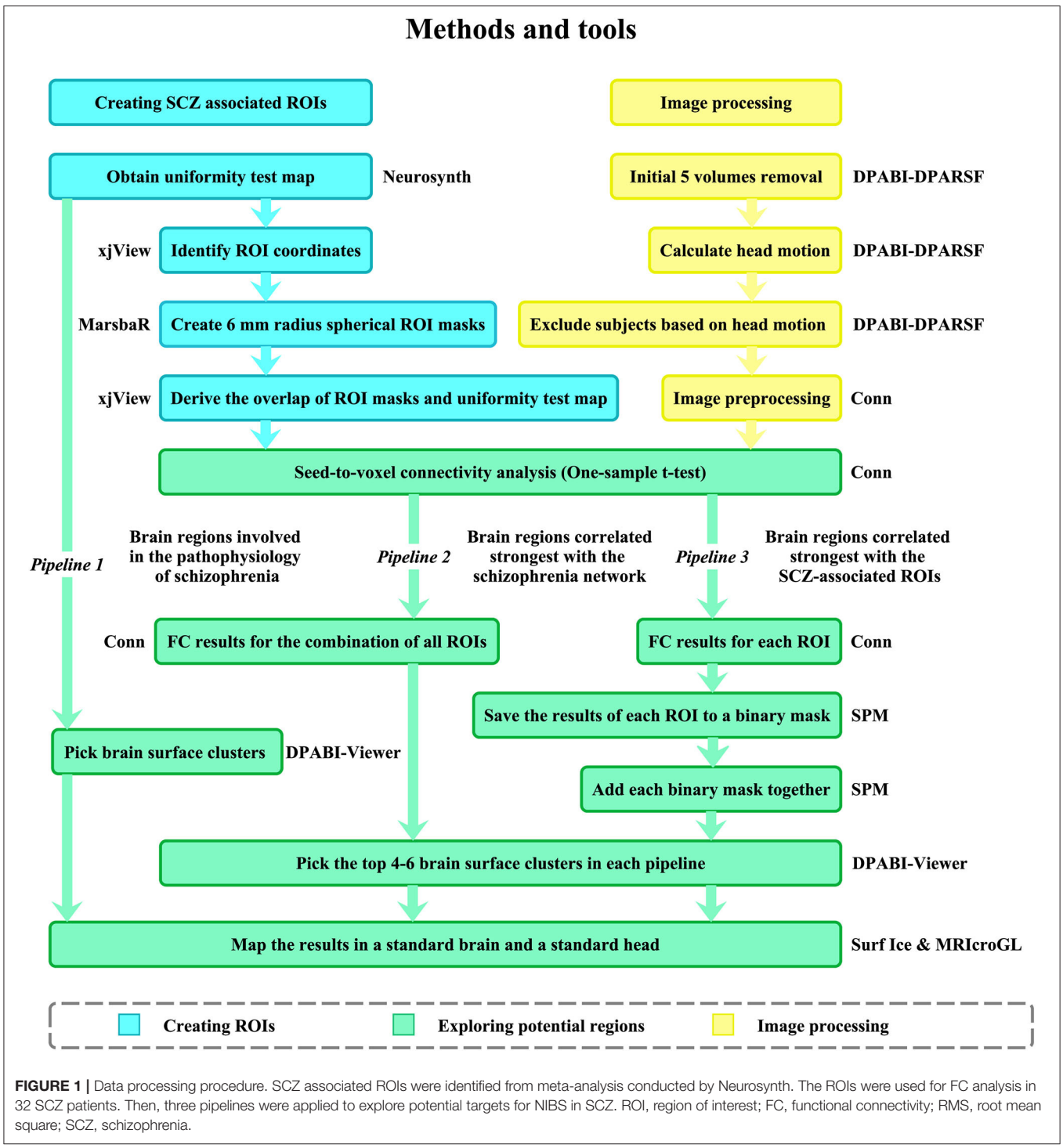

FIGURE 1 | Data processing procedure. SCZ associated ROIs were identified from meta-analysis conducted by Neurosynth. The ROIs were used for FC analysis in 32 SCZ patients. Then, three pipelines were applied to explore potential targets for NIBS in SCZ. ROI, region of interest; FC, functional connectivity; RMS, root mean square; SCZ, schizophrenia.

about the relative selectivity with which regions activate in a particular process (23). A false discovery rate (FDR) adjusted p-value of 0.01 was applied to produce the uniformity test map. Next, the coordinates with peak z-scores with all clusters larger than 50 voxels were identified by the xjview toolbox (http://www.alivelearn.net/xjview/). Finally, the 6-mm radius spherical masks centered on the specified peak coordinates were exacted by MarsBaR (http://marsbar.sourceforge.net/, version 0.44). Finally, the masks from MarsBaR and the original uniformity test map from Neurosynth were taken the overlap by xjview. The final ROIs only included the voxels from the original uniformity test map.

FC Analysis

To explore potential brain surface regions of SCZ, we conducted a seed-to-voxel FC analysis by Conn. At the subject level, the residual BOLD time course was extracted from the ROIs, and Pearson's correlation coefficients were computed between ROIs and all other brain voxels. Then, the coefficients were subsequently transformed into z-scores to increase normality. All subject-level seed maps of seed-to-voxel connectivity were included in a one sample t-test to get a group-level correlation map.

Exploring Potential NIBS Locations for SCZ

As the NIBS technique could not access whole brain regions, we used a brain surface mask created in previous studies (16, 18). The mask included the following brain regions: the bilateral pre and post-central gyrus; superior and middle frontal gyrus; superior, inferior, and middle occipital gyrus; superior and inferior parietal lobule; supramarginal gyrus; angular gyrus; superior temporal gyrus; superior temporal pole; middle temporal gyrus (MTG); middle temporal pole; inferior temporal gyrus; opercular inferior frontal gyrus (IFG); Rolandic operculum; triangular IFG; superior medial frontal gyrus; calcarine sulcus; orbital middle, superior and inferior frontal gyri; orbital medial frontal gyrus; supplementary motor area (SMA); paracentral lobule; precuneus; and cuneus. To explore the potential NIBS locations for SCZ, we picked brain surfaces from three different pipelines (**Figure 1**): (1) meta-analysis; (2) FC analysis results of SCZ network; (3) binary masks combined from each SCZ ROI FC analysis results. In pipelines 2 and 3, a voxel-wise level threshold of $p < 0.001$ and a cluster level family-wise error (FWE) of $p < 0.05$ were applied to obtain group-level correlation maps of ROIs.

Pipeline 1 Meta-Analysis

The brain surface clusters were directly picked from the Neurosynth meta-analysis (the uniformity test map) since the brain regions may be directly involved in the pathophysiology of SCZ.

Pipeline 2 FC Analysis Results of SCZ Network

The SCZ-associated ROIs were formed into an SCZ network, which was regarded as an ROI for FC analysis in CONN. Next, we excluded the clusters smaller than 20 voxels on the group-level correction map. Finally, four to six surface clusters with the largest peak z-scores were picked, with positive and negative correlation maps, respectively. These clusters represent the brain surface regions possessing the strongest correlations with the SCZ network.

Pipeline 3 Combined Binary Masks From FC Analysis Results of Each SCZ-Associated ROI

The group-level correlation map of each SCZ-associated ROI was saved to a binary mask. The binary masks of all ROIs formed a third-level map (positive and negative correlation maps, respectively). The intensity of each voxel in the third-level map represents the number of SCZ–ROIs correlated with the voxel. Finally, we identified four to six surface clusters as potential regions with the largest peak z-scores among all clusters larger than 20 voxels. These clusters represented the brain surface regions which were correlated with the largest number of SCZ-ROIs. The results of the three pipelines were mapped onto a standard brain and a standard head with the international 10–20 system in MNI space (24) using Surf Ice (www.nitrc.org/projects/surfice/) and MRIcroGL (www.mccauslandcenter.sc.edu/mricrogl/).

TABLE 1 | Coordinates of schizophrenia (SCZ) ROIs identified from meta-analysis.

ClusterID	Cluster size	T peak	Peak coordinates			Brain regions
			x	y	z	
1	188	12.68	−24	−6	−16	Amygdala_L
2	107	10.21	24	−6	−16	Amygdala_R
3	452	20.45	34	26	−4	Insula_R
4	681	20.45	−32	22	−4	Insula_L
5	118	10.91	−10	10	4	Caudate_L
6	149	10.91	14	10	4	Caudate_R
7	81	8.79	6	−14	4	Thalamus_R
8	119	11.62	−10	−16	6	Thalamus_L
9	674	17.27	−46	10	32	Precentral_L
10	97	8.44	40	38	24	Frontal_Mid_R
11	229	13.03	−2	−56	26	Precuneus_L
12	246	14.45	46	8	28	Frontal_Inf_Oper_R
13	722	16.21	0	14	48	SMA_L
14	158	11.62	−30	−56	40	Inferior Parietal_L
15	50	10.21	34	−56	44	Angular_R

L, left; R, right; SMA, supplementary motor area.

RESULTS

SCZ-Associated ROIs Identified From Meta-Analysis

Fifteen clusters with peak coordinates were identified from the meta-analysis (**Table 1**). The included studies are listed in the (**Supplementary Table S1**). These coordinates were used to create 6 mm radius spherical masks, including the bilateral amygdala, insula, thalamus, caudate, and the left caudate, precentral, precuneus, supplementary motor area (SMA), inferior parietal lobule, and the right middle frontal cortex. We took the overlap of these masks and the original meta-analysis

TABLE 2 | Potential locations for non-invasive brain stimulation (NIBS) techniques in SCZ from the three pipelines.

ID	Cluster size	Peak Intensity*	Peak coordinates			Brain regions	10–20 system locations
			x	y	z		
Pipeline 1							
1	674	17.2731	−46	10	32	dlPFC/IFG_R	Posterior to F4
2	535	16.2133	0	14	48	SMA	Midpoint to Fz-Cz
3	310	13.3871	−38	22	−6	dlPFC/IFG_L	Posterior to F3
4	246	14.447	46	8	29	dlPFC/IFG_R	
5	158	11.6208	−30	−56	40	IPL_L	P3
6	133	13.0339	−2	−56	26	Precuneus_bilateral	Anterior to Pz
7	97	8.4414	40	38	24	dlPFC/IFG_R	Posterior to F4
8	67	17.2731	34	26	−6	dlPFC/IFG_R	Posterior to F4
9	50	10.2077	34	−56	44	IPL/AG_R	P4
Pipeline 2 positive							
1	1,100	19.6838	−42	10	30	dlPFC/IFG_L	Posterior to F3
2	983	17.2673	46	14	30	dlPFC/IFG_R	Posterior to F4
3	529	16.623	−34	−54	48	IPL_L	P3
4	257	18.8981	32	−54	42	IPL_R	P4
5	597	19.5042	6	20	46	SMA	Midpoint to Fz-Cz
Pipeline 2 negative							
1	106	−5.3925	52	10	−42	TPO_R	Inferior to T4-F8
2	49	−4.9283	−50	20	−32	TPO_L	Inferior to T3-F7
3	3,888	−8.0841	−16	−90	24	SOG and MOG_bilateral	O1 to O2
4	627	−5.743	−8	62	28	mPFC	Anterior to Fz
5	24	−4.2461	14	58	38	mPFC	Anterior to Fz
Pipeline 3 positive							
1	2,724	13	NA	NA	NA	dlPFC/IFG_L	Posterior to F3
2	1,990	15	NA	NA	NA	dlPFC/IFG_R	Posterior to F4
3	857	13	NA	NA	NA	SMA	Midpoint to Fz-Cz
4	605	13	NA	NA	NA	SMG_L	Midpoint to C3-T3
5	439	12	NA	NA	NA	STG_R	Midpoint to F8-T4
6	259	12	NA	NA	NA	MTG/STG_L	Anterior to T5
Pipeline 3 Negative							
1	1,227	8	NA	NA	NA	mPFC	Anterior to Fz
2	162	8	NA	NA	NA	MTG_L	Anterior to T3
3	117	8	NA	NA	NA	TPO_R	Inferior to T4-F8
4	39	8	NA	NA	NA	MTG_R	Anterior to T4

** The intensity of voxels in each pipeline has different meanings. In pipeline 1, it represents z-score from meta-analysis conducted by Neurosynth; in pipeline 2, it represents Z-value from functional connectivity (FC) analysis conducted by Conn; in pipeline 3, it represents the number of SCZ-ROIs correlated with the voxels. Pipeline 3 has no peak intensity because the voxels in each cluster have equal intensity. L, left; R, right; NA, not applicable; IPL, Inferior Parietal Lobule; AG, angular gyrus; SMG, supramarginal gyrus SMA, supplementary motor area; dlPFC, dorsolateral prefrontal cortex; IFG, inferior frontal gyrus; mPFC, medial prefrontal cortex; MTG, middle temporal gyrus; STG, superior temporal gyrus; MTG, middle temporal gyrus; TPO, temporal pole; SOG, superior occipital gyrus; MOG, middle occipital gyrus.*

map (**Supplementary Figure S2**). Finally, the refined masks were used for seed-to-voxel connectivity analysis.

Potential NIBS Locations for SCZ

Thirty-two SCZ patients were included in this meta-analysis. The results of these three pipelines mapped on a standard brain and a standard head in the MNI space were shown in **Table 2** and **Figure 2**. The original results of each pipeline were in (**Supplementary Figures S3–S7**).

In pipeline 1, we directly picked up the brain surface regions from the meta-analysis. Finally, the bilateral dlPFC/IFG, SMA, inferior parietal lobule, and precuneus were identified as potential brain surface regions. The 10–20 system coordinates corresponding to the center of these regions were located approximately posterior to F3(F4), midpoint to Fz-Cz, P3(P4), and anterior to Pz. These brain regions may be directly involved in the pathophysiology of SCZ.

In pipeline 2, group-level FC analysis results (SCZ-network as seed) were mapped onto the head surface. Finally, the bilateral dlPFC/IFG (approximately posterior to F3/F4), inferior parietal lobule [IPL (P3/P4)], and SMA (midpoint to Fz-Cz) were found

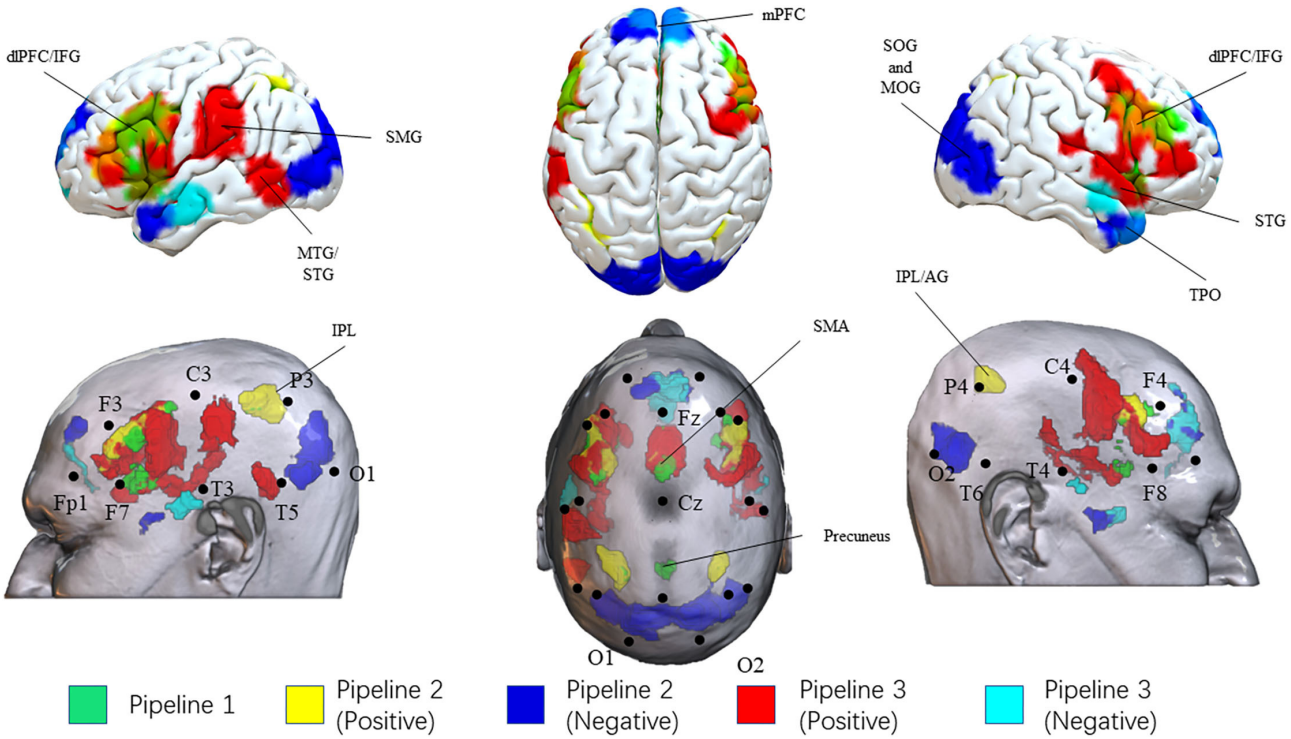

FIGURE 2 | Results of three pipelines. Brain surface regions identified from the three pipelines were presented on the top. Scalp locations corresponding to the brain surface regions were presented on the bottom. Results from pipeline 1, pipeline 2 (positive correlation), pipeline 2 (negative correlation), pipeline 3 (positive correlation), pipeline 3 (negative correlation) were presented as green, yellow, blue, red, and cyan, respectively. L, left; R, right; IPL, Inferior Parietal Lobule; AG, angular gyrus; SMG, supramarginal gyrus SMA, supplementary motor area; dlPFC, dorsolateral prefrontal cortex; IFG, inferior frontal gyrus; mPFC, medial prefrontal cortex; MTG, middle temporal gyrus; STG, superior temporal gyrus; MTG, middle temporal gyrus; TPO, temporal pole; SOG, superior occipital gyrus; MOG, middle occipital gyrus.

to be positively correlated with the SCZ network. The bilateral temporal pole, superior and middle occipital gyrus, and medial prefrontal cortex were showed overlap negatively correlated with the SCZ network. These regions were located approximately inferior to T4-F8 (T3-F7), midpoint to O1-O2, and anterior to Fz. These brain regions possessed the strongest correlations with the SCZ network.

In pipeline 3, the largest number of brain surface regions from the third-level FC analysis were picked. Finally, we found that the bilateral dlPFC/IFG, SMA, the right STG, the left MTG/STS, and the left supramarginal gyrus were positively correlated with SCZ-associated ROIs, located approximately posterior to F3(F4), midpoint to Fz-Cz, midpoint to F8-T4, anterior to T5, and midpoint to C3-T3. The bilateral MTG, medial prefrontal cortex, and the right temporal pole were potential brain surface regions positively correlated with SCZ-associated ROIs. The 10–20 system coordinates corresponding to the center of these regions were located approximately anterior to T3(T4), anterior to Fz, and inferior to T4-F8. These brain surface regions correlated with the largest number of SCZ-ROIs.

Previous NIBS Studies in SCZ

We summarized the targets used in the previous NIBS studies in SCZ from several systematic reviews (8, 25–27) in **Table 3**. The left dlPFC and the left TPJ were the most frequency targets used in the rTMS and tDCS.

DISCUSSION

In the present study, we attempt to explore potential brain regions and their corresponding scalp locations for NIBS techniques in treating SCZ. We have detected several potential brain regions by combining meta-analysis and FC analysis, which may contribute to improve the clinical efficacy of NIBS in SCZ.

The bilateral dlPFC/IFG and SMA are the most frequent targets for NIBS treatment in SCZ. Previous meta-analyses have demonstrated that high frequency rTMS and tDCS did not have a reliable improvement on treating SCZ by modulating the dlPFC (7, 70, 71). Contrary to previous clinical trials, our results showed that the location of dlPFC was posterior to F3 (F4) rather than exactly F3 (F4). The brain stimulation experiments in healthy subjects have illustrated that posterior to F3 was the optimal location for stimulating the dlPFC (72). Particularly, the Brodmann Area 9 located on the posterior to F4 in the dlPFC was remarkably associated with negative symptom severity (73). These findings suggest that stimulating the posterior to the F3 (F4) rather than the exact F3 (F4) may improve NIBS efficacy for negative symptoms.

TABLE 3 | The targets used in prior studies.

Targets	Reference	Symptoms	effect
rTMS			
TPC_L	(28–33)	AH	No
TPC_L	(34–40)	AH	Yes
TPC_R	(30)	AH	No
TPC_R	(39)	AH	Yes
TC_L/R	(41)	AH	No
TPJ_L	(4, 12)	AH	Yes
TPJ_L	(31)	Negative	No
STG_L	(14)	AH	No
PFC_R	(42)	Total	No
dlPFC_L	(43–45)	Positive	No
dlPFC_L	(43, 45–53)	Negative	Yes
dlPFC_L	(42, 44, 46, 54–56)	Negative	No
dlPFC_R	(47)	Negative	No
tDCS (Anode/Cathode)			
dlPFC_L/TPJ_L	(57–62)	Negative	No
dlPFC_L/TPJ_L	(5, 59, 63, 64)	AH	Yes
dlPFC_L/TPJ_L	(63–65)	Negative	Yes
dlPFC_L/TPJ_L	(57, 58, 60–62)	Positive	No
dlPFC_B/TPJ_B	(57)	Negative	Yes
dlPFC_L/ Fp2	(10)	Negative	No
dlPFC_L/Fp2	(66)	Negative	Yes
dlPFC_B/forearms	(67)	Negative	Yes
dlPFC_L/dlPFC_R	(68, 69)	Negative	Yes

L, left; R, right; B, bilateral; AH, auditory hallucinations; STG, superior temporal gyrus; TC, temporal cortex; TPC, temporoparietal cortex; TPJ, temporoparietal junction; dlPFC, dorsolateral prefrontal cortex; AH, auditory hallucinations; STG, superior temporal gyrus; TC, temporal cortex; TPC, temporoparietal cortex; TPJ, temporoparietal junction; dlPFC, dorsolateral prefrontal cortex.

In addition, the resting-state hyperperfusion of the SMA was considered as a marker of current catatonia in SCZ (74). Furthermore, the altered gray matter (74) and white matter volume (75) in the SMA were associated with disturbed motor behavior in SCZ. In our results, the SMA was identified in three pipelines suggesting that the SMA could serve as a considerable NIBS stimulation location for treating SCZ patients, especially those with motor abnormalities. The SMA is easily accessible using NIBS, while it is still virtually left to explore in SCZ. After reviewing the literature and registered trials, we have found just one published trial (76) and one ongoing trial — the Overcoming Psychomotor Slowing in Psychosis trial (OCoPS-P, NCT03921450) — for motor abnormalities in patients with SCZ over the SMA. The published trial, conducted by the Sebastian Walther group, has reported that inhibitory stimulation of the SMA might ameliorate psychomotor slowing in psychosis and major depression patients (76). Our data corroborated the ideas of Sebastian Walther, who suggested that NIBS stimulation of the cortical motor areas could be a practical methodology for improving and restoring motor impairment in SCZ (77).

There are other brain regions identified in our study, involving the bilateral IPL, the right temporal pole (TPO), and the medial prefrontal cortex (mPFC). IPL is one of the structures in the sense of agency and the dysconnectivity of the agency network (78), considered as a center of multisensory integration (79). The bilateral IPL, especially the angular gyrus (AG), may be directly involved in the pathophysiology of SCZ and extremely correlate with the SCZ network. A prior study has implicated that the reduction of IPL might be specific for long-term antipsychotic treatment (80). Our findings further supported that IPL could be a possible target for medication development in the future. Moreover, our results provided functional image evidence for the alteration of mPFC and TPO. The altered dopaminergic and GABAergic modulation in the mPFC is involved in SCZ progression (81). Previous meta-analysis including 4,474 individuals with SCZ has reported that only TPO thickness was negatively correlated with age, and cortical volumes at illness onset and progressive volume were declined in the temporal pole in SCZ (82). The right TPO and mPFC may strongly correlate with the SCZ network and correlate with the largest number of SCZ-associated ROIs. Despite the importance of mPFC and TPO, there remains a paucity of evidence for NIBS techniques treating SCZ over mPFC or TPO.

Interestingly, the dlPFC, SMA, and MTG are the components of the task positive network (TPN), which associates with externally oriented attention (83, 84). The mPFC, IPL, and precuneus play an important role in the default mode network (DMN) related to introspectively oriented cognitive processes, such as self-referential and reflective activity. Consistent with another study (85), we observed that TPN and DMN networks were anti-correlated. Here, our study provided the evidence to support that the anti-correlated networks were relevant to SCZ. Balancing the TPN and DMN network may have a beneficious effect in treating SCZ by NIBS to regulate neural circuits (3, 86).

Some limitations are needed to pay attention in the present study. First, excitatory or inhibitory brain regions in our study are not to be discriminated, which is essential to some NIBS techniques such as TMS. Second, the parameters used in each NIBS technique have not been studied, which may affect the efficacy. Finally, neurosynth-based meta-analysis is not flawless – potential error could occur – although several supporting analyses have been conducted to confirm the validity and sensitivity.

CONCLUSION

Combining meta-analysis and FC analysis from three pipelines, we identified several potential NIBS targets on the brain surface (with dlPFC and SMA to be the most promising regions) and locations on the scalp for treating SCZ patients. Specifically, the location of dlPFC was suggested to be posterior to F3 (F4) and not F3 (F4). Besides, we also identified that balancing the TPN and DMN might be a potential strategy to treat SCZ. These identified targets could

contribute to improving the efficacy of NIBS in treating SCZ patients.

DATA AVAILABILITY STATEMENT

The original contributions presented in the study are included in the article/**Supplementary Material**, further inquiries can be directed to the corresponding author/s.

ETHICS STATEMENT

The studies involving human participants were reviewed and approved by the Ethics Committee of Beijing Anding Hospital. The patients/participants provided their written informed consent to participate in this study.

AUTHOR CONTRIBUTIONS

HJ provided his expertise in schizophrenia, managed the data collection, and contributed to the writing of the manuscript. BZ conceived the idea and methodology for the study, designed the study, and contributed to the writing of the manuscript. YN and SZ managed data analyses and wrote the manuscript. SF was contributed to the writing of the manuscript and the graph display. All authors contributed to the article and approved the submitted version.

FUNDING

This study was supported by Beijing Natural Science Foundation (Grant No. 7212050), Capital's Funds for Health Improvement and Research (Grant Nos. 2018-1-2122, 2020-4-2126), Beijing Hospitals Authority Clinical Medicine Development of Special Funding (Grant No. ZYLX202129), Beijing Hospitals Authority's Ascent Plan (Grant No. DFL20191901), Beijing Hospitals Authority Youth Program (Grant No. QML20201901), Talents Training Fund of Beijing (Grant No. 2018000021469G292), China Academy of Chinese Medical Sciences Fund for Excellent Young Scholars (Grant No. ZZ14-YQ-017), and China Academy of Chinese Medical Sciences Innovation Fund (Grant No. CI2021A03316).

SUPPLEMENTARY MATERIAL

The Supplementary Material for this article can be found online at: https://www.frontiersin.org/articles/10.3389/fneur.2021.766736/full#supplementary-material

REFERENCES

1. Owen MJ, Sawa A, Mortensen PB. Schizophrenia. *Lancet.* (2016) 388:86–97. doi: 10.1016/S0140-6736(15)01121-6
2. Samara MT, Nikolakopoulou A, Salanti G, Leucht S. How many patients with schizophrenia do not respond to antipsychotic drugs in the short term? An analysis based on individual patient data from randomized controlled trials. *Schizophr Bull.* (2019) 45:639–46. doi: 10.1093/schbul/sby095
3. Cirillo G, Di Pino G, Capone F, Ranieri F, Florio L, Todisco V, et al. Neurobiological after-effects of non-invasive brain stimulation. *Brain Stimul.* (2017) 10:1–18. doi: 10.1016/j.brs.2016.11.009
4. Vercammen A, Knegtering H, Bruggeman R, Westenbroek HM, Jenner JA, Slooff CJ, et al. Effects of bilateral repetitive transcranial magnetic stimulation on treatment resistant auditory-verbal hallucinations in schizophrenia: a randomized controlled trial. *Schizophr Res.* (2009) 114:172–9. doi: 10.1016/j.schres.2009.07.013
5. Lindenmayer JP, Kulsa MKC, Sultana T, Kaur A, Yang R, Ljuri I, et al. Transcranial direct-current stimulation in ultra-treatment-resistant schizophrenia. *Brain Stimul.* (2019) 12:54–61. doi: 10.1016/j.brs.2018.10.002
6. Begemann MJ, Brand BA, Curčić-Blake B, Aleman A, Sommer IE. Efficacy of non-invasive brain stimulation on cognitive functioning in brain disorders: a meta-analysis. *Psychol Med.* (2020) 50:2465–86. doi: 10.1017/S0033291720003670
7. Sloan NP, Byrne LK, Enticott PG, Lum JG. Non-invasive brain stimulation does not improve working memory in schizophrenia: a meta-analysis of randomised controlled trials. *Neuropsychol Rev.* (2021) 31:115–38. doi: 10.1007/s11065-020-09454-4
8. Marzouk T, Winkelbeiner S, Azizi H, Malhotra AK, Homan P. Transcranial magnetic stimulation for positive symptoms in schizophrenia: a systematic review. *Neuropsychobiology.* (2020) 79:384–96. doi: 10.1159/000502148
9. Brunoni AR, Vanderhasselt M-A. Working memory improvement with non-invasive brain stimulation of the dorsolateral prefrontal cortex: a systematic review and meta-analysis. *Brain Cogn.* (2014) 86:1–9. doi: 10.1016/j.bandc.2014.01.008
10. Smith RC, Boules S, Mattiuz S, Youssef M, Tobe RH, Sershen H, et al. Effects of transcranial direct current stimulation (tDCS) on cognition, symptoms, and smoking in schizophrenia: a randomized controlled study. *Schizophr Res.* (2015) 168:260–6. doi: 10.1016/j.schres.2015.06.011
11. Sreeraj VS, Bose A, Chhabra H, Shivakumar V, Agarwal SM, Narayanaswamy JC, et al. Working memory performance with online-tDCS in schizophrenia: a randomized, double-blinded, sham-controlled, partial cross-over proof-of-concept study. *Asian J Psychiatr.* (2020) 50:101946. doi: 10.1016/j.ajp.2020.101946
12. Vercammen A, Knegtering H, Liemburg EJ, Den Boer JA, Aleman A. Functional connectivity of the temporo-parietal region in schizophrenia: effects of rTMS treatment of auditory hallucinations. *J Psychiatr Res.* (2010) 44:725–31. doi: 10.1016/j.jpsychires.2009.12.011
13. Blumberger DM, Christensen BK, Zipursky RB, Moller B, Chen R, Fitzgerald PB, et al. MRI-targeted repetitive transcranial magnetic stimulation of Heschl's gyrus for refractory auditory hallucinations. *Brain Stimul.* (2012) 5:577–85. doi: 10.1016/j.brs.2011.12.002
14. Schönfeldt-Lecuona C, Grön G, Walter H, Büchler N, Wunderlich A, Spitzer M, et al. Stereotaxic rTMS for the treatment of auditory hallucinations in schizophrenia. *Neuroreport.* (2004) 15:1669–73. doi: 10.1097/01.wnr.0000126504.89983.ec
15. Paillère-Martinot ML, Galinowski A, Plaze M, Andoh J, Bartrés-Faz D, Bellivier F, et al. Active and placebo transcranial magnetic stimulation effects on external and internal auditory hallucinations of schizophrenia. *Acta Psychiatr Scand.* (2017) 135:228–38. doi: 10.1111/acps.12680
16. Zhang B, Liu J, Bao T, Wilson G, Park J, Zhao B, et al. Locations for noninvasive brain stimulation in treating depressive disorders: A combination of meta-analysis and resting-state functional connectivity analysis. *Austr New Zeal J Psychiatr.* (2020) 54:582–90. doi: 10.1177/0004867420920372
17. Liu J, Zhang B, Wilson G, Kong J, Weiner MW, Aisen P, et al. New perspective for non-invasive brain stimulation site selection in mild cognitive impairment: based on meta- and functional connectivity analyses. *Front Aging Neurosci.* (2019) 11:228. doi: 10.3389/fnagi.2019.00228
18. Huang Y, Zhang B, Cao J, Yu S, Wilson G, Park J, et al. Potential locations for noninvasive brain stimulation in treating autism spectrum

disorders—a functional connectivity study. *Front Psychiatry.* (2020) 11. doi: 10.3389/fpsyt.2020.00388
19. Sheehan DV, Lecrubier Y, Sheehan KH, Amorim P, Janavs J, Weiller E, et al. The Mini-International Neuropsychiatric Interview (M.I.N.I.): the development and validation of a structured diagnostic psychiatric interview for DSM-IV and ICD-10. *J Clin Psychiatry.* (1998) 59:22–33. doi: 10.1037/t18597-000
20. Kay SR, Fiszbein A, Opler LA. The positive and negative syndrome scale (PANSS) for schizophrenia. *Schizophr Bull.* (1987) 13:261–76. doi: 10.1093/schbul/13.2.261
21. Yan C-G, Wang X-D, Zuo X-N, Zang Y-F. DPABI: data processing and analysis for (resting-state) brain imaging. *Neuroinformatics.* (2016) 14:339–51. doi: 10.1007/s12021-016-9299-4
22. Whitfield-Gabrieli S, Nieto-Castanon A. Conn: a functional connectivity toolbox for correlated and anticorrelated brain networks. *Brain Connect.* (2012) 2:125–41. doi: 10.1089/brain.2012.0073
23. Yarkoni T, Poldrack RA, Nichols TE, Van Essen DC, Wager TD. Large-scale automated synthesis of human functional neuroimaging data. *Nat Methods.* (2011) 8:665–70. doi: 10.1038/nmeth.1635
24. Cutini S, Scatturin P, Zorzi M. A new method based on ICBM152 head surface for probe placement in multichannel fNIRS. *Neuroimage.* (2011) 54:919–27. doi: 10.1016/j.neuroimage.2010.09.030
25. Osoegawa C, Gomes JS, Grigolon RB, Brietzke E, Gadelha A, Lacerda ALT, et al. Non-invasive brain stimulation for negative symptoms in schizophrenia: an updated systematic review and meta-analysis. *Schizophr Res.* (2018) 197:34–44. doi: 10.1016/j.schres.2018.01.010
26. Mehta UM, Naik SS, Thanki MV, Thirthalli J. Investigational and therapeutic applications of transcranial magnetic stimulation in schizophrenia. *Curr Psychiatry Rep.* (2019) 21:89. doi: 10.1007/s11920-019-1076-2
27. Cheng PWC, Louie LLC, Wong YL, Wong SMC, Leung WY, Nitsche MA, et al. The effects of transcranial direct current stimulation (tDCS) on clinical symptoms in schizophrenia: a systematic review and meta-analysis. *Asian J Psychiatr.* (2020) 53:102392. doi: 10.1016/j.ajp.2020.102392
28. Mcintosh AM, Semple D, Tasker K, Harrison LK, Owens DG, Johnstone EC, et al. Transcranial magnetic stimulation for auditory hallucinations in schizophrenia. *Psychiatry Res.* (2004) 127:9–17. doi: 10.1016/j.psychres.2004.03.005
29. Fitzgerald PB, Benitez J, Daskalakis JZ, Brown TL, Marston NA, De Castella A, et al. A double-blind sham-controlled trial of repetitive transcranial magnetic stimulation in the treatment of refractory auditory hallucinations. *J Clin Psychopharmacol.* (2005) 25:358–62. doi: 10.1097/01.jcp.0000168487.22140.7f
30. Jandl M, Steyer J, Weber M, Linden DE, Rothmeier J, Maurer K, et al. Treating auditory hallucinations by transcranial magnetic stimulation: a randomized controlled cross-over trial. *Neuropsychobiology.* (2006) 53:63–9. doi: 10.1159/000091721
31. Saba G, Verdon CM, Kalalou K, Rocamora JF, Dumortier G, Benadhira R, et al. Transcranial magnetic stimulation in the treatment of schizophrenic symptoms: a double blind sham controlled study. *J Psychiatr Res.* (2006) 40:147–52. doi: 10.1016/j.jpsychires.2005.02.008
32. Rosa MO, Gattaz WF, Rosa MA, Rumi DO, Tavares H, Myczkowski M, et al. Effects of repetitive transcranial magnetic stimulation on auditory hallucinations refractory to clozapine. *J Clin Psychiatry.* (2007) 68:1528–32. doi: 10.4088/JCP.v68n1009
33. Slotema CW, Blom JD, De Weijer AD, Diederen KM, Goekoop R, Looijestijn J, et al. Can low-frequency repetitive transcranial magnetic stimulation really relieve medication-resistant auditory verbal hallucinations? Negative results from a large randomized controlled trial. *Biol Psychiatry.* (2011) 69:450–6. doi: 10.1016/j.biopsych.2010.09.051
34. Hoffman RE, Boutros NN, Berman RM, Roessler E, Belger A, Krystal JH, et al. Transcranial magnetic stimulation of left temporoparietal cortex in three patients reporting hallucinated "voices". *Biol Psychiatry.* (1999) 46:130–2. doi: 10.1016/S0006-3223(98)00358-8
35. Hoffman RE, Boutros NN, Hu S, Berman RM, Krystal JH, Charney DS. Transcranial magnetic stimulation and auditory hallucinations in schizophrenia. *Lancet.* (2000) 355:1073–5. doi: 10.1016/S0140-6736(00)02043-2
36. Hoffman RE, Hawkins KA, Gueorguieva R, Boutros NN, Rachid F, Carroll K, et al. Transcranial magnetic stimulation of left temporoparietal cortex and medication-resistant auditory hallucinations. *Arch Gen Psychiatry.* (2003) 60:49–56. doi: 10.1001/archpsyc.60.1.49
37. Chibbaro G, Daniele M, Alagona G, Di Pasquale C, Cannavò M, Rapisarda V, et al. Repetitive transcranial magnetic stimulation in schizophrenic patients reporting auditory hallucinations. *Neurosci Lett.* (2005) 383:54–7. doi: 10.1016/j.neulet.2005.03.052
38. Hoffman RE, Gueorguieva R, Hawkins KA, Varanko M, Boutros NN, Wu YT, et al. Temporoparietal transcranial magnetic stimulation for auditory hallucinations: safety, efficacy and moderators in a fifty patient sample. *Biol Psychiatry.* (2005) 58:97–104. doi: 10.1016/j.biopsych.2005.03.041
39. Lee SH, Kim W, Chung YC, Jung KH, Bahk WM, Jun TY, et al. A double blind study showing that two weeks of daily repetitive TMS over the left or right temporoparietal cortex reduces symptoms in patients with schizophrenia who are having treatment-refractory auditory hallucinations. *Neurosci Lett.* (2005) 376:177–81. doi: 10.1016/j.neulet.2004.11.048
40. Bagati D, Nizamie SH, Prakash R. Effect of augmentatory repetitive transcranial magnetic stimulation on auditory hallucinations in schizophrenia: randomized controlled study. *Aust N Z J Psychiatry.* (2009) 43:386–92. doi: 10.1080/00048670802653315
41. Loo CK, Sainsbury K, Mitchell P, Hadzi-Pavlovic D, Sachdev PS. A sham-controlled trial of left and right temporal rTMS for the treatment of auditory hallucinations. *Psychol Med.* (2010) 40:541–6. doi: 10.1017/S0033291709990900
42. Klein E, Kolsky Y, Puyerovsky M, Koren D, Chistyakov A, Feinsod M. Right prefrontal slow repetitive transcranial magnetic stimulation in schizophrenia: a double-blind sham-controlled pilot study. *Biol Psychiatry.* (1999) 46:1451–4. doi: 10.1016/S0006-3223(99)00182-1
43. Hajak G, Marienhagen J, Langguth B, Werner S, Binder H, Eichhammer P. High-frequency repetitive transcranial magnetic stimulation in schizophrenia: a combined treatment and neuroimaging study. *Psychol Med.* (2004) 34:1157–63. doi: 10.1017/S0033291704002338
44. Holi MM, Eronen M, Toivonen K, Toivonen P, Marttunen M, Naukkarinen H. Left prefrontal repetitive transcranial magnetic stimulation in schizophrenia. *Schizophr Bull.* (2004) 30:429–34. doi: 10.1093/oxfordjournals.schbul.a007089
45. Cordes J, Thünker J, Agelink MW, Arends M, Mobascher A, Wobrock T, et al. Effects of 10 Hz repetitive transcranial magnetic stimulation (rTMS) on clinical global impression in chronic schizophrenia. *Psychiatry Res.* (2010) 177:32–6. doi: 10.1016/j.psychres.2009.01.014
46. Rollnik JD, Huber TJ, Mogk H, Siggelkow S, Kropp S, Dengler R, et al. High frequency repetitive transcranial magnetic stimulation (rTMS) of the dorsolateral prefrontal cortex in schizophrenic patients. *Neuroreport.* (2000) 11:4013–5. doi: 10.1097/00001756-200012180-00022
47. Jin Y, Potkin SG, Kemp AS, Huerta ST, Alva G, Thai TM, et al. Therapeutic effects of individualized alpha frequency transcranial magnetic stimulation (alphaTMS) on the negative symptoms of schizophrenia. *Schizophr Bull.* (2006) 32:556–61. doi: 10.1093/schbul/sbj020
48. Schneider AL, Schneider TL, Stark H. Repetitive transcranial magnetic stimulation (rTMS) as an augmentation treatment for the negative symptoms of schizophrenia: a 4-week randomized placebo controlled study. *Brain Stimul.* (2008) 1:106–11. doi: 10.1016/j.brs.2008.01.001
49. Prikryl R, Ustohal L, Prikrylova Kucerova H, Kasparek T, Venclikova S, Vrzalova M, et al. A detailed analysis of the effect of repetitive transcranial magnetic stimulation on negative symptoms of schizophrenia: a double-blind trial. *Schizophr Res.* (2013) 149:167–73. doi: 10.1016/j.schres.2013.06.015
50. Prikryl R, Ustohal L, Kucerova HP, Kasparek T, Jarkovsky J, Hublova V, et al. Repetitive transcranial magnetic stimulation reduces cigarette consumption in schizophrenia patients. *Prog Neuropsychopharmacol Biol Psychiatry.* (2014) 49:30–5. doi: 10.1016/j.pnpbp.2013.10.019
51. Wölwer W, Lowe A, Brinkmeyer J, Streit M, Habakuck M, Agelink MW, et al. Repetitive transcranial magnetic stimulation (rTMS) improves facial affect recognition in schizophrenia. *Brain Stimul.* (2014) 7:559–63. doi: 10.1016/j.brs.2014.04.011
52. Li Z, Yin M, Lyu X-L, Zhang L-L, Du X-D, Hung GC-L. Delayed effect of repetitive transcranial magnetic stimulation (rTMS) on negative symptoms of schizophrenia: Findings from a randomized controlled trial. *Psychiatry Res.* (2016) 240:333–5. doi: 10.1016/j.psychres.2016.04.046

53. Zhou DD, Wang W, Wang GM, Li DQ, Kuang L. An updated meta-analysis: Short-term therapeutic effects of repeated transcranial magnetic stimulation in treating obsessive-compulsive disorder. *J Affect Disord.* (2017) 215:187–96. doi: 10.1016/j.jad.2017.03.033
54. Fitzgerald PB, Herring S, Hoy K, Mcqueen S, Segrave R, Kulkarni J, et al. A study of the effectiveness of bilateral transcranial magnetic stimulation in the treatment of the negative symptoms of schizophrenia. *Brain Stimul.* (2008) 1:27–32. doi: 10.1016/j.brs.2007.08.001
55. Barr MS, Farzan F, Tran LC, Fitzgerald PB, Daskalakis ZJ. A randomized controlled trial of sequentially bilateral prefrontal cortex repetitive transcranial magnetic stimulation in the treatment of negative symptoms in schizophrenia. *Brain Stimul.* (2012) 5:337–46. doi: 10.1016/j.brs.2011.06.003
56. Wobrock T, Guse B, Cordes J, Wölwer W, Winterer G, Gaebel W, et al. Left prefrontal high-frequency repetitive transcranial magnetic stimulation for the treatment of schizophrenia with predominant negative symptoms: a sham-controlled, randomized multicenter trial. *Biol Psychiatry.* (2015) 77:979–88. doi: 10.1016/j.biopsych.2014.10.009
57. Fitzgerald PB, Mcqueen S, Daskalakis ZJ, Hoy KE. A negative pilot study of daily bimodal transcranial direct current stimulation in schizophrenia. *Brain Stimul.* (2014) 7:813–6. doi: 10.1016/j.brs.2014.08.002
58. Fröhlich F, Burrello TN, Mellin JM, Cordle AL, Lustenberger CM, Gilmore JH, et al. Exploratory study of once-daily transcranial direct current stimulation (tDCS) as a treatment for auditory hallucinations in schizophrenia. *Eur Psychiatry.* (2016) 33:54–60. doi: 10.1016/j.eurpsy.2015.11.005
59. Bose A, Shivakumar V, Agarwal SM, Kalmady SV, Shenoy S, Sreeraj VS, et al. Efficacy of fronto-temporal transcranial direct current stimulation for refractory auditory verbal hallucinations in schizophrenia: a randomized, double-blind, sham-controlled study. *Schizophr Res.* (2018) 195:475–80. doi: 10.1016/j.schres.2017.08.047
60. Koops S, Blom JD, Bouachmir O, Slot MI, Neggers B, Sommer IE. Treating auditory hallucinations with transcranial direct current stimulation in a double-blind, randomized trial. *Schizophr Res.* (2018) 201:329–36. doi: 10.1016/j.schres.2018.06.010
61. Chang CC, Kao YC, Chao CY, Chang HA. Enhancement of cognitive insight and higher-order neurocognitive function by fronto-temporal transcranial direct current stimulation (tDCS) in patients with schizophrenia. *Schizophr Res.* (2019) 208:430–8. doi: 10.1016/j.schres.2018.12.052
62. Kantrowitz JT, Sehatpour P, Avissar M, Horga G, Gwak A, Hoptman MJ, et al. Significant improvement in treatment resistant auditory verbal hallucinations after 5 days of double-blind, randomized, sham controlled, fronto-temporal, transcranial direct current stimulation (tDCS): A replication/extension study. *Brain Stimul.* (2019) 12:981–91. doi: 10.1016/j.brs.2019.03.003
63. Brunelin J, Mondino M, Gassab L, Haesebaert F, Gaha L, Suaud-Chagny MF, et al. Examining transcranial direct-current stimulation (tDCS) as a treatment for hallucinations in schizophrenia. *Am J Psychiatry.* (2012) 169:719–24. doi: 10.1176/appi.ajp.2012.11071091
64. Mondino M, Jardri R, Suaud-Chagny MF, Saoud M, Poulet E, Brunelin J. Effects of fronto-temporal transcranial direct current stimulation on auditory verbal hallucinations and resting-state functional connectivity of the left temporo-parietal junction in patients with schizophrenia. *Schizophr Bull.* (2016) 42:318–26. doi: 10.1093/schbul/sbv114
65. Valiengo L, Goerigk S, Gordon PC, Padberg F, Serpa MH, Koebe S, et al. Efficacy and safety of transcranial direct current stimulation for treating negative symptoms in schizophrenia: a randomized clinical trial. *JAMA Psychiatry.* (2020) 77:121–9. doi: 10.1001/jamapsychiatry.2019.3199
66. Palm U, Keeser D, Hasan A, Kupka MJ, Blautzik J, Sarubin N, et al. Prefrontal transcranial direct current stimulation for treatment of schizophrenia with predominant negative symptoms: a double-blind, sham-controlled proof-of-concept study. *Schizophr Bull.* (2016) 42:1253–61. doi: 10.1093/schbul/sbw041
67. Chang CC, Kao YC, Chao CY, Tzeng NS, Chang HA. Examining bi-anodal transcranial direct current stimulation (tDCS) over bilateral dorsolateral prefrontal cortex coupled with bilateral extracephalic references as a treatment for negative symptoms in non-acute schizophrenia patients: a randomized, double-blind, sham-controlled trial. *Prog Neuropsychopharmacol Biol Psychiatry.* (2020) 96:109715. doi: 10.1016/j.pnpbp.2019.109715
68. Gomes JS, Trevizol AP, Ducos DV, Gadelha A, Ortiz BB, Fonseca AO, et al. Effects of transcranial direct current stimulation on working memory and negative symptoms in schizophrenia: a phase II randomized sham-controlled trial. *Schizophr Res Cogn.* (2018) 12:20–8. doi: 10.1016/j.scog.2018.02.003
69. Jeon DW, Jung DU, Kim SJ, Shim JC, Moon JJ, Seo YS, et al. Adjunct transcranial direct current stimulation improves cognitive function in patients with schizophrenia: a double-blind 12-week study. *Schizophr Res.* (2018) 197:378–85. doi: 10.1016/j.schres.2017.12.009
70. Lefaucheur J-P, André-Obadia N, Antal A, Ayache SS, Baeken C, Benninger DH, et al. Evidence-based guidelines on the therapeutic use of repetitive transcranial magnetic stimulation (rTMS). *Clin Neurophysiol.* (2014) 125:2150–206. doi: 10.1016/j.clinph.2014.05.021
71. Pondé PH, De Sena EP, Camprodon JA, de Araújo AN, Neto MF, DiBiasi M, et al. Use of transcranial direct current stimulation for the treatment of auditory hallucinations of schizophrenia - a systematic review. *Neuropsychiatric Dis Treatment.* (2017) 13:347–55. doi: 10.2147/NDT.S122016
72. Fitzgerald PB, Maller JJ, Hoy KE, Thomson R, Daskalakis ZJ. Exploring the optimal site for the localization of dorsolateral prefrontal cortex in brain stimulation experiments. *Brain Stimul.* (2009) 2:234–7. doi: 10.1016/j.brs.2009.03.002
73. Brady RO, Gonsalvez I, Lee I, Öngür D, Seidman LJ, Schmahmann JD, et al. Breakdown of functional connectivity in cerebellar-prefrontal network underlies negative symptoms in schizophrenia. *Am J Psychiatry.* (2019) 176:512–20. doi: 10.1176/appi.ajp.2018.18040429
74. Stegmayer K, Horn H, Federspiel A, Razavi N, Bracht T, Laimböck K, et al. Supplementary motor area (SMA) volume is associated with psychotic aberrant motor behaviour of patients with schizophrenia. *Psychiatry Res.* (2014) 223:49–51. doi: 10.1016/j.pscychresns.2014.05.002
75. Walther S, Federspiel A, Horn H, Razavi N, Wiest R, Dierks T, et al. Alterations of white matter integrity related to motor activity in schizophrenia. *Neurobiol Dis.* (2011) 42:276–83. doi: 10.1016/j.nbd.2011.01.017
76. Walther S, Alexaki D, Schoretsanitis G, Weiss F, Vladimirova I, Stegmayer K, et al. Inhibitory repetitive transcranial magnetic stimulation to treat psychomotor slowing: a transdiagnostic, mechanism-based randomized double-blind controlled trial. *Schizophrenia Bull Open.* (2020) 1:sgaa020. doi: 10.1093/schizbullopen/sgaa020
77. Lefebvre S, Pavlidou A, Walther S. What is the potential of neurostimulation in the treatment of motor symptoms in schizophrenia? *Expert Rev Neurother.* (2020) 20:697–706. doi: 10.1080/14737175.2020.1775586
78. Koreki A, Maeda T, Okimura T, Terasawa Y, Kikuchi T, Umeda S, et al. Dysconnectivity of the agency network in schizophrenia: a functional magnetic resonance imaging study. *Front Psychiatry.* (2019) 10:171. doi: 10.3389/fpsyt.2019.00171
79. Smiley JF, Konnova K, Bleiwas C. Cortical thickness, neuron density and size in the inferior parietal lobe in schizophrenia. *Schizophr Res.* (2012) 136:43–50. doi: 10.1016/j.schres.2012.01.006
80. Liu N, Xiao Y, Zhang W, Tang B, Zeng J, Hu N, et al. Characteristics of gray matter alterations in never-treated and treated chronic schizophrenia patients. *Transl Psychiatry.* (2020) 10:136. doi: 10.1038/s41398-020-0828-4
81. Xu P, Chen A, Li Y, Xing X, Lu H. Medial prefrontal cortex in neurological diseases. *Physiol Genomics.* (2019) 51:432–42. doi: 10.1152/physiolgenomics.00006.2019
82. Van Erp TGM, Walton E, Hibar DP, Schmaal L, Jiang W, Glahn DC, et al. Cortical brain abnormalities in 4474 individuals with schizophrenia and 5098 control subjects via the enhancing neuro imaging genetics through meta analysis (ENIGMA) consortium. *Biol Psychiatry.* (2018) 84:644–54. doi: 10.1016/j.biopsych.2018.04.023
83. Williamson P. Are anticorrelated networks in the brain relevant to schizophrenia? *Schizophr Bull.* (2007) 33:994–1003. doi: 10.1093/schbul/sbm043
84. Liu H, Kaneko Y, Ouyang X, Li L, Hao Y, Chen EYH, et al. Schizophrenic patients and their unaffected siblings share increased resting-state connectivity in the task-negative network but not its anticorrelated task-positive network. *Schizophr Bull.* (2012) 38:285–94. doi: 10.1093/schbul/sbq074
85. Hu M-L, Zong X-F, Mann JJ, Zheng J-J, Liao Y-H, Li Z-C, et al. A review of the functional and anatomical default mode network in schizophrenia. *Neurosci Bull.* (2017) 33:73–84. doi: 10.1007/s12264-016-0090-1
86. Philip NS, Barredo J, van't Wout-Frank M, Tyrka AR, Price LH, Carpenter LL. Network mechanisms of clinical response to transcranial

magnetic stimulation in posttraumatic stress disorder and major depressive disorder. *Biol Psychiatr*. (2018) 83:263–72. doi: 10.1016/j.biopsych.2017.07.021

Conflict of Interest: The authors declare that the research was conducted in the absence of any commercial or financial relationships that could be construed as a potential conflict of interest.

The handling editor declared a past collaboration with one of the authors BZ.

Publisher's Note: All claims expressed in this article are solely those of the authors and do not necessarily represent those of their affiliated organizations, or those of the publisher, the editors and the reviewers. Any product that may be evaluated in this article, or claim that may be made by its manufacturer, is not guaranteed or endorsed by the publisher.

frontiers in Neurology

ORIGINAL RESEARCH
published: 02 March 2022
doi: 10.3389/fneur.2022.834329

The Impact of Ischemic Stroke on Gray and White Matter Injury Correlated With Motor and Cognitive Impairments in Permanent MCAO Rats: A Multimodal MRI-Based Study

Le Yang[1,2†], *Manzhong Li*[3,4†], *Yu Zhan*[1,2], *Xuefeng Feng*[1,2], *Yun Lu*[1,2], *Mingcong Li*[1,2], *Yuming Zhuang*[1,2], *Jianfeng Lei*[5] *and Hui Zhao*[1,2*]

[1] *School of Traditional Chinese Medicine, Capital Medical University, Beijing, China,* [2] *Beijing Key Lab of TCM Collateral Disease Theory Research, Beijing, China,* [3] *Department of Pharmacy, Beijing Shijitan Hospital, Capital Medical University, Beijing, China,* [4] *Beijing Key Laboratory of Bio-characteristic Profiling for Evaluation of Rational Drug Use, Beijing, China,* [5] *Medical Imaging Laboratory of Core Facility Center, Capital Medical University, Beijing, China*

OPEN ACCESS

Edited by:
Yihuai Zou,
Beijing University of Chinese Medicine, China

Reviewed by:
Yonghong Gao,
Beijing University of Chinese Medicine, China
Melissa E. Trotman-Lucas,
University of Nottingham, United Kingdom

***Correspondence:**
Hui Zhao
zhaohuishouyi@ccmu.edu.cn

[†] *These authors have contributed equally to this work*

Specialty section:
This article was submitted to Applied Neuroimaging, a section of the journal Frontiers in Neurology

Received: *13 December 2021*
Accepted: *19 January 2022*
Published: *02 March 2022*

Citation:
Yang L, Li M, Zhan Y, Feng X, Lu Y, Li M, Zhuang Y, Lei J and Zhao H (2022) The Impact of Ischemic Stroke on Gray and White Matter Injury Correlated With Motor and Cognitive Impairments in Permanent MCAO Rats: A Multimodal MRI-Based Study. Front. Neurol. 13:834329. doi: 10.3389/fneur.2022.834329

Background: Identifying the alterations of the cerebral gray and white matter is an important prerequisite for developing potential pharmacological therapy for stroke. This study aimed to assess the changes of gray and white matter after permanent middle cerebral artery occlusion (pMCAO) in rats using magnetic resonance imaging (MRI), and to correlate them with the behavior performance.

Methods: Rats were subjected to pMCAO or sham surgery and reared for 30 days. Motor and cognitive function of the rats were examined by gait and Morris water maze (MWM) tests, respectively. Multimodal MRI was conducted to examine the functional and structural changes of the gray and white matter followed with luxol fast blue (LFB) staining.

Results: The gait and MWM tests revealed significant motor and cognitive dysfunction in pMCAO rats, respectively. Magnetic resonance angiography presented abnormal intracranial arteries in pMCAO rats with reduced signal intensity of the anterior cerebral artery, anterior communicating cerebral artery, internal carotid artery, and increased basilar artery vessel signal compared with sham rats. Arterial spin labeling confirmed the decreased cerebral blood flow in the infarcted sensorimotor cortex and striatum. Structural T2-weighted imaging and T2 mapping showed brain atrophy and elevation of T2 value in the gray (sensorimotor cortex, striatum) and white (external capsule, internal capsule) matter of pMCAO rats. The results from diffusion tensor imaging (DTI) corresponded well with LFB staining showing reduced relative FA accompanied with increased relative AD and RD in the gray and white matter of pMCAO rats compared with sham rats. Fiber tracking derived from DTI further observed significantly reduced fiber density and length in the corresponding brain regions of pMCAO rats compared with sham rats. Specially, the DTI parameters (especially FA) in the relevant gray matter and white matter significantly correlated with the behavior performance in the gait and MWM tests.

Conclusion: Collectively, the gray and white matter damages could be non-invasively monitored in pMCAO rats by multimodal MRI. DTI-derived parameters, particularly the FA, might be a good imaging index to stage gray and white matter damages associated with post-stroke motor and cognitive impairments.

Keywords: ischemic stroke, white matter, gray matter, magnetic resonance imaging, rat

INTRODUCTION

Stroke is a leading cause of mortality and disability worldwide (1). Despite stroke mortality has been declining with effective thrombolysis, a large proportion of stroke survivors suffer permanent neurological deficits (2). It is worth noting that ischemic stroke causes not only gray matter damage defined by neuronal necrosis, but also elicits white matter injury (3). Clinical studies show that white matter accounts for half of the lesion volume in most cases of human stroke (3). Post-stroke white matter injury not only destroys the communications among different brain structures, but also causes remote gray matter dysfunction, ultimately leading to motor and cognitive impairments (4). In particular, the severity of white matter injury has been suggested to be an independent predictor of unfavorable outcomes in acute ischemic stroke patients undergoing endovascular therapy (5). Thus, numerous neuroprotective therapies aiming at cerebral gray matter injury (not specifically targeting the white matter characterized by axonal degeneration and demyelination) have failed to improve functional outcomes in clinically (6–8). Therefore, optimal therapies targeted at restoration of gray and white matter are critical to improve long-term neurological function after ischemic stroke.

Animal stroke models have played a unique role in developing new agents for stroke therapy. Since human ischemic stroke is often affected by occlusion of the middle cerebral artery (MCA), the occlusive MCA stroke models are closest to human ischemic stroke (9). To date, transient middle cerebral artery occlusion (MCAO) model with rats or mice is the widely used animal model for preclinical stroke research. As most large vessel occlusion patients have permanent vessel occlusion, recommendation of the Stroke Therapy Academic Industry Roundtable (STAIR) called for the permanent MCAO (pMCAO) model as the primary model for preclinical studies (10). Others in stroke research suggest that pMCAO model is of greater clinical relevance, and therapy beneficial in the pMCAO model may have a better chance of success in clinical trials (10). Thus, there is a need to develop reliable means that can characterize the structural alterations in gray and white matter which occur with post-stroke motor and cognitive impairments based on the pMCAO model.

In pharmacological studies, traditional histological staining techniques were used to assess the alterations of the ischemic gray and white matter. The main limitation is that it could not noninvasively monitor gray–white matter damage and repair after stroke (11). MRI provides a means to reveal the structural alterations of the post-stroke brain noninvasively and dynamically. For example, T2-weighted MRI is a favorable tool to real-time visualize the anatomical characteristics and pathological changes of the brain (12), and diffusion tensor imaging (DTI) informs on microstructural integrity of the gray and white matter (13). Hence, we implemented a multimodal MRI design to noninvasively characterize the changes in the perilesional gray and white matter in pMCAO rats, together with Morris water maze (MWM) and gait analysis. Furthermore, correlation analysis was carried out between behavior performances and DTI parameters from the gray and white matter at chronic stage of pMCAO, which could be reliably used for investigating potential stroke therapies that ameliorate ischemia-induced neurodegeneration.

MATERIALS AND METHODS

Animals

Twenty male Sprague–Dawley rats weighing 300–320 g (aged 8 weeks) were purchased from Vital River Laboratory Animal Technology Co. Ltd. (Beijing, China). [SCXK (jing) 2016-0011] and kept under specific pathogen free (SPF) animal research center in Capital Medical University [SYXK (jing) 2018-0003] with controlled temperature (2 ± 1°C), humidity (55 ± 10%) and 12-h light/dark cycle. The experiment was carried out after 1 week of adaptive feeding. All experiments were performed according to the National Institute of Health Guide for the Care and Use of Laboratory Animals, and approved by the Ethical Committee at Capital Medical University (permit number: AEEI-2018-052). Every effort was made to minimize the number of animals used and their suffering.

Stroke Induction and Animal Grouping

Focal cerebral ischemia was induced by permanent occlusion of the right middle cerebral artery (pMCAO) with an intraluminal filament. Briefly, 12 animals were randomly selected according to a random number list and anesthetized with isoflurane (5% for induction and 2% for maintenance) vaporized in N_2O/O_2 (70/30). The right common carotid artery (CCA), internal carotid artery (ICA), and external carotid artery (ECA) were carefully separated from the vagal nerves through a midline neck incision. A 4-0 monofilament nylon suture (Beijing Sunbio Biotech Co Ltd., China) was inserted from the ECA into the lumen of right ICA and advanced for about 16–18 mm until mild resistance was felt (14). After the incision was closed by a suture, rats were placed under a heating lamp until fully recovered and taken back to the standard cage with free access to food and water. The infarct volume was measured on the 31st day after pMCAO by T2-weighted imaging (T2WI). Rats with successful pMCAO induction were included into the pMCAO group ($N = 9$) with

the inclusion criterion setting at a lesion volume of 100 mm^3 (15). Two rats died in 3 days after the surgery and one rat with the infarct volume of less than 100 mm^3 was excluded from the study. Sham-operated animals ($N = 8$) underwent the same surgical procedure without artery occlusion.

MRI Protocols

Magnetic resonance imaging measurements were performed using a 7.0 T PharmaScan Scanner (Bruker, Germany) on the 31st day after stroke induction. Rats were initially anesthetized under 5% isoflurane mixed with N_2O/O_2 (70/30) and maintained under 2% isoflurane. During the MRI scan, the blood oxygen saturation and heart rate of rats were monitored, and the rectal temperature was kept at 37 $\pm$ 0.5°C. An experimenter blind to the group information performed the data analysis.

T2-weighted imaging was applied to determine the lesion volume of pMCAO rats using a fast spin-echo pulse sequence (16). The infarct region was defined by the area with image intensities higher than the mean+2 standard deviations of the intensity in the mirrored contralateral area (17). The infarct volume was calculated by multiplying total infarct area measured on each slice by the slice thickness using ImageJ software. Similarly, the ventricular volume and hemispheric volume were obtained. The hemispheric parenchymal volume was calculated by subtracting the ventricular and infarct volume from the hemispheric volume (18).

T2 mapping was conducted to assess the structural changes of gray and white matter with a multislice multiecho (MSME) sequence. Regions of interest (ROIs) were manually drawn in the bilateral gray matter (sensorimotor cortex and striatum) and white matter (internal capsule and external capsule) on coronal T2 relaxometry maps according to the Paxinos and Watson atlas. T2 values were obtained from each ROI and data were expressed as a percentage of the ipsilateral T2 values compared to the contralateral T2 values.

Three-dimensional time-of-flight magnetic resonance angiography (3D-TOF MRA) was conducted to detect the alterations of the intracranial arteries using a fast low angle shot sequence (16). The multiplanar reconstruction (MPR) and maximum intensity projection (MIP) images of MRA were generated by Paravision version 5.1 software (Bruker, Germany). The signal intensities of the bilateral anterior cerebral artery (ACA), anterior communicating cerebral artery (AcoA), anterior azygos cerebral artery (azACA), MCA, ICA, posterior cerebral artery (PCA), and basilar artery (BA) were obtained based on a previously described method (19).

Arterial spin labeling (ASL) was used to evaluate the regional cerebral blood flow (CBF) with an echo-planar imaging fluid-attenuated inversion recovery sequence (16). The heat map of ASL raw data and CBF map were obtained by Paravision version 5.1 software, and the regional CBF of the bilateral sensorimotor cortex and striatum was acquired according to our previous study (20). Data were expressed as the ipsilateral CBF relative to the contralateral.

Diffusion tensor imaging was performed to assess fiber integrity by an axial single-shot spin echo-planar imaging sequence (16). The DTI parametric maps including fractional anisotropy (FA), axial diffusivity (AD), and radial diffusivity (RD) were generated by Paravision version 5.1 software. ROIs were placed in the bilateral gray matter (sensorimotor cortex and striatum) and white matter (internal capsule and external capsule) on the DTI parametric maps to obtain corresponding DTI indices. Diffusion tensor tractography (DTT) was performed using Diffusion Toolkit and TrackVis software with the seeding areas placed on the corresponding brain regions (21). The mean fiber length and fiber density of the corresponding regions were measured. Data were presented as the ratio of ipsilateral value relative to the contralateral.

Gait Analysis

Gait analysis was performed with DigiGait^{TM} system (Mouse Specifics Inc., America) on the 32nd day after surgery for assessing the motor function. DigiGait^{TM} contained a transparent treadmill on which animals were restricted under a polymethyl methacrylate cover and forced to walk or run at a fixed velocity. Before the experiment, rats were trained on the treadmill to make uninterrupted runs for at least 3 step-cycles at a speed of 15 cm/s. During the experiment, each rat was placed on the treadmill repeatedly at intervals of 5 min to complete three uninterrupted runs (containing at least 3 step-cycles per run) for data analyses (22). Gait parameters including stance ratio, swing ratio, brake ratio, paw area, and stride length were automatically labeled as right forelimb (RF), right hindlimb (RH), left forelimb (LF), and left hindlimb (LH). An investigator blind to the group information analyzed gait data using DigiGait Analysis15 software.

Morris Water Maze

The Morris water maze test was performed from the 33rd to the 38th day after surgery for evaluating the learning and memory ability (23). The maze consisted of a circular tank with a transparent round platform (15 cm in diameter). The tank was divided into four virtual quadrants (quadrants I, II, III, and IV) and filled with opaque water (18–20°C).

From the 33rd to the 36th day, the platform was placed in the middle of quadrant I and 1.5 cm under the water surface for the hidden platform test. Each animal underwent four trials per day at an inter-trial interval of 60 s. For each trial, the rat was given up to 60 s to find the hidden platform. If the rat failed to find the platform within 60 s, it would be guided to the platform and kept on the platform for 10 s. The escape latency and path length by which the rat located the platform was recorded by a video tracking system (JLBehv-MWMG, Jiliang Sofware Technology Co.Ltd., Shanghai).

On the 37th day, the probe trial was performed to assess memory retention. During the probe trial, the platform was removed from the tank, and the rat was allowed to swim freely for 30 s. The percentage of escape latency and path length spent by the rat in the target quadrant (quadrant I) were calculated.

On the 38th day, rats were submitted to a platform-switched test. The submerged platform was placed in the center of quadrant II for the first trial, and then moved to quadrant III and quadrant IV for the second and third trial, respectively. For each trial, the rat was given up to 60 s to locate the hidden platform.

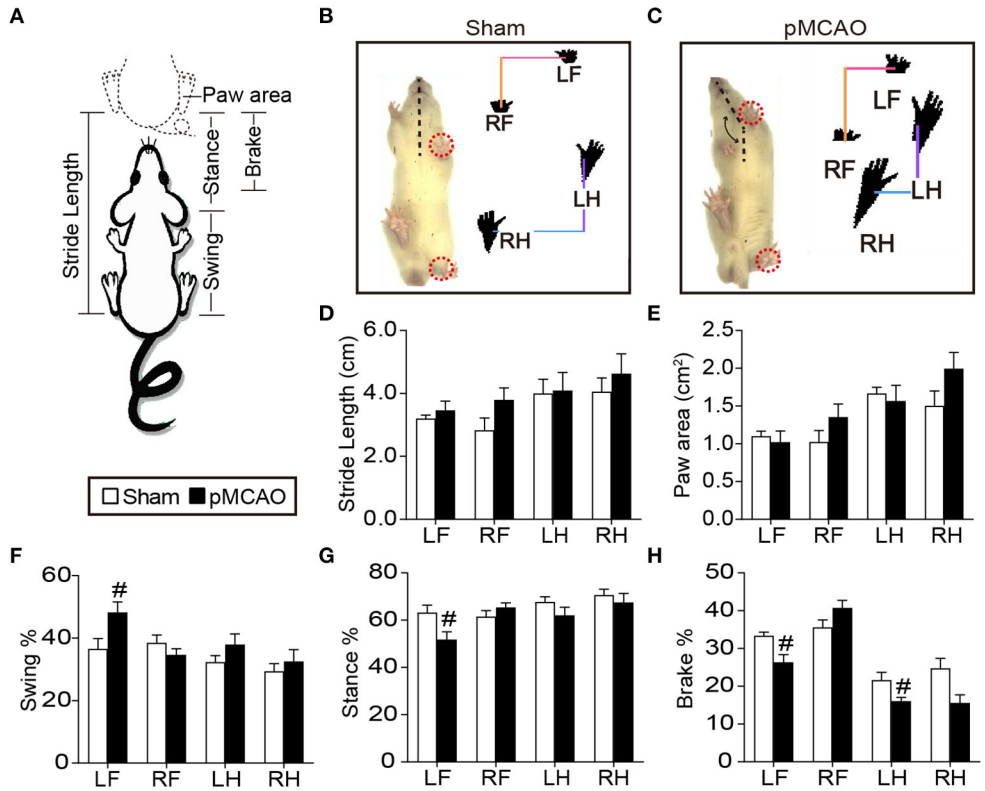

FIGURE 1 | pMCAO induced motor dysfunction in rats. **(A)** Schematic diagram of gait parameters including the stride length, paw area, swing time, stance time, and brake time. **(B,C)** Typical gait pictures captured from sham and pMCAO group. **(D–H)** Quantitative analysis of the stride length, paw area, swing time, stance time, and brake time, respectively (Student's *t*-test, $N = 8$ for the sham group and $N = 9$ for the pMCAO group). $^{\#}P < 0.05$, vs. sham group.

The escape latency and path length traveled by the rat to locate the platform was analyzed. An investigator blind to the group information analyzed data.

Immunostaining

At the end of the MWM test, rats were euthanized and transcardially perfused with 0.9% saline followed by 4% paraformaldehyde. The paraffin embedded brains were sectioned coronally to a thickness of 5 μm. Glass mounted brain sections were stained with luxol fast blue (LFB) after deparaffinization and rehydration.

Statistical Analysis

All data were expressed as mean ± standard error of the mean (SEM). The statistical analyses were performed using the SPSS 21.0 (SPSS Inc., USA) software. Data from the hidden platform test were analyzed by two-way repeated measures ANOVA (between subject factor–surgery; within subject factor–time). The gait, probe trial, platform-switched test, and MRI data were analyzed by Student's *t*-test. The DTI data were tested for correlations with gait (left hindlimb) and MWM data using Pearson linear regression analysis. Significance was defined as $P < 0.05$.

RESULTS

pMCAO Induced Motor Dysfunction in Rats

The gait analysis (**Figures 1A–C**) revealed that the right MCA occlusion induced significant increase in the percentage of swing time and decrease in the percentage of brake time and stance time of the left forelimb compared with sham group ($P < 0.05$, **Figures 1F–H**). In addition, the pMCAO rats showed reduced percentage of brake time of the left hindlimb compared with sham rats ($P < 0.05$). There was no significant difference in the paw area and stride length between the sham and pMCAO groups (**Figures 1D,E**). These results suggested that the occlusion of the right MCA led to remarkable motor impairments of the left limbs.

pMCAO Caused Cognitive Decline in Rats

In the hidden platform test, repeated measures of ANOVA showed significant main effects of time and group on the escape latency [$F_{\text{time}(3,21)} = 17.214$, $F_{\text{group}(1,7)} = 69.067$, $P < 0.001$], and path length [$F_{\text{time}(3,21)} = 4.978$, $F_{\text{group}(1,7)} = 47.673$, $P < 0.01$–0.001, **Figure 2A**], indicating all the rats showed enhanced spatial learning over training days. Group comparisons revealed that pMCAO rats took longer escape latency and path length to locate the submerged platform from the 1st to the 4th training day compared with the sham rats ($P < 0.01$–0.001, **Figures 2D,E**),

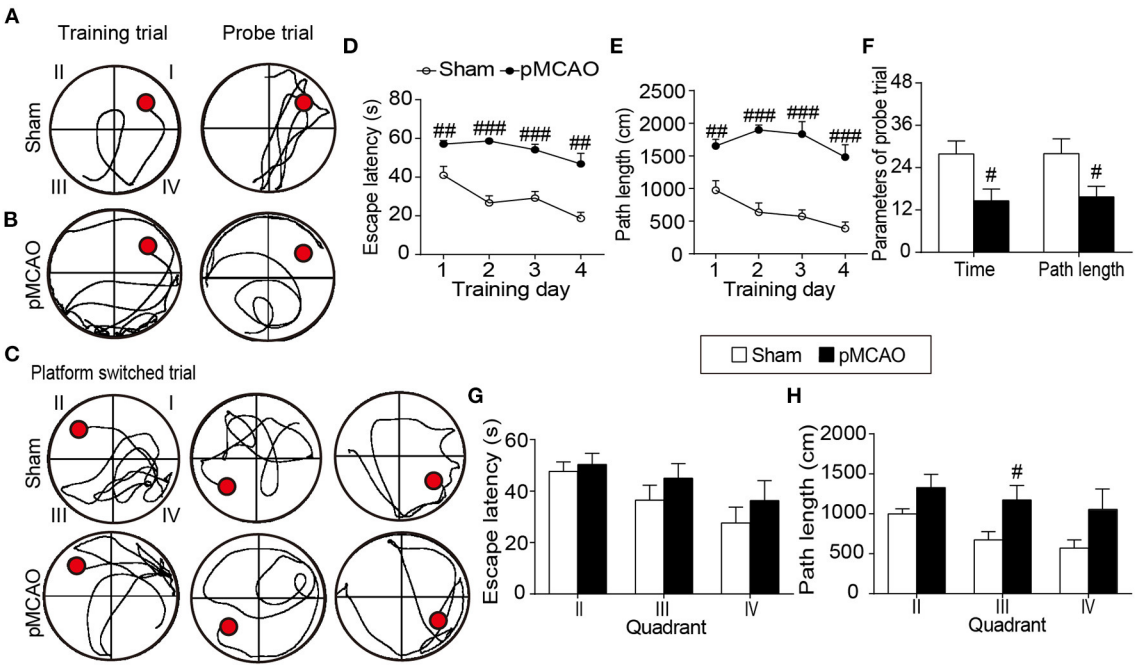

FIGURE 2 | pMCAO caused cognitive decline in rats. **(A–C)** Representative swimming traces of the sham and pMCAO rats in the training trial, probe trial, and platform switched trial, respectively. **(D,E)** Quantitative data of the escape latency and path length of rats spent to locate the submerged platform during the training trial. **(F)** Quantitative analysis of the percentage time and path length of rats spent in the original quadrant in the probe trial. **(G,H)** Quantitative analysis of the escape latency and path length of rats taken to find the switched platform during the platform switched trial (Two-way repeated measures ANOVA with between subject factor-surgery and within subject factor-time for **(D)** and **(E)**. Student's *t*-test for **(F–H)**. $N = 8$ for the sham group and $N = 9$ for the pMCAO group). $^{\#}P < 0.05$, $^{\#\#}P < 0.01$, $^{\#\#\#}P < 0.001$ vs. sham group.

suggesting impaired spatial learning ability after pMCAO. In the probe trial, pMCAO rats spent less time and covered shorter path length in the target quadrant compared with the sham rats ($P < 0.05$, **Figures 2B,F**), demonstrating disrupted memory retention after pMCAO. In the platform-switched trial, pMCAO rats took longer path length to locate the switched platform in the quadrant III than the sham rats ($P < 0.05$, **Figures 2C,G,H**), indicating impaired working memory after pMCAO.

pMCAO Resulted in Impaired Cerebrovascular Hemodynamics in Rats

The angiographic MIP maps presented the connections and morphologies of the intraluminal arteries including the AcoA, azACA, ACA, MCA, PCA, ICA, and BA (**Figure 3B**). In the pMCAO rats, the signal intensity in the right MCA starting at its origin through the distal parts was totally absent (blue arrows), suggesting the successful occlusion of the right MCA. The signal intensities of the ipsilateral ACA, AcoA, and ICA were significantly reduced in the pMCAO rats compared with the sham rats ($P < 0.001$, **Figure 3D**). Additionally, the pMCAO rats exhibited higher signal intensity in the BA than the sham rats ($P < 0.05$). Moreover, the ASL results showed that the relative CBF of the ipsilateral sensorimotor cortex and striatum were markedly decreased in the pMCAO rats compared with the sham rats ($P < 0.001$, **Figures 3A,C**), indicating that the deleterious alterations of the collateral vessels further resulted in inadequate blood supply to the corresponding brain regions.

pMCAO Induced Brain Atrophy and Structural Injury of the Gray and White Matter in Rats

Axial T2WI images exhibited obvious hyperintensity in the ipsilateral hemisphere accompanied with remarkably enlarged bilateral ventricles (**Figure 4A**). Quantitative data showed that the bilateral ventricular volumes were increased in the pMCAO rats compared with the sham rats ($P < 0.01$–0.001, **Figures 4C,E**). Moreover, rats in the pMCAO group had smaller parenchymal volume than that of sham rats ($P < 0.001$, **Figure 4D**), indicating severe brain atrophy following stroke. The relative T2 values of the ipsilateral gray matter (sensorimotor cortex, striatum) and white matter (external capsule, internal capsule) were significantly elevated in pMCAO rats compared with sham rats ($P < 0.01$–0.001, **Figures 4B,F,G**).

pMCAO Induced Microstructural Damages of the Gray and White Matter in Rats

Diffused tensor imaging results showed significantly reduced relative FA accompanied with elevated relative AD and RD in the ipsilateral sensorimotor cortex, striatum, and external capsule

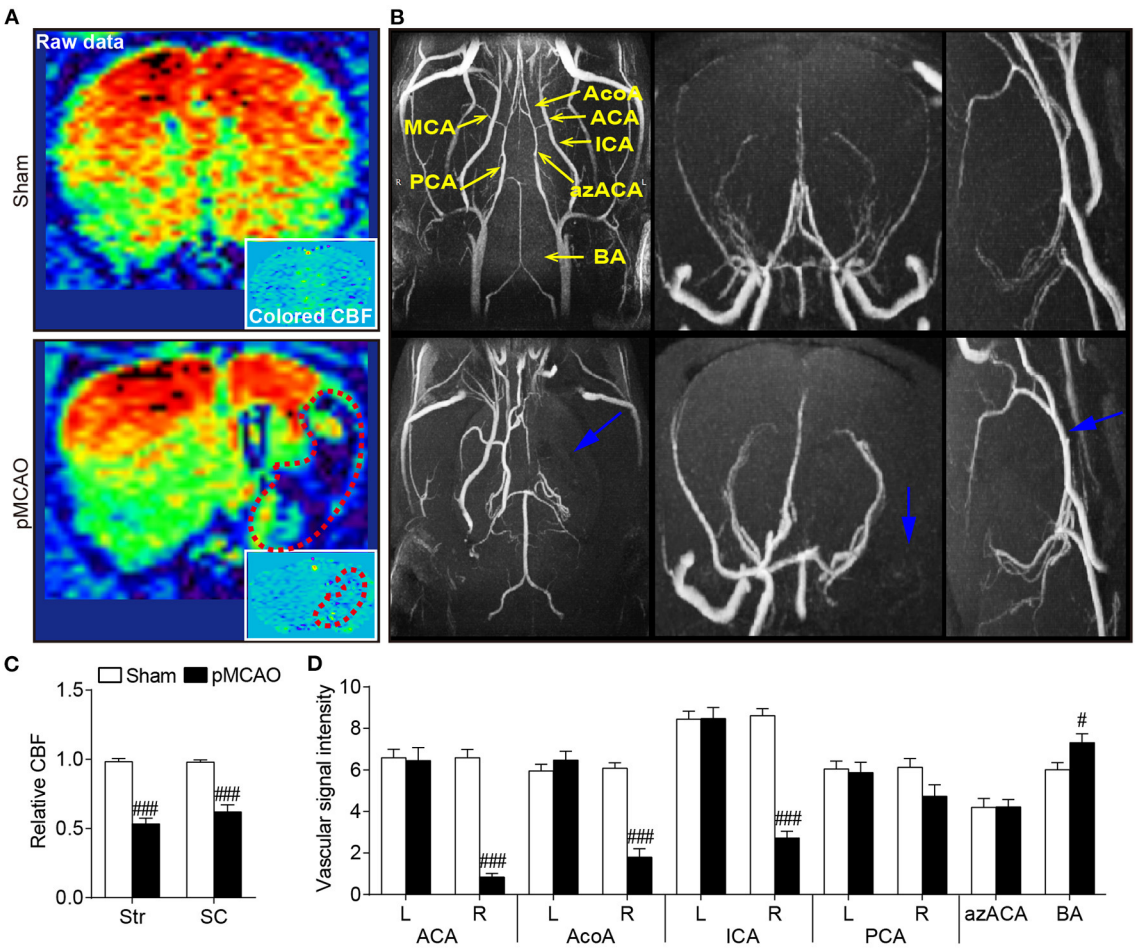

FIGURE 3 | pMCAO resulted in impaired cerebrovascular hemodynamics in rats. **(A)** Representative coronal raw data and colored CBF maps from the sham and pMCAO rats. **(B)** Typical axial, coronal, and sagittal MIP images of the sham and pMCAO rats. **(C)** Quantitative data of relative CBF in the sensorimotor cortex (SC) and striatum (Str). **(D)** Quantitative analysis of the vascular signal intensity from the bilateral anterior cerebral artery (ACA), anterior communicating cerebral artery (AcoA), internal carotid artery (ICA), posterior cerebral artery (PCA), anterior azygos cerebral artery (azACA), and basilar artery (BA) (Student's *t*-test, $N = 8$ for the sham group and $N = 9$ for the pMCAO group). $^{\#}P < 0.05$, $^{\#\#\#}P < 0.001$ vs. sham group.

of the pMCAO rats compared with the sham rats ($P < 0.01$–0.001, **Figures 5A,C–E**). Besides, the decreased relative FA and increased relative RD were also observed in the internal capsule of the pMCAO rats compared with sham rats ($P < 0.01$–0.001). The LFB staining correlated well with DTI findings showing severe axonal disorganization after pMCAO (**Figure 5B**). Fiber tracking further validated the axonal damages following pMCAO as revealed by remarkably decreased relative fiber density and fiber length in the corresponding brain regions of the pMCAO rats in comparison with the sham rats ($P < 0.01$–0.001, **Figures 5F–H**).

pMCAO Induced Motor Dysfunctions Were Correlated to Gray and White Matter Damages in Rats

The Pearson linear regression analysis revealed significant correlations between the percentage of brake time and DTI index in the cerebral gray matter including the sensorimotor cortex and striatum ($P < 0.05$–0.001, **Figures 6A,B**). The relative FA and RD of the striatum were also related to the percentage of swing and stance time ($P < 0.05$). For the cerebral white matter, there were notable correlations between the relative FA in the external capsule and gait parameters ($P < 0.05$–0.01, **Figure 6C**). The relative RD in the external capsule and relative FA in the internal capsule were also significantly correlated with the percentage of brake time ($P < 0.05$, **Figure 6D**). The significant correlations between the gait and DTI parameters were concluded in **Table 1**. These results suggested that the structural damages of the cerebral gray and white matter might contribute to post-stroke motor dysfunctions.

pMCAO Induced Cognitive Impairments Were Correlated to Gray and White Matter Injuries in Rats

For the cerebral gray matter, the relative FA, AD, and RD of the sensorimotor cortex and striatum were significantly correlated

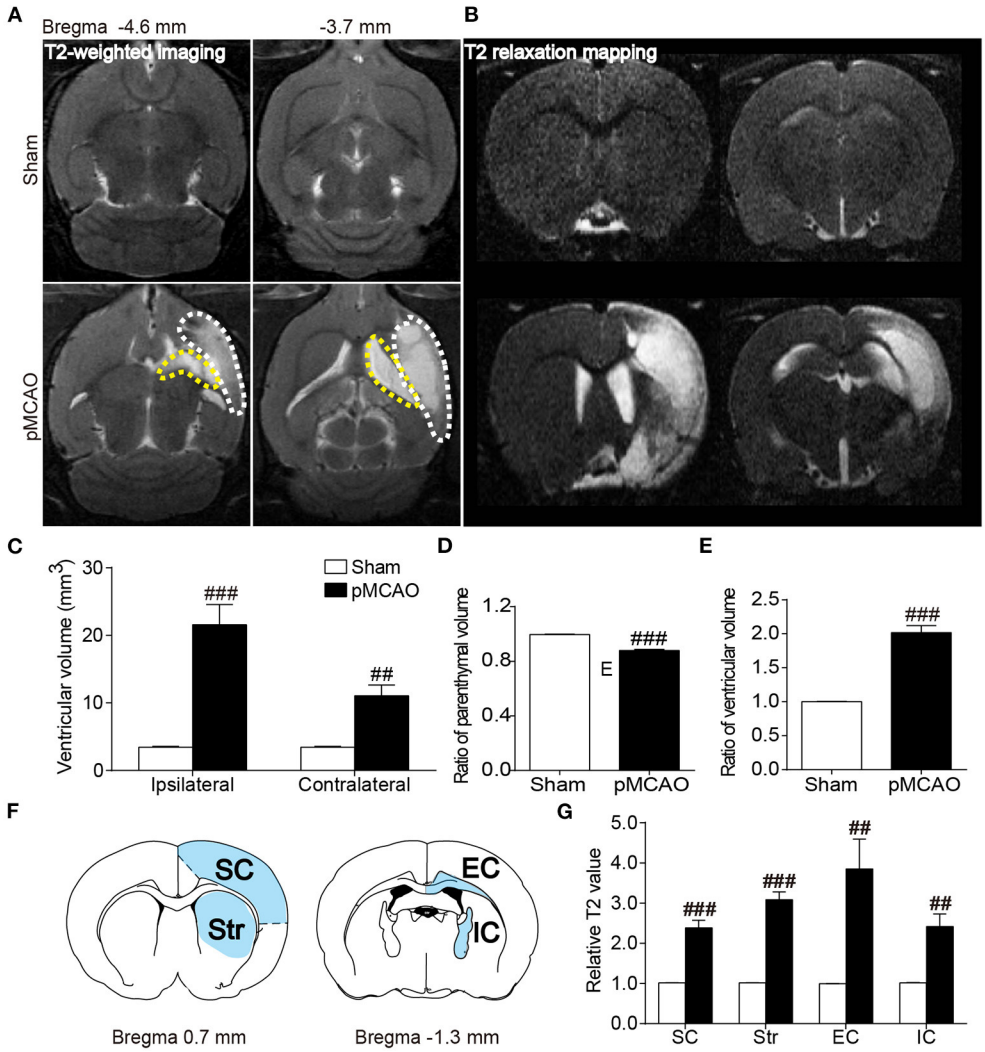

FIGURE 4 | pMCAO induced brain atrophy and structural injury of the gray and white matter in rats. **(A,B)** Representative axial T2WI and coronal T2 relaxation mapping images of the sham and pMCAO rats. **(C–E)** Quantitative analysis of the ventricular volume, ratio of parenchymal volume, and ratio of ventricular volume, respectively. **(F)** Brain atlas showing the regions of interest including sensorimotor cortex (SC), striatum (Str), external capsule (EC), and internal capsule (IC). **(G)** Quantitative analysis of the relative T2 value (Student's *t*-test, $N = 8$ for the sham group and $N = 9$ for the pMCAO group). $^{\#\#}P < 0.01$, $^{\#\#\#}P < 0.001$ vs. sham group.

with the path length in the training trial ($P < 0.01$–0.001, **Figures 7A,B**). There were also remarkable correlations between the percentage of path length in the probe trial and the relative AD and RD of the sensorimotor cortex and striatum ($P < 0.05$–0.01). Besides, relative FA in the sensorimotor cortex also related to the percentage of path length in the probe trial and path length in the platform-switched trial ($P < 0.05$). For the white matter, all the DTI index of the external capsule and the relative FA of the internal capsule were significantly correlated with all the WMW data ($P < 0.05$–0.001, **Figures 7C,D**). The significant correlations between the MWM and DTI parameters are concluded in **Table 2.** These data indicated that poststroke cognitive impairments might be attributed to the structural damages of the cerebral gray and white matter.

DISCUSSION

Cerebral ischemia is one of the most common causes of adult long-term disability, and therapeutic approaches aimed at boosting rehabilitative processes is of great concern (3). The pMCAO model is more convenient for investigating the effects of therapeutic approaches on functional recovery and structural plasticity of the gray and white matter in chronic phase after ischemic stroke (24). According to our multimodal MRI, the present study found that the structural impairments of the cerebral gray and white matter were related to motor and cognitive dysfunction in pMCAO rats on the 30th day after stroke. It was worth noting that MRI parameters, particularly the DTI parameter FA, showed significant and strong correlation

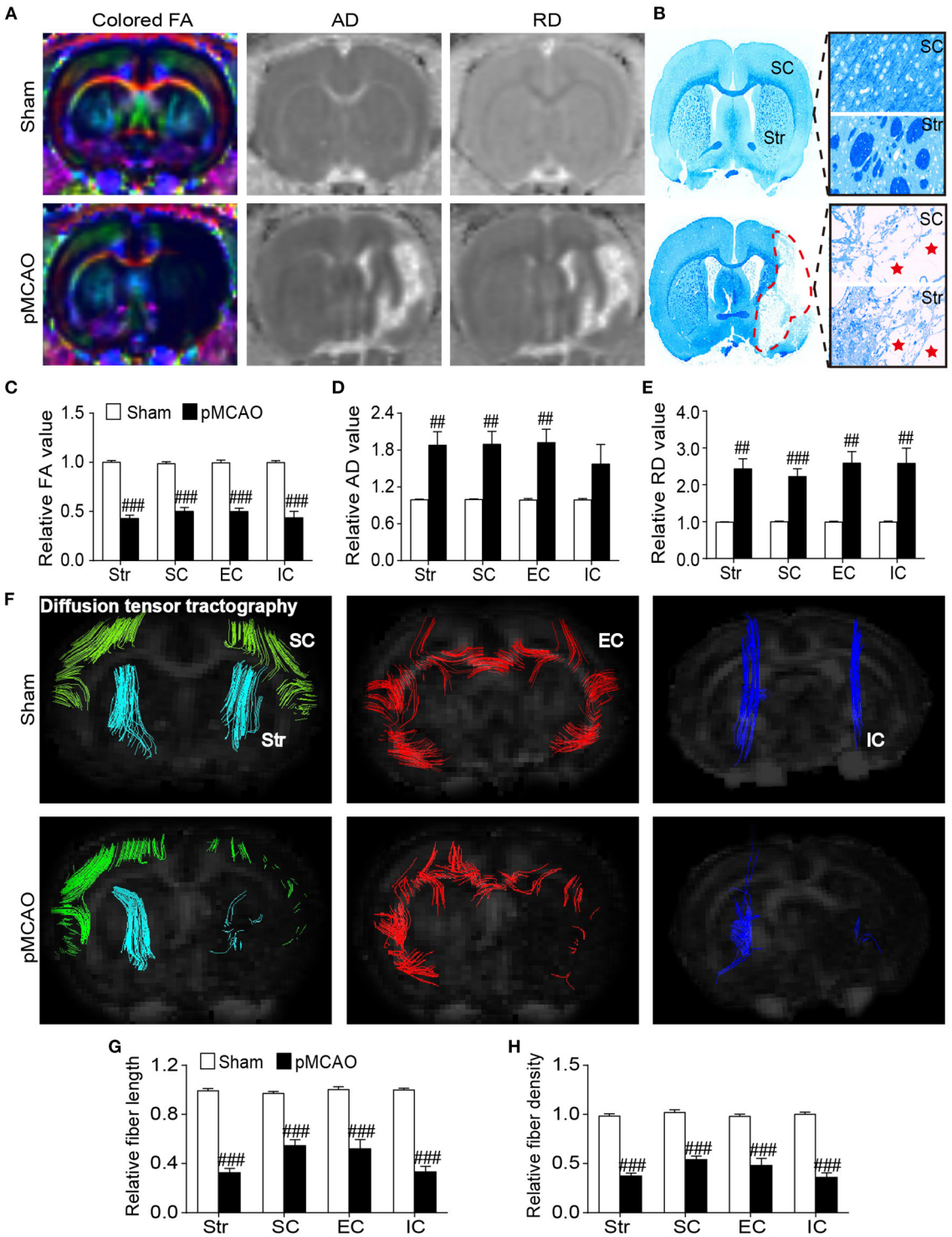

FIGURE 5 | pMCAO induced microstructural damages of the cerebral gray and white matter in rats. **(A)** Representative colored FA, AD, and RD images of the sham and pMCAO rats. **(B)** Typical LFB staining images of the sham and pMCAO rats. **(C–E)** Quantitative analysis of the relative FA, AD, and RD, respectively. **(F)** Diffusion fiber tracking with the seed placed on the bilateral sensorimotor cortex (SC), striatum (Str), external capsule (EC), and internal capsule (IC). **(G,H)** Quantitative analysis of the relative fiber length and fiber density, respectively (Student's *t*-test, $N = 8$ for the sham group and $N = 9$ for the pMCAO group). $^{\#\#}P < 0.01$, $^{\#\#\#}P < 0.001$ vs. sham group.

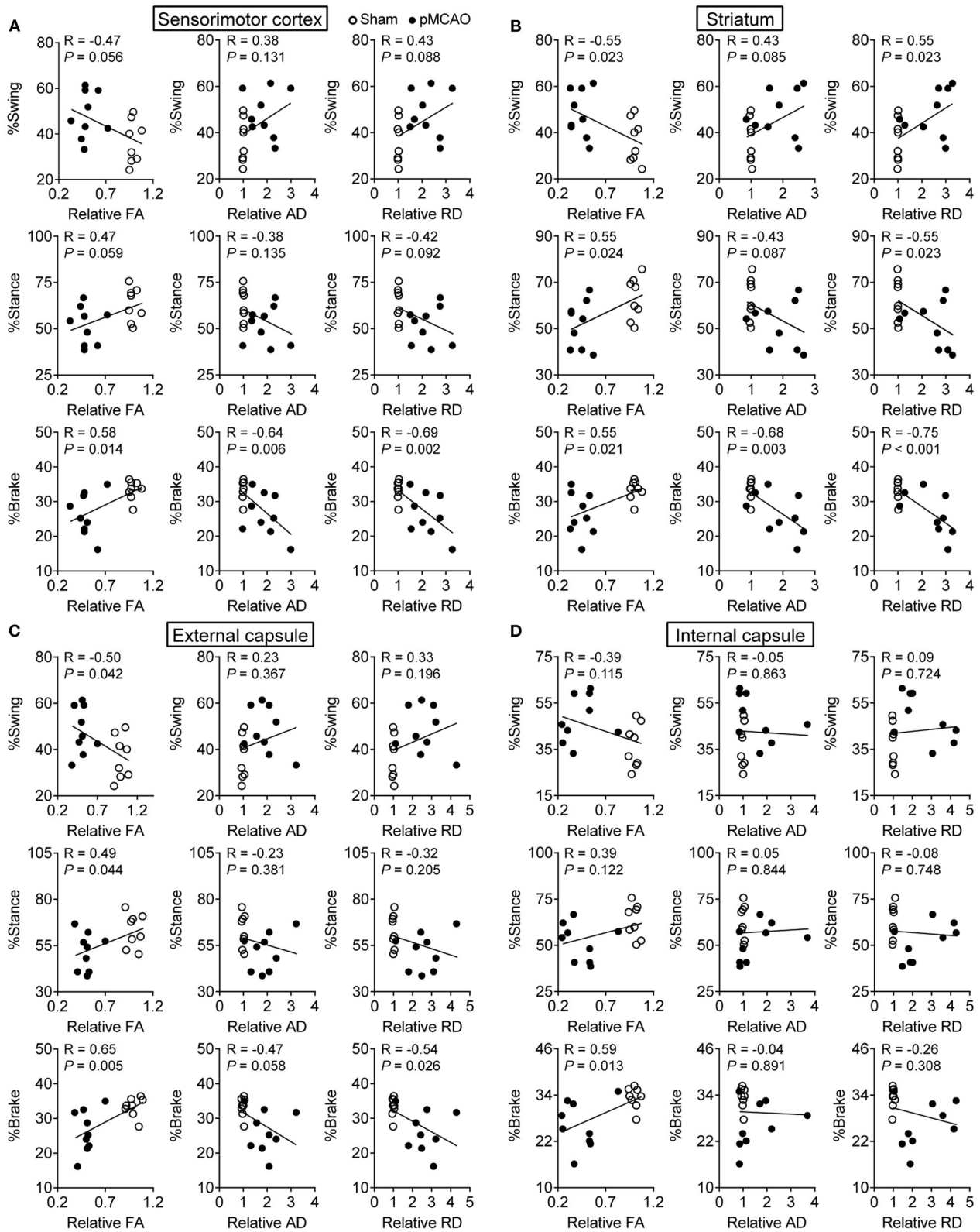

FIGURE 6 | pMCAO induced motor dysfunctions were correlated to gray and white matter damages in rats. Correlational analysis between the gait data and DTI parameters obtained from the **(A)** sensorimotor cortex, **(B)** striatum, **(C)** external capsule, and **(D)** internal capsule.

with the alterations of gait and learning-memory behavior. This indicated that the DTI parameter might be an important evaluation index for monitoring the behavioral impairment.

Ischemic stroke is most caused by stenosis or occlusion of cerebral arteries. MRA provides a non-invasive technique that allows spatiotemporally observing the changes of intracranial arteries (25). In the present study, we applied MRA to detect the brain arteries involving the circle of Willis which is the major route for the redistribution of cerebral blood flow after ischemic stroke (26). Our results showed that the unilateral MCA occlusion resulted in enhanced signal intensity of the BA, indicating that vertebrobasilar artery system might redistribute collateral flow *via* the circle of Willis in a compensatory manner (27). However, this compensation was insufficient. ASL imaging provided direct evidence showing the significantly reduced blood flow in the brain areas mainly supplied by the middle cerebral artery, especially in the sensorimotor cortex and striatum.

The continuous hypoperfusion could induce extensive tissue loss. Currently, serial T2WI images showed a large scale of infarction in the MCA-supply areas of the ipsilateral hemisphere and detected brain atrophy as evidenced by remarkably enlarged bilateral ventricles and reduced ipsilateral parenchyma volume in pMCAO rats, which was consistent with previous studies (28, 29). Specifically, T2 mapping detected significantly prolonged T2 relaxation time in both the gray matter (sensorimotor cortex, striatum) and white matter (external capsule, internal capsule). Based on this, this study strongly supported that pMCAO rats showed impairment of both gray matter and white matter.

To address the effects of pMCAO on microstructural changes in the gray and white matter, we further performed DTI analysis. DTI is considered as a sensitive tool to monitor the microstructural integrity of gray and white matter (13). FA is the most used parameter calculated from DTI that characterizes the spatial density, distribution, and connection of the nerve fibers (30). AD and RD are highly specific for characterizing the alterations of axon and myelin sheath, respectively (31). In this study, decreased FA accompanied with increased AD and RD were detected in both the ischemic gray matter (sensorimotor cortex, striatum) and white matter (external capsule, internal capsule) following stroke. Generally, decreased FA in the lesioned areas indicates demyelination and axonal injury after stroke, and increased AD and RD may result from widespread axonal disorganization and myelin degeneration, respectively (32). Moreover, the DTI-derived fiber tracking demonstrated that the ipsilateral fiber bundles were disorganized accompanied with significantly reduced fiber density and length in the corresponding regions. Correspondingly, LFB staining provided direct evidence showing the pathologic demyelination and axonal breakdown in the white and gray matter following stroke.

Due to the damage of neurons and descending fibers, most stroke survivors suffer from persistent neurological deficits with limited recovery of function (33). Motor dysfunction, characterized by decreased muscle strength and motor coordination, is one of the most common clinical manifestations in stroke. It is well-known that sensorimotor cortex and striatum play a major role in regulating muscle tension and coordinating complex movement (34). While ischemic stroke also elicits white matter injury, increasing evidence suggested that disorganized white matter tracts and the resultant loss of connectivity to the cortical regions greatly contributed to poor motor performance (35). Particularly, internal capsule is a highly concentrated part of motor and sensory conduction fibers in the corticospinal tract (36). The integrity of internal capsule is closely related to the prognosis of motor function in stroke patients (37). Moreover, the external capsule partially connects with the internal capsule, and the external capsule impairment was closely related to the lower limb spasm of stroke patients (38).

TABLE 1 | The summary of significant correlations between the gait and DTI index.

Index	Sensorimotor cortex	Striatum	External capsule	Internal capsule
%Swing	–	FA, RD	FA	–
%Stance	–	FA, RD	FA	–
%Brake	FA, AD, RD	FA, AD, RD	FA, RD	FA

Previous studies reported that gait changes observed in pMCAO rats were more similar with changes in humans following cerebral ischemia (24). Automated gait analysis is a novel method for monitoring motor deficit in animal models of stroke (13). With the information obtained from the Digi-automated gait analysis, our results were in accordance with previous studies showing that permanent right MCA occlusion induced notable left hindlimb impairments as revealed by elevated swing time accompanied with reduced stance and brake time (24).

Clinical reports showed that white matter injury detected by MRI is a stronger predictor of serious motor function symptoms in stroke patients (39). Similarly, we found there were significant correlations between the gait and DTI parameters. Especially FA in the gray matter (sensorimotor cortex, striatum) and white matter (internal capsule, external capsule) were obviously correlated with functional deficits of gait on the 31st day after pMCAO. Overall, these findings suggested that DTI parameters from gray and white matter might be appropriate noninvasive imaging biomarkers for the long-term evaluation of locomotor function deficits in pMCAO rats.

In addition to limb motor function, cognitive impairment is also a common complication following an ischemic stroke (40). In the present study, the MWM results showed significant spatial learning and memory impairments in pMCAO rats, which agreed with previous study (41). Previous reports indicated that the sensorimotor cortex and striatum were closely linked to poststroke learning and memory impairments (42–44). In addition to gray matter, damages to the white matter fibers played critical roles in the attention and executive function (45). Specially, lesion in the bilateral external capsule involved in the cognitive impairment following status epilepticus (46, 47). We analyzed the correlation between MWM and DTI parameters. Similarly, the results showed remarkable correlations between the changes in MWM data and changes

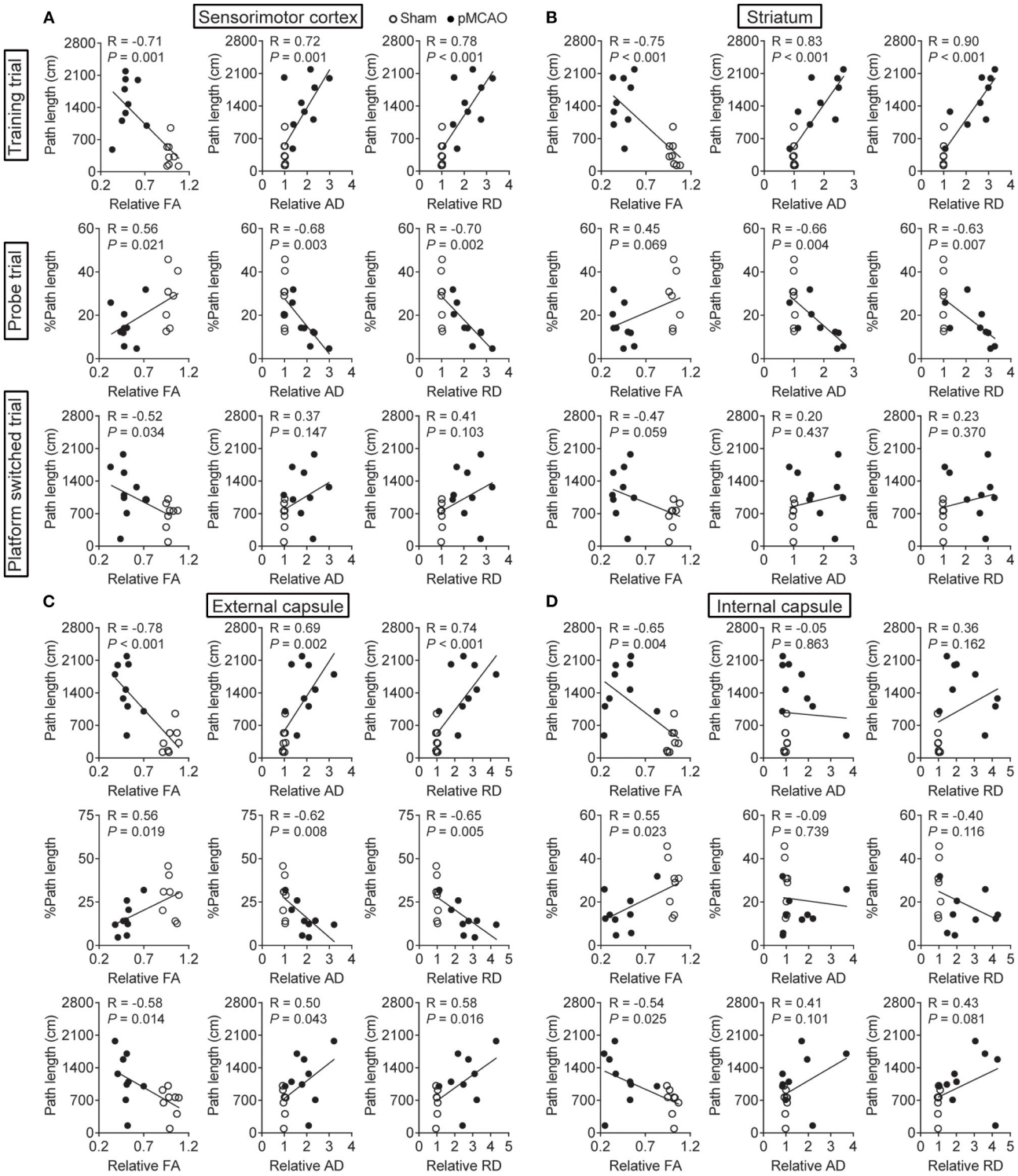

FIGURE 7 | pMCAO induced cognitive impairments were correlated to gray and white matter injuries in rats. Correlational analysis between the MWM data and DTI parameters obtained from the **(A)** sensorimotor cortex, **(B)** striatum, **(C)** external capsule, and **(D)** internal capsule.

TABLE 2 | The summary of significant correlations between the MWM and DTI index.

Index	Sensorimotor cortex	Striatum	External capsule	Internal capsule
Training trial	FA, AD, RD	FA, AD, RD	FA, AD, RD	FA
Probe trial	FA, AD, RD	AD, RD	FA, AD, RD	FA
Platform switched trial	FA	–	FA, AD, RD	FA

in DTI parameters, indicating that DTI can provide an effective method to detect learning and memory impairment in pMCAO rats.

In conclusion, the present study detected varying degrees of structural damages in the gray and white matter in pMCAO rats by multimodal MRI. Specially, the DTI parameters significantly correlated with the behavior data from gait and MWM analysis, suggesting that MRI-derived parameters could be favorable predictors of post-stroke motor and cognitive impairments. Our findings might bring some new clues for identifying gray and white matter damages associated with the decline of both motor and cognitive functions, which is imperative to evaluate the efficacy of any potential pharmacological therapy in a preclinical phase.

DATA AVAILABILITY STATEMENT

The raw data supporting the conclusions of this article will be made available by the authors, without undue reservation.

ETHICS STATEMENT

The animal study was reviewed and approved by Capital Medical University.

AUTHOR CONTRIBUTIONS

LY and MaL performed experiments, analyzed data, and drafted the manuscript. YZha and XF carried out animal experiments. LY, MiL, and JL conducted magnetic resonance imaging experiments. YZhu contributed to immunostaining. HZ designed the study, supervised the whole project, and reviewed the manuscript. All authors contributed to the article and approved the submitted version.

FUNDING

This work was supported by the National Natural Science Foundation of China (Grant nos. 82174471 and 81774381) and the Beijing Municipal Natural Science Foundation (Grant no. 7212161).

REFERENCES

1. Freitas-Andrade M, Raman-Nair J, Lacoste B. Structural and functional remodeling of the brain vasculature following stroke. *Front Physiol.* (2020) 11:948. doi: 10.3389/fphys.2020.00948
2. Dirnagl U, Endres M. Found in translation: preclinical stroke research predicts human pathophysiology, clinical phenotypes, and therapeutic outcomes. *Stroke.* (2014) 45:1510–8. doi: 10.1161/STROKEAHA.113.004075
3. Wang Y, Liu G, Hong D, Chen F, Ji X, Cao G. White matter injury in ischemic stroke. *Prog Neurobiol.* (2016) 141:45–60. doi: 10.1016/j.pneurobio.2016.04.005
4. Curtze S, Melkas S, Sibolt G, Haapaniemi E, Mustanoja S, Putaala J, et al. Cerebral computed tomography-graded white matter lesions are associated with worse outcome after thrombolysis in patients with stroke. *Stroke.* (2015) 46:1554–60. doi: 10.1161/STROKEAHA.115.008941
5. Zhang J, Puri AS, Khan MA, Goddeau RP Jr, Henninger N. Leukoaraiosis predicts a poor 90-day outcome after endovascular stroke therapy. *AJNR Am J Neuroradiol.* (2014) 35:2070–5. doi: 10.3174/ajnr.A4029
6. Chen J, Venkat P, Zacharek A, Chopp M. Neurorestorative therapy for stroke. *Front Hum Neurosci.* (2014) 8:382. doi: 10.3389/fnhum.2014.00382
7. Gladstone DJ, Black SE, Hakim AM. Heart, Stroke Foundation of Ontario Centre of Excellence in Stroke R. Toward wisdom from failure: lessons from neuroprotective stroke trials and new therapeutic directions. *Stroke.* (2002) 33:2123–36. doi: 10.1161/01.STR.0000025518.34157.51
8. Paul S, Candelario-Jalil E. Emerging neuroprotective strategies for the treatment of ischemic stroke: an overview of clinical and preclinical studies. *Exp Neurol.* (2021) 335:113518. doi: 10.1016/j.expneurol.2020.113518
9. Fluri F, Schuhmann MK, Kleinschnitz C. Animal models of ischemic stroke and their application in clinical research. *Drug Des Devel Ther.* (2015) 9:3445–54. doi: 10.2147/DDDT.S56071
10. McBride DW, Zhang JH. Precision stroke animal models: the permanent MCAO model should be the primary model, not transient MCAO. *Transl Stroke Res.* (2017) 8:397–404. doi: 10.1007/s12975-017-0554-2
11. Irving EA, Bentley DL, Parsons AA. Assessment of white matter injury following prolonged focal cerebral ischaemia in the rat. *Acta Neuropathol.* (2001) 102:627–35. doi: 10.1007/s004010100416
12. van der Zijden JP, van der Toorn A, van der Marel K, Dijkhuizen RM. Longitudinal in vivo MRI of alterations in perilesional tissue after transient ischemic stroke in rats. *Exp Neurol.* (2008) 212:207–12. doi: 10.1016/j.expneurol.2008.03.027
13. Encarnacion A, Horie N, Keren-Gill H, Bliss TM, Steinberg GK, Shamloo M. Long-term behavioral assessment of function in an experimental model for ischemic stroke. *J Neurosci Methods.* (2011) 196:247–57. doi: 10.1016/j.jneumeth.2011.01.010
14. Crupi R, Di Paola R, Esposito E, Cuzzocrea S. Middle cerebral artery occlusion by an intraluminal suture method. *Methods Mol Biol.* (2018) 1727:393–401. doi: 10.1007/978-1-4939-7571-6_31
15. Liu HS, Shen H, Harvey BK, Castillo P, Lu H, Yang Y, et al. Post-treatment with amphetamine enhances reinnervation of the ipsilateral side cortex in stroke rats. *Neuroimage.* (2011) 56:280–9. doi: 10.1016/j.neuroimage.2011.02.049
16. Zhang J, Zou H, Zhang Q, Wang L, Lei J, Wang Y, et al. Effects of Xiaoshuan enteric-coated capsule on neurovascular functions assessed by quantitative multiparametric MRI in a rat model of permanent cerebral ischemia. *BMC Complement Altern Med.* (2016) 16:198. doi: 10.1186/s12906-016-1184-z
17. Chan KC, Khong PL, Lau HF, Cheung PT, Wu EX. Late measures of microstructural alterations in severe neonatal hypoxic-ischemic encephalopathy by MR diffusion tensor imaging. *Int J Dev Neurosci.* (2009) 27:607–15. doi: 10.1016/j.ijdevneu.2009.05.012
18. Plane JM, Whitney JT, Schallert T, Parent JM. Retinoic acid and environmental enrichment alter subventricular zone and striatal neurogenesis after stroke. *Exp Neurol.* (2008) 214:125–34. doi: 10.1016/j.expneurol.2008.08.006
19. Kara F, Dongen ES, Schliebs R, Buchem MA, Groot HJ, Alia A. Monitoring blood flow alterations in the Tg2576 mouse model of Alzheimer's disease by in vivo magnetic resonance angiography at 17.6 T. *Neuroimage.* (2012) 60:958–66. doi: 10.1016/j.neuroimage.2011.12.055

20. Li MZ, Zhang Y, Zou HY, Ouyang JY, Zhan Y, Yang L, et al. Investigation of Ginkgo biloba extract (EGb 761) promotes neurovascular restoration and axonal remodeling after embolic stroke in rat using magnetic resonance imaging and histopathological analysis. *Biomed Pharmacother.* (2018) 103:989–1001. doi: 10.1016/j.biopha.2018.04.125
21. Li PC, Jiao Y, Ding J, Chen YC, Cui Y, Qian C, et al. Cystamine improves functional recovery via axon remodeling and neuroprotection after stroke in mice. *CNS Neurosci Ther.* (2015) 21:231–40. doi: 10.1111/cns.12343
22. Xu Y, Tian NX, Bai QY, Chen Q, Sun XH, Wang Y. Gait assessment of pain and analgesics: comparison of the digigait and catwalk gait imaging systems. *Neurosci Bull.* (2019) 35:401–18. doi: 10.1007/s12264-018-00331-y
23. Jing Z, Shi C, Zhu L, Xiang Y, Chen P, Xiong Z, et al. Chronic cerebral hypoperfusion induces vascular plasticity and hemodynamics but also neuronal degeneration and cognitive impairment. *J Cereb Blood Flow Metab.* (2015) 35:1249–59. doi: 10.1038/jcbfm.2015.55
24. Li S, Shi Z, Zhang H, Liu X, Chen S, Jin J, et al. Assessing gait impairment after permanent middle cerebral artery occlusion in rats using an automated computer-aided control system. *Behav Brain Res.* (2013) 250:174–91. doi: 10.1016/j.bbr.2013.04.044
25. Besselmann M, Liu M, Diedenhofen M, Franke C, Hoehn M, MR. angiographic investigation of transient focal cerebral ischemia in rat. *NMR Biomed.* (2001) 14:289–96. doi: 10.1002/nbm.705
26. Liu J, Wang Y, Akamatsu Y, Lee CC, Stetler RA, Lawton MT, et al. Vascular remodeling after ischemic stroke: mechanisms and therapeutic potentials. *Prog Neurobiol.* (2014) 115:138–56. doi: 10.1016/j.pneurobio.2013.11.004
27. van Laar PJ, Hendrikse J, Klijn CJ, Kappelle LJ, van Osch MJ, van der Grond J. Symptomatic carotid artery occlusion: flow territories of major brain-feeding arteries. *Radiology.* (2007) 242:526–34. doi: 10.1148/radiol.2422060179
28. Ding G, Jiang Q, Li L, Zhang L, Wang Y, Zhang ZG, et al. Cerebral tissue repair and atrophy after embolic stroke in rat: a magnetic resonance imaging study of erythropoietin therapy. *J Neurosci Res.* (2010) 88:3206–14. doi: 10.1002/jnr.22470
29. Jiang Q, Thiffault C, Kramer BC, Ding GL, Zhang L, Nejad-Davarani SP, et al. MRI detects brain reorganization after human umbilical tissue-derived cells (hUTC) treatment of stroke in rat. *PLoS ONE.* (2012) 7:e42845. doi: 10.1371/journal.pone.0042845
30. Kimura-Ohba S, Yang Y, Thompson J, Kimura T, Salayandia VM, Cosse M, et al. Transient increase of fractional anisotropy in reversible vasogenic edema. *J Cereb Blood Flow Metab.* (2016) 36:1731–43. doi: 10.1177/0271678X16630556
31. Pitkonen M, Abo-Ramadan U, Marinkovic I, Pedrono E, Hasan KM, Strbian D, et al. Long-term evolution of diffusion tensor indices after temporary experimental ischemic stroke in rats. *Brain Res.* (2012) 1445:103–10. doi: 10.1016/j.brainres.2012.01.043
32. Tuor UI, Morgunov M, Sule M, Qiao M, Clark D, Rushforth D, et al. Cellular correlates of longitudinal diffusion tensor imaging of axonal degeneration following hypoxic-ischemic cerebral infarction in neonatal rats. *Neuroimage Clin.* (2014) 6:32–42. doi: 10.1016/j.nicl.2014.08.003
33. Cho HM, Choi BY, Chang CH, Kim SH, Lee J, Chang MC, et al. The clinical characteristics of motor function in chronic hemiparetic stroke patients with complete corticospinal tract injury. *NeuroRehabilitation.* (2012) 31:207–13. doi: 10.3233/NRE-2012-0790
34. Fasano S, Brambilla R. Cellular mechanisms of striatum-dependent behavioral plasticity and drug addiction. *Curr Mol Med.* (2002) 2:649–65. doi: 10.2174/1566524023362005
35. Zhai F, Liu J, Su N, Han F, Zhou L, Ni J, et al. Disrupted white matter integrity and network connectivity are related to poor motor performance. *Sci Rep.* (2020) 10:18369. doi: 10.1038/s41598-020-75617-1
36. Schulz R, Park CH, Boudrias MH, Gerloff C, Hummel FC, Ward NS. Assessing the integrity of corticospinal pathways from primary and secondary cortical motor areas after stroke. *Stroke.* (2012) 43:2248–51. doi: 10.1161/STROKEAHA.112.662619
37. Hodgson K, Adluru G, Richards LG, Majersik JJ, Stoddard G, Adluru N, et al. Predicting motor outcomes in stroke patients using diffusion spectrum MRI microstructural measures. *Front Neurol.* (2019) 10:72. doi: 10.3389/fneur.2019.00072
38. Lee KB, Hong BY, Kim JS, Sul B, Yoon SC, Ji EK, et al. Which brain lesions produce spasticity? an observational study on 45 stroke patients. *PLoS ONE.* (2019) 14:e0210038. doi: 10.1371/journal.pone.0210038
39. Qiu M, Darling WG, Morecraft RJ, Ni CC, Rajendra J, Butler AJ. White matter integrity is a stronger predictor of motor function than BOLD response in patients with stroke. *Neurorehabil Neural Repair.* (2011) 25:275–84. doi: 10.1177/1545968310389183
40. Park JH, Kim BJ, Bae HJ, Lee J, Lee J, Han MK, et al. Impact of post-stroke cognitive impairment with no dementia on health-related quality of life. *J Stroke.* (2013) 15:49–56. doi: 10.5853/jos.2013.15.1.49
41. Wattanathorn J, Jittiwat J, Tongun T, Muchimapura S, Ingkaninan K. Zingiber officinale mitigates brain damage and improves memory impairment in focal cerebral ischemic rat. *Evid Based Complement Alternat Med.* (2011) 2011:429505. doi: 10.1155/2011/429505
42. Bokura H, Robinson RG. Long-term cognitive impairment associated with caudate stroke. *Stroke.* (1997) 28:970–5. doi: 10.1161/01.STR.28.5.970
43. Kesner RP, Churchwell JC. An analysis of rat prefrontal cortex in mediating executive function. *Neurobiol Learn Mem.* (2011) 96:417–31. doi: 10.1016/j.nlm.2011.07.002
44. Wei CJ, Singer P, Coelho J, Boison D, Feldon J, Yee BK, et al. Selective inactivation of adenosine A(2A) receptors in striatal neurons enhances working memory and reversal learning. *Learn Mem.* (2011) 18:459–74. doi: 10.1101/lm.2136011
45. Cumming TB, Marshall RS, Lazar RM. Stroke, cognitive deficits, and rehabilitation: still an incomplete picture. *Int J Stroke.* (2013) 8:38–45. doi: 10.1111/j.1747-4949.2012.00972.x
46. Hwang KJ, Park KC, Yoon SS, Ahn TB. Unusual lesion in the bilateral external capsule following status epilepticus: a case report. *J Epilepsy Res.* (2014) 4:88–90. doi: 10.14581/jer.14019
47. Selden NR, Gitelman DR, Salamon-Murayama N, Parrish TB, Mesulam MM. Trajectories of cholinergic pathways within the cerebral hemispheres of the human brain. *Brain.* (1998) 121:2249–57. doi: 10.1093/brain/121.12.2249

Conflict of Interest: The authors declare that the research was conducted in the absence of any commercial or financial relationships that could be construed as a potential conflict of interest.

frontiers in Neurology

ORIGINAL RESEARCH
published: 24 March 2022
doi: 10.3389/fneur.2022.827749

Transcutaneous Auricular Vagus Nerve Stimulation Modulates the Prefrontal Cortex in Chronic Insomnia Patients: fMRI Study in the First Session

Jia-Kai He[1,2†], Bao-Hui Jia[2†], Yu Wang[1], Shao-Yuan Li[1], Bin Zhao[1,3], Zeng-Guang Zhou[4], Yan-Zhi Bi[5], Mo-Zheng Wu[1], Liang Li[1], Jin-Ling Zhang[1], Ji-Liang Fang[6] and Pei-Jing Rong[1]**

[1] Department of Physiology, Institute of Acupuncture and Moxibustion, China Academy of Chinese Medical Sciences, Beijing, China, [2] Department of Acupuncture, China Academy of Chinese Medical Sciences Guang'anmen Hospital, Beijing, China, [3] Department of Acupuncture, Southern Medical University, Guangzhou, China, [4] Key Laboratory of Quantitative Remote Sensing Information Technology, Aerospace Information Research Institute, Chinese Academy of Sciences, Beijing, China, [5] Key Laboratory of Mental Health, Institute of Psychology, Chinese Academy of Sciences, Beijing, China, [6] Department of Radiology, China Academy of Chinese Medical Sciences Guang'anmen Hospital, Beijing, China

OPEN ACCESS

Edited by:
Jie Lu,
Capital Medical University, China

Reviewed by:
Hongbin Han,
Peking University Third Hospital, China
Baoci Shan,
Institute of High Energy Physics (CAS), China

***Correspondence:**
Ji-Liang Fang
fangmgh@163.com
Pei-Jing Rong
drrongpj@163.com

[†] These authors share first authorship

Specialty section:
This article was submitted to Applied Neuroimaging, a section of the journal Frontiers in Neurology

Received: 02 December 2021
Accepted: 28 February 2022
Published: 24 March 2022

Citation:
He J-K, Jia B-H, Wang Y, Li S-Y, Zhao B, Zhou Z-G, Bi Y-Z, Wu M-Z, Li L, Zhang J-L, Fang J-L and Rong P-J (2022) Transcutaneous Auricular Vagus Nerve Stimulation Modulates the Prefrontal Cortex in Chronic Insomnia Patients: fMRI Study in the First Session. Front. Neurol. 13:827749. doi: 10.3389/fneur.2022.827749

Objectives: Transcutaneous auricular vagus nerve stimulation (taVNS) has been reported to be effective for chronic insomnia (CI). However, the appropriate population for taVNS to treat insomnia is unclear.

Methods: Total twenty-four patients with CI and eighteen health controls (HC) were recruited. Rest-state functional magnetic resonance imaging (Rs-fMRI) was performed before and after 30 min' taVNS at baseline. The activated and deactivated brain regions were revealed by different voxel-based analyses, then the seed-voxel functional connectivity analysis was calculated. In the CI group, 30 min of taVNS were applied twice daily for 4 weeks. Pittsburgh Sleep Quality Index (PSQI) and Flinders Fatigue Scale (FFS) were also assessed before and after 4 weeks of treatment in the CI group. The HC group did not receive any treatment. The correlations were estimated between the clinical scales' score and the brain changes.

Results: The scores of PSQI ($p < 0.01$) and FFS ($p < 0.05$) decreased after 4 weeks in the CI group. Compared to the HC group, the first taVNS session up-regulated left dorsolateral prefrontal cortex (dlPFC) and decreased the functional connectivity (FCs) between dlPFC and bilateral medial prefrontal cortex in the CI group. The CI groups' baseline voxel wised fMRI value in the dlPFC were negatively correlated to the PSQI and the FFS score after 4 weeks treatment.

Conclusions: It manifests that taVNS has a modulatory effect on the prefrontal cortex in patients with CI. The initial state of dlPFC may predict the efficacy for taVNS on CI.

Keywords: chronic insomnia, transcutaneous auricular vagus nerve stimulation, functional magnetic resonance imaging (fMRI), biomarkers, prefrontal cortex, neuromodulation

INTRODUCTION

Chronic insomnia (CI) disorder is categorized as primary or secondary, depending on whether the sleep problem is caused by another medical and mental disorder or medication substance use (1). The main treatments for CI are medications and physical therapies. Cognitive behavioral therapy (CBT), one of the most mainstream physical therapy for insomnia, was found to reduce the Functional Connectivity (FC) between the Ventral Medial Prefrontal Cortex (vmPFC) and the striatum in patients suffering from insomnia (2). Medication also affects brain activity. In healthy participants, zolpidem reduced the neural activity in occipital lobe during visual stimulation (3). Agomelatine and mirtazapine increased the FC between right Dorsolateral Prefrontal Cortex (dlPFC) and right Precuneus in Major Depression Disorder (MDD) patients with sleep disorder (4). Physical therapies have fewer side effects and therapy dependence. Guidelines of sleep disorder recommend physical therapies as the first treatment before medications (5–8).

Insomnia is also a risk factor for depression (9). It is often accompanied by mental problems (6). Colleges have to pay close attention to some potential curative effect of neuromodulations on insomnia (10), which have been widely used in the treatment of mental diseases. Deep Brain Stimulation (DBS) and Vagus Nerve Stimulation (VNS) are invasive neuromodulations, DBS was reported to have occasionally improved a patient's sleep problems in a patient with Parkinson's disease (11). Stimulating the cat's Nucleus Tractus Solitaries (NTS), the nucleus into which sensory fibers of the vagus nerve mainly project, increases the theta and beta band power of left amygdala and prefrontal cortices. As a result, the cats performed an increase in wakefulness and a total time of rapid eye movement (REM) sleep (12). These suggest that DBS and VNS have potentially curative effect on insomnia. Acute sleep deprivation dysregulated the affective network (13–15), so it is not surprising that neuromodulations are effective on insomnia. Although many clinical trials proved their safety, surgery is still impractical for patients suffering from diseases of mild symptoms, for example, chronic insomnia (16). Transcutaneous auricular vagus nerve stimulation (taVNS) belongs to the category of neuromodulation. A clinical trial has shown the efficacy of taVNS on CI (17), but the underlying brain mechanism is still quite unclear.

Prefrontal cortex is more vulnerable to insomnia (18). The dysfunction of PFC is one of the main pathological manifestations of insomnia (19–21), neuroimaging studies reveal that sleep deprivation severely damages the PFC and reduces its ability of task execution and stimuli regulation (22). Reduced Amplitude of Low Frequency Fluctuation (ALFF) was found widely in the frontal lobe in patients with insomnia, which indicated a lower neuroexcitability. Moreover, the aberrant ALFF is related to the duration and severity of insomnia (19). Patients suffering from evening-types insomnia even have a lower metabolism and a reduced diurnal variation in PFC (23). Stimulating the peripheral branches of vagus would widely modulate the neuroexcitability through the projections from NTS to the forebrain and limbic system (24).

TABLE 1 | Sample characteristics of the participants.

Items	CI ($N = 20$)	HC ($N = 28$)	Z/χ^2	*p-value*
Age (year)	42.50 ± 15.42	43.5 ± 11.23	−0.278	0.781
Sex (M/F)	8/12	6/12	0.181	0.671
Education (year)	12.20 ± 4.62	12.83 ± 6.24	−0.179	0.858

Z, Wilcoxon rank testing; χ^2, chi-square testing. CI, chronic insomnia; HC, healthy control.

Our previous studies revealed that taVNS adjusts the frontal cortex, insular, PCC, and amygdala in patients with major depression disorder (25–28). The modulated brain regions were also closely related to sleep. According to the hyperarousal theory, patients with insomnia have an overexcited but low functioning cortex (18, 29), which leads to nocturnal sleep disturbances, daytime fatigue, and low work efficiency (29). In this study, the instant effects of taVNS would be explored. We hypothesize that taVNS would modulate the forebrain, especially brain regions related to emotion and cognition in patients with CI.

MATERIALS AND METHODS

Recruitment of Participants

A total of twenty- four patients with CI were recruited. They were diagnosed according to the Fifth Edition of the Diagnostic and Statistical Manual of Mental Disorders (DSM-V, 2015). All participants were right-handed. Before the study, they were all informed of the study protocol and volunteered to participate in the study. Patients with fMRI contraindications, severe organic or mental diseases were excluded. Patients would voluntarily quit the ongoing therapies including sleeping pills for at least 2 weeks. Healthy controls (HC) were recruited, at the same time, they were matched with patients in gender, age, and education (see **Table 1**). All participants declaimed to have taken any sleep-aid drugs or psychotropic drugs. Both the CI group and the HC group received the same clinical assessment, a session of taVNS treatment, and fMRI scans at baseline. After that the CI group received 4 weeks' of taVNS treatment while the HC group did not receive any treatment.

Ethical Review and Registration

The study was reviewed by the Ethics Committee of Institute of Acupuncture and Moxibustion under China Academy of Chinese Medical Sciences (CACMS) and registered at the Chinese Clinical Trial Registry (NO. ChiCTR-15007374).

Transcutaneous Auricular Vagus Nerve Stimulation

The electro-acupuncture stimulator (SDZ-IIB, Hwato brand, made in Su zhou, China) was attached to the bilateral cymba conchae through electrodes on the skin surface (see **Figure 1**). Parameters were set according to previous studies of taVNS (17, 27): Dilatational wave of 4/20 Hz and pulse width of 0.2 ms ± 30%. Current intensity was adjusted according to each patient's subjective feeling. Each taVNS session lasted for 30 min, twice

a day for 4 weeks, which is recommended by guidelines for short-term medications of insomnia (7, 8).

Clinical Assessments

All participants accepted Pittsburgh Sleep Quality Index (PSQI) and Flinders Fatigue Scale (FFS) before and after the 4 weeks' of treatment. To exclude the risk of depressive or anxiety symptoms, which may independently affect imaging findings, we used Hamilton Rating Scale for Depression (HAMD) and Hamilton Anxiety Rating Scale (HAMA) to estimate the mental status of all the participants. Before and after the taVNS treatment, the patient would be excluded with a total score of HAMD or HAMA >7. The process of this study is shown in **Figure 2**. In addition, we screened all patients' T2-weighted images and structural images to ruled out most of the serious metabolic or immune-related neuropsychiatric diseases, cerebrovascular diseases, inflammatory diseases of central never system, and intracranial tumors.

MRI Data Acquisition

Rest-state functional magnetic resonance imaging (Rs-fMRI) were performed before and after the first 30 min' taVNS session. Participants were told to keep their eyes closed and not fall asleep during the scan. The fMRI data was acquired by Siemens 3.0T Skyra equipment (Siemens; Munich, Germany). The scanning parameters were as follows. In functional images, the blood oxygen level-dependent gradient Echo Planar Imaging (EPI) sequence was used. One hundred and forty four volumes lasted 6 min 10 s, repeat time/echo time: 2,500/30 ms, flip angle = 90 degrees, scanning field of view: 240 mm × 240 mm, matrix: 64 × 64, number of layers: 43, layer thickness/spacing: 3.0/1.0 mm. In high-definition structure image, three-dimensional magnetization was used to prepare fast gradient echo sequence, repeat time/echo time: 2,500/2.98 ms, flip angle: 7 degree, field of view: 256 mm × 256 mm, matrix: 64 × 64, number of layers: 48; Layer thickness/spacing: 1.0/1.0 mm.

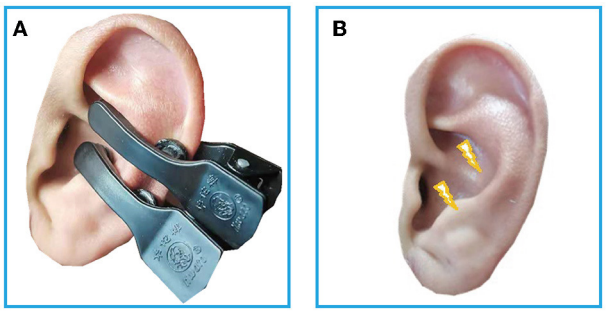

FIGURE 1 | (A) The electrodes were attached to the surface of cymba conchae. **(B)** The stimulating place of taVNS. RS-fMRI, rest-state functional Magnetic Resonance Imaging; taVNS, Transcutaneous Auricular Vagus Nerve Stimulation.

FMRI Data Preprocessing

DPABI (http://rfmri.org/DPABI) software (30), a SPM-based functional MRI preprocessing pipeline, was used for data preprocessing. The preprocessing steps were as follows. Convert DICOM file into NIFTI. Remove the first 10 time points. The remaining 134 volumes were slice-time corrected and realigned according to Friston 24-parameter model. The nuisance signals (including linear trend, head-motion, signals of cerebrospinal fluid, and white matter) were regressed out from the data (31). Then the functional images were co-registered to the T1-weighted structural images, which were segmented through Voxel Based Morphometry (VBM). Derived images were normalized to Montreal Neurological Institute (MNI) space according to transformation parameters estimated by VBM.

The limitations of the signal-to-noise ratio and disputes in sampling and preprocessing strategies for fMRI data, the existing voxel based analysis studies are sometimes contradictory. To get a better presentation of the short- time intervention, we employed ALFF, fALFF, and ReHo to reveal the reproductive results.

FMRI Data Processing

The ALFF and fALFF were calculated from the normalized images after smoothing (6 mm Gaussian kernel full width at half maximum smooth nucleus) to the MNI space. ALFF value was calculated as the average square root of the power spectrum range of 0.01–0.1 Hz and converted to a frequency domain through the fast Fourier transform process. FALFF value is the ratio of power in the specific frequency band of the whole detected frequency range. The ALFF and fALFF maps were also transferred to mean ALFF and fALFF maps by subtraction of the global mean

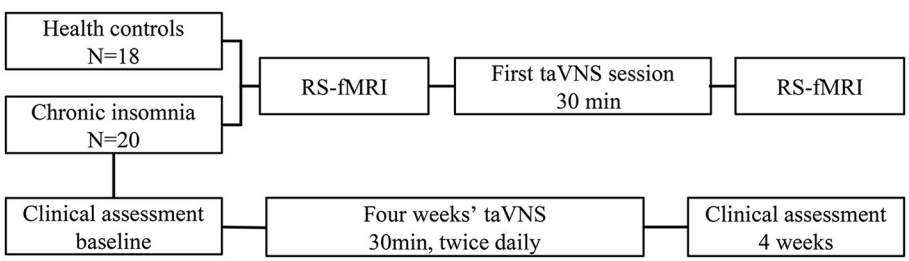

FIGURE 2 | Changes of fMRI induced by instant taVNS were measured before and after the first treatment on the two groups. Clinical scales for patients were assessed before and after the 4 weeks' taVNS treatment.

value. The mean ALFF and fALFF values were converted to Z-distribution for standardization. Then we got the zALFF and zfALFF map.

Regional homogeneity (ReHo) is calculated by voxel based on Kendall's coefficient of concordance (KCC) for the time series of a given voxel with its nearest neighbors (32). ReHo maps was calculated through the unsmoothed and filtered (0.01–0.1 Hz) images to remove physiological signals such as heartbeat and respiration. Then ReHo maps were taken to mean ReHo maps by subtraction of the mean voxel wise ReHo in the entire brain and standardized into Z-value (zReHo Maps). Calculated zReHo maps were smoothed to MNI space with 6 mm Gaussian kernel full width at half maximum smooth nucleus at last.

FC is the Pearson's correlations of the temporal fMRI signals between a Region of Interest (ROI) and all brain. Activated or deactivated regions found by the above voxel based analyses would be used as the Region of Interest (ROI) for seed to voxel FC analysis. FC were computed by voxel in the normalized image after smoothing to Montreal Neurological Institute (MNI) space (6 mm Gaussian kernel full width at half maximum smooth nucleus). All images were band-pass filtered (0.01–0.1 Hz) before FC was computed. Pearson's correlation coefficients were transformed into normally distributed scores according to the Fisher's R- to -Z transformation.

Statistics

In SPSS 25 (SPSS Inc., Chicago, IL, USA), two sample *T*-test and χ^2 tests were applied to compare the baseline characteristics between the CI and HC group. Paired *T*-test was applied to compare within group changes of PSQI and FFS scores in CI group.

For the fMRI images, the between group differences were performed with independent two sample *T*-test, with an uncorrected p-value < 0.05. Paired *T*-tests were performed to determine the within-group differences in the group, before and after the first taVNS session. For the within group comparisons, multiple comparison corrections were performance in Gaussian random field correction (GRF), combined voxel wise p-value < 0.001 with cluster p-value < 0.05 (two tailed). To clarify the behavioral associations of ALFF, fALFF, ReHo, and FC, we performed *Pearson* correlation analyses between the fMRI values and clinical scales in SPSS 25, controlling for age, sex, and education.

RESULTS

taVNS Improved PSQI and FFS Scores

Out of 24 patients, two were excluded, one because of stroke history found by structural images and the other because the patient was diagnosed with bipolar disorder. Another two patients have withdrawn from the study. At last, twenty patients completed the 4 weeks' of taVNS treatment as well as the two fMRI scan sessions. The mean duration of insomnia was 95.2 months. Both PSQI ($N = 20$, $p < 0.01$ 95%*CI*) and FFS ($N = 20$, $p < 0.05$, 95%CI) improved after the 4 weeks' taVNS treatment (see **Table 2**).

TABLE 2 | Improvement of PSQI and FFS after 4-weeks taVNS treatment ($\bar{x} \pm s$).

Items	Baseline	After treatment	*Z*	*p-value*
PSQI ($N = 20$)	12.7 ± 3.715	$9.75 \pm 4.278^{\dagger}$	3.337	0.003
FFS ($N = 20$)	14.5 ± 5.92	$11.5 \pm 4.136^{*}$	2.860	0.010

$^{*}p < 0.05$; $^{\dagger}p < 0.01$; Z, Wilcoxon rank testing; PSQI, Pittsburgh Sleep Quality Index; FFS, Flinders Fatigue Scale; Change at week 4 to baseline mean (95% CI).

First taVNS Session Activated the Similar Location in Left dlPFC and Adjusted Its FC With PFC

The CI group showed lower ALFF and fALFF in dlPFC and higher ReHo in Precuneus when compared to HC group (see **Supplementary Material 1**), which is similar to previous studies (19, 33). Three different voxel based analyses showed consistent results. Namely, the first taVNS session up- regulated left dlPFC in the CI group (see **Figures 3A,B** and **Table 3**). ALFF analysis showed the activation aroused by taVNS was higher in CI group than in the HC group (see **Figure 3C**). Then the activated dlPFC found by the ALFF, fALFF, and ReHo were merged as one ROI. The following seed to voxel FC analysis revealed decreased FC between dlPFC and bilateral dormedial prefrontal cortex (dmPFC) (see **Figures 3B,D**).

A Lower ALFF or ReHo Value in dlPFC Before the First Session Correlating With the Higher PSQI Score After 4 Weeks' of Treatment

When the correlations were examined between the clinical scales' scores and the fMRI values, several significant results were defined. At baseline, ALFF values in dlPFC were negatively correlated with the patients' PSQI ($R = -0.536$, $p < 0.01$) and FFS ($R = -0.537$, $p < 0.05$) score after 4 weeks' of treatment. The baseline ReHo values in dlPFC were also negatively correlated with the after-treatment PSQI ($R = -0.545$, $p < 0.05$) (see **Figure 3E**).

DISCUSSION

Our current study revealed that taVNS improved the CI symptoms. In the first session, the taVNS up- regulated the left dlPFC and reduced its FC with bilateral dmPFC. The baseline ReHo and ALFF values in the left dlPFC were correlated with the PSQI or FFS scores after 4 weeks' of treatment.

dlPFC Is a Potential Targeting Brain Region of taVNS Treatment on CI

According to the hyperarousal theory, the Ascending Reticular Activating System (ARAS) promotes the soberness of human brain. Patients with CI have higher FC between the thalamus and dlPFC, when compared to good sleepers. As a result, some brain regions reduce their activity to compensate for the bottom-up arousal effects originating from ARAS. For example, dlPFC

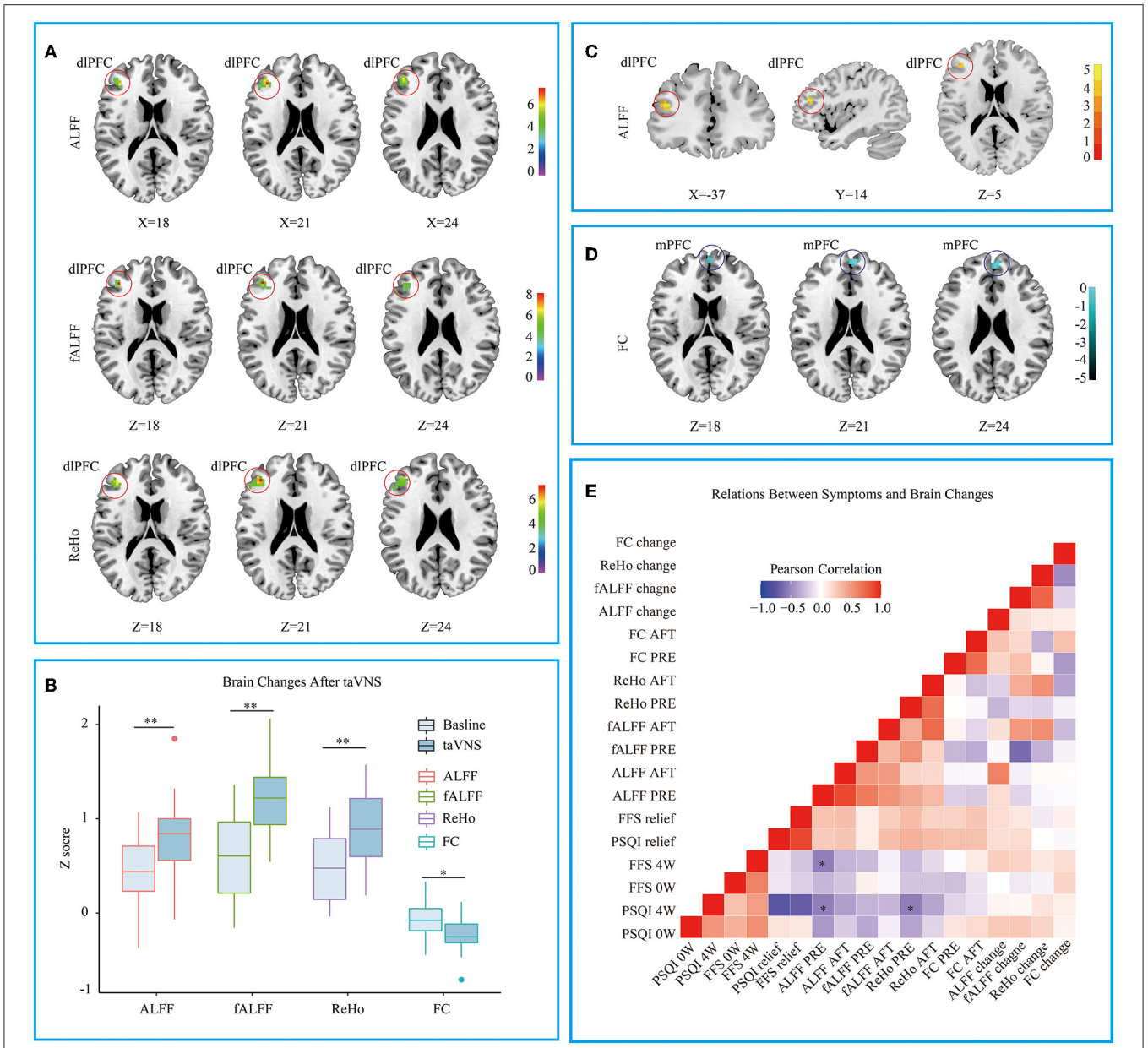

FIGURE 3 | (A) Different voxel based analyses showed similar up- regulated area in left dorsolateral prefrontal cortex. **(B)** Changes of different voxel based analyses before and after taVNS. **(C)** ALFF analysis showed taVNS aroused higher activation in the CI group than in the HC group. **(D)** The FC between the up- regulated dlPFC and bilateral dorsomedial prefrontal cortex decreased after taVNS. **(E)** Correlations between the clinical scales' scores and the fMRI values. PSQI, Pittsburgh Sleep Quality Index; FFS, Flinders Fatigue Scale; ALFF, amplitude of low frequency fluctuation; fALFF, Fractional ALFF; ReHo, Regional homogeneity; FC, Functional connectivity; 0w, before taVNS treatment; 4w, after 4 week taVNS treatment; Relief Rate, The remission rate was defined as the difference in scale scores before and after treatment divided by the scale scores before treatment. $^{*}p < 0.05$; $^{**}p < 0.01$.

show a decreased ALFF in insomniacs (21), which is similar to what we have found. DlPFC is a core region of cognitive control network (CCN) (34–37), that is why insomniacs have lower working efficiency and they are vulnerable to fatigue despite of their overexcited global status.

DlPFC is actually the most common stimulating target of transcranial magnetic stimulation (TMS). TMS on dlPFC can reduce the heart rate, the connection between the vagus and PFC is the anatomical basis of these phenomena (38). Unlike TMS, taVNS activates dlPFC indirectly. The connection offers a potent answer to what we have observed. FC Maps between dlPFC and subgenual cingulate has becoming a promising method for navigating TMS in treating depression (39). Interestingly, our study also found that patients whose initial state of dlPFC was low functioning would have a higher PSQI and FFS after 4 weeks of treatment. However, the limited sample size failed to reveal any correlation between the remission rate and ALFF values or ReHo values. A fMRI study reveals CBT increase the fALFF values in dlPFC and decrease the fALFF values in dmPFC in patient with major depression disorder (40). This phenomenon indicates

TABLE 3 | Brain changes after the first taVNS session ($N = 20$).

Items	Brain regions (AAL)	BA	Number of voxels	MNI coordinates(mm)			Peak intensity
				X	Y	Z	
ALFF	Frontal_Mid_L Frontal_Inf_Tri_L	10/46	37	−39	36	21	7.791
fALFF	Frontal_Mid_L Frontal_Inf_Tri_L	10/46	26	−39	39	21	8.305
ReHo	Frontal_Mid_L Frontal_Inf_ Tri_L	10/45/46	71	−39	39	21	7.364
FC	Frontal_Sup_ Medial_R Frontal_Sup_ Medial_L	9/10	28	3	57	21	−5.143

ALFF, Low frequency fluctuation in the left dorsolateral prefrontal lobe; fALFF, Fractional amplitude of low frequency fluctuation in the left dorsolateral prefrontal lobe; ReHo, Regional homogeneity in the left dorsolateral prefrontal lobe; FC, Functional connectivity between left dorsolateral prefrontal and medial prefrontal lobe; AAL, Anatomical Automatic Labeling; MNI, Montreal Neurological Institute; BA, Brodmann area.

increased nervous excitability in the dlPFC, which is similar to what we have found after the first session of taVNS treatment. We speculate that taVNS and CBT may share a similar brain effect on the dlPFC.

taVNS Lowered the CCN's Monitoring to Default Mode Network

Patients with CI have an abnormal FC between default mode network (DMN) and the additional brain regions when compared with good sleepers (9, 41), which aggravate the hyperarousal status of the brain. Increased ALFF values are found in brain regions related to sensation and attention (19). That is why patients with insomnia are more sensitive to external stimuli and are easier to be awakened. The FC within DMN, especially between the prefrontal lobe and the posterior DMN, decreases when we fall asleep (19, 41). The dysfunctional DMN also leads to the abnormal FCs within DMN, which impairs both the sleep structure and working memory (33, 42). DmPFC is one of the most prominent brain regions of the abnormal frontal DMN (41, 43). Study has also confirmed that dmPFC is the key area for maintaining sleep (43). Patients with CI would pay excessive attention to sleep quality, which would aggravates frustration (44). This is because mPFC is connected with the hippocampus, amygdala, nucleus accumbens, and hypothalamus. They manage reward circuit and emotions (34, 45).

Long-term sleep deprivation leads to a decompensated Salient Network (SN). CCN should allocate more resources to compensate the loosed ability of SN to modulate the aberrant DMN. The current study found that taVNS decreased the FC between left dlPFC and bilateral dmPFC, which is opposite to the pathological changes of the patients with insomnia (2, 46), indicating that CCN has lowered its monitoring to DMN, and the excessive consumption of CCN reduced. We speculate that taVNS would alleviate the symptoms of low efficiency and fatigue in patients with CI.

Electroencephalogram (EEG) has a better time resolution than fMRI. Many neuromodulations use EEG as a brain-machine interface to improve stimulating parameters. Our study found the cortex is the most outstanding brain region affected by instant taVNS. It's easier to get stable EEG signals of the cortex. Using EEG to explore biomarkers of a certain neuromodulation would be of higher translational value than fMRI.

Limitations

First, there was no obvious decrease in PSQI in the current study, which may be due to the fact that we only recruited patients with mild primary insomnia to ensure the consistency of the basic state. Second, while our study revealed that the initial status of PFC in patients with insomnia was related to curative effect, no difference were found between the changes of dlPFC and the changes of the patients' clinical scores. This may be due to the limited sample size. Transient taVNS cannot completely explain the efficacy of mechanism of taVNS. The positive results we found need a longer observation to get more convincing results. Third, a placebo control group is indeed the best designed control groups of this study. At last, the sample size was too small and we only studied the EPI sequence. Despite of the limitations, we intend to provide the potential predicting imaging biomarkers for the suitable patients who are sensitive to taVNS.

CONCLUSIONS

In this study, we found a short time taVNS aroused the left PFC in patients with insomnia. The changes of PFC could be replicated through different voxel-based analyses. The projection from NTS to forebrain might be the anatomical basis of our findings.

DATA AVAILABILITY STATEMENT

The raw data supporting the conclusions of this article will be made available by the authors, without undue reservation.

ETHICS STATEMENT

The studies involving human participants were reviewed and approved by Ethics Committee of Institute of Acupuncture and Moxibustion under China Academy of Chinese Medical Sciences. The patients/participants provided their written informed consent to participate in this study. Written informed consent was obtained from the individual(s) for the publication of any potentially identifiable images or data included in this article.

AUTHOR CONTRIBUTIONS

This article was written mainly by J-KH and B-HJ. The research scheme was designed by P-JR. Patients were recruited and assessed by LL and J-LZ. FMRI data were collected by BZ and were preprocessed by J-KH. Statistics and mapping were assisted by J-KH, Z-GZ, and Y-ZB. S-YL, YW, J-LF, and P-JR reviewed the article. Text correction was done by M-ZW. All authors contributed to the article and approved the submitted version.

FUNDING

This study was supported by the National Key Research and Development Program (No. 2018YFC1705800) and the National Natural Science Foundation (Nos. 81473780 and 81774433).

SUPPLEMENTARY MATERIAL

The Supplementary Material for this article can be found online at: https://www.frontiersin.org/articles/10.3389/fneur.2022.827749/full#supplementary-material

REFERENCES

1. Buysse DJ. Insomnia. *JAMA*. (2013) 309:706–16. doi: 10.1001/jama.2013.193
2. Lee YJG, Kim S, Kim N, Choi JW, Park J, Kim SJ, et al. Changes in subcortical resting-state functional connectivity in patients with psychophysiological insomnia after cognitive–behavioral therapy: changes in resting-state FC after CBT for insomnia patients. *Neuroimage Clin.* (2018) 17:115–23. doi: 10.1016/j.nicl.2017.10.013
3. Licata SC, Lowen SB, Trksak GH, MacLean RR, Lukas SE. Zolpidem reduces the blood oxygen level-dependent signal during visual system stimulation. *Prog Neuropsychopharmacol Biol Psychiatry*. (2011) 35:1645–52. doi: 10.1016/j.pnpbp.2011.05.015
4. Mi WF, Tabarak S, Wang L, Zhang SZ, Lin X, Du LT, et al. Corrigendum to: effects of agomelatine and mirtazapine on sleep disturbances in major depressive disorder: evidence from polysomnographic and resting-state functional connectivity analyses. *Sleep*. (2021) 44:zsaa239. doi: 10.1093/sleep/zsaa239
5. Mysliwiec V, Martin JL, Ulmer CS, Chowdhuri S, Brock MS, Spevak C, et al. The management of chronic insomnia disorder and obstructive sleep apnea: synopsis of the 2019 U.S. Department of Veterans Affairs and U.S. Department of Defense clinical practice guidelines. *Ann Intern Med.* (2020) 172:325–36. doi: 10.7326/M19-3575
6. Krystal AD, Prather AA, Ashbrook LH. The assessment and management of insomnia: an update. *World Psychiatry*. (2019) 18:337–52. doi: 10.1002/wps.20674
7. Riemann D, Baglioni C, Bassetti C, Bjorvatn B, Dolenc Groselj L, Ellis JG, et al. European guideline for the diagnosis and treatment of insomnia. *J Sleep Res.* (2017) 26:675–700. doi: 10.1111/jsr.12594
8. Qaseem A, Kansagara D, Forciea MA, Cooke M, Denberg TD, Barry MJ, et al. Management of chronic insomnia disorder in adults: a clinical practice guideline from the American college of physicians. *Ann Intern Med.* (2016) 165:125–33. doi: 10.7326/M15-2175
9. Gong L, Yu S, Xu R, Liu D, Dai X, Wang Z, et al. The abnormal reward network associated with insomnia severity and depression in chronic insomnia disorder. *Brain Imaging Behav*. (2021) 15:1033–42. doi: 10.1007/s11682-020-00310-w
10. Wang HX, Wang L, Zhang WR, Xue Q, Peng M, Sun ZC, et al. Effect of transcranial alternating current stimulation for the treatment of chronic insomnia: a randomized, double-blind, parallel-group, placebo-controlled clinical trial. *Psychother Psychosom.* (2020) 89:38–47. doi: 10.1159/000504609
11. Castillo PR, Middlebrooks EH, Grewal SS, Okromelidze L, Meschia JF, Quinones-Hinojosa A, et al. Globus pallidus externus deep brain stimulation treats insomnia in a patient with Parkinson disease. *Mayo Clin Proc.* (2020) 95:419–22. doi: 10.1016/j.mayocp.2019.11.020
12. Magdaleno-Madrigal VM, Valdés-Cruz A, Martínez-Vargas D, Martínez A, Almazán S, Fernández-Mas R, et al. Effect of electrical stimulation of the nucleus of the solitary tract on the development of electrical amygdaloid kindling in the cat. *Epilepsia.* (2002) 43:964–9. doi: 10.1046/j.1528-1157.2002.05702.x
13. Baglioni C, Spiegelhalder K, Regen W, Feige B, Nissen C, Lombardo C, et al. Insomnia disorder is associated with increased amygdala reactivity to insomnia-related stimuli. *Sleep*. (2014) 37:1907–17. doi: 10.5665/sleep.4240
14. Wang T, Li S, Jiang G, Lin C, Li M, Ma X, et al. Regional homogeneity changes in patients with primary insomnia. *Eur Radiol.* (2016) 26:1292–300. doi: 10.1007/s00330-015-3960-4
15. Huang Z, Liang P, Jia X, Zhan S, Li N, Ding Y, et al. Abnormal amygdala connectivity in patients with primary insomnia: evidence from resting state fMRI. *Eur J Radiol.* (2012) 81:1288–95. doi: 10.1016/j.ejrad.2011.03.029
16. Johnson RL, Wilson CG. A review of vagus nerve stimulation as a therapeutic intervention. *J Inflamm Res.* (2018) 11:203–13. doi: 10.2147/JIR.S163248
17. Jiao Y, Guo X, Luo M, Li S, Liu A, Zhao Y, et al. Effect of transcutaneous vagus nerve stimulation at auricular concha for insomnia: a randomized clinical trial. *Evid Based Complement Altern Med.* (2020) 2020:6049891. doi: 10.1155/2020/6049891
18. Verweij IM, Romeijn N, Smit DJA, Piantoni G, Van Someren EJW, van der Werf YD. Sleep deprivation leads to a loss of functional connectivity in frontal brain regions. *BMC Neurosci.* (2014) 15:88. doi: 10.1186/1471-2202-15-88
19. Li C, Ma X, Dong M, Yin Y, Hua K, Li M, et al. Abnormal spontaneous regional brain activity in primary insomnia: a resting-state functional magnetic resonance imaging study. *Neuropsychiatr Dis Treat.* (2016) 12:1371–8. doi: 10.2147/NDT.S109633
20. Dai XJ, Nie X, Liu X, Pei L, Jiang J, Peng DC, et al. Gender differences in regional brain activity in patients with chronic primary insomnia: evidence from a resting-state fMRI study. *J Clin Sleep Med.* (2016) 12:363–74. doi: 10.5664/jcsm.5586
21. Zou Q, Ross TJ, Gu H, Geng X, Zuo XN, Hong LE, et al. Intrinsic resting-state activity predicts working memory brain activation and behavioral performance. *Hum Brain Mapp.* (2013) 34:3204–15. doi: 10.1002/hbm.22136
22. Chuah YML, Venkatraman V, Dinges DF, Chee MWL. The neural basis of interindividual variability in inhibitory efficiency after sleep deprivation. *J Neurosci.* (2006) 26:7156–62. doi: 10.1523/JNEUROSCI.0906-06.2006
23. Hasler BP, Germain A, Nofzinger EA, Kupfer DJ, Krafty RT, Rothenberger SD, et al. Chronotype and diurnal patterns of positive affect and affective neural circuitry in primary insomnia. *J Sleep Res.* (2012) 21:515–26. doi: 10.1111/j.1365-2869.2012.01002.x
24. Shouse MN, Langer J, Bier M, Farber PR, Alcalde O, Moghimi R, et al. The α2 adrenoreceptor agonist clonidine suppresses seizures, whereas the α2 adrenoreceptor antagonist idazoxan promotes seizures: pontine microinfusion studies of amygdala-kindled kittens. *Brain Res.* (1996) 731:203–7. doi: 10.1016/0006-8993(96)00594-X
25. Fang J, Rong P, Hong Y, Fan Y, Liu J, Wang H, et al. Transcutaneous vagus nerve stimulation modulates default mode network in major depressive disorder. *Biol Psychiatry*. (2016) 79:266–73. doi: 10.1016/j.biopsych.2015.03.025
26. Fang J, Egorova N, Rong P, Liu J, Hong Y, Fan Y, et al. Early cortical biomarkers of longitudinal transcutaneous vagus nerve stimulation treatment success in depression. *NeuroImage Clin.* (2017) 14:105–11. doi: 10.1016/j.nicl.2016.12.016
27. Liu J, Fang J, Wang Z, Rong P, Hong Y, Fan Y, et al. Transcutaneous vagus nerve stimulation modulates amygdala functional connectivity in patients with depression. *J Affect Disord.* (2016) 205:319–26. doi: 10.1016/j.jad.2016.08.003
28. Tu Y, Fang J, Cao J, Wang Z, Park J, Jorgenson K, et al. A distinct biomarker of continuous transcutaneous vagus nerve stimulation treatment in major depressive disorder. *Brain Stimul.* (2018) 11:501–8. doi: 10.1016/j.brs.2018.01.006
29. Riemann D. Hyperarousal and insomnia: state of the science. *Sleep Med Rev.* (2010) 14:17. doi: 10.1016/j.smrv.2009.09.002
30. Yan CG, Wang X Di, Zuo XN, Zang YF. DPABI: Data processing & analysis for (resting-state) brain imaging. *Neuroinformatics.* (2016) 14:339–51. doi: 10.1007/s12021-016-9299-4
31. Friston KJ, Williams S, Howard R, Frackowiak RSJ, Turner R. Movement-related effects in fMRI time-series. *Magn Reson Med.* (1996) 35:346–55. doi: 10.1002/mrm.1910350312

32. Zang Y, Jiang T, Lu Y, He Y, Tian L. Regional homogeneity approach to fMRI data analysis. *Neuroimage.* (2004) 22:394–400. doi: 10.1016/j.neuroimage.2003.12.030
33. Marques DR, Gomes AA, Caetano G, Castelo-Branco M. Insomnia disorder and brain's default-mode network. *Curr Neurol Neurosci Rep.* (2017) 18:45. doi: 10.1007/s11910-018-0861-3
34. Kober H, Barrett LF, Joseph J, Bliss-Moreau E, Lindquist K, Wager TD. Functional grouping and cortical-subcortical interactions in emotion: a meta-analysis of neuroimaging studies. *Neuroimage.* (2008) 42:998–1031. doi: 10.1016/j.neuroimage.2008.03.059
35. MacDonald A, Cohen J, Stenger VA, Carter C. Functional double dissociation of dorsolateral prefrontal cortex and anterior cingulate cortex in cognitive control. *Neuroimage.* (2000) 11:1835–8. doi: 10.1126/science.288.5472.1835
36. Niendam TA, Laird AR, Ray KL, Dean YM, Glahn DC, Carter CS. Meta-analytic evidence for a superordinate cognitive control network subserving diverse executive functions. *Cogn Affect Behav Neurosci.* (2012) 12:241–68. doi: 10.3758/s13415-011-0083-5
37. Cole MW, Schneider W. The cognitive control network: integrated cortical regions with dissociable functions. *Neuroimage.* (2007) 37:343–60. doi: 10.1016/j.neuroimage.2007.03.071
38. Iseger TA, van Bueren NER, Kenemans JL, Gevirtz R, Arns M. A frontal-vagal network theory for Major Depressive Disorder: implications for optimizing neuromodulation techniques. *Brain Stimul.* (2020) 13:1–9. doi: 10.1016/j.brs.2019.10.006
39. Cash RFH, Cocchi L, Lv J, Wu Y, Fitzgerald PB, Zalesky A. Personalized connectivity-guided DLPFC-TMS for depression: advancing computational feasibility, precision and reproducibility. *Hum Brain Mapp.* (2021) 42:4155–72. doi: 10.1002/hbm.25330
40. Shu Y, Kuang L, Huang Q, He L. Fractional amplitude of low-frequency fluctuation (fALFF) alterations in young depressed patients with suicide attempts after cognitive behavioral therapy and antidepressant medication cotherapy: a resting-state fMRI study. *J Affect Disord.* (2020) 276:822–8. doi: 10.1016/j.jad.2020.07.038
41. Horovitz SG, Braun AR, Carr WS, Picchioni D, Balkin TJ, Fukunaga M, et al. Decoupling of the brain's default mode network during deep sleep. *Proc Natl Acad Sci USA.* (2009) 106:11376–81. doi: 10.1073/pnas.0901435106
42. Drummond SPA, Walker M, Almklov E, Campos M, Anderson DE, Straus LD. Neural correlates of working memory performance in primary insomnia. *Sleep.* (2013) 36:1307–16. doi: 10.5665/sleep.2952
43. Koenigs M, Holliday J, Solomon J, Grafman J. Left dorsomedial frontal brain damage is associated with insomnia. *J Neurosci.* (2010) 30:16041–3. doi: 10.1523/JNEUROSCI.3745-10.2010
44. Hamilton JP, Furman DJ, Chang C, Thomason ME, Dennis E, Gotlib IH. Default-mode and task-positive network activity in major depressive disorder: implications for adaptive and maladaptive rumination. *Biol Psychiatry.* (2011) 70:327–33. doi: 10.1016/j.biopsych.2011.02.003
45. Casement MD, Keenan KE, Hipwell AE, Guyer AE, Forbes EE. Neural reward processing mediates the relationship between insomnia symptoms and depression in adolescence. *Sleep.* (2016) 39:439–47. doi: 10.5665/sleep.5460
46. Pang R, Zhan Y, Zhang Y, Guo R, Wang J, Guo X, et al. Aberrant functional connectivity architecture in participants with chronic insomnia disorder accompanying cognitive dysfunction: a whole-brain, data-driven analysis. *Front Neurosci.* (2017) 11:259. doi: 10.3389/fnins.2017.00259

Conflict of Interest: The authors declare that the research was conducted in the absence of any commercial or financial relationships that could be construed as a potential conflict of interest.

Publisher's Note: All claims expressed in this article are solely those of the authors and do not necessarily represent those of their affiliated organizations, or those of the publisher, the editors and the reviewers. Any product that may be evaluated in this article, or claim that may be made by its manufacturer, is not guaranteed or endorsed by the publisher.

frontiers | Frontiers in Neurology

ORIGINAL RESEARCH
published: 15 April 2022
doi: 10.3389/fneur.2022.844606

Effects of Repetitive Transcranial Magnetic Stimulation on Cognitive Function in Patients With Stress-Related Depression: A Randomized Double-Blind fMRI and ^{1}H-MRS Study

Yuxin Chen[1], Xiuzhen Li[2], Lubin Wang[1], Shushi Tian[3], Yuanwang Chen[2], Feng Wang[2], Kesheng Gu[2], Ying Wang[2], Guangkai Xu[3], Shangrong Zhang[2], Jie Liu[2], Haipeng Wang[2], Zongxin Jia[2], Liqing Li[4], Xiaohui Wang[2], Fang Xie[1], Xue Wang[1], Shida Wang[1], Cong Xue[1], Yun Zhao[1] and Lingjia Qian[1]**

[1] Laboratory of Stress Medicine, Beijing Institute of Basic Medical Sciences, Beijing, China, [2] Department of Psychiatry, Hospital 984 of PLA, Beijing, China, [3] Biochemical Laboratory, Hospital 984 of PLA, Beijing, China, [4] Department of Imaging, Hospital 984 of PLA, Beijing, China

Objectives: To reveal the effects of repetitive transcranial magnetic stimulation (rTMS) on the improvement of cognitive function in patients with stress-related depression, and to enrich the neural mechanism(s) underlying rTMS so as to improve cognitive function in patients with stress-related depression.

Methods: We conducted a randomized, double-blind, placebo-controlled study of rTMS in patients with stress-related depression who were 18–40 years of age. Patients were randomly allocated to either a sham or experimental group in a 1:1 ratio. A 10-session rTMS protocol was used with 10-Hz stimulation over the left dorsolateral prefrontal cortex (DLPFC). Clinical assessments (HAMD, HAMA, DASS, MoCA), neuropsychologic (Stroop, WCST), and resting state fMRI and ^{1}H-MRS assessments were executed at two time points—baseline and after the 10th rTMS session.

Results: rTMS relieved the mental symptoms of patients in both groups. The MoCA score of patients in the experimental group increased; the number of correct answers increased significantly in Stroop testing, and the number of errors and omissions decreased significantly; the number of persistent errors decreased significantly; and the time used to complete the test decreased to an even greater extent in the WCST experimental group. The ReHo value in the lingual gyrus of the right hemisphere and the cuneus of the left and right hemispheres in the experimental group decreased after treatment. The DC value in the left and right hemispheric cuneus and postcentral gyrus of the left hemisphere in the experimental group diminished after treatment. The functional connections of these brain regions also changed as the Cho and NAA/Cr of the left

OPEN ACCESS

Edited by:
Jiliang Fang,
China Academy of Chinese Medical Sciences, China

Reviewed by:
Meiling Li,
Massachusetts General Hospital and Harvard Medical School, United States
Reza Kazemi,
Atieh Clinical Neuroscience Center, Iran

***Correspondence:**
Yun Zhao
15710282409@139.com
Lingjia Qian
newjia@vip.sina.com

Specialty section:
This article was submitted to Applied Neuroimaging, a section of the journal Frontiers in Neurology

Received: *28 December 2021*
Accepted: *14 March 2022*
Published: *15 April 2022*

Citation:
Chen Y, Li X, Wang L, Tian S, Chen Y, Wang F, Gu K, Wang Y, Xu G, Zhang S, Liu J, Wang H, Jia Z, Li L, Wang X, Xie F, Wang X, Wang S, Xue C, Zhao Y and Qian L (2022) Effects of Repetitive Transcranial Magnetic Stimulation on Cognitive Function in Patients With Stress-Related Depression: A Randomized Double-Blind fMRI and ^{1}H-MRS Study. Front. Neurol. 13:844606. doi: 10.3389/fneur.2022.844606

DLPFC changed, with alterations related to the improvement in cognitive function. The level of choline (Cho) in the left DLPFC of the experimental group was significantly lower than that of the control group, and the level of N-acetylaspartate/creatine (NAA/Cr) in the left DLPFC of the control group was significantly higher than that of the experimental group. These changes were related to the overall improvement in cognitive function.

Conclusions: Ten-Hz rTMS over the left DLPFC improved the cognitive function of patients with stress-related depression. The governing mechanism for this phenomenon may be via rTMS effects on multiple visual-related brain regions and their functional connections, and on the somatosensory cortex and its functional connection with visual and auditory cortex, reducing the level of Cho and stabilizing the level of NAA/Cr in the left DLPFC.

Keywords: stress, cognitive function, rTMS, fMRI, neurotransmitter

INTRODUCTION

Depression is one of the most common mental disorders, and its estimated global prevalence is 4.4% (1), and because of its high prevalence and social cost, it is a major focus of psychiatric research. Current research suggests that depression is caused by a combination of genetic, biological, environmental, and psychological factors. However, its underlying pathophysiologic mechanisms are still not fully understood.

Stress is a state of physical and mental tension where the body responds to a variety of adverse factors in the living environment, and studies have confirmed that stress is an important biologic cause of a variety of mental disorders. When prolonged emotional stress becomes severe, it can cause depression. When a person encounters a stressful event or situation, it could trigger a depression. The feelings of depression make it very difficult to manage and deal with stress (2, 3). Intense or long-term stress may induce depression, and many patients with stress-related depression suffer from cognitive impairment.

Repetitive transcranial magnetic stimulation (rTMS) is being used increasingly in the treatment of psychiatric disorders. High frequency rTMS applied over the left dorsolateral prefrontal cortex (DLPFC) has been shown to effectively treat depression and to potentially lead to cognitive improvement as a consequence of mood amelioration. However, whether rTMS can improve the cognitive function of patients with depression remains controversial, and its underlying regulatory mechanism(s) is arcane (4–6). Some authors have demonstrated that patients with depression in an active rTMS group improved significantly on a test of cognitive flexibility, conceptual tracking, and speed performance (4, 7). However, others have uncovered no change in neuropsychologic functioning after receiving rTMS treatment for major depression (8).

In the present study, we used 10-Hz rTMS over the left DLPFC to treat patients with stress-related depression in order to explore the effects of rTMS on their cognitive function. Furthermore, we executed fMRI and ^{1}H-MRS to explore the possible mechanism(s) by which rTMS improved cognitive function.

MATERIALS AND METHODS

Study Design

Our patients first went through one week of health screening and tests—including clinical assessments, neuropsychologic testing, resting-state fMRI, and ^{1}H-MRS. This was followed by two weeks of therapy that included daily treatment with active rTMS or sham stimulation (patients were required to remain on their original medication regimen throughout the study). Our protocol was a sham-controlled, randomized (1:1), double-blinded study. Patients were assigned to treatment arm using dynamic randomization (9) and stratified by sex, age, education, duration of illness, duration of hospitalization, first test score on the Hamilton depression rating scale (HAMD), Hamilton Anxiety Scale (HAMA), and Montreal Cognitive Assessment (MoCA). During treatment, one rTMS session was scheduled daily for five consecutive days, with a total of 10 sessions delivered over the two-week treatment period. After 10 sessions of therapy, all patients completed their second clinical assessment, neuropsychologic tests, resting-state fMRI, and ^{1}H-MRS over one week. All of the participants were on antidepressant medications at stable doses for at least two weeks prior to, during, and one week after rTMS treatment.

Characteristics of Participants

Participants

The following participants were included:

1. who were between the ages of 18 and 40 years;
2. who experienced stress prior to being diagnosed with depression;
3. who were stable after a dose of antipsychotic drugs, with a MoCA test score < 26; and
4. who were right-handed.

Patients with the following were excluded:

1. psychosis, stroke, history of seizure, head injury, or having undergone brain surgery;
2. an implanted metallic or electronic device carrier such as a cardiac pacemaker, stents, epidural or deep brain electrodes, cochlear implants, drug-infusion systems, or intracranial clips;
3. active suicidal ideation or recent suicide attempts;
4. previous substance abuse or dependence;
5. antisocial behavior or borderline personality disorder;
6. inability to complete the assessment—such as manifesting aphasia, hemiplegia, deafness, parachromatoblepsia, or hypochromatopsia;
7. current pregnancy.

Thirty-two right-handed patients participated in the study. All of the participants met criteria for unipolar (MDD, major depressive disorder) or bipolar (BD) illness and a current major depressive episode (MDE), as determined in a semi-structured clinical interview according to the Structured Clinical Interview for ICD-10. Two patients were withdrawn from the study after the rTMS series because they refused to participate. For an overview of the clinical trial, see **Figure 1**.

The study was performed in accordance with the Declaration of Helsinki and was approved by the Local Ethics Review Committee (Ethics Committee of the Hospital 984 of PLA). All of the participants provided written informed consent after the nature of the procedures had been satisfactorily explained.

rTMS Parameters and Session Procedures

For rTMS, we used a Magstim Super Rapid Magnetic Stimulator (Magstim Company Limited, Dyfed, Wales, UK) and a high-powered, figure-8-shaped magnetic coil 7 cm in mean diameter. The rTMS intervention was then conducted over a period of two weeks (10 total sessions, one session/weekday) at 10 Hz, with 80% of the individual RMT, and in four-second trains with a 56-second inter-train interval (800 pulses per session; 8,000 total pulses per patient). Single-pulse TMS was used to measure the resting motor threshold (RMT) for the Abductor Pollicis Brevis (APB) muscle using electromyographic recording. The RMT was defined as the minimum stimulator intensity that evoked a peak–peak amplitude Motor Evoked Potential (MEP) of >50 u Vin at least five out of ten consecutive trials (10, 11). Coil position over the left DLPFC was assured in the active and sham groups by a coil-positioning method using the 10–20-EEG system. In brief, the standard 10–20 EEG electrode positions were individually measured and marked, and the position of the coil center was then located at the electrode position F3 (left posterior middle frontal gyrus, BA 46) (12, 13). For active stimulation, the coil was placed at the same point tangentially to the skull, and oriented in a posterior to anterior direction. Sham treatment was delivered in the same manner as actual TMS, but with the coil angled at 90° away from the surface of the scalp. In order to minimize the side effects to patients, rTMS risk assessment was carried out for each patient prior to treatment by a 13 items questionnaire. If the patient exhibited uncomfortable symptoms during rTMS, including headache, hearing impairment, tinnitus, etc.,we withdrew them from the study in accordance with departmental procedures.

Neuropsychologic and Clinical Assessments

Clinical Assessments

To evaluate the clinical symptoms such as depression and anxiety and cognitive function, the Hamilton Rating Scale for Depression (14) and the Hamilton Anxiety Scale were conducted (15). Additional measures of symptom severity included the 21-item Depression Anxiety Stress Scale (DASS-21) (16), and all subjects completed the Montreal Cognitive Assessment (MoCA) (17). Patients were assessed at baseline (one week before rTMS treatment) and at the end of the treatment period (one week after the last session of the rTMS treatment).

Neuropsychologic Testing

To assess the patient's executive function, two neuropsychologic tests (the WCST and Stroop test), lasting ∼30 min, were administered to each patient one week before and one week after treatment. We employed the computer-based Wisconsin Card Sorting Test (WCST), which is commonly used to assess cognitive flexibility and abstract reasoning (18, 19), and the Stroop Test was implemented to assess selective attention, set shifting, and response inhibition (20, 21).

MRI Data Acquisition

Image Data Acquisition

In order to analyze the regulatory mechanism of rTMS on the spontaneous activity of brain neurons, we used an fMRI scanning procedure for functional MRI, and axial gradient-echo echo-planar imaging (EPI) to acquire images on a 3.0 Tesla Philips whole-body imaging system. Images were obtained using a standard 32-channel-head coil, where the head was stabilized with small cushions to minimize movement. During scanning, all patients were asked to keep their eyes shut but not fall asleep, remain composed, and attempt to produce no systematic cognitive or motor activity.

An EPI sequence was applied to collect resting-state functional images using the following parameters: slices = 36; slice thickness = 4 mm, slice gap = 0 mm; TE = 25 ms, TR = 2,000 ms, flip angle (FA) = 90, field of view (FOV) = 240 × 240 mm^2, matrix = 64 × 64, and voxel size = 2 × 2 × 4 mm^3. We collected 180 time points from each subject. A set of high-resolution T1-weighted structural images was collected by applying a three-dimensional fast spoiled gradient-echo (3DSPGR) sequence with the following parameters: slices = 124; slice thickness = 1.6 mm, slice ga*p* = 0 mm; TE = 2.8 ms, TR = 450 ms, FA = 15, FOV = 240 × 240 mm^2, matrix = 256 × 256 and isotropic voxel size = 1.6 × 1.6 × 1.6 mm^3.

Image Data Preprocessing

MRI data were preprocessed using the Data Processing Assistant for Resting-State fMRI Advanced Edition (DPARSF) (22), which is based on MATLAB (2013b) and SPM8. Because of the time required for magnetization equilibrium and participant adjustment to a new and noisy environment, the first 10 volumes of each functional image were deleted. The remaining 170 functional images were slice-time corrected to reduce the differences in images from different times and realigned for

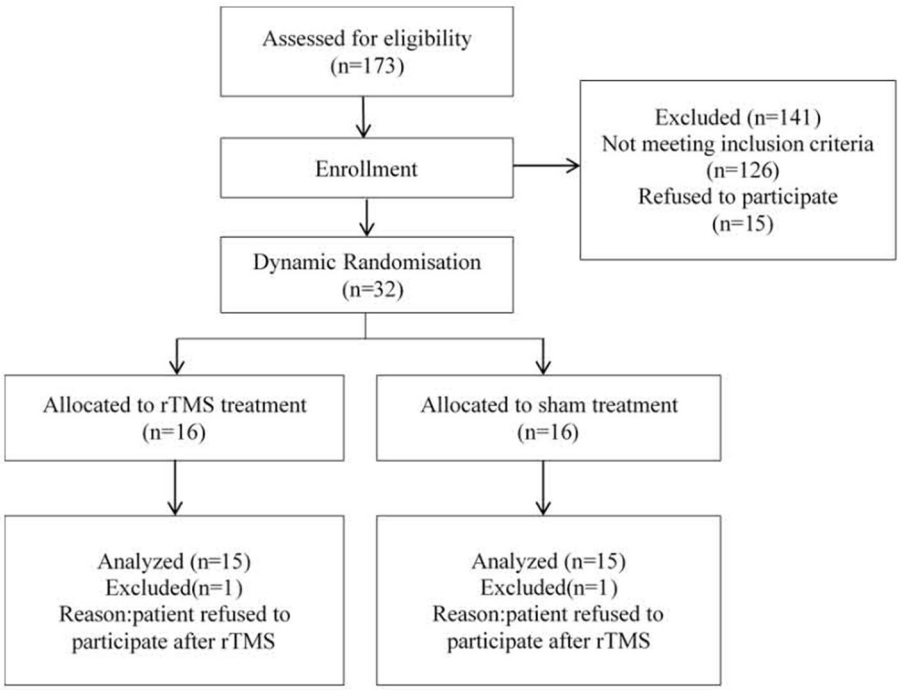

FIGURE 1 | Participant flowchart.

head motion. Subjects whose maximal head motion was beyond 2.0 mm in any direction or whose maximal head rotation was beyond 2.0° in any angular dimension were excluded. The high-resolution T1-weighted structural images were then co-registered with the functional images. Next, the entire brain was segmented into gray matter (GM), white matter (WM), and cerebrospinal fluid (CSF). Subsequently, we implemented a regression of nuisance covariates, including Friston 24-parameter correction and head-motion scrubbing with thresholds of ∼0.5 mm; noisy signals from the CSF and WM were also regressed. Retaining or removing global brain signals is controversial; we herein chose to retain the global signals. All the data were then normalized into the standard Montreal Neurological Institute (MNI) template, and each voxel size was resampled at $3 \times 3 \times 3$ mm and filtered at the 0.01–0.08-Hz band. Finally, we set a Gaussian kernel of 6-mm full-width at half-maximum (FWHM) to conduct spatial smoothing. In addition, detrending was used to remove the linear trends. The whole-brain ALFF was calculated for each subject using the preprocessed images with temporal band-pass filtering ($0.01 < f < 0.08$ Hz), which reduced low-frequency drift and high-frequency respiratory and cardiac noise. The subject-level voxel-wise ALFF map was converted into a z-score map by subtracting the mean ALFF of the whole brain and dividing by the standard deviation. The fractional low-frequency amplitude (fALFF) was obtained by dividing the ALFF signal-power spectrum by the signal-power spectrum of the entire frequency band. The fALFF value was then stronger relative to noise, with higher sensitivity and specificity (23). Regional homogeneity (ReHo) (24), degree centrality (DC) (25), and functional connectivity (FC) were also used to investigate the mechanism(s) driving rTMS effects in patients with depression.

^{1}H-MRS Data Acquisition and Quantification Protocol

Brain neurotransmitter abnormality is an important cause of mental diseases. ^{1}H-MRS is a non-invasive technique to determine the chemical composition of specific tissue areas in vivo. Magnetic resonance spectrum imaging (MRSI) data were examined using a 3.0 Tesla Philips whole-body imaging system for all patients. The MRI protocol included T1-weighted, 3D spoiled-gradient echo acquisitions in transaxial and coronal orientations, and T2- and a fluid-attenuated inversion recovery sequence in sagittal orientation. A water-suppressed, chemical shift-imaging spine echo sequence was executed using multiple voxel proton MRS. Parameters were described as follows: echo time = 135 ms, repetition time = 2,000 ms, NSA = 128, and voxel size = $1.5 \times 1.5 \times 1.5$ cm^3. Acquisition was repeated three times, with the voxel sitting in region to reduce the errors resulting from partial volume effects and to improve the signal-to-noise ratio. MRSI scans that covered the primary ROIs (left posterior middle frontal gyrus, in the BA 46) were referred to readily identifiable locations on each subject's matching high-resolution MR images (**Figure 1**). Head motion was minimized by comfortably securing subjects' heads with padding within the quadrature head coil.

A representative spectrum of a patient from the left posterior middle frontal gyrus MRSI voxel is shown in **Figure 1**. Concentrations in proton MRS studies are expressed relative to creatine, which acts as an internal reference standard in the

voxel. We evaluated each spectrum for the peak area of NAA, Cho, and Cr, and also calculated the ratios of NAA/Cr and Cho/Cr. The post-processing and quantification were performed automatically with the Philips brain imaging software package. Spectral post-processing comprised line broadening, reducing the residual water resonance, linear baseline correction, and peak integration (**Figure 2**).

Data Analysis

Neuropsychologic and Clinical Assessments, and Metabolite Data Analysis

We employed SPSS v. 24.0 statistical software to analyze the data. The balance of the two groups of patients was tested as follows: for continuous variables such as scale scores, we used an independent-sample *t* test; for naming variables such as medication and sex, we used a Chi-squared test. Treatment effects data were entered into a 2 (time of measurement, pre-treatment vs. post-treatment) × 2 (stimulation condition, active vs. sham) factorial design, with time of measurement as the within-subjects factor. Thus, for each test variable, we performed an ANOVA for repeated measures with additional post-hoc analyses using paired, two-tailed *t* tests in the case of significant results indicated by interactions in the ANOVA, with all *p*-values corrected for multiple comparisons. The scale scores and statistical significance were assigned at $P < 0.05$. Pearson's correlation analysis was applied to investigate relationships among clinical ratings (HAMD, HAMA, DASS-21, MoCA), cognitive performance (Stroop, WCST), and metabolites.

Neuroimaging Analyses

Resting fMRI index reflects the level of spontaneous activity of brain neurons in resting state, which is more suitable for the study of patients with stress disorder without clear organic lesions. The change of synchronization or difference of brain activity (network function connection characteristics, etc.) may be the main reason for the abnormality of cognitive function and emotional state. Increases in BOLD activity correlated with increases in neuronal activity, making it possible to estimate the amount and anatomic location of brain activity that occurred during a particular pathological state. Regional Homogeneity (ReHo) reaction the activity of voxel is consistent with that of its surrounding voxel neurons. Degree centrality (DC) indicates the strength of the connection between this region and other voxels in the whole brain. Fractional Amplitude of Low Frequency Fluctuations (fALFF) can reflect the strength of brain neuron activity from the perspective of energy. We analyzed the ReHo, DC, ALFF, and FC maps with DPARSF. Age, sex, and educational level were used as covariates in two-sample *t* test calculations. We used the Gaussian random field (GRF) to correct for multiple comparisons. For all of the aforementioned analyses, we set a voxel-level threshold of $p = 0.001$ and a cluster-level threshold of $p = 0.05$, and GRF correction was applied to multiple comparisons in the whole brain. In addition, a GM group mask was employed in ReHo, DC, fALFF, and FC calculations.

A seed-based, functional-connection analysis method selects significant differences in areas of ReHo, DC, and fALFF as seed points. The peak points of the ReHo, DC, and fALFF analyses were then selected as the coordinates of those regions of interest (ROIs), and the radius was set at 6 mm. We calculated seed-based FC maps between the time-courses of seed regions and the time-series for all voxels in the global brain with Pearson's correlation analyses. Finally, Fisher's *r*-to-z transformation was applied to all maps prior to statistical analysis. Pearson's correlation coefficients were calculated to assess relationships among clinical measures, neuropsychological results, ReHo, DC, ALFF, and FC maps in patients. Calculations were performed using SPSS software after eliminating the influences of age, sex, and education, and statistical significance was set to $p < 0.05$.

RESULTS

Thirty-two subjects completed the first MRI and 30 completed both scans. Subjects tolerated the rTMS treatments well, and there were no serious adverse events.

Demographic and Clinical Characteristics

There was no significant difference in demographic information, scale baseline, antipsychotic drug use, risk factors, or biochemical indices in blood between the two groups (**Table 1**).

Clinical Characteristics and Neuropsychologic Results

In this study, we uncovered a significant interaction between the total score for the MoCA and time ($p = 0.006$). After rTMS, the total score for the MoCA in the experimental group increased significantly, but there was no significant change in the control group. The scores for short-term memory and orientation to time and place (MoCA sub-factors) in the experimental group were significantly improved after rTMS ($p < 0.05$), while the scores for other sub-factors experienced no significant change. The scores for all sub-factors also underwent no significant change in the control group.

The interaction between group and time for all indices in the Stroop test was not significant. The correct numbers in the Stroop test in the experimental group increased significantly, while the numbers of errors and omissions decreased significantly ($p < 0.05$) after rTMS, and other indices did not change.

The interaction between group and time in the numbers of perseverative errors and time to complete the WCST was significant ($p = 0.048$, $p = 0.050$), and the number of perseverative errors in the experimental group decreased significantly after rTMS with no significant change in the control group. The time to complete the test by patients in both groups diminished significantly ($p < 0.01$), although the experimental group declined to a greater degree ($p = 0.001$). The total response numbers for patients in the experimental group and the number of responses needed to complete the first classification decreased significantly after rTMS ($p < 0.05$), while there was no significant change in the control group.

The interaction between group and duration of depression, anxiety, and stress subscale of the DASS, HAMD, and HAMA was not significant, but the main effect of time was significant. After treatment, the scores for depression, anxiety, and the stress subscale of the DASS, HAMD, and HAMA in the experimental

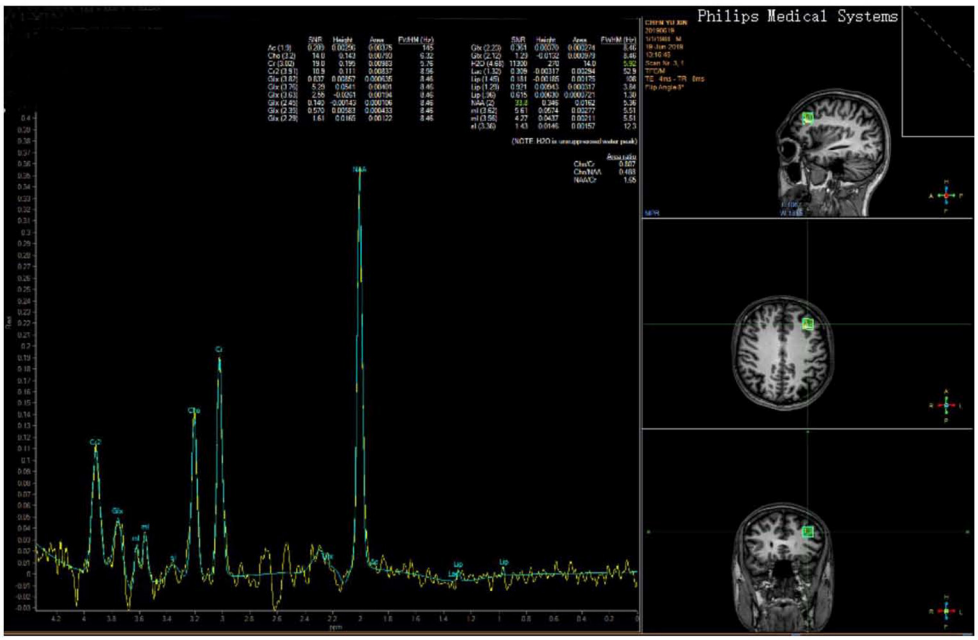

FIGURE 2 | A single voxel was placed in the left DLPFC (in BA 46, shown at right). A typical spectrum from this voxel is shown on the left and demonstrates metabolite peaks for N-acetyl-aspartate (NAA), choline (Cho), and creatine (Cr), which have been implicated in the pathophysiology of depression.

group decreased significantly, while in the control group, except for depression subscale of the DASS, the scores for the other scales also decreased significantly. We suggest that the symptoms of depression and anxiety in both groups were relieved after treatment (**Table 2**).

Cognitive Function and Mental-Symptom Outcomes

In this study, we discovered that the interaction between the total score for the MoCA and time was significant ($p = 0.006$). After rTMS, the total score for the MoCA and the scores of short-term memory and orientation to time and place (MoCA sub-factors) in the experimental group increased significantly ($p < 0.05$), while there was no significant change in the control group.

The interaction between group and time for all indices in the Stroop test was not significant. The correct numbers in the Stroop test in the experimental group increased significantly, while the numbers of errors and omissions decreased significantly ($p < 0.05$) after rTMS, and other indices did not change.

The interaction between group and time in the number of perseverative errors and time to complete the WCST was significant ($p = 0.048$, $p = 0.050$), and the number of perseverative errors in the experimental group decreased significantly after rTMS. However, there was no significant change in the control group. Moreover, the time to complete the test by patients in both groups decreased significantly ($p < 0.01$), although the improvement was more pronounced in the experimental group ($p = 0.001$). The total response numbers by patients in the experimental group and the number of responses needed to complete the first classification decreased significantly after rTMS ($p < 0.05$), while there was no significant change in the control group.

The interaction between group and the duration of depression, anxiety, and the stress subscale of the DASS, HAMD, or HAMA was not significant; however, the main effect of time was significant. After treatment, the scores for depression, anxiety, and the stress subscale of the DASS, HAMD, and HAMA in the experimental group decreased significantly, and in the control group—except for the depression subscale of DASS—the scores of the other scales were also reduced significantly. We posit that the symptoms of depression and anxiety in the two groups were relieved after treatment (**Table 2**).

ReHo, DC, and fALFF Analyses

fMRI is a useful technology that measures changes in regional CNS blood oxygenation in parallel with regional metabolic activity. Elevations in blood-oxygenation-level-dependent (BOLD) activity correlated with increases in neuronal activity, making it possible to estimate the amount and anatomic location of brain activity that occurred during a particular pathologic state.

We noted attenuated ReHo values under a resting state in the lingual gyrus of the right hemisphere and the cuneus of the left and right hemispheres in the experimental group after rTMS, there was no significant change in the ReHo value in the control group. The DC values that showed diminutions in the experimental group after rTMS were the postcentral gyrus of the left hemisphere, and the cuneus of the left and right hemispheres, but there was no significant change in the DC of the control group (**Figure 3**), nor in fALFF. We observed no significant

TABLE 1 | Clinical and socio-demographic information of study participants.

	Experimental rTMS ($n = 15$)	Sham rTMS ($n = 15$)	Statistic	p
Demographic characteristic				
Sex (male/female)	15/0	14/1	1.034	0.309
Age (years)	26.47 (6.96)	28.80 (4.94)	−1.059	0.299
Education (years)	12.07 (1.79)	13.67 (2.74)	−1.891	0.069
Duration of illness (months)	22.93 (22.27)	28.33 (22.75)	−0.657	0.517
Duration of hospitalization	2.53 (3.79)	2.77 (3.02)	−0.107	0.916
Baseline psychopathology				
HAMD	12.07 (9.06)	13.20 (9.37)	−0.337	0.739
HAMA	7.80 (7.15)	11.00 (8.98)	−1.080	0.289
DASS	66.14 (28.72)	64.80 (29.84)	0.125	0.902
MOCA	20.93 (3.51)	21.93 (2.87)	−0.854	0.400
Concomitant medication (taken/not taken)				
Sodium valproate	3/12	4/11	0.186	0.666
Olanzapine	3/12	2/13	0.240	0.624
Sertraline	3/12	0/15	3.333	0.068
Tandospirone	5/10	6/9	0.144	0.705
Dutoxetine	7/8	6/9	0.136	0.713
Mitrazapine	9/6	7/8	0.536	0.464
Oxazepam	3/12	1/14	1.154	0.283
Lithium carbonate	0/15	2/13	2.143	0.143
Escitalopram oxalate	2/13	1/14	0.370	0.543
Sulpiride	0/15	1/14	1.034	0.309
Trazodone	2/13	2/13	0.000	1.000
Quetiapine fumarate	0/15	3/12	3.333	0.068
Lorazepam	1/14	2/13	0.370	0.543
Zilacetone hydrochloride	0/15	1/14	1.034	0.309
Venlafaxine	1/14	0/15	1.034	0.309
Risk factors				
Hcy (μmol/L)	13.84 (6.84)	13.96 (6.31)	−0.050	0.961
Family history of mental illness	2/13	1/14	0.370	0.543

Student's t test for continuous data and χ^2 for categorical data.
Values in brackets reflect standard deviation of the mean.

difference using an independent-sample t test between the two groups at the same time (pre- or post-rTMS). Neither the main effects of group and time nor the interaction group × time was significant (**Table 3**, **Figure 3**).

FC Analysis

Four brain regions with significant differences in ReHo and DC values were used as seed points to analyze the functional connection with other voxels of the whole brain. We found that in the experimental group, the functional connection strength of the right cuneus and left cuneus, and the right cuneus and left and right middle occipital gyrus changed significantly after rTMS. After rTMS, there was also a significant difference in the functional connection strength of the left postcentral gyrus to the inferior temporal gyrus and supramarginal gyrus between the experimental group and the control group. Using the lingual gyrus as the seed point, we did not find any significant change in functional connectivity with other voxels (**Table 4**; **Figures 4**, **5**).

Correlations Among Clinical Data, Neuropsychologic Data and ReHo, DC, FC Values

After controlling for age, sex, and educational level, we performed a partial correlation analysis of the two group. We executed a correlation analysis of the two group of patients between ReHo, DC, and FC values and the scores on cognitive tests and psychiatric symptom scales. The ReHo value of the lingual gyrus was positively correlated with perseverative error on the WCST ($r = 0.428$, $p = 0.001$). The DC value of the postcentral gyrus was positively correlated with the time taken for the WCST and perseverative error of the WCST($r = 0.258$, $p = 0.047$; $r = 0.342$, $p = 0.07$). The ReHo value of the cuneus was positively correlated with the time taken for the WCST($r = 0.292$, $p = 0.023$), the DC value of the cuneus was positively correlated with perseverative error of the WCST and time of the WCST ($r = 0.526$, $p < 0.001$; $r = 0.277$, $p = 0.032$), and the ReHo value of the cuneus was positively correlated with DASS

TABLE 2 | Clinical characteristics and neuropsychologic assessments of the participants.

	Treatment group ($n = 15$)		Control group ($n = 15$)		p value, group	p value, time	p value interaction (time × group)
	Pre-rTMS Mean (SD)	Post-rTM Mean (SD)	Pre-rTMS Mean (SD)	Post-rTMS Mean (SD)			
Anxiety and depression							
HAMD score	12.07 (9.06)	5.73 (5.04)[a]	13.20 (9.37)	5.20 (3.59)[a]	0.894	0.000	0.556
HAMA score	7.80 (7.15)	3.07 (3.56)[a]	11.00 (8.98)	4.13 (3.02)[a]	0.264	0.000	0.41
DASS-depression score	22.80 (10.58)	15.60 (10.80)[a]	22.26 (10.00)	15.34 (11.86)	0.908	0.001	0.946
DASS-anxiety score	18.00 (10.02)	10.94 (8.34)[a]	19.20 (11.36)	12.80 (10.34)[a]	0.640	0.001	0.855
DASS-stress score	25.34 (10.66)	16.40 (11.88)[a]	23.34 (10.90)	13.60 (12.72)[a]	0.526	0.000	0.841
MoCA							
Total points	20.93 (3.51)	24.67 (2.99)[a]	21.93 (2.87)	22.77 (2.76)	0.614	0.000	0.006
Visuospatial abilities	3.26 (0.59)	3.40 (0.63)	2.77 (0.89)	2.53 (0.83)	0.006	1.000	0.263
Language	3.60 (0.99)	3.93 (1.09)	3.53 (0.99)	4.00 (0.93)	1.000	0.017	0.677
Executive functions	2.07 (1.39)	2.80 (0.86)	2.40 (1.12)	2.70 (0.98)	0.845	0.045	0.239
Attention	5.47 (0.74)	5.67 (0.49)	5.33 (1.11)	4.93 (1.09)	0.135	0.559	0.087
Short-term memory	1.67 (1.35)	3.27 (1.49)[a]	2.53 (1.36)	3.07 (1.33)	0.446	0.000	0.051
Orientation to time and place	4.87 (1.06)	5.60 (0.83)[a]	5.47 (0.74)	5.47 (0.64)	0.341	0.058	0.058
Stroop							
Accuracy of Stroop task (%)	56.97 (21.5)	76.58 (15.68)	62.87 (24.85)	72.84 (19.54)	0.872	0.000	0.191
Number correct	68.93 (26.02)	92.67 (18.98)[a]	76.07 (30.07)	88.13 (23.64)	0.872	0.000	0.191
Number of errors	20.6 (11.47)	10.40 (6.75)[a]	18.53 (13.69)	14.53 (10.53)	0.763	0.000	0.147
Number of omissions	31.13 (15.31)	17.73 (12.53)[a]	26.20 (18.69)	18.07 (13.47)	0.642	0.000	0.321
RT stroop task (ms)	994.9 (114.2)	1061.6 (85.8)	985.4 (101.9)	1035.9 (88.2)	0.539	0.012	0.716
WCST							
Trials administered	115 (16.0)	102 (22.7)[a]	121 (10.9)	112 (17.4)	0.142	0.004	0.479
Perseverative errors	6.60 (2.82)	2.20 (3.28)[a]	4.80 (3.49)	3.60 (3.42)	0.827	0.001	0.048
Percent perseverative error (%)	5.68 (2.21)	2.02 (2.95)[a]	4.14 (3.18)	3.13 (2.91)	0.782	0.002	0.062
Trials to complete first category	27.3 (19.4)	14.3 (7.32)[a]	25.2 (18.1)	19.4 (10.8)	0.717	0.015	0.328
Time (s)	753.9 (372.1)	388.3 (166.7)[a]	613.9 (190.0)	449.9 (213.5)[a]	0.612	0.000	0.05

[a] *P < 0.05, post-rTMS compared with pre-rTMS in the same groups.*

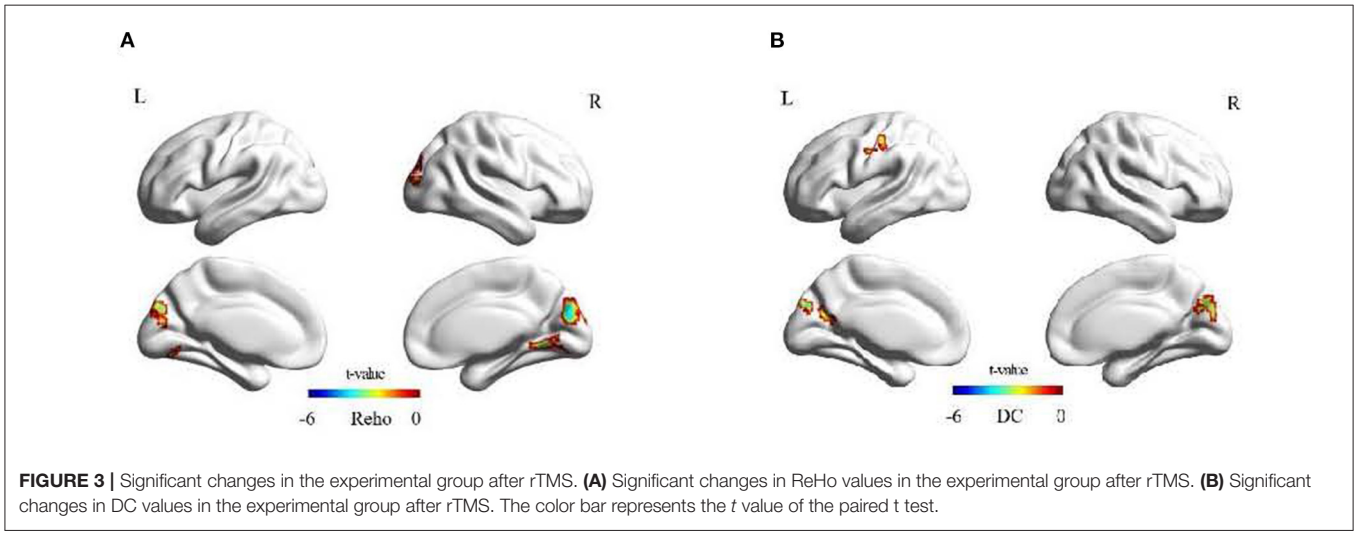

FIGURE 3 | Significant changes in the experimental group after rTMS. **(A)** Significant changes in ReHo values in the experimental group after rTMS. **(B)** Significant changes in DC values in the experimental group after rTMS. The color bar represents the *t* value of the paired t test.

score ($r = 0.254$, $p = 0.05$). The FC strength between the CUN.R and CUN.L was positively correlated with anxiety score on the DASS, depression score on the DASS, and perseverative error of the WCST ($r = 0.278$, $p = 0.031$; $r = 0.267$, $p = 0.039$; $r = 0.376$, $p = 0.003$). FC strength between the CUN.R and MOG.L was negatively correlated with RT of the Stroop task ($r =$

TABLE 3 | ReHo and DC alterations after rTMS treatment in the experimental group.

Brain region	BA	Hem	MNI peak-point coordinates			Voxels	*t* value
			x	y	z		
ReHo							
Lingual gyrus	18	R	9	−60	−3	118	−6.7456
Cuneus	18, 19	L, R	18	−84	33	202	−5.0873
DC							
Postcentral gyrus	4	L	48	−21	39	69	−6.0176
Cuneus	18, 19	L, R	15	−81	27	122	−5.5859

Gaussian random field (GRF) corrected; voxel p value < 0.001; cluster p value < 0.05; two-tailed.

TABLE 4 | Brain regions showing significantly altered FC.

Seed point	Peak area	BA	MNI peak-point coordinates			Voxels	t Value
			x	y	z		
Significantly altered FC after treatment in rTMS group							
Cuneus (18 −84 33)							
	Cuneus	18L	−6	−99	3	318	5.4351
Cuneus (15 −81 27)							
	Middle occipital gyrus	18, 19L	−30	−93	12	176	5.7132
	Middle occipital gyrus	18, 19R	24	−96	15	177	4.6835
Significantly different FC after treatment between the two groups							
Postcentral gyrus (−48 −21 39)							
	Inferior temporal gyrus	20, 37R	63	−48	15	155	5.1516
	Supramarginal gyrus	7, 39L	−36	−54	27	117	5.2488

Gaussian random field (GRF) corrected; voxel p value < 0.001; cluster p value < 0.05; two tailed.

-0.321, $p = 0.013$), FC strength between the CUN.R and MOG.R was positively correlated with perseverative error of WCST ($r = 0.266$, $p = 0.040$). FC strength between the PoCG.L and ITG.R was positively correlated with percent correct responses to the WCST ($r = 0.319$, $p = 0.013$), and it was negatively correlated with percent non-perseverative errors ($r = -0.347$, $p = 0.007$). FC strength between the PoCG.L and SMG.L was negatively correlated with the HAMA score ($r = -0.275$, $p = 0.034$), and FC strength between the IPL.R and PAL.L was positively correlated with stress score on the DASS and HAMD ($r = 0.341$, $p = 0.008$; $r = 0.369$, $p = 0.004$). An increase in the ReHo value in the lingual gyrus was positively correlated with an increase in the anxiety score in the DASS ($r = 0.439$, $p = 0.015$); an increase in the DC value in the cuneus was positively correlated with an increase in the anxiety score in the DASS ($r = 0.431$, $p = 0.018$); an increase in the ReHo value in cuneus was positively correlated with an increase of DASS Anxiety Score ($r = 0.393$, $p = 0.031$) and negatively correlated with increase in MoCA orientation score ($r = -0.361$, $p = 0.050$). An increase in FC strength between Cuneus.R and Cuneus.L was positively correlated with an increase in the depression score (DASS) ($r = 0.489$, $p = 0.006$); an increase in FC strength between Cuneus.R and Cuneus.L was positively correlated with an increase in the anxiety score (DASS) ($r = 437$, $p = 0.016$); and an increase in FC strength between PoCG.L and ITG.R was positively correlated with an increase in the MoCA score ($r = 0.449$, $p = 0.013$) (these correlation analyses are illustrated in **Figure 6**).

Metabolic Outcomes

The interaction of the three brain metabolites and their ratio between groups and time was not significant. Before rTMS, there was no significant difference in the level of choline (Cho) in the left dorsolateral prefrontal cortex between the two groups ($p = 0.394$), while after rTMS, the level of Cho in the left DLPFC in the experimental group was significantly lower than that in the control group ($p = 0.011$). Before rTMS, there was a significant difference in the ratio of N-acetylaspartate to creatine (NAA/Cr) in the left DLPFC between the two groups ($p < 0.024$), and after rTMS, the level of NAA/Cr in the left DLPFC in the experimental group was significantly higher than that in the control group ($p < 0.001$) (**Table 5**).

We performed a correlation analysis of the two groups of patients between the brain metabolic index and the scores on cognitive tests and psychiatric symptom scales (**Figure 7**). The change in Cho in the left DLPFC in the experimental group was significantly lower than that in the control group ($p = 0.168$),

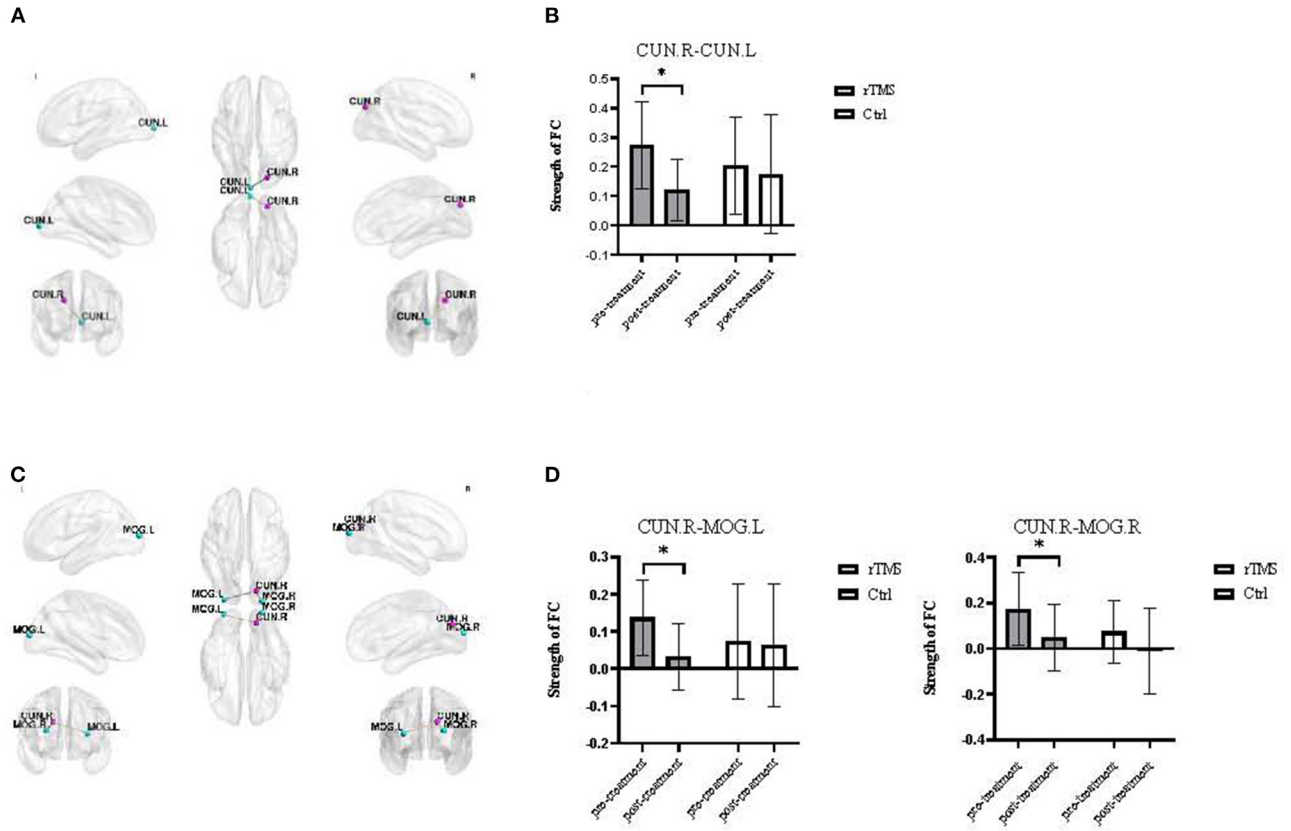

FIGURE 4 | Significantly altered FC after treatment in the rTMS group (voxel $p < 0.001$, cluster $p < 0.05$, two-tailed, GRF-corrected). **(A)** The results of functional connectivity analyses with the seed region located in the CUN.R (18 −84 33). **(B)** The panel displays the FC strength values from CUN.R to CUN.L. **(C)** The results of the functional connectivity analyses with the seed region located in the CUN.R (15 −81 27). **(D)** The panel displays the FC strength values from CUN.R to MOG.L and MOG.R. CUN, cuneus; MOG, middle occipital gyrus. *$P < 0.05$, Post-rTMS compared with pre-rTMS in the same groups.

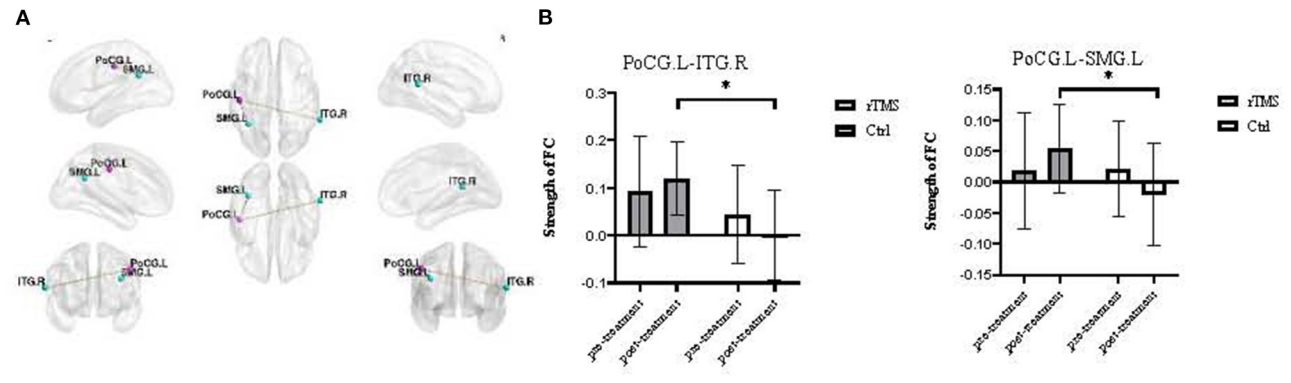

FIGURE 5 | Significantly different FC after treatment between the two groups (voxel $p < 0.01$, cluster $p < 0.05$, two-tailed, GRF-corrected). **(A)** The results of the functional connectivity analyses with the seed region located in the PoCG.L (−48 −21 39). **(B)** The panel displays the FC strength values from PoCG to ITG.R and SMG.L. PoCG, postcentral gyrus; ITG, inferior temporal gyrus; SMG, supramarginal gyrus. *$P < 0.05$, Treatment group compared with control group at the same timepoint.

and positively correlated with changes in the RT Stroop task ($r = 0.374$, $p = 0.042$). The change in NAA/Cr in the left DLPFC in the experimental group was significantly higher than that in the control group ($p = 0.067$), while the ratio was positively correlated with the correct responses rate on the WCST ($r = 0.296$, $p = 0.022$).

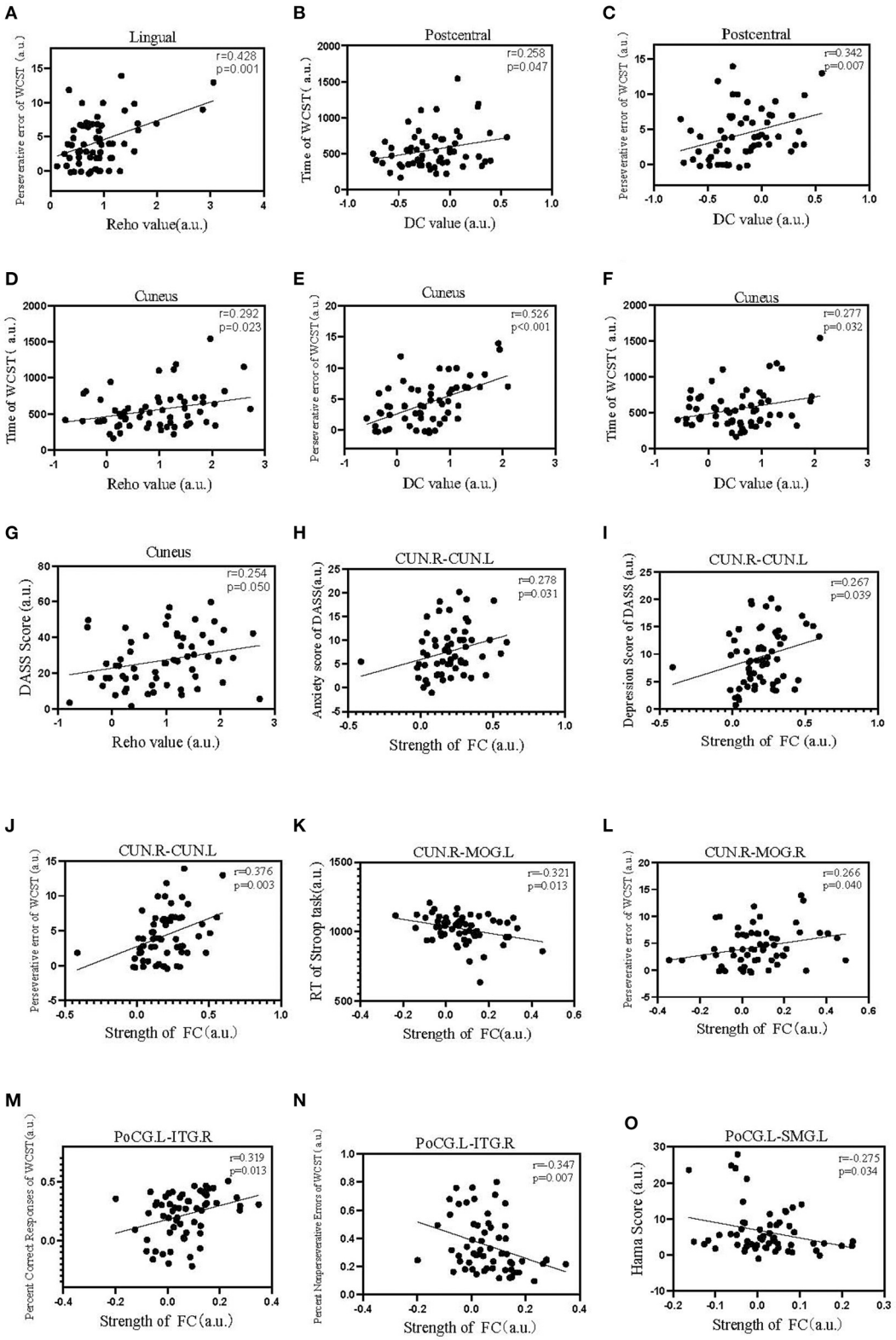

FIGURE 6 | Continued

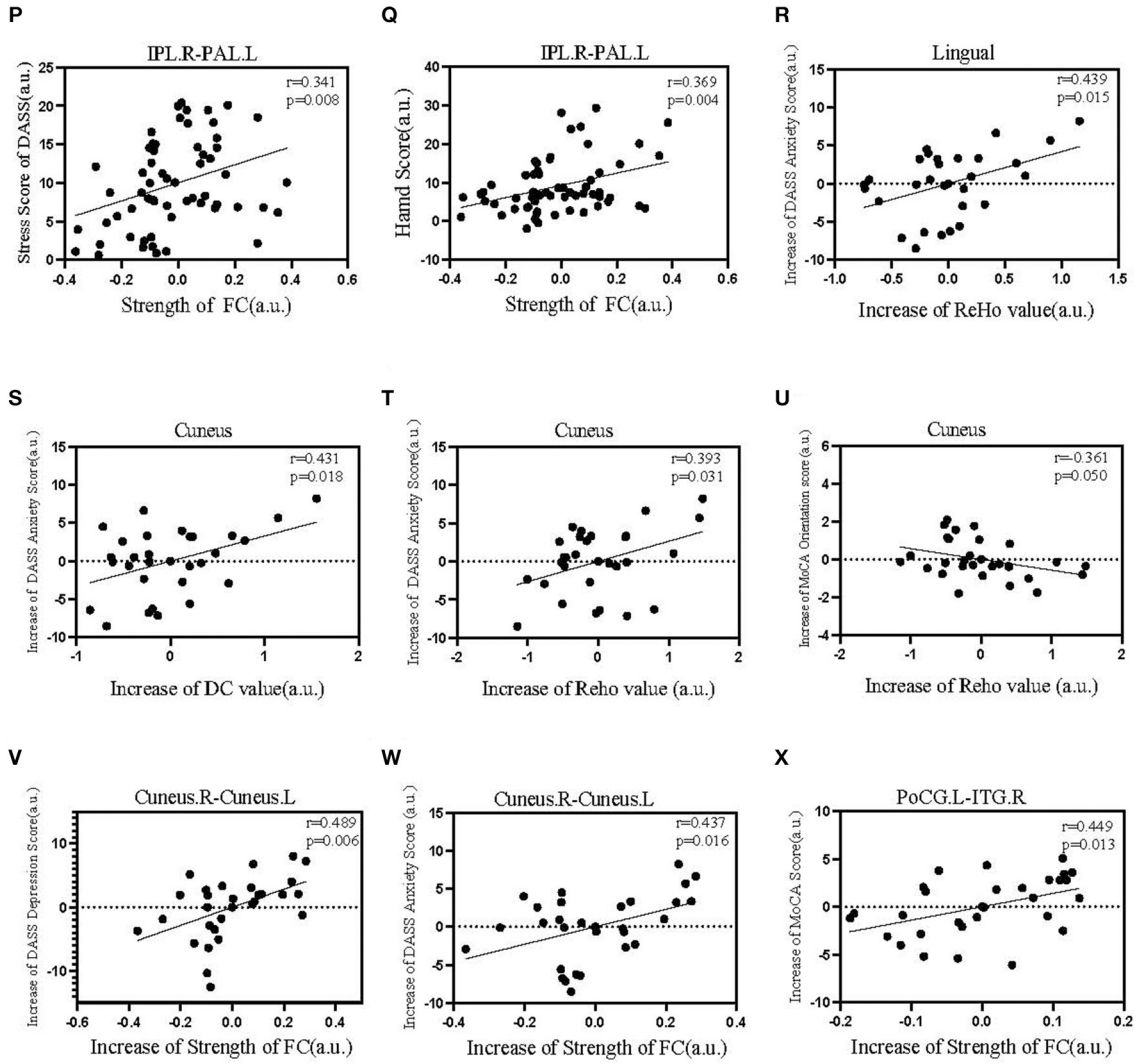

FIGURE 6 | Scatter diagrams showing significant correlations among the clinical data, neurophysiologic assessments, ReHo, DC, and FC strength for all patients (pretherapy and posttherapy). **(A)** The ReHo value of the lingual region was positively correlated with the perseverative error of the WCST. **(B,C)** The DC value of the postcentral gyrus was positively correlated with the time taken for the WCST and perseverative error of the WCST. **(D)** The ReHo value of the cuneus was positively correlated with the time taken for the WCST. **(E,F)** The DC value of the cuneus was positively correlated with perseverative error of the WCST and time of the WCST. **(G)** The ReHo value of the cuneus was positively correlated with DASS score. **(H–J)** FC strength between the CUN.R and CUN.L was positively correlated with anxiety score on the DASS, depression score on the DASS, and perseverative error on the WCST. **(K)** FC strength between the CUN.R and MOG.L was negatively correlated with reaction time (RT) on the Stroop task. **(L)** FC strength between the CUN.R and MOG.R was positively correlated with perseverative error of WCST. **(M)** FC strength between the PoCG.L and ITG.R was positively correlated with percent correct responses on the WCST. **(N)** FC strength between the PoCG.L and ITG.R was negatively correlated with percent non-perseverative errors. **(O)** FC strength between the PoCG.L and SMG.L was negatively correlated with the HAMA score. **(P,Q)** FC strength between the IPL.R and PAL.L was positively correlated with stress score of the DASS and HAMA scores. **(R)** Increase in ReHo value in lingual was positively correlated with an increase in the anxiety score in the DASS. **(S)** Increase in the DC value in cuneus was positively correlated with an increase in anxiety score in the DASS. **(T,U)** Increase in the Reho value in cuneus was positively correlated with an increase of DASS Anxiety Score and negatively correlated with increase in MoCA orientation score. **(V)** Increase in FC strength between Cuneus.R and Cuneus.L was positively correlated with an increase in depression score (DASS). **(W)** Increase in FC strength between Cuneus.R and Cuneus.L was positively correlated with an increase in anxiety score (DASS). **(X)** Increase in FC strength between PoCG.L and ITG.R was positively correlated with an increase in the MoCA score.

DISCUSSION

Effects of rTMS on Cognitive Function in Patients With Stress-Related Depression

Executive function reflects a series of cognitive processes that are necessary for cognitive control of behavior. The performance of patients with depression on the WCST, Stroop color word test, and other neuropsychologic tests has been shown to be worse than those in control groups (26–28).

The MoCA scores of the patients selected for this study ranged from 15 to 25, which indicates mild cognitive impairment. After rTMS, the MoCA scores of patients in

TABLE 5 | Comparisons of neurotransmitters in the left DLPFC by MRS between pre- and post-rTMS treatment of the two groups.

	Treatment group ($n = 15$)		Control group ($n = 15$)		p value, group	p value, time	p value interaction (time × group)
	Pre-rTMS Mean (SD)	Post-rTM Mean (SD)	Pre-rTMS Mean (SD)	Post-rTMS Mean (SD)			
NAA	0.0192 (0.0044)	0.0173 (0.0033)	0.0186 (0.0041)	0.0189 (0.0037)	0.632	0.433	0.270
NAA/Cr	1.7567 (0.2042)	1.8125 (0.1940)	1.6007 (0.1509)[b]	1.5449 (0.1066)[b]	0.001	1.000	0.067
Cho	0.0084 (0.0016)	0.0074 (0.0019)	0.0089 (0.0015)	0.0092 (0.0015)[b]	0.013	0.427	0.168
Cho/Cr	0.7805 (0.1153)	0.7881 (0.1804)	0.7720 (0.090)	0.7654 (0.1051)	0.702	0.982	0.760
Cr	0.0110 (0.0228)	0.0096 (0.0021)	0.0117 (0.0024)	0.0123 (0.0024)[b]	0.006	0.500	0.111

[b] *$P < 0.05$, Treatment group compared with control group at the same timepoints.*

the experimental group increased significantly, and the scores for short-term memory and orientation to time and place (MoCA subfactors) in the experimental group were significantly improved after rTMS. We found that after 20-Hz dTMS was focused on the DLPFC of patients with depression, there was significant improvement in the scores on spatial working memory tests in Cambridge automated neuropsychological tests (29).

The Stroop effect color word test, as a representative test of response-inhibition ability (30–32), has been widely used in patients with different diseases and of different ages (33–36). In our study, we uncovered a significant increase in the number of correct answers, while the number of errors and omissions decreased significantly in the experimental group, but there was no significant change in the control group. This illustrates the response-inhibitory capability of the patients as having been improved after rTMS. This conclusion is the same as that drawn in a previous study in which rTMS to the DLPFC in patients was used in treatment-resistant depression (TRD) (37).

In this study, we found that the number of persistent errors on the WCST in the experimental group decreased significantly after treatment, while there was no significant change in the control group, and although the test duration in the two groups decreased significantly, the experimental group decreased to an even greater extent. The number of persistent errors reflects problems such as concept formation and plasticity (29). Some researchers also found that high-frequency (at 15 Hz) rTMS stimulation over the left DLPFC in patients with treatment-resistant depression changed the performance on the WCST (38). Other investigators used intermittent theta burst stimulation (iTBS) to treat patients with treatment-resistant depression, and demonstrated that after iTBS over the left DLPFC, the correct-answer rate on the WCST and conceptual response rate increased, while the error rate declined. This indicates that iTBS exerted a positive effect on the executive function of patients with depression (39). iTBS and high-frequency rTMS stimulation can thus actively stimulate brain areas. Both our research and that of previous studies showed that the activation of the left DLPFC led to improvements in cognitive function.

Effects of rTMS on fMRI in Patients With Stress-Related Depression

The lingual gyrus is primarily responsible for letter processing, logical analysis, and visual memory processing (40). Our study revealed that the ReHo value in the right lingual gyrus of the experimental group decreased after rTMS and was positively correlated with perseverative error on the WCST. In the WCST, patients uncover rules so as to form concepts according to the shape, color, and number of cards. The above tasks require logical analysis or visual memory, and the level of gyrus activity may affect the patient's test performance. Furthermore, the ReHo value of the lingual region was positively correlated with the perseverative error of the WCST. The results showed that rTMS may affect the level of ReHo in the lingual gyrus, and thereby affect executive function in patients.

The cuneus is located in the supracalcarinal fissure of the occipital lobe and belongs to the visual cortex. We showed that the level of ReHo in the left and right cuneus of the experimental group decreased, and the level of DC in the right cuneus diminished after rTMS. The ReHo value of the cuneus was positively correlated with time of the WCST, as was the DC value of the cuneus with perseverative error on the WCST and time of the WCST. An increase in the ReHo value in the cuneus was positively correlated with an increase in the anxiety score in the DASS and negatively correlated with an increase in the orientation score (MoCA).The cuneus is principally responsible for processing visual images (40), as both the WCST and Stroop effect color word test require subjects to process visual information, and the cuneus may thus play an important role in the aforementioned tests.

After rTMS, the functional connection strength between the right cuneus and the left cuneus and between the right cuneus and the left and right middle occipital gyrus changed significantly in the experimental group. FC strength between the CUN.R and CUN.L was positively correlated with perseverative error on the WCST, FC strength between the CUN.R and MOG.L was negatively correlated with the RT of the Stroop task, and FC strength between the CUN.R and MOG.R was positively correlated with perseverative error of WCST. The middle occipital gyrus belongs to the visual cortex and is responsible for processing visual images and participating in the brain area

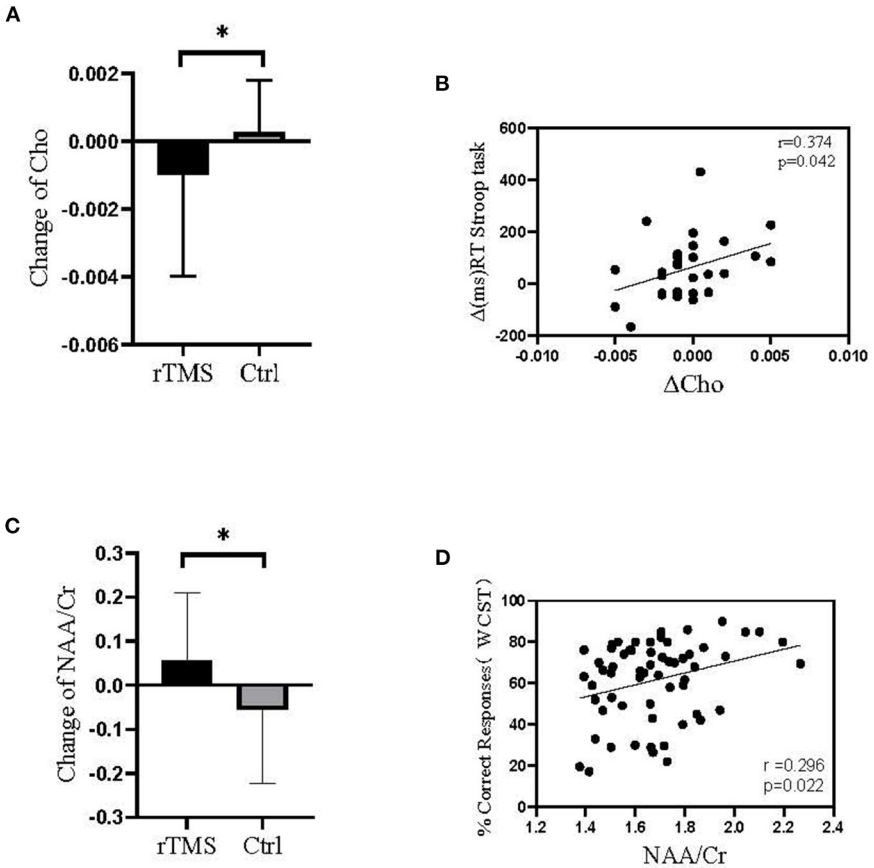

FIGURE 7 | The level of Cho and NAA/Cr in the left DLPFC before and after treatment and its relationship with cognitive testing. **(A)** The change in Cho in the left DLPFC in the experimental group was significantly lower than that in the control group. **(B)** The change in Cho in the left DLPFC was positively correlated with change in the RT on the Stroop task. **(C)** The change in NAA/Cr in the left DLPFC in the experimental group was significantly higher than that in the control group. **(D)** The NAA/Cr value in the left DLPFC was positively correlated with correct response rate on the WCST. *$P < 0.05$, Treatment group compared with control group.

associated with verbal declarative memory (40). Therefore, the functional connection strength between the right cuneus and the left cuneus, and the right cuneus and the left and right middle occipital gyrus may play important roles in the above tests. Collectively, these results suggest that rTMS may affect the functional connection strength between the right cuneus and the left cuneus, and the right cuneus and the left and right middle occipital gyrus, and thus affect executive function in patients.

The level of DC in the left postcentral gyrus of the experimental group declined after treatment, the DC value of the postcentral gyrus was positively correlated with perseverative error on the WCST and time of the WCST. After rTMS, the functional connection strength between the left postcentral gyrus and the right inferior temporal gyrus (ITG), the left postcentral gyrus, and the left supramarginal gyrus was significantly different between the two groups. FC strength between the PoCG.L and ITG.R was positively correlated with percent correct responses on the WCST, FC strength between the PoCG.L and ITG.R was negatively correlated with percent non-perseverative errors, and an increase in FC strength between PoCG.L and ITG.R was positively correlated with an increase in the MoCA score. ITG is involved in a variety of advanced cognitive functions, including visual object recognition, decision-making, vocabulary and speech comprehension, decision-making, and emotion regulation (41–44). Some studies have found that in patients with chronic schizophrenia, the reduction in bilateral inferior temporal gyrus volume may lead to semantic multimodal sensory integration and complex visual perception dysfunction (45–47).

The supramarginal gyrus belongs to the inferior parietal lobule and is related to mathematics and logic, and the inferior parietal lobule receives input from the visual and somatosensory cortex. Therefore, the inferior parietal lobule is considered to be an important area for the integration of different modal information. Injury to the inferior parietal lobule affects spatial perception and the integration of vision, movement, and other information (48). Some investigators have found that trauma-related stimuli can induce corresponding memories and often cause strong physical responses that are

involved in a variety of somatosensory information (49–51), and these can be remembered in the form of physical sensory information (52).

Studies have shown that abnormal activation of the inferior parietal lobule and postcentral gyrus in patients with PTSD precipitated abnormal sensory information processing in these patients (53, 54). The functional connectivity between the left DLPFC and the left superior parietal lobule, bilateral cuneus, and bilateral supraoccipital gyrus was significantly enhanced in PTSD patients, and there may be abnormal functional connections between the frontal lobe-parietal lobe loop and the frontal-occipital lobe loop in patients with PTSD (55). For example, EEG studies have found that primary sensory function was abnormal in PTSD patients (56–58). Abnormal automatic processing is also related to the high arousal symptoms of PTSD (59, 60), which may trigger upset in PTSD patients when exposed to a complex environment. Although the patients in our study did not meet the diagnostic criteria of PTSD, they all experienced stress-related events prior to admission.

After rTMS, the DC value of the postcentral gyrus decreased in the experimental group, and the functional connectivity strength of the left postcentral gyrus and supramarginal gyrus was negatively correlated with the HAMA score. We suggest that this connection may be related to negative emotional arousal. Our study showed that rTMS may therefore affect the level of DC in the postcentral gyrus and its functional connectivity, and then affect performance on cognitive tests.

Effects of rTMS on Brain Metabolism in Patients With Stress-Related Depression

Proton magnetic resonance spectroscopy (^{1}H-MRS) is a non-invasive method that can measure the levels of important metabolites in specific brain regions, and studies have shown that metabolites in the brain may be related to the pathophysiology of mental illness (61). The primary metabolites that we analyzed with ^{1}H-MRS were N-acetylaspartate (NAA), choline (Cho), and creatine (Cr).

We did not uncover any significant difference in the level of Cho in the left DLPFC between the two groups before rTMS, but the level of choline (Cho) in the experimental group was significantly lower than that in the control group after rTMS. Studies have shown that Cho levels and the Cho/Cr ratio in the bilateral DLPFC in young patients with depression were higher than those in healthy controls, especially with respect to the left DLPFC (62), and choline levels in the left DLPFC were abnormally elevated in children and the elderly with severe depression (63, 64). Patients with stress-related depression who participated in the current study may have had high levels of Cho in the left DLPFC, and correlation analysis showed that changes in Cho in the left DLPFC were positively correlated with changes in the RT Stroop task. rTMS may thus improve the executive function of patients by promoting the levels of Cho in the left DLPFC.

Before rTMS, the NAA/Cr ratio in the left DLPFC in the experimental group was significantly higher than that in the control group, and the gap was further augmented after treatment. The patients with a longer duration of depression exhibited a lower NAA/Cr ratio in the left DLPFC relative to those with a shorter course of disease and compared with healthy people (65). The change in memory capability has been positively correlated with the ratio of N-acetylaspartate to creatine (NAA/Cr) and the ratio of choline to creatine (Cho/Cr) in the right brain (66). After high-frequency (15-Hz) rTMS over the left DLPFC in patients with treatment-resistant depression, we noted that an improvement in the number of persistent errors on the WCST after treatment was positively correlated with an increase in NAA levels in the left anterior cingulate gyrus of the rTMS group (38). Our correlation analysis showed that the NAA/Cr ratio in the left DLPFC was positively correlated with a correct-response rate on the WCST. rTMS may therefore improve executive function in patients by stabilizing the NAA/Cr ratio in the left DLPFC.

CONCLUSIONS

Ten-Hz rTMS improved the cognitive function (executive function) of patients with stress-related depression, and this may have been due to two underlying mechanisms. One was a reduction in the activity level of sensation-related brain regions, reducing the functional connection of vision-related brain regions, improving the functional connection between somatosensory cortex and visual-auditory cortex, and stabilizing the functional connection between inferior parietal lobule and pallidus. The other mechanism appeared to be a reduction in the level of Cho and stabilization in the level of NAA/Cr in the left DLPFC.

DATA AVAILABILITY STATEMENT

The original contributions presented in the study are included in the article/supplementary material, further inquiries can be directed to the corresponding author/s.

ETHICS STATEMENT

The study was performed in accordance with the Declaration of Helsinki and was approved by the Local Ethics Review Committee (Ethics Committee of the Hospital 984 of PLA). The patients/participants provided their written informed consent to participate in this study. Written informed consent was obtained from the individual(s) for the publication of any potentially identifiable images or data included in this article.

AUTHOR CONTRIBUTIONS

YuxC designed research, conducted research, performed analysis, and wrote the paper. LQ and YZ designed research, supervised research, reviewed, and revised the manuscript, and granted research funds. XL developed clinical conception. LW performed software and data curation. ST, YuaC, FW,

KG, YW, GX, SZ, JL, HW, ZJ, LL, and XiW involved in clinical assessment and rTMS administration. FX, XuW, SW, and CX interpreted data. The authors accept responsibility for the integrity of the data and the accuracy of the data analysis. All authors contributed to the article and approved the submitted version.

FUNDING

This work was supported by the National Defense Basic Science Research Program of China (Grant No. JCKY2019548B001) and the National Defense Science and Technology Innovation Project of China (Grant No. 1716312ZT00216401).

REFERENCES

1. World Health Organization. *Depression and Other Common Mental Disorders: Global Health Estimates*. Geneva: World Health Organization (2017).
2. Bosch OG, Seifritz E, Wetter TC. Stress-related depression: neuroendocrine, genetic, and therapeutical aspects. *World J Biol Psychiatry*. (2012) 13:556–68. doi: 10.3109/15622975.2012.665477
3. Craike MJ, Coleman D, MacMahon C. Direct and buffering effects of physical activity on stress-related depression in mothers of infants. *J Sport Exerc Psychol.* (2010) 32:23–38. doi: 10.1123/jsep.32.1.23
4. Moser DJ, Jorge RE, Manes F, Paradiso S, Benjamin ML, Robinson RG. Improved executive functioning following repetitive transcranial magnetic stimulation. *Neurology*. (2002) 58:1288–90. doi: 10.1212/WNL.58.8.1288
5. Vanderhasselt MA, De Raedt R, Leyman L, Baeken C. Acute effects of repetitive transcranial magnetic stimulation on attentional control are related to antidepressant outcomes. *J Psychiatry Neurosci*. (2009) 34:119–26.
6. Nadeau SE, Bowers D, Jones TL, Wu SS, Triggs WJ, Heilman KM. Cognitive effects of treatment of depression with repetitive transcranial magnetic stimulation. *Cogn Behav Neurol.* (2014) 27:77–87. doi: 10.1097/WNN.0000000000000031
7. Ullrich H, Kranaster L, Sigges E, Andrich J, Sartorius A. Ultra-high-frequency left prefrontal transcranial magnetic stimulation as augmentation in severely ill patients with depression: a naturalistic sham-controlled, double-blind, randomized trial. *Neuropsychobiology*. (2012) 66:141–8. doi: 10.1159/000339561
8. Wajdik C, Claypoole KH, Fawaz W, Holtzheimer 3rd PE, Neumaier J, Dunner DL, et al. No Change in neuropsychological functioning after receiving repetitive transcranial magnetic stimulation treatment for major depression. *J ECT*. (2014) 30:320–4. doi: 10.1097/YCT.0000000000000096
9. Signorini DF, Leung O, Simes RJ, Beller E, Gebski VJ, Callaghan T. Dynamic balanced randomization for clinical trials. *Stat Med.* (1993) 12:2343–50. doi: 10.1002/sim.4780122410
10. Guse B, Falkai P, Gruber O, Whalley H, Gibson L, Hasan A, et al. The effect of long-term high frequency repetitive transcranial magnetic stimulation on working memory in schizophrenia and healthy controls–a randomized placebo-controlled, double-blind fMRI study. *Behav Brain Res.* (2013) 237:300–7. doi: 10.1016/j.bbr.2012.09.034
11. Fitzgerald PB, Hoy K, Daskalakis ZJ, Kulkarni J. A randomized trial of the anti-depressant effects of low- and high-frequency transcranial magnetic stimulation in treatment-resistant depression. *Depress Anxiety*. (2009) 26:229–34. doi: 10.1002/da.20454
12. Rusjan PM, Barr MS, Farzan F, Arenovich T, Maller JJ, Fitzgerald PB, et al. Optimal transcranial magnetic stimulation coil placement for targeting the dorsolateral prefrontal cortex using novel magnetic resonance image-guided neuronavigation. *Hum Brain Mapp.* (2010) 31:1643–52. doi: 10.1002/hbm.20964
13. Fitzgerald PB, Maller JJ, Hoy KE, Thomson R, Daskalakis ZJ. Exploring the optimal site for the localization of dorsolateral prefrontal cortex in brain stimulation experiments. *Brain Stimul.* (2009) 2:234–7. doi: 10.1016/j.brs.2009.03.002
14. Hamilton M. Development of a rating scale for primary depressive illness. *Br J Soc Clin Psychol.* (1967) 6:278–96. doi: 10.1111/j.2044-8260.1967.tb00530.x
15. Hamilton M. The assessment of anxiety states by rating. *Br J Med Psychol.* (1959) 32:50–5. doi: 10.1111/j.2044-8341.1959.tb00467.x
16. Taouk M, Lovibond PF, Laube R. *Psychometric Properties of a Chinese Version of the Short Depression Anxiety Stress Scales (DASS 21)*. Report for New South Wales Transcultural Mental Health Centre, Cumberland Hospital, Sydney (2001).
17. Nasreddine ZS, Phillips NA, Bédirian V, Charbonneau S, Whitehead V, Collin I, et al. The Montreal cognitive assessment, MoCA: a brief screening tool for mild cognitive impairment. *J Am Geriatr Soc.* (2005) 53:695–9. doi: 10.1111/j.1532-5415.2005.53221.x
18. Teubner-Rhodes S, Vaden KI. Jr, Dubno JR, Eckert MA. Cognitive persistence: Development and validation of a novel measure from the Wisconsin Card Sorting Test. *Neuropsychologia.* (2017) 102:95–108. doi: 10.1016/j.neuropsychologia.2017.05.027
19. Barceló F, Sanz M, Molina V, Rubia FJ. The Wisconsin Card Sorting Test and the assessment of frontal function: a validation study with event-related potentials. *Neuropsychologia.* (1997) 35:399–408. doi: 10.1016/S0028-3932(96)00096-6
20. Spreen O, Strauss E. *A Compendium of Neuropsychological Tests.* (1991). New York, USA: Oxford University Press.
21. Stroop JR. Studies of interference in serial verbal reactions. *J Exp Psychol.* (1935) 18:643–62. doi: 10.1037/h0054651
22. Yan CG, Wang XD, Zuo XN, Zang YFDPABI. Data processing and analysis for (resting-state) brain imaging. *Neuroinformatics.* (2016) 14:339–51. doi: 10.1007/s12021-016-9299-4
23. Zou QH, Zhu CZ, Yang Y, Zuo XN, Long XY, Cao QJ, et al. An improved approach to detection of amplitude of low-frequency fluctuation (ALFF) for resting-state fMRI: fractional ALFF. *J Neurosci Methods.* (2008) 172:137–41. doi: 10.1016/j.jneumeth.2008.04.012
24. Zang YF, Jiang TZ, Lu YL, He Y, Tian LX. Regional homogeneity approach to fMRI data analysis. *Neuroimage.* (2004) 22:394–400. doi: 10.1016/j.neuroimage.2003.12.030
25. Buckner RL, Sepulcre J, Talukdar T, Krienen FM, Liu H, Hedden T, et al. Cortical hubs revealed by intrinsic functional connectivity: mapping, assessment of stability, and relation to Alzheimer's disease. *J Neurosci.* (2009) 29:1860–73. doi: 10.1523/JNEUROSCI.5062-08.2009
26. Harvey PO, Le Bastard G, Pochon JB, Levy R, Allilaire JF, Dubois B, et al. Executive functions and updating of the contents of working memory in unipolar depression. *J Psychiatr Res.* (2004) 38:567–76. doi: 10.1016/j.jpsychires.2004.03.003
27. Mondal S, Sharma VK, Das S, Goswami U, Gandhi A. Neuro-cognitive functions in patients of major depression. *Indian J Physiol Pharmacol.* (2007) 51:69–75.
28. Kaneda Y. Verbal working memory impairment in patients with current episode of unipolar major depressive disorder and in remission. *Clin Neuropharmacol.* (2009) 32:346–7. doi: 10.1097/WNF.0b013e3181b130a0
29. Levkovitz Y, Harel EV, Roth Y, Braw Y, Most D, Katz LN, et al. Deep transcranial magnetic stimulation over the prefrontal cortex: Evaluation of antidepressant and cognitive effects in depressive patients. *Brain Stimul.* (2009) 2:188–200. doi: 10.1016/j.brs.2009.08.002
30. Golden CJ. Identification of brain disorders by the stroop color and word test. *J Clin Psychol.* (1976) 32:654–8.
31. Bondi MW, Serody AB, Chan AS, Eberson-Shumate SC, Delis DC, Hansen LA, et al. Cognitive and neuropathologic correlates of Stroop Color-Word Test performance in Alzheimer's disease. *Neuropsychology.* (2002) 16:335–43. doi: 10.1037/0894-4105.16.3.335
32. Stuss DT, Floden D, Alexander MP, Levine B, Katz D. Stroop performance in focal lesion patients: dissociation of processes and frontal lobe lesion location. *Neuropsychologia.* (2001) 39:771–86. doi: 10.1016/S0028-3932(01)00013-6
33. Uttl B, Graf P. Color-Word Stroop test performance across the adult life span. *J Clin Exp Neuropsychol.* (1997) 19:405–20. doi: 10.1080/01688639708403869

34. Van der Elst W, Van Boxtel MP, Van Breukelen GJ, Jolles J. The stroop color-word test: influence of age, sex, and education; and normative data for a large sample across the adult age range. *Assessment.* (2006) 13:62–79. doi: 10.1177/1073191105283427
35. Homack S, Riccio CA. A meta-analysis of the sensitivity and specificity of the Stroop Color and Word Test with children. *Arch Clin Neuropsychol.* (2004) 19:725–43. doi: 10.1016/j.acn.2003.09.003
36. Ikeda Y, Okuzumi H, Kokubun M, Haishi K. Age-related trends of interference control in school-age children and young adults in the stroop color-word test. *Psychol Rep.* (2011) 108:577–84. doi: 10.2466/04.10.22.PR0.108.2.577-584
37. Schulze L, Wheeler S. McAndrews MP, Solomon CJ, Giacobbe P, Downar J. Cognitive safety of dorsomedial prefrontal repetitive transcranial magnetic stimulation in major depression. *Eur Neuropsychopharmacol.* (2016) 26:1213–26. doi: 10.1016/j.euroneuro.2016.04.004
38. Zheng H, Jia F, Guo G, Quan D, Li G, Wu H, et al. Abnormal anterior cingulate N-acetylaspartate and executive functioning in treatment-resistant depression after rTMS therapy. *Int J Neuropsychopharmacol.* (2015) 18:pyv059. doi: 10.1093/ijnp/pyv059
39. Cheng CM, Juan CH, Chen MH, Chang CF, Lu HJ, Su TP, et al. Different forms of prefrontal theta burst stimulation for executive function of medication-resistant depression: evidence from a randomized sham-controlled study. *Prog Neuropsychopharmacol Biol Psychiatry.* (2016) 66:35–40. doi: 10.1016/j.pnpbp.2015.11.009
40. Vanni S, Tanskanen T, Seppä M, Uutela K, Hari R. Coinciding early activation of the human primary visual cortex and anteromedial cuneus. *Proc Natl Acad Sci USA.* (2001) 98:2776–80. doi: 10.1073/pnas.041600898
41. Herath, P., Kinomura, S., and Roland, P. E. (2001). Visual recognition: evidence for two distinctive mechanisms from a PET study. Hum Brain Mapp. 12, 110–9. doi: 10.1002/1097-0193(200102)12:2 < 110::AID-HBM1008>3.0.CO;2-0
42. Ishai A, Ungerleider LG, Martin A, Schouten JL, Haxby JV. Distributed representation of objects in the human ventral visual pathway. *Proc Natl Acad Sci USA.* (1999) 96:9379–84. doi: 10.1073/pnas.96.16.9379
43. Mechelli A, Gorno-Tempini ML, Price CJ. Neuroimaging studies of word and pseudo word reading: consistencies, inconsistencies, and limitations. *J Cogn Neurosci.* (2003) 15:260–71. doi: 10.1162/089892903321208196
44. Buckley MJ, Gaffan D, Murray EA. Functional double dissociation between two inferior temporal cortical areas: perirhinal cortex versus middle temporal gyrus. *J Neurophysiol.* (1997) 77:587–98. doi: 10.1152/jn.1997.77.2.587
45. Onitsuka T, Shenton ME, Salisbury DF, Dickey CC, Kasai K, Toner SK, et al. Middle and inferior temporal gyrus gray matter volume abnormalities in chronic schizophrenia:an MRI study. *Am J Psychiatry.* (2004) 161:1603–11. doi: 10.1176/appi.ajp.161.9.1603
46. Mesulam MM. From sensation to cognition. *Brain.* (1998) 121:1013–52. doi: 10.1093/brain/121.6.1013
47. Tek C, Gold J, Blaxton T, Wilk C, McMahon RP, Buchanan RW. Visual perceptual and working memory impairments in schizophrenia. *Arch Gen Psychiatry.* (2002) 59:146–53. doi: 10.1001/archpsyc.59.2.146
48. Andersen RA. Inferior parietal lobule function in spatial perception and visuomotor integration. In: *Handbook of Physiology. The Nervous System*, *p*. 483–518. Rockville, MD: American Physiological Society (1987).
49. Jones E, Vermaas RH, McCartney H, Beech C, Palmer I, Hyams K, Wessely S. Flashbacks and post-traumatic stress disorder: the genesis of a 20th-century diagnosis. *Br J Psychiatry.* (2003) 182:158–63. doi: 10.1192/bjp.182.2.158
50. Osuch EA, Benson B, Geraci M, Podell D, Herscovitch P, McCann UD, Post RM. Regional cerebral blood flow correlated with flashback intensity in patients with posttraumatic stress disorder. *Biol Psychiatry.* (2001) 50:246–53. doi: 10.1016/S0006-3223(01)01107-6
51. Hackmann A, Ehlers A, Speckens A, Clark DM. Characteristics and content of intrusive memories in PTSD and their changes with treatment. *J Trauma Stress.* (2004) 17:231–40. doi: 10.1023/B:JOTS.0000029266.88369.fd
52. van den Heuvel M, Mandl R, Hulshoff Pol H. Normalized Cut Group Clustering of Resting-State fMRI Data. *PLoS One.* (2008) 3:e2001. doi: 10.1371/journal.pone.0002001
53. Bryant RA, Felmingham KL, Kemp AH, Barton M, Peduto AS, Rennie C, et al. Neural networks of information processing in posttraumatic stress disorder: a functional magnetic resonance imaging study. *Biol Psychiatry.* (2005) 58:111–8. doi: 10.1016/j.biopsych.2005.03.021
54. Falconer E, Bryant R, Felmingham KL, Kemp AH, Gordon E, Peduto A, et al. The neural networks of inhibitory control in posttraumatic stress disorder. *J Psychiatry Neurosci.* (2008) 33:413–22.
55. Zhang Y, Liu F, Chen H, Duan LiM, Xie X, Chen B, et al. Intranetwork and internetwork functional connectivity alterations in post-traumatic stress disorder. *J Affect Disord.* (2015) 187:114–21. doi: 10.1016/j.jad.2015.08.043
56. Ge Y, Wu J, Sun X, Zhang K. Enhanced mismatch negativity in adolescents with posttraumatic stress disorder (PTSD). *Int J Psychophysiol.* (2011) 79:231–5. doi: 10.1016/j.ijpsycho.2010.10.012
57. Holstein DH, Vollenweider FX, Jäncke L, Schopper C, Csomor PA. P50 suppression, prepulse inhibition, and startle reactivity in the same patient cohort suffering from posttraumatic stress disorder. *J Affect Disord.* (2010) 126:188–97. doi: 10.1016/j.jad.2010.02.122
58. Hunter M, Villarreal G. McHaffie GR, Jimenez B, Smith AK, Calais LA, et al. Lateralized abnormalities in auditory M50 sensory gating and cortical thickness of the superior temporal gyrus in post-traumatic stress disorder: preliminary results. *Psychiatry Res.* (2011) 191:138–44. doi: 10.1016/j.pscychresns.2010.09.012
59. Clark CR, Galletly CA, Ash DJ, Moores KA, Penrose RA, McFarlane AC. Evidence-based medicine evaluation of electrophysiological studies of the anxiety disorders. *Clin EEG Neurosci.* (2009) 40:84–112. doi: 10.1177/155005940904000208
60. Heim C, Nemeroff CB. Neurobiology of posttraumatic stress disorder. *CNS Spectr.* (2009) 14:13–24.
61. Stanley JA. In vivo magnetic resonance spectroscopy and its application to neuropsychiatric disorders. *Can J Psychiatry.* (2002) 47:315–26. doi: 10.1177/070674370204700402
62. Yang XR, Langevin LM, Jaworska N, Kirton A, Lebel RM, Harris AD, et al. Proton spectroscopy study of the dorsolateral prefrontal cortex in youth with familial depression. *Psychiatry Clin Neurosci.* (2016) 70:269–77. doi: 10.1111/pcn.12392
63. Farchione TR, Moore GJ, Rosenberg DR. Proton magnetic resonance spectroscopic imaging in pediatric major depression. *Biol Psychiatry.* (2002) 52:86–92. doi: 10.1016/S0006-3223(02)01340-9
64. Kumar A, Thomas A, Lavretsky H, Yue K, Huda A, Curran J, et al. Frontal white matter biochemical abnormalities in late-life major depression detected with proton magnetic resonance spectroscopy. *Am J Psychiatry.* (2002) 159:630–6. doi: 10.1176/appi.ajp.159.4.630
65. Brambilla P, Stanley JA, Nicoletti MA, Sassi RB, Mallinger AG, Frank E, et al. 1H Magnetic resonance spectroscopy study of dorsolateral prefrontal cortex in unipolar mood disorder patients. *Psychiatry Res.* (2005) 138:131–9. doi: 10.1016/j.pscychresns.2004.12.001
66. Qiao J, Jin G, Lei L, Wang L, Du Y, Wang X. The positive effects of high-frequency right dorsolateral prefrontal cortex repetitive transcranial magnetic stimulation on memory, correlated with increases in brain metabolites detected by proton magnetic resonance spectroscopy in recently detoxified alcohol-dependent patients. *Neuropsychiatr Dis Treat.* (2016) 12:2273–8. doi: 10.2147/NDT.S106266

Conflict of Interest: The authors declare that the research was conducted in the absence of any commercial or financial relationships that could be construed as a potential conflict of interest.

frontiers | Frontiers in Neurology

ORIGINAL RESEARCH
published: 03 June 2022
doi: 10.3389/fneur.2022.858833

Altered Effective Connectivity of Resting-State Networks by Tai Chi Chuan in Chronic Fatigue Syndrome Patients: A Multivariate Granger Causality Study

Yuanyuan Li[1†], Kang Wu[1†], Xiaojie Hu[2], Tianjiao Xu[1], Zongheng Li[2], Yong Zhang[2] and Kuangshi Li[2*]*

[1] Department of Neurology and Stroke Center, Dongzhimen Hospital, Beijing University of Chinese Medicine, Beijing, China, [2] Department of Rehabilitation, Dongzhimen Hospital, Beijing University of Chinese Medicine, Beijing, China

OPEN ACCESS

Edited by:
Lijun Bai,
Xi'an Jiaotong University, China

Reviewed by:
Changwei Wu,
Taipei Medical University, Taiwan
Hongxiao Jia,
Capital Medical University, China

***Correspondence:**
Yong Zhang
zhangyong_tcm@163.com
Kuangshi Li
likuangshi89@hotmail.com

[†]These authors have contributed equally to this work and share first authorship

Specialty section:
This article was submitted to Applied Neuroimaging, a section of the journal Frontiers in Neurology

Received: *20 January 2022*
Accepted: *05 May 2022*
Published: *03 June 2022*

Citation:
Li Y, Wu K, Hu X, Xu T, Li Z, Zhang Y and Li K (2022) Altered Effective Connectivity of Resting-State Networks by Tai Chi Chuan in Chronic Fatigue Syndrome Patients: A Multivariate Granger Causality Study. Front. Neurol. 13:858833. doi: 10.3389/fneur.2022.858833

Numerous evidence has shown that patients with chronic fatigue syndrome (CFS) have changes in resting brain functional connectivity, but there is no study on the brain network effect of Tai Chi Chuan intervention in CFS. To explore the influence of Tai Chi Chuan exercise on the causal relationship between brain functional networks in patients with CFS, 21 patients with CFS and 19 healthy controls were recruited for resting-state functional magnetic resonance imaging (rs-fMRI) scanning and 36-item Short-Form Health Survey (SF-36) scale assessment before and after 1month-long training in Tai Chi Chuan. We extracted the resting brain networks using the independent component analysis (ICA) method, analyzed the changes of FC in these networks, conducted Granger causality analysis (GCA) on it, and analyzed the correlation between the difference causality value and the SF-36 scale. Compared to the healthy control group, the SF-36 scale scores of patients with CFS were lower at baseline. Meanwhile, the causal relationship between sensorimotor network (SMN) and default mode network (DMN) was weakened. The above abnormalities could be improved by Tai Chi Chuan training for 1 month. In addition, the correlation analyses showed that the causal relationship between SMN and DMN was positively correlated with the scores of Role Physical (RP) and Bodily Pain (BP) in CFS patients, and the change of causal relationship between SMN and DMN before and after training was positively correlated with the change of BP score. The findings suggest that Tai Chi Chuan is helpful to improve the quality of life for patients with CFS. The change of Granger causality between SMN and DMN may be a readout parameter of CFS. Tai Chi Chuan may promote the functional plasticity of brain networks in patients with CFS by regulating the information transmission between them.

Keywords: Tai Chi Chuan, chronic fatigue syndrome, fMRI, resting-state networks, Granger causality analysis

INTRODUCTION

Chronic fatigue syndrome (CFS) is a complex disease with a 0.2 to 2.6% prevalence rate in modern society (1). Patients with CFS usually suffer from continuous fatigue. Besides, the disease is often accompanied by sleep disorder, physical pain, exercise intolerance, cognitive dysfunction, anxiety, and other symptoms, with a consequence of serious physical and mental damage. The study by Schweitzer et al. (2) shows that CFS seriously affects the patients' quality of life, and the social model of disability of CFS patients is comparable to that of the group of stroke patients and advanced cancer patients. Until now, the etiology and pathogenesis of CFS are still unclear, and most researchers identify it today as the result of a multisystem dysfunction (3–5).

In recent years, with the proposal of central sensitization mechanism and the discovery of central nervous system's injury symptoms in CFS (6–10), it has become a new research highlight to explore the changes of brain function in patients by using functional magnetic resonance imaging (fMRI). It has been more recognized that brain dysfunction is one cause of CFS symptoms, especially the abnormality of intrinsic functional connectivity (FC) in resting-state networks (RSNs). These RSNs are composed of structurally separated but functionally connected brain regions (11), which not only play a central role in normal brain functions but also in some brain diseases (12). There are several RSNs observed in the past decades, including default mode network (DMN), sensorimotor network (SMN), left frontoparietal network (LFPN), right frontoparietal network (RFPN), executive control network (ECN), visual network (VN), auditory network (AN), salience network (SN), cerebellum network, and language network, continuously sharing information with each other and associated with the processing of cognition, emotion, action, and so on (13). A study based on DMN showed that DMN in CFS patients was impaired, which was characterized by irregular posterior cingulate cortex (PCC) activity and weakened FC of bilateral inferior parietal lobules (14). Another study (15) demonstrated that, compared to healthy women, FC between DMN and frontal lobe in CFS women decreased, while FC between SN, left temporal lobe area and medulla oblongata increased. Furthermore, the findings of a previous study (16) indicated that the FC of several brain networks in female patients with CFS was impaired, including LFPN, SMN, and SN, among which the impairment of SN showed a decline in FC with PCC. PCC is one of the important nodes of DMN. In brief, while there are a few CFS-related fMRI studies, the results, especially whether the FC of DMN is damaged or not, are still under debate. Moreover, most research focused on the intrinsic FC of a single network and neglected the interaction of extensive RSNs.

In the treatment of CFS, exercise therapy is applied as the most common measure at present (17–19). Nevertheless, given its high cost and unbearable intensity caused by the symptoms such as fatigue and pain, conventional exercise therapy is unavailable for access to clinics (19, 20). New approaches are needed for helping patients to embrace to reduce chronic fatigue and pain, improving their physical and psychological function and quality of life. As an ancient discipline involving exercise, Tai Chi Chuan is a kind of complex, multicomponent mind-body intervention with low and medium intensity, which takes advantage of safety, low cost, and is widely applicable (21), as well as provides therapeutic benefits involving improving quality of life, physical function, pain management, balance and risk of falls reduction, enhancing immune response, and improving flexibility, strength, and kinesthetic sense (22). In addition, it is reported that the Tai Chi Chuan group had a higher continuance rate at the end of the intervention and a lower drop-out rate for the ongoing class than the conventional exercise group (23). A meta-analysis (24) has also proved that Tai Chi Chuan is more beneficial in relieving fatigue than conventional treatment and low-impact exercise control. The symptoms mentioned earlier that can be alleviated by Tai Ji Chuan such as fatigue, pain, dyskinesia, and so on, are related to CFS. Other encouraging evidence (25, 26) has revealed that Tai Chi Chuan can alleviate fibromyalgia (FM) more effectively than aerobic exercise, whose symptoms are extremely similar to CFS. Some researchers believe that FM and CFS share the same pathophysiological mechanism (27–29). Thus, in our hypothesis, it might also contribute to relieving the symptoms of CFS and become an effective alternative therapy for CFS.

Positively, what can support our hypothesis are the research with fMRI revealing that Tai Chi Chuan promotes the plasticity of brain function. Brain plasticity refers to the ability to change brain structure and function under the influence of the environment (30). More evidence (31, 32) confirmed that Tai Chi Chuan had a stronger ability to remodel brain function than general aerobic exercise, which was mainly reflected in the enhancement of FC between the left middle frontal gyrus and left parietal lobe. By comparing the effects of long-term Tai Chi Chuan training and long-term walking training on the brain networks of elderly women, another work (33) found that these two kinds of exercise modes could enhance the FC of DMN, SMN, and visual network (VN) with different promotion forms. Therefore, Tai Chi Chuan has some effect on improving brain function, which requires more longitudinal studies to prove.

As mentioned earlier, there are many abnormal intrinsic FCs of RSNs in CFS patients, but there is no research studying the interaction between them. A study about Tai Chi Chuan intervention in CFS is needed accordingly. Furthermore, to move beyond the identification of regional activations toward the characterization of functional circuits is a key challenge in neuroscience. Therefore, Granger causality analysis (GCA), as a powerful method to achieve this, can not only evaluate the FC of brain networks but also examine abnormal relationships among RSNs in psychiatric patients to better understand the neurobiological basis of the disorders (34–37). In this study, we will take advantage of fMRI and GCA to study the interaction between CFS patients and healthy human brain networks. By introducing Tai Chi Chuan as an effective therapy, we would expect an improvement of the symptoms in CFS patients and its promotion of the plasticity in RSNs.

MATERIALS AND METHODS

Participants

In this study, 21 CFS patients (experimental group, 6 males and 15 females, average age 37.47 ± 12.14) and 19 healthy subjects (healthy control group, 7 males and 12 females, average age 33.31 ± 12.46) were recruited from Dongzhimen Hospital, Beijing University of Chinese Medicine. They were all right-handed, aged 25 to 65, with no previous practice history of Tai Chi Chuan and no difficulty answering and filling out the questionnaire. They had not taken psychotropic drugs for nearly a month, with no metal in the body and no contraindications for MRI examination. The experimental group met the following inclusion criteria: diagnosed as CFS of the 1994 Center for Disease Control and Prevention Case Definition (38); the course of CFS for more than 6 months; and with chronic fatigue that cannot be explained by other current diseases or drug side effects. We excluded those with major diseases, current or past psychiatric disorders, severe obesity (body mass index > 45), and any brain structure damage or abnormalities identified by MRI examinations. What's more, patients who had taken vasodilators in the past 2 weeks, who had participated in similar neuroimaging experiments within 1 month, and women who were pregnant, lactating, or menstruating were also excluded. Signed informed consent was obtained from all participants. This study was approved by the Medical Ethics Committee of Dongzhimen Hospital of Beijing University of Chinese Medicine (DZMEC-KY-2019-195).

Health-Related Quality of Life Evaluation

The 36-item Short-Form Health Survey (SF-36) was used to evaluate the health-related quality of life (HRQoL) of all subjects, which was regarded as the main index. All subjects made a self-report with an SF-36 scale before and after training in Tai Chi Chuan. This study adopted the Chinese version translated in 1991 by the Department of Social Medicine, Zhejiang University Medical College. The scale consists of eight subscales, namely Physical Functioning (PF), Role Physical (RP), Bodily Pain (BP), General Health (GH), Vitality (VT), Social Functioning (SF), Role Emotional (RE), and Mental Health (MH). The score ranges from 0 to 100. The higher the score, the better the HRQoL.

MRI Scanning

Before and after training in Tai Chi Chuan, all the subjects underwent an MRI scanning in Dongzhimen Hospital of Beijing University of Chinese Medicine with a MAGNETOM Prisma magnetic resonance scanner (Siemens, Germany). Before the scan, the patients were told in detail about the scanning time, scanning purpose, and precautions. After getting used to the indoor environment of MRI, they were told to rest on their backs for 30 min and wait until the participants were completely calm before starting scanning. Safety indicators (blood pressure, respiratory rate, heart rate, etc.) were monitored before and after each scan to evaluate the safety of the test process.

The two MRI scans adopted the same scanning sequence. The participants lay flat for 30 min to maintain complete calm. Then, they were required to stay still, think of nothing, keep eyes closed and refrain from falling asleep during scanning. In the process, earplugs were worn for noise isolation and the foam head holders were immobilized to minimize head movements. After that, the T1 structure image which is for 4 min and 10 s and the DTI image which is for 5 min and 10 s were continued.

Scanning parameters: fMRI was applied with echo-planar imaging (EPI) sequence: Repetition time (TR), 2000 ms; Echo time (TE), 30 ms; Matrix, 64 × 64; Field of view (Fov), 225 × 225 mm; Slice thickness, 3.5 mm; Gap, 0.7 mm; Phase encode direction, A>>P; Flip Angle, 90°; Fat suppr, Fat sat. The three-dimensional structure imaging scan of the whole brain was scanned using T1W1 sequence: TR, 1900 ms; TE, 2.53 ms; Fov, 250 × 250 mm; Matrix, 256 × 256; Slice thickness, 1.0 mm.

Tai Chi Chuan Training Program

To eliminate the influence of different training durations and frequencies, the training time of Tai Chi Chuan in the experimental group and the healthy control group were designed in the same way. Both the experimental group and the healthy control group were given Tai Chi Chuan training twice a week for 1 h each time. The whole process was under the guidance of therapists, with the exercise learning and repeated posture control training. The course of treatment was 4 weeks, with eight training courses in total. For the rest of the time, each participant was asked to practice Tai Chi Chuan for 30 min every day. Training Tai Chi Chuan standard movements referred to the 24-style simplified version of the General Administration of Sport of China and the Tai Chi Chuan's standard movements in Chinese Traditional Health Care Sports and Health Preservation, national teaching materials for colleges and universities citation. We selected three experienced Tai Chi Chuan coaches for systematic training, and let them know the intervention methods of Tai Chi Chuan and the basic knowledge of related diseases. During the experiment, Tai Chi Chuan's teaching was recorded to ensure the practice quality. After each training, the participants were reminded to carry out family Tai Chi Chuan exercises, video feedback of each exercise, and telephone follow-up supervision training during the research process.

Data Processing

All data processing was completed by DPABI (http://rfmri.org/dpabi) (39).

Anatomical Data Preprocessing

The T1 images were converted into the BIDS dataset. Then, they were corrected for intensity non-uniformity with N4BiasFieldCorrection (40), which was provided by Advanced Normalization Tools (ANTs) 2.3.3. The derived images were skull-stripped with OASIS30ANTs as the target template. The remaining brain tissues were segmented into the cerebrospinal fluid (CSF), white matter (WM), and gray matter (GM) by the BET (FSL 5.0.9). Brain surfaces were reconstructed using recon-all (FreeSurfer 6.0.1). A classic method, which reconciles ANTs-derived and FreeSurfer-derived segmentation of the cortical gray matter of Mindboggle (41), was applied for refining the brain mask estimated previously. Volume-based spatial normalization to one standard space (Montreal Neurological Institute, MNI) was performed through nonlinear

registration with antsRegistration (ANTs 2.3.3), using brain-extracted versions of both T1 reference and the T1 template. Meanwhile, ICBM 152 Nonlinear Asymmetrical template version 2009c was selected for spatial normalization.

Functional Data Preprocessing

First, the custom methodology of fMRIPrep (42) was used to generate the reference volume and its skull-stripped version. Susceptibility distortion correction (SDC) was omitted. Bbregister (FreeSurfer), which implements boundary-based registration, was applied for co-registering the fMRI reference and T1 reference. Moreover, slice-time was corrected using 3dTshift from AFNI and spatiotemporal filtering was conducted by mcflirt (FSL). The BOLD time series were resampled into standard space and generated a preprocessed BOLD run in MNI space. At the same time, framewise displacement (FD), DVARS, and three region-wise global signals were calculated by the preprocessed BOLD. In addition, a set of physiological regressors were extracted to allow for the component-based noise correction (CompCor). Above components were dropped from the BOLD, and frames that exceeded a threshold of 0.5 mm FD or 1.5 standardized DVARS were annotated as motion outliers. Gridded (volumetric) resampling was performed using antsApplyTransforms (ANTs), configured with Lanczos interpolation to minimize the smoothing effects of other kernels. Non-gridded (surface) resampling was performed using mri_vol2surf (FreeSurfer).

RSNs Extraction

Independent component analysis was applied to extract the RSNs by GIFT software (University of New Mexico, Albuquerque, NM). The number of independent components in all data was calculated by the method of the minimum description length (MDL) technique. Randlnit and Bootstrap operations were applied to evaluate the independent components. Then, we selected the brain networks by combining the manual selection, goodness-of-fit method (43), and the evidence which was observed in previous literature. Meanwhile, the relationship between CFS symptoms and brain network functions was also a factor to be considered. We selected six specific networks including executive control network (ECN), visual network (VN), sensory motor network (SMN), right frontoparietal network (RFPN), default mode network (DMN), and salience network (SN).

Network Analysis

To analyze the changes of FC in these six brain networks before and after Tai Chi Chuan, the images of components were normalized to Z-scores with Fisher's r-to-z transformation for acquiring the entire brain Z-score map of each subject. Meanwhile, a repeated measures model, including condition effect and interaction effect, was used to investigate the Tai Chi Chuan-induced changes in the six brain networks. The significant thresholds were set as 0.005 and family-wise error (FWE) correction for multiple comparisons at $p = 0.05$ at the cluster level was applied.

TABLE 1 | Comparison of sex, age, and BMI between the experimental group and the healthy control group.

Group	Experimental group ($N = 21$)	Healthy control group ($N = 19$)	*P*-value
Male/Female	6/15	7/12	0.557
Age ($\bar{x} \pm s$)	37.47 ± 12.14	33.31 ± 12.46	0.29
BMI ($\bar{x} \pm s$)	21.88 ± 3.49	22.98 ± 2.83	0.75

Network Granger Analysis

All the selected components were filtered between 0.01 and 0.1 Hz for multivariate Granger causal modal to explore the characteristics of networks. Meanwhile, we used the generalized partial directed coherence (GPDC) as the measured parameter (44). The method of the Akaike information criterion was applied for determining the order of Granger causality analysis. Then, comparisons between groups were done on the causal interaction of six components. We also conducted a one-sample *t*-test in each component to compute the single network imaging. An independent *t*-test was used for comparison between groups and a paired *t*-test was used for intragroup comparison. The *P*-value of the *t*-test was set as 0.05 which was corrected by the false discovery rate (FDR) for multiple comparisons. Finally, BrainNetViewer was used to display the result onto a 3D brain surface.

Correlation Analysis

Compared to the healthy subjects, there was a significant decrease in the causal relationship between SMN and DMN in CFS patients. However, after 1 month-long training in Tai Chi Chuan, the causal relationship between SMN and DMN in CFS patients was enhanced. Given the relevance of SMN and DMN to sensorimotor function, which could be best reflected by RP and BP scores, we conducted a correlation analysis between the mean Granger causality value of SMN-DMN and RP and BP scores in CFS patients. Statistical analyses were conducted using SPSS 20.0, and the threshold was set at $P < 0.05$.

RESULTS

Demographic and Clinical Information

In this study, 21 CFS patients (experimental group) and 19 healthy people (healthy control group) were recruited from Dongzhimen Hospital of Beijing University of Chinese Medicine. There were 6 males and 15 females in the experimental group, with an average age of 37.47 ± 12.14 years and an average body mass index (BMI) of 21.88 ± 3.49. The healthy control group consisted of 7 males and 12 females, with an average age of 33.31 ± 12.46 years and an average BMI of 22.98 ± 2.83. There is no statistical difference in sex, age, and BMI between the two groups. Refer to **Table 1** for details.

By observing the scores on SF-36 scale, we found that at baseline, the scores of PF, RP, BP, GH, VT, SF, and RE in the experimental group were significantly lower than those in the healthy control group ($P < 0.05$), while there was no significant

TABLE 2 | Comparison of SF-36 scores between the experimental group and the healthy control group before and after Tai Chi Chuan exercise.

SF-36	Experimental group ($N = 21$) (Mean ± SD)		Healthy control group ($N = 19$) (Mean ± SD)	
	Before	After	Before	After
MH	64.38 ± 16.39	73.52 ± 13.71$^{\#}$	72.63 ± 16.24	75.36 ± 16.18
VT	58.09 ± 16.99*	75.00 ± 15.08$^{\#}$	74.21 ± 14.83	77.89 ± 16.69
PF	85.47 ± 12.64$^{*▲}$	93.33 ± 8.42$^{\#▲}$	95.79 ± 3.82	97.11 ± 7.13
RP	30.95 ± 37.00$^{*▲}$	83.33 ± 28.87$^{\#▲}$	88.16 ± 15.29	93.42 ± 18.33
BP	59.71 ± 14.39$^{*▲}$	68.05 ± 15.16$^{\#▲}$	84.47 ± 21.69	84.00 ± 22.76
GH	45.76 ± 21.52$^{*▲}$	65.61 ± 19.39$^{\#}$	70.84 ± 21.17	79.15 ± 16.87
SF	71.95 ± 18.45$^{*▲}$	82.54 ± 15.14$^{\#}$	89.25 ± 16.37	90.01 ± 15.42
RE	36.50 ± 42.03$^{*▲}$	79.37 ± 30.69$^{\#▲}$	73.68 ± 37.80	91.23 ± 21.78

*The scores of PF, RP, BP, and RE in experimental group and the scores of PF, RP, BP, GH, SF, and RE in healthy control group are all non-normal distribution. The * represents P (experimental group–healthy control group) <0.05 before Tai Chi Chuan. The # represents P (after–before) <0.05 in experimental group. The ▲ represents using non-parametric tests based on data distribution.*

difference in the scores of MH between the two groups ($P > 0.05$). After 1month-long training in Tai Chi Chuan, the scores of PF, RP, BP, GH, VT, MH, SF, and RE in SF-36 in the experimental group were significantly higher than those before the training ($P < 0.05$). There was no obvious change in the SF-36 scale score of the healthy control group after practicing Tai Chi Chuan ($P > 0.05$). Refer to **Table 2** for details.

The RSNs

The magnetic resonance data of all participants were analyzed with independent component analysis (ICA). Six resting brain networks were selected, namely executive control network (ECN), VN, SMN, DMN, SN, and RFPN (**Figure 1A**). The specific location distribution information of these six networks is shown in the **Supplementary Information**. For all of the participants, the FC of several brain regions enhanced including the left inferior parietal cortex and posterior cingulate cortex in DMN, the left anterior cingulate/medial prefrontal cortex, inferior parietal cortex, and lateral temporal cortex in RFPN, and the bilateral paracentral lobular/mid-cingulate cortex in SMN and the FC of several brain regions weakened including the right inferior parietal cortex in RFPN and the bilateral somatosensory/motor cortex in SMN after Tai Chi Chuan (**Figure 1B** and Condition Effect in **Table 3**). Comparing the enhancement degree of FC in CFS patients with that in healthy controls after and before Tai Chi Chuan, the bilateral posterior opercular cortex in SN and the bilateral cuneus in VN were enhanced better while the left lateral temporal cortex and inferior parietal cortex RFPN and the bilateral superior temporal gyrus in SN were enhanced worse (**Figure 1C** and Interaction Effect in **Table 3**).

GCA Results

GCA indicated that the brain networks of patients with CFS showed different functional connection modes compared with healthy subjects.

As shown in **Figure 2**, in the baseline state, the healthy subjects showed six significant functional relationships, including the causal relationship between SMN and DMN, SMN and RFPN, SMN and ECN, SN and DMN, SN and VN, and RFPN and VN. Among them, SMN and SN were the main output information networks, while DMN and VN were the main input information networks. RFPN was a relay station where information flowed from SMN to VN. On the other hand, there were fewer causal relationships between brain networks of CFS patients, which were mainly manifested in the information exchange among ECN, RFPN, and VN. Meanwhile, the information transmissions of SN to DMN and SN to VN were interrupted, so that SN is isolated from other brain networks. Although the causal relationship between SMN-DMN and RFPN-VN still existed, the frequency of occurrence of them greatly decreased. Compared with healthy subjects, the causal relationship between SMN and DMN in CFS patients was significantly different ($P < 0.05$, False Discovery Rate Correction), which was mainly manifested in the weakening of the effective connection between SMN and DMN.

For healthy subjects, after 1 month of Tai Chi Chuan training, VN became the network with the most output information. The information transmission modes in the baseline state of SMN-ECN and SMN-RFPN were changed to SMN-VN-ECN and SMN-VN-RFPN, both used VN as a relay station. Interestingly, the causal relationship between RFPN and VN was reversed compared to the baseline state. However, before and after Tai Chi Chuan training, healthy subjects did not show such a significant difference in the causal relationship of brain networks (**Figure 3**).

However, for the patients with CFS, after training in Tai Chi Chuan, the information flow between brain networks was more abundant. Among them, SMN and RFPN became core networks outputting the most information, while DMN received the most information. In addition, it is not difficult to find the causal relationships among SMN-VN-RFPN, which realized the circulation of information. Although the connections between ECN-RFPN and ECN-VN were interrupted, the causality between SN and ECN is established. It is worth noting that, similar to healthy subjects, CFS patients also experienced the reversal of the causal relationship between RFPN and VN after training. Compared with before training, the effective connections of CFS patients from SMN to DMN and VN to RFPN were significantly enhanced after training ($P < 0.05$, False Discovery Rate Correction) (**Figure 4**).

Correlations

The results showed that the mean causal value of SMN-DMN was positively correlated with the scores of RP and BP (**Figures 5A,B**). Besides, the correlation analysis between SMN-DMN Granger causality value difference and RP difference before and after training showed that there was a significant positive correlation between them (**Figure 5C**).

DISCUSSION

Tai Chi Chuan was introduced as an exercise therapy, which has been proved to have the ability to promote brain plasticity (45). Accordingly, to explore the central mechanism of Tai Chi Chuan

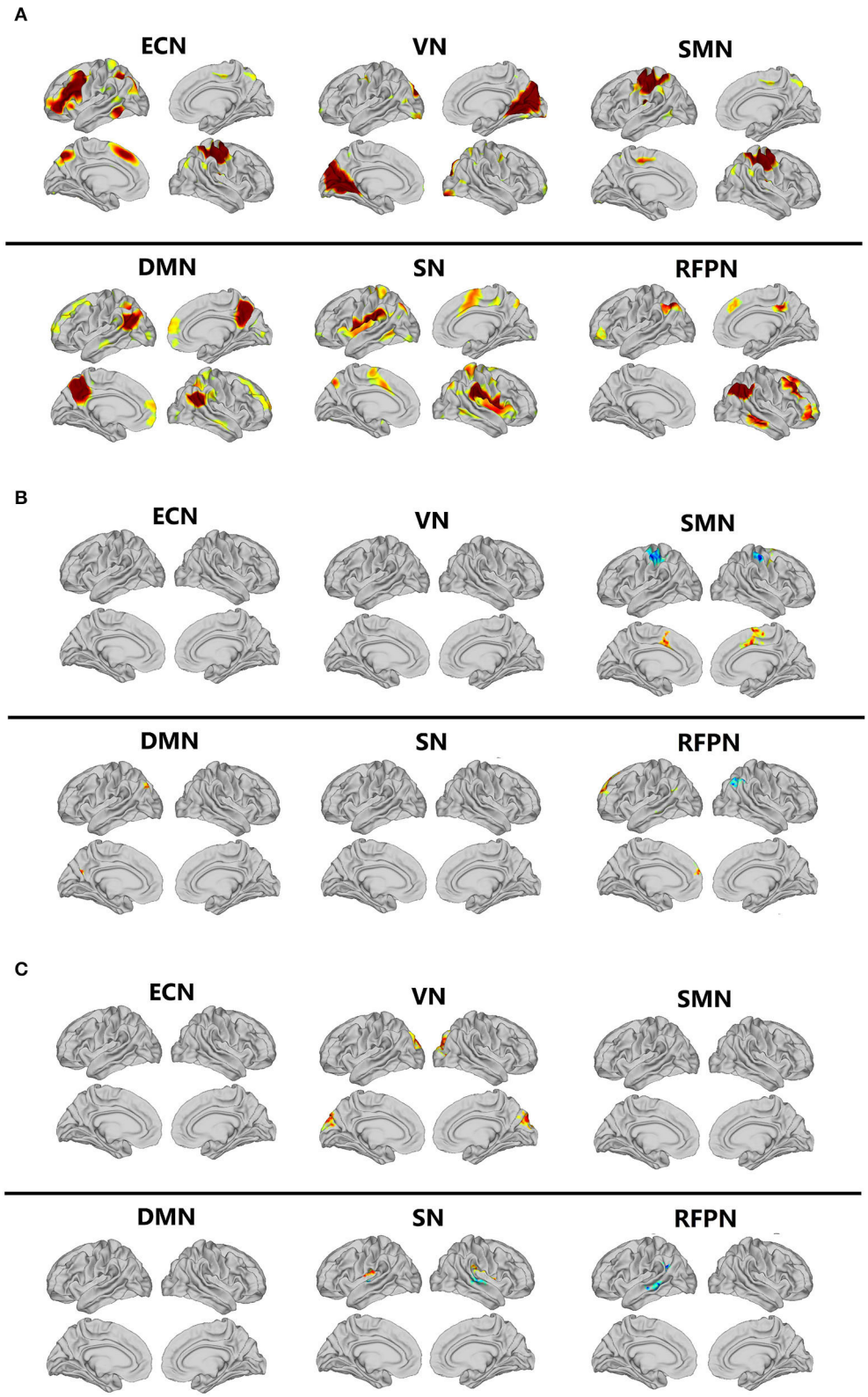

FIGURE 1 | Comparison of resting-state networks. DMN, default mode network; ECN, executive control network; ICA, independent component analysis; RFPN, right frontoparietal network; RSNs, resting-state networks; SMN, sensorimotor network; SN, salience network; VN, visual network. **(A)** The resting-state networks extracted by ICA. **(B)** Comparison of condition effect after and before Tai Chi Chuan in all participants. **(C)** Comparison of interaction effect after and before Tai Chi Chuan in CFS patients and healthy controls.

TABLE 3 | The changes of FC in RSNs before and fter Tai Chi Chuan.

Brain region	Side	MNI coordinates			t value	Area (mm^2)
		X	Y	Z		
Default mode network–condition effect: After Tai Chi > Baseline						
Inferior parietal cortex	L	−9	−65	22	4.58	128
Posterior cingulate cortex	L	−32	−79	38	4.82	120
Right frontoparietal network–condition effect: After Tai Chi > Baseline						
Anterior cingulate/ Medial prefrontal cortex	L	−12	56	24	6.43	831
Inferior parietal cortex	L	−32	−79	38	5.52	182
Lateral temporal cortex	L	−52	−26	−12	5.66	191
Right frontoparietal network–condition effect: After Tai Chi < Baseline						
Inferior parietal cortex	R	46	−52	44	−6.52	613
Sensorimotor network–condition effect: After Tai Chi > Baseline						
Paracentral lobular/ Mid cingulate cortex	L	−10	4	44	7.28	195
Paracentral lobular/ Mid cingulate cortex	R	7	−3	63	8.43	1,210
Sensorimotor network–condition effect: After Tai Chi < Baseline						
Somatosensory/Motor cortex	L	−45	−20	55	−7.12	1,867
Somatosensory/Motor cortex	R	46	−4	50	−6.32	179
Right frontoparietal network–interaction effect: CFS $_{afterTaiChi}$-CFS $_{Baseline}$ <HC $_{afterTaiChi}$-HC $_{Baseline}$						
Lateral temporal cortex	L	−51	−41	−2	−6.26	506
Inferior parietal cortex	L	−48	−54	23	−6.52	244
Salience network– interaction effect: CFS $_{afterTaiChi}$-CFS $_{Baseline}$ >HC $_{afterTaiChi}$-HC $_{Baseline}$						
Posterior opercular cortex	L	−35	−19	20	6.37	427
Posterior opercular cortex	R	42	−1	16	6.37	733
Salience network– interaction effect: CFS $_{afterTaiChi}$-CFS $_{Baseline}$ <HC $_{afterTaiChi}$-HC $_{Baseline}$						
Superior temporal gyrus	L	−55	−20	0	−5.37	176
Superior temporal gyrus	R	64	−31	11	−7.19	462
Visual network– interaction effect: CFS $_{afterTaiChi}$-CFS $_{Baseline}$ >HC $_{afterTaiChi}$-HC $_{Baseline}$						
Cuneus	L	−10	−85	33	6.24	742
Cuneus	R	7	−86	31	5.42	984

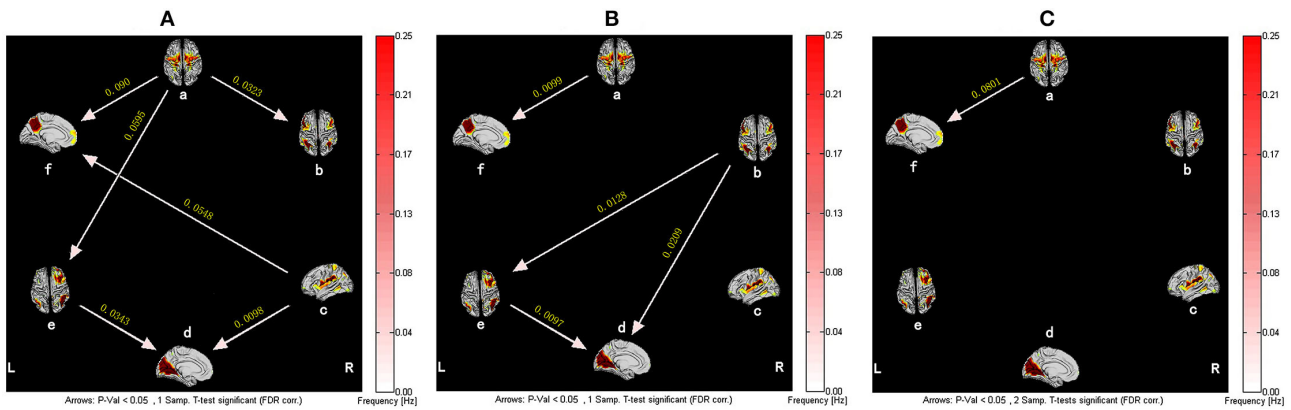

FIGURE 2 | The resting-state effective connectivity comparison between CFS patients and healthy controls. There are six resting-state networks, including: a, SMN; b, ECN; c, SN; d, VN; e, RFPN; f, DMN. Arrow directions represent causal effect between resting-state networks. Yellow numbers indicate strength of causality. Values on the color bar (corresponding with arrow colors) demonstrate frequency at which causality was found. **(A)** One-sample *t*-test result of intergroup intranetwork causal relationship of the healthy controls. **(B)** One-sample *t*-test result of intergroup intranetwork causal relationship of the CFS patients. **(C)** Two-sample *t*-test result of intergroup intranetwork causal relationship of the healthy controls minus the CFS patients.

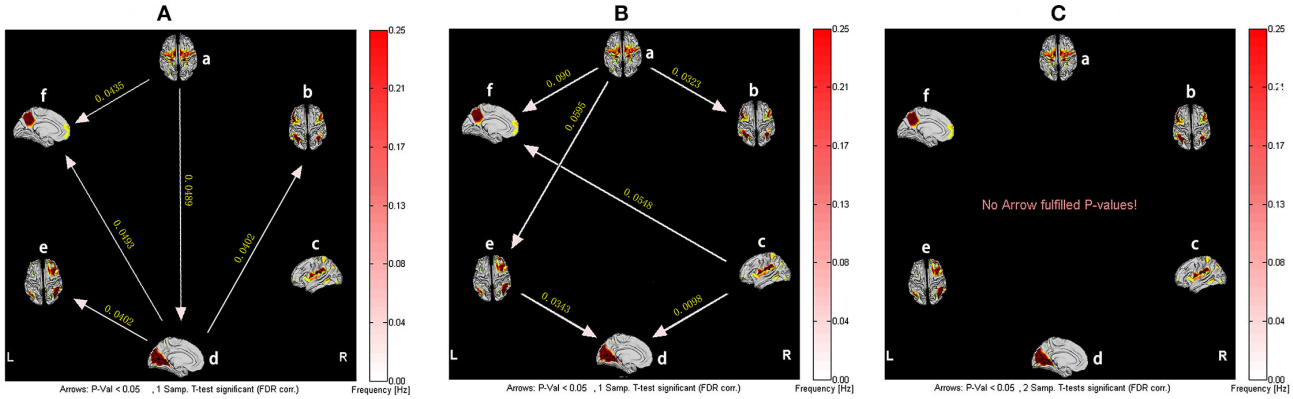

FIGURE 3 | The resting-state effective connectivity comparison of healthy subjects before and after Tai Chi Chuan training. There are six resting-state networks, including: a, SMN; b, ECN; c, SN; d, VN; e, RFPN; f, DMN. Arrow directions represent causal effect between resting-state networks. Yellow numbers indicate strength of causality. Values on the color bar (corresponding with arrow colors) demonstrate frequency at which causality was found. **(A)** One-sample *t*-test result of intergroup intranetwork causal relationship of the healthy controls after Tai Chi Chuan training. **(B)** One-sample *t*-test result of intergroup intranetwork causal relationship of the healthy controls before Tai Chi Chuan training. **(C)** Paired *t*-test result of intragroup intranetwork causal relationship of after Tai Chi Chuan training minus before Tai Chi Chuan training for healthy controls.

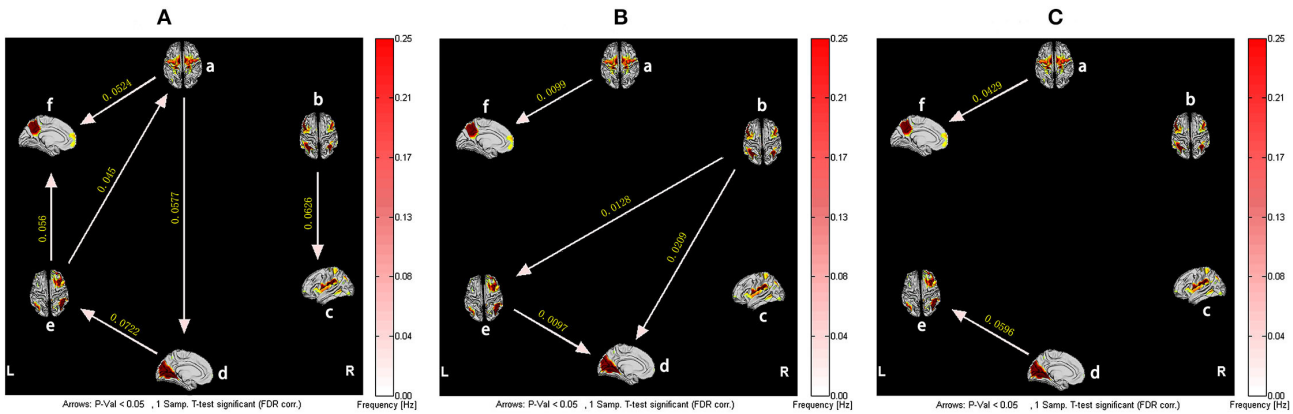

FIGURE 4 | The resting-state effective connectivity comparison of CFS patients before and after Tai Chi Chuan training. There are six resting-state networks, including: a, SMN; b, ECN; c, SN; d, VN; e, RFPN; f, DMN. Arrow directions represent causal effect between resting-state networks. Yellow numbers indicate strength of causality. Values on the color bar (corresponding with arrow colors) demonstrate frequency at which causality was found. **(A)** One-sample *t*-test result of intergroup intranetwork causal relationship of the CFS patients after Tai Chi Chuan training. **(B)** One-sample *t*-test result of intergroup intranetwork causal relationship of the CFS patients before Tai Chi Chuan training. **(C)** Paired *t*-test result of intragroup intranetwork causal relationship of after Tai Chi Chuan training minus before Tai Chi Chuan training for CFS patients.

in improving CFS, its role in promoting the plasticity of CFS patients' brain function networks was investigated for the first time in our study. Our data indicated that, compared with healthy people, patients with CFS had lower HRQoL and weaker Granger causality between RSNs. Tai Chi Chuan training could just adjust these differences, especially the information flow between SMN and DMN.

In our results, the SF-36 scale score of patients was significantly lower than that of healthy controls, which is consistent with the previous results (46, 47), indicating that the HRQoL of CFS patients has been seriously affected. However, after training in Tai Chi Chuan, the SF-36 score of CFS patients had been significantly improved compared with the baseline state, which supports the notion that Tai Chi Chuan has an obvious effect in improving HRQoL of CFS patients.

CFS, as a complex disorder composed of various symptoms, is related to many brain functions such as sensory, motor, and cognition. Our results showed a change in the effective connection between SMN and DMN in CFS patients compared with the healthy control group, which was in line with previous studies (14–16). The anterior central gyrus, posterior central gyrus, and auxiliary motor areas are the core areas of SMN, which are related to somatosensory and motor functions. Previous structural and functional MRI studies have illustrated the abnormalities of SMN. For instance, others have verified the increase in thickness of anterior central gyrus cortex in

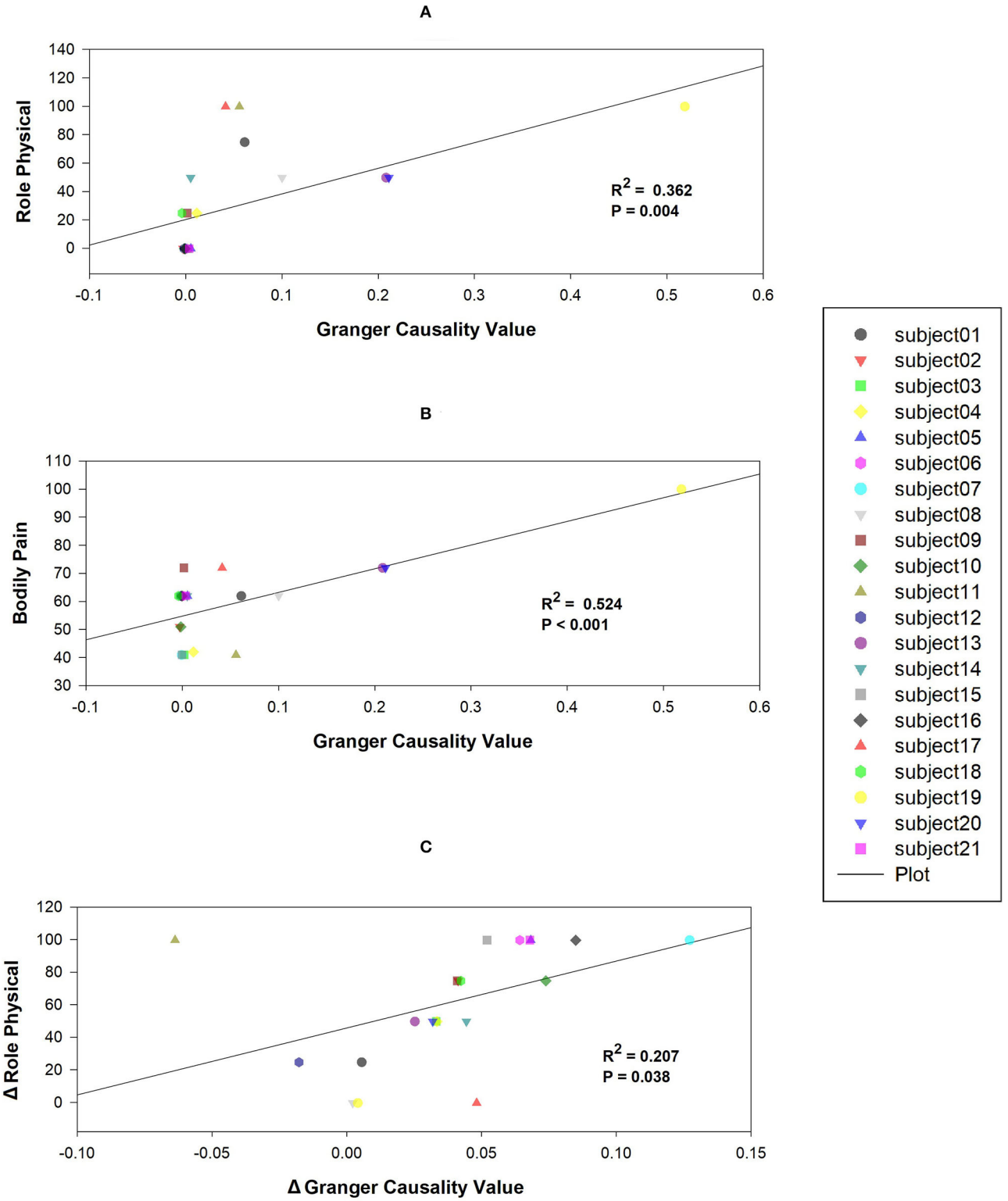

FIGURE 5 | Correlations between mean Granger causality values within abnormal casual connectivity and the scores of Role Physical and Bodily Pain. **(A)** The mean Granger causality values from SMN to DMN were positively associated with the score of Role Physical ($R^2 = 0.362$, $P = 0.004$). **(B)** The mean Granger causality values from SMN to DMN were positively associated with the score of Bodily Pain ($R^2 = 0.524$, $P < 0.001$). **(C)** The mean Granger causality difference from SMN to DMN was positively associated with the score of Role Physical difference ($R^2 = 0.207$, $P = 0.038$).

CFS patients (48). It was also established that the FC between the left anterior middle cingulate gyrus and SMN decreased in CFS patients (16). Another fMRI study (49) based on arterial spin labeling (ASL) showed that the FC between the parahippocampal gyrus, right anterior central gyrus, and the left posterior central gyrus in CFS patients was weakened. DMN plays an indispensable role in the study of resting brain networks. It is activated when the brain does not receive any stimulation or tasks, but weakened when it receives stimulation or tasks. Also, the degree of negative activation of DMN increases with the increase of task difficulty (50). DMN plays a vital role in spontaneous introspection (51) as well as advanced cognitive function (52). From the aspect of brain structures, anterior cuneiform lobe and PCC are important areas, which are related to information transmission and sensory information integration (53). The irregular activity of PCC in CFS patients observed in the past (14) may be an important reason for influencing the information transmission in DMN. This abnormal information transmission between SMN and DMN leads to the obstacle of integration of body movement and sensory information, and finally gives rise to two obvious manifestations of CFS, namely body pain and exercise intolerance. Apart from this, the correlation analysis also showed that the causal relationship between SMN and DMN was positively correlated with the RP and BP scores of SF-36 scale. Thus, the stronger the effective connection between the two networks, the stronger the physiological and somatosensory functions of patients. Hence, we suggest that the reduction of information integration between DMN and SMN may be the core mechanism of CFS.

Gratifyingly, after a month of training in Tai Chi Chuan, the SF-36 scale reflected the improvement of HRQoL of CFS patients, and the information transmission between SMN and DMN was stronger than before. Correlation analysis also showed that the change of effective connection strength between SMN and DMN had a positive correlation with the change in physiological function. A similar effect of Tai Chi Chuan has been described in another neuroimaging study (54) in which the FC between DMN and SMN was weak before rehabilitation therapy for stroke patients but enhanced after rehabilitation therapy, and the interaction between the two networks was positively correlated with motor function. In our results, it was the FC of the left inferior parietal cortex and PCC in DMN that was enhanced after Tai Chi Chuan. Therein, the inferior parietal cortex makes a critical contribution to spatial processing and cognition especially attention processing (55, 56), and PCC has a pivotal role in conscious awareness and is inactivated with painful stimulation (57). Other scholars also confirmed that Tai Chi Chuan was conducive to the functional consistency in the posterior central gyrus belonging to the SMN of employees (58), which is different from ours. What we have found is the enhanced FC of the bilateral paracentral lobular/mid-cingulate cortex and the weakened FC of the bilateral somatosensory/motor cortex in SMN. Therein, the mid-cingulate cortex is considered to be helpful to exert attentional control (59), and the interaction between somatosensory and motor cortex realized sensory processing and movement control (60, 61). These dissimilarities may own to the difference of the participants included. Taken together, Tai Chi Chuan promoted the plasticity of brain function by regulating the causal relationship between brain networks. Since there are pretty rare studies about the effect of Tai Chi Chuan in CFS, our results need to be verified by more research.

Remarkably, the reversed and strengthened causal relationship between RFPN and VN in CFS patients who often suffer from cognitive disorders (62–66) was also uncovered in our observations. In like manner, another longitudinal study (21) also found that Tai Chi Chuan changed the FC of the dorsolateral prefrontal cortex, which is a key area of both the cognitive control network and frontoparietal network (FPN). Our results, by contrast, showed the enhanced FC of the left anterior cingulate/medial prefrontal cortex, inferior parietal cortex, and lateral temporal cortex and the weakened FC of the right inferior parietal cortex in RFPN. These dissimilarities may be caused by the participants we included being CFS patients and healthy people, rather than the elderly. The information transmission between FPN and VN is closely related to cognitive function, especially the attention to visual space (67, 68). Among them, FPN plays a vital role in spatial attention and motion control, such as target-oriented hand and eye movement (69), which are exactly what the Tai Chi Chuan exercise requires. What's more, as shown in **Table 3**, enhancing the FC of the bilateral cuneus in VN by Tai Chi Chuan was more effective in CFS patients, related to visual information processing and visuomotor planning (70). Consequently, we speculate that the change in the causal relationship between RFPN and VN is the neural basis for Tai Chi Chuan to improve the cognitive function of CFS patients, especially visual-spatial attention.

There are still a few inconsistencies compared with previous studies (71–73). A prior study revealed that the FC of DMN is enhanced in female CFS patients (71). Whereas, further study (73) did not show any significant FC change of DMN in CFS adolescent patients compared with healthy controls. Differently, only significant FC change of SN in adolescent patients was found in another study (72). These inconsistencies may be due to different subjects and diagnostic criteria. Studies have proved that teenagers' brain networks are constantly changing (74), and a large-scale cross-sectional study (75) has also proved that there are differences in functional connections between male and female brain networks. Here, we mainly applied male and female gender in the age of 25 to 65 years, which would raise a significant difference to the only-female group. Moreover, different diagnostic standards, heterogeneity of population, and brain function analyses unavoidably contribute to the differences in these studies.

There are also several limitations in our research. First, the sample size is relatively small. Only 21 patients and 19 healthy people were included in our study. Second, the changes in RSNs related to cognitive function were found, but the indicators related to cognitive function were lacking. Third, GCA may not distinguish the direct causality caused by the action of the intermediate network, introducing a limited result in the brain analysis. Fourth, performing a double-blind trial on physiotherapy interventions is impossible, so there might be placebo effects. Last but not least, there's no similar large sample study before for us to refer to, and the results need to be repeated.

Future research should increase the sample size, improve the analysis method, supplement the correlation analysis between the changes in brain networks and the improvement of cognition function, and compare the effect of conventional exercise therapy with Tai Chi Chuan.

CONCLUSION

In conclusion, we recruited patients with CFS and healthy controls for fMRI scanning before and after 1-month-long training in Tai Chi Chuan. ICA and GCA were used to extract the RSNs and the changes of FC in these networks were also analyzed. Compared to the healthy control group, the causal relationship between SMN and DMN was weakened, which could be improved by Tai Chi Chuan. The findings suggest that the change of Granger causality between SMN and DMN may be a readout parameter of CFS. Tai Chi Chuan may promote the functional plasticity of brain networks in patients with CFS by regulating the information transmission between RSNs.

DATA AVAILABILITY STATEMENT

The original contributions presented in the study are included in the article/**Supplementary Material**, further inquiries can be directed to the corresponding authors.

ETHICS STATEMENT

The study involving human participants was reviewed and approved by Medical Ethics Committee of Dongzhimen Hospital of Beijing University of Chinese Medicine. The patients/participants provided their written informed consent to participate in this study.

AUTHOR CONTRIBUTIONS

KL and YZ: conceptualization, methodology, and formal analysis. YL, KW, XH, and TX: data collection and research performance. YL and KW: writing the original draft. KL: revising the original draft. YZ and ZL: research supervision. All authors contributed to the article and approved the submitted version.

FUNDING

This study was supported by the National Natural Science Foundation (Grant No. 82004437) and the Beijing Natural Science Foundation (Grant No. 7204277).

ACKNOWLEDGMENTS

We gratefully acknowledge the MRI room of Dongzhimen Hospital for providing us with scanning technical support and the rehabilitation department for providing us with training ground.

SUPPLEMENTARY MATERIAL

The Supplementary Material for this article can be found online at: https://www.frontiersin.org/articles/10.3389/fneur.2022.858833/full#supplementary-material

REFERENCES

1. Prins JB, van der Meer JWM, Bleijenberg G. Chronic fatigue syndrome. *Lancet.* (2006) 367:346–55. doi: 10.1016/S0140-6736(06)68073-2
2. Schweitzer R, Kelly B, Foran A, Terry D, Whiting J. Quality of life in chronic fatigue syndrome. *Soc Sci Med.* (1995) 41:1367–72. doi: 10.1016/0277-9536(95)00124-P
3. Fernández AA, Martín ÁP, Martínez MI, Bustillo MA, Hernández FJB, de la Cruz Labrado J, et al. Chronic fatigue syndrome: aetiology, diagnosis and treatment. *BMC psychiatry.* (2009) 9:1–11. doi: 10.1186/1471-244X-9-S1-S1
4. Kim S, Chang L. Overlap between functional GI disorders and other functional syndromes: what are the underlying mechanisms? *Neurogastroenterol Motil.* (2012) 24:895–913. doi: 10.1111/j.1365-2982.2012.01993.x
5. Deumer U-S, Varesi A, Floris V, Savioli G, Mantovani E, López-Carrasco P, et al. Myalgic encephalomyelitis/chronic fatigue syndrome (Me/cfs): an overview. *J Clin Med.* (2021) 10:4786. doi: 10.3390/jcm10204786
6. Meeus M, Nijs J. Central sensitization: a biopsychosocial explanation for chronic widespread pain in patients with fibromyalgia and chronic fatigue syndrome. *Clin Rheumatol.* (2007) 26:465–73. doi: 10.1007/s10067-006-0433-9
7. Chen R, Liang F, Moriya J, Yamakawa J, Sumino H, Kanda T, et al. Chronic fatigue syndrome and the central nervous system. *J Int Med Res.* (2008) 36:867–74. doi: 10.1177/147323000803600501
8. Meeus M, Roussel NA, Truijen S, Nijs J. Reduced pressure pain thresholds in response to exercise in chronic fatigue syndrome but not in chronic low back pain: an experimental study. *J Rehabil Med.* (2010) 42:884–90. doi: 10.2340/16501977-0595
9. Lewis I, Pairman J, Spickett G, Newton JL. Clinical characteristics of a novel subgroup of chronic fatigue syndrome patients with postural orthostatic tachycardia syndrome. *J Intern Med.* (2013) 273:501–10. doi: 10.1111/joim.12022
10. Nijs J, Ickmans K. Postural orthostatic tachycardia syndrome as a clinically important subgroup of chronic fatigue syndrome: further evidence for central nervous system dysfunctioning. *J Intern Med.* (2013) 273:498–500. doi: 10.1111/joim.12034
11. Van Den Heuvel MP, Pol HEH. Exploring the brain network: a review on resting-state fMRI functional connectivity. *Eur Neuropsychopharmacol.* (2010) 20:519–34. doi: 10.1016/j.euroneuro.2010.03.008
12. Stam CV, Van Straaten E. The organization of physiological brain networks. *Clin Neurophysiol.* (2012) 123:1067–87. doi: 10.1016/j.clinph.2012.01.011
13. Ning Y, Li K, Zhang Y, Chen P, Yin D, Zhu H, et al. Assessing cognitive abilities of patients with shift work disorder: insights from RBANS and granger causality connections among resting-state networks. *Front Psychiatry.* (2020) 11:780. doi: 10.3389/fpsyt.2020.00780
14. Shan ZY, Finegan K, Bhuta S, Ireland T, Staines DR, Marshall-Gradisnik SM, et al. Decreased connectivity and increased blood oxygenation level dependent complexity in the default mode network in individuals with chronic fatigue syndrome. *Brain Connect.* (2018) 8:33–39. doi: 10.1089/brain.2017.0549
15. Manca R, Khan K, Mitolo M, De Marco M, Grieveson L, Varley R, et al. Modulatory effects of cognitive exertion on regional functional connectivity of the salience network in women with ME/CFS: a pilot study. *J Neurol Sci.* (2021) 422:117326. doi: 10.1016/j.jns.2021.117326
16. Gay CW, Robinson ME, Lai S, O'Shea A, Craggs JG, Price DD, et al. Abnormal resting-state functional connectivity in patients with chronic

fatigue syndrome: results of seed and data-driven analyses. *Brain Connect.* (2016) 6:48–56. doi: 10.1089/brain.2015.0366
17. Rowe PC, Calkins H, DeBusk K, McKenzie R, Anand R, Sharma G, et al. Fludrocortisone acetate to treat neurally mediated hypotension in chronic fatigue syndrome: a randomized controlled trial. *JAMA.* (2001) 285:52–9. doi: 10.1001/jama.285.1.52
18. White PD, Goldsmith KA, Johnson AL, Potts L, Walwyn R, DeCesare JC, et al. Comparison of adaptive pacing therapy, cognitive behaviour therapy, graded exercise therapy, and specialist medical care for chronic fatigue syndrome (PACE): a randomised trial. *Lancet.* (2011) 377:823–36. doi: 10.1016/S0140-6736(11)60096-2
19. Clark LV, Pesola F, Thomas JM, Vergara-Williamson M, Beynon M, White PD. Guided graded exercise self-help plus specialist medical care versus specialist medical care alone for chronic fatigue syndrome (GETSET): a pragmatic randomised controlled trial. *Lancet.* (2017) 390:363–73. doi: 10.1016/S0140-6736(16)32589-2
20. Cheng CA, Chiu YW, Wu DA, Kuan YC, Chen SN, Tam KW. Effectiveness of Tai Chi on fibromyalgia patients: a meta-analysis of randomized controlled trials. *Complement Ther Med.* (2019) 46:1–8. doi: 10.1016/j.ctim.2019.07.007
21. Tao J, Chen X, Egorova N, Liu J, Xue X, Wang Q, et al. Tai chi chuan and baduanjin practice modulates functional connectivity of the cognitive control network in older adults. *Sci Rep.* (2017) 7:1–9. doi: 10.1038/srep41581
22. Klein PJ, Adams WD. Comprehensive therapeutic benefits of Taiji - a critical review. *Am J Phys Med Rehabil.* (2004) 83:735–45. doi: 10.1097/01.PHM.0000137317.98890.74
23. Yang Y, DeCelle S, Reed M, Rosengren K, Schlagal R, Greene J. Subjective experiences of older adults practicing taiji and qigong. *J Aging Res.* (2011) 2011:650210. doi: 10.4061/2011/650210
24. Xiang Y, Lu L, Chen X, Wen Z. Does Tai Chi relieve fatigue? a systematic review and meta-analysis of randomized controlled trials. *PLoS ONE.* (2017) 12:e0174872. doi: 10.1371/journal.pone.0174872
25. Wang C, Schmid CH, Rones R, Kalish R, Yinh J, Goldenberg DL, et al. A randomized trial of tai chi for fibromyalgia. *N Eng J Med.* (2010) 363:743–54. doi: 10.1056/NEJMoa0912611
26. Wang C, Schmid CH, Fielding RA, Harvey WF, Reid KF, Price LL, et al. Effect of tai chi versus aerobic exercise for fibromyalgia: comparative effectiveness randomized controlled trial. *BMJ.* (2018) 360. doi: 10.1136/bmj.k851
27. Hulens M, Rasschaert R, Vansant G, Stalmans I, Bruyninckx F, Dankaerts W. The link between idiopathic intracranial hypertension, fibromyalgia, and chronic fatigue syndrome: exploration of a shared pathophysiology. *J Pain Res.* (2018) 11:3129–40. doi: 10.2147/JPR.S186878
28. Bourke JH, Wodehouse T, Clark LV, Constantinou E, Kidd BL, Langford R, et al. Central sensitisation in chronic fatigue syndrome and fibromyalgia; a case control study. *J Psychosom Res.* (2021) 150. doi: 10.1016/j.jpsychores.2021.110624
29. Hulens M, Bruyninckx F, Dankaerts W, Rasschaert R, De Mulder P, Stalmans I, et al. High prevalence of perineural cysts in patients with fibromyalgia and chronic fatigue syndrome. *Pain Medicine.* (2021) 22:883–90. doi: 10.1093/pm/pnaa410
30. Kolb B, Whishaw IQ. Brain plasticity and behavior. *Annu Rev Psychol.* (1998) 49:43–64. doi: 10.1146/annurev.psych.49.1.43
31. Cui L, Yin H, Lyu S, Shen Q, Wang Y, Li X, et al. Tai Chi Chuan vs general aerobic exercise in brain plasticity: a multimodal MRI study. *Sci Rep.* (2019) 9:1–7. doi: 10.1038/s41598-019-53731-z
32. Cui L, Tao S, Yin H-c, Shen Q-q, Wang Y, Zhu L-n, et al. Tai Chi chuan alters brain functional network plasticity and promotes cognitive flexibility. *Front Psychol.* (2021) 2514:665419. doi: 10.3389/fpsyg.2021.665419
33. Yue C, Zhang Y, Jian M, Herold F, Yu Q, Mueller P, et al. Differential effects of tai chi chuan (motor-cognitive training) and walking on brain networks: a resting-state fMRI study in chinese women aged 60. *Healthcare.* (2020) 8:67. doi: 10.3390/healthcare8010067
34. Demirci O, Stevens MC, Andreasen NC, Michael A, Liu J, White T, et al. Investigation of relationships between fMRI brain networks in the spectral domain using ICA and Granger causality reveals distinct differences between schizophrenia patients and healthy controls. *Neuroimage.* (2009) 46:419–31. doi: 10.1016/j.neuroimage.2009.02.014
35. Stephan KE, Roebroeck A. A short history of causal modeling of fMRI data. *Neuroimage.* (2012) 62:856–63. doi: 10.1016/j.neuroimage.2012.01.034
36. Seth AK, Chorley P, Barnett LC. Granger causality analysis of fMRI BOLD signals is invariant to hemodynamic convolution but not downsampling. *Neuroimage.* (2013) 65:540–55. doi: 10.1016/j.neuroimage.2012.09.049
37. Seth AK, Barrett AB, Barnett L. Granger causality analysis in neuroscience and neuroimaging. *J Neurosci.* (2015) 35:3293–7. doi: 10.1523/JNEUROSCI.4399-14.2015
38. Fukuda K, Straus SE, Hickie I, Sharpe MC, Dobbins JG, Komaroff A. The chronic fatigue syndrome: a comprehensive approach to its definition and study. *Ann Intern Med.* (1994) 121:953–9. doi: 10.7326/0003-4819-121-12-199412150-00009
39. Yan CG, Wang XD, Zuo XN, Zang YF. DPABI: Data processing and analysis for (Resting-State) Brain Imaging. *Neuroinformatics.* (2016) 14:339–51. doi: 10.1007/s12021-016-9299-4
40. Tustison NJ, Avants BB, Cook PA, Zheng Y, Egan A, Yushkevich PA, et al. N4ITK: improved N3 bias correction. *IEEE Trans Med Imaging.* (2010) 29:1310–20. doi: 10.1109/TMI.2010.2046908
41. Klein A, Ghosh SS, Bao FS, Giard J, Hame Y, Stavsky E, et al. Mindboggling morphometry of human brains. *PLoS Comput Biol.* (2017) 13:e1005350. doi: 10.1371/journal.pcbi.1005350
42. Esteban O, Markiewicz CJ, Blair RW, Moodie CA, Isik AI, Erramuzpe A, et al. fMRIPrep: a robust preprocessing pipeline for functional MRI. *Nat Methods.* (2019) 16:111–6. doi: 10.1038/s41592-018-0235-4
43. White T, Gilleen JK, Shergill SS. Dysregulated but not decreased salience network activity in schizophrenia. *Front Hum Neurosci.* (2013) 7:65. doi: 10.3389/fnhum.2013.00065
44. Havlicek M, Jan J, Brazdil M, Calhoun VD. Dynamic Granger causality based on Kalman filter for evaluation of functional network connectivity in fMRI data. *Neuroimage.* (2010) 53:65–77. doi: 10.1016/j.neuroimage.2010.05.063
45. Wei G-X, Gong Z-Q, Yang Z, Zuo X-N. Mind-body practice changes fractional amplitude of low frequency fluctuations in intrinsic control networks. *Front Psychol.* (2017) 8:1049. doi: 10.3389/fpsyg.2017.01049
46. Evering RM, van Weering MG, Groothuis-Oudshoorn KC, Vollenbroek-Hutten MM. Daily physical activity of patients with the chronic fatigue syndrome: a systematic review. *Clin Rehabil.* (2011) 25:112–33. doi: 10.1177/0269215510380831
47. Eaton-Fitch N, Johnston S, Zalewski P, Staines D, Marshall-Gradisnik S. Health-related quality of life in patients with myalgic encephalomyelitis/chronic fatigue syndrome: an Australian cross-sectional study. *Qual Life Res.* (2020) 29:1521–31. doi: 10.1007/s11136-019-02411-6
48. Zeineh MM, Kang J, Atlas SW, Raman MM, Reiss AL, Norris JL, et al. Right arcuate fasciculus abnormality in chronic fatigue syndrome. *Radiology.* (2015) 274:517–26. doi: 10.1148/radiol.14141079
49. Boissoneault J, Letzen J, Lai S, O'Shea A, Craggs J, Robinson ME, et al. Abnormal resting state functional connectivity in patients with chronic fatigue syndrome: an arterial spin-labeling fMRI study. *Magn Reson Imaging.* (2016) 34:603–8. doi: 10.1016/j.mri.2015.12.008
50. Singh KD, Fawcett IP. Transient and linearly graded deactivation of the human default-mode network by a visual detection task. *Neuroimage.* (2008) 41:100–12. doi: 10.1016/j.neuroimage.2008.01.051
51. Andrews-Hanna JR. The brain's default network and its adaptive role in internal mentation. *Neuroscientist.* (2012) 18:251–70. doi: 10.1177/1073858411403316
52. Krajcovicova L, Marecek R, Mikl M, Rektorova I. Disruption of resting functional connectivity in Alzheimer's patients and at-risk subjects. *Curr Neurol Neurosci Rep.* (2014) 14:491. doi: 10.1007/s11910-014-0491-3
53. Chong CD, Schwedt TJ, Hougaard A. Brain functional connectivity in headache disorders: a narrative review of MRI investigations. *J Cereb Blood Flow Metab.* (2019) 39:650–69. doi: 10.1177/0271678X17740794
54. Wu CW, Lin S-HN, Hsu L-M, Yeh S-C, Guu S-F, Lee S-H, et al. Synchrony between default-mode and sensorimotor networks facilitates motor function in stroke rehabilitation: a pilot fMRI study. *Front Neurosci.* (2020) 14:548. doi: 10.3389/fnins.2020.00548
55. Husain M, Nachev P. Space and the parietal cortex. *Trends Cogn Sci.* (2007) 11:30–6. doi: 10.1016/j.tics.2006.10.011
56. Sambataro F, Doerig N, Hänggi J, Wolf RC, Brakowski J, Holtforth MG, et al. Anterior cingulate volume predicts response to psychotherapy and functional connectivity with the inferior parietal cortex in

major depressive disorder. *Eur Neuropsychopharmacol.* (2018) 28:138–48. doi: 10.1016/j.euroneuro.2017.11.008
57. Vogt BA, Laureys S. Posterior cingulate, precuneal and retrosplenial cortices: cytology and components of the neural network correlates of consciousness. *Prog Brain Res.* (2005) 150:205–17. doi: 10.1016/S0079-6123(05)50015-3
58. Wei G-X, Dong H-M, Yang Z, Luo J, Zuo X-N. Tai Chi Chuan optimizes the functional organization of the intrinsic human brain architecture in older adults. *Front Aging Neurosci.* (2014) 6:74. doi: 10.3389/fnagi.2014.00074
59. Domic-Siede M, Irani M, Valdes J, Perrone-Bertolotti M, Ossandon T. Theta activity from frontopolar cortex, mid-cingulate cortex and anterior cingulate cortex shows different roles in cognitive planning performance. *Neuroimage.* (2021) 226. doi: 10.1016/j.neuroimage.2020.117557
60. Matyas F, Sreenivasan V, Marbach F, Wacongne C, Barsy B, Mateo C, et al. Motor control by sensory cortex. *Science.* (2010) 330:1240–3. doi: 10.1126/science.1195797
61. Zagha E, Casale AE, Sachdev RNS, McGinley MJ, McCormick DA. Motor cortex feedback influences sensory processing by modulating network state. *Neuron.* (2013) 79:567–78. doi: 10.1016/j.neuron.2013.06.008
62. Jason LA, Shanks LL, Evans M, Brown A. Cognitive impairments associated with CFS and POTS. *Front Physiol.* (2013) 4:113. doi: 10.3389/fphys.2013.00113
63. Mizuno K, Watanabe Y. Neurocognitive impairment in childhood chronic fatigue syndrome. *Front Physiol.* (2013) 4:87. doi: 10.3389/fphys.2013.00087
64. Cvejic E, Birch RC, Vollmer-Conna U. Cognitive dysfunction in chronic fatigue syndrome: a review of recent evidence. *Curr Rheumatol Rep.* (2016) 18:24. doi: 10.1007/s11926-016-0577-9
65. Geraghty KJ, Blease C. Cognitive behavioural therapy in the treatment of chronic fatigue syndrome: a narrative review on efficacy and informed consent. *J Health Psychol.* (2018) 23:127–38. doi: 10.1177/1359105316667798
66. Teodoro T, Edwards MJ, Isaacs JD. A unifying theory for cognitive abnormalities in functional neurological disorders, fibromyalgia and chronic fatigue syndrome: systematic review. *J Neurol Neurosurg Psychiatry.* (2018) 89:1308–19. doi: 10.1136/jnnp-2017-317823
67. Hafkemeijer A, Möller C, Dopper EG, Jiskoot LC, Van Den Berg-Huysmans AA, Van Swieten JC, et al. A longitudinal study on resting state functional connectivity in behavioral variant frontotemporal dementia and Alzheimer's disease. *J Alzheimers Dis.* (2017) 55:521–37. doi: 10.3233/JAD-150695
68. Wang W, Wang P, Li Q, Peng Z, Wang X, Wang G, et al. Alterations of grey matter volumes and network-level functions in patients with stable chronic obstructive pulmonary disease. *Neurosci Lett.* (2020) 720:134748. doi: 10.1016/j.neulet.2020.134748
69. Xu G-Q, Lan Y, Huang D-f, Rao D-z, Pei Z, Chen L, et al. Visuospatial attention deficit in patients with local brain lesions. *Brain Res.* (2010) 1322:153–9. doi: 10.1016/j.brainres.2010.01.072
70. Su JJ, Ban SY, Wang MX, Hua FC, Wang L, Cheng X, et al. Reduced resting-state brain functional network connectivity and poor regional homogeneity in patients with CADASIL. *J Headache Pain.* (2019) 20:103. doi: 10.1186/s10194-019-1052-6
71. Kim B-H, Namkoong K, Kim J-J, Lee S, Yoon KJ, Choi M, et al. Altered resting-state functional connectivity in women with chronic fatigue syndrome. *Psychiatry Res Neuroimag.* (2015) 234:292–7. doi: 10.1016/j.pscychresns.2015.10.014
72. Wortinger LA, Endestad T, Melinder AMD, Øie MG, Sevenius A, Bruun Wyller V. Aberrant resting-state functional connectivity in the salience network of adolescent chronic fatigue syndrome. *PLoS ONE.* (2016) 11:e0159351. doi: 10.1371/journal.pone.0159351
73. Josev EK, Malpas CB, Seal ML, Scheinberg A, Lubitz L, Rowe K, et al. Resting-state functional connectivity, cognition, and fatigue in response to cognitive exertion: a novel study in adolescents with chronic fatigue syndrome. *Brain Imaging Behav.* (2020) 14:1815–30. doi: 10.1007/s11682-019-00119-2
74. Sherman LE, Rudie JD, Pfeifer JH, Masten CL, McNealy K, Dapretto M. Development of the default mode and central executive networks across early adolescence: a longitudinal study. *Dev Cogn Neurosci.* (2014) 10:148–59. doi: 10.1016/j.dcn.2014.08.002
75. Allen EA, Erhardt EB, Damaraju E, Gruner W, Segall JM, Silva RF, et al. A baseline for the multivariate comparison of resting-state networks. *Front Syst Neurosci.* (2011) 5:2. doi: 10.3389/fnsys.2011.00002

Conflict of Interest: The authors declare that the research was conducted in the absence of any commercial or financial relationships that could be construed as a potential conflict of interest.

frontiers | Frontiers in Neurology

ORIGINAL RESEARCH
published: 06 June 2022
doi: 10.3389/fneur.2022.900520

Sensorimotor Responses in Post-Stroke Hemiplegic Patients Modulated by Acupuncture at Yanglingquan (GB34): A fMRI Study Using Intersubject Functional Correlation (ISFC) Analysis

Yue Wang†, Liping Wang†, Yahui Wang, Mengxin Lu, Lingling Xu, Ruoyi Liu, Jingpei Wei, Jifeng Wan, Hua Zhang and Yihuai Zou**

Department of Neurology, Dongzhimen Hospital, Beijing University of Chinese Medicine, Beijing, China

OPEN ACCESS

Edited by:
Wei Zhang,
Peking University, China

Reviewed by:
Kai Yuan,
The Chinese University of Hong Kong, China
Jian Pei,
Shanghai University of Traditional Chinese Medicine, China

***Correspondence:**
Yihuai Zou
zouyihuai2004@163.com
Hua Zhang
nwkzhhsf@aliyun.com

†These authors have contributed equally to this work and share first authorship

Specialty section:
This article was submitted to Applied Neuroimaging, a section of the journal Frontiers in Neurology

Received: *20 March 2022*
Accepted: *02 May 2022*
Published: *06 June 2022*

Citation:
Wang Y, Wang L, Wang Y, Lu M, Xu L, Liu R, Wei J, Wan J, Zhang H and Zou Y (2022) Sensorimotor Responses in Post-Stroke Hemiplegic Patients Modulated by Acupuncture at Yanglingquan (GB34): A fMRI Study Using Intersubject Functional Correlation (ISFC) Analysis. Front. Neurol. 13:900520. doi: 10.3389/fneur.2022.900520

Motor dysfunction is common in patients with stroke. Acupuncture has become an acceptable alternative method for stroke rehabilitation. Previous studies have shown various functional connectivity changes activated by acupuncture. We introduced intersubject correlation (ISC) and intersubject functional correlation (ISFC) analyses into the functional magnetic resonance imaging (fMRI) for ischemic stroke to seek a common activation and suppression pattern triggered by acupuncture. In this study, 63 ischemic stroke patients with motor dysfunction and 42 normal controls were analyzed. Three functional scans were conducted during the resting state, motor task, and acupuncture at Yanglingquan (GB34) task. Twenty-two sensory, motor, and movement-imagination cortices in the bilateral hemispheres were selected as the region of interest (ROI). We performed ISC and ISFC analyses among these ROIs in three fMRI runs on patients and controls. Subgroup analyses by course or severity were also conducted. The results showed that acupuncture at GB34 triggered ISFC among upper limb motor, upper limb/hand/face, lower limb, tongue/larynx sensory, and movement imagination regions in the patient group. Subgroup ISC and ISFC analyses showed that patients tended to have increasing responses in the early stage of stroke (within 1 month) and decreasing responses afterward (1–3 months). Patients with mild clinical functional damage (NIHSS 2–4) tended to generate more responses *via* acupuncture than those with moderate damage (NIHSS 5–15). Our findings may help understand the clinical effects and modulatory features of acupuncture based on the group-level post-stroke neuroplasticity.

Keywords: sensorimotor cortex, Yanglingquan (GB34), acupuncture, hemiplegia, motor dysfunction, functional MRI, intersubject functional correlation, ischemic stroke

INTRODUCTION

Stroke, the third leading cause of death and disability, has been causing a serious disease burden worldwide (1). Based on current stroke trends, the World Stroke Organization (WSO) has estimated that there will be about 200 million stroke survivors in 2050 (2). The probability of post-stroke motor dysfunction is about 50–85%. Thus, functional recovery and rehabilitation,

which focus on neuronal plasticity and brain network recovery after stroke, have been the key transnational research topics (3). The current knowledge of post-stroke neuroplasticity is mainly based on invasive methods (4), which cannot be performed in clinical trials. On the contrary, non-invasive functional magnetic resonance imaging (fMRI) has been widely applied in the field of post-stroke neural plasticity with outstanding features of high spatial and temporal resolution (5, 6).

Post-stroke rehabilitation can improve motor function and regulate neuroplasticity (7, 8). Noteworthy, upper extremity function is particularly important for functional training, as it can determine whether an individual can return to his formal professional and personal life (9). Thumb-index-finger opposition is routine training for post-stroke patients with upper limb dysfunction. Both active and passive hand practices are beneficial in improving motor function (10, 11). fMRI-based research has found that 1-Hz thumb-index-finger opposition mainly activated the primary and secondary motor regions, which extended to the posterior central gyrus and anterior central sulcus (12).

Acupuncture, a traditional Chinese therapy, has a gradually increasing geographical coverage and application rate (13). The NIH Consensus Conference (14) and publications (15, 16) have demonstrated that acupuncture can improve the neurological motor deficit symptoms and become an acceptable alternative method for stroke rehabilitation. Recent research has shown that acupuncture was involved in regulating neural plasticity in patients with stroke, both functionally and structurally (17, 18). Yanglingquan (GB34), the He-Sea point of the gall bladder meridian (Foot-Shaoyang), the confluence point of tendons, is one of the main points in post-stroke acupuncture approaches, such as Wang's twelve-needling at hands and feet method and Xingnao Kaiqiao needling method (19). GB34 has been the most commonly used acupoint to study the mechanism of acupuncture stimulation in stroke based on fMRI (20). Previous studies have proposed that acupuncture at GB34 could enhance the functional connectivity (FC) between bilateral M1 cortices and increase motor-cognition connectivity (21, 22). The conventional analysis has been displayed by calculating the correlations of time series in the target regions of every single subject. In addition to the real signal induced by stimulation, FC also contains information that cannot be well-separated, such as intrinsic neural signal and non-neural noise signal (23). Therefore, capturing simpler and more accurate neural activities triggered by acupuncture among different subjects is a topic requiring attention.

The intersubject correlation (ISC) analysis provides a data-driven alternative for seeking the activity caused by complex stimuli. Based on the logic of ISC, intersubject functional correlation (ISFC) represents a new analytical method for revealing the functional connectivity of stimuli in various brain regions across subjects (24). Similar to the functional connectivity analysis, ISFC analysis targets the correlation between two response time series; however, rather than calculating the correlation between two regions within a subject, ISFC analysis calculates the same two regions across subjects. A comparative study has revealed that the data-driven ISC analysis found the same foci as the model-based general linear model (GLM) analysis and was applicable in situations where GLM was not suitable (25). Currently, this method has been widely used in studies of visual and auditory stimuli (26–28). We innovatively introduced this method into our study to further explore the common neural activities of focal brain regions in patients with post-ischemic stroke hemiplegia.

With the development of image technology and the sharing of neuroimaging information, researchers have proposed a new brain atlas, which divides the brain into 246 regions based on functional connectivity information. Unlike previous atlases that only represented specific structures and lacked fine-grained parcellations, the Brainnetome (BN) atlas has more fine-grained functional brain subregions and detailed functional connection patterns, which can help more accurately describe the locations of the activation or connectivity in the brain (29). In this study, we selected 22 sensory, motor, and movement-imagination-related cortices in bilateral anterior central gyri, posterior central gyri, and their vicinity as the regions of interest (ROI) based on the BN atlas to focus on the deficit-related rehabilitation mechanisms on hemiplegic patients by acupuncture.

This study aimed to explore the cross-subject effects of acupuncture at GB34 on functional sensorimotor activities among ischemic stroke patients with hemiplegia. Healthy subjects were recruited as normal controls. A resting-state scan was used as a background observation. Thumb-index-finger opposition was used as a reference motor task. Activation and suppression correlation responses among 22 ROIs chosen from the BN atlas were calculated and presented by applying the ISFC analysis.

MATERIALS AND METHODS

Participants

This study included 63 right-handed post-stroke inpatient subjects with hemiplegia from a single center (Dongzhimen Hospital, Beijing University of Chinese Medicine). A total of 42 age- and sex-matched healthy subjects were recruited as normal controls. All participants signed informed consent before inclusion, which explained the whole study design, including the purpose and procedures of this study, the benefits and risks of being involved, and the rights of self-data acquirement and being able to quit without conditions. Participants received a signed copy of the informed consent. Basic information (age, sex, and vital signs), National Institute of Health stroke scale (NIHSS) score, and functional and structural MRI data were collected on the same day. The subjects' demographic features and patients' lesion incidence map are shown in **Table 1** and **Figure 1**, respectively. All patients included in this study had mild to moderate (NIHSS of 0–15) neural dysfunction.

The included patients met the following criteria: (1) patients with ischemic stroke who conform to the diagnostic criteria (30) and whose course of the disease is within 3 months; (2) right-handed patients; (3) patients aged 40–75 years; (4) patients presenting first-ever post-stroke motor dysfunction in the upper or lower extremities; (5) patients in whom the infarction was located in the basal ganglia and/or the corona radiate region, side-unlimited, but not

TABLE 1 | Demographic features and clinical information of patients with stroke and normal controls.

	Number	Sex (male/female)	Age	Stroke time (day)	NIHSS score	Number of patients with right hemisphere lesion	Number of patients with left hemisphere lesion
Patient Group	63	43 / 20	59.56 ± 9.82	27.22 ± 17.53	3.81 ± 3.19	48	15
Control Group	42	22 / 20	56.64 ± 5.17	-	-	-	-

No significant distribution of age difference (two-sample t-test, $p > 0.05$) or sex difference (χ^2-test, $p > 0.05$) detected. Enumeration data are presented as mean ± standard deviation.

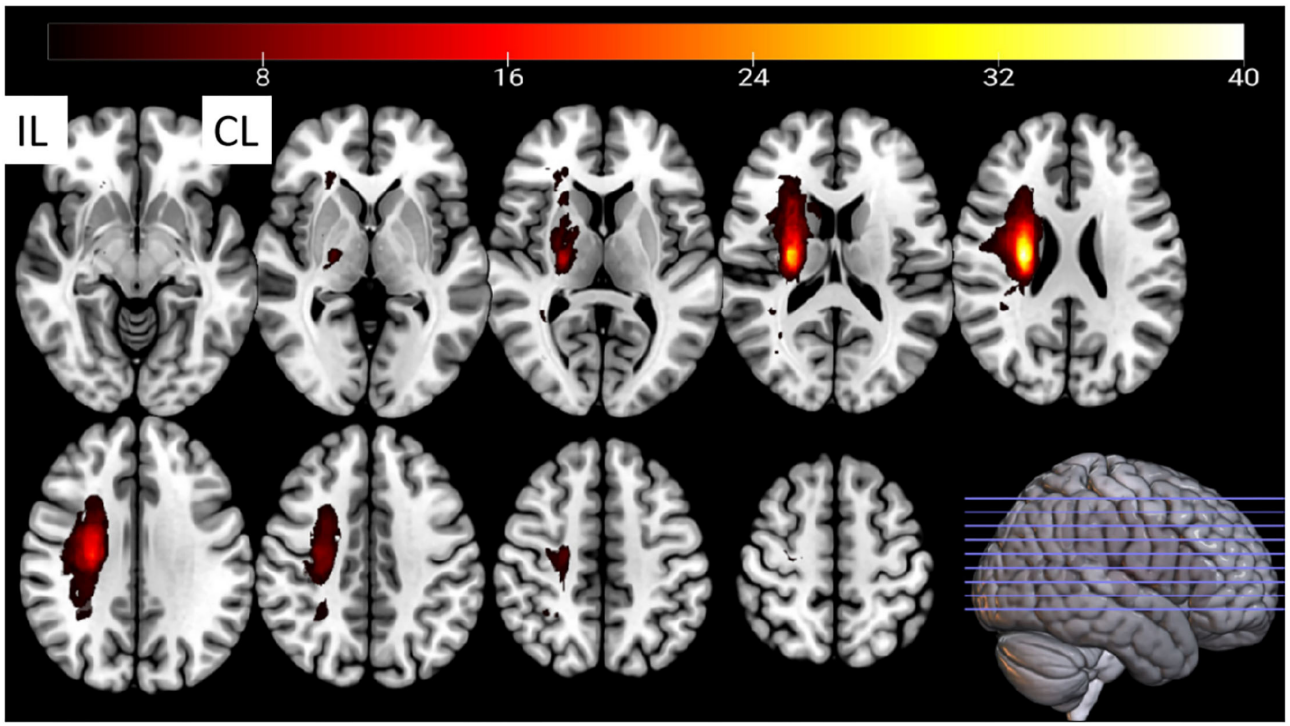

FIGURE 1 | The stroke patients' lesion-incidence map. CL, contralesional; IL, ipsilesional. Fifteen lesions from the left hemisphere were flipped to the right hemisphere.

caused by embolism; (6) patients without other central nervous system diseases (e.g., epilepsy, Parkinson's disease, Alzheimer's disease, and vascular dementia), psychiatric disorders (e.g., depression and schizophrenia), or any other serious primary diseases (e.g., tumors, organ failure, atrial fibrillation, and thrombotic diseases); (7) patients without unremovable metallic implants or contraindication of magnetic resonance examination.

The included healthy controls met the following criteria: (1) right-handed people; (2) people aged 40–75 years; (3) people proved to be healthy by a medical examination (without organic or significant functional diseases); (4) people without a family history of mental or neural system inheritance; (5) people without experience of joining research similar to this experiment; (6) people without physical abnormalities (e.g., cold, headache, and cough) during the trial; (7) people not taking any excitatory medications within the past 2 months; and (8) people without unremovable metallic implants or contraindication of magnetic resonance examination.

Task Design

The participants were told to close their eyes without engaging in any mental task. According to participants' reports after the scanning, they were affirmed to keep awake during the whole scanning procedure. Three fMRI runs were conducted. The first run was in a resting state for 6 min and 10 s. The second run occurred during the motor task with passive thumb-index-finger opposition on the affected side in patients or the left side in normal controls. The task was performed as a "rest-move-rest-move-rest-move-rest" pattern by two researchers. Each time slice lasted for 20 s for a total of 2 min and 20 s. The "move" period allowed the participants' thumb and index fingertips touching-and-parting at a frequency of 1 Hz (31). The "rest" period had no intervention, only relaxation. The third run occurred during the acupuncture operation on the affected side in patients or the left side in normal controls. The needles were disposable sterile silver needles (specification parameter: $\phi 0.40 \times 40$ mm) purchased from Beijing Zhongyantaihe Medical Instrument Co., LTD., and manufactured by Suzhou Shenlong

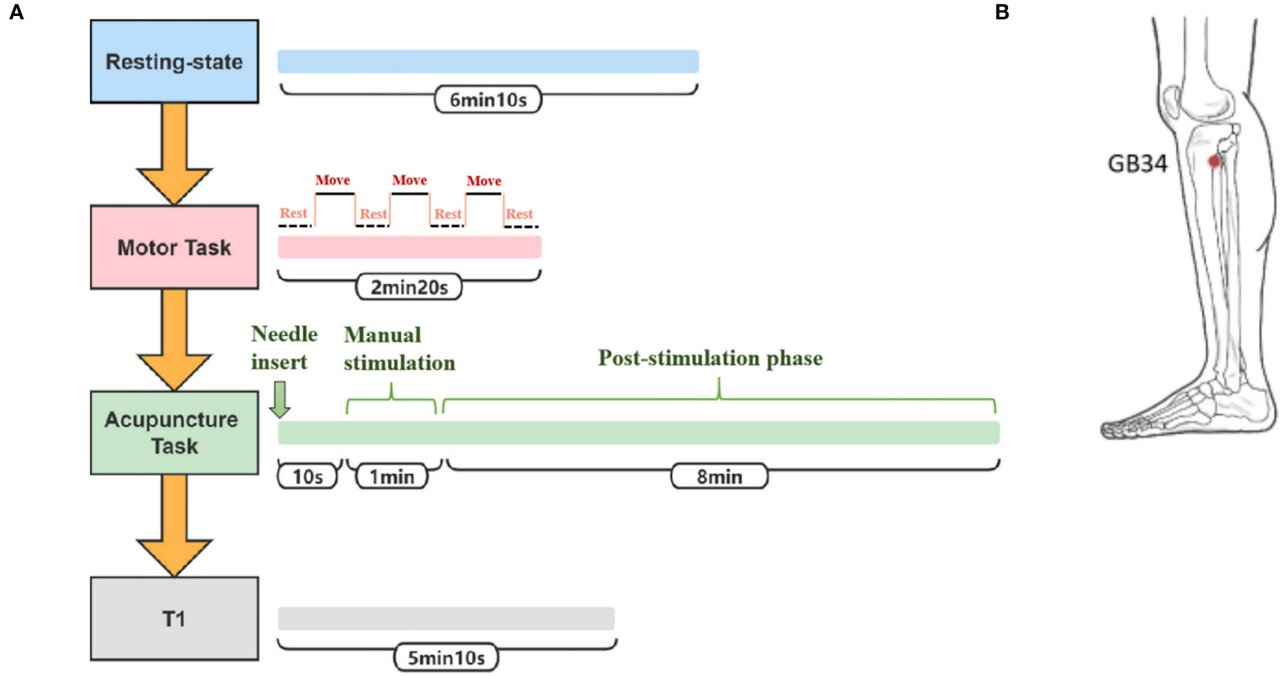

FIGURE 2 | Study design. **(A)** The scanning protocol. **(B)** The location of Yanglingquan (GB34).

Medical Instrument Co., LTD. Acupoint selection was performed according to the National standard GB/T 12346-2006 Name and Location of Acupoints. Yanglingquan (GB34) is located on the outside of the lower leg, in the middle of the concavity of the anterior and inferior parts of the fibula head. After routine skin disinfection, the needle was vertically inserted for 1.5–2 Cun (about 25–40 mm depending on the height and weight of a participant) at GB34. There was a 10-s post-onset phase of the resting state with the needle inserted, followed by a 1-min manual stimulation phase by using the mild reinforcing–reducing method at a frequency of 1 Hz. Then, an 8-min post-stimulation phase occurred with the needle remaining inside the leg. The needle was removed and disposed of after the acupuncture scanning. In the end, the T1-weighted structural image was acquired. The scanning protocol and position of GB34 are shown in **Figures 2A,B**, respectively. At the end of the MRI scanning procedure, NIHSS scores of patients with ischemic stroke were evaluated by an experienced neurologist.

fMRI Parameters

All scans were performed by a 3.0 Tesla scanner (Siemens, Verio, Germany) in Dongzhimen Hospital. The scanning parameters were as follows: fMRI was applied with echo-planar imaging (EPI) sequence with a repetition time (TR) of 2,000 ms; echo time (TE) of 30 ms; matrix of 64 × 64; field of view (Fov) of 225 × 225 mm; slice thickness of 3.5 mm; a gap of 0.7 mm; phase encode direction of A >> P; flip angle of 90°; and fat suppr of fat sat. The three-dimensional structure imaging scan of the whole brain was scanned using the following T1W1 sequence: TR of 1,900 ms; TE of 2.53 ms; Fov of 250 × 250 mm; matrix of 256 × 256; and slice thickness of 1.0 mm.

Data Processing

For each of the 3 BOLD runs per subject, the following preprocessing was performed (32). First, a reference volume and its skull-stripped version were generated. BOLD runs were slice-time corrected to 0.971 s using 3dTshift from AFNI (RRID:SCR_005927). Head-motion parameters with respect to the BOLD reference were estimated using mcflirt (FSL 5.0.11). The BOLD time series were resampled onto their original native space by applying the transforms to correct for head motion. The BOLD reference was then co-registered to the T1w reference using bbregister (FreeSurfer) with 6 degrees of freedom. Framewise displacement (FD), DVARS, and 3 region-wise global signals within the cerebrospinal fluid, the white matter, and the whole-brain masks were calculated. Additionally, a set of physiological regressors was extracted to allow component-based noise correction. Finally, these masks were resampled into BOLD space and binarized by thresholding at 0.99. The BOLD time series were resampled onto the fsnative. Automatic removal of motion artifacts using an independent component analysis (ICA-AROMA) was performed on the preprocessed BOLD on the Montreal Neurological Institute (MNI) space-time series after the removal of non-steady state volumes and spatial smoothing with an isotropic Gaussian kernel of 6 mm FWHM (full-width half-maximum). Imaging data were filtered (bandpass, 0.01–0.1 Hz; **Supplementary Material 1**).

TABLE 2 | Information of 22 ROIs based on Brainnetome Atlas.

No.	Name	Hemisphere	Description	Location
0	A4ul_L	Left	Upper limb region	Precentral gyrus
1	A4ll_L	Left	Lower limb region	Paracentral lobe
2	A4tl_L	Left	Tongue/larynx region	Precentral gyrus
3	A4t_L	Left	Trunk region	Precentral gyrus
4	A1/2/3ulhf_L	Left	Upper limb/hand/face region	Postcentral gyrus
5	A1/2/3ll_L	Left	Lower limb region	Paracentral lobe
6	A1/2/3tonla_L	Left	Tongue/larynx region	Postcentral gyrus
7	A1/2/3tru_L	Left	Trunk region	Postcentral gyrus
8	A2_L	Left	S2 sensory	Postcentral gyrus
9	A6m_L	Left	Medial area 6	Superior frontal gyrus
10	A7r_L	Left	Rostral area 7	Superior parietal lobe
11	A4ul_R	Right	Upper limb region	Precentral gyrus
12	A4ll_R	Right	Lower limb region	Paracentral lobe
13	A4tl_R	Right	Tongue/larynx region	Precentral gyrus
14	A4t_R	Right	Trunk region	Precentral gyrus
15	A1/2/3ulhf_R	Right	Upper limb/hand/face region	Postcentral gyrus
16	A1/2/3ll_R	Right	Lower limb region	Paracentral lobe
17	A1/2/3tonla_R	Right	Tongue/larynx region	Postcentral gyrus
18	A1/2/3tru_R	Right	Trunk region	Postcentral gyrus
19	A2_R	Right	S2 sensory	Postcentral gyrus
20	A6m_R	Right	Medial area 6	Superior frontal gyrus
21	A7r_R	Right	Rostral area 7	Superior parietal lobe

Statistical Analysis

The BN atlas was downloaded from https://atlas.brainnetome.org/index.html and used to define the location of the ROIs of all three fMRI datasets. The average time series of the voxel in each ROI were calculated according to the spatial coordinates. For the 15 patients with left-sided lesions, we exchanged the data symmetrically between the two hemispheres. The chosen ROIs were motor, sensory, and movement-imagination cortices (**Table 2** and **Figure 3**). Also, the exchange of the data would not concern the specific dysfunction of the dominant hemisphere, such as aphasia. By this step, all 63 patients with right hemisphere lesions received affected-side passive finger movement and GB34 acupuncture operation.

Then ROIs time series were extracted from the preprocessed fMRI data. ISC and ISFC for each functional run were calculated and analyzed across the subjects from each group by using Brain Imaging Analysis Kit (BrainIAK, https://brainiak.org) implemented in Python rather than computing the correlations across the ROIs within one subject. We used the isc function in BrainIAK with a leave-one-out approach comprising BOLD time series for one ROI across multiple subjects and returns ISC values for ROIs for each subject. For the ISFC analysis, we supplied BOLD time-series data for 22 ROIs across the subjects to the isfc function. By using the leave-one-out approach, we plotted the ROI-by-ROI ISFC matrix for each subject. Then, we used the bootstrap_isc function (applying a bootstrap hypothesis test) to perform group-level statistical tests on the subject-level ISC/ISFC values. We computed confidence intervals as 95%, random state as 1,000, and resampling iterations as 1,000 in this step and obtained group-level ROI-to-ROI p-values and mean ISC/ISFC values. For the group comparison, we conducted the Monte Carlo approximate permutation tests between the two groups (e.g., patients with stroke vs. normal controls, motor task vs. acupuncture task). False discovery rate (FDR) correction was used for multiple tests across the ROIs.

RESULTS

Resting-State ISC and ISFC

The patterns of ISC and ISFC across the ROIs in the patient and control groups were first observed. We generated the functional correlation matrix across all 22 ROIs (**Figure 4A**). The off-diagonal values in the matrix were time-series correlations between the ROIs. The diagonal values were correlations between subjects of one particular ROI (ISC). In the control group, the correlations varied and were distributed evenly, having more negative values than positive values. Statistical analysis of ISC showed that region A4ul_L was spontaneously activated in the control group ($p < 0.05$, FDR-corrected; **Figure 4C**). ISFC analysis showed several negative correlations between the ROIs in the control group ($p < 0.05$, FDR-corrected; **Figure 4D**): A1/2/3ulhf_L and A4ul_L, A1/2/3ulhf_L and A4t_R, A1/2/3ulhf_L and A6m_R, A1/2/3ulhf_R and A4t_R, A1/2/3ll_R and A4t_R, A1/2/3ll_R and A6m_R. These pairs were between the upper body sensory cortex, trunk motor and sensory cortex, and movement–imagination cortex, which indicated that there were only a few spontaneous negative connectivities in normal controls. In contrast, the ISFC matrix in the patient

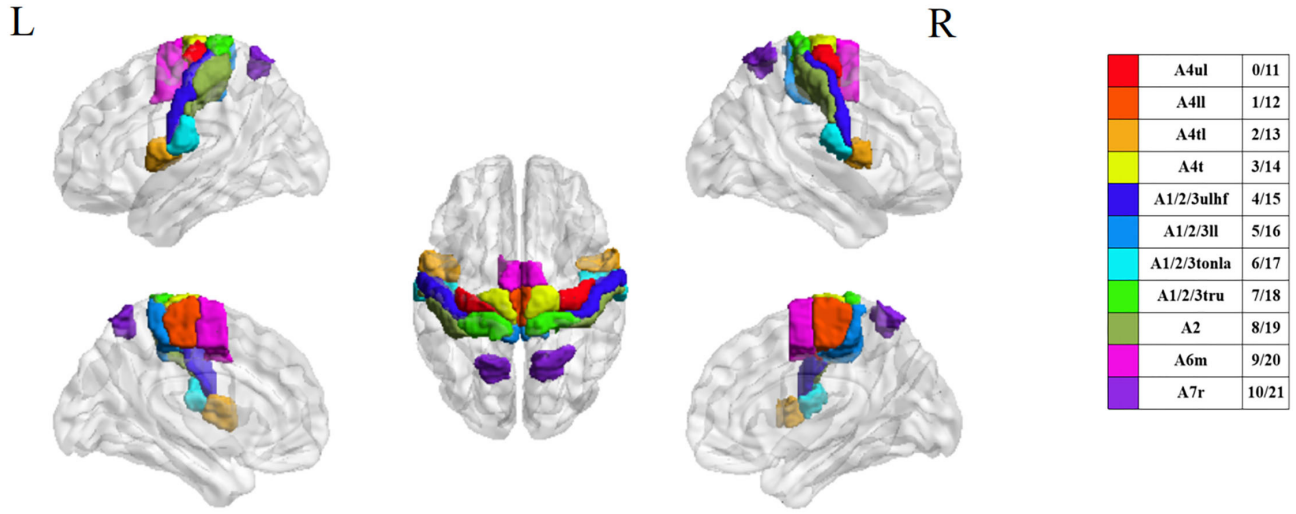

FIGURE 3 | ROI distribution.

group (**Figure 4B**) had a relatively consistent pattern of positive values. Notably, mild positive values were universal between the ROIs within the contralesional (left) hemisphere. Additionally, negative correlations were a handful and gentle across the matrix. There were no significant ROIs or ROI pairs found in the patient group by statistical analysis ($p > 0.05$, FDR-corrected). These findings proved that ISFC analysis could filter out individual and stimulus-unrelated neural signals. Furthermore, patients had less shared response between the regions than controls in the resting state.

Motor Task-Stimulated ISC and ISFC

Functional correlation matrices based on the motor task were observed in both groups (**Figures 5A,B**). The motor task triggered a large scope of responses in both groups. Patients with stroke and normal controls had high-level positive correlations between the ROIs in the ipsilesional (right) hemisphere, especially between A4ul_R, A1/2/3ulhf_R, A2_R, and A6m_R, which were hand-related sensorimotor and imagination cortices. Patients tended to have higher positive correlations among the ROIs in the ipsilesional hemisphere than normal controls except for regions A1/2/3ll_R and A7r_R, which had zero or negative values with others. Within the contralesional hemisphere, both groups had a similar pattern as in the resting state, having lower values among the ROIs. For the inter-hemisphere correlations, the two groups had similar patterns.

Statistical analysis demonstrated a substantial amount of significant ISCs and ISFCs ($p < 0.01$, FDR-corrected). In the ISC analysis, patients had a wider activation range than normal controls, with activated bilateral upper limb motor regions (A4ul_R, A4ul_L; **Figures 5C,D**). In ISFC analysis (**Figures 5E,F**), the findings were (1) most ROIs time series positively correlated with others within the ipsilesional hemisphere in both groups; (2) there was an equal amount of negative and positive correlations between the hemispheres in both groups. In contrast, in the control group, regions A4ul_L and A4ll_L tended to have many negative correlations with others, which were not seen in the patient group. Our study of ISCs and ISFCs during the motor task demonstrated that one-side passive thumb-index-finger opposition movement could activate shared positive correlations of sensorimotor cortices within the contralateral hemisphere and several negative correlations between the bilateral hemispheres. On comparing the groups, patients had more significant pairs within the contralateral side and more positive and less negative pairs between the bilateral upper/lower body ROIs. The differences we observed were in line with the common knowledge that disturbances after stroke not only occur in the vicinity of the lesion but also between remote cortical areas in the affected and unaffected hemispheres (33). Additionally, when we narrowed down the statistical p-value to $p < 0.001$ (FDR-corrected), the patient group retained almost entirely significant ISFCs from the level of $p < 0.01$ (**Figure 5G**), while the control group showed no significant values. The cortical functional connections under pathological conditions seemed to be more accordant.

Acupuncture Task-Stimulated ISC and ISFC

The acupuncture task demonstrated unique patterns of correlation distributions (**Figures 6A,B**), different from either the resting state or the motor task in both groups. In the control group, unlike in the motor task, the positive and negative values were distributed evenly within and between the hemispheres. Unlike in the resting state, more positive values were observed during the acupuncture procedure. Patients' ISFCs showed even distribution as well, differing from either the resting state (positive values within the unaffected hemisphere) or motor task (positive values within the affected hemisphere). The matrix of patients was visibly weaker than normal controls, which indicated that patients had slighter connectivity changes.

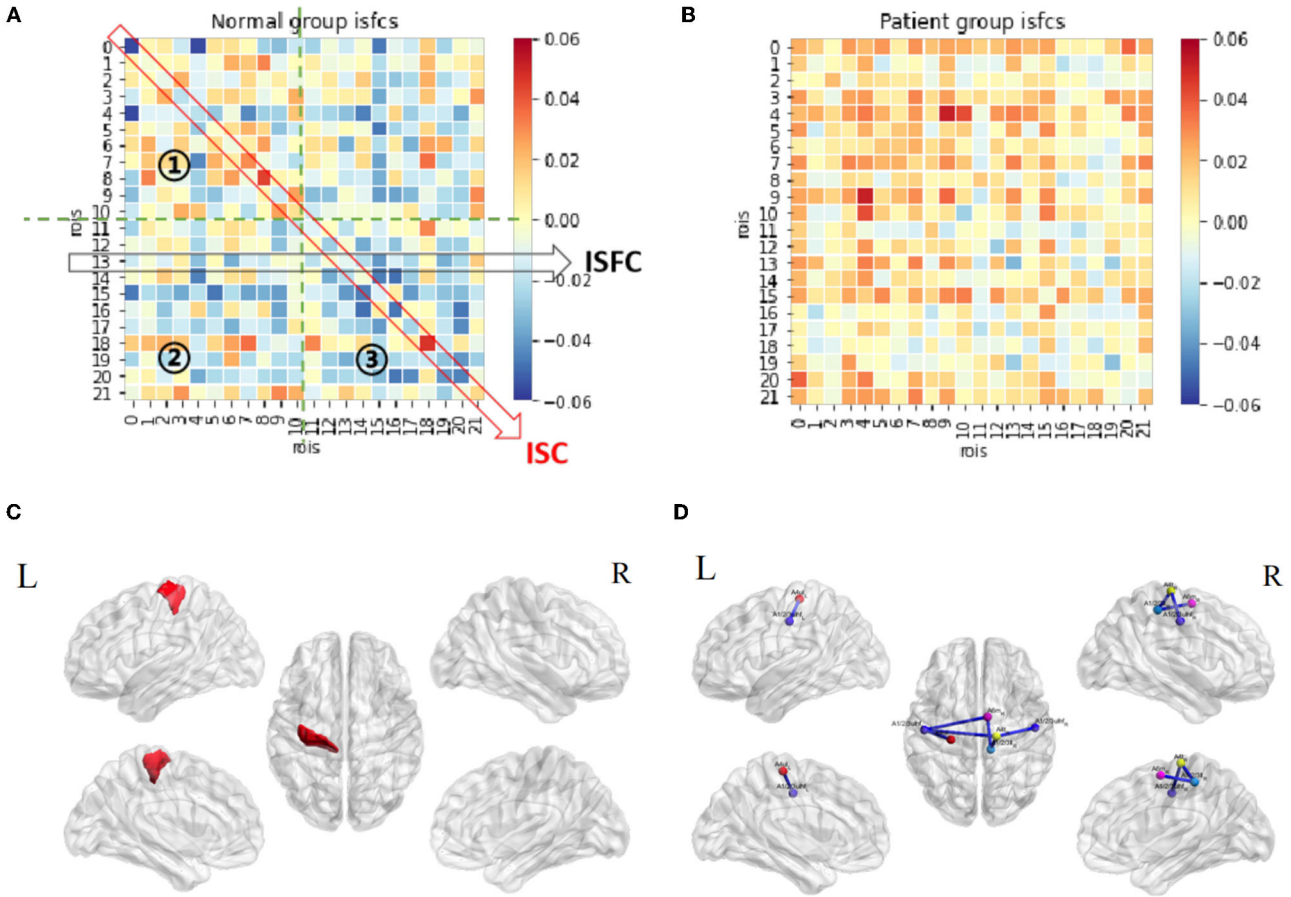

FIGURE 4 | Resting-state ISC and ISFC. **(A)** The ISFC matrix of 22 ROIs during resting state in the control group. The off-diagonal values represent intersubject functional correlations between ROIs, while the diagonal values represent intersubject correlation within each ROI. ①, ②, and ③ represent the area of contralesional hemisphere, between hemispheres, and ipsilesional hemisphere (the other matrices in this article follow this law). **(B)** ISFC matrix of 22 ROIs during resting state in the patient group. **(C)** Significant ROI at resting-state in the control group ($p < 0.05$, FDR-corrected). **(D)** Significant negative ISFCs (lines in blue) between ROIs in the control group ($p < 0.05$, FDR-corrected).

Statistical analysis in the control group showed that regions A1/2/3tonIa_L, A4tl_R, and A1/2/3tonIa_R were activated by acupuncture ($p < 0.05$, FDR-corrected; **Figure 6C**). Surprisingly, no significant ROI pairs appeared ($p > 0.05$, FDR-corrected). Although subjects had various responses and their tongue/larynx sensorimotor areas were activated during acupuncture, no synchronous functional correlation between the ROIs across all subjects existed. The significantly increased functionally connected pairs stimulated by acupuncture in patients were A1/2/3ulhf_L and A1/2/3ll_R, A1/2/3ll_L and A6m_R, and decreased pairs were A4ul_L and A1/2/3tonIa_L, A1/2/3ulhf_L and A7r_L, A7r_R and A1/2/3tonIa_L, A7r_R and A1/2/3ulhf_R (**Figure 6D**; $p < 0.05$, FDR-corrected). The regulation mainly occurred within the contralesional hemisphere and between the hemispheres.

By putting the significant maps during the motor and acupuncture tasks in patients with stroke side by side, we noticed a common trend of opposite activation of bilateral A7r with sensory regions. While the movement stimulus had a strong and targeted stimulation on the ROIs we obtained, immediate acupuncture stimulation at GB34 presented a relatively less, but comprehensive response. Comparison between the two tasks in both groups showed consistent higher correlations among ROI pairs (**Figures 6E,F**; $p < 0.01$, FDR-corrected). Thus, the motor task activated significantly more abundant connections than the acupuncture stimulus, especially in the affected hemisphere, whereas the negative correlations triggered by the two tasks were not significantly different.

Subgroup Analyses of Acupuncture Tasks in Patients

We performed a subgroup analysis based on the time course of stroke and neurological damage to further explore the cross-subject bilateral sensorimotor connections in patients with stroke during acupuncture. Subgroup characteristics are reported in **Table 3**.

Firstly, 63 patients were divided into 3 groups based on the course: group C1, within 0.5 month (16 subjects); group

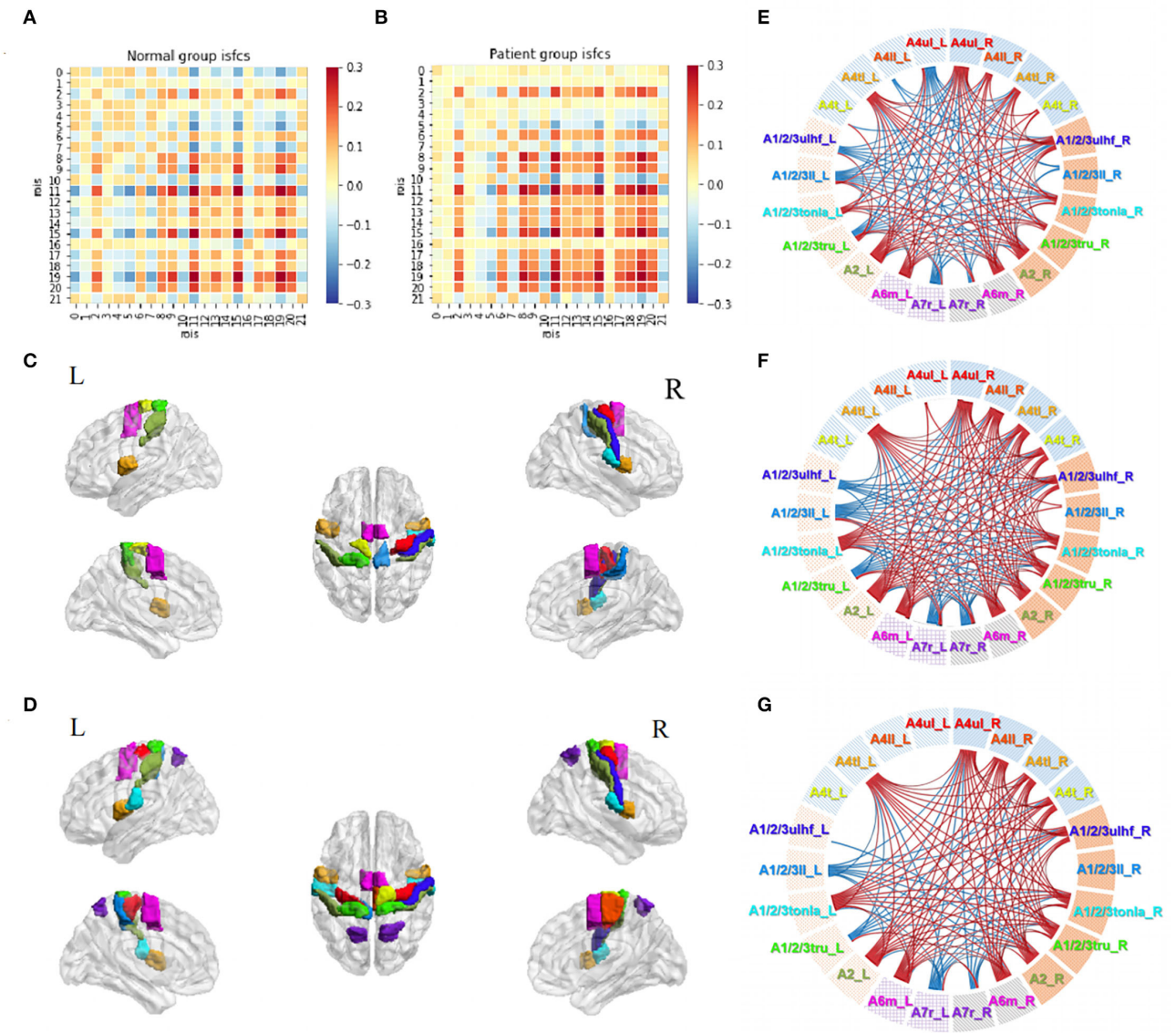

FIGURE 5 | Motor task-stimulated ISC and ISFC. **(A)** ISFC matrix of 22 ROIs during motor task in the control group. **(B)** ISFC matrix of 22 ROIs during motor task in the patient group. **(C)** Significantly stimulated ROIs in the control group ($p < 0.01$, FDR-corrected). **(D)** Significantly stimulated ROIs in the patient group ($p < 0.01$, FDR-corrected). **(E)** Significant positive (lines in red) and negative (lines in blue) ISFCs between ROIs in the control group ($p < 0.01$, FDR-corrected). **(F)** Significant ISFCs between ROIs in the patient group ($p < 0.01$, FDR-corrected). **(G)** Significant ISFCs between ROIs in the patient group ($p < 0.001$, FDR-corrected).

C2, 0.5–1 month (24 subjects); and group C3, 1–3 months (23 subjects). Correlations in three subgroups were stronger than themselves when calculated as a whole group. The connection degrees showed a trend of strong to weak distributions from group C1 to group C3 (**Figures 7A–C**). Significant activities in ROIs and ROI pairs were different across the groups ($p < 0.05$, FDR-corrected). Specifically, C1 group patients had their regions A4ul_R (ipsilesional upper limb motor area), A4tl_R, and A4tl_L (bilateral tongue/larynx motor area), A2_L, A6m_L, and A1/2/3tru_R activated by acupuncture (**Figure 7D**). ROI pairs in the contralesional hemisphere negatively correlated with each other. There were several positive pairs within the ipsilesional hemisphere and between the bilateral hemispheres (tongue/larynx sensorimotor area with the ipsilesional motor area and contralesional sensory area; **Figure 7F**). Group C2 patients had the activation at regions A4tl_L and A6m_R (**Figure 7E**). They showed numerous negative correlations over the ROI pairs. The majority of the correlations existed between the upper and lower body regions within the ipsilesional hemisphere and between the hemispheres. A few positive connections were observed between bilateral upper limb motor regions (A4ul_L and A4ul_R) and between A4ul_L, A4ul_R,

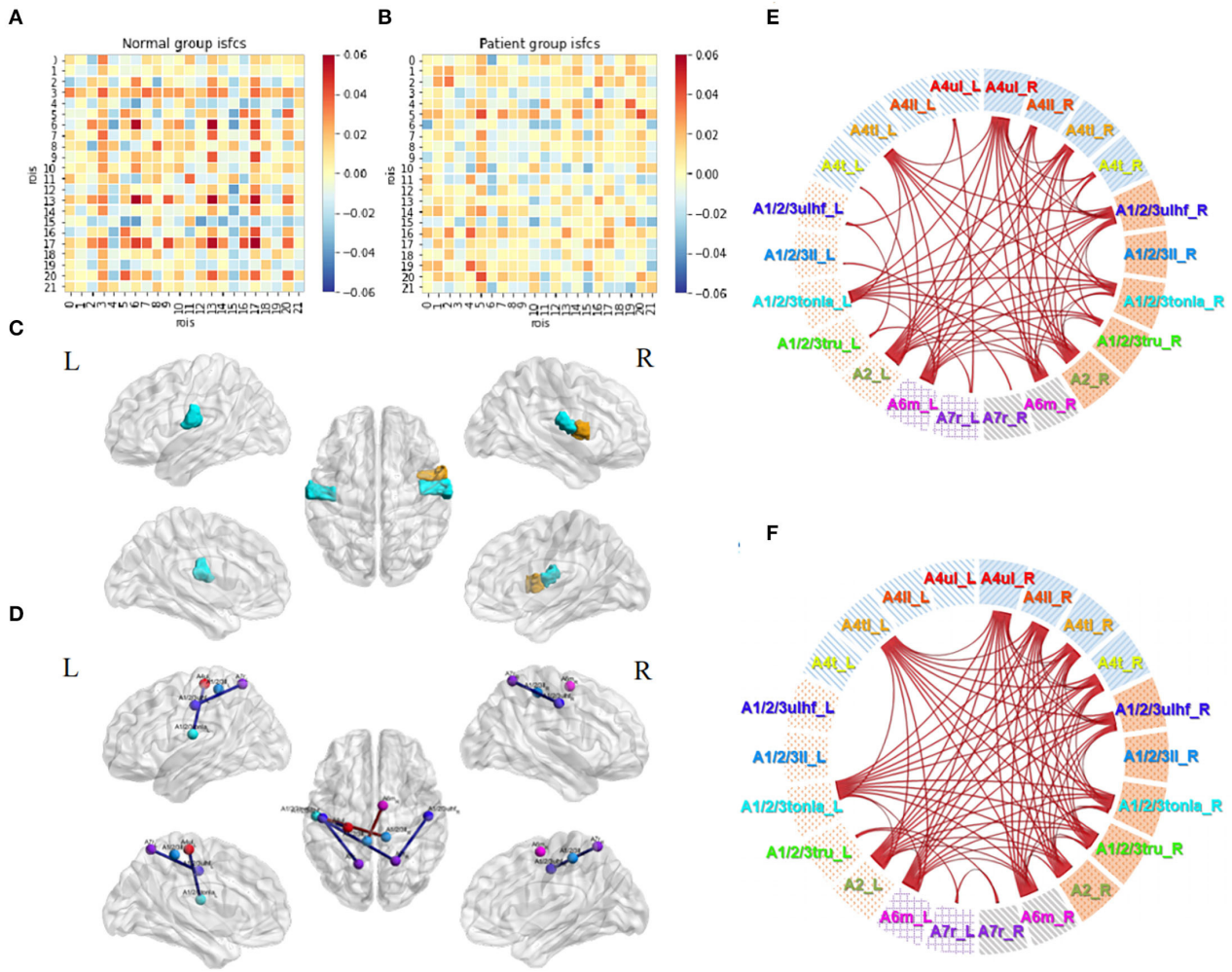

FIGURE 6 | Acupuncture task-stimulated ISC and ISFC. **(A)** ISFC matrix of 22 ROIs during acupuncture task in the control group. **(B)** ISFC matrix of 22 ROIs during acupuncture task in the patient group. **(C)** Significant ROIs in the control group during acupuncture ($p < 0.05$, FDR-corrected). **(D)** Significant positive (lines in red) and negative (line in blue) ISFCs during acupuncture in the patient group ($p < 0.05$, FDR-corrected). **(E)** Significant ISFCs between motor task vs. acupuncture task in the control group ($p < 0.01$, FDR-corrected). **(F)** Significant ISFCs between motor task vs. acupuncture task in the patient group ($p < 0.01$, FDR-corrected).

and A4tl_L, and other regions (**Figure 7G**). Group C3 presented no significant ISC and much fewer significant ISFCs than the other two groups (**Figure 7H**). Positive correlations existed between ipsilesional lower limb and tongue and larynx, A6m_R and A1/2/3ll_L, and A6m_R and A4tl_R. Negative correlations existed mostly between the ipsilesional upper limb sensory area (A1/2/3ulhf_R) and contralesional cortices. Comparison among the subgroups demonstrated that stronger correlations existed in group C1 vs. group C2 (**Figure 7I**; $p < 0.05$, FDR-corrected). In conclusion, patients obtained strong and various stimulation by acupuncture at GB34 within 0–0.5 and 0.5–1 month, while fewer responses were activated by acupuncture after 1 month.

Then, we divided the patients into three subgroups based on NIHSS severity: group Nih1 with NIHSS score of 0–1 (nearly no neural dysfunction, 18 subjects); group Nih2 with NIHSS score of 2–4 (mild dysfunction, 21 subjects); and group Nih3 with NIHSS score of 5–15 (moderate dysfunction, 24 subjects). The number and degree of the positive ISFCs decreased from the group Nih1 to Nih3 within the contralesional hemisphere and bilateral hemispheres and increased within the ipsilesional side (**Figures 8A–C**). Statistical analysis ($p < 0.05$, FDR-corrected) showed that the upper limb motor cortex on the unaffected side (A4ul_L) was significantly activated across the subjects in the group Nih1 (**Figure 8D**). Significant positive functional connectivities were mainly within bilateral upper/lower limb motor, trunk sensory, and holistic sensory regions (**Figure 8F**). A4ll_L, A1/2/3tonIa_L, A4tl_R, and A7r_R were activated by acupuncture in the group Nih2 (**Figure 8E**). The numerous significant positive connections mainly occurred within the unaffected side and between the sides. Negative correlations were mostly seen between the hemispheres (**Figure 8G**). In contrast, the group Nih3 showed only a few significant ISFCs involving

TABLE 3 | Demographic features and clinical data of subgroup patients.

Subgroup	Number	Sex (male/female)	Age (year)	Course (day)	NIHSS
C1	16	13 / 3	57.44 ± 11.10	8.81 ± 3.17	3.44 ± 2.94
C2	24	14 / 10	59.21 ± 9.99	20.54 ± 4.16	3.38 ± 3.57
C3	23	16 / 7	61.39 ± 8.76	47 ± 11.68	4.52 ± 2.92
Nih1	18	12 / 6	55.56 ± 6.56	22.28 ± 16.68	0.44 ± 0.51
Nih2	21	17 / 4	61.48 ± 9.11	24.38 ± 14.18	2.9 ± 0.77
Nih3	24	14 / 10	60.88 ± 11.76	33.42 ± 19.52	7.13 ± 2.37

Enumeration data are presented as mean ± standard deviation. No significant different NIHSS scores were detected among subgroup C (ANOVA, $p > 0.05$). No significant different course was detected among subgroup Nih (ANOVA, $p > 0.05$).

the tongue and larynx area and the affected upper/lower limb motor area. Positive values mainly existed within the ipsilesional side (**Figure 8H**). Group comparison found numerous higher correlations in the contralesional side in the Nih1 group vs. the Nih3 group (**Figure 8I**) and between the hemispheres in the Nih2 group vs. the Nih3 group (**Figure 8J**). These results indicated that more and stronger isochronous connections existed in patients with lighter neural damage during acupuncture.

DISCUSSION

ISC and ISFC Analyses

The ISC/ISFC analysis is a promising approach. Unlike GLM, which requires setting up *a priori* hypothetical model, the ISC/ISFC analysis provides a data-driven solution. It filters out intrinsic correlations and noise, revealing the mechanisms of brain effects induced by the task (34). Currently, this method is mostly applied to analyze fMRI data during complex stimulation or tasks. It has been proved to have less noise by previous studies (24). Current studies on the neural mechanisms of acupuncture include the effects of different experimental designs, acupuncture manipulation modality, and acupoint specificity in healthy individuals or patients. Due to the different limitations of the studies, results are often heterogeneous (35). The ISC/ISFC method, by linking the individual's brain activity to group-level activities, weakens the specificity of subjects and focuses more on the common changes induced by stimuli or tasks, making the results relatively reliable. In this study, the ISC/ISFC method was applied to describe the impaired functional activations in patients with stroke modulated by acupuncture for the first time.

Patient Specificity

We observed huge differences in sensorimotor cortex neuroactivities during 3 fMRI runs in patients with stroke vs. normal controls. After cerebral infarction at the motor pathway, the inhibition and activation of the affected hemisphere and motor-related brain areas showed a pathological process of unilateral instability and bilateral compensation. Compared to the negative functional connectivity status at resting state in healthy subjects, patients with stroke presented positive ISFC across all ROIs, especially within the unaffected hemisphere. Research has shown that the left passive motor task activated the healthy subject's right primary sensory cortex, primary motor cortex, and somatosensory motor area (36). Based on the BN template, we described the activated regions more precisely with similar results in the control group. However, patients had a wider range of responses than normal controls. Additionally, the negative functional connectivity between the contralesional upper and lower limb motor cortex and other regions disappeared in patients compared with normal controls. Previous studies have shown that ipsilesional corticomotor excitability was initially suppressed but increased over time, brain area activation in the affected hemisphere was reduced, and activation in the unaffected hemisphere was increased after cerebral infarction (37). The impairment caused contralateral motor impairment and inter-hemispheric imbalance due to the contralesional hemisphere hyperexcitability (38). Our results agreed with this research in that the infarction increased the excitability in the contralesional motor cortices and disabled the suppression effects between the bilateral cortices. After needling at GB34, we observed broad correlation changes and significant activation at the bilateral tong/larynx area but no significant increased or decreased functional connectivity in the healthy group. A previous study has found that acupuncture at GB34 in healthy volunteers enhanced regional homogeneity (ReHo) in the right inferior parietal lobule and right frontal gyrus and reduced ReHo in the left inferior frontal gyrus (39). Our results showed trends of intersubject activation and suppression among the bilateral sensorimotor cortices stimulated by acupuncture; however, no significant between-region effects were detected. In patients with stroke, acupuncture significantly increased and decreased the ISFCs within the bilateral sensory areas, and between sensory areas and movement-imagination areas, respectively. The results in the patients agreed with previous research. The acupuncture stimulus may have individual irritants in healthy subjects rather than the common regulating effects we observed in hemiplegic patients with stroke.

Acupuncture Effect

We designed the motor task as a reference task to explore the similar and diverse neural response patterns stimulated by acupuncture across patients or normal controls. Acupuncture triggered unique responses in the sensorimotor cortex in post-stroke hemiplegia patients. Our results showed that functional connectivities between regions A1/2/3ulhf_L and A1/2/3ll_R, A1/2/3ll_L and A6m_R increased, and A4ul_L and A1/2/3tonIa_L, A1/2/3ulhf_L and A7r_L, A7r_R

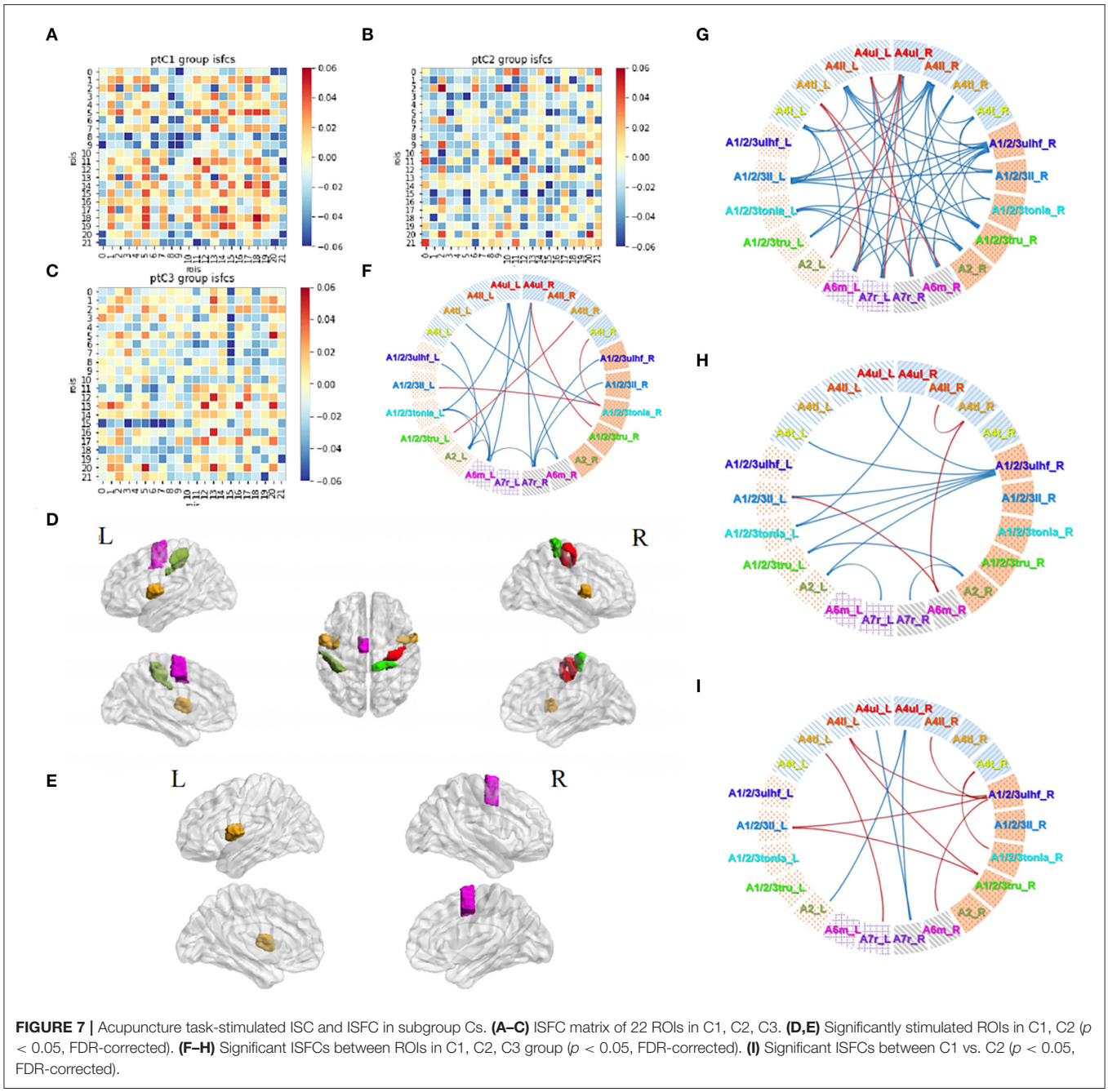

FIGURE 7 | Acupuncture task-stimulated ISC and ISFC in subgroup Cs. **(A–C)** ISFC matrix of 22 ROIs in C1, C2, C3. **(D,E)** Significantly stimulated ROIs in C1, C2 ($p < 0.05$, FDR-corrected). **(F–H)** Significant ISFCs between ROIs in C1, C2, C3 group ($p < 0.05$, FDR-corrected). **(I)** Significant ISFCs between C1 vs. C2 ($p < 0.05$, FDR-corrected).

and A1/2/3tonIa_L, A7r_R and A1/2/3ulhf_R decreased during the acupuncture stimulation. Previous studies of conventional FC analyses have proven that motor disorders were associated with functional connectivity abnormalities in the sensorimotor cortex in patients with stroke (40). Additionally, studies have shown that acupuncture on one side could stimulate bilateral regions (41) and increase the sensorimotor network functional connectivity in humans (42) and rats (43). Research has also shown that acupuncture increases the pain-related connectivity in the sensorimotor network after ischemic stroke or inhibits neural inflammation in the sensorimotor cortex (44, 45). A meta-analysis collected by the BN research team (29) has demonstrated that regions A1/2/3tonIa_L and A7r_L/A7r_R were involved in pain monitoring/discrimination and spatial/location discrimination, respectively. Our results indicated that the mechanism of acupuncture at GB34 in patients with stroke might include sensorimotor cortices and probably act through pain and discrimination-related responses.

Few studies have set a motor task as control of the acupuncture task. However, in Traditional Chinese Medicine theory, both procedures were used to regulate "qi" and

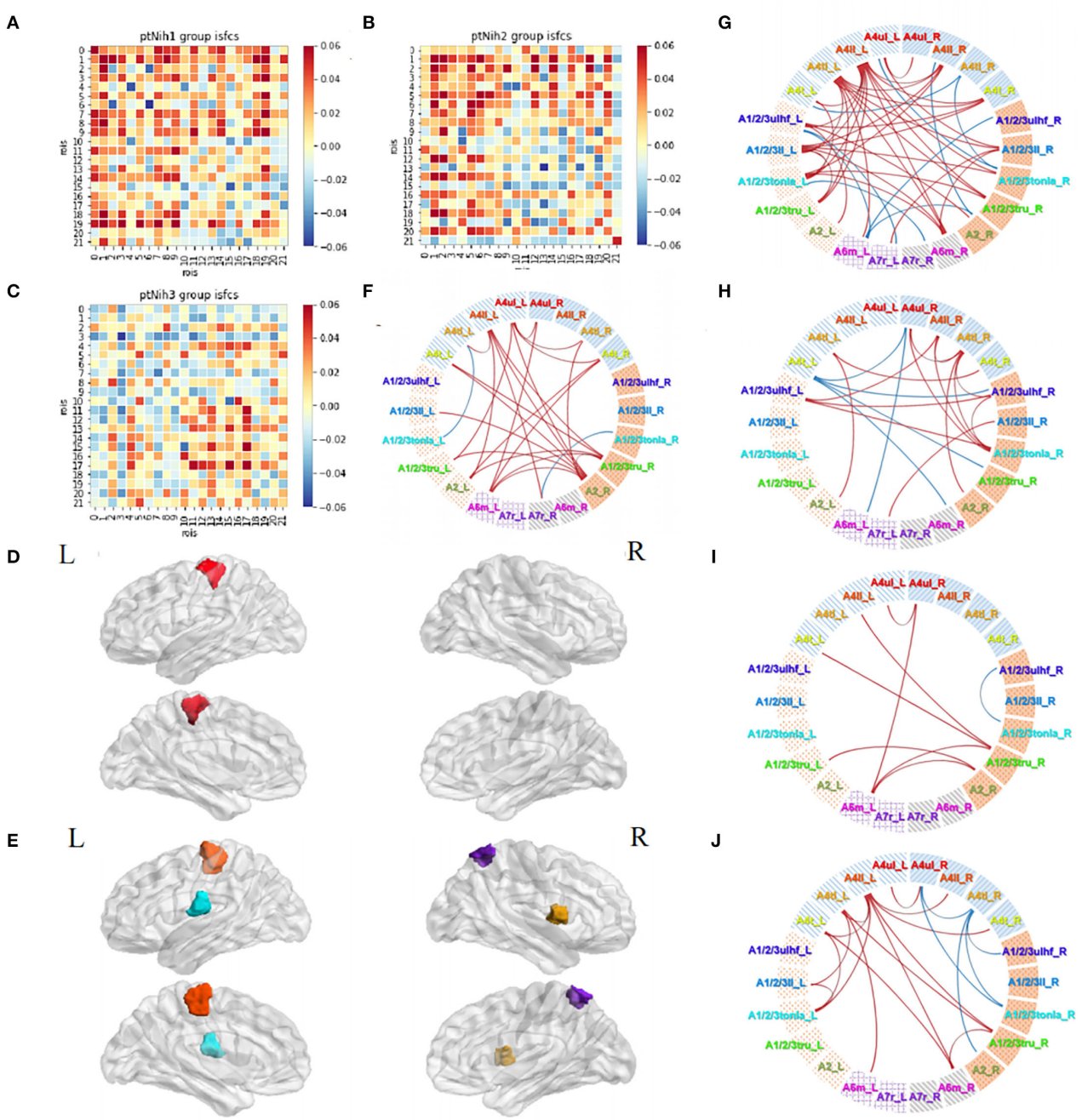

FIGURE 8 | Acupuncture task-stimulated ISC and ISFC in subgroup Nihs. **(A–C)** ISFC matrix of 22 ROIs in Nih1, Nih2, and Nih3. **(D,E)** Significantly stimulated ROI in Nih1, Nih2 ($p < 0.05$, FDR-corrected). **(F–H)** Significant ISFCs in Nih1, Nih2, Nih3 group ($p < 0.05$, FDR-corrected). **(I)** Significant ISFCs between Nih1 vs. Nih3 ($p < 0.05$, FDR-corrected). **(J)** Significant ISFCs between Nih2 vs. Nih3 ($p < 0.05$, FDR-corrected).

"blood" circulation, contracting or relaxing muscles and meridians. We discovered wide-range distributions of positive ISFCs among the ROIs in the motor task vs. acupuncture. Yet, no negative values existed in the comparison map. Acupuncture may produce slighter upregulated but even downregulated stimulation compared with motor rehabilitation methods.

Patients' Subgroup Acupuncture Effect

Subgroup calculations presented diverse features of acupuncture stimulus. Patients at the early stage of recovery (within 0.5 month) presented activation mainly in the ipsilesional motor cortex (A4ul_R) and bilateral tongue/larynx motor regions, along with negative correlations within the contralesional hemisphere. At this stage, acupuncture mainly activated the functional

correlations within the affected side and between the bilateral sides (the C1 group vs. the C2 group showed positive ISFCs). From 0.5–1 month, patients developed activation in A4tl_L and A6m_R. Noticeably, patients generated significant positive correlations between the bilateral upper limb motor cortices (A4ul_R and A4ul_L) and many other negative connections between the bilateral hemispheres. Acupuncture precisely activated the bilateral upper limb regions but suppressed the widespread overreacted connections within and across the hemisphere. As the course prolonged (1–3 months), negative connections evidently reduced, with several bilateral connections between the upper body sensory cortex and other regions and a small number of positive correlations. Patients at this stage tend to have relatively smooth conditions and slow motor improvements. The acupuncture effects became personalized and lost their track from the ISFC map.

Neuroplasticity plays a crucial role during the recovery process of patients with stroke. Reorganization may be the principal process responsible for post-stroke recovery. Previous research has shown that ipsilesional corticomotor excitability was initially suppressed and increased over time in patients with stroke (37). Longitudinal studies have shown that the resting-state functional connectivity between the bilateral sensorimotor cortices decreased in the early stage and then increased in a few weeks or months during the motor recovery in patients with stroke (46, 47). In studies that performed seed-based analyses on the primary motor cortex (M1) area, the results have revealed that acupuncture increased functional connectivity between the left M1 and right M1 along with the premotor cortex (PMC), supplementary motor area (SMA), thalamus, and cerebellum (48, 49). Several Chinese clinical trials have demonstrated that patients tended to receive better motor recovery with earlier involvement in acupuncture therapy [including GB34; (50–52)]. However, no study has focused on the immediate effects of acupuncture in different time courses of ischemic stroke. Our results agreed with previous findings and identified more patterns than before. The distinct responses we observed in the subgroup Cs may be related to the pathological features of the sensorimotor cortex during motor recovery.

Visualizing the data from another angle by the severity of neural dysfunction, we found a majority of intersubject positive correlations among all three subgroups. Patients with nearly no functional damage tended to have less increased and decreased connections within the contralesional hemisphere and between the bilateral hemispheres, while patients with mild functional damage (NIHSS 2–4) had the most and strongest activation within the contralesional hemisphere and between the bilateral hemispheres. The focal regions, the contralesional upper and lower limb cortex (A4ul_L and A4ll_L) were respectively activated across the patients in the subgroups Nih1 and Nih2. Surprisingly, patients with moderate neural damage (NIHSS 5–15) activated fewer connections by acupuncture. Acupuncture generates fewer effects in the sensorimotor cortex under serious conditions.

Changes in connectivity of brain regions and between the bilateral primary sensory cortices have been significantly correlated with changes in NIHSS (53, 54). One study (55) has demonstrated that patients with an Action Research Arm Test score of 29–57 (mildly to moderately affected) presented lower connectivities in the sensorimotor network than patients with a score of 0–28 (severely affected), indicating that patients with stroke had different resting-state connectivity patterns according to severity levels. One clinical trial has found that after 10 days of acupuncture therapy, patients in the mild to moderate motor deficit group presented significantly increased functional connectivity between bilateral M1s, while the severe group had no significant change between bilateral M1s (56). Another research (57) that has focused on the immediate effects of acupuncture on the affected side-GB34 found a different enhanced and reduced response pattern of connectivity between bilateral M1, dorsal premotor cortex (PMd), and ventral premotor cortex (PMv) between the mild to moderate and severe motor deficit groups. Our findings of acupuncture effects in different subgroups by NIHSS scores may be accompanied by the characteristics of neuroplasticity (58).

Limitations

In this study, we observed the immediate acupuncture effect at one acupoint, GB34. Although GB34 is an important acupoint in Traditional Chinese Medicine theory and alternative therapy for motor dysfunction treatment, studies have testified different effects caused by diverse acupoints. Our study provided a perspective to explore the complex mechanisms of acupuncture therapy.

We have noticed that both subgroup analyses showed distinct results from the whole patient group analysis. One reason that may explain this difference is that some of the acupuncture effects were hidden during the ISFC calculation in the whole patient group. With more homogeneity background (similar stroke time or neural damage), the patients tend to have more common reacting models to acupuncture. Another reason could be the narrowed sample size of the subgroups. One publication (59) has suggested that with 20 subjects, on average, the ISC statistics had converged close to a large sample ISC statistics with 130 subjects, however, in healthy subjects. This was the first-time application of ISFC analysis in patients with stroke. Thus, we were unsure about the reliable sample size. There should be more influence factors to consider in the further exploration.

CONCLUSION

We innovatively applied ISFC approach to analyze the immediate effects of acupuncture at GB34 in sensorimotor-related cortices in post-stroke patients with motor dysfunction and normal controls. The ISFC analysis could filter out noise during the resting state. We observed special correlation patterns in patients apart from normal controls in all functional runs. Compared with the resting state and motor task results, we found that the acupuncture task triggered ISFC among the upper limb motor region, upper limb/hand/face, lower limb, and tongue/larynx sensory regions, and movement imagination regions in the patient group. The subgroup ISC and ISFC

analyses of patients' acupuncture tasks showed how acupuncture stimulation changed according to disease progression and condition. Patients tended to have increased responses in the early stage of stroke (within 1 month) and decreasing responses afterward (1–3 months). Patients with mild clinical functional damage (NIHSS 2–4) tended to generate more responses *via* acupuncture than those with moderate damage (NIHSS 5–15). Our findings may help understand the clinical effects and modulatory features of acupuncture based on group-level post-stoke neuroplasticity.

The challenge we are facing is to learn more about the mechanisms of plasticity and the characteristics of acupuncture to be able to modulate them to obtain the best rehabilitation efficacy for patients with post-stroke hemiplegia. In the future, such analyses of cross-subject studies could help to optimize acupuncture regimens based on the common features under particular patients' conditions, thereby ensuring the expectations based on the possible response and outcome.

DATA AVAILABILITY STATEMENT

The raw data supporting the conclusions of this article will be made available by the authors, without undue reservation.

ETHICS STATEMENT

The studies involving human participants were reviewed and approved by the Ethics Committee of Dongzhimen Hospital, Beijing University of Chinese Medicine. The patients/participants provided their written informed consent to participate in this study.

AUTHOR CONTRIBUTIONS

YuW and LW were involved in literature search, data analyses, and writing of the manuscript. YaW and ML contributed to the experimental design. LX and RL contributed to the subjects' recruitment. JWe and JWa were involved in clinical diagnosis for patients with stroke and NIHSS evaluations. HZ designed the study approaches and consulted through the study. YZ designed the study protocol and sought funding. All authors read and approved the final manuscript.

FUNDING

This work was supported by grants from the National Natural Science Foundation of China (Nos. 81873257 and 81473667).

ACKNOWLEDGMENTS

The authors would like to thank the Natural Scientific Foundation of China for its financial support. We thank the Brainnetome Atlas, fMRIPrep, and BrainIAK software for the free usage. We thank Dr. Kun Ou from the University of Hong Kong for the English writing guidance. This manuscript was edited for the English Language by Charlesworth Author Services (www.cwauthors.com).

SUPPLEMENTARY MATERIAL

The Supplementary Material for this article can be found online at: https://www.frontiersin.org/articles/10.3389/fneur.2022.900520/full#supplementary-material

REFERENCES

1. GBD 2019 Stroke Collaborators. Global, regional, and national burden of stroke and its risk factors, 1990-2019: a systematic analysis for the Global Burden of Disease Study 2019. *Lancet Neurol.* (2021) 20:795–820. doi: 10.1016/S1474-4422(21)00252-0
2. Brainin M, Feigin VL, Norrving B, Martins SCO, Hankey GJ, Hachinski V. Global prevention of stroke and dementia: the WSO Declaration. *Lancet Neurol.* (2020) 19:487–8. doi: 10.1016/S1474-4422(20)30141-1
3. Norrving B, Barrick J, Davalos A, Dichgans M, Cordonnier C, Guekht A. Action plan for stroke in Europe 2018-2030. *Eur Stroke J.* (2018) 3:309–36. doi: 10.1177/2396987318808719
4. Cheatwood JL, Emerick AJ, Kartje GL. Neuronal plasticity and functional recovery after ischemic stroke. *Top Stroke Rehabil.* (2008) 15:42–50. doi: 10.1310/tsr1501-42
5. Yourganov G, Stark BC, Fridriksson J, Bonilha L, Rorden C. Effect of stroke on contralateral functional connectivity. *Brain Connect.* (2021) 11:543–52. doi: 10.1089/brain.2020.0901
6. Mekbib DB, Zhao Z, Wang J, Xu B, Zhang L, Cheng R. Proactive motor functional recovery following immersive virtual reality-based limb mirroring therapy in patients with subacute stroke. *Neurotherapeutics.* (2020) 17:1919–30. doi: 10.1007/s13311-020-00882-x
7. Cassidy JM, Mark JI, Cramer SC. Functional connectivity drives stroke recovery: shifting the paradigm from correlation to causation. *Brain.* (2021) 2021:awab469. doi: 10.1093/brain/awab469
8. Chen J, Sun D, Zhang S, Shi Y, Qiao F, Zhou Y. Effects of home-based telerehabilitation in patients with stroke: a randomized controlled trial. *Neurology.* (2020) 95:e2318–30. doi: 10.1212/WNL.0000000000010821
9. Micera S, Caleo M, Chisari C, Hummel FC, Pedrocchi A. Advanced neurotechnologies for the restoration of motor function. *Neuron.* (2020) 105:604–20. doi: 10.1016/j.neuron.2020.01.039
10. Fang Q, Mahmoud SS, Gu X, Fu J. A novel multistandard compliant hand function assessment method using an infrared imaging device. *IEEE J Biomed Health Inform.* (2019) 23:758–65. doi: 10.1109/JBHI.2018.2837380
11. Villafane JH, Taveggia G, Galeri S, Bissolotti L, Mulle C, Imperio G, et al. Efficacy of short-term robot-assisted rehabilitation in patients with hand paralysis after stroke: a randomized clinical trial. *Hand.* (2018) 13:95–102. doi: 10.1177/1558944717692096
12. Askim T, Indredavik B, Haberg A. Internally and externally paced finger movements differ in reorganization after acute ischemic stroke. *Arch Phys Med Rehabil.* (2010) 91:1529–36. doi: 10.1016/j.apmr.2010.07.217
13. Candon M, Nielsen A, Dusek JA. Trends in insurance coverage for acupuncture, 2010–2019. *J Am Med Assoc Netw Open.* (2022) 5:e2142509. doi: 10.1001/jamanetworkopen.2021.42509
14. NIH Consensus Conference. Acupuncture. *J Am Med Assoc.* (1998) 280:1518–24. doi: 10.1001/jama.280.17.1518
15. Zhang S, Wu B, Liu M, Li N, Zeng X, Liu H, et al. Acupuncture efficacy on ischemic stroke recovery: multicenter randomized controlled trial in China. *Stroke.* (2015) 46:1301–6. doi: 10.1161/STROKEAHA.114.007659
16. Xu M, Li D, Zhang S. Acupuncture for acute stroke. *Cochrane Database Syst Rev.* (2018) 3:CD003317. doi: 10.1002/14651858.CD003317.pub3

17. Lv Q, Xu G, Pan Y, Liu T, Liu X, Miao L. Effect of acupuncture on neuroplasticity of stroke patients with motor dysfunction: a meta-analysis of fMRI studies. *Neural Plast.* (2021) 2021:8841720. doi: 10.1155/2021/8841720
18. Zhang J, Lu C, Wu X, Nie D, Yu H. Neuroplasticity of acupuncture for stroke: an evidence-based review of MRI. *Neural Plast.* (2021) 2021:2662585. doi: 10.1155/2021/2662585
19. Yang ZX, Xie JH, Liu DD. Xingnao Kaiqiao needling method for acute ischemic stroke: a meta-analysis of safety and efficacy. *Neural Regen Res.* (2017) 12:1308–14. doi: 10.4103/1673-5374.213551
20. Zhang J, Li Z, Li Z, Li J, Hu J, Xu QJ, et al. Progress of acupuncture therapy in diseases based on magnetic resonance image studies: a literature review. *Front Hum Neurosci.* (2021) 15:694919. doi: 10.3389/fnhum.2021.694919
21. Chen X, Zhang H, Zou YH. A functional magnetic resonance imaging study on the effect of acupuncture at GB34 (Yanglingquan) on motor-related network in hemiplegic patients. *Brain Res.* (2015) 1601:64–72. doi: 10.1016/j.brainres.2015.01.011
22. Ning YZ, Li KS, Fu CH, Ren Y, Zhang Y, Liu HW, et al. Enhanced functional connectivity between the bilateral primary motor cortices after acupuncture at yanglingquan (GB34) in right-hemispheric subcortical stroke patients: a resting-state fMRI study. *Front Hum Neurosci.* (2017) 11:178. doi: 10.3389/fnhum.2017.00178
23. Nastase SA, Gazzola V, Hasson U, Keysers C. Measuring shared responses across subjects using intersubject correlation. *Soc Cogn Affect Neurosci.* (2019) 14:667–85. doi: 10.1093/scan/nsz,037
24. Simony E, Honey CJ, Chen J, Lositsky O, Yeshurun Y, Wiesel A. Dynamic reconfiguration of the default mode network during narrative comprehension. *Nat Commun.* (2016) 7:12141. doi: 10.1038/ncomms12141
25. Pajula J, Kauppi JP, Tohka J. Inter-subject correlation in fMRI: method validation against stimulus-model based analysis. *PLoS ONE.* (2012) 7:e41196. doi: 10.1371/journal.pone.0041196
26. Wen Z, Yu T, Yang X, Li Y. Goal-directed processing of naturalistic stimuli modulates large-scale functional connectivity. *Front Neurosci.* (2018) 12:1003. doi: 10.3389/fnins.2018.01003
27. Bolton TAW, Jochaut D, Giraud AL, Van De Ville D. Dynamic inter-subject functional connectivity reveals moment-to-moment brain network configurations driven by continuous or communication paradigms. *J Vis Exp.* (2019) 2019:59083. doi: 10.3791/59083
28. Bolton TAW, Jochaut D, Giraud AL, Van De Ville D. Brain dynamics in ASD during movie-watching show idiosyncratic functional integration and segregation. *Hum Brain Mapp.* (2018) 39:2391–404. doi: 10.1002/hbm.24009
29. Fan L, Li H, Zhuo J, Zhang Y, Wang J, Chen L, et al. The human brainnetome atlas: a new brain atlas based on connectional architecture. *Cereb Cortex.* (2016) 26:3508–26. doi: 10.1093/cercor/bhw157
30. Chinese Neurology Branch of Medical Association CDG, Neurology Branch, and Chinese Medical Association. Chinese guidelines for the diagnosis and treatment of acute ischemic stroke. *Chin J Neurol.* (2015) 48:12. doi: 10.3760/cma.j
31. Cramer SC, Mark A, Barquist K, Nhan H, Stegbauer KC, Price R. Motor cortex activation is preserved in patients with chronic hemiplegic stroke. *Ann Neurol.* (2002) 52:607–16. doi: 10.1002/ana.10351
32. Esteban O, Markiewicz CJ, Blair RW, Moodie CA, Isik AI, Erramuzpe A. fMRIPrep: a robust preprocessing pipeline for functional MRI. *Nat Methods.* (2019) 16:111–6. doi: 10.1038/s41592-018-0235-4
33. Rehme AK, Grefkes C. Cerebral network disorders after stroke: evidence from imaging-based connectivity analyses of active and resting brain states in humans. *J Physiol.* (2013) 591:17–31. doi: 10.1113/jphysiol.2012.243469
34. Kauppi JP, Pajula J, Tohka J. A versatile software package for inter-subject correlation based analyses of fMRI. *Front Neuroinform.* (2014) 8:2. doi: 10.3389/fninf.2014.00002
35. He T, Zhu W, Du SQ, Yang JW, Li F, Yang BF. Neural mechanisms of acupuncture as revealed by fMRI studies. *Auton Neurosci.* (2015) 190:1–9. doi: 10.1016/j.autneu.2015.03.006
36. Nasrallah FA, Mohamed AZ, Campbell ME, Yap HK, Yeow CH, Lim JH. Functional connectivity of brain associated with passive range of motion exercise: proprioceptive input promoting motor activation? *Neuroimage.* (2019) 202:116023. doi: 10.1016/j.neuroimage.2019.116023
37. Stinear CM, Petoe MA, Byblow WD. Primary motor cortex excitability during recovery after stroke: implications for neuromodulation. *Brain Stimul.* (2015) 8:1183–90. doi: 10.1016/j.brs.2015.06.015
38. Dodd KC, Nair VA, Prabhakaran V. Role of the contralesional vs. ipsilesional hemisphere in stroke recovery. *Front Hum Neurosci.* (2017) 11:469. doi: 10.3389/fnhum.2017.00469
39. Liu L, Chen S, Zeng D, Li H, Shi C, Zhang L. Cerebral activation effects of acupuncture at Yanglinquan (GB34) point acquired using resting-state fMRI. *Comput Med Imaging Graph.* (2018) 67:55–8. doi: 10.1016/j.compmedimag.2018.04.004
40. Liu H, Tian T, Qin W, Li K, Yu C. Contrasting evolutionary patterns of functional connectivity in sensorimotor and cognitive regions after stroke. *Front Behav Neurosci.* (2016) 10:72. doi: 10.3389/fnbeh.2016.00072
41. Chen SQ, Cai DC, Chen JX, Yang H, Liu LS. Altered brain regional homogeneity following contralateral acupuncture at Quchi (LI 11) and Zusanli (ST 36) in ischemic stroke patients with left hemiplegia: an fMRI study. *Chin J Integr Med.* (2020) 26:20–5. doi: 10.1007/s11655-019-3079-6
42. Cai RL, Shen GM, Wang H, Guan YY. Brain functional connectivity network studies of acupuncture: a systematic review on resting-state fMRI. *J Integr Med.* (2018) 16:26–33. doi: 10.1016/j.joim.2017.12.002
43. Li Z, Yang M, Lin Y, Liang S, Liu W, Chen B, et al. Electroacupuncture promotes motor function and functional connectivity in rats with ischemic stroke: an animal resting-state functional magnetic resonance imaging study. *Acupunct Med.* (2021) 39:146–55. doi: 10.1177/0964528420920297
44. Liu P, Qin W, Zhang Y, Tian J, Bai L, Zhou G, et al. Combining spatial and temporal information to explore function-guide action of acupuncture using fMRI. *J Magn Reson Imaging.* (2009) 30:41–6. doi: 10.1002/jmri.21805
45. Liu W, Wang X, Yang S, Huang J, Xue X, Zheng Y. Electroacupuncture improves motor impairment *via* inhibition of microglia-mediated neuroinflammation in the sensorimotor cortex after ischemic stroke. *Life Sci.* (2016) 151:313–22. doi: 10.1016/j.lfs.2016.01.045
46. Golestani AM, Tymchuk S, Demchuk A, Goodyear BG, Group VS. Longitudinal evaluation of resting-state FMRI after acute stroke with hemiparesis. *Neurorehabil Neural Repair.* (2013) 27:153–63. doi: 10.1177/1545968312457827
47. Xu H, Qin W, Chen H, Jiang L, Li K, Yu C. Contribution of the resting-state functional connectivity of the contralesional primary sensorimotor cortex to motor recovery after subcortical stroke. *PLoS ONE.* (2014) 9:e84729. doi: 10.1371/journal.pone.0084729
48. Bai LJ, Tao Y, Wang D, Wang J, Sun CZ, Hao NX. Acupuncture induces time-dependent remodelling brain network on the stable somatosensory first-ever stroke patients: combining diffusion tensor and functional MR imaging. *Evid Based Complement Alternat Med.* (2014) 2014:740480. doi: 10.1155/2014/740480
49. Li YX, Wang Y, Liao CX, Huang WH, Wu P. Longitudinal brain functional connectivity changes of the cortical motor-related network in subcortical stroke patients with acupuncture treatment. *Neural Plast.* (2017) 2017:5816262. doi: 10.1155/2017/5816263
50. Xu JF, Shi XM, Bian JL, Li J, Li Y. Clinical observation on different courses of Stroke treated by Acupuncture method of "Xing Nao Kai Qiao". *J Tianjin Univ Tradition Chinese Med.* (2005) 1:33. doi: 10.3969/j.issn.1673-9043.2005.01.017
51. Wang HG, Cai HC. Clinical observation of ultra- early intervention of acupuncture in the treatment of acute cerebral infarction. *J Clin Acupunct Moxibust.* (2015) 31:31–2. doi: 10.3969/j.issn.1005-0779.2015.03.012
52. Xiong J, Li YD, Zhang Y. Dynamic observation on the clinical effect of "Xingnao Kaiqiao" acupuncture on neurological impairment after cerebral infarction. *Shanxi J Tradition Chinese Med.* (2006) 22:33–5. doi: 10.3969/j.issn.1000-7156.2006.02.021
53. Ovadia-Caro S, Villringer K, Fiebach J, Jungehulsing GJ, van der Meer E, Margulies DS. Longitudinal effects of lesions on functional networks after stroke. *J Cereb Blood Flow Metab.* (2013) 33:1279–85. doi: 10.1038/jcbfm.2013.80
54. Frías I, Starrs F, Gisiger T. Interhemispheric connectivity of primary sensory cortex is associated with motor impairment after stroke. *Sci Rep.* (2018) 8:12601. doi: 10.1038/s41598-018-29751-6

55. Bonkhoff AK, Espinoza FA, Gazula H, Vergara VM, Hensel L, Michely J. Acute ischaemic stroke alters the brain's preference for distinct dynamic connectivity states. *Brain.* (2020) 143:1525–40. doi: 10.1093/brain/awaa101
56. Chen TZ, Zou YH, Du ZM. Effect of "hand and foot acupuncture with twelve needles contralateral acupuncture at Quchi (LI 1imary motor areas of the brain and cerebellum in patients with hemiplegia after ischemic stroke. *J Tradition Chinese Med.* (2021) 62:1514–21. doi: 10.13288/j.11-2166/r.2021.17.010
57. Lu MX. *Acupuncture Effects on Different Motor Dysfunction Degrees After Cerebral Infarction.* (Master's thesis). Beijing: Beijing University of Chinese Medicine (2020).
58. Grefkes C, Fink GR. Connectivity-based approaches in stroke and recovery of function. *Lancet Neurol.* (2014) 13:206–16. doi: 10.1016/S1474-4422(13)70264-3
59. Pajula J, Tohka J. How many is enough? Effect of sample size in inter-subject correlation analysis of fMRI. *Comput Intell Neurosci.* (2016) 2016:2094601. doi: 10.1155/2016/2094601

Conflict of Interest: The authors declare that the research was conducted in the absence of any commercial or financial relationships that could be construed as a potential conflict of interest.

frontiers | Frontiers in Neurology

ORIGINAL RESEARCH
published: 11 July 2022
doi: 10.3389/fneur.2022.912923

Modulation of Brain Activity and Functional Connectivity by Acupuncture Combined With Donepezil on Mild-to-Moderate Alzheimer's Disease: A Neuroimaging Pilot Study

Yijun Zhan[1†], Qinhui Fu[1†], Jian Pei[1], Mingxia Fan[2], Qiurong Yu[2], Miao Guo[2], Houguang Zhou[3], Tao Wang[4], Liaoyao Wang[1] and Yaoxin Chen[1]*

[1] Department of Acupuncture, Longhua Hospital, Shanghai University of Traditional Chinese Medicine, Shanghai, China, [2] Shanghai Key Laboratory of Magnetic Resonance, Department of Physics, East China Normal University, Shanghai, China, [3] Department of Geriatrics, Huashan Hospital, Fudan University, Shanghai, China, [4] Alzheimer's Disease and Related Disorders Center, Shanghai Mental Health Center, School of Medicine, Shanghai Jiaotong University, Shanghai, China

OPEN ACCESS

Edited by:
Jiliang Fang,
China Academy of Chinese Medical Sciences, China

Reviewed by:
Zhi Wen,
Renmin Hospital of Wuhan University, China
Siyi Yu,
Chengdu University of Traditional Chinese Medicine, China

***Correspondence:**
Jian Pei
longhuaacup@aliyun.com

[†] These authors have contributed equally to this work and share first authorship

Specialty section:
This article was submitted to Applied Neuroimaging, a section of the journal Frontiers in Neurology

Received: 05 April 2022
Accepted: 14 June 2022
Published: 11 July 2022

Citation:
Zhan Y, Fu Q, Pei J, Fan M, Yu Q, Guo M, Zhou H, Wang T, Wang L and Chen Y (2022) Modulation of Brain Activity and Functional Connectivity by Acupuncture Combined With Donepezil on Mild-to-Moderate Alzheimer's Disease: A Neuroimaging Pilot Study. Front. Neurol. 13:912923. doi: 10.3389/fneur.2022.912923

Background: Functional brain imaging changes have been proven as potential pathophysiological targets in early-stage AD. Current longitudinal neuroimaging studies of AD treated by acupuncture, which is one of the growingly acknowledged non-pharmacological interventions, have neither adopted comprehensive acupuncture protocols, nor explored the changes after a complete treatment duration. Thus, the mechanisms of acupuncture effects remain not fully investigated.

Objective: This study aimed to investigate the changes in spontaneous brain activity and functional connectivity and provide evidence for central mechanism of a 12-week acupuncture program on mild-to-moderate AD.

Methods: A total of forty-four patients with mild-to-moderate AD and twenty-two age- and education-level-matched healthy subjects were enrolled in this study. The forty-four patients with AD received a 12-week intervention of either acupuncture combined with Donepezil (the treatment group) or Donepezil alone (the control group). The two groups received two functional magnetic resonance imaging (fMRI) scans before and after treatment. The healthy subject group underwent no intervention, and only one fMRI scan was performed after enrollment. The fractional amplitude of low-frequency fluctuation (fALFF) and functional connectivity (FC) were applied to analyze the imaging data. The correlations between the imaging indicators and the changed score of Alzheimer's Disease Assessment Scale-Cognitive Section (ADAS-cog) were also explored.

Results: After the 12-week intervention, compared to those in the control group, patients with AD in the treatment group scored significantly lower on ADAS-cog value. Moreover, compared to healthy subjects, the areas where the fALFF value decreased in patients with AD were mainly located in the right inferior temporal gyrus, middle/inferior frontal gyrus, middle occipital gyrus, left precuneus, and bilateral superior temporal

gyrus. Compared with the control group, the right precuneus demonstrated the greatest changed value of fALFF after the intervention in the treatment group. The difference in ADAS-cog after interventions was positively correlated with the difference in fALFF value in the left temporal lobe. Right precuneus-based FC analysis showed that the altered FC by the treatment group compared to the control group was mainly located in the bilateral middle temporal gyrus.

Conclusion: The study revealed the key role of precuneus in the effect of the combination of acupuncture and Donepezil on mild-to-moderate AD for cognitive function, as well as its connection with middle temporal gyrus, which provided a potential treating target for AD.

Trial Registration Number: NCT03810794 (http://www.clinicaltrials.gov).

Keywords: Alzheimer's disease, acupuncture, Donepezil, functional magnetic resonance imaging (fMRI), fractional amplitude of low-frequency fluctuation (fALFF), functional connectivity (FC)

INTRODUCTION

Alzheimer's disease (AD), with high disability and mortality, leads to huge burden throughout the world (1, 2). To effectively break the progression of the disease, it is urgent to discover the key treating target for AD. Since the research diagnosis criteria of AD published by International Working Group (IWG)-2 in 2014 raised magnetic resonance imaging (MRI) as one of the topographical markers (3), studies based on functional magnetic resonance imaging (fMRI) technique have been laid growing emphasis on. Recently, functional brain imaging changes have been proven as potential targets in early-stage AD (4), among which fractional amplitude of low-frequency fluctuation (fALFF) and functional connectivity (FC) are the most commonly used imaging indexes. Both fALFF, directly reflecting spontaneous brain activity, and FC decreased as early as in the preclinical AD stage of subjective cognitive decline (5). A study has carried out combined analysis of fALFF with FC, seeking precisely-significant seed point through the former method and applying it in the latter analysis, to investigate the pathological mechanisms of AD as rigorously as possible (5). Several brain regions, including the hippocampus, posterior cingulate cortex, precuneus, pre-frontal cortex, temporal lobe, and angular gyrus, have been reported and well known as the core brain regions involved in the pathophysiology of AD (6–8).

In view of the huge challenges the new drug development for AD is now facing, the effects of non-pharmacological interventions are gaining attention. Our previous review has showed that acupuncture therapy, exercise intervention, and repetitive transcranial magnetic stimulation could bring benefits to patients with AD not only in cognition function, but also in daily living ability and life quality (9). Specifically, acupuncture, with a history of over 3,000 years, is gradually acknowledged in its therapeutic effects and regulation of neuroplasticity in AD (10).

When it comes to the mechanisms of acupuncture treating AD, neuroimaging studies in the recent decade have demonstrated that acupuncture could induce positive modulation of specific brain regions and neuroplastic reorganization of brain functional networks in AD or mild cognitive impairment (11–14). There were several regions that show activated changes in patients with MCI and AD after immediate manual or electro-acupuncture stimulation, including the default-mode network (DMN), left frontal parietal network, right frontal parietal network, visual network, sensorimotor network, and auditory network (15). Moreover, there is certain correlation between the changes in cognitive function and alteration in functional connectivity. However, low consistency revealed in current research results, due to the differences in study designs, scanning parameters, and selection of seed point. Current neuroimaging studies of acupuncture for AD have not adopted comprehensive acupuncture protocols, nor have explored the changes after a complete treatment duration. As a part of a multicenter randomized controlled trial, this neuroimaging pilot study was carried out to obtain scientific and objective evidence for the central mechanism of acupuncture program combined with Donepezil on AD.

Abbreviations: AD, Alzheimer's disease; ADAS-cog, Alzheimer's Disease Assessment Scale-Cognitive Section; DMN, default-mode network; DPARSF, Data Processing Assistant for Resting-State fMRI; DTI, diffusion tensor imaging; fALFF, fractional amplitude of low-frequency fluctuation; FC, functional connectivity; FOV, field of view; MNI, Montreal Neurological Institute; MTA-scale, medial temporal lobe atrophy; NINCDS-ADRDA, Neurological Communicative Disorders and Stroke and the Alzheimer's Disease and Related Disorders Association; PET, positron emission tomography; SD, standard deviation; SPSS, Statistical Packing for the Social Sciences; TE, echo time; TPN, tau pathology network; TR, repetition time.

MATERIALS AND METHODS

Participants

This pilot study was approved by the Medical Ethics Committee of Longhua Hospital, Shanghai University of Traditional Chinese Medicine (no. 2018LCSY060). In this study, 44 right-handed patients with AD and 22 age-, gender-, and education-matched healthy subjects were enrolled. The

patients were recruited from March 2019 to December 2020 at the Department of Acupuncture Longhua Hospital, Shanghai University of Traditional Chinese Medicine, the Department of Geriatrics, Huashan Hospital, Fudan University, and Alzheimer's Disease and Related Disorders Center, the Department of Geriatrics, Shanghai Mental Health Center, School of Medicine, Shanghai Jiaotong University. The healthy subjects were recruited from the local community by advertisements.

Patients with AD met the diagnostic criteria of Neurological Communicative Disorders and Stroke and the Alzheimer's Disease and Related Disorders Association (NINCDS-ADRDA) for AD, with Mini-Mental State Examination (MMSE) evaluated as mild-to-moderate AD (11 to 22 for primary school education, 11 to 26 for middle school education, or above). The patients' scale for medial temporal lobe atrophy (MTA-scale) was required to be no <2 for those under 75 years old, and no <3 for those over 75 years old. Exclusion criteria for patients with AD included cognitive impairment caused by other factors, such as frontotemporal dementia, dementia with Lewy bodies, vascular dementia, severe depression, cerebrovascular disease, tumors, poisoning, metabolic diseases, and infections; severe chronic disorders, such as Parkinson's disease, epilepsy, myocardial infarction, heart failure, malignant tumor, severe infection, impaired hepatic or renal function; aphasia, disturbance of consciousness, or failure to cooperate with the related examinations due to physical disability; anticoagulant treatments, such as warfarin or heparin; and the use of pacemakers or receiving acupuncture in the past 2 weeks.

The matched healthy subjects had a normal cognitive function, with MMSE evaluated as above 27, whereas subjects with severe chronic disorders mentioned above were excluded.

For all the participants, those with contraindications to undergoing an MRI scan should be excluded, such as claustrophobia or pacemaker implantation. Written informed consent was provided by every participant.

Interventions

The 44 patients with AD were randomly assigned into either the treatment group (acupuncture combined with Donepezil) or the control group (Donepezil along). Both groups took Donepezil 5 mg one time daily before bed time for 12 weeks.

Patients in the treatment group received additional acupuncture treatment. Disposable stainless steel needles (0.25 mm×25 mm) were used. Based on our previous studies on the acupoint selection and the clinical experience (9), the main acupoints of this study were Shenting (DU24), Yintang (EX-HN3), Baihui (DU20), Sishencong (EX-HN1), Wangu (GB12), Shenmen (HT7), Zhaohai (KI6), and Xuanzhong (GB39). The detailed information for the locations of the acupoints is presented in **Supplementary Table S1**. Among them, DU24 and GB12 were electrically stimulated as a pair, with a disperse-dense wave of 2/50 Hz, 0.5 mA. The treatment included thirty-six 30-min sessions over 12 weeks.

Resting-State fMRI Imaging Acquisition

Image acquisitions were performed in Shanghai Key Laboratory of Magnetic Resonance on a 3T MR scanner (Discovery MR750 3.0T scanner, GE Healthcare, US) with a 64 channel head coil. A high-resolution three-dimensional T1-weighted imaging was performed with the following parameters: slice number = 192, slice thickness = 1 mm, repetition time (TR) = 2,530 ms, echo time (TE) = 2.98 ms, field of view (FOV) = 224 mm × 224 mm, gap = 0 mm, acquisition matrix = 64×64.

Resting-state data were performed with the following parameters: slice number = 35, slice thickness = 3.5 mm, repetition time (TR) = 500 ms, echo time (TE) = 30 ms, field of view (FOV) = 224 mm × 224 mm, gap = 0.525 mm, acquisition matrix = 64×64, flip angle = 60°, total time = 8 min 7 s.

During the scan, participants were asked to relax with their eyes closed but not to fall asleep. Images of patients with AD were acquired at baseline and week 12, respectively. Healthy subjects received the fMRI scan only one time at baseline.

Data Preprocessing

Preprocessing of the rs-fMRI data was performed using SPM12 (http://www.fil.ion.ucl.ac.uk/spm/) and Data Processing Assistant for Resting-State fMRI (DPARSF) (16). The first 40 volumes were discarded from a total of 960 volumes to allow for signal equilibrium of the initial magnetic resonance signals and adaptation of the subjects to the circumstances. Then, slice timing correction was carried out; realignment for head-motion correction, coregistration of the functional images to DARTEL template, spatial normalization to the Montreal Neurological Institute (MNI) 24 template (resampling voxel size = 3 mm×3 mm ×3 mm), and smoothing with an isotropic Gaussian kernel (full width at half maximum = 8 mm), detrending and regression out covariables were performed in order. Any subject with a head motion >2.0-mm translation or a 2.0° rotation in any direction was excluded.

Primary Measurements

fALFF Analysis

In this study, the DPARSF software package was used to calculate the fALFF value on MATLAB R2016a. The calculation principle was used to transform the time series of the image into the frequency domain through fast Fourier transform and obtain the power spectrum. At each frequency point, the square root of the power spectrum was calculated, and then, the average square root was obtained at 0.01–0.08 Hz of each voxel. The fALFF value of the image was calculated as the ratio of the low-frequency power spectrum to the power spectrum of the whole frequency range.

Seed-Based FC Analysis

The FC analysis method based on seed points was used to explore the features of functional connectivity of the brain regions of interest in patients with AD. Before conducting FC, the images were filtered between 0.01 and 0.08 Hz to control noise interference. The brain area most significantly related to the AD in the fALFF analysis result was selected as the seed point,

and the DPARSF software package was applied to perform the whole-brain FC analysis on the MATLAB R2016a platform.

Secondary Measurement

Alzheimer's Disease Assessment Scale-Cognitive Section (ADAS-Cog)

Alzheimer's Disease Assessment Scale-Cognitive Section is a general neuropsychological measurement tool for evaluating cognitive function (17), which is the most widely used scale in clinical trials for AD. It can keenly identify the cognitive changes and therapeutic effects of subjects with mild-to-moderate AD. The main evaluation indicators include 11 cognitive and 1 non-cognitive items. The highest score is 70 points. The higher the score, the worse the cognitive function.

Statistical Analysis

The statistical analysis of demographic characteristics and clinical measurements was carried out using the Statistical Packing for the Social Sciences (SPSS) version 19.0 (IBM Corp., Armonk, NY, USA). The analysis of variance (ANOVA) was used for continuous variable, and the chi-square test was used for categorical variables.

SPM12 software was used to carry out the statistical analysis of fALFF and FC. The one-way ANOVA was used to analyze the differences between different groups. The statistical significance level was set as $p < 0.001$. The false discovery rate (FDR) or family-wise error (FWE) theory was used for multiple comparison corrections (voxel-wise $p < 0.01$, cluster-wise $p < 0.05$). *Post hoc* analysis was also performed with the Bonferroni correction to evaluate the differences between the different groups ($p < 0.05$). Taking gender, age, and education level as covariates, multiple regression analysis was used to analyze the correlation between the changes of fALFF and FC with the differences in ADAS-cog before and after treatment in patients with AD. The xjview software (http://www.alivelearn.net/xjview) was utilized to display the results as images.

RESULTS

Demographic and Clinical Information

A total of 44 patients with AD and 22 healthy subjects were included in the study. The subjects in the treatment group and control group completed all the treatment procedures. Then, 1 case in healthy subject group was terminated due to the tendency of claustrophobia during the scan. In preprocessing period, 2 cases in the treatment group, 2 cases in the control group, and 1 case in the healthy subject group were excluded because of head movement translation$>$2 mm and/or rotation$>2^{\circ}$. Finally, 20 cases in each group were included in the statistical analysis. Demographic and clinical characteristics of these participants are shown in **Table 1**. There were no significant differences in age, education level, personal history, and past history across the three groups (**Table 1**).

Group Differences in fALFF

The Difference in fALFF Value Between Patients With AD and Healthy Subjects

Compared with the healthy subject, decreased fALFF values of patients with AD were detected in the right inferior temporal gyrus, middle/inferior frontal gyrus, postcentral gyrus, middle occipital gyrus; the left precuneus; and the bilateral

TABLE 1 | Baseline characteristics of participants.

Characteristics	Treatment group ($N = 20$)	Control group ($N = 20$)	Healthy subject group ($N = 20$)
Age, years (mean ± SD)	61.82 ± 6.118	60.52 ± 7.420	60.97 ± 7.274
Sex, male [count (%)]	9 (45.0%)	8 (40.0%)	10 (50.0%)
Course, months [M(IQR)]	15 (12)	14 (14)	/
Education level [count (%)]			
illiteracy	2 (10.0%)	2 (10.0%)	2 (10.0%)
Primary school	5 (25.0%)	3 (15.0%)	4 (20.0%)
Middle school	4 (20.0%)	7 (35.0%)	5 (25.0%)
High school	5 (25.0%)	3 (15.0%)	4 (20.0%)
College	4 (20.0%)	5 (25.0%)	5 (25.0%)
Past medical history [count(%)]			
Hypertension	9 (45.0%)	10 (50.0%)	9 (45.0%)
Heart disease	4 (20.0%)	5 (25.0%)	4 (20.0%)
Diabetes	5 (25.0%)	5 (25.0%)	4 (20.0%)
Hyperlipidemia	8 (40.0%)	7 (35.0%)	7 (35.0%)
Alcohol [count (%)]	3 (15.0%)	2 (10.0%)	3 (15.0%)
Tobacco [count (%)]	5 (25.0%)	4 (20.0%)	4 (20.0%)
MMSE [M(IQR)]	17 (5)	18 (6)	27 (4)

superior temporal gyrus (**Table 2** and **Figure 1**, $p < 0.05$, FDR-corrected).

Comparison of fALFF Difference Within the Treatment Group and Control Group Before and After Intervention

It was shown that significant differences in fALFF value before and after intervention in the treatment group were located in the right precuneus, middle frontal gyrus, and superior temporal gyrus; and those in the control group were located in the right lingual gyrus and middle frontal gyrus and the left inferior temporal gyrus, lingual gyrus, and thalamus (**Supplementary Tables S2**, **S3**, **Supplementary Figures S1**, **S2**, $p < 0.05$, FDR-corrected).

Comparison of fALFF Difference Between the Treatment Group and Control Group Before and After Intervention

Compared with the control group, significant differences in fALFF value before and after intervention in the treatment group were located in the right precuneus and the left inferior temporal gyrus, lingual gyrus, and thalamus, whereas did not

TABLE 2 | Regions showing significant fALFF value differences between healthy subject and AD.

Brain region	R/L	BA	MNI (Peak point)			T value	Voxel
			X	Y	Z		
Inferior temporal gyrus	R	37	48	−70	−4	−7.03	68
Inferior frontal gyrus	R	/	45	5	26	−6.63	16
Superior temporal gyrus	R	22	66	−43	11	−5.94	22
Postcentral gyrus	R	3	45	−22	53	−5.95	155
Middle frontal gyrus	R	6	30	−1	50	−5.54	30
Middle occipital gyrus	R	19	39	−79	8	−5.01	18
Superior temporal gyrus	L	/	−57	8	2	−4.83	14
Precuneus	L	/	−9	−73	35	−4.76	14

R, right; L, left; MNI, Montreal Neurological Institute. $p < 0.05$, FDR–corrected.

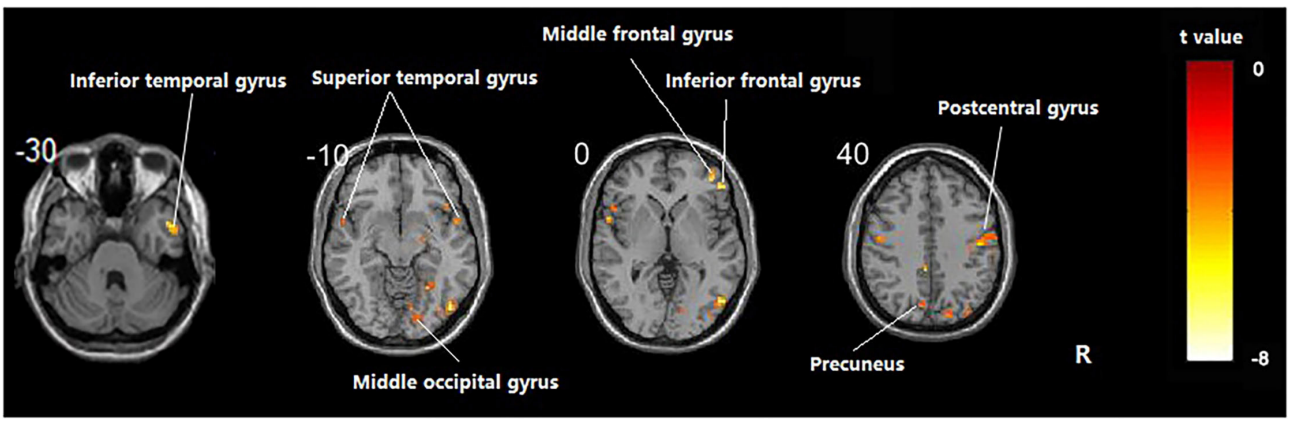

FIGURE 1 | Regions showing significant fALFF value differences between healthy subjects and AD. The results were FDR-corrected with $p<0.05$.

TABLE 3 | Regions showing significant fALFF value changes between the treatment group and control group.

Brain region	R/L	BA	MNI (Peak point)			*T*-value	Voxel
			X	Y	Z		
Precuneus	R	/	6	−58	65	8.94	15
Inferior temporal gyrus	L	/	−51	−46	−25	8.08	27
Lingual gyrus	L	/	−18	−82	−22	7.89	9
Thalamus	L	/	−12	−10	11	7.30	6

R, right; L, left; MNI, Montreal Neurological Institute. $p < 0.001$, uncorrected.

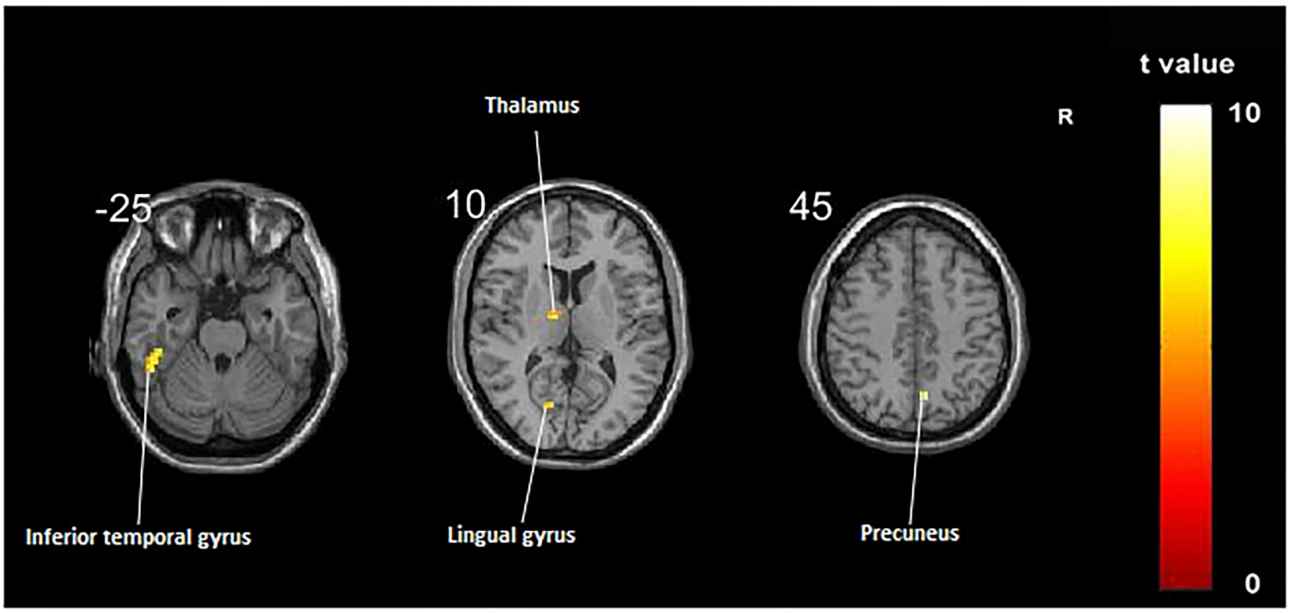

FIGURE 2 | Regions showing significant fALFF value changes between the treatment group and control group. The results were uncorrected with $p<0.001$.

TABLE 4 | Change in ADAS–cog values within and between groups (mean ± SD).

	Treatment group ($n = 20$)	Control group ($n = 20$)
Week 0	19.32 ± 1.89	19.98 ± 1.59
Week 12	16.52 ± 1.47[ab]	18.08 ± 1.49[a]
ΔWeek 12–Week 0	2.80 ± 1.51[b]	1.90 ± 1.36

[a]$p < 0.05$ within group; [b]$p < 0.05$ between groups.

pass the FDR or FWE correction (**Table 3**, **Figure 2**, $p < 0.001$, uncorrected).

Correlation Analysis Between fALFF Difference and ADAS-Cog Difference in Treatment Group

The differences in ADAS-cog before and after the intervention within and between the treatment group and control group groups were both statistically significant (**Table 4**, $p < 0.05$).

Multiple regression analysis, with covariates of age, gender, and educational level removed, showed that ADAS-cog difference caused by acupuncture combined with Donepezil was positively correlated with the change in ADAS-cog value in the left inferior temporal gyrus ($r = 0.8779$, $p < 0.001$, FWE-corrected) and was negatively correlated with the right middle temporal gyrus ($r = -0.9485$, $p < 0.001$, FWE-corrected) (**Table 5**, **Figure 3**).

Group Differences in FC

Selection of Seed Points

The results of the fALFF analysis above revealed that the right precuneus was the significant point in the effect of acupuncture combined with Donepezil, as well as in the comparison between the treatment group and the control group. It was then hypothesized that the right precuneus might be the key point in the treatment of AD. Therefore, it was selected as the seed point to analyze the FC with the whole brain, locating at the MNI coordinates (6, −58, 65), with the radius of 6 mm, which was the frequently-used volume for a seed point (**Figure 4**).

Comparison of FC Difference Between the Treatment Group and Control Group Before and After Intervention

Compared with the control group, significant differences in FC value before and after intervention in the treatment group were located in the bilateral middle temporal gyrus and left middle frontal gyrus, whereas did not pass the FDR or FWE correction (**Table 6**, **Figure 5**, $p < 0.001$, uncorrected).

Correlation of Functional Connection of the Whole Brain and Right Precuneus and Cognitive Function Improvement in the Treatment Group

Multiple regression analysis, with covariates of age, gender, and educational level removed, showed that ADAS-cog difference caused by acupuncture combined with Donepezil was negatively correlated with the right precuneus-based FC of the right superior temporal gyrus ($r = -0.8809$, $p < 0.001$, FDR-corrected), right superior occipital gyrus ($r = -0.8866$, $p < 0.001$, FDR-corrected), and left precuneus ($r = -0.9757$, $p < 0.001$, FDR-corrected) (**Table 7**, **Figure 6**).

DISCUSSION

Our study implied that the treatment of acupuncture combined with Donepezil on patients with AD could mainly upregulate the abnormally decreased spontaneous neural activity of the left precuneus and its functional connectivity with the

TABLE 5 | Regions showing significant correlation in the change in fALFF in the treatment group to the change in ADAS–cog.

Brain region	R/L	BA	MNI (Peak point)			*T*-value	Voxel
			X	Y	Z		
Inferior temporal gyrus	L	/	−24	−45	0	7.57	7
Middle temporal gyrus	R	/	42	−78	21	−5.06	6

R, right; L, left; MNI, Montreal Neurological Institute. $p < 0.05$, FWE–corrected.

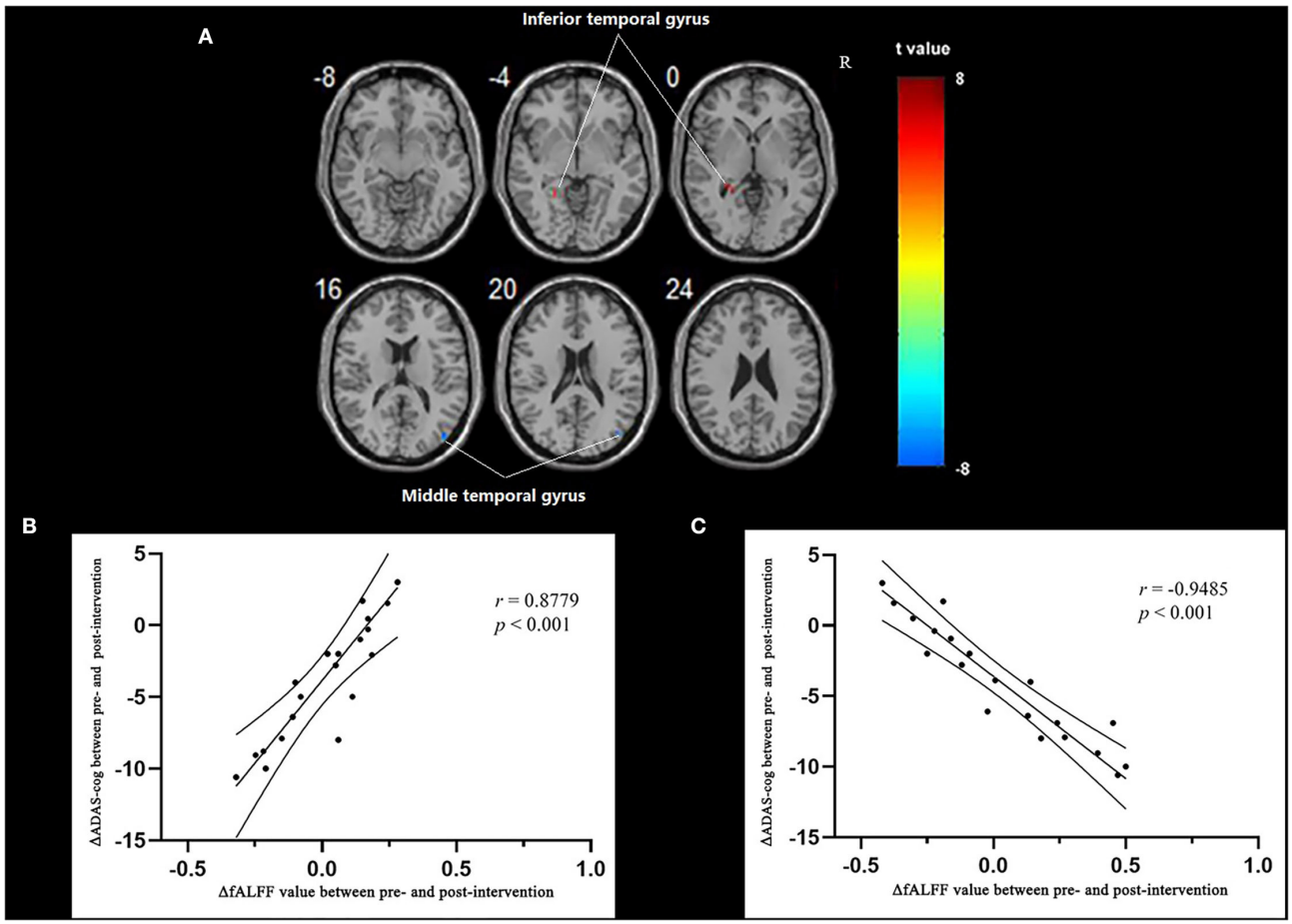

FIGURE 3 | Regions showing significant correlation in the change in fALFF in the treatment group to the change in ADAS-cog. **(A)** Multiple regression correlation results of significant correlation between fALFF value changes and ADAS-cog value changes in the treatment group ($p<0.001$, FWE-corrected). **(B)** Pearson correlation results of the change in fALFF value of the left inferior temporal gyrus and the change in ADAS-cog value. **(C)** Pearson correlation results of the change in fALFF value of the right middle temporal gyrus and the change in ADAS-cog value.

temporal gyrus, which were correlated with the improvement in cognitive function. Our results, to some extent, provide a potential brain region target for precise therapies, such as transcranial magnetic stimulation (TMS). Moreover, the brain region could be taken as the target for evaluating the effect of various therapies. The conclusions drawn in this study are basically consistent with the results of existing AD pathology studies. Decreased fALFF values were often detected in the precuneus, angular gyrus, hippocampus, superior frontal gyrus, paracentral lobule, occipitotemporal cortex, parietal lobule, etc. (18–20) In a cross-sectional study, patients with AD showed a clear reduction of cortical gray matter in the temporal lobe, precuneus, cingulate gyrus, and inferior frontal gyrus (21). These brain regions are at the center of many brain function networks and are closely related to the progression of AD (22). As the condition develops, the functional connectivity of the above brain areas is gradually weakened (23).

The precuneus and temporal gyrus are the main brain regions of the default-mode network, closely related to AD cognitive function. FC disruption within this network is associated with cognitive decline in patients. Then, the damage of DMN can

appear in the early period of AD, which is manifested as the decrease in network connection and the decline of network integrity (24, 25).

The precuneus has been confirmed to demonstrate structural or functional abnormalities in patients with AD, such as cortical atrophy and metabolic impairment (26, 27). Pathologically, the precuneus is involved in Braak's IV and V stages, closely related to the process of AD from the appearance of the initial symptoms to the end period. The precuneus was also found to be involved in the tau deposition pathology of AD. Positron emission tomography (PET) studies were compared and analyzed to reveal that the tau pathology network (TPN) overlapped with DMN, and the tau distribution peak in the TPN was located in the precuneus (28). Recent research raised that the precuneus might be dually involved in both memory and perceptual metacognition due to the close relationship shared between the precuneus and perceptual metacognition (29, 30).

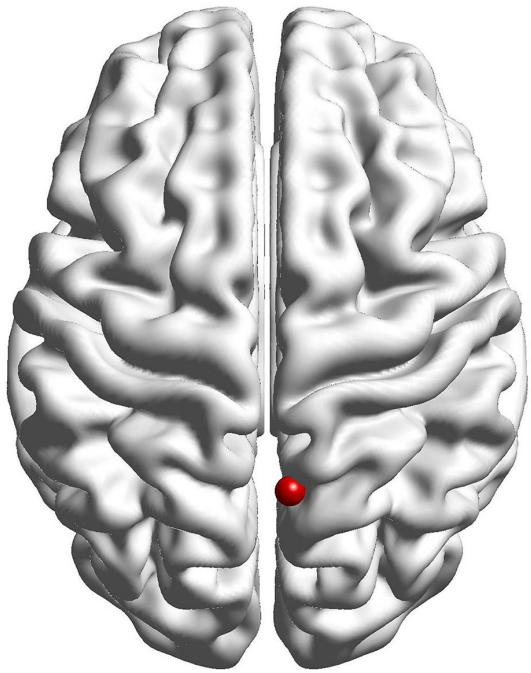

FIGURE 4 | Seed point of the right precuneus for functional connection analysis.

The temporal lobe, including the structure of hippocampus, is well accepted as one of the most critical brain regions relating to AD. Connectivity changes in the posterior-medial and anterior-temporal hippocampal networks were found to contribute together to the cognitive decline in Alzheimer's disease (31), which were proved to be key in episodic memory formation (32). Studies based on dynamic functional connectivity showed that the continuous cognitive impairment in AD leads to a gradual loss of meta-stable state in the whole brain, and the brain regions with significantly reduced effective functional connectivity were mainly located in the temporal lobe (33). Another acupuncture study on AD showed that the intervention could improve cognitive function by increasing the neuronal activity of the low frontotemporal lobe, especially the hippocampus (34).

Another finding of our study was that the increased FC between left and right precuneus correlated with the improvement in cognitive function by acupuncture combined with Donepezil, which could be explained by the functional region transfer by corpus callosum. A similar result had been drawn by an experiment of acupuncture on mouse models of vascular dementia, which implied the effect of acupuncture's ameliorating white matter damage in the corpus callosum (35). A previous study had shown that the significant alterations in white matter microstructural metrics caused by AD could be detected by the technology of diffusion tensor imaging (DTI), and the alteration indexes were closely related to the cognitive function degree of AD (36). The results above hint that further

TABLE 6 | Regions showing significant FC changes between the treatment group and control group.

Brain region	R/L	BA	MNI (Peak point)			*T*-value	Voxel
			X	Y	Z		
Middle temporal gyrus	R	/	51	−42	−3	10.84	5
Middle temporal gyrus	L	21	−57	−48	3	7.86	5
Middle frontal gyrus	L	/	−12	42	24	6.15	7

R, right; L, left; MNI; Montreal Neurological Institute. $p < 0.001$, uncorrected.

TABLE 7 | Regions showing significant correlation in the change in FC in the treatment group to the change in ADAS–cog.

Brain region	R/L	BA	MNI (Peak point)			*T*-value	Voxel
			X	Y	Z		
Superior occipital gyrus	R	/	21	−102	6	−4.42	12
Superior temporal gyrus	R	41	48	−33	9	−6.07	18
Precuneus	L	/	−12	−57	51	−8.00	34

R, right; L, left; MNI, Montreal Neurological Institute. $p < 0.001$, FDR–corrected.

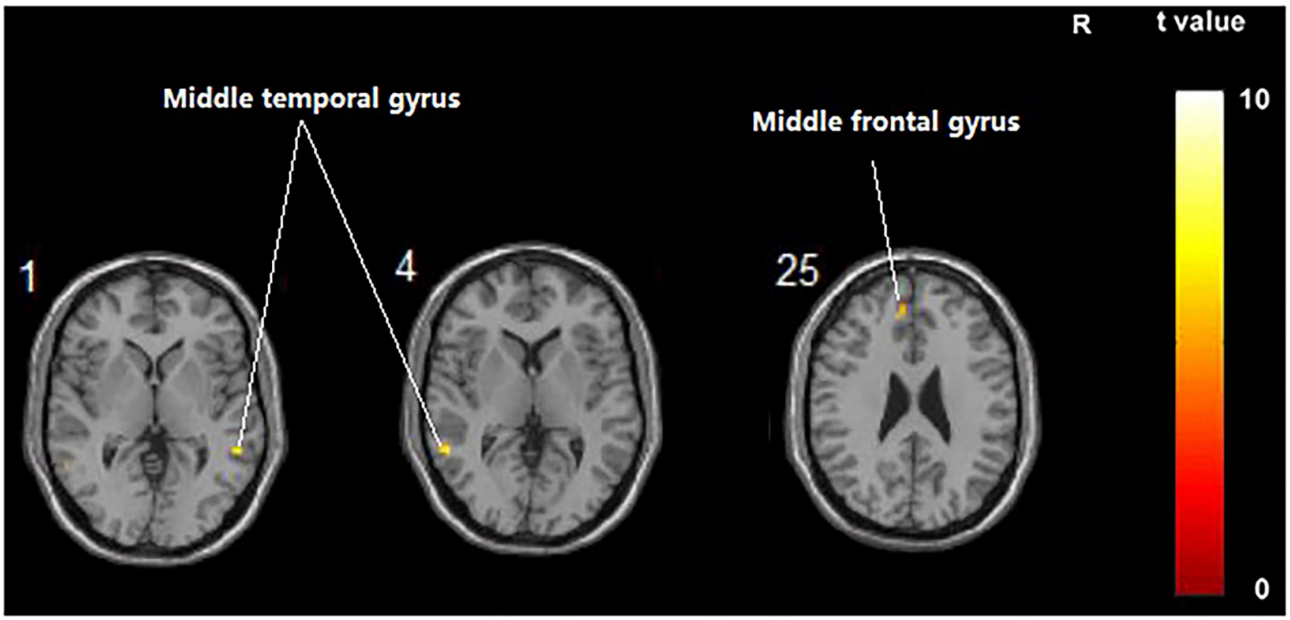

FIGURE 5 | Regions showing significant FC changes between the treatment group and control group. The results were uncorrected with $5<0.001$.

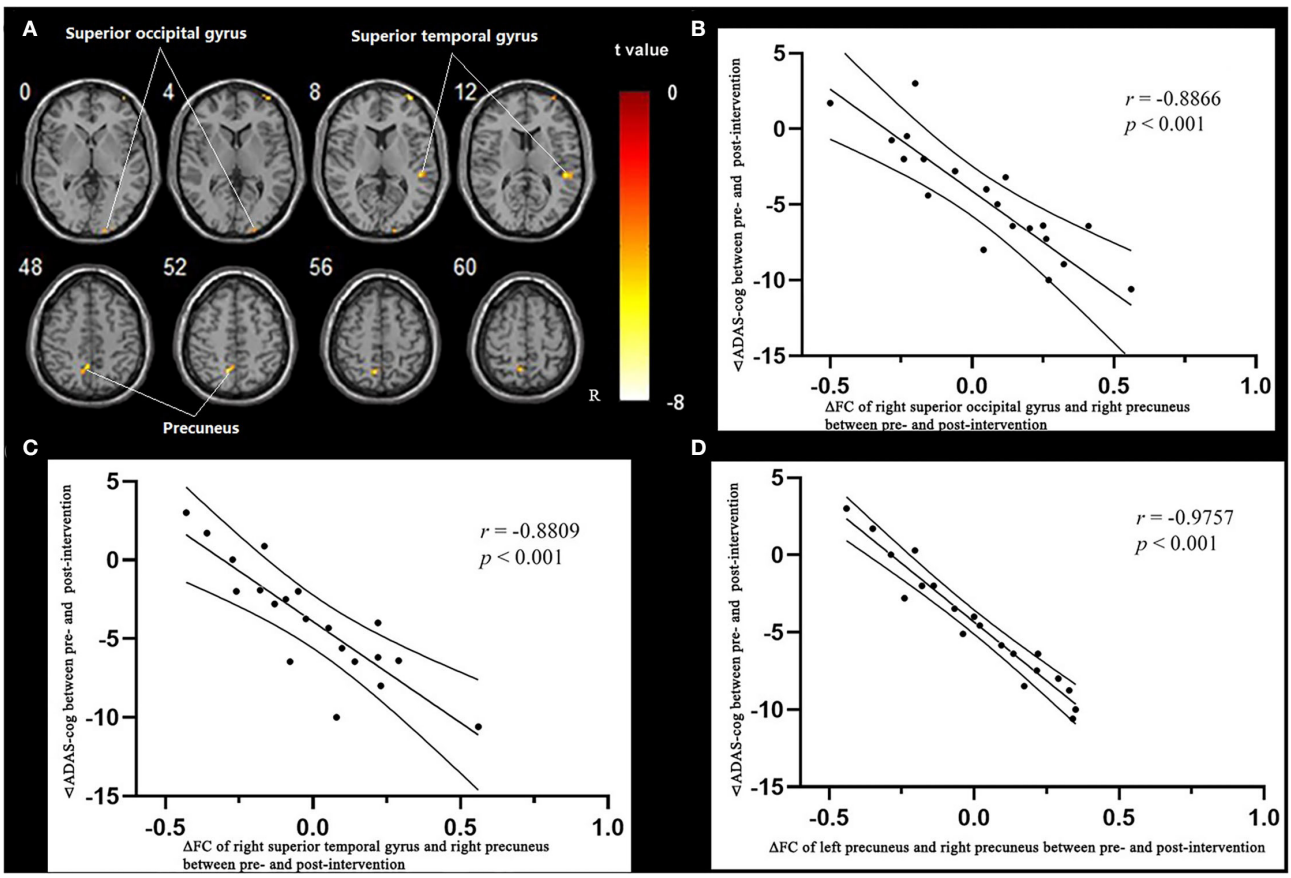

FIGURE 6 | Regions showing significant correlation in the change in FC in the treatment group to the change in ADAS-cog. **(A)** Multiple regression correlation results of significant correlation between FC changes and ADAS-cog value changes in the treatment group ($p < 0.001$, FDR-corrected). **(B)** Pearson correlation results of the change in FC to the right superior occipital gyrus and the change in ADAS-cog value. **(C)** Pearson correlation results of the change in FC to the right superior temporal gyrus and the change in ADAS-cog value. **(D)** Pearson correlation results of the change in FC to the right superior temporal gyrus and the change in ADAS-cog value.

studies might apply DTI technology to investigate and prove the effect of acupuncture on the diffusivity of white matter fiber tracts.

LIMITATIONS

A precise parameter for electroacupuncture has not been taken into consideration, which plays a key role in the clinical effect. A study has implied that high-frequency electrical acupuncture has a stronger protective effect on hippocampal synaptic plasticity and spatial learning and memory ability in AD rats, compared with low-frequency or intermediate-frequency stimulation (37). It is suggested that the crucial factors for the clinical effect and mechanism of acupuncture on AD should be included in the future study designs, such as frequency and intensity of electro-/manual acupuncture, and even the evaluation of *Deqi*.

CONCLUSION

The central mechanism of acupuncture combined with Donepezil improving the cognitive dysfunction of patients with AD lied in the regulation of the abnormal reduction in spontaneous neuron activity and functional connectivity in the precuneus and temporal gyrus, which provided a potential treating target for AD, as well as a target with monitoring value in the progression of acupuncture intervention on AD.

DATA AVAILABILITY STATEMENT

The raw data supporting the conclusions of this article will be made available by the authors, without undue reservation.

ETHICS STATEMENT

The studies involving human participants were reviewed and approved by the Medical Ethics Committee of Longhua Hospital, Shanghai University of Traditional Chinese Medicine. The patients/participants provided their written informed consent to participate in this study.

AUTHOR CONTRIBUTIONS

JP, YZ, and MF designed this study. QF, HZ, and TW collected and analyzed the clinical data. LW and YC scanned the imaging data. YZ, MF, QY, and MG analyzed the imaging data. YZ and QF wrote the manuscript. All authors contributed to the article and approved the submitted version.

FUNDING

This work was supported by the key Scientific Research Program of the Science and Technology Commission of Shanghai Municipality (18401970500), the Financing Scheme of Arising Interdisciplinary Subjects of TCM of Shanghai Municipal Health Bureau (Shxxjcxk201709), the TCM genre program of Shanghai Municipal Health Bureau [YZ (2018–2020)-CCCX-1006], and the National Natural Science Foundation of China (81603697).

ACKNOWLEDGMENTS

We would like to thank all the patients, acupuncture and rehabilitation practitioners who participated.

SUPPLEMENTARY MATERIAL

The Supplementary Material for this article can be found online at: https://www.frontiersin.org/articles/10.3389/fneur.2022.912923/full#supplementary-material

Supplementary Figure S1 | Regions showing significant fALFF value changes within the treatment group before and after treatment. The results were corrected with $p<0.05$, FDR-corrected.

Supplementary Figure S2 | Regions showing significant fALFF value changes within the control group before and after treatment. The results were corrected with $p<0.05$, FDR-corrected.

REFERENCES

1. Scheltens P, De Strooper B, Kivipelto M, Holstege H, Chételat G, Teunissen CE, et al. Alzheimer's disease. *Lancet.* (2021) 397:1577–90. doi: 10.1016/S0140-6736(20)32205-4
2. GBD 2016 Dementia Collaborators. Global, regional, and national burden of Alzheimer's disease and other dementias, 1990-2016: a systematic analysis for the global burden of disease study 2016. *Lancet Neurol.* (2019) 18:88–106. doi: 10.1016/S1474-4422(18)30403-4
3. Dubois B, Feldman HH, Jacova C, Hampel H, Molinuevo JL, Blennow K, et al. Advancing research diagnostic criteria for Alzheimer's disease: the IWG-2 criteria. *Lancet Neurol.* (2014) 13:614–29. doi: 10.1016/S1474-4422(14)70090-0
4. Habib M, Mak E, Gabel S, Su L, Williams G, Waldman A, et al. Functional neuroimaging findings in healthy middle-aged adults at risk of Alzheimer's disease. *Ageing Res Rev.* (2017) 36:88–104. doi: 10.1016/j.arr.2017.03.004
5. Zhang Q, Wang Q, He C, Fan D, Zhu Y, Zang F, et al. Altered regional cerebral blood flow and brain function across the alzheimer's disease spectrum: a potential biomarker. *Front Aging Neurosci.* (2021) 13:630382. doi: 10.3389/fnagi.2021.630382
6. Kawagoe T, Onoda K, Yamaguchi S. Subjective memory complaints are associated with altered resting-state functional connectivity but not structural atrophy. *Neuroimage Clin.* (2019) 21:101675. doi: 10.1016/j.nicl.2019.101675
7. Xue C, Yuan B, Yue Y, Xu J, Wang S, Wu M, et al. Distinct disruptive patterns of default mode subnetwork connectivity across the spectrum of preclinical Alzheimer's Disease. *Front Aging Neurosci.* (2019) 11:307. doi: 10.3389/fnagi.2019.00307
8. Zheng W, Cui B, Han Y, Song H, Li K, He Y, et al. Disrupted regional cerebral blood flow, functional activity and connectivity in Alzheimer's Disease: a combined ASL perfusion and resting state fMRI study. *Front Neurosci.* (2019) 13:738. doi: 10.3389/fnins.2019.00738
9. Wang LY, Pei J, Zhan YJ, Cai YW. overview of meta-analyses of five non-pharmacological interventions for Alzheimer's Disease. *Front Aging Neurosci.* (2020) 12:594432. doi: 10.3389/fnagi.2020.594432

10. Ji S, Duan J, Hou X, Zhou L, Qin W, Niu H, et al. The role of acupuncture improving cognitive deficits due to Alzheimer's Disease or vascular diseases through regulating neuroplasticity. *Neural Plast.* (2021) 2021:8868447. doi: 10.1155/2021/8868447
11. Zheng W, Su Z, Liu X, Zhang H, Han Y, Song H, et al. Modulation of functional activity and connectivity by acupuncture in patients with Alzheimer disease as measured by resting-state fMRI. *PLoS ONE.* (2018) 13:e0196933. doi: 10.1371/journal.pone.0196933
12. Wang Z, Nie B, Li D, Zhao Z, Han Y, Song H, et al. Effect of acupuncture in mild cognitive impairment and Alzheimer disease: a functional MRI study. *PLoS ONE.* (2012) 7:e42730. doi: 10.1371/journal.pone.0042730
13. Wang Z, Liang P, Zhao Z, Han Y, Song H, Xu J, et al. Acupuncture modulates resting state hippocampal functional connectivity in Alzheimer disease. *PLoS ONE.* (2014) 9:e91160. doi: 10.1371/journal.pone.0091160
14. Liang P, Wang Z, Qian T, Li K. Acupuncture stimulation of Taichong (Liv3) and Hegu (LI4) modulates the default mode network activity in Alzheimer's disease. *Am J Alzheimers Dis Other Demen.* (2014) 29:739–48. doi: 10.1177/1533317514536600
15. Ji S, Zhang H, Qin W, Liu M, Zheng W, Han Y, et al. Effect of acupuncture stimulation of hegu (LI4) and Taichong (LR3) on the resting-state networks in alzheimer's disease: beyond the default mode network. *Neural Plast.* (2021) 2021:8876873. doi: 10.1155/2021/8876873
16. Yan CG, Wang XD, Zuo XN, Zang YF, DPABI. Data processing&analysis for (resting-state) brain imaging. *Neuroinformatics.* (2016) 14:339–51. doi: 10.1007/s12021-016-9299-4
17. Rosen WG, Mohs RC, Davis KL. A new rating scale for Alzheimer's disease. *Am J Psychiatry.* (1984) 141:1356–64. doi: 10.1176/ajp.141.11.1356
18. Zhen D, Xia W, Yi ZQ, Zhao PW, Zhong JG, Shi HC, et al. Alterations of brain local functional connectivity in amnestic mild cognitive impairment. *Transl Neurodegener.* (2018) 7:26. doi: 10.1186/s40035-018-0134-8
19. Yang L, Yan Y, Wang Y, Hu X, Lu J, Chan P, et al. Gradual disturbances of the Amplitude of Low-Frequency Fluctuations (ALFF) and fractional ALFF in Alzheimer spectrum. *Front Neurosci.* (2018)12:975. doi: 10.3389/fnins.2018.00975
20. Ding C, Du W, Zhang Q, Wang L, Han Y, Jiang J. Coupling relationship between glucose and oxygen metabolisms to differentiate preclinical Alzheimer's disease and normal individuals. Hum Brain Mapp. (2021)42:5051–62. doi: 10.1002/hbm.25599
21. Dicks E, Vermunt L, van der Flier WM, Visser PJ, Barkhof F, Scheltens P, et al. Modeling grey matter atrophy as a function of time, aging or cognitive decline show different anatomical patterns in Alzheimer's disease. *Neuroimage Clin.* (2019) 22:101786. doi: 10.1016/j.nicl.2019.101786
22. Cauda F, Nani A, Manuello J, Premi E, Palermo S, Tatu K, et al. Brain structural alterations are distributed following functional, anatomic and genetic connectivity. *Brain.* (2018) 141:3211–32. doi: 10.1093/brain/awy252
23. Wu Z, Peng Y, Hong M, Zhang Y. Gray matter deterioration pattern during Alzheimer's disease progression: a regions-of-interest based surface morphometry study. *Front Aging Neurosci.* (2021) 13:593898. doi: 10.3389/fnagi.2021.593898
24. Leech R, Sharp DJ. The role of the posterior cingulate cortex in cognition and disease. *Brain.* (2014) 137:12–32. doi: 10.1093/brain/awt162
25. Utevsky AV, Smith DV, Huettel SA. Precuneus is a functional core of the default-mode network. *J Neurosci.* (2014) 34:932–40. doi: 10.1523/JNEUROSCI.4227-13.2014
26. Dickerson BC, Bakkour A, Salat DH, Feczko E, Pacheco J, Greve DN, et al. The cortical signature of Alzheimer's disease: regionally specific cortical thinning relates to symptom severity in very mild to mild AD dementia and is detectable in asymptomatic amyloid-positive individuals. *Cereb Cortex.* (2009) 19:497–510. doi: 10.1093/cercor/bhn113
27. Yokoi T, Watanabe H, Yamaguchi H, Bagarinao E, Masuda M, Imai K, et al. Involvement of the precuneus/ posterior cingulate cortex is significant for the development of Alzheimer's Disease: a PET (THK5351, PiB) and resting fMRI study. *Front Aging Neurosci.* (2018) 10:304. doi: 10.3389/fnagi.2018.00304
28. Hoenig MC, Bischof GN, Seemiller J, Hammes J, Kukolja J, Onur ÖA, et al. Networks of tau distribution in Alzheimer's disease. *Brain.* (2018) 141:568–81. doi: 10.1093/brain/awx353
29. Morales J, Lau H, Fleming SM. Domain-General and domain-specific patterns of activity supporting metacognition in human prefrontal cortex. *J Neurosci.* (2018) 38:3534–46. doi: 10.1523/JNEUROSCI.2360-17.2018
30. Ye Q, Zou F, Lau H, Hu Y, Kwok SC. Causal evidence for mnemonic metacognition in human precuneus. *J Neurosci.* (2018) 38:6379–87. doi: 10.1523/JNEUROSCI.0660-18.2018
31. Dautricourt S, de Flores R, Landeau B, Poisnel G, Vanhoutte M, Delcroix N, et al. Longitudinal changes in hippocampal network connectivity in alzheimer's disease. *Ann Neurol.* (2021) 90:391–406. doi: 10.1002/ana.26168
32. Cooper RA, Ritchey M. Cortico-hippocampal network connections support the multidimensional quality of episodic memory. *eLife.* (2019) 8:e45591. doi: 10.7554/eLife.45591
33. Demirtaş M, Falcon C, Tucholka A, Gispert JD, Molinuevo JL, Deco G, et al. whole-brain computational modeling approach to explain the alterations in resting-state functional connectivity during progression of Alzheimer's disease. *Neuroimage Clin.* (2017) 16:343–54. doi: 10.1016/j.nicl.2017.08.006
34. Shan Y, Wang JJ, Wang ZQ, Zhao ZL, Zhang M, Xu JY, et al. Neuronal specificity of acupuncture in Alzheimer's Disease and mild cognitive impairment patients: a functional MRI Study. *Evid Based Complement Alternat Med.* (2018) 2018:7619197. doi: 10.1155/2018/7619197
35. Ahn SM, Kim YR, Kim HN, Shin YI, Shin HK, Choi BT. Electroacupuncture ameliorates memory impairments by enhancing oligodendrocyte regeneration in a mouse model of prolonged cerebral hypoperfusion. *Sci Rep.* (2016) 6:28646. doi: 10.1038/srep28646
36. Mayo CD, Garcia-Barrera MA, Mazerolle EL, Ritchie LJ, Fisk JD, Gawryluk JR. Relationship between DTI metrics and cognitive function in Alzheimer's Disease. *Front Aging Neurosci.* (2019) 10:436. doi: 10.3389/fnagi.2018.00436
37. Wang Y, Kong L, Li W, Zhang K, Shen F, Wang Y, et al. Effects and mechanisms of different frequencies of electroacupuncture for learning and memory ability of Alzheimer's rats. Zhongguo Zhen Jiu. (2017) 37:629–36. doi: 10.13703/j.0255-2930.2017.06.016

Conflict of Interest: The authors declare that the research was conducted in the absence of any commercial or financial relationships that could be construed as a potential conflict of interest.

frontiers | Frontiers in Neurology

TYPE Original Research
PUBLISHED 26 July 2022
DOI 10.3389/fneur.2022.947379

OPEN ACCESS

EDITED BY
Lijun Bai,
Xi'an Jiaotong University, China

REVIEWED BY
Liu Lan Ying,
Tongde Hospital of Zhejiang Province, China
Yongjun Chen,
Shangdong University of Traditional Chinese Medicine, China

*CORRESPONDENCE
Hongxiao Jia
jhxlj@ccmu.edu.cn

†These authors have contributed equally to this work

SPECIALTY SECTION
This article was submitted to Applied Neuroimaging, a section of the journal Frontiers in Neurology

RECEIVED 18 May 2022
ACCEPTED 06 July 2022
PUBLISHED 26 July 2022

CITATION
Ning Y, Zheng S, Feng S, Yao H, Feng Z, Liu X, Dong L and Jia H (2022) The altered intrinsic functional connectivity after acupuncture at shenmen (HT7) in acute sleep deprivation. *Front. Neurol.* 13:947379. doi: 10.3389/fneur.2022.947379

The altered intrinsic functional connectivity after acupuncture at shenmen (HT7) in acute sleep deprivation

Yanzhe Ning[1,2†], Sisi Zheng[1,2†], Sitong Feng[1,2], Hao Yao[1,2], Zhengtian Feng[1,2], Xinzi Liu[1,2], Linrui Dong[1,2] and Hongxiao Jia[1,2*]

[1]The National Clinical Research Center for Mental Disorders and Beijing Key Laboratory of Mental Disorders, Beijing Anding Hospital, Capital Medical University, Beijing, China, [2]Advanced Innovation Center for Human Brain Protection, Capital Medical University, Beijing, China

Introduction: Accumulating evidence has shown that acupuncture could significantly improve the sleep quality and cognitive function of individuals suffering from insufficient sleep. Numerous animal studies have confirmed the effects and mechanisms of acupuncture on acute sleep deprivation (SD). However, the role of acupuncture on individuals after acute SD remains unclear.

Methods: In the current study, we recruited 30 healthy subjects with regular sleep. All subjects received resting-state fMRI scans during the rested wakefulness (RW) state and after 24 h of total SD. The scan after 24 h of total SD included two resting-state fMRI sessions before and after needling at Shenmen (HT7). Both edge-based and large-scale network FCs were calculated.

Results: The edge-based results showed the suprathreshold edges with abnormal between-network FC involving all paired networks except somatosensory motor network (SMN)-SCN between the SD and RW state, while both decreased and increased between-network FC of edges involving all paired networks except frontoparietal network (FPN)-subcortical network (SCN) between before and after acupuncture at HT7. Compared with the RW state, the large-scale brain network results showed decreased between-network FC in SMN-Default Mode Network (DMN), SMN-FPN, and SMN-ventral attention network (VAN), and increased between-network FC in Dorsal Attention Network (DAN)-VAN, DAN-SMN between the RW state and after 24 h of total SD. After acupuncture at HT7, the large-scale brain network results showed decreased between-network FC in DAN-VAN and increased between-network FC in SMN-VAN.

Conclusion: Acupuncture could widely modulate extensive brain networks and reverse the specific between-network FC. The altered FC after acupuncture at HT7 may provide new evidence to interpret neuroimaging mechanisms of the acupuncture effect on acute SD.

KEYWORDS

large scale brain networks, sleep deprivation (SD), fMRI, functional connectivity, acupuncture

Introduction

With the rapid economic development, many individuals are undergoing insufficient sleep due to work or neuropsychological problems (1, 2). It has been reported that 30% of adults on average sleep <7 h per day (3). Sleep deprivation (SD) becomes a prevailing problem for many individuals in modern societies, leading to lower working performance, accidents in life, and a high risk of illness (4). In addition, SD interferes with the cognitive function and emotion of individuals (5). Due to acute SD, brain functions are damaged and subsequently promote the development of psychiatric and neurodegenerative diseases (6). It is critical that developing an efficacious intervention combats these negative consequences of SD.

There are several interventions for treating SD, such as pharmacological therapy, cognitive behavior therapy, and other complementary and alternative therapies (7). Acupuncture acts as the most important clinical treatment modality of traditional Chinese medicine, progressed through thousands of years in clinical practice (8). Accumulating evidence has shown that acupuncture could significantly improve the sleep quality and cognitive function of individuals suffering from insufficient sleep (9). Numerous animal studies had also confirmed the effects and mechanisms of acupuncture on acute SD (10, 11). Nonetheless, the role of acupuncture on individuals after SD remains unclear.

To test the role of acupuncture on individuals after acute SD, we first explored the single acupoint immediate effect on acute SD individuals. HT7 (Shenmen) is one of the most frequently used acupoints in improving sleep quality and cognitive impairments. Also, recent clinical studies have revealed that acupuncture at HT7 had a beneficial effect on sleep disorders among Chinese people (12). Furthermore, one animal study on rats after 72 h of SD revealed significant improvements in cognitive abilities and brainwaves after acupuncture at HT7 (10). However, little is known about the effect of acupuncture at HT7 on acute SD individuals.

The use of functional magnetic resonance imaging (fMRI) is effective to explore the effect of acupoint HT7 intervening acute SD. Increasing studies have investigated the aberrant activity of brain regions in diverse paradigms and imaging, concerning acute or chronic SD (13, 14). Specifically, brain-imaging studies have revealed that SD could convert the activities of several brain regions and change the connectivity of brain regions (15). Functional brain networks can display correlated activities when an individual is awake or at rest (16). Functional connectivity (FC) is the direct approach to calculate the connectivity between seed areas or brain networks (1). The altered FC within and between brain networks have been confirmed after SD, involving the Default Mode Network (DMN), Salience Network (SN), Dorsal Attention Network (DAN), and Frontoparietal Network (FPN) (17, 18). DMN is preferentially activated when people are engaged in internally-oriented tasks, e.g., daydreaming and retrieving memories (19). Numerous fMRI studies have revealed that SD reduces intrinsic connectivity within DMN and anti-correlated networks (i.e., Attention Network) (17, 20). After SD, the connection between FPN and DMN showed a decreased disposition (15, 18). SN is capable to detect and integrate emotional and sensory stimuli, regulating the DMN and central executive network (21). In short, numerous fMRI studies have reported the abnormal FC among these aforementioned large-scale functional brain networks in SD. However, to date, there was no study reporting FC changes between large-scale networks after acupuncture at HT7 on acute SD.

According to the controversial acupuncture modulation hypothesis, the acute SD subjects should be different from the RW subjects in intrinsic network FC, part of which would be reversed after acupuncture at HT7. In this study, we recruited 30 healthy subjects with regular sleep and detected 2 times resting-state fMRI scans during the rested wakefulness (RW) state and after 24 h of total SD. The scan after 24 h of total SD included two resting-state fMRI sessions before and after acupuncture at Shenmen (HT7). Both edge-based and large-scale network FCs were calculated between the RW state and after 24 h of total SD, before and after acupuncture at HT7, and RW state and after acupuncture at HT7.

Materials and methods

Subjects

Thirty healthy subjects (14 females) studying in the college, aged 20–30 years (25.20 ± 2.20 years) with an education duration of 18.10 ± 2.45 years, were recruited. All subjects must meet the following criteria: (1) had no symptoms associated with sleep disorders and Pittsburgh Sleep Quality Index score < 5; (2) normal sleep patterns and not extreme morning or evening types according to Horne-Ostberg Morningness-Eveningness Questionnaire; (3) right-handed; (4) no history of neurologic or psychiatric disorders; (5) no history of trauma stimuli for the latest 1 year; (6) no addiction of coffee, smoking, and alcohol; (7) no MRI contraindications. Our study protocol had been approved by the Ethics Committee of Beijing Anding Hospital. All enrolled subjects were required to sign the informed consent before the beginning of this study.

Study procedure

All recruited subjects were required to visit our laboratory twice. A brief introduction to the study protocol was provided and signed the informed consent at the first visit. During the second visit after a week, the subjects returned to the laboratory for 24 h SD from 8:00 am on the 1st day to 8:00 am on the 2nd day. During the SD, all subjects were required to stay awake all the time and not take tea, coffee, or alcohol. The members

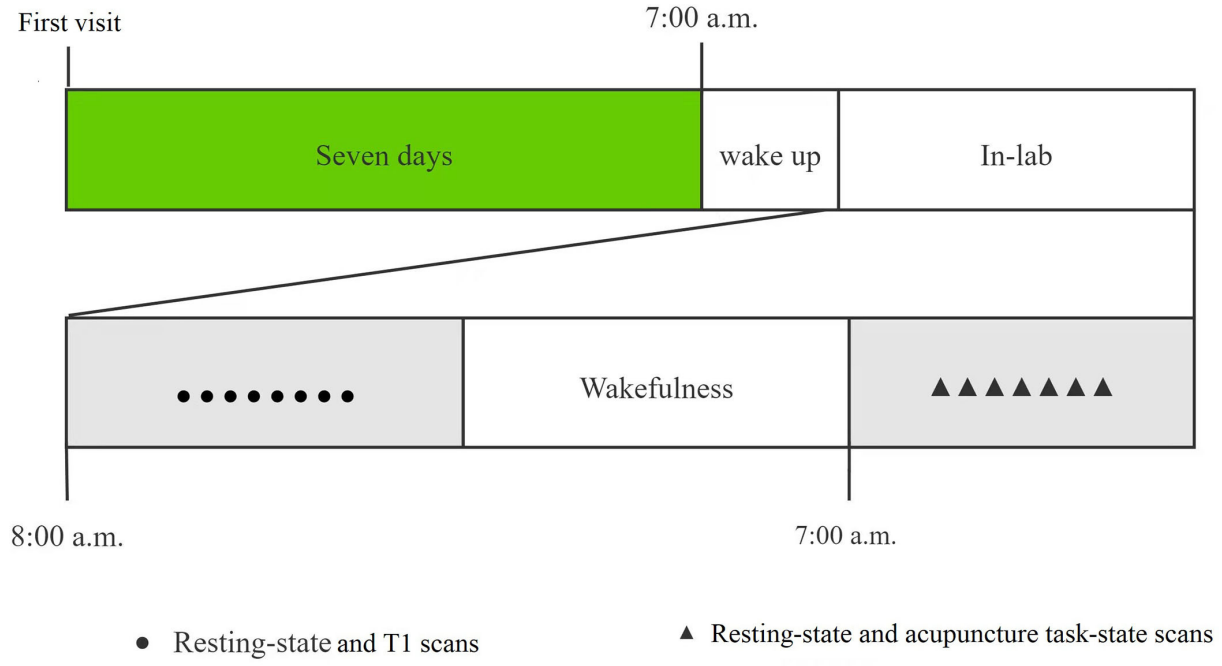

FIGURE 1
The flowchart of study procedure.

of our research group monitored in turns, to prevent subjects from falling asleep. They would be waked up immediately if they showed any signs of falling asleep. All subjects were required to complete twice MRI scans at the beginning of the study and after 24 h of SD. At the first MRI scanning, we performed the 490-s resting-state and 250-s T1 scans, while the 490-s resting-state and 550-s acupuncture task-state scan at the second MRI scanning after 7:00 am the next day. We would remind the participants not to fall asleep during scanning before each scan sequence, and rule out the participant who reported falling asleep during the fMRI scan. The study procedure was shown in Figure 1.

Acupuncture task-state fMRI design

In our study, the non-repeated event-related fMRI design was employed to detect the effects of acupuncture, which was in line with our previous studies (22, 23). According to our previous study, we performed a 60-s acupuncture manipulation and then a 490-s resting-state scan (without manipulation). We would compare the two resting-state scans before and after acupuncture at HT7 to detect the acupuncture effect on SD.

Acupuncture was performed at bilateral Shenmen (HT7, located on the palmar ulnar end of the transverse crease of the wrist and on the radial aspect of the tendon of the ulnar flexor). The needling was conducted by inserting two sterile, single-use silver needles (0.5 mm in diameter and 40 mm in length) vertically into bilateral HT7s to a depth of 20–30 mm. The needling operation included rotating the needle clockwise and counterclockwise at 1 Hz with even reinforcing and reducing manipulation for 60 s. All needling operations were conducted by the same two licensed and skilled acupuncturists.

MRI acquisition

In this study, we employed a 3.0 Tesla Prisma MRI scanner (Siemens) to acquire MRI scans at Beijing Anding Hospital. Subjects were required to stay still, keep their eyes closed, and refrain from falling asleep during the scan. Meanwhile, the foam head holders were immobilized to reduce head movements.

The high-resolution structural information for anatomical localization was obtained by applying 3D MRI sequences before the functional scanning. The resting-state and acupuncture task-state fMRI data were collected with a single-shot, gradient-recalled echo-planar imaging sequence with the following parameters: echotime = 30 ms, repetition time = 2,000 ms, flip angle = 90°, matrix = 64 × 64, gap = 1 mm, field of view = 225 × 225 mm, slice thickness = 3.5 mm, 32 interleaved axial

TABLE 1 Number and ratio of decreased and increased ROI-wise FC between the acute SD and RW states.

Number Percent	VN	SMN	DAN	VAN	SCN	FPN	DMN
Decreased ROI-wise FC							
VN	0						
	0%						
SMN	2	0					
	0.3%	0%					
DAN	4	0	1				
	1.3%	0%	1.1%				
VAN	1	3	0	0			
	0.28%	0.65%	0%	0%			
SCN	0	0	0	0	0		
	0%	0%	0%	0%	0%		
FPN	3	3	2	1	1	0	
	0.65%	0.49%	0.68%	0.30%	0.68%	0%	
DMN	2	3	4	0	1	1	2
	0.28%	0.31%	0.87%	0%	0.14%	0.14%	0.38%
Increased ROI-wise FC							
VN	0						
	0%						
SMN	1	0					
	0.16%	0%					
DAN	0	1	1				
	0%	0.25%	1.1%				
VAN	1	0	1	0			
	0.28%	0%	0.45%	0%			
SCN	0	0	1	2	1		
	0%	0%	1.02%	1.79%	4.76%		
FPN	1	2	2	1	1	0	
	0.22%	0.33%	0.68%	0.3%	0.68%	0%	
DMN	3	1	3	3	4	3	6
	0.41%	0.10%	0.65%	0.57%	1.73%	0.43%	1.14%

Values in the first line of each cell are the count number of suprathreshold edges belonging to each pair of networks for the significant cluster obtained from the NBS analysis; while values in the second line are the ratio (in percent) of that number to the number of full connections for each pair of networks. VN, visual network; SMN, somatosensory network; DAN, dorsal attention network; VAN, ventral attention network; SCN, subcortical network; FPN, frontoparietal network; DMN, default mode network, FC, functional connectivity; RW, rested wakefulness; SD, sleep deprivation; ROI, region of interest.

slices and 180 volumes. The high-resolution structural scan was acquired with the following parameters: voxel size = 1 mm^3, TR = 2,530 ms, TE = 3.39 ms, flip angle = 90°, matrix = 256 × 256, field of view = 256 × 256 mm, slice thickness = 1 mm.

Data processing

All data processing was completed by DPABI (24) with the methods in the article published by Li et al. (25).

Anatomical data preprocessing

The T1 images were converted into the BIDS dataset. Then they were corrected for intensity non-uniformity with N4BiasFieldCorrection (26), which was provided by ANTs 2.3.3. The derived images were skull-stripped with OASIS30ANTs as the target template. The remaining brain tissues were segmented into the cerebrospinal fluid (CSF), white-matter (WM), and gray-matter (GM) by the BET (FSL 5.0.9). A classic method, which reconciles ANTs- and FreeSurfer-derived segmentation of the cortical gray-matter of Mindboggle (27), was applied for refining the brain mask estimated

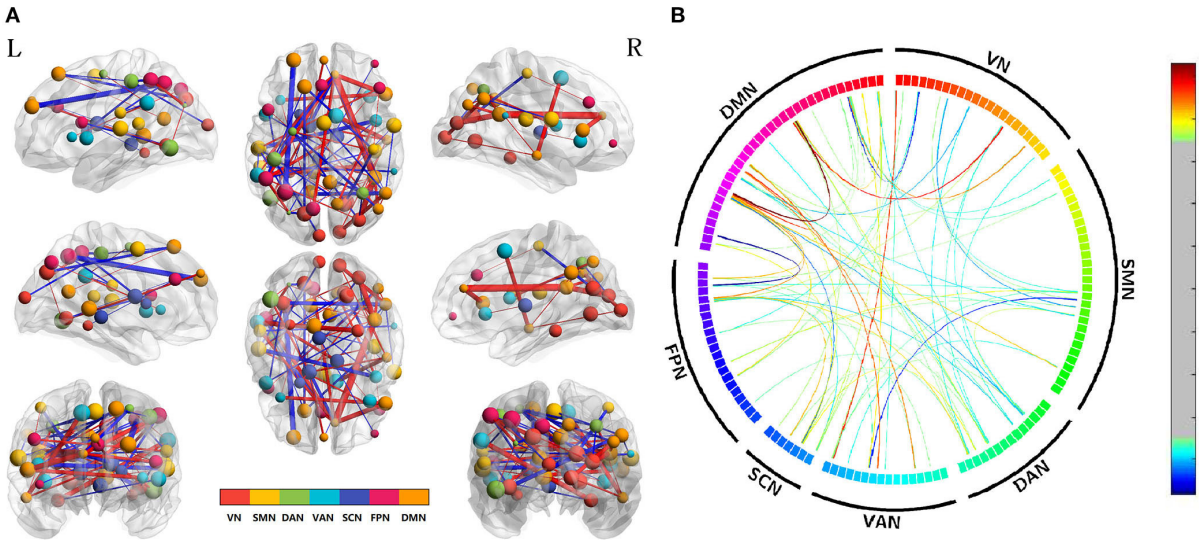

FIGURE 2
Altered edge-based functional connectivity between the acute SD and RW states. **(A)** The brain maps show the affected edges (lines) and their connecting nodes (spheres) from several perspectives. The size of a node indicates how many affected edges are connected to this sphere. Bigger nodes have more affected edges than smaller ones. The color of a node indicates which network it belongs to. The warm color of edges indicates the increased FC after acute SD, while the cold color of edges indicates the decreased FC. **(B)** ROI to ROI connectivity of seven networks in panels. The result was corrected by NBS ($p < 0.01$, two-tailed, permutation with 5,000 iterations). DAN, dorsal attention network; DMN, default mode network; FC, functional connectivity; FPN, frontoparietal network; L, left; R, right; SCN, subcortical network; SMN, somatosensory network; VAN, ventral attention network; VN, visual network; RW, rested wakefulness; SD, sleep deprivation.

previously. Volume-based spatial normalization to one standard space (MNI152NLin2009cAsym) was conducted *via* non-linear registration with antsRegistration (ANTs 2.3.3), using brain-extracted versions of T1 reference and template. Meanwhile, we selected ICBM 152 Non-linear Asymmetrical template version 2009c for spatial normalization.

Functional data preprocessing

First, we used the custom methodology of fMRIPrep (28) to generate the reference volume and skull-stripped version. Susceptibility distortion correction (SDC) was omitted. Bbregister, which implements boundary-based registration, was applied for co-registering the fMRI reference and T1 reference. Moreover, slice-time was corrected using 3dT shift from AFNI and spatiotemporal filtering was conducted by mcflirt (FSL). The BOLD time series were resampled into standard space and generated a preprocessed BOLD run in MNI 152 NLin2009c Asym space. At the same time, framewise displacement (FD), DVARS, and three region-wise global signals were calculated by the preprocessed BOLD. Additionally, a set of physiological regressors were extracted to allow for component-based noise correction (CompCor). Above components were dropped from the BOLD and frames that exceeded a threshold of 0.5 mm FD or 1.5 standardized DVARS were annotated as motion outliers. Gridded (volumetric) resampling was performed using ants Apply Transforms (ANTs), configured with Lanczos interpolation to minimize the smoothing effects of other kernels. We used bandpass filter (0.01–0.08 Hz) to reduce the high-frequency physiological noise and low-frequency drift.

Edge-based FC calculation

The Dosenbach atlas (29), which contained 160 regions of interest (ROIs) and deleted 18 ROIs in the cerebellum, was selected to extract the BOLD signals which averaged across all voxels in the ROIs. Each node of the atlas was a 5 mm-radius sphere. Pearson's correlation coefficient of the BOLD signals was computed to define the FC for any pair of two ROIs. Meanwhile, the value of FC was transformed into z-scores by Fisher's r-to-z formula. Network-Based Statistic (NBS) with paired *T*-tests were applied to compare the FC inter and intra group ($p < 0.01$, two-tailed, permutation with 5,000 iterations). For exploring the relationship of each large-scale network, we classified suprathreshold edges by their membership in the networks according to Li et al. (25) and Yeo et al. (30).

Large-scale network FC calculation

The seven networks are the visual network (VN, 22 ROIs), subcortical network (SCN, seven ROIs), DAN (14

TABLE 2 Number and ratio of decreased and increased ROI-wise FC for acute SD subjects between after and before acupuncture.

Number Percent	VN	SMN	DAN	VAN	SCN	FPN	DMN
Decreased ROI-wise FC							
VN	3						
	1.30%						
SMN	11	8					
	1.72%	1.97%					
DAN	7	10	2				
	2.27%	2.46%	2.20%				
VAN	12	6	7	3			
	3.41%	1.29%	3.13%	2.50%			
SCN	1	3	4	3	0		
	0.65%	1.48%	4.08%	2.68%	0.00%		
FPN	3	5	3	8	0	4	
	0.65%	0.82%	1.02%	2.38%	0.00%	1.90%	
DMN	6	16	5	14	4	9	11
	0.83%	1.67%	1.08%	2.65%	1.73%	1.30%	2.08%
Increased ROI-wise FC							
VN	2						
	0.87%						
SMN	6	5					
	0.94%	1.23%					
DAN	7	4	0				
	2.27%	0.99%	0.00%				
VAN	4	11	3	3			
	1.14%	2.37%	1.34%	2.50%			
SCN	2	3	2	1	0		
	1.30%	1.48%	2.04%	0.89%	0.00%		
FPN	12	11	7	7	4	2	
	2.60%	1.81%	2.38%	2.08%	2.72%	0.95%	
DMN	9	18	7	12	1	13	5
	1.24%	1.88%	1.52%	2.27%	0.43%	1.88%	0.95%

Values in the first line of each cell are the count number of suprathreshold edges belonging to each pair of networks for the significant cluster obtained from the NBS analysis; while values in the second line are the ratio (in percent) of that number to the number of full connections for each pair of networks. VN, visual network; SMN, somatosensory network; DAN, dorsal attention network; VAN, ventral attention network; SCN, subcortical network; FPN, frontoparietal network; DMN, default mode network; FC, functional connectivity; RW,SD, sleep deprivation; ROI, region of interest.

ROIs), FPN (21 ROIs), somatosensory-motor network (SMN, 29 ROIs), ventral attention network (VAN, 16 ROIs), and DMN (33 ROIs). Finally, we counted the number of edges within these networks and between these networks. Besides, we verified the above results by using a large-scale network FC analysis. Averaging the FC z-scores across all involved edges was applied for evaluating the FC among the seven networks. *T*-tests were used to compare the FC within and between groups ($p < 0.05$, False Discovery Rate Correction).

Results

Edge-based FC

NBS analysis ($p < 0.01$, two-tailed, permutation with 5,000 iterations) was used to calculate the edge-based FC among 142 ROIs. After conducting the differences in edge-based FC between the acute SD and RW states, we found that the suprathreshold edges with abnormal within-network FC involving DAN, SCN, DMN, and between-network FC involving

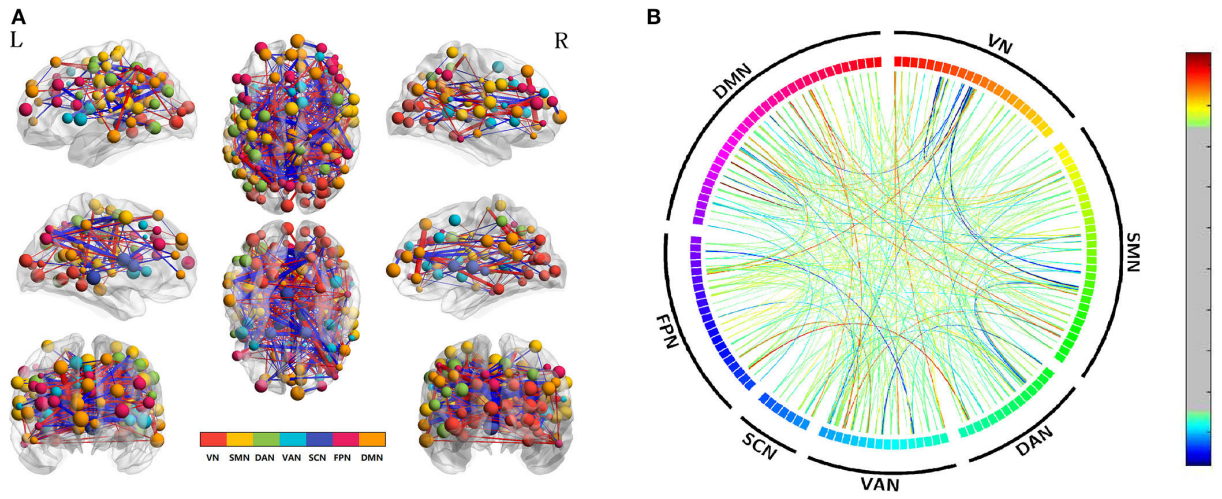

FIGURE 3
Altered edge-based functional connectivity for acute SD subjects between after and before acupuncture. **(A)** The brain maps show the affected edges (lines) and their connecting nodes (spheres) from several perspectives. The size of a node indicates how many affected edges are connected to this sphere. Bigger nodes have more affected edges than smaller ones. The color of a node indicates which network it belongs to. The warm color of edges indicates the increased FC after acupuncture, while the cold color of edges indicates the decreased FC. **(B)** ROI to ROI connectivity of seven networks in panels. The result was corrected by NBS ($p < 0.01$, two-tailed, permutation with 5,000 iterations). DAN, dorsal attention network; DMN, default mode network; FC, functional connectivity; FPN, frontoparietal network; L, left; R, right; SCN, subcortical network; SMN, somatosensory network; VAN, ventral attention network; VN, visual network; SD, sleep deprivation.

all paired networks except SMN-SCN, which suggested the widespread impact of SD on brain networks. Most of the affected ROI connections between two networks included both decreased FC and increased FC of edges. While there was only decreased ROI-wise FC between networks involving VN-DAN and SMN-VAN. The only increased ROI-wise FC between networks included SMN-DAN, DAN-VAN, DAN-SCN, VAN-SCN, and VAN-DMN. Moreover, we found that SD subjects demonstrated only increased within-network FC of the SCN, while both increased and decreased within-network FC of the DAN and DMN. The details are shown in Table 1 and Figure 2.

To explore acupuncture effects on acute SD, we then examined the differences in edge-based FC for SD between before and after acupuncture at HT7. Compared with SD before acupuncture at HT7, we found the suprathreshold edges with abnormal within-network FC involving all brain networks except SCN, and both decreased and increased between-network FC of edges involving all paired networks except FPN-SCN. Moreover, we found that SD subjects demonstrated only increased within-network FC of the DAN after acupuncture at HT7, while both increased and decreased within-network FC of the VN, SMN, VAN, FPN, and DMN. The details were shown in Table 2 and Figure 3.

We also compared the differences between SD after acupuncture and RW state. Compared with SD, we found both decreased and increased between-network FC of suprathreshold edges involving DAN only and decreased or increased between-network FC of edges involving all paired networks except SMN-SCN. The details are shown in Table 3 and Figure 4.

Large-scale network FC

To validate acupuncture effects, we furtherly analyzed large-scale within- and between-network FC. First, we compared the differences in large-scale network FC between the acute SD and RW states. We found that SD subjects showed a significant decrease in network FC in SMN-DMN, SMN-FPN, and SMN-VAN, and increased between-network FC in DAN-VAN, DAN-SMN. No abnormal within-network FC was found in acute SD subjects. We then conducted the comparisons between before and after acupuncture at HT7. Results revealed that the SD subjects showed significantly decreased between-network FC in DAN-VAN, increased between-network FC in SMN-VAN after acupuncture at HT7. There was no altered within-network FC in SD subjects after acupuncture. At last, we compared large-scale within- and between-network FC between acute SD after acupuncture and RW, and found no significant difference between the two states. The details are shown in Table 4 and Figure 5.

TABLE 3 Number and ratio of decreased and increased ROI-wise FC between acute SD after acupuncture and RW state.

Number Percent	VN	SMN	DAN	VAN	SCN	FPN	DMN
Decreased ROI-wise FC							
VN	0						
	0.00%						
SMN	3	0					
	0.47%	0.00%					
DAN	1	3	1				
	0.32%	0.74%	1.10%				
VAN	1	2	0	1			
	0.28%	0.43%	0.00%	0.83%			
SCN	0	0	0	2	0		
	0.00%	0.00%	0.00%	1.79%	0.00%		
FPN	1	1	2	2	0	0	
	0.22%	0.16%	0.68%	0.60%	0.00%	0.00%	
DMN	3	0	7	3	1	5	0
	0.41%	0.00%	1.52%	0.57%	0.43%	0.72%	0.00%
Increased ROI-wise FC							
VN	2						
	0.87%						
SMN	0	1					
	0.00%	0.25%					
DAN	2	0	1				
	0.65%	0.00%	1.10%				
VAN	1	1	3	0			
	0.28%	0.22%	1.34%	0.00%			
SCN	1	0	1	0	0		
	0.65%	0.00%	1.02%	0.00%	0.00%		
FPN	2	1	0	2	2	2	
	0.43%	0.16%	0.00%	0.60%	1.36%	0.95%	
DMN	5	1	3	1	4	4	3
	0.69%	0.10%	0.65%	0.19%	1.73%	0.58%	0.57%

Values in the first line of each cell are the count number of suprathreshold edges belonging to each pair of networks for the significant cluster obtained from the NBS analysis; while values in the second line are the ratio (in percent) of that number to the number of full connections for each pair of networks. VN, visual network; SMN, somatosensory network; DAN, dorsal attention network; VAN, ventral attention network; SCN, subcortical network; FPN, frontoparietal network; DMN, default mode network; FC, functional connectivity; RW,SD, sleep deprivation; ROI, region of interest.

Discussion

In the current study, we recruited 30 healthy subjects with regular sleep to compare their network FC between RW state and after 24 h of total SD, and before and after acupuncture at HT7. The edge-based results showed the suprathreshold edges with abnormal between-network FC involving all paired networks except SMN-SCN between the RW and after 24 h of total SD, while both decreased and increased between-network FC of edges involving all paired networks except FPN-SCN between before and after acupuncture at HT7. Compared with the RW state, the large-scale brain network results showed decreased between-network FC in SMN-DMN, SMN-FPN, SMN-VAN, and increased between-network FC in DAN -VAN, DAN-SMN between the RW state and after 24 h of total SD. After acupuncture at HT7, the large-scale brain network results showed decreased between-network FC in DAN-VAN, and increased between-network FC in SMN-VAN. In a word, our results may preliminarily provide new evidence to interpret the effect of acupuncture at HT7 on acute SD individuals.

In comparison with RW subjects, the FC in widespread brain regions and brain networks altered after 24 h of SD in our study. In line with our results, previous studies had demonstrated that functional brain networks in SD were abnormal involving SMN,

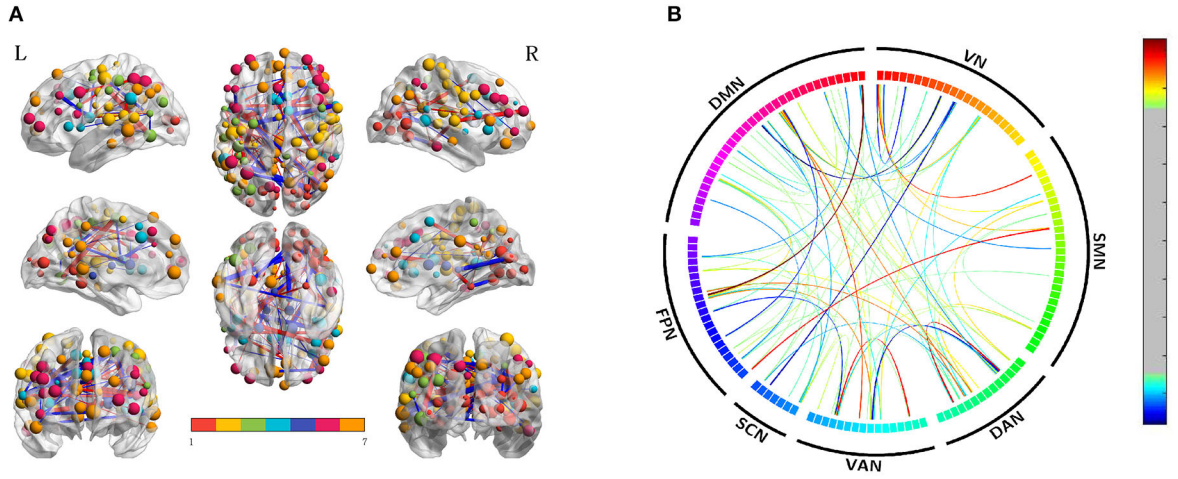

FIGURE 4
Altered edge-based functional connectivity between the acute SD after acupuncture and RW state. **(A)** The brain maps show the affected edges (lines) and their connecting nodes (spheres) from several perspectives. The size of a node indicates how many affected edges are connected to this sphere. Bigger nodes have more affected edges than smaller ones. The color of a node indicates which network it belongs to. The warm color of edges indicates the increased FC after acupuncture, while the cold color of edges indicates the decreased FC. **(B)** ROI to ROI connectivity of seven networks in panels. The result was corrected by NBS ($p < 0.01$, two-tailed, permutation with 5,000 iterations). DAN, dorsal attention network; DMN, default mode network; FC, functional connectivity; FPN, frontoparietal network; L, left; R, right; SCN, subcortical network; SMN, somatosensory network; VAN, ventral attention network; VN, visual network; RW, rested wakefulness.

TABLE 4 Large scale between-network FC changes.

Between networks	*t*	*p*
SD > RW		
VAN-SMN	−2.18	0.04
SMN-DAN	2.15	0.04
SMN-VAN	−2.18	0.04
DAN-VAN	2.32	0.03
SMN-FPN	−2.36	0.03
SMN-DMN	−2.05	0.05
After > before acupuncture		
VAN-SMN	2.8	0.01
VAN-DAN	−2.3	0.03

VN, visual network; SMN, somatosensory network; DAN, dorsal attention network; VAN, ventral attention network; SCN, subcortical network; FPN, frontoparietal network; DMN, default mode network, FC, functional connectivity; RW, rested wakefulness; SD, sleep deprivation.

DMN, Salience Network (SN), DAN, and FPN (17, 18, 31). A graph theory-based study on the whole brain networks also revealed that the small-world property of resting-state networks was significantly enhanced after acute SD (32). DMN is an internally directed network, which has been reported decreased FC within the network after acute SD (17). It is important that DMN can impact rest-stimulus interactions in corresponding sensory cortices (33), which may explain the decreased FC in DMN-SMN after SD. Also, it had been observed that SD could impact DAN which is associated with the top-down deployment of attention (34, 35). Several fMRI studies have revealed that SD could change the intrinsic connectivity within the DAN and its related anti-correlated network (i.e., DMN) (17, 20). FPN, which mainly supports the control of information processing, can contribute to verbal expression, memory, and cognitive control (36). After acute SD, the decreased FC in FPN-DMN was found, which was associated with working-memory performance (18). Notably, the SMN was found to be more affected (more pairs of large-scale networks) than other networks in the current study. Brain regions of the SMN control motor, somatosensory and auditory processing, and are responsible for external stimuli and internally generated movement. It has been demonstrated that the brain networks related to sleep and wake are modulated by sensory inputs, meanwhile, both sensory information and deprivation may induce changes in brain networks relative to sleep and waking up (37). One study revealed the decreased FC between the putamen and the main brain regions of SMN after acute SD, which in turn impaired motor perception and fine motor control. Another previous study also illustrated that the connection between the SMN and SN was reduced after acute SD (38). Thus, our results may support the notion that the SMN is the core network of altered large scale networks due to sleep loss. In short, we speculated that the abnormal FC within and between networks after acute SD might explain SD-induced impairments in cognitions and emotional discrimination, and be interpreted as a possible compensatory adaptation of the human brain that could enable partial recovery of certain behaviors.

Acupuncture, as the key component of Traditional Chinese Medicine, has been reported to modulate FC across the brain networks (8, 39, 40). Previous neuroimaging studies

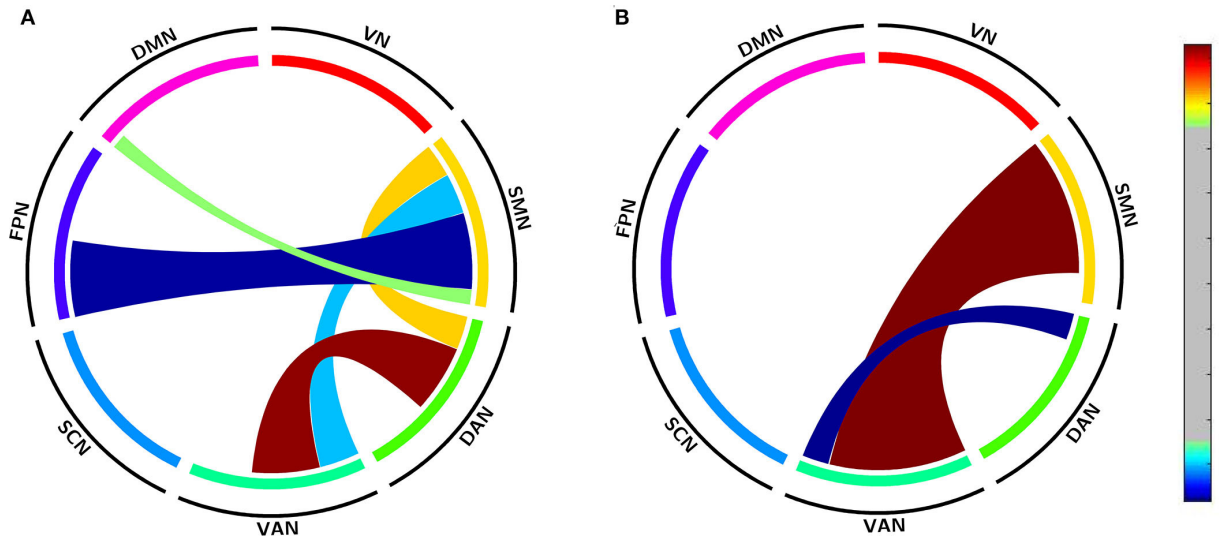

FIGURE 5
Altered large-scale network functional connectivity. **(A)** Altered large-scale network functional connectivity between SD and RW state; **(B)** Altered large-scale network functional connectivity for SD between after and before acupuncture. For the *T*-value color bar, blue indicates functional connectivity decrease while red indicates functional connectivity increase. The result was corrected by FDR-corrected $p < 0.05$ (two-tailed). DAN, dorsal attention network; DMN, default mode network; FC, functional connectivity; FPN, frontoparietal network; L, left; R, right; SCN, subcortical network; SMN, somatosensory network; VAN, ventral attention network; VN, visual network; RW, rested wakefulness; SD, sleep deprivation.

have also illustrated remarkable changes in brain activities responsive to acupuncture at the "Shenmen" point intervening on SD (10, 41). In this study, we found all seven networks were affected by acupuncture at HT7. According to previous neuroimaging studies, acupuncture stimuli could modulate extensive brain regions involving somatosensory, cognitive, and affective processing (8). A meta-analysis study on brain activities responding to acupuncture revealed that acupuncture could activate SMN and deactivate the limbic-paralimbic neocortical network (42). Apart from the activation/deactivation, the FC within and between networks could also be modulated by acupuncture (43, 44). These findings demonstrated that acupuncture could modulate multi-scale brain functions across the brain regions and networks, which was in line with our edge-based results. Moreover, we found the decreased FC in DAN-VAN and increased FC in SMN-VAN by large-scale network analysis. The DAN controls goal-oriented top-down deployment of attention (45), while the VAN partly overlapping with SN mediates stimulus-driven bottom-up attentional reorienting (46). The interaction between the two networks was competitive among multiple stimuli in the visual cortex and mediated the selection of behaviorally relevant information (47). One study on major depressive disorders revealed the increased clustering coefficient and small-worldness of DAN and VAN (48). Another study on healthy subjects demonstrated granger causal influences from VAN to DAN are negatively associated with attention performance (49). Hence, we speculated that the decreased FC between VAN and DAN might be interpreted as the treatment effect on the attention deficits of SD subjects. Regions of the SMN are spatially adjacent to regions of the DAN and VAN in the brain and cooperate with DAN and VAN during external tasks (30). The decreased FC in SMN-VAN after 24 h of total SD suggested abnormal performances during cognitive tasks. Previous neuroimaging studies confirmed that acupuncture could modulate SMN in low back pain and stroke patients, which represented the effects of acupuncture on diseases (50, 51). Thus, the enhanced FC in SMN-VAN after acupuncture could be interpreted as the treatment effects on acute SD. Together with changes in the DAN-VAN and SMN-VAN, no change between DMN and other networks (no significant pairs of large-scale networks) may suggest that acupuncture mainly modulates intrinsic FC of the externally directed networks. Taken together, the altered FC in SD-induced brain networks after acupuncture may indicate the mechanism of acupuncture on acute SD.

As to the analysis method in the current study, the surface-based preprocessing method was applied, which was better than the volume-based method for registration, reproducibility of algorithms, and surface reconstructions (52). Differing from previous neuroimaging studies on SD by employing seed-based FC analysis (18, 53), we applied both NBS and large-scale brain network analyses to explore SD-related abnormalities and acupuncture effects on intrinsic FC in large-scale brain networks. Hereby, our results could reveal the altered FC of large-scale brain networks after acupuncture at HT7.

However, there were still some limitations. First, as a preliminary study to explore the effect of acupuncture on SD, we only investigated the immediate effect at a single acupoint. Further studies on the long-term effects of acupuncture with group acupoints will be needed to explore the relationship between cognitive function improvements and FC changes. Secondly, without a control group of SD subjects with sham acupuncture treatment, we could not precisely quantify the effect of acupuncture on large-scale brain network FC. Nevertheless, in line with previous neuroimaging studies without the control group (22, 25, 54), our results indicated the possible mechanisms of the modulatory effects of acupuncture on SD. Furthermore, it is a challenge to set up sham acupuncture, which is not only difficult to implement but also has some specific efficacy, thus underestimating the therapeutic effect of acupuncture in the trial (55). Finally, numerous studies suggested that longer resting-state scans could improve reliability and replicability (56, 57). In the current study, we collected 490-s resting-state data. Future studies with longer resting-state scans will be needed to validate our results.

Conclusion

The edge-based results detected both decreased and increased between-network FC of edges involving most of the paired networks after acupuncture at HT7. The large-scale brain network results demonstrated that acupuncture could reverse the altered between-network FC of DAN-VAN and SMN-VAN. In short, acupuncture could widely modulate all brain networks and reverse the specific between-network FC.

Data availability statement

The raw data supporting the conclusions of this article will be made available by the authors, without undue reservation.

Ethics statement

The studies involving human participants were reviewed and approved by Ethics Committee of Beijing Anding Hospital. The patients/participants provided their written informed consent to participate in this study.

Author contributions

YN and HJ: conception and design. SZ, HY, ZF, XL, and LD: data collection. YN and SZ: data analysis. YN and SF: writing. SF: english-language revision. HJ and YN: revision. All authors contributed to the final version of the manuscript and approved the submitted version.

Funding

This study was supported by National Natural Science Foundation (Grant no. 81904120), Beijing Hospitals Authority Youth Program (Grant no. QML20201901), Beijing Natural Science Foundation (Grant no. 7212050), Beijing Hospitals Authority Clinical Medicine Development of Special Funding (Grant no. ZYLX202129), Beijing Hospitals Authority's Ascent Plan (Grant no. DFL20191901), and Talents Training Fund of Beijing (Grant no. 2018000021469G292).

Conflict of interest

The authors declare that the research was conducted in the absence of any commercial or financial relationships that could be construed as a potential conflict of interest.

Publisher's note

References

1. Mu Q, Nahas Z, Johnson KA, Yamanaka K, Mishory A, Koola J, et al. Decreased cortical response to verbal working memory following sleep deprivation. *Sleep.* (2005) 28:55–67. doi: 10.1093/sleep/28.1.55

2. Hirshkowitz M, Whiton K, Albert SM, Alessi C, Bruni O, DonCarlos L, et al. National Sleep Foundation's sleep time duration recommendations: methodology and results summary. *Sleep Health.* (2015) 1:40–3. doi: 10.1016/j.sleh.2014.12.010

3. Schoenborn CA, Adams PE. Health behaviors of adults: United States, 2005-2007. *Vital Health Stat.* (2010) 10:1–132.

4. Philip P, Akerstedt T. Transport and industrial safety, how are they affected by sleepiness and sleep restriction? *Sleep Med Rev.* (2006) 10:347–56. doi: 10.1016/j.smrv.2006.04.002

5. Yarkoni T, Poldrack RA, Nichols TE, Van Essen DC, Wager TD. Large-scale automated synthesis of human functional neuroimaging data. *Nat Methods.* (2011) 8:665–70. doi: 10.1038/nmeth.1635

6. Medic G, Wille M, Hemels ME. Short- and long-term health consequences of sleep disruption. *Nat Sci Sleep.* (2017) 9:151–61. doi: 10.2147/NSS.S134864

7. Kansagra S. Sleep disorders in adolescents. *Pediatrics.* (2020) 145:S204–9. doi: 10.1542/peds.2019-2056I

8. Zhang Y, Zhang H, Nierhaus T, Pach D, Witt CM, Yi M. Default mode network as a neural substrate of acupuncture: evidence, challenges and strategy. *Front Neurosci.* (2019) 13:100. doi: 10.3389/fnins.2019.00100

9. Yin X, Gou M, Xu J, Dong B, Yin P, Masquelin F, et al. Efficacy and safety of acupuncture treatment on primary insomnia: a randomized controlled trial. *Sleep Med.* (2017) 37:193–200. doi: 10.1016/j.sleep.2017.02.012

10. Li J, Liu JP. [Effects of acupuncture at "Shenmen" (HT 7) on brainwaves and cognitive ability in rats with sleep deprivation]. *Zhen Ci Yan Jiu.* (2017) 42:502–6. doi: 10.13702/j.1000-0607.2017.06.006

11. Li J, Ran X, Cui C, Xiang C, Zhang A, Shen F. Instant sedative effect of acupuncture at GV20 on the frequency of electroencephalogram alpha and beta waves in a model of sleep deprivation. *Exp Ther Med.* (2018) 15:5353–8. doi: 10.3892/etm.2018.6123

12. Wang C, Xu WL, Li GW, Fu C, Li JJ, Wang J, et al. Impact of acupuncture on sleep and comorbid symptoms for chronic insomnia: a randomized clinical trial. *Nat Sci Sleep.* (2021) 13:1807–22. doi: 10.2147/NSS.S326762

13. Dai XJ, Jiang J, Zhang Z, Nie X, Liu BX, Pei L, et al. Plasticity and susceptibility of brain morphometry alterations to insufficient sleep. *Front Psychiatry.* (2018) 9:266. doi: 10.3389/fpsyt.2018.00266

14. Zhang L, Shao Y, Jin X, Cai X, Du F. Decreased effective connectivity between insula and anterior cingulate cortex during a working memory task after prolonged sleep deprivation. *Behav Brain Res.* (2021) 409:113263. doi: 10.1016/j.bbr.2021.113263

15. Gujar N, Yoo SS, Hu P, Walker MP. The unrested resting brain: sleep deprivation alters activity within the default-mode network. *J Cogn Neurosci.* (2010) 22:1637–48. doi: 10.1162/jocn.2009.21331

16. Greicius MD, Krasnow B, Reiss AL, Menon V. Functional connectivity in the resting brain: a network analysis of the default mode hypothesis. *Proc Natl Acad Sci USA.* (2003) 100:253–8. doi: 10.1073/pnas.0135058100

17. De Havas JA, Parimal S, Soon CS, Chee MW. Sleep deprivation reduces default mode network connectivity and anti-correlation during rest and task performance. *Neuroimage.* (2012) 59:1745–51. doi: 10.1016/j.neuroimage.2011.08.026

18. Dai C, Zhang Y, Cai X, Peng Z, Zhang L, Shao Y, et al. Effects of sleep deprivation on working memory: change in functional connectivity between the dorsal attention, default mode, fronto-parietal networks. *Front Hum Neurosci.* (2020) 14:360. doi: 10.3389/fnhum.2020.00360

19. Buckner RL. The serendipitous discovery of the brain's default network. *Neuroimage.* (2012) 62:1137–45. doi: 10.1016/j.neuroimage.2011.10.035

20. Yeo BT, Tandi J, Chee MW. Functional connectivity during rested wakefulness predicts vulnerability to sleep deprivation. *Neuroimage.* (2015) 111:147–58. doi: 10.1016/j.neuroimage.2015.02.018

21. Downar J, Crawley AP, Mikulis DJ, Davis KD. A multimodal cortical network for the detection of changes in the sensory environment. *Nat Neurosci.* (2000) 3:277–83. doi: 10.1038/72991

22. Zhang Y, Li K, Ren Y, Cui F, Xie Z, Shin JY, et al. Acupuncture modulates the functional connectivity of the default mode network in stroke patients. *Evid Based Complement Alternat Med.* (2014) 2014:765413. doi: 10.1155/2014/765413

23. Ning Y, Li K, Fu C, Ren Y, Zhang Y, Liu H, et al. Enhanced functional connectivity between the bilateral primary motor cortices after acupuncture at yanglingquan (GB34) in right-hemispheric subcortical stroke patients: a resting-state fMRI study. *Front Hum Neurosci.* (2017) 11:178. doi: 10.3389/fnhum.2017.00178

24. Yan CG, Wang XD, Zuo XN, Zang YF. DPABI: data processing & analysis for (resting-state) brain imaging. *Neuroinformatics.* (2016) 14:339–51. doi: 10.1007/s12021-016-9299-4

25. Li L, Su YA, Wu YK, Castellanos FX, Li K, Li JT, et al. Eight-week antidepressant treatment reduces functional connectivity in first-episode drug-naive patients with major depressive disorder. *Hum Brain Mapp.* (2021) 42:2593–605. doi: 10.1002/hbm.25391

26. Tustison NJ, Avants BB, Cook PA, Zheng Y, Egan A, Yushkevich PA, et al. N4ITK: improved N3 bias correction. *IEEE Trans Med Imaging.* (2010) 29:1310–20. doi: 10.1109/TMI.2010.2046908

27. Klein A, Ghosh SS, Bao FS, Giard J, Hame Y, Stavsky E, et al. Mindboggling morphometry of human brains. *PLoS Comput Biol.* (2017) 13:e1005350. doi: 10.1371/journal.pcbi.1005350

28. Esteban O, Markiewicz CJ, Blair RW, Moodie CA, Isik AI, Erramuzpe A, et al. fMRIPrep: a robust preprocessing pipeline for functional MRI. *Nat Methods.* (2019) 16:111–6. doi: 10.1038/s41592-018-0235-4

29. Dosenbach NU, Nardos B, Cohen AL, Fair DA, Power JD, Church JA, et al. Prediction of individual brain maturity using fMRI. *Science.* (2010) 329:1358–61. doi: 10.1126/science.1194144

30. Yeo BT, Krienen FM, Sepulcre J, Sabuncu MR, Lashkari D, Hollinshead M, et al. The organization of the human cerebral cortex estimated by intrinsic functional connectivity. *J Neurophysiol.* (2011) 106:1125–65. doi: 10.1152/jn.00338.2011

31. Krause AJ, Simon EB, Mander BA, Greer SM, Saletin JM, Goldstein-Piekarski AN, et al. The sleep-deprived human brain. *Nat Rev Neurosci.* (2017) 18:404–18. doi: 10.1038/nrn.2017.55

32. Liu H, Li H, Wang Y, Lei X. Enhanced brain small-worldness after sleep deprivation: a compensatory effect. *J Sleep Res.* (2014) 23:554–63. doi: 10.1111/jsr.12147

33. Menon V. Large-scale brain networks and psychopathology: a unifying triple network model. *Trends Cogn Sci.* (2011) 15:483–506. doi: 10.1016/j.tics.2011.08.003

34. Zhou X, Wu T, Yu J, Lei X. Sleep deprivation makes the young brain resemble the elderly brain: a large-scale brain networks study. *Brain Connect.* (2017) 7:58–68. doi: 10.1089/brain.2016.0452

35. Hutton JS, Dudley J, Horowitz-Kraus T, DeWitt T, Holland SK. Functional connectivity of attention, visual, and language networks during audio, illustrated, and animated stories in preschool-age children. *Brain Connect.* (2019) 9:580–92. doi: 10.1089/brain.2019.0679

36. Zhu W, Chen Q, Xia L, Beaty RE, Yang W, Tian F, et al. Common and distinct brain networks underlying verbal and visual creativity. *Hum Brain Mapp.* (2017) 38:2094–111. doi: 10.1002/hbm.23507

37. Velluti RA. Interactions between sleep and sensory physiology. *J Sleep Res.* (1997) 6:61–77. doi: 10.1046/j.1365-2869.1997.00031.x

38. Tsvetanov KA, Henson RN, Tyler LK, Razi A, Geerligs L, Ham TE, et al. Extrinsic and intrinsic brain network connectivity maintains cognition across the lifespan despite accelerated decay of regional brain activation. *J Neurosci.* (2016) 36:3115–26. doi: 10.1523/JNEUROSCI.2733-15.2016

39. Dhond RP, Yeh C, Park K, Kettner N, Napadow V. Acupuncture modulates resting state connectivity in default and sensorimotor brain networks. *Pain.* (2008) 136:407–18. doi: 10.1016/j.pain.2008.01.011

40. Yu S, Xie M, Liu S, Guo X, Tian J, Wei W, et al. Resting-state functional connectivity patterns predict acupuncture treatment response in primary dysmenorrhea. *Front Neurosci.* (2020) 14:559191. doi: 10.3389/fnins.2020.559191

41. Chen D, Zhang Y, Wang C, Wang X, Shi J, Zhang J, et al. Modulation of hippocampal dopamine and synapse-related proteins by electroacupuncture improves memory deficit caused by sleep deprivation. *Acupunct Med.* (2020) 38:343–51. doi: 10.1177/0964528420902147

42. Chae Y, Chang DS, Lee SH, Jung WM, Lee IS, Jackson S, et al. Inserting needles into the body: a meta-analysis of brain activity associated with acupuncture needle stimulation. *J Pain.* (2013) 14:215–22. doi: 10.1016/j.jpain.2012.11.011

43. Shi Y, Zhang S, Li Q, Liu Z, Guo S, Yang J, et al. A study of the brain functional network of Deqi via acupuncturing stimulation at BL40 by rs-fMRI. *Complement Ther Med.* (2016) 25:71–7. doi: 10.1016/j.ctim.2016.01.004

44. Han X, Jin H, Li K, Ning Y, Jiang L, Chen P, et al. Acupuncture modulates disrupted whole-brain network after ischemic stroke: evidence based on graph theory analysis. *Neural Plast.* (2020) 2020:8838498. doi: 10.1155/2020/8838498

45. Corbetta M, Patel G, Shulman GL. The reorienting system of the human brain: from environment to theory of mind. *Neuron.* (2008) 58:306–24. doi: 10.1016/j.neuron.2008.04.017

46. Fox MD, Corbetta M, Snyder AZ, Vincent JL, Raichle ME. Spontaneous neuronal activity distinguishes human dorsal and ventral attention systems. *Proc Natl Acad Sci USA.* (2006) 103:10046–51. doi: 10.1073/pnas.0604187103

47. McMains S, Kastner S. Interactions of top-down and bottom-up mechanisms in human visual cortex. *J Neurosci.* (2011) 31:587–97. doi: 10.1523/JNEUROSCI.3766-10.2011

48. Chen H, Liu K, Zhang B, Zhang J, Xue X, Lin Y, et al. More optimal but less regulated dorsal and ventral visual networks in patients with major depressive disorder. *J Psychiatr Res.* (2019) 110:172–8. doi: 10.1016/j.jpsychires.2019.01.005

49. Wen X, Yao L, Liu Y, Ding M. Causal interactions in attention networks predict behavioral performance. *J Neurosci.* (2012) 32:1284–92. doi: 10.1523/JNEUROSCI.2817-11.2012

50. Lee J, Eun S, Kim J, Lee JH, Park K. Differential influence of acupuncture somatosensory and cognitive/affective components on functional brain connectivity and pain reduction during low back pain state. *Front Neurosci.* (2019) 13:1062. doi: 10.3389/fnins.2019.01062

51. Zhang J, Lu C, Wu X, Nie D, Yu H. Neuroplasticity of acupuncture for stroke: an evidence-based review of MRI. *Neural Plast.* (2021) 2021:2662585. doi: 10.1155/2021/2662585

52. Coalson TS, Van Essen DC, Glasser MF. The impact of traditional neuroimaging methods on the spatial localization of cortical areas. *Proc Natl Acad Sci USA.* (2018) 115:E6356–65. doi: 10.1073/pnas.1801582115

53. Chen WH, Chen J, Lin X, Li P, Shi L, Liu JJ, et al. Dissociable effects of sleep deprivation on functional connectivity in the dorsal and ventral default mode networks. *Sleep Med.* (2018) 50:137–44. doi: 10.1016/j.sleep.2018.05.040

54. Zhao T, Pei L, Ning H, Guo J, Song Y, Zhou J, et al. Networks are associated with acupuncture treatment in patients with diarrhea-predominant irritable bowel syndrome: a resting-state imaging study. *Front Hum Neurosci.* (2021) 15:736512. doi: 10.3389/fnhum.2021.736512

55. Fei YT, Cao HJ, Xia RY, Chai QY, Liang CH, Feng YT, et al. Methodological challenges in design and conduct of randomised controlled trials in acupuncture. *BMJ.* (2022) 376:e064345. doi: 10.1136/bmj-2021-064345

56. Birn RM, Molloy EK, Patriat R, Parker T, Meier TB, Kirk GR, et al. The effect of scan length on the reliability of resting-state fMRI connectivity estimates. *Neuroimage.* (2013) 83:550–8. doi: 10.1016/j.neuroimage.2013.05.099

57. Laumann TO, Gordon EM, Adeyemo B, Snyder AZ, Joo SJ, Chen MY, et al. Functional system and areal organization of a highly sampled individual human brain. *Neuron.* (2015) 87:657–70. doi: 10.1016/j.neuron.2015.06.037

frontiers | Frontiers in Neurology

TYPE Original Research
PUBLISHED 18 August 2022
DOI 10.3389/fneur.2022.952405

OPEN ACCESS

EDITED BY
Yihuai Zou,
Beijing University of Chinese Medicine, China

REVIEWED BY
Xuanang Xu,
Rensselaer Polytechnic Institute, United States
Jing Xia,
National University of Singapore, Singapore

*CORRESPONDENCE
Hui-miao Sun
sunhuimiao99@163.com
Fan Wang
fan.wang@xjtu.edu.cn

†These authors share first authorship

SPECIALTY SECTION
This article was submitted to Applied Neuroimaging, a section of the journal Frontiers in Neurology

RECEIVED 25 May 2022
ACCEPTED 18 July 2022
PUBLISHED 18 August 2022

CITATION
Sun H-m, Li Q-y, Xiao R-y, Zhang Z-d, Yang X-y, Yang J, Jin B, Wen J-x, Wu Y-j, Yang H and Wang F (2022) A structural MRI study of global developmental delay in infants (<2 years old). *Front. Neurol.* 13:952405. doi: 10.3389/fneur.2022.952405

A structural MRI study of global developmental delay in infants (<2 years old)

Hui-miao Sun[1*†], Qian-yun Li[2†], Ru-yi Xiao[3], Ze-dong Zhang[2], Xiao-yan Yang[1], Jie Yang[1], Bo Jin[1], Jia-xiang Wen[1], Yan-jun Wu[1], Hong Yang[1] and Fan Wang[3*]

[1]Department of Magnetic Resonance Imaging (MRI), Children Hospital of Shanxi Province (Shanxi Maternal and Child Health Hospital), Taiyuan, China, [2]College of Medical Imaging, Shanxi Medical University, Taiyuan, China, [3]Key Laboratory of Biomedical Information Engineering of Ministry of Education, Xi'an Jiaotong University, Xi'an, China

Objective: To use structural magnetic resonance imaging (3D-MRI) to evaluate the abnormal development of the cerebral cortex in infants with global developmental delay (GDD).

Methods: The GDD group includes 67 infants aged between 112 and 699 days with global developmental delay and who underwent T1-weighted MRI scans in Shanxi Children's Hospital from December 2019 to March 2022. The healthy control (HC) group includes 135 normal developing infants aged between 88 and 725 days in Shanxi Children's Hospital from September 2020 to August 2021. Whole-brain T1-weighted MRI scans were carried out with a 3.0-T magnetic resonance scanner, which was later processed using InfantSurfer to perform MR image processing and cortical surface reconstruction. Two morphological features of the cortical surface of the 68 brain regions were computed, i.e., the cortical thickness (CT) and cortical surface area (SA), and compared between the GDD and HC groups.

Results: With regard to the CT, the HC group showed a rapid decrease at first and then a slow increase after birth, and the CT of the GDD group decreased slowly and then became relatively stable. The GDD group showed bilaterally higher hemispherical average CT than those in the HC group. In detail, for the left hemisphere, except in the entorhinal and temporal poles in which the average CT values of the two brain regions were lower than those of the HC group, the CT of the 26 brain regions in the GDD group was higher than those of the HC group ($p < 0.05$). For the right hemisphere, the CT of the entorhinal in the GDD group was lower than that in the HC group. Otherwise, the CT of the remaining 28 brain regions was higher than those in the HC group ($p < 0.05$). With regard to the SA, both groups showed a rapid increase after birth till 23 months and remained quite stable afterward. The GDD group shows lower SA bilaterally than that in the HC group. In detail, SA in the GDD group was lower in most cortical regions of both hemispheres than in the HC group ($p < 0.05$), except for the right temporal pole and entorhinal. When testing for brain asymmetry, we found that the HC group showed obvious asymmetry of CT and SA, while only a few cortical regions in the GDD group showed asymmetry.

KEYWORDS

global developmental delay, infant, cortical surface, CT, SA, MRI

Introduction

The diagnostic criteria of the 5th edition of the Diagnostic and Statistical Manual of Mental Disorders (DSM-V) issued by the American Psychiatric Association on 18 May 18 2013 classify global developmental delay (GDD) as a neurodevelopmental disorder, which refers to underdevelopment in more than two aspects, including skills like motor, language, cognitive and social communication, and adjusts the diagnostic age to <5 years old (1). The prevalence of GDD is around 3%, and 5–10% of healthy children experience GDD early in development. Most cases often have several causes, which are mutually transformed and causative. There is a study that has shown that GDD is associated with genetic defects (2), and Li et al. show the subtle structural changes of each brain area in children with GDD by the change of ADC value (3) to indirectly understand the location and degree of brain injury in children. In a functional imaging study, the UF and SCP WMT showed microstructural changes suggestive of compromised white matter maturation in children with GDD (4). Current international scientific research and clinical evaluation of GDD is mostly based on the Gesell development diagnosis scale, which evaluates the development in five aspects, such as gross movement, fine movement, speech, human ability, and response-ability. The infant is diagnosed with GDD when the development quotient (DQ) is lower than 70 in two or more aspects. The current research regards the age of 0–3 as the key period for the early identification of infants with GDD. Lack of early diagnosis and intervention may introduce further intellectual disability, such as cerebral palsy, autism spectrum disorder (ASD), or attention deficit hyperactivity disorder (ADHD) (5). In particular, the development of language is combined with cognition, which is proceeded for up to 21 months. After 3 years old, cognitive and language development training becomes more difficult, recovery is slow, and the possibility of curing children with GDD is significantly reduced (6). The diagnosis and imaging study of the GDD is of great significance to the choice of treatment, prognosis, risk assessment of recurrence, and the implementation of prevention programs. At present, few studies are focusing on GDD with whole-brain structure MR images.

The first 2 years of life are a period of abnormal dynamic development of the structure and functions of the human brain. Babies' brains reach 80% of their adult size at the age of 2 (7). Studies have shown that many neurodevelopmental and mental disorders are caused by abnormal brain development at this stage. The cerebral cortex, which makes up the largest part of the human brain, has the topology of a 2-D sheet and a highly folded geometry (8). Surface-based morphometry (SBM) is widely used and mature in estimating cortical morphological indexes such as volume, cortical thickness, and surface area. Cortical thickness (CT) and surface area (SA) are important components that measure cortical morphometry. CT and SA abnormalities are commonly observed in neurodevelopmental disorders, including bipolar disorder (9), schizophrenia (10), autism (11), and attention-deficit/hyperactivity disorder (12). Shaw et al. used 3D-T1WI's longitudinal study of the correlation between intelligence and cortical thickness in normal children and adolescents and found that in early childhood, there was a significant negative correlation between intelligence and cortical thickness, while with age, they gradually showed a positive correlation (13). Therefore, the selection of these two indicators for quantitative analysis of children with GDD is helpful to further explore the relevant pathophysiological mechanism.

An MRI can associate the development of the brain structure with the behavior of infants, making it convenient to evaluate the lesions. In particular, 3D-MRI uses three-dimensional volume scanning with high spatial resolution and good tissue contrast and can display brain structure at the submillimeter level, which is convenient for the establishment of a visual map of the human brain. Infant FreeSurfer (14) is the most advanced special cortex analysis software for infants, which can calculate the morphological parameters of any position of the brain or other related data. The purpose of this study is to quantitatively analyze the CT and SA of infants with GDD by using whole-brain 3D-MRI, draw the developmental trajectory maps, and analyze the hemispheric asymmetry to help find the brain structural changes related to the disease and further reveal the potential pathophysiological mechanism of GDD.

Global developmental delay is a temporary diagnosis, which can be returned to normal after a timely clinical intervention. The use of structural magnetic resonance imaging (3D-MRI) to evaluate the abnormal development of the cerebral cortex in children with global developmental delay is conducive to providing early imaging evidence for the clinic and analyzing the differences in different brain regions, providing support for the study of the mechanism of related neuropsychiatric disorders.

Data and methods

General information

The experimental group selected 67 infants who underwent 3D-T1WI MRI examination in Shanxi Children's Hospital from December 2019 to March 2022 as the GDD group. They were aged between 112 and 699 d and included the following criteria: (1) met the diagnostic criteria of GDD in DSM-V; (2) the age was between 0 and 2 years old; (3) there was no previous neurotrophic factor drug therapy; (4) the image quality was good, and accurate data could be obtained. Exclusion criteria: infantile schizophrenia, obsessive-compulsive disorder, autism spectrum disorder, Asperger's syndrome, and other diseases. In the HC group, 145 infants were selected who underwent T1-weighted brain MRI examination in Shanxi Children's Hospital from September 2020 to August 2021, aged from 88 to 725 days. Inclusion criteria were as follows: (1) full-term natural delivery;

(2) no family history of mental or neurological disease; (3) no intracranial space occupying or congenital disease by clinical and imaging examination; (4) normal motor and cognitive function tested by development scale. All children complete the examination under sedation. This study was approved by the ethics committee of Shanxi Children's Hospital.

Inspection method

For the 3D-T1WI data collection, all subjects were given an enema with 5% chloral hydrate, a dose of 1 ml/kg, equipped with a hearing protection device, and scanned after deep sleep.

The GDD group was examined with GEDISCOVERY MR750W3.0T magnetic resonance machine and the head matrix coil. Sweep parameters were as follows: (1) regular MRI: T1WI: TR = 1,750 ms, TE = 27 ms; T2WI: TR = 5,231 ms, TE = 129 ms; T2-FLAIR: TR = 7,800 ms, TE = 89 ms. *All sequences*: FOV = 200 × 200 mm^2, matrix = 256 × 256 mm^2, slice spacing = 1.2 mm, slice thickness = 5.0 mm, excitation times = 2. (2) 3D-T1WI sequence: TR = 7.7 ms, TE = 2.8 ms, FOV = 240 × 240 mm^2, matrix = 256 × 256 mm^2, slice spacing = 0 mm, slice thickness = 1.0 mm, excitation times = 1.

The HC group was examined with PhilipsAchieva3.0T magnetic resonance machine and the head matrix coil. MR scan sequences include: (1) 3D-T1WI: using gradient echo sequence, TR = 600 ms, TE = 27 ms, FOV = 250 × 250 mm^2, slice spacing = −0.55 mm, slice thickness = 1.1 mm. (2) T2WI: TR = 2,651 ms, TE = 105 ms, FOV = 180 × 180 mm^2, matrix = 0.9 × 0.9 mm^2, slice spacing = 0.5 mm, slice thickness = 4.0 mm, excitation times = 2. (3) T2-FLAIR: TR = 7,800 ms, TE = 89 ms, TI = 2,300 ms, FOV = 180 × 180 mm^2, matrix = 0.9 × 0.9 mm^2, slice spacing = 0.5 mm, slice thickness = 4.0 mm, excitation times = 2.

Data processing

In this experiment, the Infant FreeSurfer software (11) was used to reconstruct the three-dimensional cortical surface of all 3D-T1WI magnetic resonance image data, including image intensity correction, head stripping, brain tissue segmentation, left and right cerebral dissection, reconstruction of the inner and outer surface of the cerebral cortex, and so on. To ensure the quality of skull dissection and the accuracy of gray matter/white matter boundary segmentation, the results of skull dissection and brain tissue segmentation were examined by two skilled anatomical operators. After the cortical reconstruction was completed, the left and right hemispheres were divided into 33 brain regions according to the FreeSurfer cortical atlas (15), and the average CT and the summed SA of each brain region were calculated. Linear mixed effect (LME) (16) models were used to model the development trajectory, and three models (linear, quadratic, and logistic curve) were used to fit the trajectory. After fitting different models, the best model was selected as the development trajectory according to the Akaike Information Criterion (AIC). In this study, based on this model, the developmental trajectories of CT and SA of two groups of subjects with age were fitted, respectively.

Statistical methods

MATLAB software was used to analyze the differences in the CT and SA between the two groups and the asymmetry between the left and right hemispheres of the two groups. Double-sample unpaired *t*-test was used for the difference between the groups, and paired *t*-test was used for hemispheric asymmetry. $P < 0.05$ was statistically significant.

Results

Developmental trajectories of CT

Figure 1 shows the comparative maps of the CT developmental trajectory of bilateral cerebral hemispheres between the two groups. Figure 2 shows the CT developmental trajectories of some representative regions of the two groups. Red represents the HC group and the blue line represents the GDD group. Different from the trend of rapid decrease and then slow increase of average CT in the HC group, the average CT of the GDD group decreases slowly and then remains stable. From the developmental trajectory maps, it can be seen that the average CT values of both sides of the brain in the GDD group are higher than those in the HC group.

Developmental trajectories of SA

Figure 3 shows the comparative maps of the hemispherical SA developmental trajectory between the two groups. Figure 4 shows the SA developmental trajectories of some representative regions of the two groups. Red represents the HC group and the blue line represents the GDD group. The average SA of both groups increases rapidly at first, reaches the peak at about 23 months, and then remains stable. From the developmental trajectory maps, it can be seen that the average SA value of both sides of the brain in the GDD group is lower than that in the HC group.

Differences in CT between two groups

Table 1 shows brain regions with significant differences in cortical thickness (CT) of bilateral cerebral hemispheres between the two groups. As shown in Table 1, for the left cerebral

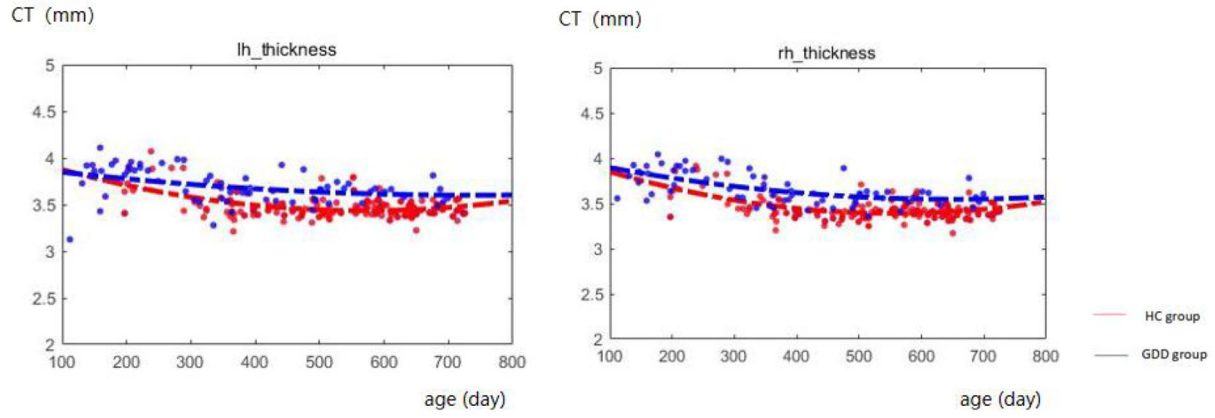

FIGURE 1
Hemispherical CT developmental trajectories of the two groups. The red line represents the HC group, and the blue line represents the GDD group (lh, left hemisphere; rh, right hemisphere).

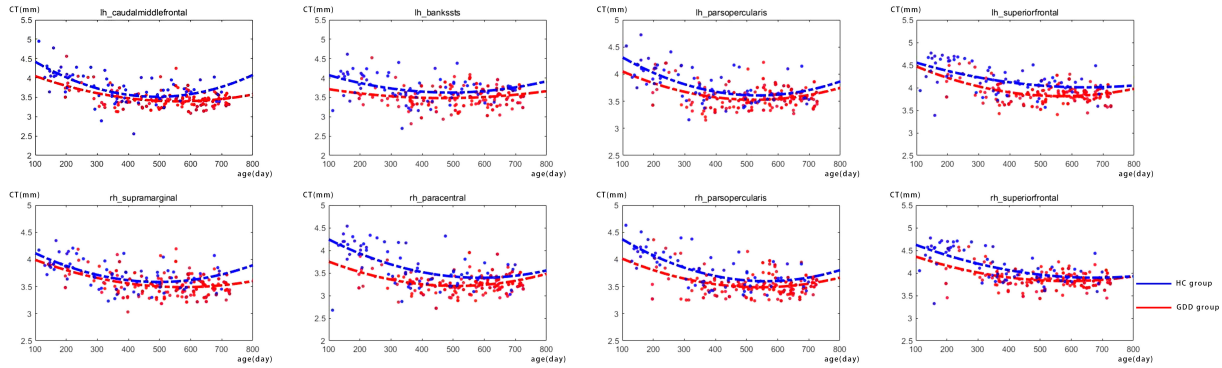

FIGURE 2
There are the CT developmental trajectories of some representative regions of the two groups. The red line represents the HC group, and the blue line represents the GDD group (lh, left hemisphere; rh, right hemisphere).

hemisphere, except for the average CT values of the entorhinal and temporal pole are lower than that of the HC group, the CT values of 26 brain regions such as caudal middle frontal, postcentral, pars-triangularis, supra-marginal, and bankssts in the GDD group are higher than those of the HC group, while for the right cerebral hemisphere, except that the CT value of entorhinal is lower than that of the HC group, the CT values of 28 brain regions such as superior temporal, posterior cingulate, inferior parietal, precentral and transverse temporal in the GDD group are higher than those of the HC group.

Differences in SA between two groups

Table 2 shows brain regions with significant differences in cortical surface areas (SA) of bilateral cerebral hemispheres between the two groups. As shown in Table 2, for the left hemisphere, SA values in all 33 brain regions in the GDD group are lower than those in the HC group; for the right hemisphere, SA values in 31 brain regions in the GDD group are also lower than those in the HC group, except the entorhinal and temporal pole.

Asymmetry of CT and SA of the two groups

The medial and lateral views of Figures 5A,C show the asymmetry of CT and SA between the left and right hemispheres of the HC group. The medial and lateral views of Figures 5B,D show the asymmetry of CT and SA between the left and right hemispheres of the GDD group. All results are shown

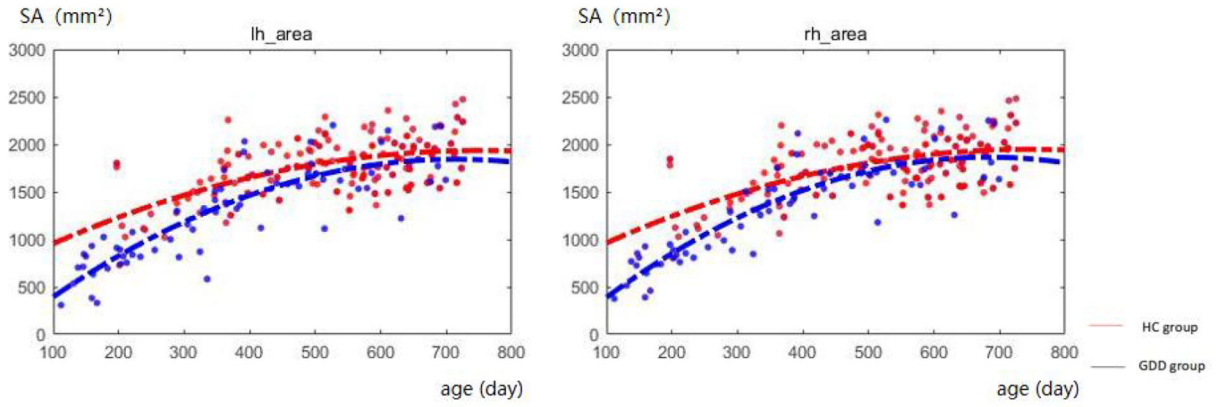

FIGURE 3
Hemispherical SA developmental trajectory between the two groups. The red line represents the HC group, and the blue line represents the GDD group (lh, left hemisphere; rh, right hemisphere).

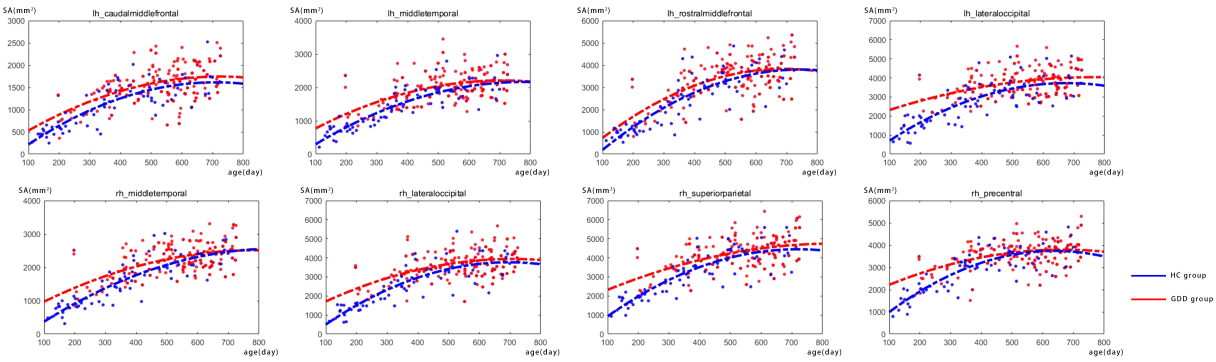

FIGURE 4
There are the SA developmental trajectories of some representative regions of the two groups. The red line represents the HC group, and the blue line represents the GDD group (lh, left hemisphere; rh, right hemisphere).

on the average central cortical surface of the age-matched left hemisphere. On the medial and lateral surfaces, the overall patterns in the left greater than the right (red), and the right greater than the left (blue) are relatively consistent in all ages.

As shown in Figure 5B and Table 3, the significantly asymmetric brain regions of CT in the GDD group are the lateral orbitofrontal, pars-orbitalis, pericalcarine, and posterior cingulate, all of which are larger on the left side than on the right side.

As shown in Figure 5D and Table 4, the significantly asymmetric brain regions of SA in the GDD group are pars-triangularis, pars-orbitalis, frontal pole, caudal anterior cingulate, and transverse temporal, all of which are larger on the right side than on the left side except transverse temporal.

Comparing Figures 5A,C with Figures 5B,D, it can be seen that the asymmetry area of the brain in the GDD group is less than that in the HC group. Except that the CT of the pericalcarine in the GDD group is larger than that on the right side, the asymmetry of other brain regions is consistent with that of the HC group.

Discussion

As we all know, the development of the cerebral cortex is closely related to the realization of various functions of the human body. For example, the frontal lobe is the area of executive function, attention, and motor coordination; the parietal lobe is involved in the development of spatial

TABLE 1 Brain cortical regions that show significant differences in cortical thickness (CT) between the two groups.

Brain region	CT (mm)		*P*	
	Left hemisphere (GDD/HC)	Right hemisphere (GDD/HC)	Left	Right
Caudal middle frontal	3.76/3.46	3.80/3.44	<0.0001**	<0.0001**
Entorhinal	2.27/3.08	2.56/3.07	<0.0001**	0.0005**
Postcentral	3.20/2.83	3.20/2.81	<0.0001**	<0.0001**
Pars triangularis	3.89/3.68	3.93/3.60	<0.0001**	<0.0001**
Supra marginal	3.81/3.63	3.73/3.54	<0.0001**	<0.0001**
Bankssts	3.74/3.51	3.85/3.58	<0.0001**	<0.0001**
Lateral orbitofrontal	4.11/4.12	3.84/3.92	0.9246	0.0464*
Pars orbitalis	4.22/4.03	4.02/3.90	<0.0001**	0.0112*
Middle temporal	4.05/3.74	4.09/3.78	<0.0001**	<0.0001**
Pericalcarine	3.43/2.93	3.31/2.92	<0.0001**	<0.0001**
Paracentral	3.61/3.22	3.66/3.27	<0.0001**	<0.0001**
Medial orbitofrontal	4.03/4.05	4.09/3.99	0.799	0.0406*
Frontalpole	4.51/4.37	4.52/4.38	0.0446*	0.0037**
Cuneus	3.82/3.25	3.71/3.23	<0.0001**	<0.0001**
Inferior temporal	4.04/3.68	4.05/3.69	<0.0001**	<0.0001**
Rostral middle frontal	4.12/3.74	4.08/3.70	<0.0001**	<0.0001**
Isthmus cingulate	2.91/2.66	2.86/2.62	<0.0001**	<0.0001**
Lateral occipital	3.86/3.16	3.81/3.16	<0.0001**	<0.0001**
Lingual	3.57/3.24	3.51/3.23	<0.0001**	<0.0001**
Superior parietal	3.73/3.26	3.70/3.23	<0.0001**	<0.0001**
Pars opercularis	3.80/3.58	3.83/3.54	<0.0001**	<0.0001**
Fusiform	3.86/3.53	3.72/3.49	<0.0001**	<0.0001**
Superior frontal	4.19/3.88	4.16/3.88	<0.0001**	<0.0001**
Temporalpole	3.86/4.09	3.85/3.95	0.0018**	0.1032
Precuneus	3.92/3.52	3.81/3.51	<0.0001**	<0.0001**
Transverse temporal	3.26/3.09	3.31/3.15	<0.0001**	0.0002**
Precentral	3.36/3.06	3.32/3.01	<0.0001**	<0.0001**
Inferior parietal	3.92/3.64	3.90/3.59	<0.0001**	<0.0001**
Posterior cingulate	3.37/3.13	3.17/2.91	<0.0001**	<0.0001**
Superior temporal	3.70/3.49	3.77/3.46	<0.0001**	<0.0001**
Insula	3.73/3.68	3.76/3.72	0.14	0.2719
Rostral anterior cingulate	3.29/3.40	3.11/3.09	0.1156	0.6732
Caudal anterior cingulate	3.05/3.03	2.99/2.92	0.7688	0.2132

*$P < 0.05$, **$P < 0.01$.

TABLE 2 Brain cortical regions that show significant differences in cortical surface area (SA) between the two groups.

Brain region	SA (mm^2)		*P*	
	Left hemisphere (GDD/HC)	Right hemisphere (GDD/HC)	Left	Right
Caudal middle frontal	1087.77/1549.43	1132.23/1448.11	<0.0001**	<0.0001**
Entorhinal	123.46/164.58	172.18/151.78	0.0076**	0.5221
Postcentral	2713.43/3385.09	2839.90/3212.46	<0.0001**	<0.0001**
Pars triangularis	619.24/856.49	849.88/1022.06	<0.0001**	<0.0001**
Supra marginal	2073.40/2682.30	2191.27/2560.47	<0.0001**	<0.0001**
Insula	1376.64/1669.19	1336.84/1566.32	<0.0001**	<0.0001**
Bankssts	509.30/719.18	491.03/676.99	<0.0001**	<0.0001**
Lateral orbitofrontal	1095.04/1384.28	1373.65/1475.09	<0.0001**	<0.0001**
Pars orbitalis	262.99/375.67	400.81/466.79	<0.0001**	<0.0001**
Middle temporal	1389.69/1991.66	1728.52/2211.28	<0.0001**	<0.0001**
Pericalcarine	640.50/971.46	786.29/1076.84	<0.0001**	<0.0001**
Paracentral	842.28/1021.16	1014.06/1128.39	<0.0001**	<0.0001**
Medial orbitofrontal	873.94/1048.12	943.83/1094.34	<0.0001**	<0.0001**
Frontalpole	120.06/158.83	190.28/206.51	<0.0001**	<0.0001**
Cuneus	721.13/1079.72	915.14/1137.95	<0.0001**	<0.0001**
Inferior temporal	1355.59/1951.14	1485.49/1877.82	<0.0001**	<0.0001**
Rostral middle frontal	2368.85/3392.16	2823.70/3521.96	<0.0001**	<0.0001**
Rostral anterior cingulate	369.22/498.77	370.93/464.99	<0.0001**	<0.0001**
Isthmus cingulate	751.63/1056.92	802.35/1008.20	<0.0001**	<0.0001**
Lateral occipital	2644.76/3719.88	2846.88/3600.93	<0.0001**	<0.0001**
Lingual	1409.71/2100.67	1695.88/2121.28	<0.0001**	<0.0001**
Superior parietal	3070.07/4349.31	3429.06/4196.36	<0.0001**	<0.0001**
Pars opercularis	782.91/1094.37	775.27/968.42	<0.0001**	<0.0001**
Fusiform	1296.44/2002.08	1465.54/1932.85	<0.0001**	<0.0001**
Caudal anterior cingulate	373.16/464.14	479.48/570.34	<0.0001**	<0.0001**
Superior frontal	3445.20/4450.62	3795.94/4287.15	<0.0001**	<0.0001**
Temporal pole	251.08/297.65	308.28/266.77	0.0026**	0.9663
Precuneus	1900.47/2825.29	2326.39/3033.29	<0.0001**	<0.0001**
Transverse temporal	294.05/372.20	241.71/294.85	<0.0001**	<0.0001**
Precentral	2840.55/3590.41	3055.08/3590.00	<0.0001**	<0.0001**
Inferior parietal	2187.09/3243.82	2868.38/3747.84	<0.0001**	<0.0001**
Posterior cingulate	712.06/928.79	790.42/957.84	<0.0001**	<0.0001**
Superior temporal	2155.62/2789.43	2304.05/2754.76	<0.0001**	<0.0001**

**$P < 0.01$.

orientation, speech and language, and attention; the temporal lobe is associated with memory integration; and the occipital lobe is the visual center (17), while the insular lobe connects the other lobes to participate in the realization of cognitive and sensory functions. Developmental disorders in any part of the cerebral cortex can lead to motor, language, and cognitive disorders.

At present, there are various forms of research on the cerebral cortex, and surface-based morphometry (SBM) is more in line with the goal of this study. We selected two indexes: cortical thickness and cortical surface area. Panizzon and other studies have shown that cortical thickness and cortical surface area are genetically related, but there is no genetic relationship between them (18), which further proves that they are indeed driven by different cellular mechanisms, which is consistent with the results of Rakic (16, 19). There have been similar studies on the properties of normal human brain structural networks, which have proved that the description of surface area and cortical thickness reveal different properties of human brain network structures (20). Grasby et al. showed that genetic factors had opposite effects on surface area and thickness and observed that there was a significant positive genetic correlation and two-way causality between total surface area and general cognitive function and education level, and a significant negative correlation between total surface area and insomnia, attention deficit hyperactivity disorder, depressive symptoms, major depressive disorder, and neuroticism (21). Therefore, this study compared the normal development of infants from the results of statistical differences between the two indicators, respectively, to explore the mechanism of neurodevelopmental disorders related to general developmental delay.

To eliminate the possible research differences caused by different scanning devices, homogenization of the data of different devices was carried out. We collected the image data of nineteen normally developing infants aged between 78 and 940 days who were examined by GEDISCOVERYMR750W3.0T magnetic resonance machine and met the inclusion criteria. The scanning parameters are the same as those of GEDISCOVERYMR750W3.0T magnetic resonance machine in the study. A new control group was formed between the above subjects and the control subjects examined by PhilipsAchieva3.0T magnetic resonance machine in the study. The new control group and the experimental group scanned by GEDISCOVERYMR750W3.0T magnetic resonance machine in the study used the same data processing method to compare the difference between CT and SA in each brain area of the same bilateral brain. Only one of the brain regions on both sides showed different results compared to existing results, but the differences were not significant. In summary, we believe that the influence of different scanning devices on the research results can be ignored.

GDD and HC show different development trajectories

In this study, the average CT of the bilateral brain in the GDD group was slightly different from that in the HC group, which decreased rapidly after birth and then kept stable. This is different from the results of some literature works. Wang et al. showed that in the first 2 years after birth, the average CT development of the whole cerebral cortex followed an "inverted U-shaped" trajectory, and CT increased dynamically in the first year but changed slightly in the second year (22). It may be related to genetic, dietary, and environmental factors due to the different sources of the subjects. On the other hand, the average SA development trajectory of both sides of the brain in the GDD group was similar to that in the HC group, which increased rapidly at first after birth, reached a peak at about 23 months, and remained quite stable afterward. It is suggested that the SA expansion pattern of children with global developmental delay is similar to that of normal children.

In addition, from the developmental trajectory map, we can see that the average CT value of both hemispheres in the GDD group is higher than that in the HC group, and the average SA value in the bilateral brain in the GDD group is lower than that in the HC group. The relevant content is further analyzed in the following content.

GDD and HC show differences in CT

This study found that for the left cerebral hemisphere, except for insula, the lateral orbitofrontal cortex, medial orbitofrontal cortex, caudal anterior cingulate, and rostral anterior cingulate, the CT values of other brain regions in the GDD group were different from those in the HC group. The CT values of the entorhinal and temporal pole in the GDD group were lower than those in the HC group, while the CT values in the other frontal, temporal, parietal, and occipital lobes were higher than those in the HC group. For the right cerebral hemisphere, except insula, temporal pole, caudal anterior cingulate, and rostral anterior cingulate, the CT values of other brain regions in the GDD group were different from those in the HC group, in which the entorhinal CT value in the GDD group was lower than that in the HC group, while the CT values in the other frontal, temporal, parietal and occipital lobes were higher than those in the HC group. Since the global developmental delay may evolve into autism spectrum disorder and hyperactive attention deficit to a certain extent, the author studies a similar mechanism.

The results of this study showed that the CT values of superior frontal, caudal middle frontal, pars-opercularis, pars-orbitalis, and posterior cingulate increased in both hemispheres compared with those of the HC group. The lateral orbitofrontal cortex and medial orbitofrontal cortex also showed an increase

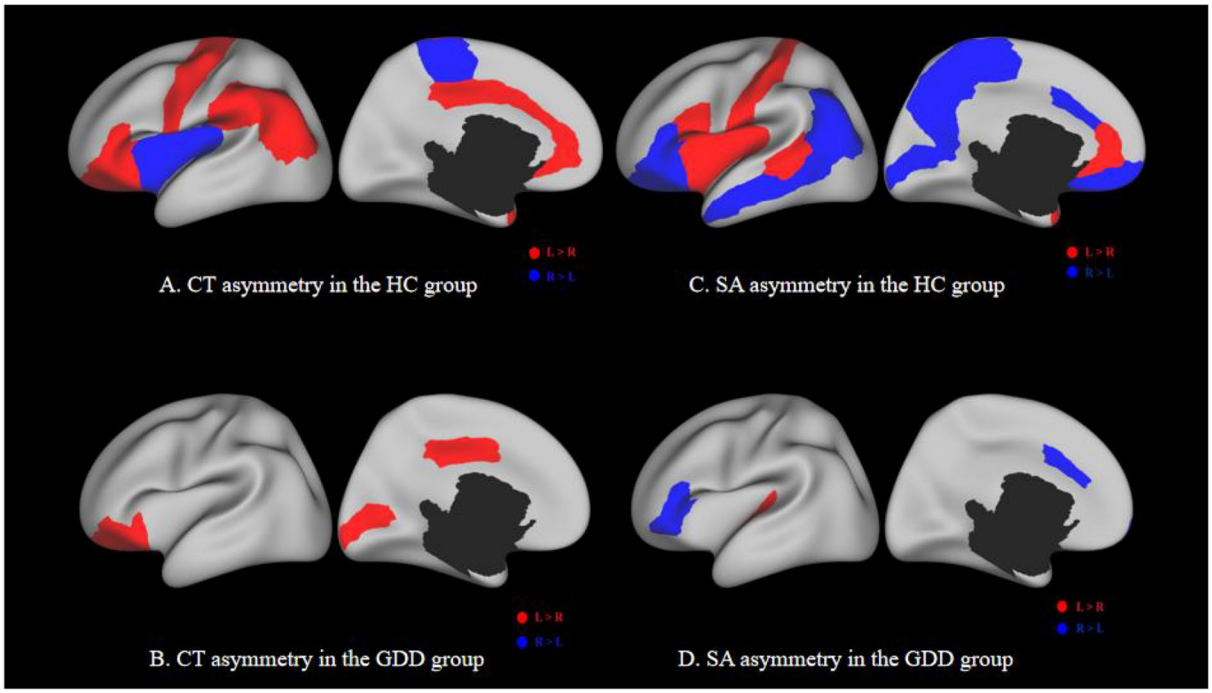

FIGURE 5
(A,C) show the asymmetry of CT and SA between two hemispheres of the HC group. **(B,D)** show the asymmetry of CT and SA between two hemispheres of the GDD group. Each image has a lateral view on the left and a medial view on the right. Red indicates a higher CT/SA in the left hemisphere of the same region than the right, while blue indicates the opposite. The black hole in the medial view indicates the medial wall between two hemispheres.

TABLE 3 Brain cortical regions that show significant asymmetry in cortical thickness (CT) in the GDD group.

Brain hemisphere	CT (mm)		*P*
	Left hemisphere	Right hemisphere	
Lateral orbitofrontal	4.13	3.87	0.0017**
Pars orbitalis	4.26	4.08	0.0237*
Pericalcarine	3.46	3.31	0.0489*
Posterior cingulate	3.37	3.18	0.0177*

*$P < 0.05$, **$P < 0.01$.

TABLE 4 Brain cortical regions that show significant asymmetry in cortical surface area (SA) in the GDD group.

Brain hemisphere	SA (mm^2)		*P*
	Left hemisphere	Right hemisphere	
Pars triangularis	604.62	751.4	0.0174*
Pars orbitalis	258.57	349.88	0.0016**
Frontalpole	114.72	163.92	0.0003**
Caudal anterior cingulate	364.02	430.44	0.0327*
Transverse temporal	283.14	208.17	0.0008**

*$P < 0.05$, **$P < 0.01$.

on the right. In van Rooij's study on autism (23), the same results were observed in the same areas, which may indicate that the children with global developmental delay have the same motor and cognitive control disorder mechanism, resulting in a developmental delay in the corresponding dimension.

In Yang et al.'s study, it was found that the thinning of the right superior frontal gyrus was consistent with the typical symptoms of ADHD. These structural abnormalities may correspond to disorders of attention, executive function, and cognitive control (24). In this study, the increase in CT value of the right superior frontal may indicate that part of the neurodevelopmental disorder mechanism of motor execution and cognition in children with global developmental delay is opposite to that of ADHD. In addition, compared with the results of this study, Kong et al. also found an increase in cortical thickness in the right frontal pole, right medial orbitofrontal gyrus, and right anterior and posterior central gyrus in children with Tourette syndrome (25). The frontal pole and medial orbitofrontal cortex belong to the prefrontal cortex, which is related to the thinking and execution of the brain, while the precentral gyrus and postcentral gyrus belong

to the sensorimotor cortex. The increased cortical thickness in these areas may indicate that the neurons in these areas are structurally dense and can increase the ability to regulate convulsions (21). These findings may show a compensatory effect, but it may also be due to the inhibition of exercise and other abilities caused by a too thick CT, which needs further study.

The upper parietal lobe is part of the default mode network. The default mode network has a functional connection to the caudate nucleus through dopamine projection. The striatal dopaminergic circuit may regulate cognition and emotion by regulating this network. In this study, it was found that the CT value of the bilateral parietal lobe was higher than that of the HC group, which may cause cognitive impairment in children with global developmental delay. This is similar to the related results of Zhang et al. on depression (26).

This study found that CT increased and SA decreased in the bilateral temporal lobe and fusiform, which may cause the disturbance of social perception. Adolphs believes that the higher sensory cortex, such as the fusiform gyrus and superior temporal sulcus, is involved in detailed sensory processing (27). Zilbovicius's study of autism spectrum disorders has also shown that the superior temporal sulcus is a major participant in social perception (28). In the study of ADHD, Hoogman et al. found that the surface area of children with ADHD was lower, mainly in the frontal lobe, cingulate gyrus, and temporal lobe, and the thickness of the fusiform gyrus and temporal pole cortex was also lower (29). However, this study is contrary to the results in terms of cortical thickness. Due to the differences in cellular mechanisms between CT and SA, it is not possible to determine which role or the combined effect of the two causes the corresponding dysfunction.

GDD and HC show differences in SA

The results of this study showed that except for the right entorhinal and the temporal pole, the SA in all brain regions of the other bilateral hemispheres was lower than that of normal children. During the development of normal children, the lateral temporal lobe, lateral parietal lobe, and medial prefrontal lobe were highly dilated, and the medial temporal lobe was poorly dilated. Sensory-specific correlative cortex such as supraoccipital gyrus (visual correlation), superior temporal gyrus/middle gyrus (auditory correlation), and superior parietal gyrus (sensory/tactile correlation/spatial correspondence) also showed a significant increase in SA (30). Fjell et al. showed that several regions in the frontal cortex, especially the anterior cingulate, showed high expansion in both development and evolution (31), in which the area of these regions was related to intellectual functions in humans. The lack of cortical dilatation in children with global developmental delay may indicate developmental disorders in the corresponding brain regions.

In SA-related studies of autism, cortical dilatation occurs in high-risk infants with ASD from June to 12 months, and excessive brain volume growth is associated with the occurrence and severity of social deficits in autism (32). The data of this study show that the SA of multiple brain regions of both hemispheres is lower than that of normal children, indicating that the decreased social ability of children with global developmental delay may be different from the pathophysiological mechanism of ASD expansion in SA. In a study on subjective cognitive decline, it was found that the decrease in total cortical volume and cortical surface area in patients (33) may suggest the pathophysiological mechanism of decreased cortical surface area in children with global developmental delay. Another study on autism spectrum disorders showed a significant decrease in SA in the orbitofrontal cortex and posterior cingulate gyrus (34), which is consistent with the results of this study, suggesting that the decline in executive power may be related to this.

At present, most of the research results on neurodevelopmental disorders are focused on adolescents and adults, and they are different from the results of this study and there are not many references, so the mechanism of SA reduction in children with global developmental delay needs further research.

GDD and HC show different asymmetry patterns

The asymmetrical areas of the brain in the GDD group were less than those in the HC group. The CT of the GDD group showed significant left deviation in lateral orbitofrontal, pars-orbitalis, peri-calcarine, and posterior cingulate. The SA of the GDD group showed significant left deviation in transverse temporal and significant right deviation in pars-triangularis, pars-orbitalis, frontal pole, and caudal anterior cingulate.

Normal children show obvious left deviation in the early stage of infants (35), but in this study, the number of lateral brain areas in the GDD group is less than that in the HC group, which may be caused by underdevelopment, indicating that there may be maturation disorders in the corresponding brain regions. Asymmetry between the left and right hemispheres is an important aspect of human brain tissue, which may be changed under various neurodevelopmental abnormalities (35).

The left hemisphere responsible for language specialization is one of the earliest observed brain asymmetries. Some aspects of language generation and syntactic processing are then mainly located in the triangle and operculum of the inferior frontal gyrus (36). The results of this study show that the

left tilting areas of CT and SA in the whole frontal lobe, including the inferior frontal gyrus, are fewer than those in the HC group, indicating that the decrease in lateralization may lead to the corresponding language development delay. Glasser's neurography analysis using diffusion imaging data showed that the arcuate bundle connecting the superior temporal gyrus (STG) and the middle temporal gyrus (MTG) to the inferior frontal lobe was asymmetrical to the left, and the left STG and MTG pathways were involved in speech processing and lexical-semantic processing, respectively (37). This left deviation was significantly reflected in the CT hemispheric asymmetry of middle temporal in the HC group, but not in the GDD group. It is further proved that the language cortex of the left hemisphere may not be fully activated, which is related to the underdevelopment of language in children.

Li et al. showed the leftward asymmetries in the medial prefrontal, paracentral, and anterior cingulate cortices, which expanded substantially during the first 2 years of normal infants (38). In this study, we have not seen the leftward asymmetries in the same regions. Postema et al. showed that ASD was significantly associated with alterations of cortical thickness asymmetry mostly in the medial frontal, orbitofrontal, cingulate, and inferior temporal areas, and also with asymmetry of the orbitofrontal surface area (39). This study does not show the same results. This may indicate that children with GDD have a disorder in the lateralization of the relevant cortex, but also avoid the risk of ASD to a certain extent.

Some studies have shown that children with attention deficits have consistent functional disorders in the right inferior frontal gyrus and anterior cingulate cortex (40, 41). The results of this study showed that the lateralization of the corresponding areas in the GDD group was normal, and the thickness of the bilateral anterior cingulate cortex was not different from that in the HC group, indicating that the GDD group may not have cortical dysfunction in the corresponding regions.

Conclusion

The results of this study show that compared with normal developmental children, the whole brain average developmental trajectory of GDD infants is similar to that of HC infants, but there is an increase in CT and a decrease in SA in many brain regions on both sides of the brain. There may be no correlation between the two aspects, and the specific pathophysiological mechanism needs to be further studied.

The results of this study are helpful for further analyzing the mechanism of neurodevelopmental disorders in children with GDD, providing visual imaging data for clinical diagnosis and treatment, prognosis evaluation, efficacy evaluation and correlation analysis with clinical score, and facilitating further research work related to infant brain development.

Limitation

Because our sample size is limited, there is no grouping according to etiology and backwardness dimensions, so the final result can only be an overall difference. Next, we will expand the sample size, take etiology and other factors into correlation considerations, and study the specific mechanisms of neurodevelopmental disorders in different dimensions of developmental backwardness.

Data availability statement

The original contributions presented in the study are included in the article/Supplementary material, further inquiries can be directed to the corresponding author/s.

Ethics statement

Written informed consent was obtained from the individual(s), and minor(s)' legal guardian/next of kin, for the publication of any potentially identifiable images or data included in this article.

Author contributions

H-mS: project guidance, data collection and analysis, and article writing and modification. Q-yL: project implementation, data collection and analysis, and article writing and revision. RX: data post-processing, statistical analysis, and article modification. Z-dZ and J-xW: clinical data collection. X-yY: interpretation of results. JY, BJ, and Y-jW: image data collection. HY: image examination and scanning. FW: project guidance, data post-processing, and article modification. All authors contributed to the article and approved the submitted version.

Funding

This work was funded by Key Research and Development Program of Shanxi Province (Project No.: 201903D321051).

Conflict of interest

The authors declare that the research was conducted in the absence of any commercial or financial relationships that could be construed as a potential conflict of interest.

Publisher's note

References

1. American Psychiatric Association. *Diagnostic and Statistical Manual of Mental Disorders (DSM-5)*. 5th ed. Arlington VA: American Psychiatric Association (2013). 79 p.

2. Duncan AR, Vitobello A, Collins SC, Vancollie VE, Lelliott CJ, Rodan L, et al. Heterozygous variants in KDM4B lead to global developmental delay and neuroanatomical defects. *Am J Hum Genet.* (2020) 107:1170–7. doi: 10.1016/j.ajhg.2020.11.001

3. Li L, Zhao JS, Gao ZF, Ma CY, Dong CH, Zhang HW. Application of apparent diffusion coefficient in children with intellectual disability/global developmental delay aged 2-12 years with normal brain MRI. *Chin J Contemp Pediatr.* (2019) 21:541–6. doi: 10.7499/j.issn.1008-8830.2019.06.008

4. Ramli N, Yap A, Muridan R, Seow P, Rahmat K, Fong CY, et al. Microstructural abnormalities found in uncinate fasciculus and superior cerebellar tracts in children with global developmental delay: a feasibility study. *Clin Radiol.* (2020) 75:77.e15–22. doi: 10.1016/j.crad.2019.09.134

5. Li XJ. *Children's Rehabilitation Undergraduate rehabilitation IFI*. Beijing: People's Medical Publishing House (2018).

6. Xu YH. *Risk Factors, Clinical Features and Prognosis of 185 Patients With Global Developmental Delay* (master's thesis). Anhui: Anhui Medical University (2016).

7. Knickmeyer RC, Gouttard S, Kang C, Evans D, Wilber K, Smith JK, et al. structural MRI study of human brain development from birth to 2 years. *J Neurosci.* (2008) 28:12176–82. doi: 10.1523/JNEUROSCI.3479-08.2008

8. Dale AM, Fischl B, Sereno MI. Cortical surface-based analysis. I Segmentation and surface reconstruction. *Neuroimage.* (1999) 9:179–94. doi: 10.1006/nimg.1998.0395

9. Kuang L, Gao W, Long Z, Cao W, Cui D, Guo Y, et al. Common and specific characteristics of adolescent bipolar disorder types I and II: a combined cortical thickness and structural covariance analysis. *Front Psychiatry.* (2022) 12:750798. doi: 10.3389/fpsyt.2021.750798

10. Neilson E, Shen X, Cox SR, Clarke TK, Wigmore EM, Gibson J, et al. Impact of polygenic risk for schizophrenia on cortical structure in UK biobank. *Biol Psychiatry.* (2019) 86:536–44. doi: 10.1016/j.biopsych.2019.04.013

11. Hazlett HC, Poe MD, Gerig G, Styner M, Chappell C, Smith RG, et al. Early brain overgrowth in autism associated with an increase in cortical surface area before age 2 years. *Arch Gen Psychiatry.* (2011) 68:467–76. doi: 10.1001/archgenpsychiatry.2011.39

12. Shaw P, Malek M, Watson B, Sharp W, Evans A, Greenstein D. Development of cortical surface area and gyrification in attention-deficit/hyperactivity disorder. *Biol Psychiatry.* (2012) 72:191–7. doi: 10.1016/j.biopsych.2012.01.031

13. Shaw P, Greenstein D, Lerch J, Clasen L, Lenroot R, Gogtay N, et al. Intellectual ability and cortical development in children and adolescents. *Nature.* (2006) 440:676–9. doi: 10.1038/nature04513

14. Zöllei L, Iglesias JE, Ou Y, Grant PE, Fischl B. Infant FreeSurfer: an automated segmentation and surface extraction pipeline for T1-weighted neuroimaging data of infants 0-2 years. *Neuroimage.* (2020) 218:116946. doi: 10.1016/j.neuroimage.2020.116946

15. Bérard N, Landis BN, Legrand L, Tyrand R, Grouiller F, Vulliémoz S, et al. Electrical stimulation of the medial orbitofrontal cortex in humans elicits pleasant olfactory perceptions. *Epilepsy Behav.* (2021) 114(Pt A):107559. doi: 10.1016/j.yebeh.2020.107559

16. Rakic P. The radial edifice of cortical architecture: from neuronal silhouettes to genetic engineering. *Brain Res Rev.* (2007) 55:204–19. doi: 10.1016/j.brainresrev.2007.02.010

17. Gogtay N, Giedd JN, Lusk L, Hayashi KM, Greenstein D, Vaituzis AC, et al. Dynamic mapping of human cortical development during childhood through early adulthood. *Proc Natl Acad Sci USA.* (2004) 101:8174–9. doi: 10.1073/pnas.0402680101

18. Panizzon MS, Fennema-Notestine C, Eyler LT, Jernigan TL, Prom-Wormley E, et al. Distinct genetic influences on cortical surface area and cortical thickness. *Cereb Cortex.* (2009) 19:2728–35. doi: 10.1093/cercor/bhp026

19. Rakic P. A small step for the cell, a giant leap for mankind: a hypothesis of neocortical expansion during evolution. *Trends Neurosci.* (1995) 18:383–8. doi: 10.1016/0166-2236(95)93934-P

20. Sanabria-Diaz G, Melie-García L, Iturria-Medina Y, Alemán-Gómez Y, Hernández-González G, Valdés-Urrutia L, et al. Surface area and cortical thickness descriptors reveal different attributes of the structural human brain networks. *Neuroimage.* (2010) 50:1497–510. doi: 10.1016/j.neuroimage.2010.01.028

21. Grasby KL, Jahanshad N, Painter JN, Colodro-Conde L, Bralten J, et al. The genetic architecture of the human cerebral cortex. *Science.* (2020) 367:eaay6690. doi: 10.1126/science.aay6690

22. Wang F, Lian C, Wu Z, Zhang H, Li T, Meng Y, et al. Developmental topography of cortical thickness during infancy. *Proc Natl Acad Sci USA.* (2019) 116:15855–60. doi: 10.1073/pnas.1821523116

23. van Rooij D, Anagnostou E, Arango C, Auzias G, Behrmann M, Busatto GF, et al. Cortical and subcortical brain morphometry differences between patients with autism spectrum disorder and healthy individuals across the lifespan: results from the ENIGMA ASD Working Group. *Am J Psychiatry.* (2018) 175:359–69. doi: 10.1176/appi.ajp.2017.17010100

24. Yang XR, Carrey N, Bernier D, MacMaster FP. Cortical thickness in young treatment-naive children with ADHD. *J Atten Disord.* (2015) 19:925–30. doi: 10.1177/1087054712455501

25. Kong L, Lv B, Wu T, Zhang J, Fan Y, Ouyang M, et al. Altered structural cerebral cortex in children with Tourette syndrome. *Eur J Radiol.* (2020) 129:109119. doi: 10.1016/j.ejrad.2020.109119

26. Zhang FF, Peng W, Sweeney JA, Jia ZY, Gong QY. Brain structure alterations in depression: psychoradiological evidence. *CNS Neurosci Ther.* (2018) 24:994–1003. doi: 10.1111/cns.12835

27. Adolphs R. Cognitive neuroscience of human social behaviour. *Nat Rev Neurosci.* (2003) 4:165–78. doi: 10.1038/nrn1056

28. Zilbovicius M, Meresse I, Chabane N, Brunelle F, Samson Y, Boddaert N. Autism, the superior temporal sulcus and social perception. *Trends Neurosci.* (2006) 29:359–66. doi: 10.1016/j.tins.2006.06.004

29. Hoogman M, Muetzel R, Guimaraes JP, Shumskaya E, Mennes M, Zwiers MP, et al. Brain imaging of the cortex in ADHD: a coordinated analysis of large-scale clinical and population-based samples. *Am J Psychiatry.* (2019) 176:531–42. doi: 10.1176/appi.ajp.2019.18091033

30. Lyall AE, Shi F, Geng X, Woolson S, Li G, Wang L, et al. Dynamic development of regional cortical thickness and surface area in early childhood. *Cereb Cortex.* (2015) 25:2204–12. doi: 10.1093/cercor/bhu027

31. Fjell AM, Westlye LT, Amlien I, Tamnes CK, Grydeland H, Engvig A, et al. High-expanding cortical regions in human development and evolution are related to higher intellectual abilities. *Cereb Cortex.* (2015) 25:26–34. doi: 10.1093/cercor/bht201

32. Hazlett HC, Gu H, Munsell BC, Kim SH, Styner M, Wolff JJ, et al. Early brain development in infants at high risk for autism spectrum disorder. *Nature.* (2017) 542:348–51. doi: 10.1038/nature21369

33. Sun Y, Wang X, Wang Y, Dong H, Lu J, Scheininger T, et al. Anxiety correlates with cortical surface area in subjective cognitive decline: APOE ε4 carriers versus APOE ε4 non-carriers. *Alzheimers Res Ther.* (2019) 11:50. doi: 10.1186/s13195-019-0505-0

34. Ecker C, Ginestet C, Feng Y, Johnston P, Lombardo MV, Lai MC, et al. Brain surface anatomy in adults with autism: the relationship between surface area, cortical thickness, and autistic symptoms. *JAMA Psychiatry.* (2013) 70:59–70. doi: 10.1001/jamapsychiatry.2013.265

35. Choe MS, Ortiz-Mantilla S, Makris N, Gregas M, Bacic J, Haehn D, et al. Regional infant brain development: an MRI-based morphometric analysis in 3 to 13 month olds. *Cereb Cortex.* (2013) 23:2100–17. doi: 10.1093/cercor/bhs197

36. Toga AW, Thompson PM. Mapping brain asymmetry. *Nat Rev Neurosci.* (2003) 4:37–48. doi: 10.1038/nrn1009

37. Glasser MF, Rilling JK, DTI. tractography of the human brain's language pathways. *Cereb Cortex.* (2008) 18:2471–82. doi: 10.1093/cercor/bhn011

38. Li G, Lin W, Gilmore JH, Shen D. Spatial patterns, longitudinal development, and hemispheric asymmetries of cortical thickness in infants from birth to 2 years of age. *J Neurosci.* (2015) 35:9150–62. doi: 10.1523/JNEUROSCI.4107-14.2015

39. Postema MC, van Rooij D, Anagnostou E, Arango C, Auzias G, Behrmann M, et al. Altered structural brain asymmetry in autism spectrum disorder in a study of 54 datasets. *Nat Commun.* (2019) 10:4958. doi: 10.1038/s41467-019-13005-8

40. Rubia K, Criaud M, Wulff M, Alegria A, Brinson H, Barker G, et al. Functional connectivity changes associated with fMRI neurofeedback of right inferior frontal cortex in adolescents with ADHD. *Neuroimage.* (2019) 188:43–58. doi: 10.1016/j.neuroimage.2018.11.055

41. Hart H, Radua J, Nakao T, Mataix-Cols D, Rubia K. Meta-analysis of functional magnetic resonance imaging studies of inhibition and attention in attention-deficit/hyperactivity disorder: exploring task-specific, stimulant medication, and age effects. *JAMA Psychiatry.* (2013) 70:185–98. doi: 10.1001/jamapsychiatry.2013.277

frontiers | Frontiers in Neurology

TYPE Original Research
PUBLISHED 22 August 2022
DOI 10.3389/fneur.2022.913193

OPEN ACCESS

EDITED BY
Jiliang Fang,
China Academy of Chinese Medical Sciences, China

REVIEWED BY
Francesco Cauteruccio,
Marche Polytechnic University, Italy
Nathan Churchill,
St. Michael's Hospital, Canada
Jan Egger,
University Hospital Essen, Germany

*CORRESPONDENCE
Dechang Peng
pengdcdoctor@163.com

†These authors have contributed equally to this work

SPECIALTY SECTION
This article was submitted to Applied Neuroimaging, a section of the journal Frontiers in Neurology

RECEIVED 05 April 2022
ACCEPTED 25 July 2022
PUBLISHED 22 August 2022

CITATION
Liu X, Wei Z, Chen L, Duan W, Li H, Kong L, Shu Y, Li P, Li K, Xie W, Zeng Y, Huang L, Long T and Peng D (2022) Effects of 3-month CPAP therapy on brain structure in obstructive sleep apnea: A diffusion tensor imaging study. *Front. Neurol.* 13:913193. doi: 10.3389/fneur.2022.913193

Effects of 3-month CPAP therapy on brain structure in obstructive sleep apnea: A diffusion tensor imaging study

Xiang Liu[1†], Zhipeng Wei[2†], Liting Chen[3], Wenfeng Duan[1], Haijun Li[1], Linghong Kong[1], Yongqiang Shu[1], Panmei Li[1], Kunyao Li[1], Wei Xie[1], Yaping Zeng[1], Ling Huang[1], Ting Long[1] and Dechang Peng[1*]

[1]Department of Radiology, The First Affiliated Hospital of Nanchang University, Nanchang, China, [2]Department of Radiology, The Second Affiliated Hospital of Nanchang University, Nanchang, China, [3]Medical Imaging Center, First Affiliated Hospital of Jinan University, Guangzhou, China

White matter (WM) fiber alterations in patients with obstructive sleep apnea (OSA) is associated with cognitive impairment, which can be alleviated by continuous positive airway pressure (CPAP). In this study, we aimed to investigate the changes in WM in patients with OSA at baseline (pre-CPAP) and 3 months after CPAP adherence treatment (post-CPAP), and to provide a basis for understanding the reversible changes after WM alteration in this disease. Magnetic resonance imaging (MRI) was performed on 20 severely untreated patients with OSA and 20 good sleepers. Tract-based spatial statistics was used to evaluate the fractional anisotropy (FA), mean diffusion coefficient, axial diffusion coefficient, and radial diffusion coefficient (RD) of WM. To assess the efficacy of treatment, 20 patients with pre-CPAP OSA underwent MRI again 3 months later. A correlation analysis was conducted to evaluate the relationship between WM injury and clinical evaluation. Compared with good sleepers, patients with OSA had decreased FA and increased RD in the anterior thalamic radiation, forceps major, inferior fronto-occipital tract, inferior longitudinal tract, and superior longitudinal tract, and decreased FA in the uncinate fasciculus, corticospinal tract, and cingulate gyrus ($P < 0.05$). No significant change in WM in patients with post-CPAP OSA compared with those with pre-CPAP OSA. Abnormal changes in WM in untreated patients with OSA were associated with oxygen saturation, Montreal cognitive score, and the apnea hypoventilation index. WM fiber was extensively alteration in patients with severe OSA, which is associated with cognitive impairment. Meanwhile, cognitive recovery was not accompanied by reversible changes in WM microstructure after short-term CPAP therapy.

KEYWORDS

CPAP, diffusion tensor imaging, white matter fibers, TBSS, cognitive impairment

Introduction

Obstructive sleep apnea (OSA) is a common sleep disorder that is characterized by repeated partial collapse and obstruction of the upper respiratory tract, resulting in intermittent hypoxia, hypercapnia, and sleep fragmentation (1). Chronic intermittent hypoxemia and sleep fragmentation lead to a cascade of pathophysiological processes, including oxidative stress, systemic inflammation, neuroinflammation, and neuronal death (2, 3). Hypoxemia, inflammation, and oxidative stress are widely recognized to be associated with cognitive impairment in patients with OSA (4–6). Although clinical and pathophysiological support for OSA may lead to damage to white matter (WM) structures, the exact neural mechanisms underlying cognitive impairment in patients with OSA are complex and unclear.

Continuous positive airway pressure (CPAP) is currently considered the first-line treatment for OSA (7). CPAP therapy can significantly improve daytime sleepiness in patients with OSA and partially recover their cognitive dysfunction (8). The efficacy of CPAP therapy in asymptomatic, mild, and severe patients with OSA has not been fully established, particularly in the recovery of cognitive dysfunction (9). Therefore, determining whether OSA treatment is stable and whether brain function and structure are reversed has become a hot topic.

Neuroimaging methods can explore brain changes after CPAP therapy and provide new insights into the recovery from cognitive dysfunction in patients with OSA after treatment. A study on voxel-based morphometry showed increased hippocampal and frontal gray matter (GM) volume and no significant increase in total intracranial GM volume after 3 months of CPAP therapy, whereas another study found no change in GM volume after 6 months of CPAP therapy (10). Concerns have been raised regarding the factors that might affect the effectiveness of CPAP therapy. Castronovo et al. demonstrated that WM fiber is changed in patients with OSA in the baseline group. Moreover, they reported that fractional anisotropy (FA) and mean diffusion coefficient (MD) in some brain regions can be recovered after 12 months of CPAP therapy and are also associated with attention, executive performance, and short-term memory recovery. This confirmed the reversible WM structural changes in patients with OSA after long-term CPAP therapy (11). Damage to the WM myelin sheath is associated with persistent daytime sleepiness, which was also demonstrated in another CPAP study (12). Our previous study showed that after 1 month of CPAP treatment, spontaneous brain activity in the bilateral posterior cerebellar lobe, right superior temporal gyrus, left anterior central gyrus, and other brain regions was reversed, which was related to cognitive function and drowsiness. Such reversible spontaneous brain activity is related to the adaptive compensation of OSA (13). However, few studies were conducted on whether WM structure is reversed after CPAP therapy.

Diffusion tensor imaging (DTI) is a new imaging method based on diffusion-weighted imaging that can describe changes in brain structure (14). DTI can analyze the dispersion movement of water molecules in tissues in three-dimensional space and non-invasively observe the changes in WM structure and fiber bundles in the brain (15), which is used to study the pathophysiological changes in the early brain (16). Based on the advantages of voxel and trajectory analysis, tract-based spatial statistics (TBSS) has been widely applied in studies of various neurological diseases, such as Parkinson's disease (17), chronic spinal cord injury in children (18), multiple sclerosis (19), schizophrenia (20), and preoperative evaluation of tumor (21). Macey et al. (22) showed that OSA is more likely to damage WM fibers (bilateral cingulate, right terminal striatum) in women, and this differential damage helps explain the sex differences in symptoms, particularly anxiety and depression. Kumar et al. (23) reported that the MD values of multiple brain regions in patients with OSA are significantly reduced, which is related to the pathological mechanism of ischemia and hypoxia induction. We believe that TBSS can provide new insights into OSA-related WM fiber damage and its underlying neuropathological mechanisms.

In this study, we aimed to evaluate the changes in WM microstructure in patients with OSA after short-term treatment and explore the correlation between the partially reversed areas of WM and the recovery of neurocognitive function in patients with OSA.

Materials and methods

Patients

This was a short-term, longitudinal study. Figure 1 shows the recruitment of patients with OSA. The sleep health group was assessed only at baseline. Good sleepers (GSs) were recruited through community advertisement. All patients with OSA were enrolled in the Sleep Monitoring Center, Department of Respiratory Medicine, The First Affiliated Hospital of Nanchang University, from August 2020 to March 2022. The diagnostic criteria were the 2017 American Academy of Sleep Medicine Clinical Practice Guidelines for obstructive respiratory sleep apnea in adults (24). The inclusion criteria were as follows: apnea hypoventilation index (AHI) >15, age 20-60 years, right-handedness, and standard CPAP therapy for 3 months, 4 h per night, at least 5 days per week. The exclusion criteria for all participants were as follows: (1) sleep disorders other than OSA; (2) respiratory disease, hypertension, diabetes, hypothyroidism, and prior CPAP treatment; (3) history of central nervous system diseases, including neurodegenerative diseases, epilepsy, brain tumors, cerebral infarction, and traumatic brain injury; (4)

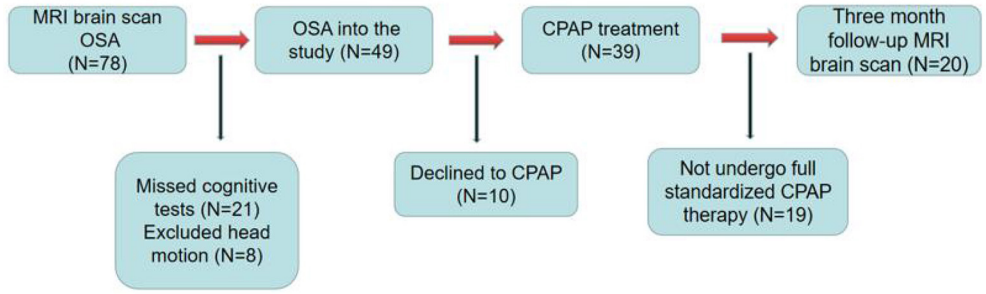

FIGURE 1
Schematic diagram of OSA patients process in this study.

abuse of illegal drugs or current use of psychoactive drugs; (5) MRI contraindications, such as internal metal implants and claustrophobia; (6) motion artifacts; and (7) loss to follow-up. Finally, 20 GSs, and 20 patients with OSA who had complied with CPAP therapy for 3 months were included in the analysis. We adhered to the principles of the Declaration of Helsinki. This study was approved by the Medical Ethics Committee of the First Affiliated Hospital of Nanchang University [2020 (94)]. All participants provided written informed consent.

Neuropsychological assessment and polysomnography

All patients with OSA completed neuropsychological assessments, including the Montreal cognitive assessment (MoCA), Epworth sleepiness scale (ESS), and Pittsburgh sleep quality index, at baseline and at 3-month follow-up. MoCA includes visual space and execution, naming, memory, attention, language, abstract thinking, computation, and direction (25). The highest MoCA score was 30, with a score of <26 indicating the presence of cognitive impairment. If the number of years of education was <12, one point was added to the total score to adjust the education level. The ESS contains eight different categories used to assess daytime sleepiness in patients with OSA. The overall ESS score was 24 points (3 points for each category), with 0, 6, 11, and 16 corresponding to four different levels of sleepiness (26). The PSQI is used to assess sleep quality on a scale of 0–21, with higher scores indicating poorer sleep quality (27). The Hamilton anxiety scale (HAMA) and Hamilton depression scale were used to assess anxiety and depression, respectively. In general, a HAMA score of >14 indicates clinically significant anxiety symptoms. A HAMD score of <7 is normal; a score of 7–17, possible depression; an overall score of 17–24, definite depression; and a total score of >24, major depression.

To rule out sleep disorders other than OSA, all subjects with OSA and GSs were required to undergo polysomnography (PSG) with a physiological monitoring system (Alice 5 LE; Respironics, Orlando, FL, USA), the detection contents included electroencephalogram, electroophthalmogram, electrocardiogram, oxygen saturation (SaO_2), etc. The day before polysomnography, all participants avoided hypnotics, alcohol, and coffee, and the test was performed from 10 p.m. to 6 a.m. the following day. According to the American Academy of Sleep Medicine's clinical practice guidelines for adult OSA, an AHI between 5 and 15 is classified as mild; AHI ≥15/h but <30/h, moderate; and AHI ≥30/h, severe (28).

CPAP treatment

An automatic CPAP equipment (YH-480; Yuwell, Jiangsu, China) was used to explain the basic functions of the CPAP machine operation in patients with OSA who met the inclusion criteria, and an appropriate mask interface was selected. The equipment can monitor breathing levels and automatically adjust the pressure. The treatment pressure of the ventilator was set to 4–20 cm H_2O. All subjects with OSA received standard CPAP therapy for 3 months with compliance of ≥4 h per night for at least 5 days per week. The built-in SIM card of the ventilator can upload user data in real time *via* a wireless transmission function, including the usage duration, AHI, and mask leakage.

MRI data acquisition

All participants were scanned on a 3.0 Tesla MRI system with an eight-channel phased-array head coil (Siemens, Munich, Germany) between 7 and 9 p.m. The scans included conventional MRI and DTI of the head. During the examination, subjects were required to lie quietly on the examination bed, wear ear plugs and eye masks throughout the examination to reduce external interference, fix their heads with sponges to prevent head movement, and breathe through the nose to

minimize the interference of head artifacts caused by mouth opening breathing. Routine MRI data were collected from the brain: axis T2WI [pulse repetition time (TR) = 3,000 ms, echo time (TE) = 122 ms, field of view (FOV) = 240 mm × 240 mm, matrix = 256 × 256, layer thickness = 5 mm], axial T1WI (TR = 600 ms, TE = 10 ms, FOV = 240 mm × 240 mm, matrix = 256 × 256, layer thickness = 5 mm), and axial T2-FLAIR (TR = 3,000 ms, TE = 122 ms, FOV = 240 mm × 240 mm, matrix = 256 × 256, layer thickness = 5 mm). Conventional craniocerebral MRI was used to exclude cerebral parenchymal structural lesions such as cerebral infarction, large cysts, and tumors, and was performed by two imaging physicians with senior professional titles. Subsequently, DTI was performed: single-shot spin echo-echo planar image of pulse spin-echo diffusion-weighted image sequence of subjects was obtained, and its parameters were as follows: TR = 7,700 ms, TE = 104 ms, FOV = 230 × 230 mm, voxel size = 1.8 × 1.8 × 2.0 mm, matrix = 128 × 128, excitation number = 2, and layer thickness = 2.0 mm. Sixty-four non-linear diffusion gradient directions were applied with b values of 0 and 1,000 s/mm^2.

Data preprocessing

All DTI data were preprocessed using FSL V5.0.9 (FMRIB Software Library, http://www.fmri.ox.au.uk/fsl) developed by the Functional Magnetic resonance Imaging Center of the University of Oxford (29), and TBSS was used for voxel statistical analysis (30). The following preprocessing steps were performed. First, the format of the original DTI data was converted (from DICOM to NIFTI format), and the data quality of the generated files was checked layer by layer to evaluate the basic parameters of the data, including image artifacts, image layers, and data head movement. Second, head eddy current correction and gradient direction correction were performed to align the data generated in the previous step with image B = 0, and the corresponding gradient direction correction was performed on the original dispersion gradient table. Third, to strip and remove images outside the brain, the threshold was set to 0.2(BET tool using FSL software). Finally, the DTI tensor index was calculated; FA, MD, axial diffusion coefficient (AD), and radial diffusion coefficient (RD) were generated.

DTI data processing was based on TBSS: (1) All FA values were registered in the standard MNI space using non-linear registration parameters. The FMRIB58_FA_1 mm template of the FSL was used as the registration image. (2) The average FA value images of all the test data were generated, and the WM fiber skeleton was then extracted, and the WM fiber skeleton was constructed based on the self-generated data. (3) The FA images formed after previous registration were projected onto the WM fiber skeleton constructed by the data in this study to generate individual FA maps for further statistical analysis. The average FA threshold was 0.2. (4) A design comparison matrix was created, and a randomization tool was used to perform a permutation test on the two groups of FA image data. We set the number of permutations to 5,000, with multiple comparisons correction using threshold-free cluster enhancement (to control type I errors). (5) The differential WM area of the FA map was extracted ($p < 0.05$). The location of the differential WM area could be checked using the DTI-81 WM template of the International Consortium for Brain Mapping (31); (6) Similarly, MD, AD, and RD values were calculated using the NON-FA DTI index based on the FA skeleton foundation, and subsequent statistical analysis was conducted.

Statistic analysis

Statistical analysis was performed using IBM SPSS Statistics for Windows (version 23.0), and statistical significance was set at $P < 0.05$. Demographic data and clinical psychological scores are expressed as the mean ± standard deviation. The Kolmogorov–Smirnov test was used to determine whether the data conformed to a normal distribution. To compare the differences in clinical indicators between OSA and GSs, pre-CPAP, and post-CPAP, a two-sample *t* test was used for normally distributed data, and the Mann–Whitney U test was used for non-normally distributed data. Spearman correlation analysis was conducted between FA, MD, AD, and RD values of patients with OSA with abnormal brain regions and the clinical evaluation results.

Results

Demographic, clinical, and neurocognitive scales

Detailed demographic and clinical assessments of the two groups are shown in Table 1. No significant difference was found in age and years of education between the OSA and GSs groups. However, significant differences were noted in body mass index, AHI, minimum blood oxygen saturation, mean blood oxygen saturation, SaO_2 < 90%, ESS, and MoCA between the two groups. Demographic and clinical evaluations of pre- and post-CPAP are shown in Table 2. Significant differences were found in ESS, MoCA, HAMA, Hamilton depression scale, Pittsburgh sleep quality index, and other aspects between pre- and post-CPAP.

TBSS

Compared with GSs, FA and RD were significantly different in the OSA group ($P < 0.05$; Figure 2). In the OSA group, the FA values of the bilateral anterior thalamic radiation (ATR), corticospinal tract (CST), inferior fronto-occipital tract

TABLE 1 Demographic and clinical data of OSA and GSs.

Category	OSA ($n = 20$)	GSs ($n = 20$)	*t*-value	*P*-value
Gender (male/female)	19/1	19/1	n/a	n/a
Age (year)[a]	40.81 ± 8.61	39.75 ± 12.36	−0.312	0.855
BMI (Kg/m^2)[b]	27.12 ± 3.98	23.50 ± 1.90	−3.662	0.001
Education (year)[b]	11.60 ± 2.56	10.75 ± 2.82	−0.996	0.325
AHI, /hour[b]	46.80 ± 19.69	2.54 ± 1.24	−10.03	<0.001
$LSaO_2$ (%)[b]	71.89 ± 10.27	93.80 ± 3.28	9.078	<0.001
$MSaO_2$ (%)[b]	94.05 ± 3.08	97.25 ± 1.94	3.920	<0.001
SaO_2 < 90%[b]	32.33 ± 15.87	0.25 ± 0.18	−9.037	<0.001
MoCA[b]	23.25 ± 2.57	28.25 ± 1.20	7.867	0.001
ESS[b]	10.40 ± 5.13	3.15 ± 2.13	−5.832	<0.001

GSs, normal sleep group; AHI, apnea hypopnea index; LSaO2, minimum blood oxygen saturation; MSaO2, average blood oxygen saturation; SaO2 < 90%, percentage of total sleep time with oxygen saturation <90; ESS, Epworth sleepiness scale; [a], Student, t-test; [b], Mann-Whitney U-test. n/a indicates the no statistics.

TABLE 2 Demographic and clinical data of pre-CPAP and post-CPAP.

Category	pre-CPAP ($n = 20$)	post-CPAP ($n = 20$)	*t*-value	*P*-value
Gender (male/female)	19/1	19/1	n/a	n/a
Age (year)[a]	40.8 ± 8.61	n/a	n/a	n/a
BMI (Kg/m^2)[a]	27.12 ± 3.98	27.01 ± 3.91	−0.82	0.805
Education (year)[b]	10.75 ± 2.82	n/a	n/a	n/a
AHI, /hour[a]	46.80 ± 19.69	n/a	n/a	n/a
$LSaO_2$ (%)[a]	71.89 ± 10.27	n/a	n/a	n/a
$MSaO_2$ (%)[a]	94 ± 3.08	n/a	n/a	n/a
SaO2 < 90%[a]	32.33 ± 15.87	n/a	n/a	n/a
MoCA[a]	23.25 ± 2.57	25.65 ± 2.70	2.87	0.007
HAMA[b]	7.30 ± 5.11	3.60 ± 2.47	−2.91	0.006
HAMD[b]	4.85 ± 2.56	3.15 ± 2.15	−2.27	0.029
PSQI[b]	6.25 ± 1.80	5.1 ± 1.58	−2.142	0.039
ESS[a]	10.4 ± 5.13	7.15 ± 3.34	−3.372	0.023

AHI, apnea hypopnea index; $LSaO_2$, minimum blood oxygen saturation; $MSaO_2$, average blood oxygen saturation; SaO_2 < 90%, percentage of total sleep time with oxygen saturation <90; ESS, Epworth sleepiness scale; HAMA, Hamilton anxiety scale; HAMD, Hamilton depression scale; PSQI, Pittsburgh sleep quality index. [a], Student, t-test; [b], Mann-Whitney U-test. n/a indicates the no statistics.

(IFO), forceps major (FM), superior longitudinal fasciculus (SLF), inferior longitudinal fasciculus (ILF), uncinate fasciculus (UNC), and right cingulate gyrus (CGC) decreased (Table 3). In the OSA group, ATR on the left side, and RD values of the bilateral IFO, FM, ILF, and SLF increased (Table 4). No significant differences were found in FA, AD, RD, and MD between pre- and post-CPAP WM fibers ($P > 0.05$; Figure 3).

Relationship between DTI changes and clinical evaluation in patients with OSA

Relationship between FA value and clinical scale in OSA group at baseline. SaO_2 < 90% was positively correlated with clusters 13 ($r = -0.458$, $P = 0.042$, 95% CI: −0.787,−0.025). In the RD value of the OSA group, the MoCA scale was positively correlated with cluster 3 ($r = 0.446$, $P = 0.049$, 95%CI: 0.028, 0.718) and negatively correlated with cluster 7 ($r = -0.597$, $P = 0.005$, 95%CI: −0.724,−0.339), AHI was positively correlated with clusters 3 ($r = 0.481$, $P = 0.032$, 95%CI: −0.170, 0.654) (Figure 4).

Discussion

In recent years, whether CPAP therapy can improve brain function and structure has attracted extensive research interest, prompting researchers to study the neuropathological mechanisms of WM alterations in patients with OSA after CPAP therapy. The results showed that, first, extensive changes occurred in WM fiber in patients with OSA before treatment, confirming that WM fiber alterations were related to OSA, mainly involving the ATR, CST, FM, IFO, ILF, UNC, SLF, and CGC. Second, OSA symptoms and cognitive impairment improved 3 months after CPAP treatment in patients with OSA, but WM fiber did not significantly change. The change of WM fiber may be associated with the individual differences in OSA patients and the degree of response to treatment. Third, at baseline, we found that WM fibers were significantly correlated with SaO2 < 90%, AHI, and MoCA, indicating that WM alterations were related to cognitive impairment, and intermittent hypoxia was one of the causes of WM alterations.

At baseline, patients with OSA showed extensive WM fiber abnormalities. Long-term intermittent hypoxia is well-known to cause pathological changes such as oxidative stress and ischemia reperfusion in the brain, which leads to WM fiber alteration in the brain (32). WM structural alterations are associated with extensive and chronic cell damage, including decreased synaptic and axon density, neurodegeneration, and cell death (33). Consistent with these findings, we found that the FA values of WM fiber tracts were reduced and RD value increased in patients with OSA, which may be related to the different underlying pathophysiological processes of OSA. Reduced FA is related to the number and density of axons, and increased RD is related to myelin sheath injury (34). The study by Zhang et al. (35) showed that impaired integrity of the anterior corpus callosum fiber bundle is related to early myelination and unique fiber composition, which explains the different susceptibilities of different structures to intermittent hypoxic environments. Mei et al. (36) reported that WM integrity abnormality is only found in children with moderate-to-severe OSA, and WM impairment is accompanied by cognitive decline, confirming

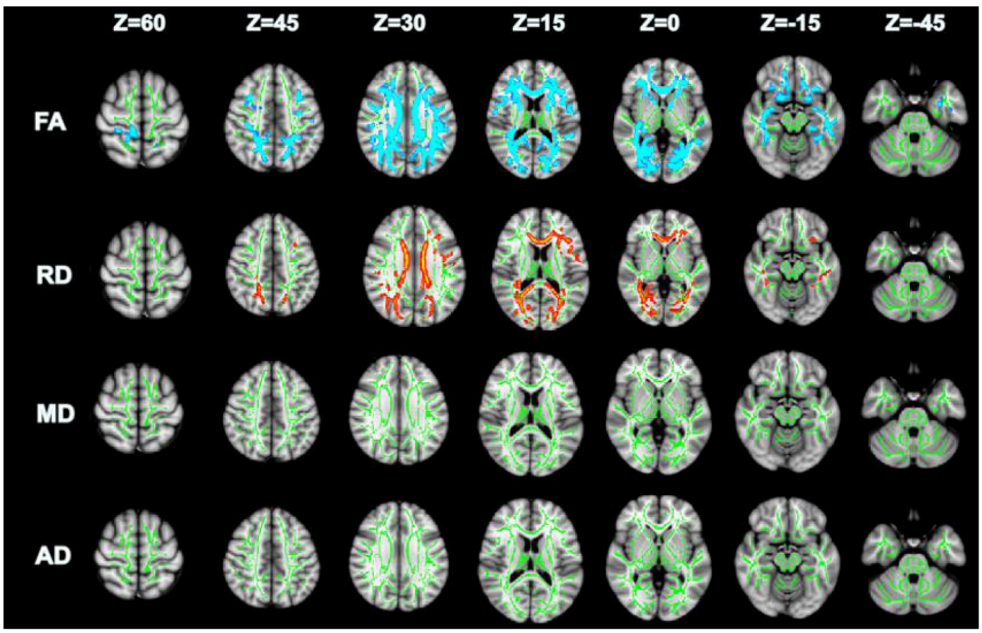

FIGURE 2
TBSS analysis of OSA and GSs differential white matter fibers, green: mean fractional anisotropy (FA) skeleton; Blue and red represent changed areas (FA and RD) of DTI value in OSA group compared with control group, $P < 0.05$.

TABLE 3 Distribution of FA differences in brain regions between OSA and GSs before treatment.

Base line	Cluster	Voxel	*P*-value	MNI			L/R	WM
				X	Y	Z		
	15	32,990	0.001	−2	−29	18	L	ATR, FM, IFO, SLF
	14	5,656	0.013	30	19	11	R	ATR, UNC, SLF, IFO
	13	1,482	0.034	−44	−27	−14	L	ILF, SLF, UNC
	12	382	0.036	11	−35	62	R	CST
	11	171	0.037	21	18	−20	R	UNC, IFO
	10	127	0.039	−33	−46	10	L	ATR, IFO, ILF, SLF
	9	123	0.039	−28	−35	19	L	ATR, SLF
	8	66	0.040	25	−90	−1	R	FM, IFO, ILF
	7	54	0.040	30	−4	−14	R	IFO, ILF, UNC
	6	40	0.040	−28	−10	25	L	CST, SLF
	5	39	0.040	10	−51	17	R	CGC

ATR, Anterior thalamic radiation; CST, Corticospinal tract; FM, Forceps major; IFO, Inferior fronto-occipital fasciculus; ILF, Inferior longitudinal fasciculus; UNC, Uncinate fasciculus; SLF, Superior longitudinal fasciculus; CGC, Cingulate gyrus.

that WM fiber impairment is related to OSA severity. Therefore, we hypothesized that OSA severity, age, and physiological and anatomical structures were related to the susceptibility and degree of WM fiber bundle alteration.

The CGC is involved in the control of autonomic nervous functions, including respiration, blood pressure, and salivation (37). During breathing, neurons in the CGC fire in sync with breathing and are associated with the central network that controls breathing (38). Taylor et al. (39) showed that the structural changes in the CGC are related to an increase in sympathetic discharge when awake, and that sympathetic excitatory stimulation can cause changes in the central nervous system and thus participate in the regulation of blood pressure and respiration. The corticospinal tract originates from the motor-related cortical region, mainly carries motor-related information, and mediates voluntary movement (40). Previous

TABLE 4 Distribution of RD differences in brain regions between OSA and GSs before treatment.

Base line	Cluster	Voxel	*P*-value	MNI			L/R	WM
				X	Y	Z		
	9	17,745	0.006	−5	−27	21	L	ATR, FM, IFO, ILF, SLF
	8	2,579	0.028	28	−54	6	R	FM, IFO, ILF, SLF
	7	237	0.045	38	−35	−20	L	ILF
	6	171	0.046	33	−79	−4	L	IFO, ILF
	5	90	0.047	−34	−49	11	L	ATR, IFO, ILF, SLF
	4	75	0.047	−54	−26	−13	L	ILF, SLF
	3	73	0.047	−55	−40	−5	L	SLF

ATR, Anterior thalamic radiation; FM, Forceps major; IFO, Inferior fronto-occipital fasciculus; ILF, Inferior longitudinal fasciculus; SLF, Superior longitudinal fasciculus.

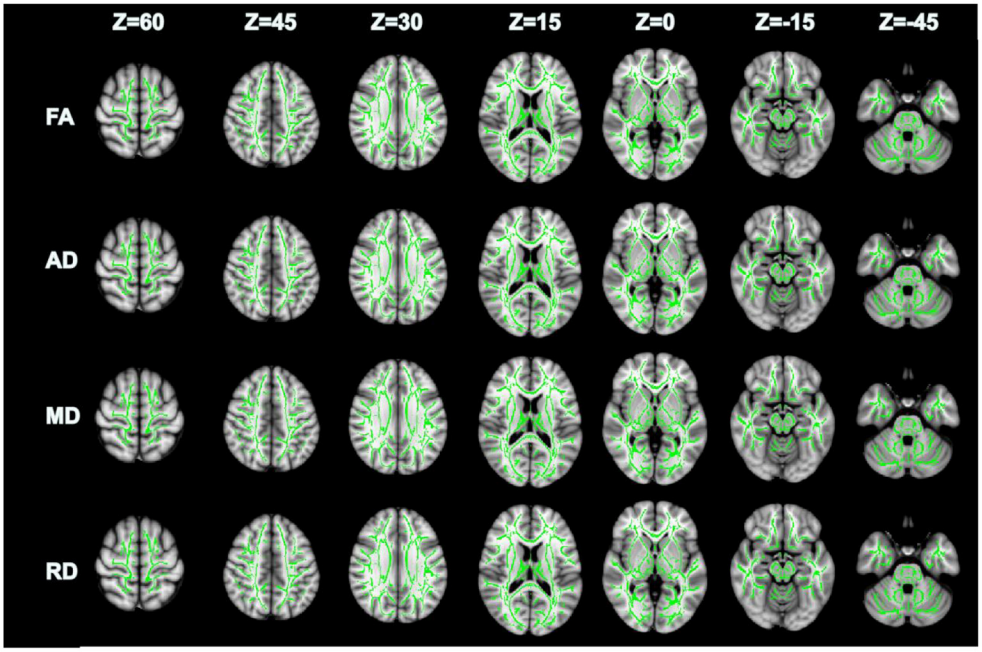

FIGURE 3
There were no significant differences in FA, AD, MD and RD between pre-CPAP and post-CPAP after TBSS analysis, $P > 0.05$.

studies have shown that impaired peripheral muscle movement in patients with OSA is associated with decreased corticospinal excitability (41). Marillier et al. (42) showed that intermittent hypoxia and hypercapnia during sleep lead to increased corticospinal tract inhibition in patients with OSA, partially explaining the neuromuscular mechanism of OSA limb muscle dysfunction. Similar to previous results, our study further confirmed fiber alteration in the CGC and corticospinal tract. Therefore, we speculate that sleep disruption in patients with OSA may lead to intermittent hypoxia and hypercapnia, which may indirectly affect the autonomic nerves related to respiration and lead to muscle movement disorders, which may be one of the risk factors for exacerbating the progression of OSA.

In addition, we found that WM fiber alterations in ATR, FM, IFO, ILF, UNC, SLF, and other regions. Numerous studies have shown that various cognitive functions, including reading, intelligence, information processing, visuospatial memory, attention, and response inhibition, are associated with different WM microstructures (43, 44). The ATR and SLF are involved in speech production disorders (45). The UNC is involved in bidirectional information transmission between the frontal and parietal cortex (46), and the FM is associated with delayed memory disorders (47), The damage of the ILF is significantly associated with depression (48), and the IFO plays an important role in semantic processing (49). Our results provide more evidence of WM microfiber structural

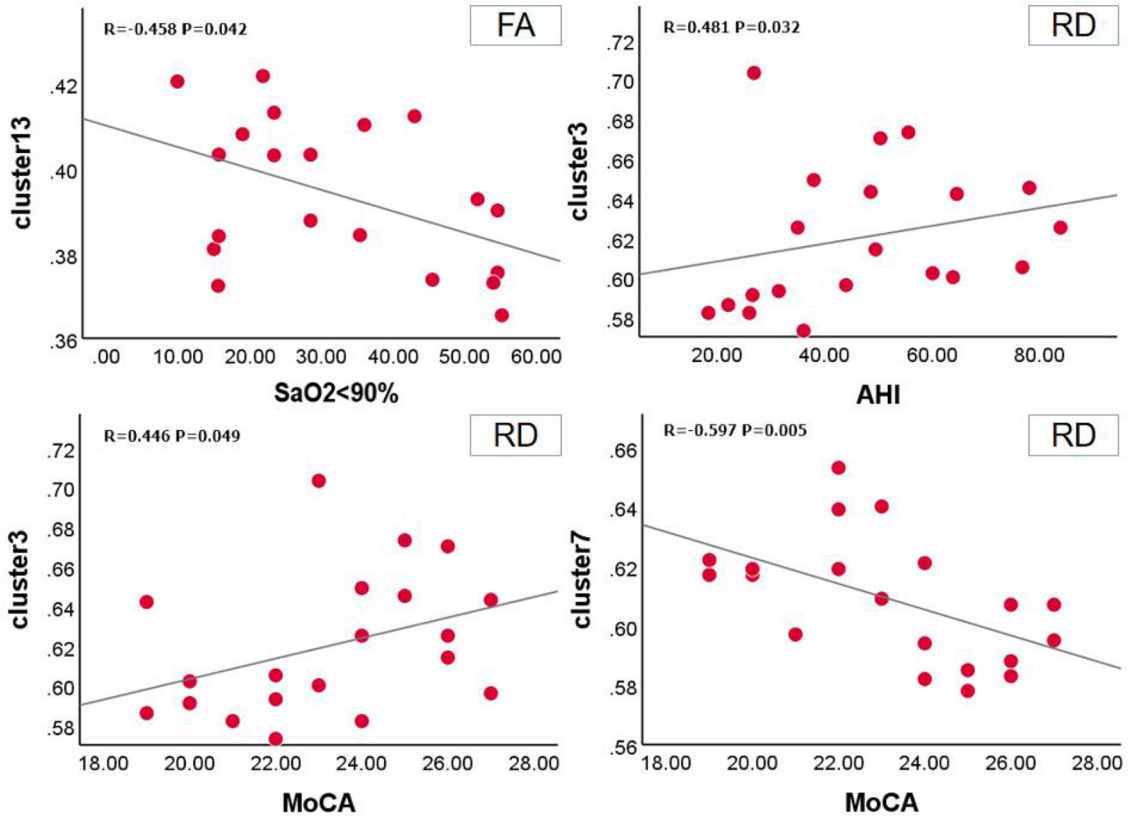

FIGURE 4
Correlation between FA, RD and clinical assessment scale in OSA before the treatment.

alteration in patients with OSA. At the same time, fiber alterations in these different white matter areas may provide more explanations for the heterogeneity of OSA cognitive impairment and symptoms (50). We also found that extensive WM fiber alteration was significantly correlated with SaO2 < 90% time, AHI, and MoCA. This further explained that intermittent hypoxia and severity of OSA led to extensive WM fiber bundle damage and contributed to further understanding of the neuroimaging mechanism of WM fiber bundle integrity affecting cognitive function.

In the current study, 3 months of CPAP therapy did not cause in alteration WM in the brain. Understanding whether CPAP therapy for OSA is likely to stabilize and reverse brain structural changes is important because it can provide clinical guidance and motivate patients to adhere to treatment. Studies on the recovery of brain function and structure after OSA treatment have shown inconsistent results. Canessa et al. (51) demonstrated that increased GM volume in the hippocampus, medial orbitofrontal anterior lobe, and superior frontal gyrus is associated with improvements in visuospatial short-term memory, attention, and executive function after 3 months of treatment, confirming that changes in the GM are associated with cognitive improvement. Contrary to the findings of Donoghue et al. (52) no significant difference was found in the GM between the pretreatment and control groups (52). In a voxel-based morphometry study of patients with OSA after surgical treatment, alterations in some brain WM structures were not significant, but were compensated by changes in other cortical areas (53). A recent DTI study showed that some WM tracts reversibly recover after 3 months of short-term treatment (54). The different results of previous studies may be due to the relatively individual difference and varied responses of different patients to CPAP therapy (12).

Limitation

This study has several limitations. First, this was a short-term CPAP therapy, and We only used DTI to discuss the alterations of WM structure. DTI technology can only show the alterations of WM non-specifically, and cannot confirm the existence of

tiny recovery of nerve cells. Second, we examined the general population, which was dominated by men, whose results cannot be extended. Finally, our sample size was relatively small which may cause potential statistical bias.

Conclusion

This study was based on the spatial statistics of trajectory to investigate the reversible changes in WM microstructure in the brain before and after short-term CPAP treatment. We observed extensive abnormalities in the WM in patients with severe OSA before treatment, and these areas included the autonomic nerves involved in respiration. No significant reversible WM alteration was found after short-term CPAP therapy. Therefore, further longitudinal studies are warranted to explore the reversible alterations in WM microstructure in the brain after long-term treatment and to provide potential imaging markers for clinical treatment.

Data availability statement

The original contributions presented in the study are included in the article/supplementary material, further inquiries can be directed to the corresponding author.

Ethics statement

The study was approved by the Ethics Committee of The First Affiliated Hospital of Nanchang University. The patients/participants provided their written informed consent to participate in this study.

Author contributions

XL and ZW wrote, reviewed, and revised the manuscript. DP guided and designed the MRI experiment. ZW analyzed DTI data. XL and WD analyzed and discussed the ideas of the paper. XL analyzed the results and wrote the manuscript. LC, TL, LH, HL, LK, YS, PL, WX, and YZ collected DTI data and applied for the ethics approval. All authors contributed to the article and approved the submitted version.

Funding

This study was supported by the National Natural Science Foundation of China (Grant Nos. 81860307 and 81560285); the Natural Science Foundation Project of Jiangxi, China (Grant Nos. 20202BABL216036, 20181ACB20023, and 20171BAB205070); Education Department Project of Jiangxi provincial, China (Grant Nos. 700544006 and GJJ190133); and Department of Health Project and Jiangxi provincial, China (Grant No. 20181039).

Conflict of interest

The authors declare that the research was conducted in the absence of any commercial or financial relationships that could be construed as a potential conflict of interest.

Publisher's note

References

1. Franklin KA, Lindberg E. Obstructive sleep apnea is a common disorder in the population-a review on the epidemiology of sleep apnea. *J Thorac Dis.* (2015) 7:1311–22. doi: 10.3978/j.issn.2072-1439.2015.06.11

2. Unnikrishnan D, Jun J, Polotsky V. Inflammation in sleep apnea: an update. *Rev Endocr Metab Disord.* (2015) 16:25–34. doi: 10.1007/s11154-014-9304-x

3. Yang Q, Wang Y, Feng J, Cao J, Chen B. Intermittent hypoxia from obstructive sleep apnea may cause neuronal impairment and dysfunction in central nervous system: the potential roles played by microglia. *Neuropsychiatr Dis Treat.* (2013) 9:1077–86. doi: 10.2147/NDT.S49868

4. Blackwell T, Yaffe K, Laffan A, Redline S, Ancoli-Israel S, Ensrud KE, et al. Associations between sleep-disordered breathing, nocturnal hypoxemia, and subsequent cognitive decline in older community-dwelling men: the osteoporotic fractures in men sleep study. *J Am Geriatr Soc.* (2015) 63:453–61. doi: 10.1111/jgs.13321

5. Lee MH, Lee SK, Thomas RJ, Yoon JE, Yun CH, Shin C. Deep Learning-Based assessment of brain connectivity related to obstructive sleep apnea and daytime sleepiness. *Nat Sci Sleep.* (2021) 13:1561–72. doi: 10.2147/NSS.S327110

6. Zhou L, Chen P, Peng Y, Ouyang R. Role of oxidative stress in the neurocognitive dysfunction of obstructive sleep apnea syndrome. *Oxid Med Cell Longev.* (2016) 2016:9626831. doi: 10.1155/2016/9626831

7. Senaratna CV, Perret JL, Lodge CJ, Lowe AJ, Campbell BE, Matheson MC, et al. Prevalence of obstructive sleep apnea in the general population: a systematic review. *Sleep Med Rev.* (2017) 34:70–81. doi: 10.1016/j.smrv.2016.07.002

8. Wang ML, Wang C, Tuo M, Yu Y, Wang L, Yu JT, et al. Cognitive effects of treating obstructive sleep apnea: a meta-analysis of randomized controlled trials. *J Alzheimers Dis.* (2020) 75:705–15. doi: 10.3233/JAD-200088

9. Baril AA, Martineau-Dussault ME, Sanchez E, Andre C, Thompson C, Legault J, et al. Obstructive sleep apnea and the brain: a focus on gray and white matter structure. *Curr Neurol Neurosci Rep.* (2021) 21:11. doi: 10.1007/s11910-021-01094-2

10. Huynh NT, Prilipko O, Kushida CA, Guilleminault C. Volumetric brain morphometry changes in patients with obstructive sleep apnea syndrome: effects of CPAP treatment and literature review. *Front Neurol.* (2014) 5:58. doi: 10.3389/fneur.2014.00058

11. Castronovo V, Scifo P, Castellano A, Aloia MS, Iadanza A, Marelli S, et al. White matter integrity in obstructive sleep apnea before and after treatment. *Sleep.* (2014) 37:1465–75. doi: 10.5665/sleep.3994

12. Zhang J, Weaver TE, Zhong Z, Nisi RA, Martin KR, Steffen AD, et al. White matter structural differences in OSA patients experiencing residual daytime sleepiness with high CPAP use: a non-Gaussian diffusion MRI study. *Sleep Med.* (2019) 53:51–9. doi: 10.1016/j.sleep.2018.09.011

13. Li H, Li L, Kong L, Li P, Zeng Y, Li K, et al. FrequencySpecific regional homogeneity alterations and cognitive function in obstructive sleep apnea before and after short-term continuous positive airway pressure treatment. *Nat Sci Sleep.* (2021) 13:2221–38. doi: 10.2147/NSS.S344842

14. Yu Q, Lin K, Liu Y, Li X. Clinical uses of diffusion tensor imaging fiber tracking merged neuronavigation with lesions adjacent to corticospinal tract: a retrospective cohort study. *J Korean Neurosurg Soc.* (2020) 63:248–60. doi: 10.3340/jkns.2019.0046

15. Xiao X, Kong L, Pan C, Zhang P, Chen X, Sun T, et al. The role of diffusion tensor imaging and tractography in the surgical management of brainstem gliomas. *Neurosurg Focus.* (2021) 50:E10. doi: 10.3171/2020.10.FOCUS20166

16. Shaikh S, Kumar A, Bansal A. Diffusion tensor imaging: an overview. *Neurol India.* (2018) 66:1603–11. doi: 10.4103/0028-3886.246233

17. Arevalo-Saenz A, Lopez-Manzanares L, Navas-Garcia M, Pastor J, Vega-Zelaya L, Torres CV. Deep brain stimulation in Parkinson's disease: analysis of brain fractional anisotropy differences in operated patients. *Rev Neurol.* (2022) 74:125–34. doi: 10.33588/rn.7404.2021196

18. Fisher J, Alizadeh M, Middleton D, Matias CM, Mulcahey MJ, Calhoun-Thielen C, et al. Brain white matter abnormality induced by chronic spinal cord injury in the pediatric population: a preliminary tract-based spatial statistic study. *Top Spinal Cord Inj Rehabil.* (2021) 27:1–13. doi: 10.46292/sci20-00018

19. Gharaylou Z, Sahraian MA, Hadjighassem M, Kohanpour M, Doosti R, Nahardani S, et al. Widespread disruptions of white matter in familial multiple sclerosis: DTI and NODDI study. *Front Neurol.* (2021) 12:678245. doi: 10.3389/fneur.2021.678245

20. Abdolalizadeh A, Ostadrahimi H, Ohadi M, Saneei SA, Bayani EA. White matter microstructural associates of apathy-avolition in schizophrenia. *J Psychiatr Res.* (2021) 142:110–6. doi: 10.1016/j.jpsychires.2021.07.042

21. Manan AA, Yahya N, Idris Z, Manan HA. The utilization of diffusion tensor imaging as an Image-Guided tool in brain tumor resection surgery: a systematic review. *Cancers.* (2022) 14:2466. doi: 10.3390/cancers14102466

22. Macey PM, Kumar R, Yan-Go FL, Woo MA, Harper RM. Sex differences in white matter alterations accompanying obstructive sleep apnea. *Sleep.* (2012) 35:1603–13. doi: 10.5665/sleep.2228

23. Kumar R, Chavez AS, Macey PM, Woo MA, Yan-Go FL, Harper RM. Altered global and regional brain mean diffusivity in patients with obstructive sleep apnea. *J Neurosci Res.* (2012) 90:2043–52. doi: 10.1002/jnr.23083

24. Kapur VK, Auckley DH, Chowdhuri S, Kuhlmann DC, Mehra R, Ramar K, et al. Clinical practice guideline for diagnostic testing for adult obstructive sleep apnea: an american academy of sleep medicine clinical practice guideline. *J Clin Sleep Med.* (2017) 13:479–504. doi: 10.5664/jcsm.6506

25. Chen KL, Xu Y, Chu AQ, Ding D, Liang XN, Nasreddine ZS, et al. Validation of the chinese version of montreal cognitive assessment basic for screening mild cognitive impairment. *J Am Geriatr Soc.* (2016) 64:e285–90. doi: 10.1111/jgs.14530

26. Johns MW. A new method for measuring daytime sleepiness: the Epworth sleepiness scale. *Sleep.* (1991) 14:540–5. doi: 10.1093/sleep/14.6.540

27. Backhaus J, Junghanns K, Broocks A, Riemann D, Hohagen F. Test-retest reliability and validity of the pittsburgh sleep quality index in primary insomnia. *J Psychosom Res.* (2002) 53:737–40. doi: 10.1016/S0022-3999(02)00330-6

28. Berry RB, Brooks R, Gamaldo C, Harding SM, Lloyd RM, Quan SF, et al. AASM scoring manual updates for 2017 (Version 2.4). *J Clin Sleep Med.* (2017) 13:665–6. doi: 10.5664/jcsm.6576

29. Jenkinson M, Beckmann CF, Behrens TE, Woolrich MW, Smith SM. Fsl. *Neuroimage.* (2012) 62:782–90. doi: 10.1016/j.neuroimage.2011.09.015

30. Smith SM, Jenkinson M, Johansen-Berg H, Rueckert D, Nichols TE, Mackay CE, et al. Tract-based spatial statistics: voxelwise analysis of multi-subject diffusion data. *Neuroimage.* (2006) 31:1487–505. doi: 10.1016/j.neuroimage.2006.02.024

31. Mori S, Oishi K, Jiang H, Jiang L, Li X, Akhter K, et al. Stereotaxic white matter atlas based on diffusion tensor imaging in an ICBM template. *Neuroimage.* (2008) 40:570–82. doi: 10.1016/j.neuroimage.2007.12.035

32. Jelic S, Padeletti M, Kawut SM, Higgins C, Canfield SM, Onat D, et al. Inflammation, oxidative stress, and repair capacity of the vascular endothelium in obstructive sleep apnea. *Circulation.* (2008) 117:2270–8. doi: 10.1161/CIRCULATIONAHA.107.741512

33. Lee MH, Yun CH, Min A, Hwang YH, Lee SK, Kim DY, et al. Altered structural brain network resulting from white matter injury in obstructive sleep apnea. *Sleep*. (2019) 42:zsz120. doi: 10.1093/sleep/zsz120

34. Budde MD, Xie M, Cross AH, Song SK. Axial diffusivity is the primary correlate of axonal injury in the experimental autoimmune encephalomyelitis spinal cord: a quantitative pixelwise analysis. *J Neurosci.* (2009) 29:2805–13. doi: 10.1523/JNEUROSCI.4605-08.2009

35. Zhang B, Zhu DM, Zhao W, Zhang Y, Yang Y, Zhang C, et al. Selective microstructural integrity impairments of the anterior corpus callosum are associated with cognitive deficits in obstructive sleep apnea. *Brain Behav.* (2019) 9:e1482. doi: 10.1002/brb3.1482

36. Mei L, Li X, Wang S, Si R, Ji T, Xu Z, et al. The impacts of obstructive sleep apnea severity on brain white matter integrity and cognitive functions in children: a diffusion tensor imaging study. *Nat Sci Sleep.* (2021) 13:2125–35. doi: 10.2147/NSS.S329408

37. Joo EY, Tae WS, Lee MJ, Kang JW, Park HS, Lee JY, et al. Reduced brain gray matter concentration in patients with obstructive sleep apnea syndrome. *Sleep.* (2010) 33:235–41. doi: 10.1093/sleep/33.2.235

38. Johnson AK, Zhang Z, Clayton SC, Beltz TG, Hurley SW, Thunhorst RL, et al. The roles of sensitization and neuroplasticity in the long-term regulation of blood pressure and hypertension. *Am J Physiol Regul Integr Comp Physiol.* (2015) 309:R1309–25. doi: 10.1152/ajpregu.00037.2015

39. Taylor KS, Millar PJ, Murai H, Haruki N, Kimmerly DS, Bradley TD, et al. Cortical autonomic network gray matter and sympathetic nerve activity in obstructive sleep apnea. *Sleep*. (2018) 41:1–10 doi: 10.1093/sleep/zsx208

40. Welniarz Q, Dusart I, Roze E. The corticospinal tract: evolution, development, and human disorders. *Dev Neurobiol.* (2017) 77:810–29. doi: 10.1002/dneu.22455

41. Joo EY, Kim HJ, Lim YH, Koo DL, Hong SB. Altered cortical excitability in patients with untreated obstructive sleep apnea syndrome. *Sleep Med.* (2010) 11:857–61. doi: 10.1016/j.sleep.2010.02.015

42. Marillier M, Gruet M, Baillieul S, Roux Mallouf TLE, Wuyam, B., et al. Neuromuscular dysfunction and cortical impairment in sleep apnea syndrome. *Med Sci Sports Exerc*. (2018) 50:1529–39. doi: 10.1249/MSS.0000000000001625

43. Madden DJ, Bennett IJ, Burzynska A, Potter GG, Chen NK, Song AW. Diffusion tensor imaging of cerebral white matter integrity in cognitive aging. *Biochim Biophys Acta.* (2012) 1822:386–400. doi: 10.1016/j.bbadis.2011.08.003

44. Schmithorst VJ, Yuan W. White matter development during adolescence as shown by diffusion MRI. *Brain Cogn.* (2010) 72:16–25. doi: 10.1016/j.bandc.2009.06.005

45. Cipolotti L, Molenberghs P, Dominguez J, Smith N, Smirni D, Xu T, et al. Fluency and rule breaking behaviour in the frontal cortex. *Neuropsychologia.* (2020) 137:107308. doi: 10.1016/j.neuropsychologia.2019.107308

46. Chaddock-Heyman L, Erickson KI, Voss MW, Powers JP, Knecht AM, Pontifex MB, et al. White matter microstructure is associated with cognitive control in children. *Biol Psychol.* (2013) 94:109–15. doi: 10.1016/j.biopsycho.2013.05.008

47. Liu Z, Kang L, Zhang A, Yang C, Liu M, Wang J, et al. Injuries in left corticospinal tracts, forceps major, and left superior longitudinal fasciculus (Temporal) as the quality indicators for major depressive disorder. *Neural Plast.* (2021) 2021:2348072. doi: 10.1155/2021/2348072

48. Olvet DM, Delaparte L, Yeh FC, DeLorenzo C, McGrath PJ, Weissman MM, et al. A comprehensive examination of white matter tracts and connectometry in major depressive disorder. *Depress Anxiety.* (2016) 33:56–65. doi: 10.1002/da.22445

49. Duffau H. The anatomo-functional connectivity of language revisited. new insights provided by electrostimulation and tractography. *Neuropsychologia.* (2008) 46:927–34. doi: 10.1016/j.neuropsychologia.2007.10.025

50. Lee SA, Kim SJ, Lee SY, Kim HJ. Periodic limb movements during sleep are associated with poor health-related quality of life in patients with obstructive sleep apnea. *Sleep Breath.* (2021). doi: 10.1007/s11325-021-02469-y

51. Canessa N, Castronovo V, Cappa SF, Aloia MS, Marelli S, Falini A, et al. Obstructive sleep apnea: brain structural changes and neurocognitive function before and after treatment. *Am J Respir Crit Care Med.* (2011) 183:1419–26. doi: 10.1164/rccm.201005-0693OC

52. O'Donoghue FJ, Briellmann RS, Rochford PD, Abbott DF, Pell GS, Chan CH, et al. Cerebral structural changes in severe obstructive sleep apnea. *Am J Respir Crit Care Med.* (2005) 171:1185–90. doi: 10.1164/rccm.200406-738OC

53. Lin WC, Huang CC, Chen HL, Chou KH, Chen PC, Tsai NW, et al. Longitudinal brain structural alterations and systemic inflammation in obstructive sleep apnea before and after surgical treatment. *J Transl Med.* (2016) 14:139. doi: 10.1186/s12967-016-0887-8

54. Salsone M, Caligiuri ME, Castronovo V, Canessa N, Marelli S, Quattrone A, et al. Microstructural changes in normal-appearing white matter in male sleep apnea patients are reversible after treatment: a pilot study. *J Neurosci Res.* (2021) 99:2646–56. doi: 10.1002/jnr.24858

frontiers | Frontiers in Neurology

TYPE Study Protocol
PUBLISHED 01 September 2022
DOI 10.3389/fneur.2022.977112

OPEN ACCESS

EDITED BY
Jiliang Fang,
Guang'anmen Hospital, China Academy of Chinese Medical Sciences, China

REVIEWED BY
Taipin Guo,
Yunnan University of Traditional Chinese Medicine, China
Hailong Fan,
Hohhot Hospital of Mongolian Medicine and Traditional Chinese Medicine, China

*CORRESPONDENCE
Di Zhang
erinzd53@126.com

†These authors have contributed equally to this work and share first authorship

SPECIALTY SECTION
This article was submitted to Applied Neuroimaging, a section of the journal Frontiers in Neurology

RECEIVED 24 June 2022
ACCEPTED 04 August 2022
PUBLISHED 01 September 2022

CITATION
Zhang D, Wang YS, Li HP, Ma J, Sun JF, Wu ZP, Zhang GL and Jin S (2022) The central-peripheral coupling effect of ocular acupuncture kinesitherapy in post-stroke dyskinesia: A functional neuroimaging and neurotic electrophysiology study protocol. *Front. Neurol.* 13:977112. doi: 10.3389/fneur.2022.977112

The central-peripheral coupling effect of ocular acupuncture kinesitherapy in post-stroke dyskinesia: A functional neuroimaging and neurotic electrophysiology study protocol

Di Zhang[1*†], Yongshen Wang[2†], Hongpeng Li[3], Jiang Ma[4], Jianfeng Sun[1], Zhipeng Wu[1], Guilong Zhang[5†] and Song Jin[1†]

[1]Department of Rehabilitation, Hospital of Chengdu University of Traditional Chinese Medicine, Chengdu, China, [2]School of Health Preservation and Rehabilitation, Chengdu University of Traditional Chinese Medicine, Chengdu, China, [3]School of Medicine and Life Science, Chengdu University of Traditional Chinese Medicine, Chengdu, China, [4]Medical Rehabilitation Department, Affiliated Sport Hospital of Chengdu Sport University, Chengdu, China, [5]Department of Orthopedics, Hospital of Chengdu University of Traditional Chinese Medicine, Chengdu, China

Background: Dyskinesia is a common manifestation after stroke. Motor functional rehabilitation after stroke is of great significance to the maintenance of national health. Ocular Acupuncture Kinesitherapy (OAKT) can repair nerve injuries, improve motor function, reduce rehabilitation time, and promote dyskinesia recovery after stroke. The mechanism, however, remains a mystery, necessitating urgent research. The M1-thalamus-spinal cord neural signaling pathway is linked to limb motor function. Bold-fMRI can represent the cerebral functional state, and TMS-MEP is of certain practical utility for assessing motor neural function and prognosis. Combining fMRI scanning with TMS-MEP detection is predicted to advance brain-spinal cord regulation and muscle response linkage control mechanism research, as well as completely investigate the central-peripheral coupling effect of Ocular Acupuncture Kinesitherapy on dyskinesia after stroke (PSD).

Methods: This is a prospective functional neuroimaging and neurotic electrophysiological study with a case-control design between the PSD with the HC groups and a randomized controlled design within the 3 PSD groups (OAKT group, ocular acupuncture group, and kinesitherapy group). Using fMRI scans and TMS-MEP approach, we will assess the central-peripheral neural function alterations in PSD as well as the coupling effects of OAKT on PSD. We plan to enroll 90 participants at the Hospital of Chengdu University of Traditional Chinese Medicine from Aug 31, 2022, to Dec 31, 2023, including 45 PSD and 45 HC subjects. After enrollment and on the last day after 4-weeks of waiting (HC subjects) or intervention (PSD subjects), all eligible subjects will be evaluated using fMRI scanning, TMS-MEP detection, and the MMT and Fugl-Mayer scales assessment. The MMT and Fugl-Meyer

scores will be recorded, and a Pearson correlation analysis will be performed to assess the correlation between clinical and imaging outcomes.

Discussion: Findings of this study will help to explain the central-peripheral coupling effect of OAKT on PSD and to further provide the neural processing of acupuncture kinesitherapy covering the entire pathway from peripheral to central nervous system.

Clinical trial registration: This study is registered with an identifier (ChiCTR2200060483) at the Chinese Clinical Trial Registry in June 2022. http://www.chictr.org.cn/index.aspx.

KEYWORDS

ocular acupuncture kinesitherapy, dyskinesia after stroke, fMRI, TMS-MEP, central-peripheral coupling effect

Introduction

Dyskinesia after stroke (PSD), a typical result of cerebrovascular accident, is characterized by abnormal muscle strength and tension in the unilateral upper and lower limbs, affecting the patient's ability to sit, stand, walk, and other motor actions. With more than 13 million new cases per year, stroke has become the second leading cause of death and disability worldwide, with high morbidity, mortality, and disability rate. Half of the surviving patients suffer from physical dysfunction to varying degrees, such as motor dysfunction, sensory dysfunction, balance disorder, and so on (1, 2), posing a substantial social and economic burden as well as a significant health risk to humans (3–5). According to one study, PSD has the most recommended recommendations for stroke rehabilitation, with 257 suggestions in six dimensions (6). Actively fostering rehabilitation of post-stroke dyskinesia has an important role in restoring healthy life, enhancing utilization efficiency and logical allocation of medical resources, and lowering the economic burden of patients, families, and even society as a whole (7).

Acupuncture paired with exercise training is a type of integrated Chinese and western therapy that has been shown to dramatically repair nerve injury after stroke, alleviate affected limb functioning, and improve patients' quality of life. Acupuncture has been generally recognized by medical science for its certain success in the treatment of stroke (8, 9), particularly the consciousness and resuscitation restoring needling method, which has been widely used for stroke patients (10–12). Acupuncture with varied techniques based on the level of muscular tension has been found (13) to considerably alleviate the neurological deficit after stroke, and acupuncture has been considered the principal TCM therapy for post-stroke dyskinesia rehabilitation. Exercise training stresses the use of a combination of passive and active exercises to significantly improve neural activity, vascular endothelial function, aerobic metabolism capacity, exercise tolerance, and cardiopulmonary function (14). Muscle strength, proprioception, range of motion, joint stability, and limb motion stimulation can all be improved with exercise training (15). It has become a core means of rehabilitation therapy for a variety of illnesses affecting the skeletal muscle system, endocrine system, cardio-cerebrovascular system, and nervous system. Traditional acupuncture followed by exercise training can improve motor function for PSD more effectively than single acupuncture or exercise training; however, due to the long treatment time, multiple manipulated meridians and acupoints, obvious pain, and complicated steps, it is not conducive to patient long-term persistence and affects the follow-up rehabilitation.

Ocular Acupuncture Kinesitherapy (OAKT) is a form of moving acupuncture in which exercise training is carried out while ocular acupuncture needles are embedded in the orbital tissues. Ocular acupuncture, an acupuncture treatment manipulated on orbit with 8 areas and 13 acupoints, has been approved by the Standardization Administration of China in 2009 (16). As a sort of micro-acupuncture, ocular acupuncture can activate the meridians, invigorate blood, relieve pain and regulate viscera functions by stimulating acupoints around the orbital margin (17–19). Conducting physical therapy (PT), occupational therapy (OT), speech therapy (ST), swallowing training, and other therapies during ocular needle retention can manipulate at fewer points with low pain and simple steps for PSD patients (20), demonstrating the advantages of rapid onset and high patient tolerance. It is advantageous to reduce the treatment length and rehabilitation course, reduce stroke morbidity, and dramatically increase short and long-term efficacy (21–29). In northeast China, OAKT has gradually gained popularity and has become the primary approach for PSD rehabilitation. OAKT has been proven more efficient than traditional acupuncture followed by exercise training in alleviating limb spasms, reducing limb muscle tension, alleviating motor dysfunction, restoring clinical nerve function,

and improving daily living ability in PSD (30–36). It has societal significance for its ease of operation, safety and efficiency in treatment, and high patient compliance. The National Administration of Traditional Chinese Medicine established the Operating Standards for OAKT in 2018, clarifying the indications, operating specifications, processes, and precautions in the treatment of stroke and promoting it as a suitable technology for TCM in China. However, because OAKT has such a short application period, it is unclear how it promotes dyskinesia recovery after a stroke.

The brain, as a sophisticated neurological center, can process and integrate input signals by processing and exchanging materials, energy, and information between neurons and synapses to control numerous peripheral organ functions. As a significant input-output channel of motor neuron signal transmission, the Primary Motor Cortex (M1)-Thalamus-Spinal cord is strongly associated with motor functions, such as target-oriented activities of controlling limbs, motor proficiency, coordinated movement, and motor learning (37). The corpus callosum white matter fiber connecting the bilateral primary motor cortex and associated with motor function score was destroyed in post-stroke dyskinesia patients, as was the structural integrity of the right upper longitudinal fasciculus. According to the findings, the cerebral cortex dysfunction of PSD is related to the damaged structure, whereas the contralateral cortex and other brain regions compensate (38), and left upper limb activity and self-paced finger motoring can activate the injured corpus callosum white matter fiber connecting the bilateral primary motor cortex (39).

Functional magnetic resonance imaging (fMRI), a non-interventional functional neuroimaging technique with simultaneous imaging of structure and function, high spatial-temporal resolution, and non-radioactivity, is useful for quantifying cerebral neuronal state and providing an objective reflection of brain functional activities (40). Transcranial Magnetic Stimulation-Motor Evoked Potential (TMS-MEP) is a transcranial magnetic stimulation technique that targets motor cells in the cerebral cortex, spinal nerve roots, and peripheral nerves to record compound action potentials on the relevant muscles, reflecting the functional status of the pyramidal tract. It can be utilized to assess limb motor dysfunction and dynamically monitor recovery conditions due to the great penetration, deep location, and less discomfort of magnetic stimulation (41, 42). TMS-MEP concentrates on the assessment of motor neuronal function, whereas fMRI primarily reflects brain anatomy and functional status. The combination of fMRI and TMS-MEP is intended to thoroughly examine brain functional activity, cortical excitability, and motor neural conduction in pursuit of objective evaluation of motor function from central to peripheral nerves.

We intend to perform fMRI scanning and TMS-MEP technique to observe the OAKT in cerebral function, motor neural function, and dyskinesia improvement to determine the potential mechanism of OAKT in the rehabilitation of PSD. Through correlation analysis of functional neuroimaging, neurotic electrophysiological, and clinical data, it will be contributed to investigating the central-peripheral coupling effect of OAKT on PSD and to further clarify the neurological processing of acupuncture kinesitherapy covering the entire pathway from peripheral to central nervous system.

Methods

Study setting

This is a prospective functional neuroimaging and neurotic electrophysiological study with a case-control design between the PSD with the HC groups and a randomized controlled design within the 3 PSD groups (OAKT group, ocular acupuncture group, and kinesitherapy group). Using fMRI scanning and the TMS-MEP technique, we will assess the central-peripheral neuronal function changes of PSD as well as the coupling effects of OAKT on them. This trial was authorized by the Institutional Review Board of Chengdu University of Traditional Chinese Medicine in April 2022 (reference number: 2022KL-027) and registered (ChiCTR2200060483) at the Chinese Clinical Trial Registry in June 2022. We plan to enroll 90 participants at the Hospital of Chengdu University of Traditional Chinese Medicine from Aug 31, 2022, to Dec 31, 2023. All eligible subjects will be evaluated by fMRI scanning, TMS-MEP examination, and the MMT and Fugl-Mayer assessment following enrollment and on the last day after 4-weeks of waiting (for HC subjects) or intervention (ocular acupuncture, kinesitherapy, or OAKT for PSD subjects, respectively). MMT and Fugl-Meyer score, ReHo value, cluster size, active or positive brain regions and their MNI coordinates, amplitude (AMP), potential latency (PL), and central motor conduction time (CMCT) in the cortical region will be measured, and Pearson correlation analysis will be performed to assess the relationship between clinical and imaging outcomes. This trial will be conducted in accordance with the Standard Protocol Items: Recommendations for Interventional Trials (SPIRIT) (43). Figure 1 displays a flow diagram.

Subjects

Patients with post-stroke dyskinesia (PSD) and healthy controls (HC) from the hospital of Chengdu University of Traditional Chinese Medicine and social recruitment, respectively, served as the study's subjects. The diagnostic criteria for patients in this study are based on the Chinese Guidelines for Diagnosis and Treatment of Acute Intracerebral Hemorrhage 2019 (44) and the Chinese Guidelines for Diagnosis and Treatment of Acute Ischemic Stroke 2018 (45). During

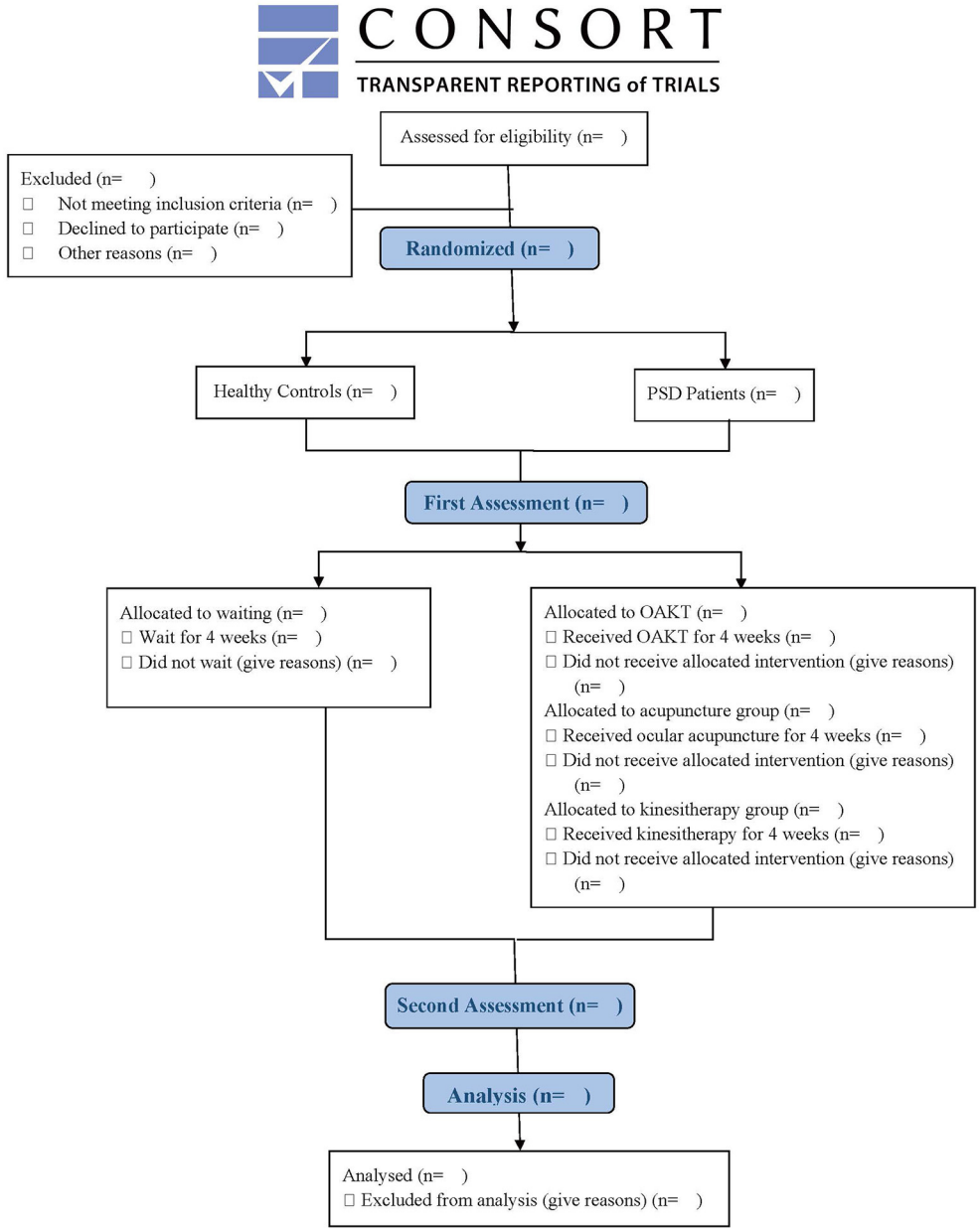

FIGURE 1
Flow diagram.

the anticipated enrollment period from Aug 31, 2022, to December 31, 2023, patients matching the diagnosis standards and satisfying the inclusion and exclusion criteria will be recruited for the study. Table 1 lists the stroke diagnostic criteria.

PSD participants

This study will exclude dyskinesia brought on by progressive supranuclear palsy, hepatolenticular degeneration, essential tremor, multiple system atrophy, chorea, tossing syndrome, myoclonus, dystonia, Tourette syndrome, and other conditions.

PSD participants that meet the following criteria: (1) have unilateral dyskinesia and a fresh stroke diagnosis; (2) are right-handed and aged 30–80; (3) have no fMRI or TMS contraindications, and no metallic objects inside the body; (4) haven't undergone acupuncture or exercise therapy for a disease-related condition in the previous month; (5) comprehend and agree with the relevant research content and volunteer to sign the informed consent form can be included

TABLE 1 Diagnostic criteria of stroke.

Ischemic stroke	1. Acute onset
	2. Usually focal or sometimes complete neurologic impairment (unilateral facial or body weakness or numbness, language barriers, and so on)
	3. Imaging lesions or symptoms/signs lasting more than 24 h
	4. Exclude non-vascular etiology
	5. Exclude cerebral hemorrhage by brain CT/MRI scanner
Hemorrhagic stroke	1. Acute onset
	2. Usually focal or sometimes complete neurologic impairment accompanied with headache, vomiting, elevated blood pressure, and different degrees of consciousness disorders
	3. Brain CT/MRI scanner showed hemorrhagic focus
	4. Exclude non-vascular etiology.

in this study. While those who (1) have serious illnesses like uncontrollable hypertension, arrhythmia, serious coronary heart disease, uncontrolled diabetes complications, epilepsy, serious organ failure, and a second stroke, etc.; (2) have unstable vital signs; (3) are vulnerable to co-infection, bleeding, tumor, pregnant women, and postoperative dysfunction; (4) receive other Traditional Chinese Medicine rehabilitation interventions besides acupuncture during treatment; (5) with linguistic or cognitive impairment; (6) with a history of mental illness or long-term sedative use; (7) with conditions that prevent exercise will be excluded.

Healthy controls

Healthy controls that satisfy the requirements: (1) have no history of stroke or impaired motor function; (2) are right-handed between the ages of 30 and 80; (3) have no metallic objects in their bodies and no fMRI or TMS contraindications; (4) have not undergone disease-related acupuncture or exercise therapy in the previous month; (5) understand and agree with relevant research content and volunteer to sign the informed consent form can be included in this study.

While those (1) with significant conditions, such as uncontrollable hypertension, arrhythmia, major coronary heart disease, or diabetes complications are not well-controlled, or have epilepsy, serious organ failure, and second attack of stroke, etc.; (2) with unstable vital signs; (3) are susceptible to co-infection, hemorrhage, tumor, pregnant women, postoperative dysfunction patients; (4) get other Traditional Chinese Medicine rehabilitation intervention other than acupuncture during the waiting period; (5) with linguistic or cognitive impairment; (6) with a history of mental illness or long-term sedative use; (7) with conditions that prevent exercise will be excluded.

Interventions

PSD participants will be randomized to the ocular acupuncture (OA) group, the kinesitherapy (KT) group, or the OAKT group after enrollment.

Subjects in the OAKT group will undergo kinesitherapy after receiving ocular acupuncture stimulation at the "Upper-Jiao Area" (ACU 1), "Lower-Jiao Area" (ACU 2), "Liver Area" (ACU 3), and "Kidney Area" (ACU 4) (16) (Figure 2). This involves a series of advised exercise training consisting of warm-up exercises (low levels of aerobic exercise), exercise training (including aerobic training, walking training, treadmill training, resistance training, upper limb flexion adduction-abduction exercise, lower extremity knee flexion-extension exercise, flexibility training), and relaxation training (stretching exercise) (46). Needles for ocular acupuncture will remain embedded until the day's exercise training is finished. OAKT will be manipulated once a day, 5 days a week, for 4 weeks, with 2 days off between courses. Sweating, breathing, pulse, and blood pressure measures will be used to adjust the exercise prescription.

Subjects in the OA group will receive ocular acupuncture stimulation at the same acupoints of that in the OAKT group, without any exercise training of any kind.

Subjects in the KT group will undertake the same kinesitherapy as well as that in the OAKT group, without ocular acupuncture stimulation.

Healthy subjects will only get clinical, functional imaging, and electrophysiological evaluation without any therapy after enrollment and on the last day of the fourth week.

Outcomes

Clinical outcomes

MMT Freehand Muscle Strength Grading and Simplify Fugl-Meyer grading will be evaluated at baseline and study completion. With 11 grades, MMT is used for measuring muscle contraction force based on muscle ability to accomplish gravity-support, anti-gravity, or anti-resistance tasks. Muscle strength increases with grade level. Fugl-Meyer is a motor function evaluation scale that consists of 33 upper-limb and 17 lower-limb subscales. Each subscale is worth 0 to 2 points, for a total score of 100. The motor function improves with a higher score.

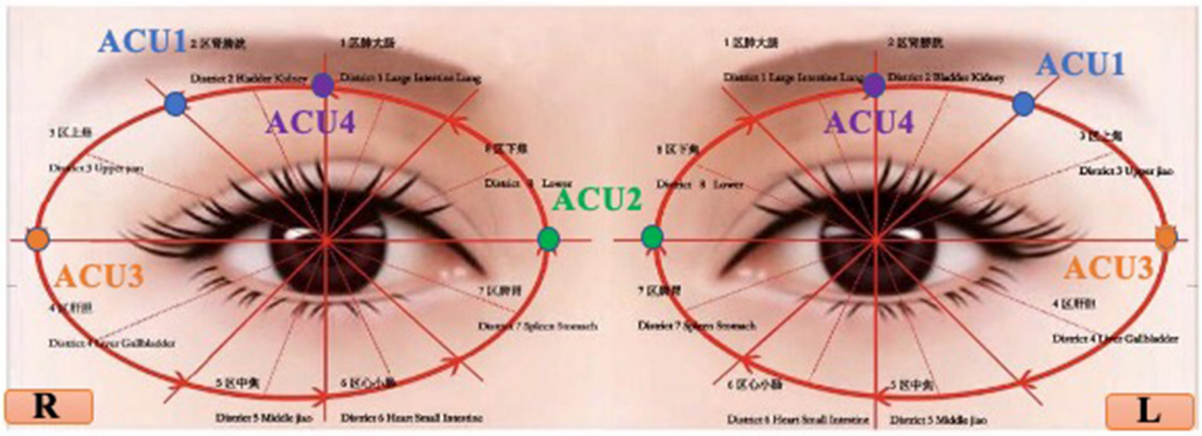

FIGURE 2
Location of ocular acupoints.

Functional neuroimaging outcomes

A 3.0 Tesla high-field full-body magnetic resonance imaging system will be used for functional neuroimaging. Bold-fMRI data is acquired in the resting state following structural image scanning with a three-dimensional fast-spoiled gradient-recalled sequence and functional image scanning with a Gradient-Echo-Planar Imaging for 10 min, covering the entire brain, cerebellum, and brain stem. The parameters for scanning structural images include layer a thickness of 1 mm, a Repetition Time/Echo Time (TR/TE) of 2,700 ms/3.39 ms, Field of Vision (FOV) of 256 mm^2, Matrix of 256 × 256, a Flip Angle of 7°, and an in-plane resolution of 1 × 1 mm. The settings for functional image scanning include a slice thickness of 5 mm, a TR/TE of 2,000 ms/30 ms, Matrix of 64 x 64, FOV of 240 mm^2, and a Flip Angle of 90°.

The original fMRI data in DICOM format will be copied to a computer and converted by MRIcro software into an analyzable.img file format. The software packages Data Processing Assistant for Resting-State fMRI (DPARSF) and the statistical parametric mapping software package (SPM12) in Matlab (Mathworks, Inc., Natick, Massachusetts) will be utilized to preprocess the fMRI data. Preprocessing steps include (1) realign, all images of each selected subject whose translation in all directions (x, y, z) is <1 mm and rotation angle is <1 degree will be aligned with its first image for further analysis; (2) Spatial normalization, registers images of all subjects to the standard template of Montreal Neurological Institute (MNI) neurological spatial coordinates and re-cuts the voxel to 3 mm 3 for data standardization and individual comparability; (3) slice-timing correction, uses a mathematical approach to collect all images at the same time point by default, with the intermediate time point as the reference layer; (4) smoothing with an 8 mm full width at half maximum (FWHM) kernel to reduce spatial noise, as well as errors caused by spatial normalization; (5) Detrending with linear regression and filtering with a frequency window of 0.01–0.08 Hz to remove low frequency noise caused by respiration, heartbeat, and other physiological factors, as well as high frequency noise from the MRI scanner itself.

Regional homogeneity (ReHo), a typical fMRI analysis, can indirectly reflect the time synchronization of spontaneous neural function activities in a specific brain region. The Kendall's Coefficient Concordance (KCC) will be used to quantify the local consistency of time series between each voxel in the entire brain and the nearest 26 voxels around it by using REST software in Matlab. Each individual receives a ReHo image by computing the KCC value of each voxel. After normalization, the average ReHo image of each subject will be derived by dividing the KCC value of each voxel by the average KCC value of the entire brain. The estimated ReHo value corresponds to the KCC value, which runs from 0 to 1. The closer it is to 1, the more consistent this voxel's activity is in time series with its neighboring voxels, reflecting brain local neuronal activity synchronization. The calculation is expressed as follows:

$$\mathrm{ReHo} = \frac{\sum(R_i)^2 - n(R)^2}{k^2(n^3 - n)/12}$$

The SPM12 in Matlab will be used to analyze the obtained ReHo value. MNI coordinates of the associated regions, the size of the clusters, and the active or positive brain regions will all be noted before and after the intervention.

Neurotic electrophysiology outcomes

Transcranial magnetic stimulation of motor evoked potential (TMS-MEP) examination will be used for neurotic electrophysiology. Cortical magnetic stimulation will be performed using the Keypoint evoked potential instrument and the magnetic stimulator MagII PR030 with standard circular

coil and single puls form. The subjects assume a calm supine or seated position. The compound action potentials of the hand muscle (abductor pollicis brevis) will be recorded using a magnetic stimulator center at 175 px on both sides in the C3 and C4 areas, as well as a spinal cord stimulation center in the C7 area. Simultaneously, the compound action potential of the lower extremity muscle (tibialis anterior) will be recorded, with the coil center situated between 2 and 150 px in front of the CZ region. The intensity of the stimulus should gradually increase from low to 65–75% of the maximum output intensity on the scalp and 65–80% of the maximum output intensity on the lower limbs. Varying limbs can be stimulated at different positions and angles depending on the subject's condition. In order to establish the strong repeatability of compound muscle action potential (CMAP) waves, the complete inspection should measure 4–5 CMAP waves. The highest amplitude, shortest latency, and clearest waveform should be recorded.

The cortical region's amplitude (AMP), potential latency (PL), and central motor conduction time (CMCT) serve as the main markers of TMS-MEP. The outcomes can be categorized into 4 levels: (1) no MEP wave with strong repeatability and a clear and stable waveform is evoked during cortical stimulation; (2) prolonged PL in cortical stimulation; (3) prolongation of CMCT; (4) AMP in the affected side drops by more than half when compared to the healthy side. The last three are categorized as prolonged in this study and will be treated as aberrant MEP.

Safety outcomes

The incidence of adverse events, primarily fainting, bent needle, and subcutaneous hematoma during ocular acupuncture, tinnitus, chest tightness, palpitation produced by fMRI scanning noise, and muscle soreness or weariness induced by excessive exercise training, will be recorded for safety evaluation.

Participant timeline

All participants are scheduled to finish the trial by December 2023 once recruitment and data collecting start in Aug 2022. Enrollment, interventions, and participant assessments are depicted in a temporal schematic diagram (Figure 3).

Sample size

This is a central-peripheral coupling mechanism study rather than a clinical trial. As human-based neuroimaging mechanism studies differ from clinical trials, sample size cannot be estimated using clinical trial computational methods. According to the sample size calculation of imaging studies at home and abroad (47), the sample size is usually 6–12 cases in each group. We determined the sample size as 15 cases per group in accordance with the minimum statistical requirements, considering the drop-out that could be brought on by subjects' compliance and removing the scenario that patients' excessive head movement might influence the data in the statistical analysis progress during fMRI scanning. To keep the statistical results accurate and reliable, 45 healthy controls must be matched simultaneously. In total, 90 subjects-−15 in the OAKT group, 15 in the OA group, 15 in the KT group, and 45 in the HC group—are required for this study.

Recruitment

All participants are scheduled to finish the trial by December 2023 once recruitment and data collecting start in Aug 2022. Participants who meet the inclusion and exclusion criteria will be recruited after signing an informed consent form prior to the trial. They are free to decide whether or not to take part in the study. Subjects have the option to refuse or withdraw from the study at any time during the procedure. The DMC or researchers may suspend subjects' participation in the study at any time for their good.

Data collection and management

One researcher (DZ), using a paper version of case report forms (CRF), will gather and document clinical, neurotic electrophysiological, and side-effect information throughout the study. Another researcher (JFS) will copy functional neuroimaging data from the fMRI system using prescribed CDs and record it in an electronic Microsoft Office Excel form with passwords. All data will subsequently be captured and managed using the Research Electronic Data Capture (REDCap) system (48). A researcher (YSW) will enter the data into the REDCap Database, which will then be double-checked by a second researcher (HPL). To ensure accurate data collection and proper data export for further analyses, the statistician (ZPW) will review the database. The Hospital of Chengdu University of Traditional Chinese Medicine will store all information in paper form for 10 years and back it up on various network drives.

Statistical methods

Only subjects with complete data after 4 weeks of intervention or waiting and pre-post evaluation will be statistically analyzed.

	STUDY PERIOD										
	Enrolment	Allocation	Post-allocation								Close-out
TIMEPOINT**	*-7day~ -1day*	0 day	*1 day*	*5 day*	*8 day*	*12 day*	*15 day*	*19 day*	*22 day*	*26 day*	*27 day*
ENROLMENT:											
Eligibility screen	X										
Informed consent	X										
INTERVENTIONS:											
[OAKT for PSD]			—	—	—	—	—	—	—	—	
[OA for PSD]			—	—	—	—	—	—	—	—	
[KT for PSD]			—	—	—	—	—	—	—	—	
[Waiting for HC]			—	—	—	—	—	—	—	—	
ASSESSMENTS:											
[fMRI TMS-MEP MMT Fugl-Mayer]		X								X	
[Adverse Events]										X	

FIGURE 3
Time schematic diagram of enrolment, interventions, and assessments.

Clinical and electrophysiological data analysis

SPSS 23.0 will be used for data analysis. For measurement data, the *T*-test or ANOVA with 95% confidence intervals will be used to compare groups if the distribution is normal, else a Non-parametric Test will be performed. For enumeration data, a chi-square test will be used. A two-sided threshold of $P < 0.05$ will be considered statistically significant.

Neuroimaging data analysis

SPM12 software will be used to perform paired *t*-tests on the acquired ReHo value. The statistical threshold voxel-level will be $P < 0.001$ with multiple comparisons corrected by FEW (family-wise error), cluster level $\alpha < 0.05$. More than 10 continuous voxels will be significant.

Correlation analysis between clinical and imaging data

The MATLAB software will be used to conduct the correlation analysis between ReHo values and clinical indexes of PSD. Gender, age, and course will be included as covariates in a Pearson correlation study between the MMT score, Fugl-Meyer score, and ReHo values of PSD. The statistical threshold of $P < 0.05$ will be considered statistically significant.

Data monitoring

Adverse events include fainting, bent needles, and subcutaneous hematomas during ocular acupuncture, tinnitus, chest tightness, palpitation induced by fMRI scanning noise, and muscle pain and weariness caused by excessive exercise training.

An independent data monitoring committee (DMC) comprised of a study statistician, external stroke researcher, and external rehabilitation therapist will oversee the study and review adverse events. The DMC will constantly monitor the entire study procedure and make suggestions for quality assurance, as well as consider and recommend either stopping or continuing the study if adverse events occur. Once the study or data analysis is finished, the study team will be unblinded.

Auditing

Once a year, independent staff from the Chengdu University of Traditional Chinese Medicine will monitor and audit the prudent use of project money.

Discussion

A major side effect of the cerebrovascular accident is PSD, which impairs motor function and places a heavy financial, psychological, and physical burden on patients, families, and society. Rehabilitation after a stroke is crucial to maintaining overall health. Sun (49) verified the superior effects of acupuncture combined with exercise training on neurological function and movement problems in patients with cerebral infarction compared to exercise training alone by measuring Fugl-Meyer score, BI score, Berg score, and NISS score changes ($P < 0.05$). The combination therapy can play a better role in terms of effectiveness and symptom function improvement, with fewer adverse events and good safety, compared to acupuncture or Bobath therapy alone, according to Liu's systematic review of spastic paralysis after stroke (50). The greatest improvement in motor function can be achieved when acupuncture is used in conjunction with exercise training. However, this approach necessitates acupuncture manipulation first, followed by training, which hinders patient long-term perseverance and has an impact on follow-up rehabilitation due to the lengthy treatment time, numerous manipulated meridians and acupoints, obvious pain sensations, and complex steps. By combining ocular acupuncture and exercise training simultaneously, OAKT can ease limb spasms, decrease muscle tension, alleviate motor dysfunction, etc. in PSD patients with improved outcomes. It can minimize the treatment duration and rehabilitation course, and improve short- and long-term efficacy by making use of the advantages of fewer stimulation acupoints, low pain feelings, simple manipulation steps, rapid onset, and high patient tolerance. Unfortunately, due to the short application period, it is yet unclear how OAKT promotes PSD recovery, necessitating urgent research in this area. Therefore, the first scientific challenge of this work is how to appropriately conduct the OAKT mechanism research on PSD.

Through the exchange and fusion of matter, energy, and information, the brain, the higher neurological center, can regulate various functional activities of peripheral organs. The M1-THA-SPC, a crucial input-output pathway of motor neuron signal transmission, can assist in limb goal-oriented motor control, achieving motor proficiency, coordinating movement, and motor learning through the mapping of neurons. Muscle serves as both the peripheral target organ and the primary executive body of the movement in this signaling pathway, the function cannot be carried out without the command and regulation of the higher and secondary centers (brain and spinal cord) (SPC). As a result, we intend to conduct a central-peripheral linkage control study in conjunction with brain-spinal cord regulation and muscular response to understand the mechanism of OAKT on PSD.

fMRI, a non-invasive neuroimaging technique for studying cerebral function, can quantitatively detect the functional activity of brain neurons to reflect the functional state of the brain objectively. Previous fMRI studies have shown that the function of motor-related brain areas, particularly the primary motor cortex, as well as the degree of linkage between the thalamus and other cortical motor networks, is aberrant in stroke patients, and changed dramatically after acupuncture intervention. TMS-MEP is a type of neurotic electrophysiological detection method for recording compound action potentials on the appropriate muscles by transcranial magnetic stimulation of cortical motor cells, spinal nerve roots, and peripheral nerves. It can objectively reflect the current state of cerebral cortex function and is useful in assessing subjects' motor neural function and prognosis. For these reasons, this study will combine fMRI scanning with TMS-MEP detection to realize brain-spinal cord regulation and muscle response linkage control mechanism research, as well as completely investigate the central-peripheral coupling effect of OAKT on PSD.

Two advances in this study are the idea and the methodology. For the idea, we propose to conduct a prospective functional neuroimaging and neurotic electrophysiological study based on a case-control study in the PSD and HC groups as well as a self-control study in the PSD group. The primary motor cortex (higher center), the thalamus (higher center), the spinal cord (secondary center), and the muscle (peripheral) motor neural signal transmission channel are the targets of our assessment of PSD's abnormal central-peripheral neural function and the coupling effects of OAKT on PSD. For the technique, we propose doing a curative effect evaluation and mechanism investigation based on fMRI scanning, TMS-MEP examination, and the MMT and Fugl-Mayer scale assessment to examine the effects of OAKT on brain function, motor nerve function, and degree of motor dysfunction in PSD. Pearson analysis will also be performed between the MMT score, Fugl-Meyer score, and ReHo values of PSD to investigate the association of imaging, neurotic electrophysiological, and clinical outcomes, and to finally exploit the central-peripheral linkage control mechanism and coupling effect of OAKT on PSD from functional imaging and neurotic electrophysiology perspectives.

Confidentiality

The Hospital of Chengdu University of Traditional Chinese Medicine will maintain complete custody of all participant medical documents (study records/CRF, laboratory sheets, data CDs, etc.). Researchers, ethical committees, and statisticians will have access to medical records. Personal identity will not be disclosed in any public report on the results of this study. We will do everything within the law to protect the privacy of participants' personal medical information.

Ancillary and post-trial care

The study team will bear all testing and treatment costs for this study.

Any potential harm from this study will be prevented and treated as best we can. The DMC will decide whether a study-related adverse event is caused by the trial's protocol or by the treatment if it occurs. In accordance with the Chinese Quality Management Standards for Drug Clinical Trials, the sponsor will pay for medical expenses and other financial compensation for any harm caused by the testing procedure.

Ethics statement

The studies involving human participants were reviewed and approved by the Institutional Review Board of Chengdu University of Traditional Chinese Medicine has granted ethics approval for this study, which will be carried out in Aug 2022 in accordance with the Declaration of Helsinki's principles (reference number: 2022KL-027). The patients/participants provided their written informed consent to participate in this study.

Author contributions

DZ, HL, and YW take responsibility for the concept, design, and integrity of the data. JM, JS, ZW, and GZ: investigation. DZ and YW: methodology. HL: statistical analysis. DZ: project administration, writing–original draft, and funding acquisition. SJ: supervision. GZ: writing–review and editing. All authors contributed to the article and approved the submitted version.

Funding

This study was supported by the Sichuan Administration of Traditional Chinese Medicine (No. 2020LC0081), the Hospital of Chengdu University of Traditional Chinese Medicine (No. 20ZL02), and the Chengdu University of Traditional Chinese Medicine (No. MPRC2021044).

Conflict of interest

The authors declare that the research was conducted in the absence of any commercial or financial relationships that could be construed as a potential conflict of interest.

Publisher's note

References

1. Wu SM, Wu B, Liu M, Chen ZM, Wang WZ, Anderson CS, et al. Stroke in China: advances and challenges in epidemiology, prevention, and management. *Lancet Neurol.* (2019) 18:394–405. doi: 10.1016/S1474-4422(18)30500-3

2. Li ZY, Fang SZ, Yu LQ, Nie PY, Liu F. Meta-analysis of effects of trunk muscle training on lower extremity function in patients with stroke hemiplegia. *Fujian Med J.* (2020) 42:134–8.

3. GBD 2016 Dementia Collaborators. Global, regional, and national burden of Alzheimer's disease and other dementias, 1990–2016: A systematic analysis for the global burden of disease study 2016. *Lancet Neurol.* (2019) 18:88–106. doi: 10.1016/S1474-4422(18)30403-4

4. Lindsay P, Norrving B, Sacco RL, Brainin M, Hacke W, Martins S, et al. World stroke organization (WSO): global stroke fact sheet 2019. *Int J Stroke.* (2019) 14:806–17. doi: 10.1177/1747493019881353

5. Ekker MS, Boot EM, Singhal AB, Tan KS, Debette S, Tuladhar AM, et al. Epidemiology, aetiology, and management of ischaemic stroke in young adults. *Lancet Neurol.* (2018) 17:790–801. doi: 10.1016/S1474-4422(18)30233-3

6. Zhang ZX, Lv M, Luo XF, Yu X, Lu ZY, Wang L, et al. Recommendations of clinical practice guidelines of stroke rehabilitation. *Chin J Rehabil Theory Pract.* (2020) 26:170–80. doi: 10.3969/j.issn.1006-9771.2020.02.007

7. World Health Organization, Qiu ZY, Guo JX, Li L. Rehabilitation in the health service system. *Chin J Rehabil Theory Pract.* (2020) 26:1–14. doi: 10.3969/j.issn.1006-9771.2020.01.003

8. Yang A, Wu HM, Tang JL, Xu L, Yang M, Liu G. Acupuncture for stroke rehabilitation. *Cochrane Database Syst Rev.* (2016) 8:CD004131. doi: 10.1002/14651858.CD004131.pub3

9. Winstein CJ, Arena R, Bates B, Cherney LR, Cramer SC, Deruyter F, et al. Guidelines for adult stroke rehabilitation and recovery: a guideline for healthcare professionals from the American heart association/American stroke association. *Stroke.* (2016) 47:e98–l69. doi: 10.1161/STR.0000000000000098

10. Shi XM. Clinical study of "Xingnao Kaiqiao" acupuncture on 9005 cases of apoplexy. *Guiding J Tradit Chin Med Pharmacol.* (2005) 11:3–5. doi: 10.3969/j.issn.1672-951X.2005.01.003

11. Kou P, Shi XM. Review of the curative effect of acupuncture on stroke treated by "Xingnao Kaiqiao" method and analysis of NIHSS scale. *Shanxi J Tradit Chin Med.* (2015) 13:41–42+55.

12. Zhu CT, Shi N, Shi XM. *Clinical* study on the intervention time of xing nao kai qiao needling method for hemorrhagic stroke. *Shanghai J Acupunct Moxibustion.* (2017) 36:1277–80. doi: 10.13460/j.issn.1005-0957.2017.11.1277

13. Yu XP, Yan J, Zou W. Clinical observation on the muscle tension staged acupuncture for stroke hemiplegia. *Chin Acupunct Moxibustion.* (2018) 38:1035–8. doi: 10.13703/j.0255-2930.2018.10.002

14. Zhang Q. *Literature analysis of TCM intervention in chronic heart failure and clinical effect of exercise rehabilitation.* [dissertation]. Shenyang: Liaoning University of Traditional Chinese Medicine (2018).

15. Li SC, Fu L, Guo XC, Meng TT, Zhang SJ, Wang P. Efficacy of exercise therapy on recovery of moto function after anterior cruciate ligament reconstruction: a meta-analysis. *Chin J Evid Based Med.* (2019) 19:1086–92.

16. Affiliated Hospital of Liaoning University of Traditional Chinese Medicine, Che J, Tian WZ, Hai Y, Tian Y, Zhang SW, et al. *Standardized Manipulations of Acupuncture and Moxibustion—Part 15: Ophthalmic Acupuncture Techniques. National Public Service Platform for Standards Information.* (2021). Available online at: https://std.samr.gov.cn/gb/search/gbDetailedid=D4BEFFF4EA7AB241E05397BE0A0AF581

17. Wang TD, Hai Y. The progress of eye acupuncture relieve pain effect in clinical survey. *J Pract Trad Chin Int Med.* (2021) 27:182–3. doi: 10.13729/j.issn.1671-7813.2015.07.82

18. Wang PQ, Ju QB, Zhou HF, Wang J. Study of the theoretical basis of ocular acupuncture therapy based on literature clinical experiment: eye colludes in the brain and regulate viscera. *Chin J Basic Med Tradit Chin Med.* (2011) 17:1133–4.

19. Yang T, Wang PQ. Study of the specificity of acupoint area based on meridians and anatomy. *Hunan J Tradit Chin Med.* (2014) 30:99–101.

20. Li TY, Xing HJ, Xu YY Shi J, Wang JL, Sun YH, et al. *Features of clinical application of eye acupuncture therapy revealed by data mining. Acupunct Res.* (2019) 44:377–82.

21. Tian LR, Wang PQ, Zhang JM. Analysis of eye acupuncture combined with rehabilitation training for the treatment of stroke. *J Emerg Tradit Chin Med.* (2021) 30:1970–3. doi: 10.3969/j.issn.1004-745X.2021.11.022

22. Kong Y. *Clinical Study of Eye Acupuncture Combined With Body Acupuncture Therapy in the Treatment of Limb Motor Dysfunction in Patients With Wind-Yang Disturbance Stroke Hemiplegia*. Shenyang: Liaoning University of Traditional Chinese Medicine (2021).

23. Cui C, Wang PQ, Shao Y, Liu J. Effects of transcranial direct current stimulation combined with eye acupuncture exercise therapy on recovery of limb motor dysfunction after stroke. *J Liaon Univ Tradit Chin Med.* (2021) 23:123–6. doi: 10.13194/j.issn.1673-842x.2021.05.028

24. Sun Y, Li BL, Hu N. Observation on the curative effect of eye acupuncture combined with needle retention rehabilitation training in treating hemiplegic limb dysfunction after stroke. *Jilin J Chin Med.* (2021) 41:272–4. doi: 10.13463/j.cnki.jlzyy.2021.02.036

25. Gong B. *Observation of the Curative Effect of the Rehabilitation Therapy of Eye Acupuncture Retaining Needle on Patients With Spastic Hemiplegia After Stroke.* Shenyang: Liaoning University of Traditional Chinese Medicine (2020).

26. Wang Y, Zhou HF, Wang Z. A randomized controlled study of periocular acupuncture "inducing resuscitation and unblocking meridians" technique on limb dyskinesia in the acute phase of ischemic stroke. *J Liaon Univ Tradit Chin Med.* (2020) 22:72–5.

27. Yang W. *Clinical Study of Curative Effect of Eye Acupuncture With Acupuncture Rehabilitation Training in Treating Spastic Hemiplegia of Lower Limbs After Stroke*. Shenyang: Journal of Liaoning University of Traditional Chinese Medicine (2020).

28. Yang S. *Clinical Application and Time-Effect Relationship of Rehabilitation With Eye-Acupuncture in Patients With Spasm Stage of Stroke*. Shenyang: Liaoning University of Traditional Chinese Medicine (2020).

29. Zou L, Bo Q. Clinical observation eye-acupuncture combine with rehabilitation exercise in the treatment of qi deficiency and blood stasis type stroke hemiplegia at the recovery stage. *Clin J Tradit Chin Med.* (2018) 30:1247–9. doi: 10.16448/j.cjtcm.2018.0381

30. Yuan Q. *Clinical Study of Eye Acupuncture Combined With Rehabilitation Exercise For Spastic Hemiplegia After Stroke*. Hefei: Anhui University of Traditional Chinese Medicine (2016).

31. Liu H. *Clinical Study of Eye Acupuncture With Acupuncture Rehabilitation Therapy on Shoulder Hand Syndrome After Stroke*. Shenyang: Liaoning University of Traditional Chinese Medicine (2018).

32. Wang YR. *Clinical Effect of Ophthalmic Needle and Needle Rehabilitation on Apoplexy and Law of Bulbar Conjunctiva Microcirculation*. Shenyang: Liaoning University of Traditional Chinese Medicine (2019).

33. Xu H, Wang PQ, Chen YG. *Clinical* observation on eye-acupuncture combined with motion functional training in treatment of ischemic stroke. *J Liaon Univ Tradit Chin Med.* (2014) 16:123–5.

34. Li H, Lv YX. Clinical observation on 28 cases of motor aphasia caused by cerebral infarction treated by eye acupuncture therapy combined with speech rehabilitation. *J N Chin Med.* (2014) 46:174–80.

35. Tian YC, Zhang SQ. *Clinical observation on eye acupuncture* combined with exercise therapy for treating cerebral infarction of spastic hemiplegia. *Chin Arch Tradit Chin Med.* (2013) 31:674–5.

36. Duan YP. *Controlled* clinical observation of eye acupuncture therapy combined with recovery training on hemiplegia after stroke clinical. *J Pract Tradit Chin Int Med.* (2012) 26:70–2.

37. Castañeda RM, Zingg B, Matho KS, Chen XY, Wang QX, Foster NN, et al. Cellular anatomy of the mouse primary motor cortex. *Nature.* (2021) 598:159–66. doi: 10.1038/s41586-021-03970-w

38. Zhang Y, Li KS, Ning YZ, Fu CH, Liu HW, Han X, et al. Altered structural and functional connectivity between the bilateral primary motor cortex in unilateral subcortical stroke. *Medicine.* (2016) 95:e4534. doi: 10.1097/MD.0000000000004534

39. Cui FY. *fMRI and DTI Imaging of Hemiplegic Limb Movement and Acupuncture at Yanglingquan Point in brain Functional Remodeling*. Beijing: Beijing University of Chinese Medicine (2009).

40. Fang JL, Wang XL. International progress of fMRI study on brain acupuncture effect. *Chin Imag J Integ Tradit West Med.* (2013) 11:197–202. doi: 10.3969/j.issn.1672-0512.2013.02.033

41. Chen R, Cros D, Curra A, Lazzaro VD, Lefaucheur JP, Magistris MR, et al. The clinical diagnostic utility of transcranial magnetic stimulation: report of an IFCN committee. *Clin Neurophysiol.* (2008) 1l9:504–32. doi: 10.1016/j.clinph.2007.10.014

42. Kong XZ, Wang YH, Li YM, Wang YY, Meng L, et al. Study on motor evoked potential evaluation of brain function after acute cerebral infarction. *Mod J Integ Tradit Chin West Med.* (2011) 20:2360–1. doi: 10.3969/j.issn.1008-8849.2011.19.009

43. Chan AW, Tetzlaff JM, Gøtzsche PC, Altman DG, Mann H, Berlin JA, et al. SPIRIT 2013 explanation and elaboration: guidance for protocols of clinical trials. *BMJ.* (2013) 013:1501–7. doi: 10.1136/bmj.e7586

44. Chinese Society of Neurology, Chinese Stroke Society. Chinese guidelines for diagnosis and treatment of acute intracerebral hemorrhage 2019. *Chin J Neurol.* (2019) 12:994–1005. doi: 10.3760/cma.j.issn.1006-7876.2019.12.003

45. Chinese Society of Neurology, Chinese Stroke Society. Chinese guidelines for diagnosis and treatment of acute ischemic stroke 2018. *Chin J Neurol.* (2018) 9:666–82. doi: 10.3760/cma.j.issn.1006-7876.2018.09.004

46. Chen JY, Chen YD, Han YL. Expert consensus of exercise rehabilitation after percutaneous coronary intervention. *Chin J Interv Cardiol.* (2016) 24:361–9.

47. Desmond JE, Gary HG. Estimating sample size in functional MRI (fMRI) neuroimaging studies: statistical power analyses. *J Neurosci Methods.* (2002) 118:115–28. doi: 10.1016/S0165-0270(02)00121-8

48. Harris PA, Taylor R, Thielke R, Payne J, Gonzalez N, Conde JG. Research electronic data capture (REDCap)—a metadata-driven methodology and workflow process for providing translational research informatics support. *J Biomed Inform.* (2009) 42:377–81. doi: 10.1016/j.jbi.2008.08.010

49. Sun S. *Effect of* acupuncture combined with rehabilitation training on neurological function and dyskinesia in patients with cerebral infarction. *Chin Med Mod Dist Educ China.* (2020) 18:111–3. doi: 10.3969/j.issn.1672-2779.2020.13.044

50. Liu DY, Ren JW. *Acupuncture* combined with bobath therapy in treating post-stroke spastic paralysis: A systematic review and meta-analysis. *J Guangzhou Univ Tradit Chin Med.* (2019) 36:1967–74. doi: 10.13359/j.cnki.gzxbtcm.2019.12.021

frontiers | Frontiers in Neurology

TYPE Original Research
PUBLISHED 01 September 2022
DOI 10.3389/fneur.2022.931838

OPEN ACCESS

EDITED BY
Wei Zhang,
Peking University, China

REVIEWED BY
Jie Yang,
Central South University, China
Ivan V. Brak,
State Scientific Research Institute of Physiology and Basic Medicine, Russia

*CORRESPONDENCE
Yong Liu
1909768139@qq.com
Jiliang Fang
Fangmgh@163.com

†These authors have contributed equally to this work and share first authorship

SPECIALTY SECTION
This article was submitted to Applied Neuroimaging, a section of the journal Frontiers in Neurology

RECEIVED 29 April 2022
ACCEPTED 19 July 2022
PUBLISHED 01 September 2022

CITATION
Ma Y, Wang Z, He J, Sun J, Guo C, Du Z, Chen L, Luo Y, Gao D, Hong Y, Zhang L, Liu Y and Fang J (2022) Transcutaneous auricular vagus nerve immediate stimulation treatment for treatment-resistant depression: A functional magnetic resonance imaging study.
Front. Neurol. 13:931838.
doi: 10.3389/fneur.2022.931838

Transcutaneous auricular vagus nerve immediate stimulation treatment for treatment-resistant depression: A functional magnetic resonance imaging study

Yue Ma[1,2†], Zhi Wang[1,2†], Jiakai He[2,3], Jifei Sun[1,2], Chunlei Guo[1,2], Zhongming Du[4], Limei Chen[1,2], Yi Luo[1,2], Deqiang Gao[1], Yang Hong[1], Lei Zhang[1], Yong Liu[5]* and Jiliang Fang[1]*

[1]Guang'anmen Hospital, China Academy of Chinese Medical Sciences, Beijing, China, [2]Graduate School of China Academy of Chinese Medical Sciences, Beijing, China, [3]Institute of Acupuncture and Moxibustion, China Academy of Chinese Medical Sciences, Beijing, China, [4]Dongzhimen Hospital, Beijing University of Chinese Medicine, Beijing, China, [5]Affiliated Hospital of Traditional Chinese Medicine, Southwest Medical University, Luzhou, China

Objective: Transcutaneous auricular vagus nerve stimulation (taVNS) is effective for treatment-resistant depression (TRD). In the current study, we observed the immediate modulating brain effect of taVNS in patients with TRD using rest-state functional magnetic resonance imaging (rs-fMRI).

Method: Forty patients with TRD and forty healthy controls (HCs) were recruited. Rs-fMRI was performed before and after 30 min of taVNS at baseline. The brain regions that presented significantly different the Regional Homogeneity (ReHo) between the TRD patients and HCs were selected as the ROI to calculate the functional connectivity (FC) of full brain. The correlations were estimated between the clinical scales' score and the functional brain changes.

Results: Following taVNS stimulation treatment, TRD patients showed significantly reduced ReHo in the medial orbital frontal cortex (mOFC) ($F = 18.06$, $P < 0.0001$), ANCOVA of the mOFC-Based FC images revealed a significant interaction effect on the left inferior parietal gyrus (IPG) and left superior marginal gyrus (SMG) ($F = 11.6615$, $P < 0.001$, $F = 16.7520$, $P < 0.0001$). Among these regions, the HAMD and HAMA scores and ReHo/FC changes were not correlated.

Conclusion: This study applied rs-fMRI technology to examine the effect of taVNS stimulation treatment on the brain activity of TRD. These results suggest that the brain response of TRD patients to taVNS treatment may

be associated with the functional modulation of cortical regions including the medial orbital frontal cortex, the left inferior parietal gyrus, and the left superior marginal regions. Changes in these neuroimaging indices may represent the neural mechanisms underlying taVNS Immediate Stimulation treatment in TRD.

KEYWORDS

treatment-resistant depression, transcutaneous auricular vagus nerve stimulation, rest-state functional magnetic resonance imaging (rs-fMRI), amplitude of low-frequency fluctuations, regional homogeneity, functional connectivity, orbital frontal cortex

Introduction

Major depressive disorder (MDD) is a common clinical disorder of the psychiatric system, characterized by persistent depressed mood, reduced interest and cognitive function, anhedonia, and somatic disturbances (1). MDD contributes significantly to the global disease burden, with up to one-third being treatment-resistant patients (2). In clinical treatment, about 35% of patients with depression exhibit poor efficacy even after a complete course of treatment with two or more antidepressants that possess different chemical structures; this type of depression is categorized as treatment-resistant depression (TRD) (3). In addition, the disability and fatality rates of TRD patients are significantly higher than those of ordinary depression patients (4). Serretti et al. (5) reported six most likely risk factors for TRD, including long course of disease, slow onset, comorbid anxiety, advanced age, episode severity, and depressive characteristics. Therefore, TRD is a hot but difficult research topic for psychiatrists at present.

TRD is a complex disorder for which the pathogenesis is not fully understood. Studies have demonstrated TRD is associated with functional abnormalities in brain neural circuits related to emotional and cognition processing, self-representation, and reward processing, these brain regions include the medial orbital frontal cortex (mOFC), amygdala, inferior parietal gyrus (IPG), and superior marginal gyrus (SMG) (6–9). It was reported that anhedonia is associated with neurological dysfunctions in the reward system (10). Additional studies (11–13) revealed the reward loop nervous system carries emotional or cognitive information and decision-making information in the prefrontal cortex. The mOFC is a key part that mediates pain experience and motivation to avoid pain.

TRD treatment is mainly based on drug therapy combined with non-drug treatment. Most antidepressants cause adverse reactions, such as cardiovascular disease and metabolic syndrome (14). Non-drug treatments mainly include psychotherapy, electroconvulsive therapy (ECT), repetitive transcranial magnetic stimulation (rTMS), deep brain stimulation (DBS), and vagus nerve stimulation (VNS). VNS is an FDA-approved somatic treatment for treatment-resistant depression (TRD) that can produce clinically significant antidepressant effects (15). However, the application is limited by the involvement of surgery and potential side effects. To overcome the potential barriers to applying VNS, a non-invasive transcutaneous vagus nerve stimulation (taVNS) method has been developed. The rationale for using taVNS on the ear is based on anatomical studies that suggest the ear is the only place on the surface of the human body where there is afferent vagus nerve distribution (16, 17). Thus, direct stimulation of the afferent nerve fibers on the ear should produce an effect similar to classic VNS in reducing depressive symptoms but without the burden of surgical intervention (18, 19). Our previous research group (20–22) discovered that taVNS is clinically effective in treating TRD and further observed that taVNS has a significant synergistic effect on TRD patients in maintaining drug treatment. The taVNS therapeutic mechanism may be related to the modulating brain default mode network (DMN), reward network and salience network. However, the mechanism of the immediate effect of taVNS in the treatment of TRD remains unclear.

Resting-state functional magnetic resonance imaging (rs-fMRI) is a neuroimaging technique based on blood oxygenation level dependent (BOLD) levels to detect brain activity patterns and is one of the main methods to study the brain effects of acupuncture (23). Additionally, rs-fMRI has been gradually applied in the field of bipolar disorder (24), schizophrenia (25), autism (26), and other psychiatric disorders. Also, rs-fMRI has been applied to study the subtypes of depression (27–29). ReHo is used to assess the level of coordination of neural activity in local brain regions by calculating ReHo values, which indirectly reflect the spontaneous activity of local neurons in time synchronization (30). Functional connectivity (FC), which is a fMRI method for observing the functional association between different brain regions by analyzing the statistical correlation between the time series of different brain regions (31), has also been used in major depressive disorder research.

Materials and methods

Recruitment of participants

Forty adult patients aged between 18 and 70 years with a Diagnostic and Statistical Manual of Mental Disorders-IV-Text

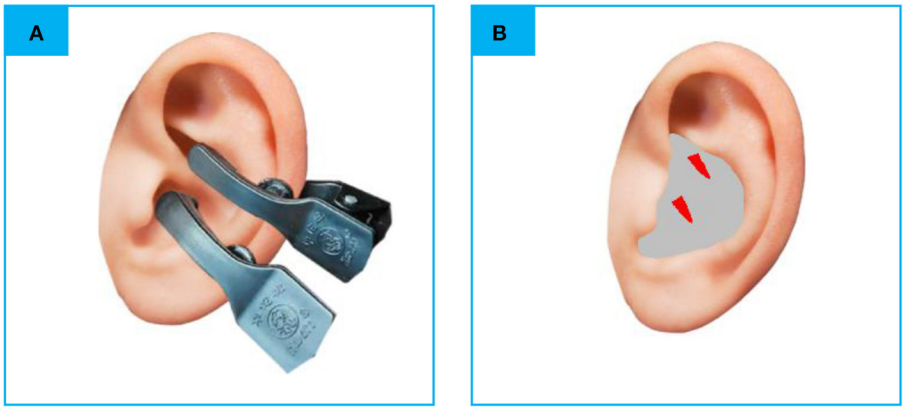

FIGURE 1
(A) The electrodes were attached to the surface of cymba conchae. **(B)** The stimulating place of taVNS. rs-fMRI, rest-state functional Magnetic Resonance Imaging; taVNS, Transcutaneous Auricular Vagus Nerve Stimulation (the red color areas).

Revision or 5 (DSM-IV-TR or 5) diagnosis of major depressive disorder who had failed to respond to at least two different antidepressants with adequate dosage and treatment duration (i.e., fluoxetine $\geq$ 20 mg/day for $\geq$ 60 consecutive days) were included in our study. Forty healthy controls (HCs) were recruited and matched with patients in sex, age, and education. The HCs had no lifetime history of major or minor psychiatric disorders. In addition, the TRD patients and HCs did not have major medical or neurological illnesses, or a history of alcohol or substance abuse. All participants were right-handed. Before the study, they were all informed of the study protocol and volunteered to participate in the study. Participants with fMRI contraindications and severe organic or mental diseases were excluded.

Ethical review and registration

The present study was reviewed and approved by the Ethics Committee of Guang'anmen Hospital, China Academy of Chinese Medical sciences (No. 2017-021-SQ) and registered at the Chinese Clinical Trial Registry (No. ChiCTR-1800014277).

Transcutaneous auricular vagus nerve stimulation

The electro-acupuncture stimulator (SDZ-IIB, Hwato brand, manufactured in Su Zhou, China) was attached to the bilateral cymba conchae through electrodes on the skin surface (Figure 1). Parameters were set according to previous studies of taVNS (32, 33): Dilatational wave of 4/20 Hz and pulse width of 0.2 ms $\pm$ 30%. The current intensity was adjusted according to each patient s subjective feeling. Each taVNS session lasted for 30 min. Before treatment, the patient's ear armor was routinely disinfected with 75% alcohol.

Clinical assessments

All participants accepted Hamilton Rating Scale for Depression (HAMD) and Hamilton Anxiety Rating Scale (HAMA) to estimate the mental status of all the participants. Inclusion in the current study required patients to score >17, and the HCs would be excluded with a total score of HAMD or HAMA >7. The process of the current study is shown in Figure 2. In addition, we screened all patients' T2-weighted and structural images to rule out most of the severe metabolic or immune-related neuropsychiatric diseases, cerebrovascular diseases, inflammatory diseases of the central never system, and intracranial tumors.

Scan acquisition

Rest-state functional magnetic resonance imaging (rs-fMRI) was performed before and after the first 30 min taVNS session. Participants were told to keep their eyes closed and not fall asleep during the scan. The fMRI data were acquired by Siemens 3.0T Skyra scanner (Siemens; Munich, Germany). The scanning parameters were as follows. The BOLD gradient Echo Planar Imaging (EPI) sequence was used in functional images. Two hundred volumes lasted 6 min and 10 s, repeat time/echo time: 2,000/30 ms, flip angle = 90°, scanning field of view: 224 mm × 224 mm, matrix: 64 × 64, number of layers: 32, layer thickness/spacing: 3.5/0.6 mm. In a high-definition structure image, three-dimensional magnetization was used to prepare a fast gradient-echo sequence, repeat time/echo time: 2,530/2.98 ms, flip angle: 7 degrees, field of view: 256 mm

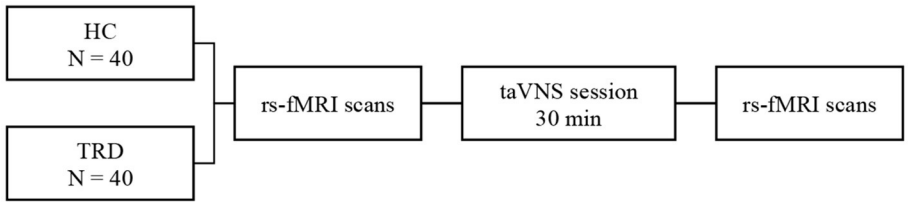

FIGURE 2
fMRI for instant taVNS were measured before and after the first treatment on the two groups.

× 256 mm, matrix: 64 × 64, and Layer thickness/spacing: 1.0/0 mm. We obtained 192 images.

Image processing

fMRI data pre-processing

DPABI (http://rfmri.org/DPABI) software (34), an SPM-based functional MRI pre-processing pipeline, was used for data pre-processing. The pre-processing steps were as follows. DICOM file was converted into NIFTI, and the first 10 time points were removed. The remaining 190 time points were slice-time corrected and realigned according to the Friston 24-parameter model. The nuisance signals, including linear trend, head-motion, signals of cerebrospinal fluid, and white matter, were regressed from the data (35). Then, the functional images were co-registered to the T1-weighted structural images, segmented through Voxel-Based Morphometry (VBM). Derived images were normalized to Montreal Neurological Institute (MNI) space according to transformation parameters estimated by VBM. All data used in this study satisfied the criteria of spatial movement in any direction <1.5 mm or degree. Subjects demonstrated no significant group differences in head-motion parameters. In this study, we failed to find significant differences in FD between groups ($F = 0.4939$, $P = 0.4843$).

The limitations of the signal-to-noise ratio and disputes in sampling and pre-processing strategies for fMRI data in the existing voxel-based analysis studies are sometimes contradictory. To better present the short-time intervention, we employed ReHo and FC to reveal the reproductive results.

Regional homogeneity (ReHo) is calculated using voxel-based Kendall's coefficient of concordance (KCC) for the time series of a given voxel with its nearest neighbors (24). ReHo maps were calculated using the unsmoothed and filtered (0.01–0.08Hz) images to remove physiological signals, such as heartbeat and respiration. Then ReHo maps were taken to mean ReHo maps by subtracting the mean voxel-wise ReHo in the entire brain and standardized into Z-value (zReHo Maps). Calculated zReHo maps were smoothed to MNI space with 6 mm Gaussian kernel full width at the half maximum smooth nucleus.

FC is the Pearson's correlations of the temporal fMRI signals between a Region of Interest (ROI) and all brain. Positive brain regions after ReHo statistics found by the above voxel based analyses would be used as the ROI for seed to voxel FC analysis. The AAL template of the WFU_Pick Atlas_v3.0 software was used to extract the seed points of the differential brain regions (36), Calculate the correlation coefficient (r) between the average time series of different brain regions and the time series of other voxels in the whole brain, Pearson's correlation coefficients were transformed into normally distributed scores according to the Fisher's R- to -Z transformation. Statistical inferences were the same as in the ReHo analysis.

Statistics

Clinical data analysis

Clinical data were analyzed using the SPSS 23.0 statistical software (IBM Corporation, Somers, New York). One-way analysis of variance (ANOVA) was used to compare age and education level among the groups, and the chi-square test was used to compare sex. A two-sample t-test was used to compare HAMD-17 and HAMA scores between the two groups, with $P < 0.05$ (two-tailed) as the threshold for statistical significance.

fMRI data analysis

In SPSS 25 (SPSS Inc., Chicago, IL, USA), two-sample *t*-tests and $\chi 2$ tests were applied to compare the baseline characteristics between the TRD and HC groups.

For the fMRI data, to determine the group × stimulation interaction effect between the two groups and the two scans, the main effects of group (the TRD group and the HC group) and time (baseline and post taVNS stimulation period), Covariates in the repeated measures ANCOVA and *post hoc* analyses were performed. Gender, age, education level, and framewise displacement (FD) metric (derived from Jenkinson's formula) of the four groups of subjects were used as covariates. The brain regions showing significant time differences in the HC group were excluded (37). The result

for ANCOVA was the performance in Gaussian random field correction (GRF), combined voxel-wise P-value <0.01 with cluster P-value <0.05 (two-tailed). We performed *post-hoc t*-test analysis using DPARSF 5.1 software for two-by-two comparisons between groups, and Bonferroni correction was applied to the results, setting a threshold of $P < 0.0125(0.05/4)$ for statistical significance.

TABLE 1 Demographic and clinical characteristics of the study participants.

Items	TRD ($N = 40$)	HC ($N = 40$)	Z/χ^2	P-value
Age (year)	43.01 ± 11.90	38.33 ± 13.04	1.764	0.082
Sex (M/F)	16/24	13/27	0.487	0.32
Education(year)	13.59 ± 3.63	15.07 ± 5.38	−1.489	0.141
HAMD	22.10 ± 4.33	2.40 ± 1.82	−7.688	*<0.01*
HAMA	23.97 ± 8.95	2.85 ± 2.39	−7.512	*<0.01*

Z, Wilcoxon rank testing; χ 2, chi-square testing. TRD, treatment-resistant depression; HC, healthy control. HAMD, Hamilton rating scale for depression; HAMA, Hamilton anxiety rating scale.

To clarify the behavioral associations of brain function, we performed Pearson correlation analyses between the fMRI values and clinical scales in SPSS 25.

Results

Demographic characteristics and clinical results

The demographic and behavioral data are provided in Table 1, in which no significant differences in age and sex between TRD patients and HCs were observed. However, the HAMD and HAMA scores were higher for the TRD patients group ($n = 40{:}40$, $P < 0.01$).

fMRI results

ReHo

Group × stimulation interaction differences in ReHo are shown in Figure 3A and Tables 2, 3. Significant group ×

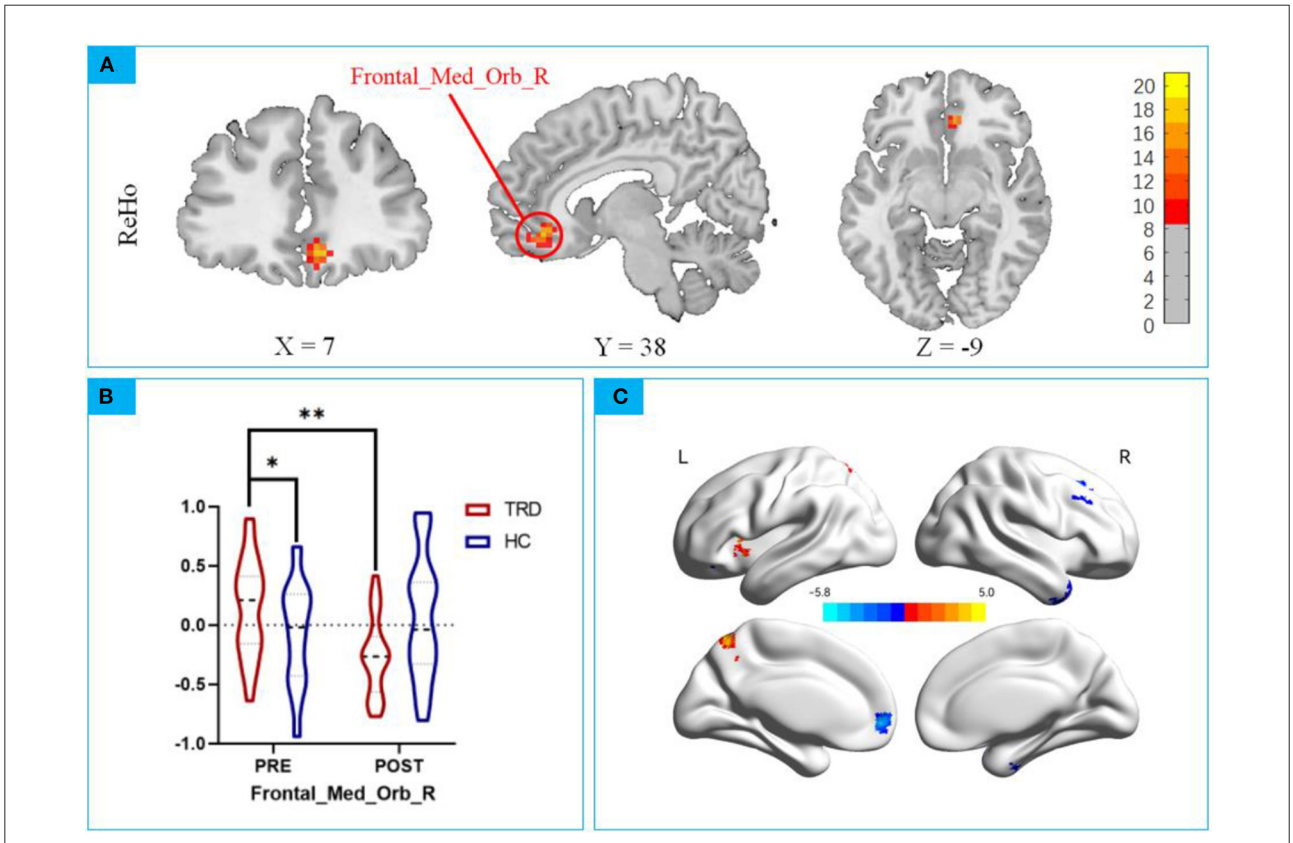

FIGURE 3
(A) Significant group × stimulation interactions on ReHo were observed in the right medial orbital frontal cortex; **(B)** *post hoc* analysis showed taVNS decreased lower activation in the TRD group than baseline. * $p < 0.01$; ** $p < 0.001$. **(C)** Main Effect of Time on ReHo. Blue colors represent decreased ReHo in after taVNS stimulation compared to before, while the hot colors represent the opposite.

TABLE 2 Brain changes with Group × stimulation interaction.

Items	Brain regions (AAL)	BA	MNI (mm)			Number of voxels	Peak intensity
			X	*Y*	*Z*		
ReHo	Frontal_Med_Orb_R	11	6	39	−12	42	16.1717

ReHo, Regional homogeneity in the right medial orbital frontal; AAL, Anatomical Automatic Labeling; MNI, Montreal Neurological Institute; BA, Brodmann area.

TABLE 3 Repeated measures ANCOVA of TRD and HC at baseline and post taVNS stimulation period.

Variables	*F*	*P*
Time	4.870	0.0303
Group	0.1349	0.7143
Time×Group	18.06	<0.0001

Covariates in the repeated measures ANCOVA include gender, age, education level, and FD.

stimulation interactions on ReHo were observed in the right medial orbital frontal cortex.

Repeated measures ANCOVA revealed a significant interaction effect on the right medial orbital frontal cortex ($F = 18.06$, P < 0.0001, Figure 3A), *post hoc* analyses confirmed that the Reho value in the mOFC of the TRD group was significantly higher in the HC group in the baseline ($t = 2.402$, $P < 0.001$; Figure 3B). After instant taVNS stimulation, the ReHo value was significantly decreased ($t = -4.314$, $P < 0.001$; Figure 3B), Before and after treatment in the HC group, the difference was not statistically significant ($t = 1.155$, $P = 0.2515$; Figure 3B).

Significant main effect on time was found, Compared to before taVNS stimulation, in the right posterior lobes of the cerebellum, temporal inferior gyrus, left medial orbital frontal, and right superior frontal gyrus of the ReHo value decreased, Left precentral gyrus of the ReHo value increased (Table 4). No significant main effect on group effect was found. The 3D map is produced by the BrainNet Viewer toolbox (38) (Figure 3C).

FC

According to the ReHo results, we defined the right medial orbital frontal regions as ROI for the FC analyses (39). Repeated measures ANCOVA revealed a significant interaction effect on the left inferior parietal gyrus and left superior marginal gyrus ($F = 11.6615$, $P < 0.001$, $F = 16.7520$, $P < 0.0001$; Figure 4A; Tables 5, 6).

ANCOVA of the mOFC-Based FC images showed that the group×time interaction effect of the mOFC with IPG showed statistical significance. *Post hoc* analyses confirmed that the FC strength in the TRD group was significantly lower in the HC group in the baseline ($t = 2.133$, $P < 0.001$; Figure 4B), after instant taVNS stimulation, the FC strength was significantly increased ($t = -4.314$, $P < 0.001$; Figure 4B). Before and after treatment in the HC group, the difference was not statistically significant ($t = 1.155$, $P = 0.2515$; Figure 4B).

ANCOVA of the mOFC-Based FC showed that the group×time interaction effect of the mOFC with the SMG showed statistical significance. *Post hoc* analyses confirmed that the FC strength in the TRD group was significantly lower in the HC group in the baseline ($t = 3.236$, $P < 0.01$; Figure 4B), after instant taVNS stimulation, the FC strength was increased ($t = 1.623$, $P = 0.11339$; Figure 4B), but the difference was not statistically significant. Furthermore, after treatment in the HC group, the FC strength was significantly lower in the baseline ($t = 8.704$, $P < 0.001$; Figure 4B).

No significant main effect was found in functional connection of mOFC and IPG. However Significant main effect on time was found in mOFC and SMG (Table 7), Compare before taVNS stimulation in the left middle Cingulate Gyrus, left middle frontal gyrus, and left Inferior parietal of the FC strength decreased. No significant main effect on group effect was found. The 3D map is produced by the BrainNet Viewer toolbox (38) (Figure 4C).

Correlation analyses

The HAMD and HAMA scores and ReHo/FC changes in the above-mentioned brain regions were not correlated (Figure 5).

Discussion

This study applied rs-fMRI technology to examine the effect of taVNS stimulation treatment on the brain activity of TRD. Our current study revealed that following taVNS stimulation treatment, TRD patients showed significantly reduced ReHo in the medial orbital frontal cortex (mOFC). ANCOVA of the mOFC-Based FC images revealed a significant interaction effect on the left inferior parietal gyrus (IPG) and left superior marginal gyrus (SMG). Among these regions, the HAMD and HAMA scores and ReHo/FC changes were not correlated.

TABLE 4 Anatomical Locations of Significant Main Effect of Group on ReHo.

Items	Brain regions (AAL)	BA	MNI (mm)			Number of voxels	Peak intensity
			X	*Y*	*Z*		
ReHo	Cerebelum_Crus2_R	–	33	−81	−48	205	−5.8082
ReHo	Temporal_Inf_R	20	42	−6	−39	168	−3.8751
ReHo	Frontal_Med_Orb_L	11	−12	54	−3	160	−4.9271
ReHo	Frontal_Sup_R	9	24	15	39	141	−4.5308
ReHo	Precuneus_L	7	−9	−63	60	128	4.8316

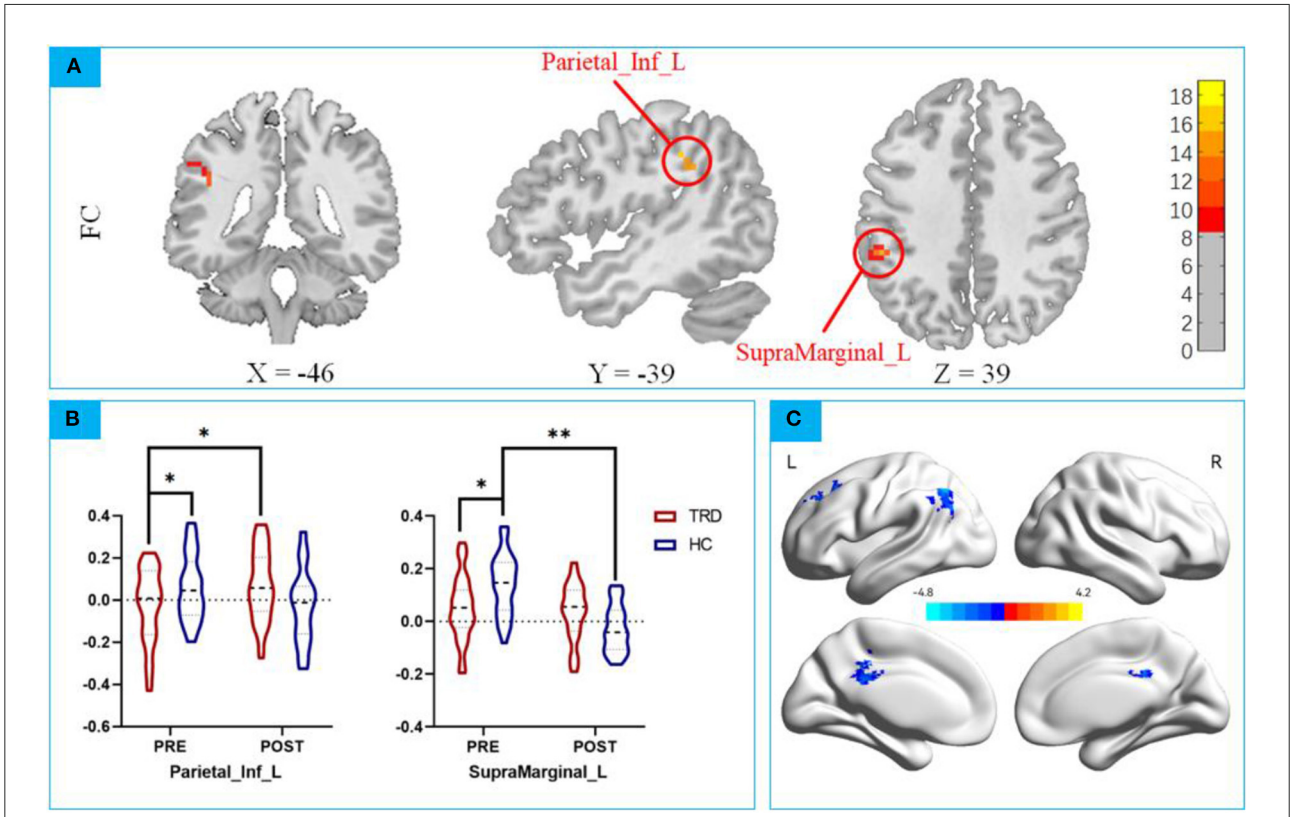

FIGURE 4
(A) Repeated measures ANCOVA revealed a significant interaction effect on the left inferior parietal gyrus and left superior marginal gyrus; **(B)** *post hoc* analysis mOFC-Based FC between the mOFC and IPG; *post hoc* analysis mOFC-Based FC between the mOFC and SMG. * $p < 0.01$; ** $p < 0.001$; **(C)** Main Effect of Time on FC of mOFC and SMG. Blue colors represent decreased FC of mOFC and SMG in POST-taVNS stimulation compared to PRE-taVNS.

TABLE 5 Group × Time Interaction on the mOFC-Based FC.

Items	Brain regions (AAL)	BA	MNI (mm)			Number of voxels	Peak intensity
			X	*Y*	*Z*		
FC	Parietal_Inf_L	40	−54	−40	39	20	15.466
FC	SupraMarginal_L	48	−48	−40	33	20	15.466

FC, Functional connection in the left inferior parietal gyrus and left superior marginal gyrus; AAL, Anatomical Automatic Labeling; MNI, Montreal Neurological Institute; BA, Brodmann area.

taVNS can immediately regulate the synchrony of neuronal activity in the mOFC brain region of TRD patients

Several studies have confirmed that patients with TRD tend to have lower reward sensitivity (40). The mOFC is an integral part of the reward network and is associated with emotional information and sensory stimuli (41, 42). Fang et al. (43) illustrated that abnormal OFC-default network functional connection regulation was significantly related to relieving depressive symptoms. Studies have also demonstrated that the gray matter volume of OFC and the functional connection of OFC-amygdala in TRD patients are positively correlated, reflecting that TRD patients may suffer from greater stress and depression, and must call OFC more frequently to regulate the amygdala response to negative emotions (44). Compared with the HC group, it was found that ReHo in the mOFC brain region of TRD patients was decreased by taVNS immediate treatment. Based on previous studies (20–22), taVNS may have an immediate regulation effect on the spontaneous brain activity of mOFC in TRD patients to improve the status of the limbic system and reward circuit. The mOFC is also a key brain region involved in safety and risk decision-making. When TRD shows overactivation of OFC in the resting state, it will overreact to social rejection signals, thus increasing the risk of suicidal behavior. In addition, from the perspective of neural circuits, mOFC is also involved in the motivation control of punishment avoidance conditions, suggesting that its significant activation may simultaneously mediate the process of individuals' high avoidance motivation for pain (45). More than half of TRD patients report suicidal thoughts (46). After taVNS treatment, TRD patients' ReHo value immediately decreased, and the synchronization of neuronal activity was significantly reduced, which means that taVNS can effectively inhibit negative emotions such as suicidal tendencies in TRD patients. In conclusion, taVNS treatment may activate the emotion cognitive regulation function involved in mOFC and jointly regulate the negative emotions of TRD patients.

TABLE 6 Repeated measures ANCOVA of TRD and HC at baseline and post taVNS stimulation period.

Variables	Parietal_Inf_L		SupraMarginal_L	
	F	*P*	*F*	*P*
Time	0.0193	0.8898	4.4858	0.0374
Group	0.1269	0.7226	0.2614	0.6106
Time×Group	11.6615	*0.0010*	16.7520	*0.0001*

taVNS has an immediate regulatory effect on brain regions and brain networks related to the regulation of emotion

In this study, ANCOVA of the mOFC-Based FC images revealed a significant interaction effect on the left inferior parietal gyrus (IPG) and left superior marginal gyrus (SMG). Furthermore, Main Effect of Time on ReHo, Compared before taVNS stimulation, in the right posterior lobes of the cerebellum, temporal inferior gyrus, left medial orbital

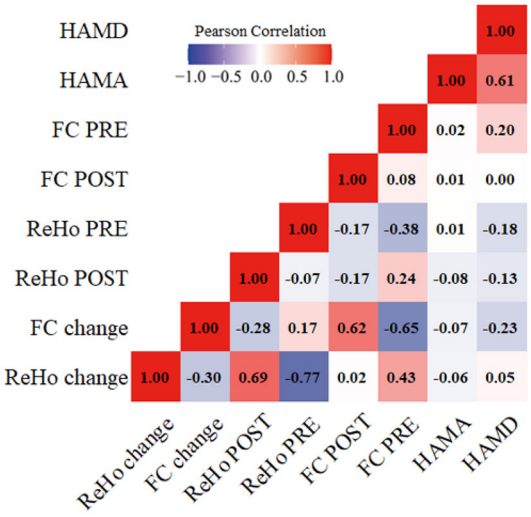

FIGURE 5
Correlations between the clinical scales' scores and the fMRI values. HAMD, Hamilton rating scale for depression; HAMA, Hamilton anxiety rating scale. ReHo, Regional homogeneity; FC, Functional connectivity; ReHo PRE/FC PRE, before taVNS treatment; ReHo POST/FC POST, after taVNS treatment; ReHo change/FC change, the difference in value before and after treatment.

TABLE 7 Anatomical Locations of Significant Main Effect of Group on mOFC-based FC of mOFC and SMG.

Items	Brain regions (AAL)	BA	MNI (mm)			Number of voxels	Peak intensity
			X	*Y*	*Z*		
FC	Cingulum_Mid_L	23	−6	−39	39	159	−4.3617
FC	Parietal_Inf_L	40	−45	−60	48	165	−4.7134
FC	Frontal_Mid_L	9	−24	33	39	132	−3.9720

frontal and right superior frontal gyrus of the ReHo value decreased, left precentral gyrus of the ReHo value increased. Main Effect of Time on FC of mOFC and SMG, compare before taVNS stimulation, in the left middle Cingulate Gyrus, left middle frontal gyrus, and left Inferior parietal of the FC strength decreased. Abnormalities in these regions have also been extensively reported in previous studies, and the present study has accumulated more evidence for the relevant results (47–49). Previous studies have posited that rumination may play a pivotal role in the psychopathology of TRD (50, 51), Default mode network (DMN), such as the medial prefrontal cortex (MPFC) and posterior cingulate cortex/precuneus. Frontoparietal control network (FPCN) regions, including the inferior parietal lobule (IPL), dorsal lateral prefrontal cortex (DLPFC), and superior marginal gyrus (SMG) (52). DMN and FPCN are closely related to emotion and cognitive processing (53), Silani et al. (54) showed that the SMG is a key brain area for emotion control. The FPCN anatomically connects the DMN and the dorsal attention network (DAN), and its function is to integrate stored internal representations with external environmental information, and to simultaneously resolve multiple interdependent emergencies and response mappings to conflicting stimuli, assigning work. Memory and attention resources. Our study found that the FC strength in the TRD group was significantly lower in the HC group in the baseline that the top-down regulation of TRD emotion is abnormal. And taVNS treatment can reduce the neural activity level of the mOFC and increase the neural activity intensity of the SMG and the IPL, which has a dynamic regulatory effect on the brain function of TRD patients. This suggests that taVNS can regulate the negative emotions of TRD from bottom to top (55). In conclusion, taVNS has an immediate regulatory effect on brain regions and brain networks related to the regulation of emotion.

Interestingly, we also found that after taVNS intervention in the HC group, the FC strength was significantly lower in the baseline. The taVNS immediate stimulation also had modulating effects in healthy individuals. Previous studies have also found short-term antidepressant therapy for healthy individuals reduce activity in the amygdala, OFC, superior frontal gyrus, and precentral gyrus, and SMG during emotional stimulation. These brain regions are associated with the negative affective of depression (56–64). Our taVNS treatment is consistent with studies on the regulatory effect of antidepressants on healthy individuals, which is worthy of further study.

Limitations

First, the study's sample size is small, and thus the results may be biased. Fewer brain areas are immediately adjusted to cause changes, which may be different from those after long-term treatment. Second, this study only used the commonly used research indicators of resting-state fMRI to observe the changes in the immediate effect mechanism of the brain, and the indicators used are not comprehensive enough.

In our future studies, the sample size will be expanded, and a variety of functional imaging research methods will be used to further explore the brain mechanism of the efficacy of taVNS on TRD patients. More indicators, including arterial spin labeling (ASL), GABA and other indicators of TRD patients, will need to be carried out for statistical analysis to improve the scientific value of this study.

Conclusions

In this study, we found taVNS can immediately regulate the synchrony of neuronal activity in the mOFC brain region of TRD patients. ANCOVA of the mOFC-Based FC images revealed a significant interaction effect on the IPG and SMG. In summary, the potential mechanism of taVNS treatment for TRD may be to enhance the function of emotion regulation circuits, monitor and manage negative emotions. Activity of emotion-processing networks, reduces the processing of negative emotions in TRD. Through taVNS treatment, the abnormal brain regions in TRD can be normalized, or even reversed, which may play a compensatory role in the reduction of depressive symptoms and involving DMN, FPCN and Reward Network.

Data availability statement

The original contributions presented in the study are included in the article/supplementary material, further inquiries can be directed to the corresponding authors.

Ethics statement

The studies involving human participants were reviewed and approved by Ethics Committee of Guang'anmen Hospital, China Academy of Chinese Medical Sciences, China (No. 2017-021-SQ). The patients/participants provided their written informed consent to participate in this study. Written informed consent was obtained from the individual(s) for the publication of any potentially identifiable images or data included in this article.

Author contributions

JF conceived and designed this experiment. This article was written mainly by YM and ZW. Patients were recruited and assessed by JS and CG. fMRI data were collected by ZW and JH. YM and ZD drew the diagrams and carried out the statistical analysis of data. YH and LZ performed fMRI on the subjects. JF and YLi reviewed the article. Text correction was done by YLu and LC. All authors contributed to the article and approved the submitted version.

Funding

This research was supported by the Science and Technology Innovation Project of China Academy of Chinese Medical Sciences (CI2021A03301), National Natural Science Foundation of China (82174282 and 81774433), and National Key Research and Development Program of China (2018YFC1705800).

Acknowledgments

The authors would like to thank TopEdit (www.topeditsci.com) for its linguistic assistance during the preparation of this manuscript.

Conflict of interest

The authors declare that the research was conducted in the absence of any commercial or financial relationships that could be construed as a potential conflict of interest.

Publisher's note

References

1. Hasin DS, Sarvet AL, Meyers JL, Saha TD, Ruan WJ, Stohl M, et al. Epidemiology of adult DSM-5 major depressive disorder and its specifiers in the United States. *JAMA Psychiatry.* (2018) 75:336–46. doi: 10.1001/jamapsychiatry.2017.4602

2. Ahmed HU, Hossain MD, Aftab A, Soron TR, Alam MT, Chowdhury MW, et al. Suicide and depression in the World Health Organization South-East Asia Region: a systematic review. *WHO South-East Asia J Public Health.* (2017) 6:60:6. doi: 10.4103/2224-3151.206167

3. Gaynes BN, Lux L, Gartlehner G, Asher G, Forman-Hoffman V, Green J, et al. Defining treatment-resistant depression. *Depress Anxiety.* (2020) 37:134–45. doi: 10.1002/da.22968

4. Bergfeld IO, Mantione M, Figee M, Schuurman PR, Lok A, Denys D, et al. Treatment-resistant depression and suicidality. *J Affect Disord.* (2018) 235:362–7. doi: 10.1016/j.jad.2018.04.016

5. Serretti A, Fabbri C. 6 Signs your patient is at risk for treatment-resistant depression. *Psychiatric Times.* (2017). Available online at: https://www.psychiatrictimes.com/view/6-signs-your-patient-risk-treatment-resistant-depression (accessed August 30, 2017).

6. Murphy JA, Sarris J, Byrne GJA. Review of the conceptualisation and risk factors associated with treatment-resistant depression. *Depress Res Treat.* (2017) 2017:4176825. doi: 10.1155/2017/4176825

7. Bennabi D, Aouizerate B, El-Hage W, Doumy O, Moliere F, Courtet P, et al. Risk factors for treatment resistance in unipolar depression: a systematic review. *J Affect Disord.* (2015) 171:137–41. doi: 10.1016/j.jad.2014.09.020

8. Fife D, Blacketer C, Reps JM, Ryan, P. Database Studies of Treatment-Resistant Depression Should Take Account of Adequate Dosing. *Prim Care Companion CNS Disord.* (2018) 20:18m02274. doi: 10.4088/PCC.18m02274

9. Cepeda MS, Reps J, Ryan P. Finding factors that predict treatment-resistant depression: results of a cohort study. *Depress Anxiety.* (2018) 35:668–73. doi: 10.1002/da.22774

10. Der-Avakian A, Markou A. The neurobiology of anhedonia and other reward-related deficits. *Trends Neurosci.* (2012) 35:68–77. doi: 10.1016/j.tins.2011.11.005

11. Bracht T, Mertse N, Walther S, Lüdi K, Breit S, Federspiel A, et al. Link between structural connectivity of the medial forebrain bundle, functional connectivity of the ventral tegmental area, and anhedonia in unipolar depression. *NeuroImage Clin.* (2022) 34:102961. doi: 10.1016/j.nicl.2022.102961

12. Yee DM, Crawford JL, Lamichhane B, Braver TS. Dorsal anterior cingulate cortex encodes the integrated incentive motivational value of cognitive task performance. *J Neurosci.* (2021) 41:3707–20. doi: 10.1523/JNEUROSCI.2550-20.2021

13. Jackson SA, Horst NK, Pears A, Robbins TW, Roberts AC. Role of the perigenual anterior cingulate and orbitofrontal cortex in contingency learning in the marmoset. *Cerebral Cortex (New York, NY).* (2016) 26:3273–84. doi: 10.1093/cercor/bhw067

14. Khawam EA, Laurencic G, Malone DA. Side effects of antidepressants: an overview. *Cleve Clin J Med.* (2006) 73:351–61. doi: 10.3949/ccjm.73.4.351

15. Chen LM, Li XJ, Xu K, Guo CL, Zhang GL, Han M, et al. Functional MRI-based study on neuromechanism of trans-auricular vagus nerve stimulation for treatment-resistant depression. *Acupuncture Res.* (2021) 46:869–74. doi: 10.13702/j.1000-0607.20210241

16. Henry TR. Therapeutic mechanisms of vagus nerve *stimulation.Neurology.* (2002) 59:S3–14. doi: 10.1212/WNL.59.6_suppl_4.S3

17. Peuker ET, Filler TJ. The nerve supply of the human auricle. *Clin Anat.* (2002) 15:35–7. doi: 10.1002/ca.1089

18. Hein, E, Nowak, M, Kiess, O, Biermann, T, and Bayerlein, K. Kornhuber J,Kraus T. Auricular transcutaneous electrical nerve stimulation in depressed patients: a randomized controlled pilot study. *J Neural Transm.* (2013) 120:821–7. doi: 10.1007/s00702-012-0908-6

19. Rong PJ, Fang JL, Wang LP, Meng H, Liu J, Ma YG, et al.Transcutaneous vagus nerve stimulation for the treatment of depres-sion: A study protocol for a double blinded randomized clinical trial. *BMC Complement Altern Med.* (2012) 12:255. doi: 10.1186/1472-6882-12-255

20. Rong P, Liu J, Wang L, Liu R, Fang J, Zhao J, et al. Effect of transcutaneous auricular vagus nerve stimulation on major depressive disorder: A nonrandomized controlled pilot study. *J Affect Disord.* (2016) 195:172–9. doi: 10.1016/j.jad.2016.02.031

21. Fang J, Hong Y, Fan Y, Liu J. Brain response to transcutaneous electronical stimulation on auricular concha of the healthy subjects using fmri. *Chin J Magnetic Reson Imaging.* (2014) 5:416–22. doi: 10.3969/j.issn.1674-8034.2014.06.003

22. Xu K, Li XJ, Fang JL, Chen LM, Gao DQ, Hong Y. Clinical observation on effect in auricular electro-acupuncture on treatment-resistant depression. *Medica-World Sci Technol.* (2019) 21:2266–71. doi: 10.11842/wst.20190718004

23. Pandarakalam JP. Challenges of treatment-resistant depression. *Psychiatr Danub.* (2018) 30:273–84. doi: 10.24869/psyd.2018.273

24. Chen CH, Suckling J, Lennox BR, Ooi C, Bullmore ET. A quantitative meta-analysis of fMRI studies in bipolar disorder. *Bipolar Disord.* (2011) 13:1–15. doi: 10.1111/j.1399-5618.2011.00893.x

25. Mwansisya TE, Hu A, Li Y, Chen X, Wu G, Huang X, et al. Task and resting-state fMRI studies in first-episode schizophrenia: a systematic review. *Schizophr Res.* (2017) 189:9–18. doi: 10.1016/j.schres.2017.02.026

26. Dapretto M, Davies MS, Pfeifer JH, Scott AA, Sigman M, Bookheimer SY, et al. Understanding emotions in others: mirror neuron dysfunction in children with autism spectrum disorders. *Nat Neurosci.* (2006) 9:28–30. doi: 10.1038/nn1611

27. Drysdale AT, Grosenick L, Downar J, Dunlop K, Mansouri F, Meng Y, et al. Resting-state connectivity biomarkers define neurophysiological subtypes of depression. *Nat Med.* (2017) 23:28–38. doi: 10.1038/nm.4246

28. Borserio BJ, Sharpley CF, Bitsika V, Sarmukadam K, Fourie PJ, Agnew LL, et al. Default mode network activity in depression subtypes. *Rev Neurosci.* (2021) 32:597–613. doi: 10.1515/revneuro-2020-0132

29. Guo CC, Hyett MP, Nguyen VT, Parker GB, Breakspear MJ. Distinct neurobiological signatures of brain connectivity in depression subtypes during natural viewing of emotionally salient films. *Psychol Med.* (2016) 46:1535–45. doi: 10.1017/S0033291716000179

30. Zang Y, Jiang T, Lu Y, He Y, Tian L. Regional homogeneity approach to fMRI data analysis. *Neuroimage.* (2004) 22:394–400. doi: 10.1016/j.neuroimage.2003.12.030

31. Friston KJ, Frith CD, Liddle PF, Frackowiak RSJ. Functional connectivity: the principal-component analysis of large (PET) data sets. *J Cereb Blood Flow Metab.* (1993) 13:5–14. doi: 10.1038/jcbfm.1993.4

32. Jiao Y, Guo X, Luo M, Li S, Liu A, Zhao Y, et al. Effect of transcutaneous vagus nerve stimulation at auricular concha for insomnia: a randomized clinical trial. *Evid Based Complement Altern Med.* (2020) 2020:6049891. doi: 10.1155/2020/2536573

33. Liu J, Fang J, Wang Z, Rong P, Hong Y, Fan Y, et al. Transcutaneous vagus nerve stimulation modulates amygdala functional connectivity in patients with depression. *J Affect Disord.* (2016) 205:319–26. doi: 10.1016/j.jad.2016.08.003

34. Yan CG, Wang XD, Zuo XN, Zang YF. DPABI: Data Processing and Analysis for (Resting-State) Brain Imaging. *Neuroinformatics.* (2016) 14:339–51. doi: 10.1007/s12021-016-9299-4

35. Friston KJ, Williams S, Howard R, Frackowiak RS, Turner R. Movement-related effects in fMRI time-series. *Magnetic Resonan Med.* (1996) 35:346–55. doi: 10.1002/mrm.1910350312

36. Maldjian JA, Laurienti PJ, Kraft RA, Burdette JH. An automated method for neuroanatomic and cytoarchitectonic atlas-based interrogation of fMRI data sets. *Neuroimage.* (2003) 19:1233–9. doi: 10.1016/S1053-8119(03)00169-1

37. Wang L, Li X, Li K, Su Y, Zeng Y, Zhang Q, et al. Mapping the effect of escitalopram treatment on amplitude of low-frequency fluctuations in patients with depression: a resting-state fMRI study. *Metab Brain Dis.* (2017) 32:147–54. doi: 10.1007/s11011-016-9871-5

38. Xia M, Wang J, He Y. BrainNet Viewer: A Network Visualization Tool for Human Brain Connectomics. *PLoS ONE.* (2013) 8. doi: 10.1371/journal.pone.0068910

39. Deng R, Yang X, Meng Y, Tao Y, Wang H, Li X, et al. Data-driven study on resting-state functional magnetic resonance imaging during early abstinence of alcohol dependence in male patients and its predictive value for relapse. *BMC Psychiatry.* (2022) 22. doi: 10.1186/s12888-022-03782-w

40. Klawohn J, Joyner K, Santopetro N, Brush CJ, Hajcak G. Depression reduces neural correlates of reward salience with increasing effort over the course of the progressive ratio task. *J Affect Disord.* (2022) 307:294–300. doi: 10.1016/j.jad.2022.03.051

41. Klawohn J, Burani K, Bruchnak A, Santopetro N, Hajcak G. Reduced neural response to reward and pleasant pictures independently relate to depression. *Psychol Med.* (2021) 51:741–9. doi: 10.1017/S0033291719003659

42. Rappaport BI, Kandala S, Luby JL, Barch DM. Brain reward system dysfunction in adolescence: current, cumulative, and developmental periods of depression. *Am J Psychiatry.* (2020) 177:754–63. doi: 10.1176/appi.ajp.2019.19030281

43. Fang J, Rong P, Hong Y, Fan Y, Liu J, Wang H, et al. Transcutaneous vagus nerve stimulation modulates default mode network in major depressive disorder. *Biol Psychiatry.* (2016) 79:266–73. doi: 10.1016/j.biopsych.2015.03.025

44. Mao Y, Zuo XN, Ding C, Qiu J. OFC and its connectivity with amygdala as predictors for future social anxiety in adolescents. *Dev Cogn Neurosci.* (2020) 44:100804. doi: 10.1016/j.dcn.2020.100804

45. Taylor WD, Zald DH, Felger JC, Christman S, Claassen DO, Horga G, et al. Influences of dopaminergic system dysfunction on late-life depression. *Mol Psychiatry.* (2022) 27:180–91. doi: 10.1038/s41380-021-01265-0

46. Kalin NH. Insights into suicide and depression. *Am J Psychiatry.* (2020) 177:877–80. doi: 10.1176/appi.ajp.2020.20081207

47. Gong J, Wang J, Qiu S, Chen P, Luo Z, Wang J, et al. Common and distinct patterns of intrinsic brain activity alterations in major depression and bipolar disorder: voxel-based meta-analysis. *Transl Psychiatry.* (2020) 10. doi: 10.1038/s41398-020-01036-5

48. Zhang Y, Shao J, Wang X, Chen Z, Liu H, Pei C, et al. Functional impairment-based segmentation of anterior cingulate cortex in depression and its relationship with treatment effects. *Human Brain Mapp.* (2021) 42:4035–47. doi: 10.1002/hbm.25537

49. Zhang B, Qi S, Liu S, Liu X, Wei X, Ming D, et al. Altered spontaneous neural activity in the precuneus, middle and superior frontal gyri, and hippocampus in college students with subclinical depression. *BMC Psychiatry.* (2021) 21. doi: 10.1186/s12888-021-03292-1

50. Vidal S, Jermann F, Aubry J, Richard-Lepouriel H, Kosel M. Effect of Ketamine on Rumination in Treatment-Resistant Depressive Patients. *J Clin Psychopharmacol.* (2020) 40:607–10. doi: 10.1097/JCP.0000000000001305

51. Foroughi A, Sadeghi K, Parvizifard A, Parsa Moghadam A, Davarinejad O, Farnia V, et al. The effectiveness of mindfulness-based cognitive therapy for reducing rumination and improving mindfulness and self-compassion in patients with treatment-resistant depression. *Trends Psychiatry Psychother.* (2020) 42:138–46. doi: 10.1590/2237-6089-2019-0016

52. Rai S, Griffiths KR, Breukelaar IA, Barreiros AR, Chen W, Boyce P, et al. Default-mode and fronto-parietal network connectivity during rest distinguishes asymptomatic patients with bipolar disorder and major depressive disorder. *Transl Psychiatry.* (2021) 11:547. doi: 10.1038/s41398-021-01660-9

53. Dai Z, Shao J, Zhou H, Chen Z, Zhang S, Wang H, et al. Disrupted fronto-parietal network and default-mode network gamma interactions distinguishing suicidal ideation and suicide attempt in depression. *Progr Neuro-Psychopharmacol Biol Psychiatry.* (2022) 113:110475. doi: 10.1016/j.pnpbp.2021.110475

54. Silani G, Bird G, Brindley R, Singer T, Frith CD, Frith U, et al. Levels of emotional awareness and autism: An fMRI study. *Soc Neurosci.* (2008) 3:112–97. doi: 10.1080/17470910701577020

55. Kaiser R, Andrews-Hanna JR, Wager TD, Pizzagalli DA. Large-scale network dysfunction in major depressive disorder: a meta-analysis of resting-state functional connectivity. *JAMA Psychiatry.* (2015) 72:603–11. doi: 10.1001/jamapsychiatry.2015.0071

56. Del-Ben CM, Deakin JF, McKie S, Delvai NA, Williams SR, Elliott R, et al. The effect of citalopram pretreatment on neuronal responses to neuropsychological tasks in normal volunteers: an FMRI study. *Neuropsychopharmacology.* (2005) 30:1724–34. doi: 10.1038/sj.npp.1300728

57. Takahashi H, Yahata N, Koeda M, Takano A, Asai K, Suhara T, et al. Effects of dopaminergic and serotonergic manipulation on emotional processing: a pharmacological fMRI study. *Neuroimage.* (2005) 27:991–1001. doi: 10.1016/j.neuroimage.2005.05.039

58. Harmer CJ, Mackay CE, Reid CB, Cowen PJ, Goodwin GM. Antidepressant drug treatment modifies the neural processing of nonconscious threat cues. *Biol Psychiatry.* (2006) 59:816–20. doi: 10.1016/j.biopsych.2005.10.015

59. Anderson IM, Del-Ben CM, Mckie S, Richardson P, Williams SR, Elliott R, et al. Citalopram modulation of neuronal responses to aversive face emotions: a functional MRI study. *Neuroreport.* (2007) 18:1351–5. doi: 10.1097/WNR.0b013e3282742115

60. Bigos KL, Pollock BG, Aizenstein HJ, Fisher PM, Bies RR, Hariri AR, et al. Acute 5-HT reuptake blockade potentiates human amygdala reactivity. *Neuropsychopharmacology.* (2008) 33:3221–5. doi: 10.1038/npp.2008.52

61. Simmons AN, Arce E, Lovero KL, Stein MB, Paulus MP. Subchronic SSRI administration reduces insula response during affective anticipation in healthy volunteers. *Int J Neuropsychopharmacol.* (2009) 12:1009–20. doi: 10.1017/S1461145709990149

62. Murphy SE, Norbury R, O'Sullivan U, Cowen PJ, Harmer CJ. Effect of a single dose of citalopram on amygdala response to emotional faces. *Br J Psychiatry.* (2009) 194:535–40. doi: 10.1192/bjp.bp.108.056093

63. Brühl AB, Kaffenberger T, Herwig U. Serotonergic and noradrenergic modulation of emotion processing by single dose antidepressants. *Neuropsychopharmacology.* (2010) 35:521–33. doi: 10.1038/npp.2009.159

64. Windischberger C, Lanzenberger R, Holik A, Spindelegger C, Stein P, Moser U, et al. Area-specific modulation of neural activation comparing escitalopram and citalopram revealed by pharmaco-fMRI: a randomized cross-over study. *Neuroimage.* (2010) 49:1161–70. doi: 10.1016/j.neuroimage.2009.10.013

frontiers | Frontiers in Neurology

TYPE Original Research
PUBLISHED 14 September 2022
DOI 10.3389/fneur.2022.950718

OPEN ACCESS

EDITED BY
Yihuai Zou,
Beijing University of Chinese Medicine, China

REVIEWED BY
Aamir Malik,
Brno University of Technology, Czechia
Zhenxiang Han,
Seventh People's Hospital of Shanghai, China

*CORRESPONDENCE
Woo-Kyoung Yoo
mdwooky@gmail.com;
wooky@hallym.ac.kr

SPECIALTY SECTION
This article was submitted to Applied Neuroimaging, a section of the journal Frontiers in Neurology

RECEIVED 23 May 2022
ACCEPTED 17 August 2022
PUBLISHED 14 September 2022

CITATION
An H, Bashir S, Cha E, Lee J, Ohn SH, Jung K-I and Yoo W-K (2022) Continuous theta-burst stimulation over the left posterior inferior frontal gyrus induced compensatory plasticity in the language network. *Front. Neurol.* 13:950718. doi: 10.3389/fneur.2022.950718

Continuous theta-burst stimulation over the left posterior inferior frontal gyrus induced compensatory plasticity in the language network

HyunJung An[1], Shahid Bashir[2], Eunsil Cha[3], Jeongeun Lee[3], Suk Hoon Ohn[3], Kwang-Ik Jung[3] and Woo-Kyoung Yoo[1,3]*

[1]Hallym Institute for Interdisciplinary Program Molecular Medicine, Hallym University College of Medicine, Chunchon, South Korea, [2]Neuroscience Center, King Fahad Specialist Hospital Dammam, Dammam, Saudi Arabia, [3]Department of Physical Medicine and Rehabilitation, Hallym University Sacred Heart Hospital, Anyang, South Korea

Introduction: Continuous theta-burst stimulation (cTBS) has been used as an effective tool in inducing inhibitory aftereffect within a short time periods in the motor cortex; this has been demonstrated in the language network to a limited degree with controversial effect. In this study, we aimed to delineate the offline effect of cTBS-induced changes to the left posterior inferior frontal gyrus (pIFG) in healthy subjects using functional magnetic resonance imaging (fMRI).

Methods: Twenty healthy, normal subjects (mean age: 30.84 years) were recruited. They all were right-handed and had no contra-indications for fMRI or cTBS. They were randomly assigned into the treatment group or the sham control group.

Results: ANOVA showed that cTBS had a significant main effect only when the sham treatment was subtracted from the real stimulation in left superior temporal, left inferior frontal gyrus, thalamus, and right insular cortex (uncorrected $p < 0.002$). The subjects' post-cTBS condition differed significantly from their pre-cTBS condition in the left pIFG (uncorrected $p < 0.002$). There were interactions in the pIFG, bilateral superior parietal lobules, left superior temporal, left supramarginal, and left cuneus areas. The application of cTBS induced increased BOLD signals in language-related networks by stimulating the left pIFG (BA 44). This implies that inhibiting the pIFG led to increased use of language network resources.

Conclusion: This study demonstrated cTBS-induced changes in the language network caused by stimulation of the left pIFG. Based on these findings, future studies on the therapeutic effects of cTBS on the right Broca's homolog area are warranted.

KEYWORDS

inhibition, Broca area, virtual lesion, naming, non-invasive brain stimulation, repetitive transcranial magnetic stimulation

Introduction

Repetitive transcranial magnetic stimulation (rTMS) is a non-invasive and relatively painless neuromodulation technique used to temporarily disrupt cortical neuronal activity. It can be used to study numerous cognitive functions and to clarify the relationship between the brain and behavior (1, 2). A novel variant form of rTMS, continuous theta burst stimulation (cTBS) (3), has various advantages, including rapid application and the ability to produce behavioral effects and induce robust neurophysiological aftereffects that are thought to involve neuronal mechanisms similar to those of long-term depression (LTD) (2–6). cTBS has an inhibitory effect that can reduce motor cortical excitability, denoted by the suppression of motor evoked potentials (MEPs), in a way that imitates the mechanisms of LTD (3, 7–11).

Functional magnetic resonance imaging (fMRI) and clinical and neurophysiological findings of non-invasive brain stimulation has been shown that the posterior inferior frontal gyrus (pIFG) plays a key role in different language functions and networks. Multiple line of evidence has been shown that the conventional rTMS on Broca's homolog area were effective for the purpose of improving aphasia after stroke (7, 12–18). Like conventional rTMS, cTBS studies mostly reported improvement of naming performance in healthy subjects (19, 20), as well as in post-stroke aphasia patients (21) by right Broca's homolog area stimulation. It is essential to have understanding how stimulation of Broca's area cause suppression or facilitation in the language network by cTBS protocol, however, it has been seldomly reported. There was one study that applied off-line cTBS over the left pIFG in healthy subjects, which suppressed activity in the left pIFG and increased activity in the right pIFG during repetition of auditory and visual words and pseudowords (22). This finding is somewhat different to note that facilitation of motor cortex using facilitatory protocol namely the intermittent TBS, which resulted reduced activity in fMRI (23), although one considers the difference of the stimulated cortex.

Combining TMS-evoked neuronal responses with cerebral hemodynamics is a valuable approach for exploring how TMS impacts neuronal activity in the targeted and remote areas that are required for specific tasks (22, 24). This approach can be used to probe the immediate effect of TMS on regional neuronal activity across the whole brain, which then makes it possible to draw inferences about the contribution of the targeted area to a specific task or function (22, 24, 25). In the current study, concurrent cTBS-fMRI was employed to investigate the effect of short bursts of high-frequency cTBS to the left pIFG on the blood-oxygen-level-dependent (BOLD) response during a picture-naming task. We aimed to assess whether real, cTBS (in contrast to sham cTBS) applied to an intact left pIFG could induce changes or modulate task-related activities in the language network during a picture-naming task (PNT).

Methods and materials

Participants

Twenty healthy subjects (4 females; mean age 30.2 ± 4.5 years) were recruited for this study. The subjects were randomly assigned to one of two groups: the real cTBS (treatment) group or the sham cTBS (control) group. All subjects were native Korean speakers. All were assessed as right-handed using the Edingurgh Inventory for Handedness (EHI) (26). Participants who were age between 20 and 35, didn't had any sign or history of neurological or psychiatric conditions and acute medical illness were included in this study. The exclusion criteria were use of psychotropic medication, an average use of more than three alcoholic beverages, pregnancy, previous history of head trauma or brain surgery, ferromagnetic metal in the head, implanted cardiac pacemaker or neurostimulator. All participants provided written informed consent before participating but after the study procedure was fully explained to them. The study was approved by the local research ethics committee and conducted in accordance with the Declaration of Helsinki.

Experimental setup and design

The stimulation set-up consisted of a magnetic stimulator STM 9000 (ATES MEDICA Device, Italy) that administered single-pulse TMS and cTBS. A figure-8 coil was placed tangentially over the subject's left primary motor cortex with the handle pointing at a 45° angle posterolaterally. To measure MEP, a surface electromyography (EMG) was performed using pre-gelled, disposable Ag/AgCl electrodes. The active electrode was placed on the contralateral first dorsal interosseous (FDI) muscle, the reference electrode on the metacarpophalangeal joint, and the ground electrode on the wrist. The EMG signal was acquired at 3 kHz, filtered (10–500 Hz), amplified, and stored for offline analysis.

During the procedure, the participants sat in a comfortable chair with a headrest; their hands rested on their laps. They were monitored for drowsiness and asked to keep their eyes open during TMS. All participants wore earplugs to protect them from possible acoustic trauma due to the noise from the discharge of the TMS coil.

All participants underwent baseline tests (MMSE, EHI) and imaging study (structural MRI and fMRI) followed by baseline TMS measurement [resting motor threshold (RMT) and active motor threshold (AMT)] (Figure 1). Pre-cTBS fMRI was done using PNT. Then participants moved to another room and received cTBS on left pars opercularis for 40 s. Right after cTBS procedure, the participants undergone post-cTBS fMRI using same task with different set of pictures (Figure 1).

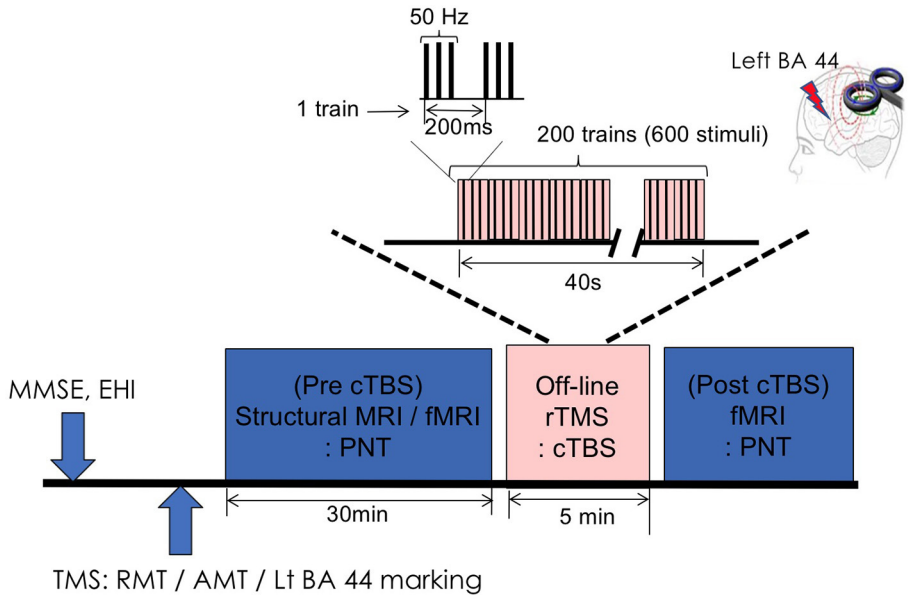

FIGURE 1
Experimental design. MMSE, Mini Mental Status Examination; EHQ, Edinburgh Handedness Inventory; TMS, transcranial magnetic stimulation; RMT, resting motor threshold; AMT, active motor threshold; BA, Brodmann area; rTMS, repetitive transcranial magnetic stimulation; cTBS, continuous theta-burst stimulation; PNT, picture naming task.

Task and FMRI procedure

The participants completed a PNT that used pictures of simple, white-on-black line drawings (27). Thirty pictures were selected for the fMRI overt naming task; the pictures were controlled for difficulty and frequency. We prepared five different picture sets of 100 images with a moderate level of use frequency and word complexity. Different pictures were used for the pre- and post-fMRI tasks. The pictures were presented on a screen that was reflected by a mirror placed in front of the participant. Each participant performed three scanning fMRI runs with a block design of ∼5 min for each. Within each run, there were five task blocks. Each block consisted of 30 s of rest and 30 s for each task (PNT). Within each task block, each trial began with 200 ms fixation; the picture was then presented for 100 ms. This was followed by a 200-ms response period during which participants were asked to name the presented picture as quickly and accurately as possible. We measured the correctness of the responses by recording participants' responses through a speaker outside the scanner. For the behavioral task, two investigators independently count the behavioral response. We only counted both investigators' positive answers.

FMRI acquisition

FMRI was acquired using a single-shot gradient echo planar imaging (EPI) sequence. The vast majority of fMRI performed at field strengths of 3T and below uses single-shot EPI, in which the k-space representation of an excited slice is read out in a single extended echo train. These extended readout periods make EPI sequences very efficient in terms of SNR per unit time, and thus highly sensitive to functional activation (28). The scanning parameters were as follows: 190 EPI volumes per block; repetition time (TR)/echo time (TE) = 2,000/35 ms; flip angle (FA) = 90°; field of view (FoV) = 240 mm; matrix = 64 × 64; resolution = 3 × 3 × 3 mm^3; and 35 slices. A high-resolution structural T1-weighted image was obtained using a magnetization-prepared rapid acquisition gradient echo (MP-RAGE) sequence with the following scanning parameters: TR/TE = 8.1/2.3 ms; thickness = 1 mm; FoV = 256 mm; FA = 90°; matrix size = 256 × 256, and resolution = 1 × 1 × 1 mm^3.

FMRI analysis

The data were analyzed using the Statistical Parametric Mapping software (SPM8, Wellcome Department of Imaging Neuroscience, London, UK) with Matlab version 2009a (Mathworks, Natick, MA). Prior to analysis, all images were preprocessed. The images were realigned to the mean functional image in the time series using mean frame-wise displacement, co-registered with each individual's structural image, spatially normalized to the MNI space, and spatially smoothed using a Gaussian kernel (8 mm, full width at half maximum). Poor-quality scans due to excessive head movement (≥3 mm) were excluded from the analysis. One case in sham condition showed excessive head movement, we excluded it.

For the subject-level analysis of the fMRI data, a general linear model (GLM) was used to calculate individual contrasts. The design matrix consisted of the PNT and rest periods. Motion parameters were included in the design as regressor variables of no interest to exclude variance related to head movement. Contrast maps for each condition were created for all participants.

For the group-level analysis, a full-factorial ANOVA with two independent variables (pre- and post-cTBS) and two dependent variables (real and sham cTBS) was conducted. The statistical contrast maps were thresholded. The height threshold was $p < 0.002$ (uncorrected) at the voxel level, and the extent threshold was 10 voxels with a false-discovery rate (FDR) correction at the cluster level of $p < 0.05$.

ROIs and analysis

Since we targeted the left pars opercularis gyrus (BA 44) for stimulation, changes to the network related to the left BA 44 were our main interest. To explore the effects of real and sham cTBS pre- and post-stimulation, we determined functionally defined regions of interest (ROIs) (left BA 45 [−48, 24, −10]; left BA 44 [−38, 16, 50]; right BA 45 [52, 22, −10]; right BA 44 [44, 8, 54]) using the Automated Anatomical Labeling (AAL-90) atlas (29). We then extracted the contrast estimate for each subject individually.

TMS stimulation

TMS was conducted in a separate, quiet room near the MRI center. This study was designed to explore the offline effect of cTBS, so we conducted an fMRI on each subject before and immediately after cTBS was applied to Broca's area.

The RMT was obtained over M1, where the lowest stimulus intensity evoked TMS-induced motor evoked potentials (MEPs) of at least 50 μV in the target muscle in five out of 10 consecutive trials. The TMS sessions were conducted in accordance with the published safety guidelines (30, 31). The targeted area for the stimulation (left pars opercularis gyrus) was identified using MRIcro software after a 3D T1 magnetic resonance image (MRI) was obtained with a surface marker located near both pIFG (BA 44). An offline-cTBS was administered with 40-s trains of 3 bursts at 50 Hz pulses, interleaved by 200 ms, for a total of 600 pulses. The mean stimulator output was delivered at 90% of the individual AMT. For each session, AMT was calculated for the left first dorsal interosseous and defined as the minimum stimulator output intensity required to produce motor evoked potentials (MEP) of at least 200 μV at 20% of maximum muscle contraction (3).

Sham group received stimulation by tilting the stimulator coil 45 degree so that subjects feel the pressure on the scalp along with a same auditory input.

Statistical analysis

For the subject-level analysis of the fMRI data, a general linear model (GLM) was used to calculate individual contrasts. For the group-level analysis, a full-factorial ANOVA with two independent variables (pre- and post-cTBS) and two dependent variables (real and sham cTBS) was conducted. The height threshold was $p < 0.002$ (uncorrected) at the voxel level, and the extent threshold was 10 voxels with a false-discovery rate (FDR) correction at the cluster level of $p < 0.05$. The accuracy of PNT in fMRI session was compared between real and sham group using independent t-test.

Results

fMRI whole-brain analysis

ANOVA showed increased activation in the right insula, right pIFG, left superior temporal gyrus, left middle temporal gyrus, and left middle frontal area in the real cTBS group (uncorrected $p < 0.002$) (Figure 2A); there was no significant increase in activation in the sham cTBS group. The post-cTBS MRI showed significantly increased activation only in the left pIFG (uncorrected $p < 0.002$) (Figure 2B). There was no significant activation in the pre-cTBS compared to post-cTBS condition. A significant interaction effect between condition and time was observed in the left pIFG, the left superior temporal gyrus, both superior parietal lobules, the left angular gyrus, and the left cuneus; in all these areas, activation increased significantly post-cTBS in the treatment group (uncorrected $p < 0.002$) (Table 1) (Figure 2C).

fMRI ROI analysis

The ROI analysis focusing on the language areas showed increased activation only in left BA 45 and 44 areas of the post cTBS stimulation condition (uncorrected $p < 0.005$) (Figure 3).

Behavioral results

All subjects in both groups achieved 100% accuracy on the picture-naming task; no behavioral differences between the two groups were observed.

Discussion

The current work aimed to investigate the impact of cTBS applied to the left pIFG on the hemodynamic response during a PNT. We found that cTBS had a significant effect on the left pIFG, left superior temporal gyrus, bilateral superior parietal

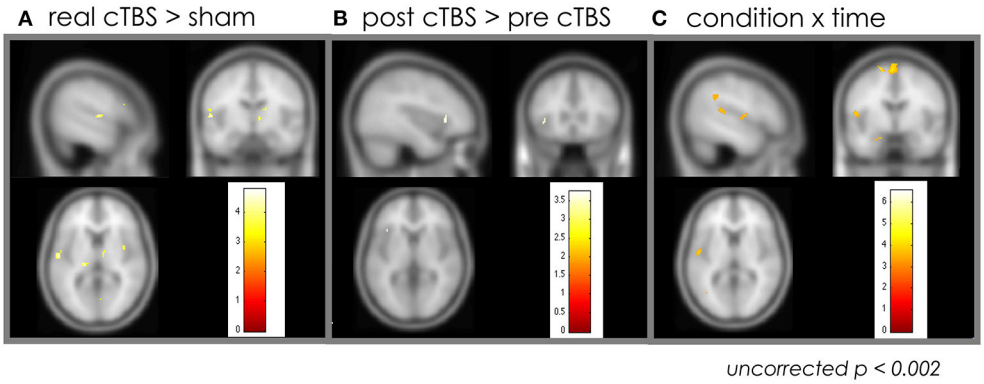

FIGURE 2
Effect of the cTBS: whole brain analysis. **(A)** Increased activation in the right insula, right pIFG, left superior temporal gyrus, left middle temporal gyrus, and left middle frontal area in the real cTBS group compared to sham group. **(B)** The post-cTBS MRI showed significantly increased activation only in the left pIFG compared to pre-cTBS. **(C)** A significant interaction effect between condition and time was observed in the left pIFG, the left superior temporal gyrus, both superior parietal lobules, the left angular gyrus, and the left cuneus. cTBS, continuous theta-burst stimulation; pIFG, posterior inferior frontal gyrus; MRI, magnetic resonance imaging.

TABLE 1 The area of increased activation by the interaction effect between condition and time.

Region	BA	x	y	z	*P*-value
Left posterior inferior frontal gyrus	44	−51	7	9	<0.001
superior temporal gyrus	22	−52	−34	15	<0.001
angular gyrus	39	−44	−46	33	<0.001
cuneus	19	−13	−74	28	<0.001
superior parietal lobule	7	−6	−35	66	<0.001
Right superior parietal lobule	7	13	−64	52	<0.001

BA, Brodmann area.

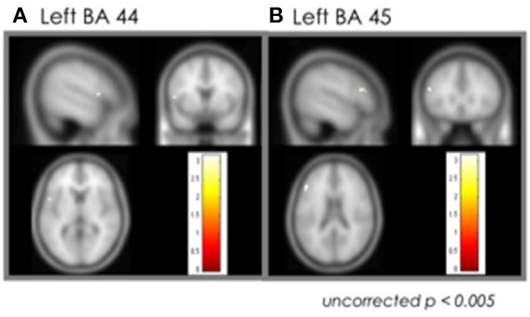

FIGURE 3
Effect of the cTBS: ROI analysis. **(A)** Left BA 44. **(B)** Left BA 45. cTBS, continuous theta-burst stimulation; BA, Brodmann area.

lobule, left angular gyrus, and left cuneus. These findings suggest two possible interpretations. First, offline-cTBS may have increased neuronal activity in the stimulated area (left pIFG) and in other brain regions within the language network during the PNT. This would indicate that the inhibitory effect of cTBS led to the recruitment of additional resources to achieve similar performance (12–16). Second, the inhibitory aftereffect of cTBS may have modulated intrahemispheric cortical connectivity; this explanation aligns with recent previous work done using TMS-EEG (32).

Administering cTBS at 80% of AMT to the left pIFG has been reported to lead to no change in behavioral outcomes on a speech repetition task (33). Other studies have found that cTBS induced a significant decrease in pIFG and M1 effective connectivity during a listening task (34), suppressed activity in the left pIFG and increased activity in the right pIFG during repetition of words and pseudowords (22) and led to changes in interhemispheric and intrahemispheric TMS-evoked synchrony as measured by electroencephalogram (EEG) (32). In this study, since we used a higher intensity (90% of AMT), it is not surprising that we observed changes in the stimulated area and in the related network. It is interesting, however, that activation in the target area increased rather than decreased; this contrasts with previous reports (22). The different tasks used in this and previous studies (picture naming vs. contrasting words and pseudowords repetition) and differences in stimulation intensity (90% vs. 80% of AMT) cannot be excluded as explanations for this contradiction. Moreover, since the basic principle of activation in fMRI is that activation depends on the potential effectiveness of the resource, this finding could be interpreted to indicate decreased effectiveness in the stimulated hemisphere since more resources were recruited to perform the task (we observed no additional activation in the right inferior frontal area). This explanation would align with previous studies of iTBS stimulation to the motor cortex (23).

The language related other nodes were increased after cTBS that includes left posterior part of superior temporal gyrus and

left angular gyrus. Among left superior temporal gyrus, posterior and ventral to Heschel's gyrus portion has been reported to have a phonological priming effect, which is lateralized speech selective response (35). The angular gyrus is one of the node of semantic retrieval network, which is widely distributed in a left-lateralized network including in the inferior temporal gyrus, anterior fusiform, hippocampus, pars orbitalis, superior and middle temporal gyri, and the right cerebellum (36). Especially, left angular gyrus is related to word comprehension in both speaking and writing (37).

Together with both bilateral superior parietal lobule and cuneus involved in visuospatial attention, above language network would be used to increase activity to compensate inhibition induced by cTBS by use of phonological and semantic resources as well as by increasing signal to noise ration with attention.

PNT is a sequential process of relation of visual recognition of picture by semantic network into lexical network, which represents concepts' names leading to speech production (38). In this semantic retrieval process, semantically related words showed reduced activity in the left pars orbitalis than phonologically related words (39). In this study, the significant interaction effect was located at BA 44 [−51, 7, 9]. This region has been reported to have relation to articulating planning (40, 41). As this area is also involved in working memory increased activity in the real cTBS condition might have related to difficult speech comprehension that reflects top-down predictions about the possible articulatory codes associated with the words (42, 43).

One main strength of this work is that it combined rTMS with fMRI to probe the impact of short bursts of high-frequency stimulation (cTBS) to the left pIFG on the BOLD hemodynamic response during a language task. However, this study has some limitations. First, caution must be used when interpreting fMRI in general, because of the small number of participants. Second, this study obtained limited behavioral data, which is a major drawback. Behavioral data (i.e., reaction time on a millisecond scale) could not be recorded due to background noise, so only the correctness of the responses was acquired. Third, the criteria of head motion that we excluded from the analysis might be too loose, which couldn't exclude to have artifacts instead of real activations, although we included the estimated motion parameters in the design as regressor of no interest in the first level GLM, which can reduce the sensitivity to detect noise as well as activations. Finally, the fMRI data were associated only with the onsets of correct trials in the PNT. Analyzing behavioral data and correlating them with the fMRI data would expand the current findings by relating them to behavioral measures. Future work should employ online and offline TMS coupled with fMRI data to explore the effects of TMS on electrophysiological measures (i.e., MEP amplitude), behavioral measures with more sensitive behavioral task to reduce the ceiling effect (i.e., reaction time and error rate) and on regional brain hemodynamic neuronal activity.

Conclusion

This study demonstrated cTBS-induced inhibition in the language network caused by stimulation of the left pIFG, which induced increased use of resources of language and attention network to maintain same performance in PNT.

Data availability statement

The original contributions presented in the study are included in the article/supplementary material, further inquiries can be directed to the corresponding author/s.

Ethics statement

The studies involving human participants were reviewed and approved by Ethics Committee of Hallym University Sacred Heart Hospital. The patients/participants provided their written informed consent to participate in this study.

Author contributions

W-KY and HA: design study and analysis the data. W-KY, HA, and EC: collect the data. W-KY, SB, EC, JL, SO, and K-IJ wrote the main manuscript text. All authors reviewed the manuscript.

Funding

This research was supported by the National Research Foundation of Korea, Basic Research Promotion Fund (NRF-2013R1A1A2012562) and Hallym University Research Fund.

Conflict of interest

The authors declare that the research was conducted in the absence of any commercial or financial relationships that could be construed as a potential conflict of interest.

Publisher's note

References

1. Kobayashi M, Hutchinson S, Schlaug G, Pascual-Leone A. Ipsilateral motor cortex activation on functional magnetic resonance imaging during unilateral hand movements is related to interhemispheric interactions. *Neuroimage.* (2003) 20:2259–70. doi: 10.1016/S1053-8119(03)00220-9

2. Pascual-Leone A, Valls-Solé J, Wassermann EM, Hallett M. Responses to rapid-rate transcranial magnetic stimulation of the human motor cortex. *Brain.* (1994) 117:847–58. doi: 10.1093/brain/117.4.847

3. Huang YZ, Edwards MJ, Rounis E, Bhatia KP, Rothwell JC. Theta burst stimulation of the human motor cortex. *Neuron.* (2005) 45:201–6. doi: 10.1016/j.neuron.2004.12.033

4. Pascual-Leone A, Freitas C, Oberman L, Horvath JC, Halko M, Eldaief M, et al. Characterizing brain cortical plasticity and network dynamics across the age-span in health and disease with TMS-EEG and TMS-fMRI. *Brain Topogr.* (2011) 24:302–15. doi: 10.1007/s10548-011-0196-8

5. Hallett M. Transcranial magnetic stimulation: a primer. *Neuron.* (2007) 55:187–99. doi: 10.1016/j.neuron.2007.06.026

6. Suppa A, Huang YZ, Funke K, Ridding MC, Cheeran B, Lazzaro VD, et al. Ten years of theta burst stimulation in humans: established knowledge, unknowns and prospects. *Brain Stimul.* (2016) 9:323–35. doi: 10.1016/j.brs.2016.01.006

7. Lazzaro VD, Pilato F, Saturno E, Oliviero A, Dileone M, Mazzone P, et al. Theta-burst repetitive transcranial magnetic stimulation suppresses specific excitatory circuits in the human motor cortex. *J Physiol.* (2005) 565:945–50. doi: 10.1113/jphysiol.2005.087288

8. Di Lazzaro V, Dileone M, Pilato F, Capone F, Musumeci G, Ranieri F, et al. Modulation of motor cortex neuronal networks by rTMS: comparison of local and remote effects of six different protocols of stimulation. *J Neurophysiol.* (2011) 105:2150–6. doi: 10.1152/jn.00781.2010

9. Allen EA, Pasley BN, Duong T, Freeman RD. Transcranial magnetic stimulation elicits coupled neural and hemodynamic consequences. *Science.* (2007) 317:1918–21. doi: 10.1126/science.1146426

10. Gentner R, Wankerl K, Reinsberger C, Zeller D, Classen J. Depression of human corticospinal excitability induced by magnetic theta-burst stimulation: evidence of rapid polarity-reversing metaplasticity. *Cereb Cortex.* (2008) 18:2046–53. doi: 10.1093/cercor/bhm239

11. Huang, Y.-Z., Chen, R.-S., Rothwell JC, Wen, et al.-Y. The after-effect of human theta burst stimulation is NMDA receptor dependent. *Clin Neurophysiol.* (2007) 118:1028–32. doi: 10.1016/j.clinph.2007.01.021

12. Naeser MA, Martin PI, Baker EH, Hodge SM, Sczerzenie SE, Nicholas M, et al. Overt propositional speech in chronic nonfluent aphasia studied with the dynamic susceptibility contrast fMRI method. *Neuroimage.* (2004) 22:29–41. doi: 10.1016/j.neuroimage.2003.11.016

13. Naeser MA, Martin PI, Nicholas M, Baker EH, Seekins H, Kobayashi M, et al. Improved picture naming in chronic aphasia after TMS to part of right Broca's area: an open-protocol study. *Brain Lang.* (2005) 93:95–105. doi: 10.1016/j.bandl.2004.08.004

14. Naeser MA, Martin PI, Nicholas M, Baker EH, Seekins H, Helm-Estabrooks N, et al. Improved naming after TMS treatments in a chronic, global aphasia patient–case report. *Neurocase.* (2005) 11:182–93. doi: 10.1080/13554790590944663

15. Martin PI, Naeser MA, Ho M, Doron KW, Kurland J, Kaplan J, et al. Overt naming fMRI pre- and post-TMS: two nonfluent aphasia patients, with and without improved naming post-TMS. *Brain Lang.* (2009) 111:20–35. doi: 10.1016/j.bandl.2009.07.007

16. Turkeltaub PE, Coslett HB, Thomas AL, Faseyitan O, Benson J, Norise C, et al. The right hemisphere is not unitary in its role in aphasia recovery. *Cortex.* (2012) 48:1179–86. doi: 10.1016/j.cortex.2011.06.010

17. Harvey DY, Podell J, Turkeltaub PE, Faseyitan O, Coslett HB, Hamilton RH. Functional reorganization of right prefrontal cortex underlies sustained naming improvements in chronic aphasia via repetitive transcranial magnetic stimulation. *Cogn Behav Neurol.* (2017) 30:133–44. doi: 10.1097/WNN.0000000000000141

18. Bucur M, Papagno C. Are transcranial brain stimulation effects long-lasting in post-stroke aphasia? A comparative systematic review and meta-analysis on naming performance. *Neurosci Biobehav Rev.* (2019) 102:264–89. doi: 10.1016/j.neubiorev.2019.04.019

19. Nicolo P, Fargier R, Laganaro M, Guggisberg AG. Neurobiological correlates of inhibition of the right broca homolog during new-word learning. *Front Hum Neurosci.* (2016) 10:371. doi: 10.3389/fnhum.2016.00371

20. Harvey DY, Mass JA, Shah-Basak PP, Wurzman R, Faseyitan O, Sacchetti DL, et al. Continuous theta burst stimulation over right pars triangularis facilitates naming abilities in chronic post-stroke aphasia by enhancing phonological access. *Brain Lang.* (2019) 192:25–34. doi: 10.1016/j.bandl.2019.02.005

21. Miniussi C, Thut G. Combining TMS and EEG offers new prospects in cognitive neuroscience. *Brain Topogr.* (2009) 22:249–56.

22. Hartwigsen G, Saur D, Price CJ, Ulmer S, Baumgaertner A, Siebner HR. Perturbation of the left inferior frontal gyrus triggers adaptive plasticity in the right homologous area during speech production. *Proc Natl Acad Sci.* (2013) 110:1–6. doi: 10.1073/pnas.1310190110

23. Cardenas-Morales L, Nowak DA, Kammer T, Wolf RC, Schonfeldt-Lecuona C. Mechanisms and applications of theta-burst rTMS on the human motor cortex. *Brain Topogr.* (2010) 22:294–306. doi: 10.1007/s10548-009-0084-7

24. Bergmann TO, Karabanov A, Hartwigsen G, Thielscher A, Siebner HR. Combining non-invasive transcranial brain stimulation with neuroimaging and electrophysiology: current approaches and future perspectives. *Neuroimage.* (2016) 140:4–19. doi: 10.1016/j.neuroimage.2016.02.012

25. Andoh J, Paus T. Combining functional neuroimaging with off-line brain stimulation: modulation of task-related activity in language areas. *J Cogn Neurosci.* (2011) 23:349–61. doi: 10.1162/jocn.2010.21449

26. Oldfield RC. The assessment and analysis of handedness: the Edinburgh inventory. *Neuropsychologia.* (1971) 9:97–113. doi: 10.1016/0028-3932(71)90067-4

27. Snodgrass JG, Vanderwart M. A standardized set of 260 pictures: norms for name agreement, image agreement, familiarity, visual complexity. *J Exp Psychol Hum Learn.* (1980) 6:174–215. doi: 10.1037/0278-7393.6.2.174

28. Swisher JD, Sexton JA, Gatenby JC, Gore JC, Tong F. Multishot versus single-shot pulse sequences in very high field fMRI: a comparison using retinotopic mapping. *PLoS ONE.* (2012) 7:e34626. doi: 10.1371/journal.pone.0034626

29. Tzourio-Mazoyer N, Landeau B, Papathanassiou D, Crivello F, Etard O, Delcroix N, et al. Automated anatomical labeling of activations in SPM using a macroscopic anatomical parcellation of the MNI MRI single-subject brain. *Neuroimage.* (2002) 15:273–89. doi: 10.1006/nimg.2001.0978

30. Rossi S, Hallett M, Rossini PM, Pascual-Leone A, Safety of TMS Consensus Group. Safety, ethical considerations, and application guidelines for the use of transcranial magnetic stimulation in clinical practice and research. *Clin Neurophysiol.* (2009) 120:2008–39. doi: 10.1016/j.clinph.2009.08.016

31. Wassermann EM, Wang B, Zeffiro TA, Sadato N, Pascual-Leone A, Toro C, et al. Locating the motor cortex on the MRI with transcranial magnetic stimulation and PET. *Neuroimage.* (1996) 3:1–9. doi: 10.1006/nimg.1996.0001

32. Ahn HJ, Bashir S, Martin P, Naeser MA, Pascual-Leone A, Yoo WK. cTBS effect on language reorganization verified by fMRI and chronometry TMS in an aphasia patient. *Neurol Clin Neurosci.* (2020) 8:74–8. doi: 10.1111/ncn3.12353

33. Restle J, Murakami T, Ziemann U. Facilitation of speech repetition accuracy by theta burst stimulation of the left posterior inferior frontal gyrus. *Neuropsychologia.* (2012) 50:2026–31. doi: 10.1016/j.neuropsychologia.2012.05.001

34. Murakami T, Restle J, Ziemann U. Effective connectivity hierarchically links temporoparietal and frontal areas of the auditory dorsal stream with the motor cortex lip area during speech perception. *Brain Lang.* (2012) 122:135–41. doi: 10.1016/j.bandl.2011.09.005

35. Vaden KI Jr., Muftuler LT, Hickok G. Phonological repetition-suppression in bilateral superior temporal sulci. *Neuroimage.* (2010) 49:1018–23. doi: 10.1016/j.neuroimage.2009.07.063

36. Price CJ. The anatomy of language: a review of 100 fMRI studies published in 2009. *Ann N Y Acad Sci.* (2010) 1191:62–88. doi: 10.1111/j.1749-6632.2010.05444.x

37. Brownsett SL, Wise RJ. The contribution of the parietal lobes to speaking and writing. *Cereb Cortex.* (2010) 20:517–23. doi: 10.1093/cercor/bhp120

38. Roelofs A. A spreading-activation theory of lemma retrieval in speaking. *Cognition.* (1992) 42:107–42. doi: 10.1016/0010-0277(92)90041-F

39. De Zubicaray GI, Mcmahon KL. Auditory context effects in picture naming investigated with event-related fMRI. *Cogn Affect Behav Neurosci.* (2009) 9:260–9. doi: 10.3758/CABN.9.3.260

40. Heim S, Eickhoff SB, Amunts K. Different roles of cytoarchitectonic BA 44 and BA 45 in phonological and semantic verbal fluency as

revealed by dynamic causal modelling. *Neuroimage.* (2009) 48:616–24. doi: 10.1016/j.neuroimage.2009.06.044

41. Zheng ZZ, Munhall KG, Johnsrude IS. Functional overlap between regions involved in speech perception and in monitoring one's own voice during speech production. *J Cogn Neurosci.* (2010) 22:1770–81. doi: 10.1162/jocn.2009.21324

42. Obleser J, Kotz SA. Expectancy constraints in degraded speech modulate the language comprehension network. *Cereb Cortex.* (2010) 20:633–40. doi: 10.1093/cercor/bhp128

43. Friederici AD, Kotz SA, Scott SK, Obleser J. Disentangling syntax and intelligibility in auditory language comprehension. *Hum Brain Mapp.* (2010) 31:448–57. doi: 10.1002/hbm.20878

frontiers | Frontiers in Neurology

TYPE Original Research
PUBLISHED 27 September 2022
DOI 10.3389/fneur.2022.990686

OPEN ACCESS

EDITED BY
Jiliang Fang,
China Academy of Chinese Medical Sciences, China

REVIEWED BY
Yanlu Wang,
Karolinska Institutet (KI), Sweden
Ankit Khambhati,
University of California, San Francisco, United States

*CORRESPONDENCE
Xiaodong Wang
dongdongdexx@163.com
Lun Dong
lundongu571@163.com

†These authors have contributed equally to this work

SPECIALTY SECTION
This article was submitted to Applied Neuroimaging, a section of the journal Frontiers in Neurology

RECEIVED 10 July 2022
ACCEPTED 05 September 2022
PUBLISHED 27 September 2022

CITATION
Zhang J, Zhang H, Yan F, Zhang H, Zhang E, Wang X, Wei M, Pei Y, Yang Z, Li Y, Dong L and Wang X (2022) Investigating the mechanism and prognosis of patients with disorders of consciousness on the basis of brain networks between the thalamus and whole-brain. *Front. Neurol.* 13:990686. doi: 10.3389/fneur.2022.990686

Investigating the mechanism and prognosis of patients with disorders of consciousness on the basis of brain networks between the thalamus and whole-brain

Jun Zhang[1,2†], Hongying Zhang[3†], Fuli Yan[2†], Hengzhu Zhang[2], Enpeng Zhang[2], Xingdong Wang[2], Min Wei[2], Yunlong Pei[2], Zhijie Yang[2], Yuping Li[2], Lun Dong[2*] and Xiaodong Wang[2*]

[1]Department of Neurosurgery, Huashan Hospital, Shanghai Medical College, Fudan University, Shanghai, China, [2]Department of Neurosurgery, Clinical Medical College of Yangzhou University, Yangzhou, China, [3]Department of Radiology, Clinical Medical College of Yangzhou University, Yangzhou, China

Purpose: This study aimed to investigate the changes in the functional connectivity between the bilateral thalamus and the whole-brain in patients with severe traumatic brain injury (sTBI) patients suffering from disorders of consciousness (DOC) and to explore their potential prognostic representation capacity.

Methods: The sTBI patients suffering from DOC and healthy controls underwent functional magnetic resonance imaging. We defined patients with the Extended Glasgow Outcome Score (GOS-E) ≥ 3 as the wake group and GOS-E $= 2$ as the coma group. The differences in functional connectivity between sTBI and healthy controls and between wake and coma groups were compared. Based on the brain regions with altered functional connectivity between wake and coma groups, they were divided into 26 regions of interest. Based on the Z-values of regions of interest, the receiver operating characteristic analysis was conducted to classify the prognosis of patients.

Results: A total of 28 patients and 15 healthy controls were finally included. Patients who had DOC indicated a significant disruption of functional connectivity between the bilateral thalamus and the whole-brain (FDR corrected, $P < 0.0007$). The functional connectivity strength (bilateral thalamus to whole-brain) was significantly different between coma patients who went on to wake and those who were eventually non-awake at 6 months after sTBI (Alphasim corrected, $P < 0.05$). Furthermore, the 26 regions of interest had a similar or even better prognostic distinction ability than the admission Glasgow coma score.

10.3389/fneur.2022.990686

Conclusion: The thalamus-based system of consciousness of sTBI patients suffering from DOC is disrupted. There are differences in the thalamus-to-whole-brain network between wake and coma groups and these differences have potential prognostic characterization capability.

KEYWORDS

disorders of consciousness, severe traumatic brain injury, thalamus, brain networks, resting state functional magnetic resonance (rs-fMRI)

Introduction

Severe traumatic brain injury (sTBI), affecting millions of people each year, is a serious global public health problem (1, 2). sTBI is a leading cause of death, especially among young people (3). For survivors, however, disorders of consciousness (DOC) is a major challenge (4). Currently, there is no consensus on why sTBI causes DOC (5). Knowing the structure and composition of the normal consciousness networks is the basis and premise for the study of DOC caused by sTBI.

Consciousness is an interesting but controversial scientific issue. From a neuroscience perspective, consciousness originates from the brain, which is a kind of information processing based on the hardware of the brain and is regulated by the consciousness control system (6). From an anatomical point of view, similar to other cortical-subcortical systems, such as the sensory, motor, or limbic systems, the brain networks dedicated to regulating the level of consciousness could be referred to as the "consciousness system" (7). The cortical regions of the consciousness system included medial (medial frontal, anterior cingulate, posterior cingulate, precuneus, and retrosplenial cortex) and lateral (lateral frontal, anterior insula, orbital frontal, and lateral temporal-parietal association cortex) brain surface (6). In addition, the major subcortical components of the consciousness system include the midbrain, superior pons, thalamus, hypothalamus, and basal forebrain (6). In the consciousness system as a whole, the higher-order cortex interacts with the subcortical arousal system (*via* a series of parallel systems), exerting regulation and control on the overall level of consciousness, arousal, and attention (6).

Once the consciousness system is disconnected or the balance is disturbed, a DOC can occur. The advent of resting-state functional magnetic resonance imaging (fMRI) sheds light on DOC exploration. Several studies investigated the features of brain networks in patients with DOC (8–11). Although there is significant methodological heterogeneity among the studies, the study content is based on the consciousness system. Evidence from graph theory indicated that cortical regions in the hubs of the brain networks in health become non-hubs of the brain networks in DOC patients (8). The study by Vanhaudenhuyse et al. (9) analyzed differences in default mode networks in patients with different degrees of DOC. The finding suggested that the functional connectivity strength of the default mode networks was correlated with the level of consciousness (9). In fact, the study indicated that significant impairment of effective connectivity in the fronto-parietal brain network was one of the causes of DOC (10). Whether based on neuroanatomy or functional neural-brain networks theory, scholars agree that the thalamus plays an important role in consciousness (11). Further study revealed that thalamus-related functional connectivity was attenuated in DOC patients (11). The above studies analyzed the DOC mechanism based on multiple disease types (cerebral hemorrhage, brain trauma, cerebral infarction, cerebrovascular disease, etc.), but did not elaborate on a single disease (such as sTBI). The findings of studies may not be fully applicable to traumatic DOC.

In summary, given the bilateral thalamus's crucial role in the generation of consciousness, the purpose of this study was to investigate the changes in the functional connectivity between the bilateral thalamus and the whole-brain in patients with sTBI-type DOC. In addition, most of the studies only explained the DOC-related mechanisms, and the ability of brain networks between the bilateral thalamic and whole-brain to assess patients' wake (6 months after DOC) is unclear, so our study attempts to clarify this.

Abbreviations: sTBI, Severe traumatic brain injury; DOC, Disorders of consciousness; fMRI, Functional magnetic resonance imaging; GCS, Glasgow coma score; MRI, Magnetic resonance imaging; GOS-E, Extended Glasgow Outcome Score; AAL, Automated anatomical labeling; FDR, False discovery rate; ROC, Receiver operating characteristic; AUC, Area under the curve.

Materials and methods

Participants

The study was a prospective, single-center study. A total of 30 sTBI patients with DOC and 15 health controls were initially included from June 2020 to June 2021.

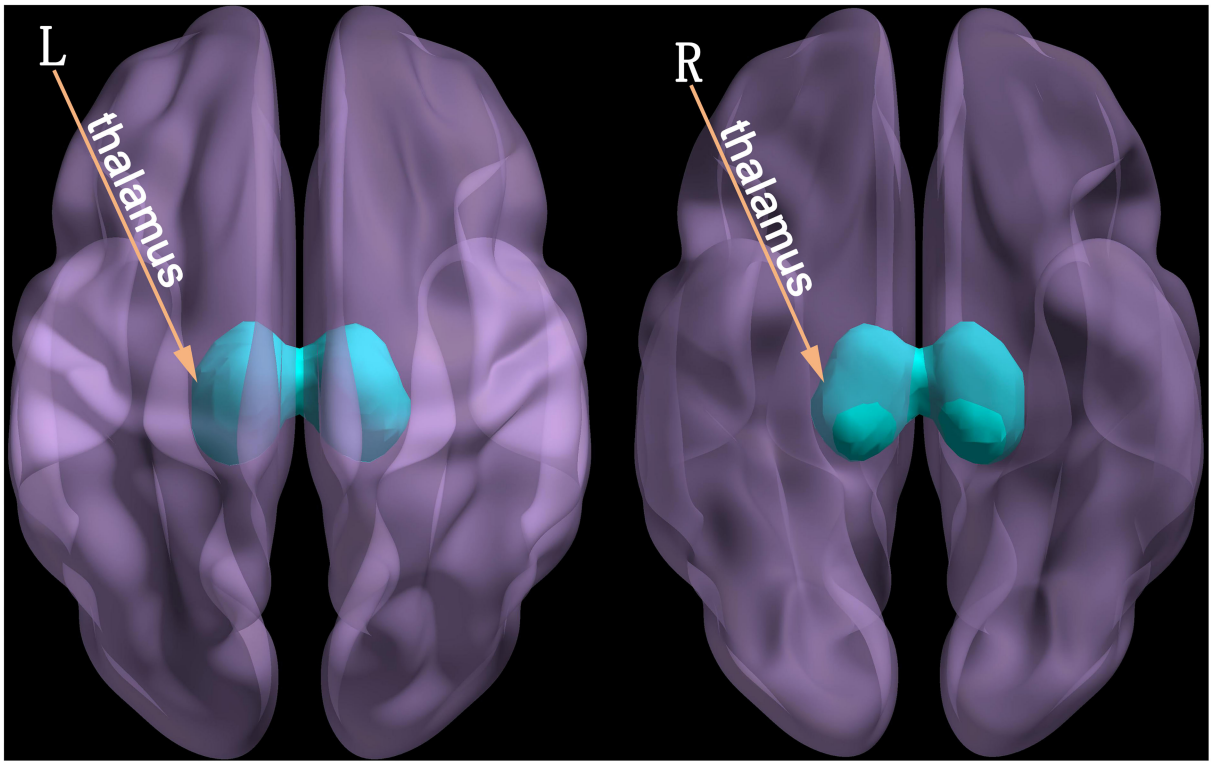

FIGURE 1
The seed point for functional connectivity analysis - the thalamus (L, left; R, right).

Inclusion criteria of patients: (1) Age 18–80 years old; (2) the diagnosis of sTBI patients with DOC was confirmed by history, scale—Glasgow coma score (GCS) $\leq$ 8, and brain imaging data (12, 13); (3) in the 1st to 4th weeks after injury; (4) the work and communication before the sTBI was normal; (5) right-handed; (6) stable spontaneous breathing and vital signs; (7) all guardians agreed to performed this research and signed an informed consent form. Exclusion criteria of patients: (1) Comorbidities other neurological and or psychiatric diseases; (2) non-traumatic DOC; (3) with severe multiple injuries; (4) contraindications for Magnetic resonance imaging (MRI) detection; (5) history of alcohol and drug abuse.

Inclusion criteria of healthy controls: (1) the baseline characteristics were partially matched (age could be moderately biased) with the DOC patients; (2) all controls be informed of the study protocol and signed the consent form; (3) no history of alcohol and drug abuse; (4) no familial neurological and/or psychiatric diseases; (5) no contraindications for MRI detection.

Prognosis assessment

A professionally trained neurosurgeon was masked to access the neurological prognosis outcomes of DOC patients for 6 months by telephone (close family members were investigated) and/or outpatient follow-up. The Extended Glasgow Outcome Score (GOS-E) was applied to evaluate DOC patients' prognosis (14). We defined patients with GOS-E $\geq$ 3 as the wake group and GOS-E = 2 as the DOC group (15).

fMRI data acquisition

The fMRI data of DOC patients (1–4 weeks after sTBI) were collected. The fMRI data were acquired with an 8-channel head coil on a 3.0 Tesla MRI system (Discovery MR750; GE Medical Systems, Milwaukee, WI, USA) located in the Neuroradiology Center. The 8 min fMRI resting-state sequence applied the following parameters: percent phase field view = 100, echo time = 30 ms, repetition time = 2,000 ms, flip angle = 90°, matrix = 64 × 64, slice thickness = 3.5 mm, spacing between slices = 4.2 mm, field of view = 300 × 300 mm, and slices = 33.

Whole-brain three-dimensional structural images were acquired using magnetization-prepared rapid acquisition gradient-echo T1-weighted sequence. The parameters were as follows: echo time = 3.18 ms, repetition time = 8.16 ms, flip angle =12°, matrix = 256 × 256, slice thickness = 1 mm, and slices = 168.

TABLE 1 Baseline characteristics of the study subjects.

Term	Healthy controls	DOC patients	Wake group	DOC group	*P*-value
Age, (Mean ± SD)	45.07 ± 17.65	58.00 ± 15.39	52.23 ± 17.22	59.38 ± 15.98	0.02[a]; 0.36[b]
Gender, male (%)	10 (66.7)	19 (67.9)	7 (87.5)	8 (61.5)	0.94[a]; 0.20[b]
Right-handed, N (%)	15 (100.0)	28 (100.0)	13 (100.0)	8 (100.0)	-
aGCS, (Mean ± SD)	-	5.00 ± 2.45	5.85 ± 2.38	2.88 ± 1.36	0.002[b]
GOS-E, (Mean ± SD)	-	3.00 ± 1.93	4.69 ± 1.49	2.00 ± 0.00	< 0.001[b]

DOC, disorders of consciousness; aGCS, admission Glasgow coma score; GOS-E, Glasgow outcome score expansion (a. healthy controls vs. DOC patients; b. wake group vs. DOC group).

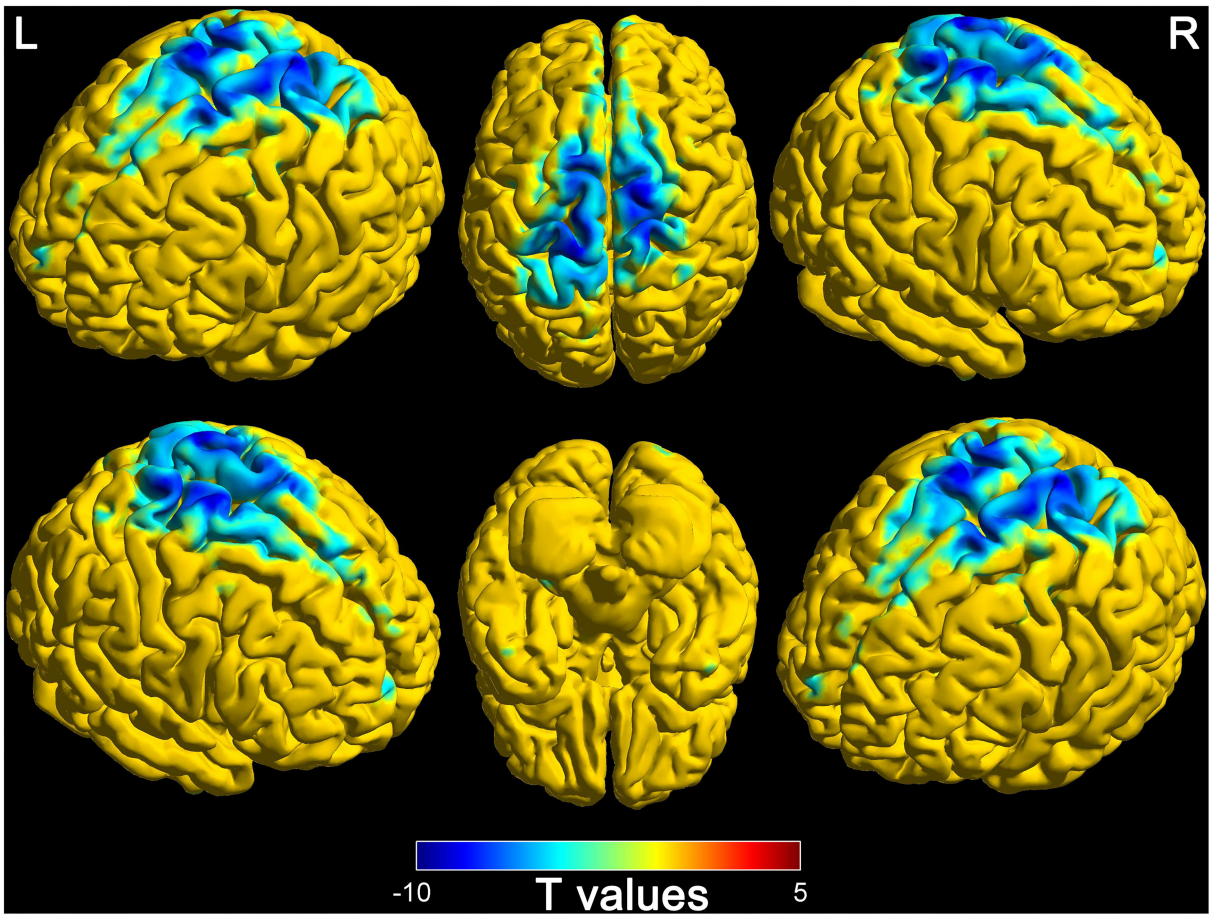

FIGURE 2
Differences of functional connectivity in thalamus and whole-brain between disorders of consciousness patients and healthy controls (L, left; R, right).

fMRI data preprocessing

The resting-state fMRI data were preprocessed by Statistical Parametric Mapping 12 (SPM 12) (https://www.fil.ion.ucl.ac.uk/spm/software/). The preprocessing steps included the following processes: (1) Convert Digital Imaging and Communications in Medicine format to Neuroimaging Informatics Technology Initiative format; (2) eliminate the functional data at the first 10 time points; (3) adjust the original position of the structure image to anterior commissure; (4) use the 33rd level layer as the reference layer for slice timing; (5) exclude data with head translation > 2 mm and rotation > 2° and realign head movements; (6) segment the structure image into gray matter, white matter, and cerebrospinal fluid; (7) normalize image to Montreal standard head anatomic space (reslice by 3 × 3 × 3 mm); (8) apply the Gauss kernel of 4 mm with full width

TABLE 2 Altered functional connectivity between the thalamus and whole-brain in patients with disorders of consciousness.

Cluster	Regions	Peak MNI	*T*-value	*P* value
		x y z		
DOC patients < Health controls				
1	Cerebelum 8	15, −63,−57	−4.27	FDR < 0.0007
2	Cerebellum posterior lobe	−12, −81, −54	−6.25	FDR < 0.0007
3	Left cerebellum, cerebellum inferior	−39, −81, −48	−4.83	FDR < 0.0007
4	Putamen	−30, −9, −51	−5.35	FDR < 0.0007
5	Inferior temporal gyrus	33, −9, −51	−5.36	FDR < 0.0007
6	Cerebellar tonsil, cerebellum anterior lobe	−30, −36, −39	−4.37	FDR < 0.0007
7	Midbrain	6, −30, −9	−4.71	FDR < 0.0007
8	Midbrain, thalamus, sub-thalamic nucleus, substania nigra, red nucleus	−6, −12, −9	−4.17	FDR < 0.0007
9	Middle occipital gyrus, lingual gyrus	27, −102, −9	−5.43	FDR < 0.0007
10	Inferior frontal gyrus, insula, middle frontal gyrus, claustrum	−36, 30, 9	−4.96	FDR < 0.0007
11	Superior temporal gyrus, transverse temporal gyrus, middle temporal gyrus	−42, −30, 6	−4.46	FDR < 0.0007
12	Superior frontal gyrus, medial frontal gyrus	12, 66, 15	−4.83	FDR < 0.0007
13	Inferior parietal lobule, supramarginal gyrus	−48, −42, 15	−4.38	FDR < 0.0007
14	Caudate, lentiform nucleus	−18, −3, 18	−4.67	FDR < 0.0007
15	Precentral gyrus, inferior frontal gyrus	−48, 0, 30	−4.44	FDR < 0.0007
16	Superior frontal gyrus, postcentral gyrus, precentral gyrus, limbic lobe, precuneus, cingulate gyrus, paracentral lobule, middle frontal gyrus, superior parietal lobule, inferior parietal lobule	−15, −39, 78	−10.14	FDR < 0.0007
17	Superior frontal gyrus, medial frontal gyrus	0, 57, 39	−4.22	FDR < 0.0007
18	Precuneus, superior parietal gyrus, superior occipital gyrus	−9, −81, 51	−4.26	FDR < 0.0007

DOC, disorders of consciousness; MNI, Montreal neurological institute.

and half height for smoothing; (9) delete the linear trend; (10) low-frequency filter 0.01–0.08 Hz.

fMRI data post-processing

Rest 1.8 (http://www.restfmri.net/forum/REST_V1.8) software was used to post-process the fMRI data. The bilateral thalamus (Figure 1) was extracted as a region of interest based on the automated anatomical labeling (AAL) template (16). Then, the average time series of the voxels in regions of interest were calculated and Pearson's correlation analysis was used on the time series of each voxel in the whole-brain (17). Therefore, the functional connectivity matrix between the bilateral thalamus and the whole-brain voxel was obtained. However, the functional connectivity value was the *R* correlation coefficient (non-normal distribution). Thus, the Fisher's was performed to convert it into a *Z*-value conforming to the normal distribution (18).

A two-sample *t*-test was applied by the Rest 1.8 based on the functional connectivity (DOC patients *vs.* health controls and wake group *vs.* DOC group). The multiple comparison correction was performed using the AlphaSim (clusters > 154, $P < 0.05$) (19, 20) or false discovery rate (FDR) ($P < 0.05$) to correct functional connectivity values and we adjusted for nuisance covariates (cerebrospinal fluid, white matter, head motion coefficient, age, and gender) (19, 21). The areas of different functional connectivity (wake group *vs.* DOC group) were taken as regions of interest. Based on brain regions with altered functional connectivity, 26 regions of interest were manually defined (seed point as the origin and 1.5 mm as the radius). The manual definition process was as follows: (1) The brain regions with altered functional connectivity were identified; (2) Based on xjView (https://www.alivelearn.net/xjview/), allowed the mouse to click the

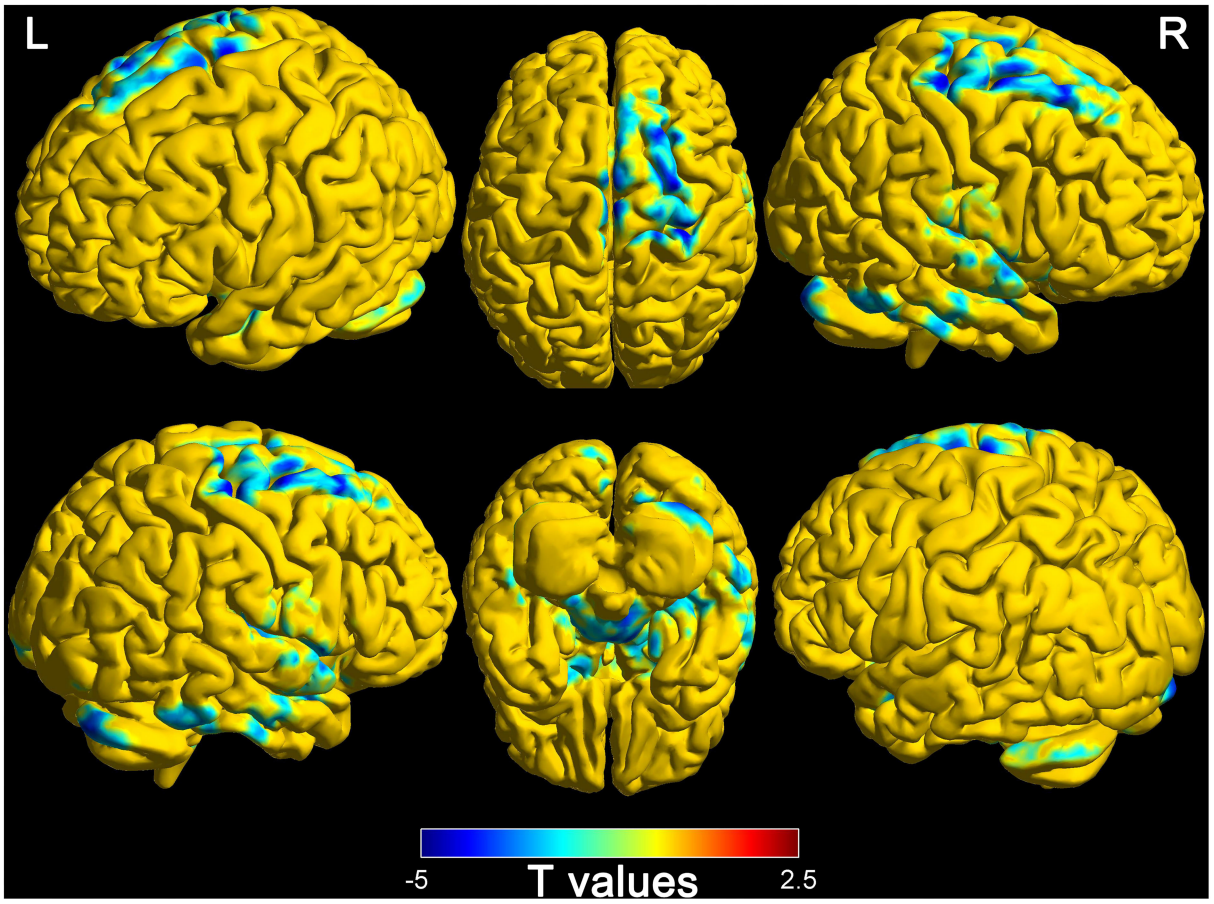

FIGURE 3
Differences of functional connectivity (thalamus to whole-brain) between wake and DOC groups (L, left; R, right).

abnormal functional connectivity map one by one; (3) During intensive clicking, and if a different brain region is revealed, it will be recorded as a region of interest. In addition, the AAL template was adopted and aimed to divide the whole brain into 116 regions of interest to examine the robustness of manual segmentation results. The *Z*-values of each region of interest were extracted as variables for prognostic prediction by Rest 1.8.

Pearson's correlation coefficients between each region of interest pair were calculated to form a matrix of *R*-values. Then, similarly, Fisher's was applied to convert the *R*-values matrix into a *Z*-values matrix conforming to the normal distribution (22). A two-sample *t*-test was performed to compare the Z matrix differences between the wake and DOC groups. Differences between groups were presented as a matrix of *P*-values. Furthermore, based on statistical values, a node-side-node brain network was employed to further visualize functional connectivity differences. The nodes represent brain areas, the edges represent interregional functional connectivity, and the diameters of the edges represent functional connection strength.

Statistics analysis

SPSS 26 (https://www.ibm.com/support/pages/downloading-ibm-spss-statistics-26) and MedCalc (https://www.medcalcsoftware.com/) software were conducted for data analysis. The Kolmogorov-Smirnov was performed to test the normality of measurement data. Normally distributed data were represented by mean ± standard, and comparisons between two groups were by a two-sample *t*-test. Otherwise, the median and its quartile were used, and the rank sum test was applied to compare groups. The Chi-square test was applied to the comparison of count data between groups. Each region of interest and GCS were evaluated for their ability to classify the prognosis using the receiver operating characteristic (ROC) curve. Statistical significance was set at $P < 0.05$.

TABLE 3 Decreased functional connectivity (thalamus to whole-brain) in wake group.

Cluster	Regions	Peak MNI	T value	*P* value
		x y z		
Wake group < DOC group				
1	Cerebellum posterior lobe, declive, pons, occipital lobe, cerebellum anterior lobe, brainstem, limbic lobe, parahippocampa gyrus, lingual gyrus, fusiform gyrus, inferior temporal gyrus, lentiform nucleus, pallidum, midbrain, hippocampus, cerebellar tonsil, putamen, amygdala, inferior occipital gyrus, insula, inferior frontal gyrus, thalamus, middle temporal gyrus, olfactory cortex, medial frontal gyrus, subthalamic nucleus, cuneus, caudate	39, −87, −24	−5.46	Alphasim < 0.05
2	Extra nuclear, insula, rolandic operculum, superior temporal gyrus, postcentral gyrus, superior temporal gyrus, limbic lobe, transverse temporal gyrus, cingulate gyrus, heschl gyrus, superior temporal gyrus, precentral gyrus, thalamus, middle temporal gyrus, lentiform nucleus, inferior frontal gyrus, pallidum, inferior parietal lobule, anterior and median cingulate and paracingulate gyri, claustrum, amygdala, medial dorsal nucleus	45, −24, 9	−4.29	Alphasim < 0.05
3	Superior temporal gyrus, middle temporal gyrus, inferior temporal gyrus, precentral gyrus, insula, inferior frontal gyrus, postcentral	45, 6, −18	−4.70	Alphasim < 0.05
4	Precentral gyrus, superior frontal gyrus, middle frontal gyrus, postcentral gyrus, middle frontal gyrus, paracentral lobule	30, 21, 60	−4.96	Alphasim < 0.05
5	Supplementary motor area, superior frontal gyrus, medial frontal gyrus, paracentral lobule	0, −6, 72	−4.80	Alphasim < 0.05

DOC, disorders of consciousness; MNI, Montreal neurological institute.

Results

Basic characteristics

A total of 28 DOC patients were finally included, after excluding two patients with significant head movement. Fifteen healthy controls were also included in this study. Baseline characteristics of participants are provided in Table 1. The differences in terms of gender and right-handedness were not statistically significant between DOC patients and healthy controls. However, the difference was statistically significant in age (DOC patients vs. Health controls) ($P = 0.02$). Additionally, the mean value of GCS at admission and GOS-E at 6 months was 5 and 3, respectively, in DOC patients.

The patients were divided into wake ($n = 13$) and DOC ($n = 8$) groups according to their GOS-E scores at 6 months. Furthermore, seven patients had died by the final follow-up. Basal demographic characteristics of the two groups (wake and DOC) are shown in Table 1. There were no significant differences between groups in terms of age, gender, and right-handedness. As expected, the differences were statistically significant in admission GCS ($P = 0.002$) and GOS-E at 6 months ($P < 0.001$).

Differences of connectivity (thalamus to whole-brain) in DOC patients and healthy controls

The comparison results between DOC patients and healthy controls are shown in Figure 2. The functional connectivity between the thalamus and some brain regions was decreased in DOC patients, compared with healthy controls (FDR corrected, $P < 0.0007$). The brain regions with weakened functional connectivity were mainly distributed in the core region of the global brain including the frontal lobe, temporal lobe, parietal lobe, occipital lobe, limbic system, cerebellum, and brain stem. The specific brain region features (name, peak point coordinates, statistics *T*-values, and FDR corrected *P*-values) are displayed in Table 2.

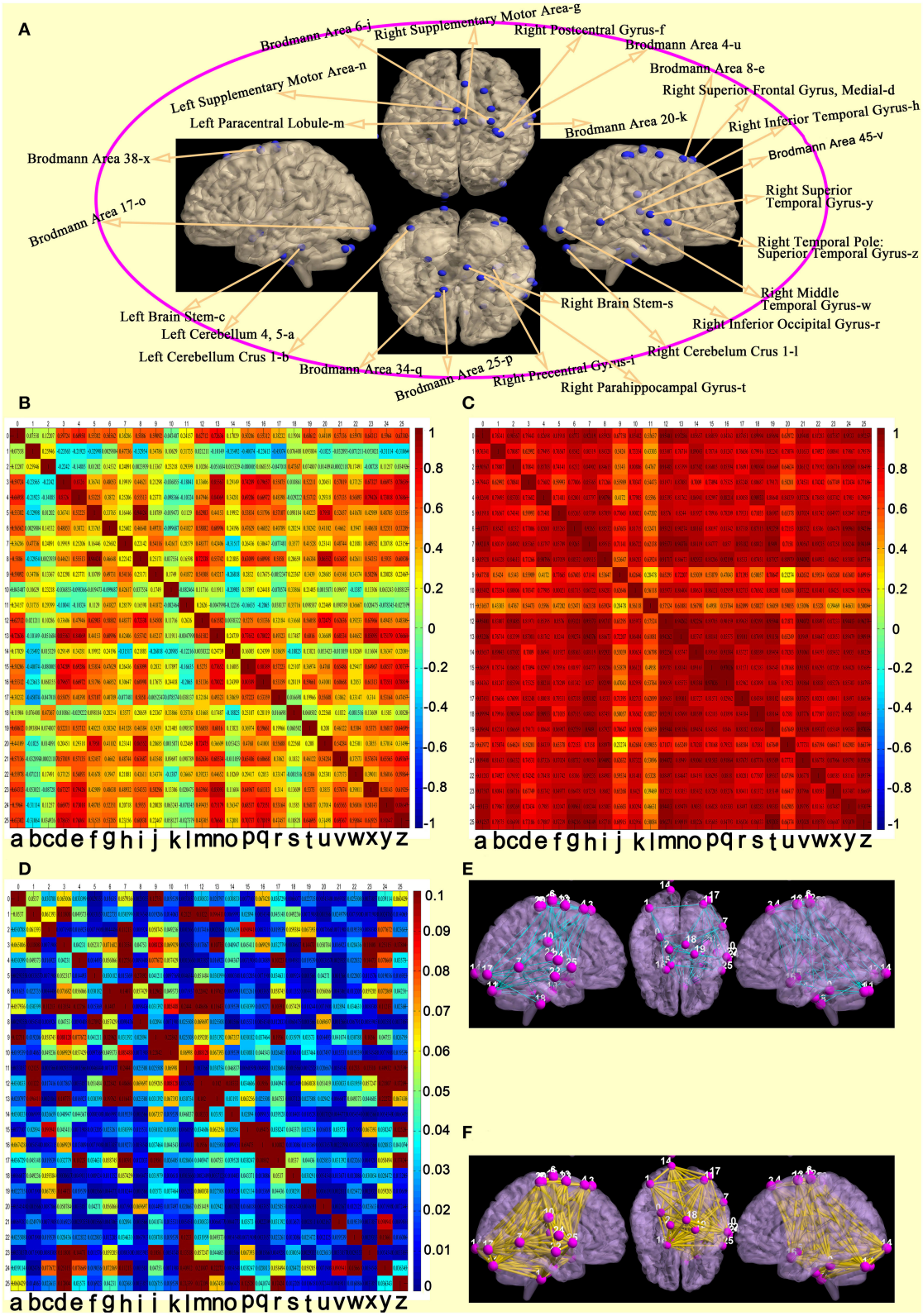

FIGURE 4
Features of functional connectivity between each regions of interest pair. **(A)** 26 regions of interest. **(B)** matrix of Pearson's correlation coefficients between each regions of interest pair in the awake group. **(C)** matrix of Pearson's correlation coefficients between each regions of *(Continued)*

FIGURE 4 (Continued)
interest pair in the DOC group. **(D)** differences of a matrix of *Z*-values between awake and DOC groups. **(E)** compared with the wake group, the strength of functional connectivity between some regions of interest pairs in the DOC group were similar. **(F)** compared with the wake group, the strength of functional connectivity between many regions of interest pairs in the DOC group were enhanced).

TABLE 4 Quantitative analysis of regions of interests in wake and DOC groups.

Brain regions	Wake group	DOC group	*P*-value
Left cerebellum 4, 5	1.218 ± 0.346	1.632 ± 0.196	0.006
Left cerebellum crus1	0.473 ± 0.325	0.853 ± 0.449	0.036
Left brain stem	0.758 ± 0.397	1.312 ± 0.507	0.011
Right superior frontal gyrus, medial	0.496 ± 0.346	0.947 ± 0.423	0.015
Brodmann area 8	0.712 ± 0.266	1.371 ± 0.384	< 0.001
Right postcentral gyrus	0.769 ± 0.313	1.354 ± 0.365	0.001
Right supplementary motor area	0.384 ± 0.354	0.99 ± 0.477	0.003
Right inferior temporal gyrus	0.737 ± 0.443	1.219 ± 0.340	0.017
Right precentral gyrus	0.782 ± 0.358	1.448 ± 0.358	0.001
Brodmann area 6	0.496 ± 0.345	0.961 ± 0.658	0.046
Brodmann area 20	0.763 ± 0.573	1.379 ± 0.170	0.002
Right cerebelum crus 1	0.318 ± 0.299	0.816 ± 0.272	0.001
Left paracentral lobule	0.860 ± 0.447	1.424 ± 0.339	0.007
Left supplementary motor area	0.680 ± 0.370	1.229 ± 0.355	0.003
Brodmann area 17	0.621 ± 0.335	1.050 ± 0.532	0.034
Brodmann area 25	0.842 ± 0.493	1.311 ± 0.209	0.008
Brodmann area 34	0.934 ± 0.445	1.428 ± 0.235	0.004
Right inferior occipital gyrus	0.561 ± 0.479	1.006 ± 0.461	0.049
Right brain stem	0.627 ± 0.409	1.294 ± 0.408	0.002
Right parahippocampal gyrus;	0.882 ± 0.372	1.441 ± 0.299	0.002
Brodmann area 4	0.553 ± 0.346	1.232 ± 0.422	0.001
Brodmann area 45	1.126 ± 0.426	1.722 ± 0.564	0.013
Right middle temporal gyrus	0.898 ± 0.617	1.565 ± 0.290	0.004
Brodmann area 38	0.569 ± 0.299	1.247 ± 0.435	< 0.001
Right superior temporal gyrus	0.976 ± 0.417	1.498 ± 0.445	0.0014
Right temporal pole: superior temporal gyrus	0.972 ± 0.399	1.539 ± 0.516	0.011

DOC, disorders of consciousness.

Differences of connectivity in thalamus and whole-brain between wake and DOC groups

Based on the thalamus and whole-brain functional connectivity, there were statistically significant differences between wake and DOC groups (Alphasim corrected, $P < 0.05$). The findings are presented in Figure 3. The brain regions of decreased functional connectivity in the wake group are the frontal lobe, temporal lobe, parietal lobe, occipital lobe, limbic system, cerebellum, and brain stem. Detailed characteristics are provided in Table 3.

Features of functional connectivity between each region of interest pair

The 26 regions of interest were selected, according to the above comparison results of the wake and DOC groups (Figure 4A). Compared with the wake group (Figure 4B), the DOC group (Figure 4C) had a higher Pearson's correlation coefficients (*R*-values) between each region of interest pair. The difference between groups was statistically significant (FDR corrected, $P < 0.05$) (Figure 4D). The visualization findings indicated that, compared with the wake group, the strength of functional connectivity between some regions of interest pairs (28.99%) in the DOC group was similar (Figure 4E),

while many regions of interest (71.01%) were enhanced (Figure 4F).

Quantitative analysis of regions of interest in wake and DOC groups

Z-values of regions of interest were extracted for quantitative comparison between wake and DOC groups. Twenty-six regions of interest were obtained from the comparison results between the wake and DOC groups. The findings of the quantitative analysis are presented in Table 4. Statistically significant differences were found between both groups ($P < 0.05$).

The prognostic assessment ability of the indicators

The ROC curve analysis was applied to assess the prognostic power of 26 regions of interest and GCS by comparing the area under the curve (AUC) for each ROC. The results of AUC are presented in Figure 5. The prognostic discriminative power of the 26 regions of interest fluctuated between 0.721 and 0.933. Among them, the right postcentral gyrus has the strongest prognostic prediction ability for DOC patients (AUC = 0.933) and Brodmann Area 6 has the weakest power to assess the prognosis of patients with DOC (AUC = 0.721). In addition, the performance of GCS in the prognostic assessment of DOC patients was modest (AUC = 0.827).

Robustness analysis

The AAL template was used and we aimed to divide the whole-brain into 116 regions of interest. The *Z*-values for functional connectivity of these regions of interest were extracted. Then, the 6-month prognosis of DOC patients was differentiated based on the *Z*-values. The results of the prognostic assessment were performed as for Figure 6. There were five brain regions that could effectively classify (AUC ranging 0.740 from to 0.865) the 6-month prognosis of patients with DOC. The findings are moderately robust (not only do brain regions overlap but also AUC values are similar).

Discussion

In this study, resting-state brain network findings, based on sTBI patients suffering from DOC, indicated that functional connectivity of the bilateral thalamus to the whole-brain was disrupted in DOC patients. In addition, the functional connectivity between the bilateral thalamus and the whole-brain of the DOC group was different compared with the wake group, and the differences in functional connectivity were associated with prognosis.

Survivors after sTBI may develop DOC, such as vegetative state/unresponsive arousal syndrome or minimally conscious state. Our findings found that the functional connectivity of the thalamus to midbrain, cerebellum, insula, basal ganglia area, frontal lobe, temporal lobe, superior parietal lobule, inferior parietal lobule, limbic lobe, precuneus, cingulate gyrus, paracentral lobule, and occipital lobe was reduced in DOC patients compared with healthy controls. Similar to our results, previous studies showed that thalamic structural integrity and the thalamic-cortical networks were disrupted in DOC (23, 24).

The complex structure of the thalamus determines its functional richness. The thalamus as a relay station plays a critical role in consciousness (23, 24). The thalamus can be divided into a specific projection and a non-specific projection system according to the different types of fiber-endings projecting to the cerebral cortex from various parts of the thalamus and their differences in distribution. The non-specific projection system is closely related to the brainstem reticular system (25). Within the brainstem, neurons of the reticular formation stimulate cortical activation by exciting the widespread projecting neurons of the non-specific thalamocortical projection system (25). Therefore, its main function is to transmit and distribute the upward activation effect originating from the reticular system of the brainstem to almost all cortical areas, maintaining and regulating the excitatory state of the cerebral cortex (influencing the overall level of cortical arousal) (6). Moreover, the formation of consciousness relies on the synergy of multiple parallel systems (6). Once the parallel system is disrupted or interrupted, it may lead to DOC (6, 26).

The cortical network of the consciousness system is very extensive, and mainly includes bilateral cerebral hemispheres, especially the lateral frontal, anterior insula, lateral parietal (adjacent temporo-occipital cortex), medial frontal, medial parietal (precuneus) lobes, anterior lobe, and cingulate cortex (6). Therefore, once trauma involves cortical areas or non-specific projection systems, DOC may appear. Furthermore, due to the devastating violence and widespread spread of violence, the patient's cortical consciousness system was easily disrupted. This may explain the extremely high incidence of DOC in sTBI patients.

Ascending excitatory projections from the thalamus, basal forebrain, and brainstem reticular activating systems (subcortical system) play a serious role in normal cortical excitation during the awake, conscious state (27). The subcortical consciousness system is also not immune to the effects of devastating violence. Evidence from Yu et al. (24) that the microstructural integrity of the thalamus is a critical factor in the generation of consciousness and axonal damage may be the main cause of the disconnection between the thalamus and

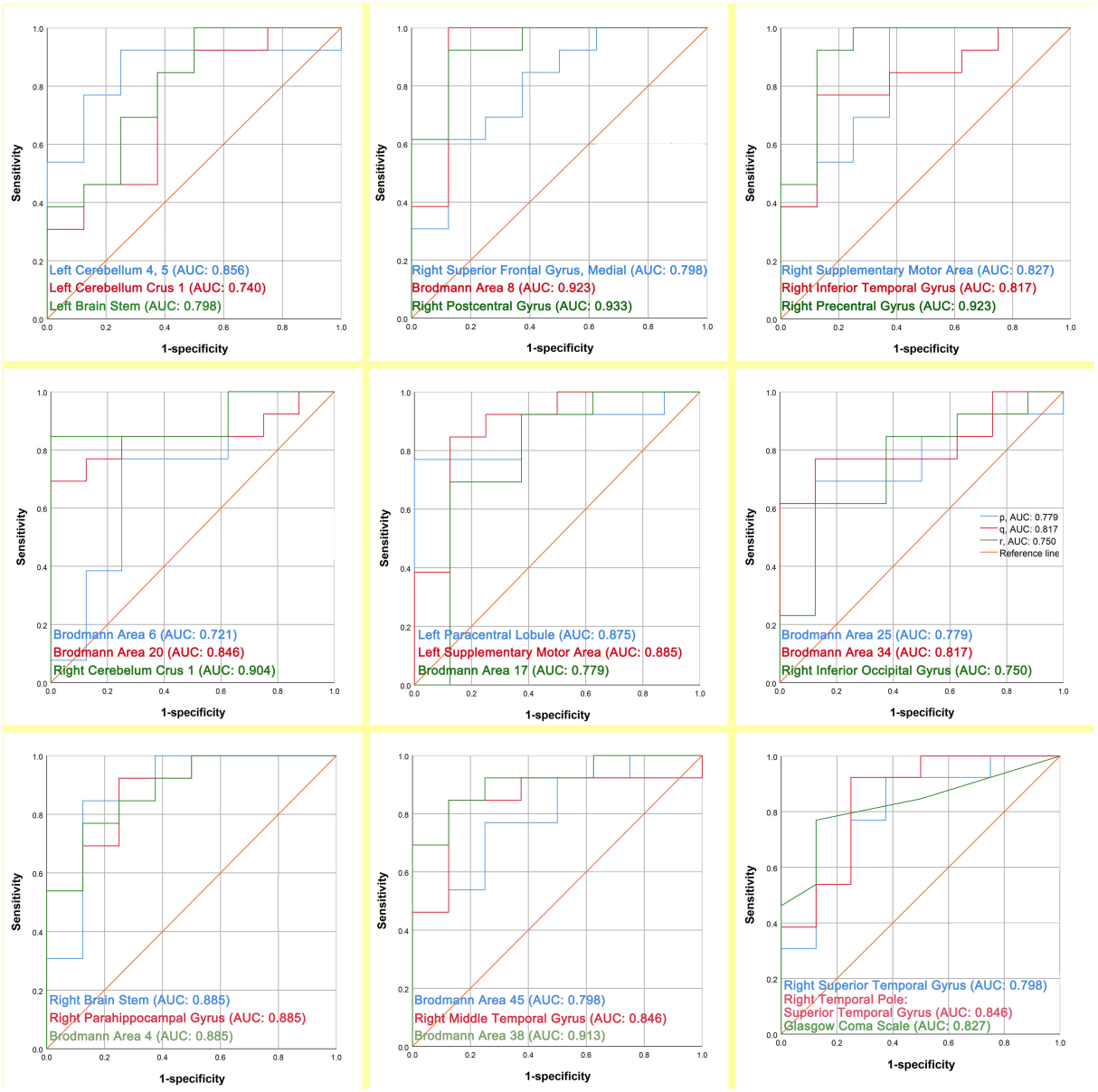

FIGURE 5
The prognostic assessment ability of the 26 regions of interest and GCS respectively for the outcome of DOC patients (AUC: area under the curve).

the cortex. In addition, some additional subcortical structures also play important roles in consciousness and alertness. The superior colliculus and pretectal regions form a core circuit with the pulvinar involved in directed attention (28). The basal ganglia area is reciprocal connections with the thalamic nucleus and this circuit may also be involved in arousal and attention functions (29). In addition, the claustrum nucleus, with extensive cortical connections, has been demonstrated to play a significant role in the maintenance of consciousness and attention (6). The cerebellum is interconnected with the prefrontal cortex to participate in attention and consciousness (30). The results of our study also confirm this, although this finding is presently controversial.

The precuneus and posterior cingulate cortex as the core components of the default mode network are involved in consciousness, introspection, episodic memory, and self-processing (31). A previous study based on diffusion magnetic resonance imaging suggested that the connection between the thalamus and pisteromedial cortex (precuneus and posterior cingulate) white matter cellulose was disrupted in DOC patients

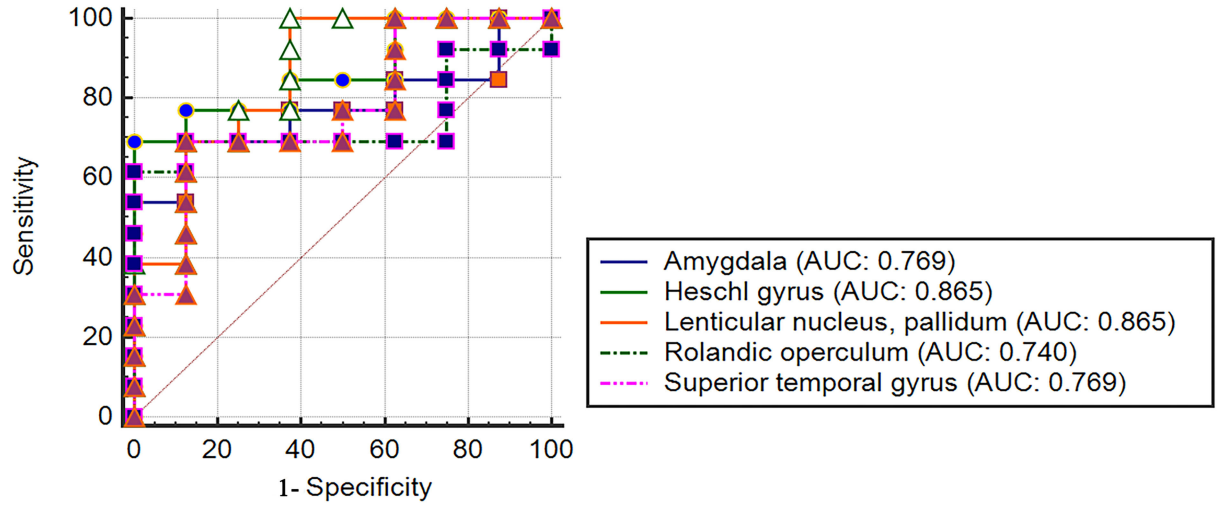

FIGURE 6
Robustness analysis of prognosis prediction based on AAL template.

(31). This provides a rationale for our findings that structure determines function. However, it should be pointed out that the coupling of structure and function in the field of brain science is not a one-to-one match. Although we are unable to reveal the mechanism of the coupling between brain structure and function, we deeply realize that biophysical and network communication models with optimized structure-function coupling will be more conducive to explain the above findings. Therefore, a scientific and rigorous circuit brain network model of biophysical communication is urgently needed in the DOC field.

Based on the above findings, we further analyzed the network of the thalamus-to-whole-brain in patients with different prognoses (wake group *vs.* DOC group) 6 months after sTBI. As expected, the functional connectivity of the thalamus to the whole-brain was abnormally increased in the DOC group compared with the wake group. This may be related to the disconnection between the thalamus and consciousness system (the cortex and the cortical subconscious) in DOC group patients. On the surface, the functional connectivity of patients with DOC is enhanced and in essence, there is no causal relationship between the both, but the local brain activity of compensatory synchronicity self-enhanced between the brain regions after the loss of connectivity (32). Disruption of long-range structural connection (white matter cellulose or neurotransmitter conduction) of the thalamus to the whole-brain is considered a plausible explanation in the acute phase of DOC (32). To clarify the above theory, we manually divided 26 regions of interest based on brain regions with peak differences between wake and DOC groups, and performed functional connectivity analysis of local and distant brain areas. The results showed that most of the adjacent brain regions had enhanced functional connectivity. Although this is an exploratory analysis, it further clarifies our findings. Therefore, it is necessary to further perform long-range causal connectivity and white matter cellulose tracing analysis about acute patients with sTBI in future studies.

Functional connectivity between the thalamus and the whole-brain may be applied as an imaging marker for the prognosis assessment of DOC patients, and it could also be used as an evaluation index for the remaining brain network about latent consciousness function. Differences in neurological outcomes (wake or persistent DOC) in patients with DOC may be associated with their residual brain networks of consciousness systems. Therefore, we cautiously believe that protecting and remodeling the remaining brain consciousness network is the key to improving the wake. Furthermore, the 26 regions of interest defined according to the functional connectivity differences (wake group *vs.* DOC group) had a similar or even better wake representation ability than the admission GCS and a supplementary analysis using an AAL also demonstrated the robustness of the results of this study. Notably, brainstem regions were not included in the AAL template. Thus, a core template based on brainstem areas is urgently needed in the DOC field, although this is moderately challenging. The GCS score is a standardly used measure of neurological status and prognosis (33). However, GCS scores are relatively subjective and are greatly affected by external factors. If the GCS is complemented with functional connectivity (relatively objective and effectively reflect brain activity), their prognostic assessment ability may be more stable and reliable. Based on this protocol in future studies, it is potentially feasible to introduce machine learning to identify the prognosis of sTBI-type DOC patients.

However, our study had several shortcomings. First, the sample size in this study was small. Therefore, machine learning and linear model for prognostic assessment are relatively constrained. Second, DOC is just a general term for the vegetative state, unresponsive arousal syndrome, minimally conscious state, etc. This study failed to further differentiate and compare them. Third, the age mismatch between healthy controls and DOC patients, although adjusted for its effect, may also have biased the results. Fourth, coupling the structural and functional networks is an ideal protocol for in-depth exploration of DOC mechanisms and performing prognostic assessments. However, limited to the study protocol, we failed to make further explorations.

Conclusion

The thalamus-based system of consciousness of sTBI patients suffering from DOC is disrupted. There are differences in the thalamus-to-whole-brain network between wake and DOC groups. These differences may set the tone for the direction of neurological outcomes in patients and have potential prognostic characterization capability. Future studies with larger sample sizes, ideal structure-function coupling protocol, and machine learning model are needed to clarify mechanisms and prognostic classification ability.

Data availability statement

The raw data supporting the conclusions of this article will be made available by the authors, without undue reservation.

Ethics statement

The studies involving human participants were reviewed and approved by Ethics Committee of Clinical Medical College of Yangzhou University (2020KY-179). The patients/participants provided their written informed consent to participate in this study.

Author contributions

Conception and design: LD, JZ, and XiaW. Data collection: JZ, LD, and HYZ. Data analysis: JZ. Drafting: JZ, HZZ, and FLY. Helping with drafting: EPZ, ZJY, and YPL. Draft revision: YLP, MW, XinW, and XiaW. All authors contributed to the article and approved the submitted version.

Funding

This study was funded by the Jiangsu Province High-level Health Talents Six Ones Project Top-notch Talent Research Project (LGY2018031) and the Hospital Level Support Projects (Fcjs202050).

Acknowledgments

We thank Frontiers in Neurology for providing such an excellent academic exchange platform.

Conflict of interest

The authors declare that the research was conducted in the absence of any commercial or financial relationships that could be construed as a potential conflict of interest.

Publisher's note

References

1. Bolte AC, Dutta AB, Hurt ME, Smirnov I, Kovacs MA, McKee CA, et al. Meningeal lymphatic dysfunction exacerbates traumatic brain injury pathogenesis. *Nat Commun.* (2020) 11:4524. doi: 10.1038/s41467-020-18113-4

2. Zhang K, Jiang W, Ma T, Wu H. Comparison of early and late decompressive craniectomy on the long-term outcome in patients with moderate and severe traumatic brain injury: a meta-analysis. *Br J Neurosurg.* (2016) 30:251–7. doi: 10.3109/02688697.2016.1139052

3. Liu X, Donnelly J, Czosnyka M, Aries MJH, Brady K, Cardim D, et al. Cerebrovascular pressure reactivity monitoring using wavelet analysis in traumatic brain injury patients: a retrospective study. *PLoS Med.* (2017) 14:e1002348. doi: 10.1371/journal.pmed.1002348

4. Ham TE, Bonnelle V, Hellyer P, Jilka S, Robertson IH, Leech R, et al. The neural basis of impaired self-awareness after traumatic brain injury. *Brain.* (2014) 137:586–97. doi: 10.1093/brain/awt350

5. Wu X, Zou Q, Hu J, Tang W, Mao Y, Gao L, et al. Intrinsic functional connectivity patterns predict consciousness level and recovery outcome in acquired brain injury. *J Neurosci.* (2015) 35:12932–46. doi: 10.1523/JNEUROSCI.0415-15.2015

6. Blumenfeld H. *Chapter 1-Neuroanatomical Basis of Consciousness. Neurology of Conciousness*. New Haven, CT: Academic Press (2016).

7. Blumenfeld H. Impaired consciousness in epilepsy. *Lancet Neurol.* (2012) 11:814–26. doi: 10.1016/S1474-4422(12)70188-6

8. Achard S, Delon-Martin C, Vértes PE, Renard F, Schenck M, Schneider F, et al. Hubs of brain functional networks are radically reorganized in comatose patients. *Proc Natl Acad Sci USA.* (2012) 109:20608–13. doi: 10.1073/pnas.1208933109

9. Vanhaudenhuyse A, Noirhomme Q, Tshibanda LJ, Bruno MA, Boveroux P, Schnakers C, et al. Default network connectivity reflects the level of consciousness in non-communicative brain-damaged patients. *Brain.* (2010) 133:161–71. doi: 10.1093/brain/awp313

10. Boly M, Tshibanda L, Vanhaudenhuyse A, Noirhomme Q, Schnakers C, Ledoux D, et al. Functional connectivity in the sefault network during resting state is preserved in a vegetative but not in a brain dead patient. *Hum Brain Mapp.* (2009) 30:2393–400. doi: 10.1002/hbm.20672

11. Marino S, Bonanno L, Giorgio A. Functional connectivity in disorders of consciousness: methodological aspects and clinical relevance. *Brain Imaging Behav.* (2016) 10:604–8. doi: 10.1007/s11682-015-9417-1

12. Maas AIR, Menon DK, Adelson PD, Andelic N, Bell MJ, Belli A, et al. Traumatic brain injury: integrated approaches to improve prevention, clinical care, and research. *Lancet Neurol.* (2017) 16:987–1048. doi: 10.1016/S1474-4422(17)30371-X

13. Cooper DJ, Nichol AD, Bailey M, Bernard S, Cameron PA, Pili-Floury S, et al. Effect of early sustained prophylactic hypothermia on neurologic outcomes among patients with severe traumatic brain injury: the polar randomized clinical trial. *JAMA.* (2018) 320:2211–20. doi: 10.1001/jama.2018.17075

14. Wilson JTL, Pettigrew LEL, Teasdale GM. Structured interviews for the Glasgow outcome scale and the extended glasgow outcome scale: guidelines for their use. *J Neurotrauma.* (1998) 15:573–85. doi: 10.1089/neu.1998.15.573

15. Guo H, Liu R, Sun Z, Liu B, Xiang Y, Mao J, et al. Evaluation of prognosis in patients with severe traumatic brain injury using resting-state functional magnetic resonance imaging. *World Neurosurg.* (2019) 121:e630–9. doi: 10.1016/j.wneu.2018.09.178

16. Tzourio-Mazoyer N, Landeau B, Papathanassiou D, Crivello F, Etard O, Delcroix N, et al. Automated anatomical labeling of activations in SPM using a macroscopic anatomical parcellation of the MNI MRI single-subject brain. *Neuroimage.* (2002) 15:273–89. doi: 10.1006/nimg.2001.0978

17. Johnen VM, Neubert FX, Buch ER, Verhagen L, O'Reilly JX, Mars RB, et al. Causal manipulation of functional connectivity in a specific neural pathway during behavior and at rest. *Elife.* (2015) 4:e04585. doi: 10.7554/eLife.04585

18. Fisher RA. Frequency distribution of the values of the correlation coefficient in samples from an indefinitely large population. *Biometrika.* (1915) 10:507–21. doi: 10.1093/biomet/10.4.507

19. Muschelli J, Nebel MB, Caffo BS, Barber AD, Pekar JJ, Mostofsky SH. Reduction of motion-related artifacts in resting state fMRI using aCompCor. *Neuroimage.* (2014) 96:22e35. doi: 10.1016/j.neuroimage.2014.03.028

20. Lim SL, Cherry JB, Davis AM, Balakrishnan SN, Ha OR, Bruce JM, et al. The child brain computes and utilizes internalized maternal choices. *Nat Commun.* (2016) 24:11700. doi: 10.1038/ncomms11700

21. Warthen KG, Boyse-Peacor A, Jones KG, Sanford B, Love TM, Mickey BJ. Sex differences in the human reward system: convergent behavioral, autonomic and neural evidence. *Soc Cogn Affect Neurosci.* (2020) 15:789–801. doi: 10.1093/scan/nsaa104

22. Lee SY, Kim H, Lee JY, Kim JH, Lee DY, Mook-Jung I, et al. Effects of chronic tinnitus on metabolic and structural changes in subjects with mild cognitive impairment. *Front Aging Neurosci.* (2020) 12:594282. doi: 10.3389/fnagi.2020.594282

23. Yu Y, Zheng W, Tan X, Li X, Zhang X, Gao J, et al. Microstructural profiles of thalamus and thalamocortical connectivity in patients with disorder of consciousness. *J Neurosci Res.* (2021) 99:3261–73. doi: 10.1002/jnr.24921

24. Annen J, Heine L, Ziegler E, Frasso G, Bahri M, Di Perri C, et al. Function-structure connectivity in patients with severe brain injury as measured by MRI-DWI and FDG-PET. *Hum Brain Mapp.* (2016) 37:3707–20. doi: 10.1002/hbm.23269

25. Gutmann B, Mierau A, Hülsdünker T, Hildebrand C, Przyklenk A, Hollmann W, et al. Effects of physical exercise on individual resting state EEG alpha peak frequency. *Neural Plast.* (2015) 3:717312. doi: 10.1155/2015/717312

26. Zhang J, Zhang E, Yuan C, Zhang H, Wang X, Yan F, et al. Abnormal default mode network could be a potential prognostic marker in patients with disorders of consciousness. *Clin Neurol Neurosurg.* (2022) 218:107294. doi: 10.1016/j.clineuro.2022.107294

27. Englot DJ, Yang L, Hamid H, Danielson N, Bai X, Marfeo A, et al. Impaired consciousness in temporal lobe seizures: role of cortical slow activity. *Brain.* (2010) 133:3764–77. doi: 10.1093/brain/awq316

28. Krauzlis RJ, Lovejoy LP, Zenon A. Superior colliculus and visual spatial attention. *Annu Rev Neurosci.* (2013) 36:165–82. doi: 10.1146/annurev-neuro-062012-170249

29. Dreher JC, Grafman J. The roles of the cerebellum and basal ganglia in timing and error prediction. *Eur J Neurosci.* (2002) 16:1609–19. doi: 10.1046/j.1460-9568.2002.02212.x

30. Baumann O, Mattingley JB. Effects of attention and perceptual uncertainty on cerebellar activity during visual motion perception. *Cerebellum.* (2014) 13:46–54. doi: 10.1007/s12311-013-0519-2

31. Cui Y, Song M, Lipnicki DM, Yang Y, Ye C, Fan L, et al. Subdivisions of the posteromedial cortex in disorders of consciousness. *Neuroimage Clin.* (2018) 20:260–6. doi: 10.1016/j.nicl.2018.07.025

32. Palacios EM, Sala-Llonch R, Junque C, Roig T, Tormos JM, Bargallo N, et al. Resting-state functional magnetic resonance imaging activity and connectivity and cognitive outcome in traumatic brain injury. *JAMA Neurol.* (2013) 70:845–51. doi: 10.1001/jamaneurol.2013.38

33. Majdan M, Steyerberg EW, Nieboer D, Mauritz W, Rusnak M, Lingsma HF. Glasgow coma scale motor score and pupillary reaction to predict six-month mortality in patients with traumatic brain injury: comparison of field and admission assessment. *J Neurotrauma.* (2015) 32:101–8. doi: 10.1089/neu.2014.3438

frontiers | Frontiers in Neurology

TYPE Original Research
PUBLISHED 01 December 2022
DOI 10.3389/fneur.2022.956931

OPEN ACCESS

EDITED BY
Jiliang Fang,
Guang'anmen Hospital, China Academy of Chinese Medical Sciences, China

REVIEWED BY
Jie Jia,
Fudan University, China
Huangan Wu,
Shanghai University of Traditional Chinese Medicine, China

*CORRESPONDENCE
Jingling Chang
ear6979@163.com
Ying Gao
gaoying973@126.com

SPECIALTY SECTION
This article was submitted to Applied Neuroimaging, a section of the journal Frontiers in Neurology

RECEIVED 30 May 2022
ACCEPTED 10 October 2022
PUBLISHED 01 December 2022

CITATION
Xu M, Gao Y, Zhang H, Zhang B, Lyu T, Tan Z, Li C, Li X, Huang X, Kong Q, Xiao J, Kranz GS, Li S and Chang J (2022) Modulations of static and dynamic functional connectivity among brain networks by electroacupuncture in post-stroke aphasia. *Front. Neurol.* 13:956931. doi: 10.3389/fneur.2022.956931

Modulations of static and dynamic functional connectivity among brain networks by electroacupuncture in post-stroke aphasia

Minjie Xu[1,2], Ying Gao[1,3]*, Hua Zhang[1], Binlong Zhang[1], Tianli Lyu[1], Zhongjian Tan[1], Changming Li[1], Xiaolin Li[1], Xing Huang[1], Qiao Kong[1], Juan Xiao[1], Georg S. Kranz[4,5,6], Shuren Li[7] and Jingling Chang[1,3]*

[1]Department of Neurology, Dongzhimen Hospital, Beijing University of Chinese Medicine, Beijing, China, [2]Key Laboratory of Chinese Internal Medicine Ministry of Education, Beijing University of Chinese Medicine, Beijing, China, [3]Institute for Brain Disorders, Beijing University of Chinese Medicine, Beijing, China, [4]Department of Rehabilitation Sciences, The Hong Kong Polytechnic University, Hong Kong, Hong Kong SAR, China, [5]The State Key Laboratory of Brain and Cognitive Sciences, The University of Hong Kong, Hong Kong, Hong Kong SAR, China, [6]Department of Psychiatry and Psychotherapy, Comprehensive Center for Clinical Neurosciences and Mental Health, Medical University of Vienna, Vienna, Austria, [7]Division of Nuclear Medicine, Department of Biomedical Imaging and Image-Guided Therapy, Medical University of Vienna, Vienna, Austria

Introduction: Post-stroke aphasia (PSA) is a language disorder caused by left hemisphere stroke. Electroacupuncture (EA) is a minimally invasive therapeutic option for PSA treatment. Tongli (HT5) and Xuanzhong (GB39), two important language-associated acupoints, are frequently used in the rehabilitation of patients with PSA. Preliminary evidence indicated functional activation in distributed cortical areas upon HT5 and GB39 stimulation. However, research on the modulation of dynamic and static functional connectivity (FC) in the brain by EA in PSA is lacking.

Method: This study aimed to investigate the PSA-related effects of EA stimulation at HT5 and GB39 on neural processing. Thirty-five participants were recruited, including 19 patients with PSA and 16 healthy controls (HCs). The BOLD signal was analyzed by static independent component analysis, generalized psychophysiological interactions, and dynamic independent component analysis, considering variables such as age, sex, and years of education.

Results: The results revealed that PSA showed activated clusters in the left putamen, left postcentral gyrus (PostCG), and left angular gyrus in the salience network (SN) compared to the HC group. The interaction effect on temporal properties of networks showed higher variability of SN ($F = 2.23$, positive false discovery rate [pFDR] = 0.017). The interaction effect on static FC showed increased functional coupling between the right calcarine and right lingual gyrus ($F = 3.16$, pFDR = 0.043). For the dynamic FC, at the region level, the interaction effect showed lower variability and higher frequencies of circuit 3, with the strongest connections between the supramarginal gyrus and posterior cingulum ($F = 5.42$, pFDR = 0.03), middle cingulum and PostCG ($F = 5.27$, pFDR = 0.036), and triangle inferior frontal and lingual

gyrus ($F = 5.57$, pFDR $= 0.026$). At the network level, the interaction effect showed higher variability in occipital network–language network (LN) and cerebellar network (CN) coupling, with stronger connections between the LN and CN ($F = 4.29$, pFDR $= 0.042$). Dynamic FC values between the triangle inferior frontal and lingual gyri were anticorrelated with transcribing, describing, and dictating scores in the Chinese Rehabilitation Research Center for Chinese Standard Aphasia Examination.

Discussion: These findings suggest that EA stimulation may improve language function, as it significantly modulated the nodes of regions/networks involved in the LN, SN, CN, occipital cortex, somatosensory regions, and cerebral limbic system.

KEYWORDS

electroacupuncture, brain networks, post stroke aphasia, functional connectivity, psychophysiological interaction analysis, independent component analysis

Introduction

Post-stroke aphasia (PSA) is a clinical syndrome caused by a left hemisphere stroke that results in the loss of language skills and consequently has an impact on daily life (1). Even mild aphasia can have a negative effect on functional outcomes, such as mood, quality of life, and ability to return to work (2). Language is a critical cognitive skill supported by large-scale brain networks (3). In addition to the direct effect of focal lesions on important cortical regions, damage to other remote areas within language networks and non-language-specific networks also leads to the occurrence and development of aphasia (4, 5). It has been suggested that focal stroke lesions can affect language comprehension by altering the functional connectivity (FC) of multiple networks and subnetworks in PSA (6–8).

Acupuncture is an ancient Chinese treatment that has been systematically used for 2000 years (9). It is rapidly gaining recognition for its therapeutic properties in the treatment of PSA and several other neurological conditions (10–13). Electroacupuncture (EA) is a modern form of acupuncture that features a small current passing between pairs of acupuncture needles. To observe the immediate effect of acupuncture on brain activity, several recent studies have applied EA during functional magnetic resonance imaging (fMRI) (14–16). Block design is one of the most commonly used scanning methods for exploring the potential mechanisms of EA in fMRI studies (17–20). Tongli (HT5) and Xuanzhong (GB39) are important language-implicated acupoints used in Chinese medicine. They are commonly used in PSA rehabilitation therapy because they are tailored to language-processing systems. Previous fMRI studies of EA treatment demonstrated that stimulation at HT5 and GB39 resulted in activation of language regions and the somatosensory cortex in both cerebral hemispheres and that it might modulate speech function through effects on brain networks in healthy individuals (21–23).

It is worth noting that the emergence of acupuncture as a treatment stem from its function in patients rather than in healthy people (24). Modulation of information processing in the brain through acupuncture may differ between patients with PSA and healthy individuals and occurs mainly in disorder-related areas (24). A direct comparison of the effect on neural networks between patients with PSA and healthy individuals involved in the processing of EA stimulation at HT5 and GB39 is virtually absent from the present research. Moreover, although the aforementioned studies have focused on localizing a series of brain regions showing activation patterns during the processing of EA stimulation in healthy individuals, a rapidly growing body of neuroimaging literature suggests that the effect of acupuncture in patients with stroke may be attributed to modulation of disrupted patterns of the whole-brain network rather than in one or two confined brain regions (25, 26).

Therefore, this study aimed to explore and compare how EA stimulation modulates FC and temporal properties in patients with PSA and healthy individuals. To address this question, independent component analysis (ICA) and general psychophysiological interaction (gPPI) were used to reveal static and dynamic FC changes at the levels of the region of interest (ROI) and large-scale network.

Abbreviations: PSA, post stroke aphasia; HC, healthy control; EA, electroacupuncture; PPI, Psychophysiological Interaction; static ICA, static independent component analysis; dyn, ICA, dynamic independent component analysis; DMN, default mode network; SMN, sensorimotor network; CRRCAE, Chinese Rehabilitation Research Center for Chinese Standard Aphasia test; BDAE, Boston Diagnostic Aphasia Examination; VN, visual network; SN, salience network; DAN, dorsal attention network; FPN, frontoparietal network; LN, language network; CN, cerebellar network. AG, angular gyrus; SMG, supramarginal gyrus; PostCG, postcentral gyrus; ANTs, Advanced Neuroimaging Tools.

Materials and methods

Participants and ethics statements

Based on previous study results, 35 right-handed participants were recruited between August 2013 and February 2021, including 19 patients with PSA (33–78 years, 13 men) and 16 demographically matched healthy volunteers (24–63 years, right-handed, eight men). Patients with PSA were recruited from the Department of Neurology at Dongzhimen Hospital with complaints of language disorders. Healthy controls (HCs) were recruited from the local community.

The Medical Research Ethics Committee of Dongzhimen Hospital (reference number: ECPJ-BDY-2015-04) approved this study, and all participants provided written consent to participate. An overview of the study design is shown in Figure 1.

Clinical evaluation and speech and language testing

Demographic factors, sex, age, handedness, years of education (Edu), and scores on the Boston Diagnostic Aphasia Examination were reviewed for each patient. Twelve patients with motor aphasia were diagnosed by the Chinese Rehabilitation Research Center for Chinese Standard Aphasia Examination (CRRCAE), a battery of language tests designed according to the Mandarin rules. As a result of testing the reliability and validity of the CRRCAE in a prior study, it was found to have good sensitivity and reliability and may be used as a quantitative table for the diagnosis of aphasia in Mandarin speakers (27, 28). Thirty subscales including comprehension, speaking, writing, calculation, copy, and repeating comprise the scale (28).

Stimuli and scanning procedure

Acupuncture procedures and needling sensation recording

Both the PSA and HC groups received EA stimulation at the HT5 and GB39 acupoints during fMRI acquisition. Before the start of the scan, the participants positioned themselves on the fMRI scanner bed on their backs, and needles were placed at the GB39 and HT5 acupoints. According to the "Name and Location of Acupoints" (GB/T 12346-2006), two acupoints were located on both sides. HT5 was situated radially to the flexor carpi ulnaris tendon on the anteromedial side of the forearm, 33 mm proximal to the palmar wrist crease, with insertion depths ranging from 10 to 30 mm. GB39 was needled at an insertion depth of 33 mm, 100 mm above the external malleolus tip, on the anterior fibula border (Figure 2A). A professional acupuncturist performed acupuncture. All participants reported their experience ("Deqi") with acupuncture stimulation. Deqi featured aching, pressure, heaviness, fullness, and numbness among other feelings (23–29). The acupuncturist used 0.40 × 40-mm sterile silver acupuncture needles (Guizhou, China) with the EA technique. Han's acupoint nerve stimulator (model LH-202H) was situated outside the fMRI room, with one end of the acupoint wire linked to the acupuncture needle handle and the other end connected to it. The EA frequency was 2 Hz, and the electric current was 2 mA. As previously mentioned, the stimulation waveform is the dilatational wave (23).

fMRI scanning

All fMRI data were acquired using the 3 Tesla Siemens MRI scanner (Erlangen, Germany) at Dongzhimen Hospital. A high-resolution T1-weighted structural image was obtained using an isotropic multi-echo magnetization-prepared rapid acquisition sequence (repetition time: 1900 ms, echo time: 2.13 ms, field of view: 250 mm, flip angle: 90°, voxel size: 1.0 × 1.0 × 1.0 mm, slice thickness: 1.0 mm, matrix: 256 × 256, number of slices: 176). Functional images were acquired using a single shot gradient-recalled echo planar imaging sequence (31 interleaved axial slices, repetition time: 2,000 ms, echo time: 30 ms, flip angle: 90°, field of view: 225 × 225 mm^2, interslice gap: 0.7 mm, matrix: 64 × 64 mm^2, slice thickness: 3.5 mm, voxel size: 3.5 × 3.5 × 3.5 mm^3). The fMRI experimental design was a classic resting/stimulation block design divided between a 30-s resting interval and a 30-s stimulation period; such blocks were repeated for six cycles, six acupuncture blocks, and six rest blocks out of a total of 12 blocks that were completed in one session (30) (Figure 2B).

Data processing

The Resting-State fMRI Data Analysis Toolkit (REST plus, version 1.24; http://www.restfmri.net/forum/RESTplus) (31) and task-fMRI images were preprocessed using the Statistical Parametric Mapping 12 software suite (SPM12, http://www.fil.ion.ucl.ac.uk/spm). First, we discarded the first 10 volumes for each participant to avoid the negative impact of magnetic disequilibrium on data quality. Subsequently, all functional images were preprocessed [slice acquisition time, head motion, and a 6-mm Gaussian kernel with full width at half maximum (FWHM) smoothing]. All data had head motions <3 mm or 3°. Next, using Advanced Normalization Tools (ANTS1.9, https://www.nitrc.org/projects/ants), the functional images were spatially normalized to the Montreal Neurological Institute space in the Linux platform. Temporal filtering was also applied, which allowed a frequency band of 0.01–0.1 Hz to pass. Subsequently, each participant was subjected to linear

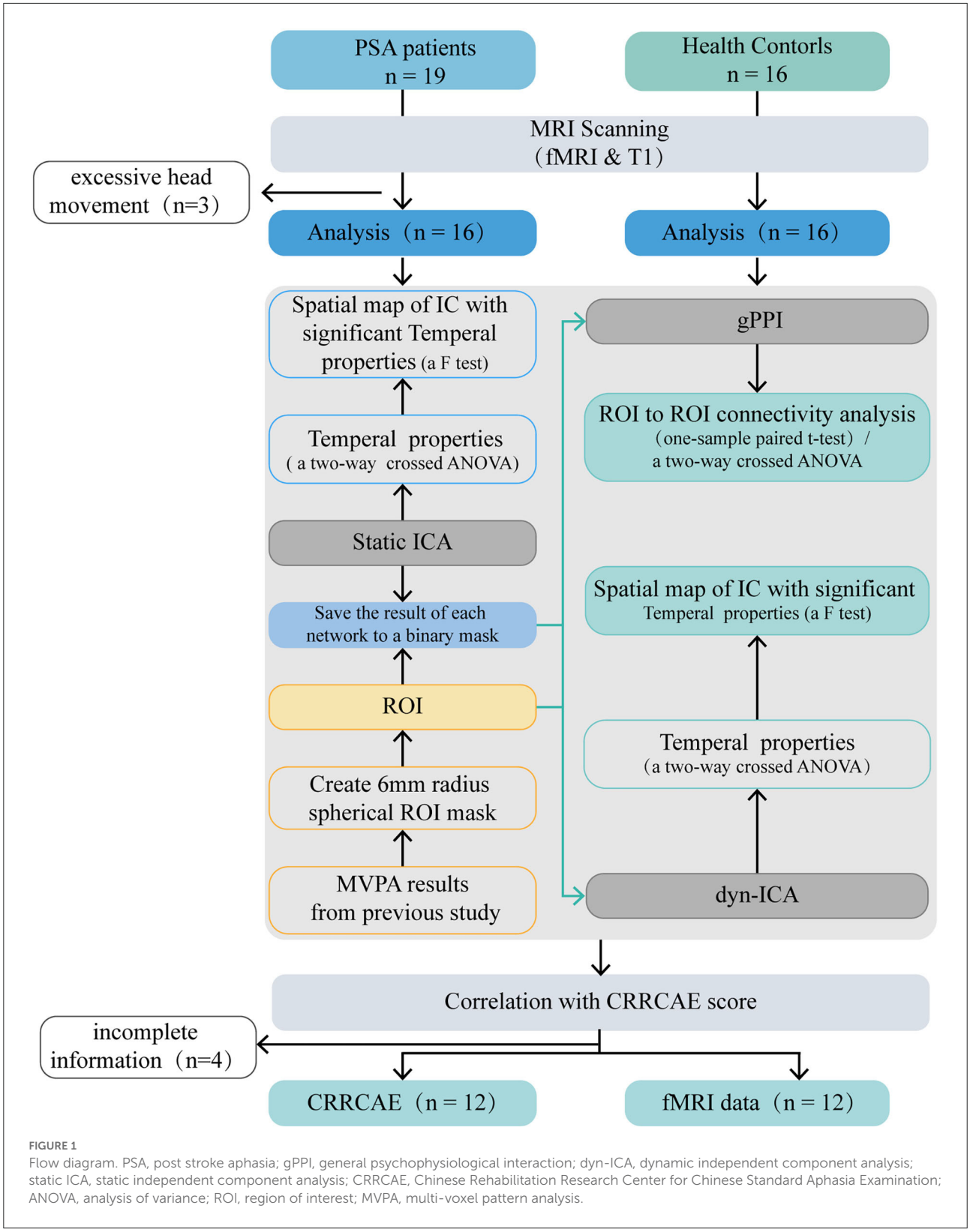

FIGURE 1
Flow diagram. PSA, post stroke aphasia; gPPI, general psychophysiological interaction; dyn-ICA, dynamic independent component analysis; static ICA, static independent component analysis; CRRCAE, Chinese Rehabilitation Research Center for Chinese Standard Aphasia Examination; ANOVA, analysis of variance; ROI, region of interest; MVPA, multi-voxel pattern analysis.

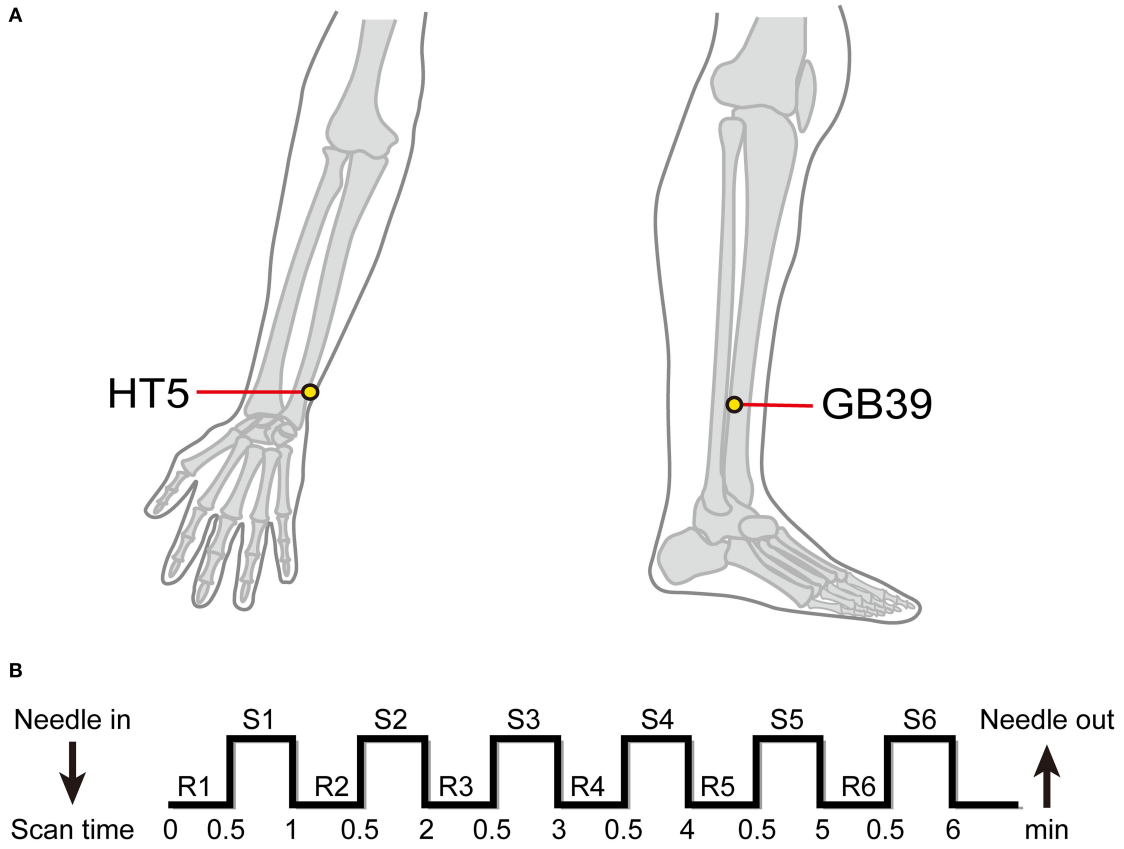

FIGURE 2
Location of acupuncture points and electroacupuncture stimulation procedure. **(A)** Location of HT5 and GB39. **(B)** n-Block design of task-based fMRI. R, rest; S, stimulation.

detrending to remove any residual effect of low-frequency drift or high-frequency physiological noise.

Statistical analysis

All statistical analyses were performed using the CONN toolbox (32). We examined the effects of EA on FC using a condition main effect (group: any effect, condition: EA stimulation > rest at baseline), the PSA-related effect using a group main effect (group: PSA-HC, condition: any effect), and the interaction effect using a two-way crossed analysis of variance (ANOVA), with years of Edu, age, and sex as covariates, with a within-subjects factor (condition: EA stimulation vs. rest at baseline) and a between-subjects factor (group: patients with PSA vs. HCs). At a threshold of $p < 0.05$, the false discovery rate-corrected results were considered statistically significant.

Static-independent component analysis

Implemented in CONN 18b, static-ICA employs the Fast-ICA method and GICA3 back projection to estimate independent components (ICs) and subject-level spatial map estimation (33). Twenty estimated components were chosen (34). The spatial maps and time courses were normalized to z-scores for future analyses.

Spatial components

The dorsal attention network (DAN), default mode network (DMN), sensorimotor network (SMN), salience network (SN), visual network (VN), frontoparietal network, language network (LN), and cerebellar network (CN) were identified within each component using spatial sorting and a correlational spatial match-to-template approach (spatial correlation and spatial overlap of suprathreshold areas/dice coefficient) (35). Nine components were chosen from a total of 20 ICs to represent the brain networks (Figure 3A). Among them, instead of calling network 9 the VN, we chose to call it the occipital network, as there was no visual stimulus in this study. From now on, we shall refer to components as "networks" and we will identify components by referring to their label (e.g., DMN); component descriptions are listed in Supplementary Table 1. For the spatial map, we examined how

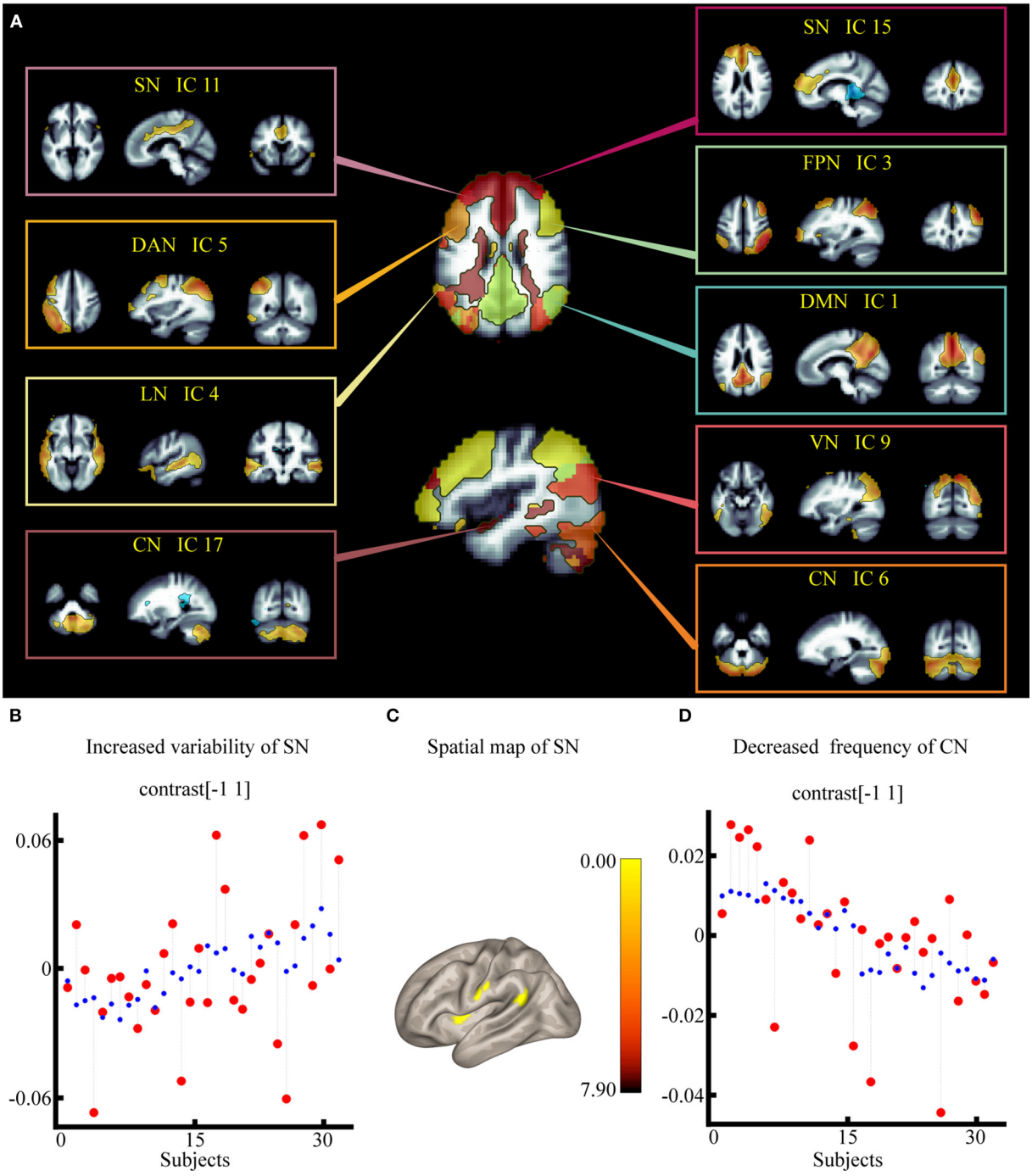

FIGURE 3
Effect of electroacupuncture stimulation on static independent component analysis. **(A)** Nine spatial maps of intrinsic resting-state networks in 32 subjects. **(B)** Changes in temporal properties varies of SN within each group and condition. **(C)** Spatial map of SN for the contrast of post stroke aphasia group vs. healthy control group. **(D)** Changes in temporal properties varies of VN within each group and condition. DMN, default mode network; SMN, sensorimotor network; VN, visual network; SN, salience network; DAN, dorsal attention network; FPN, frontoparietal network; LN, language network; CN, cerebellar network.

the PSA-related network structure differed between the two groups using a voxel-wise F-test (group main effect), as in previous studies (36).

Temporal components

First, for each individual, a set of nine beta coefficients for each of the two condition regressors was derived, indicating

the degree to which the task regressor relates to a specific network. Then, to verify the interaction effect (group × condition) on BOLD signal fluctuations in each brain network, we performed a two-way crossed ANOVA test for the nine remaining networks using the temporal properties implemented in the CONN toolbox.

GPPI-based FC analyses

Unsmoothed (37) but preprocessed (refer to data processing) fMRI data were inputted into the CONN toolbox for additional preprocessing and gPPI analysis (38). Before conducting the gPPI analysis, we used a component-based noise correction method to remove artifacts from the fMRI data. To investigate how EA stimuli alter brain functional architecture at the ROI (Supplementary Figure 1) and large-scale network levels (static ICA results), we used gPPI analysis according to Lee Masson et al. (23–39). The regression model used in the gPPI analysis was as follows: $Y = X_1 \times \beta + X_2 \times \beta G + error$, where Y = time-series BOLD response of the seed, X_1 = the hemodynamic response function (HRF) convolved gPPI terms (i.e., time-series BOLD response of the seed × the psychological regressor as dictated by onset and duration of EA stimulus), β = the strength of FC (i.e., the beta estimates of gPPI terms), X_2 = $X_1 \times$ HRF convolved psychological regressor × covariates of no interest (age, Edu, and sex regressors), and βG = the beta estimates of the HRF-convolved time-series BOLD response of the seeds. Individual results were transformed into z-scores using the Fisher z-transformation for the group-level analysis. First, we evaluated how FC was modulated by the stimuli in each group using a one-sample paired t-test. Second, we used a two-way crossed ANOVA to assess the interaction effect on FC strength (40).

Dynamic independent component analysis

Dynamic connectivity measures were used to examine and characterize the sources of FC variability. Dyn-ICA runs an ICA on the connection time series and returns ICs that most accurately represent FC modulation over time (41, 42). For first-level signal processing, Dyn-ICA matrices (circuits) are created using dynamic connectivity measures. Seeds used to build the matrices were obtained from our previous multi-voxel pattern analysis results (23) (Supplementary Figure 1) and static ICA results in this study (Figure 3A). Then, the aggregated data were divided into 12 circuits using Dyn-ICA with 30 smoothing kernels, in line with a previous study's method (43). This processing produces multiple outputs, including the individual subject-level matrices gamma and the variability and frequency of the dynamic circuit time series. For the second level, we statistically evaluated (1) the frequency of each component (temporal component time-series frequency averaged across all participants) and (2) the variability of each component (temporal component time-series standard deviation averaged across all participants), and the spatial properties (defined as gPPI interaction terms). A two-way crossover ANOVA test was used to assess the interaction effect of temporal data on the frequency and variability of dynamic circuits with Edu, age, and sex as covariates of no interest. Finally, a main effect of condition was performed to assess the EA stimulus-dependent spatial characteristics of circuits with significant temporal properties.

TABLE 1 Demographic data and clinical characteristics of the PSA and HCs groups.

Characteristics	PSA patients	HCs	*P*-values
Gender, female/male, *n*	5:11	3:13	0.41
Handedness, right/left, *n*	16:0	16:0	1.00
Age, years, mean ± SD	58.56 ± 12.14	42.81 ± 13.38	0.16
Edu, years mean ± SD	12 ± 2.52	15.25 ± 4.22	0.00
Listening mean ± SD	25 ± 9		
Repeating mean ± SD	20 ± 7		
Speaking mean ± SD	11 ± 10		
Reading aloud mean ± SD	17 ± 7		
Reading comprehension mean ± SD	21 ± 10		
Transcribing mean ± SD	3 ± 4		
Describing mean ± SD	2 ± 4		
Dictating mean ± SD	1 ± 2		
Calculating mean ± SD	3 ± 4		
BDAE, mean	2		

Edu, years of education; EA, electroacupuncture; LN, language network; CN, cerebellar network; SN, salience network; ROI, region of interest; SMG, supramarginal gyri; PostCG, postcentral gyri; PSA, post stroke aphasia; HC, healthy control; DMN, default mode network; positive false discovery rate, p-FDR; MNI, montreal neurological institute; R, right; L, left.

TABLE 2 Spatial map of SN for the contrast of PSA group vs. HC group.

Regions	Clusters			Size	Side	*F*	*p*-FDR
	x	*y*	*z*				
Putamen	−30	−06	06	54	left	−3.92	0.003
AG	−57	−51	15	53	left	−4.45	0.003
PostCG	−60	−15	30	39	left	−4.00	0.010

Edu, years of education; EA, electroacupuncture; LN, language network; CN, cerebellar network; SN, salience network; ROI, region of interest; SMG, supramarginal gyri; PostCG, postcentral gyri; PSA, post stroke aphasia; HC, healthy control; DMN, default mode network; positive false discovery rate, p-FDR; MNI, montreal neurological institute; R, right; L, left.

Correlation analysis between behavioral data and fMRI data during EA stimulation

To evaluate the correlation between brain network modulation during EA and behavioral data (CRRCAE scores) in patients with PSA, we conducted a rank correlational analysis. Please note that the correlation analyses were exploratory;

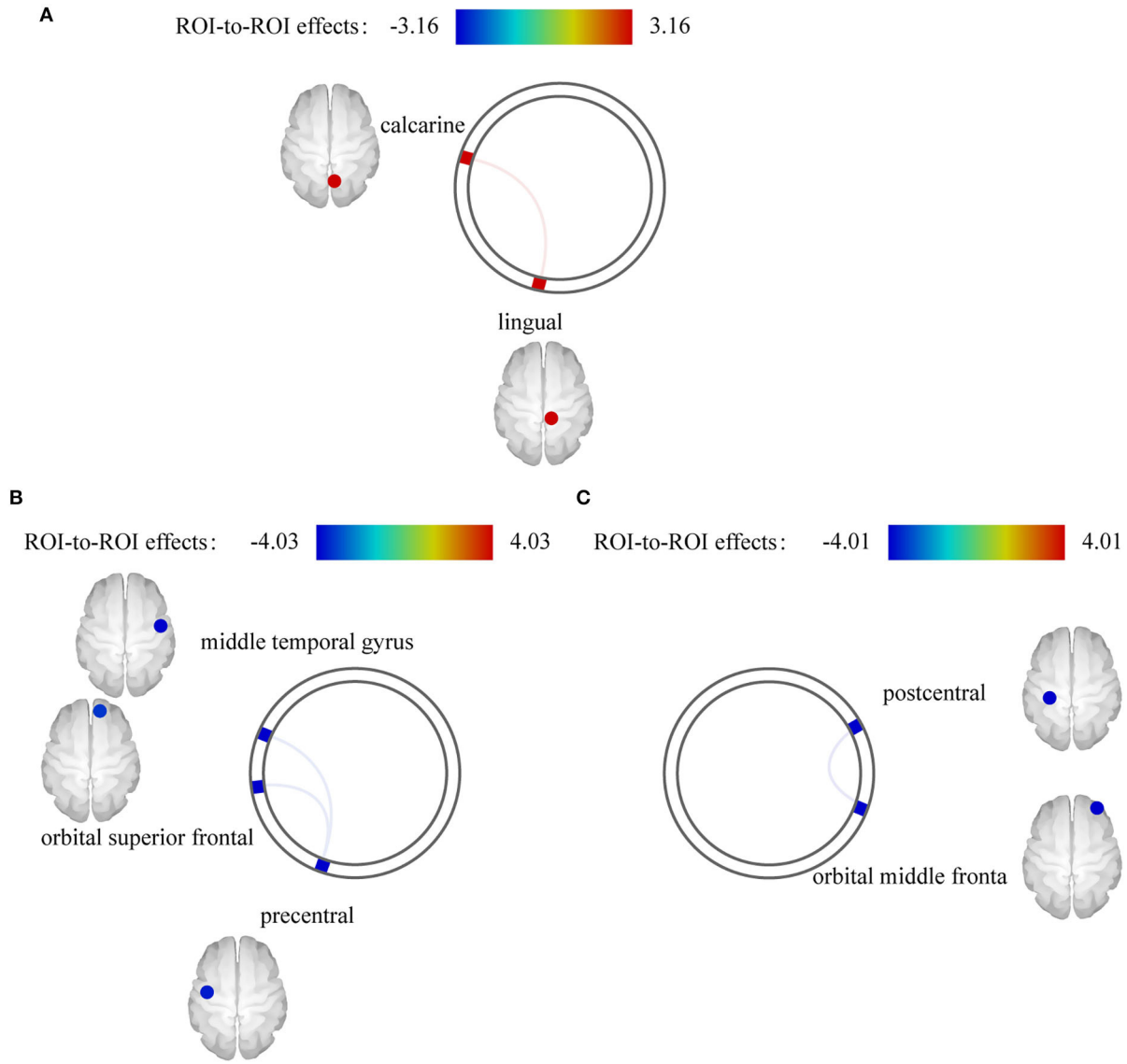

FIGURE 4
Effect of electroacupuncture (EA) stimulation on static functional connectivity (FC). **(A)** Interaction effect on static FC. **(B)** EA stimulus-dependent changes in FC for the contrast of EA stimulation vs. rest at baseline in post stroke aphasia group. **(C)** EA stimulus-dependent changes in FC for the contrast of EA stimulation vs. rest at baseline in healthy control group.

thus, a p-value < 0.05 with no corrections for multiple comparisons was implemented, in line with a previous study's methods (44). Correlation analysis was performed using the R software package (The R Project for Statistical Computing, Vienna, Austria).

Results

Clinical characteristics and indices

Detailed clinical characteristics and indices are summarized in Table 1. Patients with PSA and the HCs exhibited no significant differences in age or sex, but they showed significant differences in Edu ($p \leq 0.001$).

Spatial map and temporal properties of each IC

Varied interaction effect of temporal properties

According to the results of the two-way crossed ANOVA test, there was a significant effect on the degree of synchronization, including increased variability of SN [$F = 2.23$, positive false discovery rate (pFDR) $= 0.017$] (Figure 3B) and lower

TABLE 3 Significant static FC values during EA stimulation.

Regions	Side	MNI coordinates			Regions	Side	MNI coordinates			*F*	*p*-FDR
		x	*y*	*z*			*x*	*y*	*z*		
EA stimulation > rest at baseline in PSA											
Precentral	L	−44	−9	41	Middle temporal gyrus	R	52	−4	−20	−4.03	0.024
					Orbital superior frontal	R	14	55	−17	−3.35	0.048
EA stimulation > rest at baseline in HC											
Postcentral	L	−32	−31	67	Orbital middle frontal	R	37	54	−5	−4.01	0.025
Group × condition interaction effect											
Calcarine	L	−3	−93	11	Lingual	R	12	−39	0	3.16	0.043

Edu, years of education; EA, electroacupuncture; LN, language network; CN, cerebellar network; SN, salience network; ROI, region of interest; SMG, supramarginal gyri; PostCG, postcentral gyri; PSA, post stroke aphasia; HC, healthy control; DMN, default mode network; positive false discovery rate, p-FDR; MNI, montreal neurological institute; R, right; L, left.

frequency of CN [$F = -2.93$, pFDR = 0.006] (Figure 3D; Supplementary Table 1).

Spatial map for the comparison of the PSA and HC groups

According to the results of the group main effect, different contributions from certain brain regions in the nine networks were detected. We found that the PSA group showed activated clusters in the left putamen, left postcentral gyrus (PostCG), and left angular gyrus (AG) in the SN compared to the HC group. No significant differences were observed in CN. Results are summarized in Figure 3C and Table 2.

Static FC during EA stimulation

Interaction effect on static FC

We found an interaction effect on functional coupling between the right calcarine and right lingual gyrus [$F_{(14,27)} = 3.16$, pFDR = 0.043] (Figure 4A; Table 3). However, no significant differences were observed at the network level.

Changes in FC between EA stimulation and rest in each group

We also separately identified the FCs between ROIs during EA stimulation in each group. EA stimulation reduced FC between the left precentral and right middle temporal gyrus [$F_{(4,13)} = -4.03$, pFDR = 0.024] and right orbital superior frontal gyrus [$F_{(4,11)} = -3.35$, pFDR = 0.048] in PSA (Figure 4B). Additionally, ROI-based gPPI analysis of the HC group revealed that EA stimulation reduced FC between the left postcentral and right orbital middle frontal regions [$F_{(3,5)} = -4.01$, pFDR = 0.025], compared with the rest condition (Figure 4C). The results are presented in Table 3. Network-based gPPI analysis revealed no significant differences in either HC groups or PSA groups.

Dynamic FC during EA stimulation

Results of the interaction effects at the network level

The outlook of the 12 components is shown in Supplementary Figure S2. Patients with PSA had higher variability of occipital network LN and CN coupling (Figure 5A), with stronger connections between the LN and CN ($F = 4.29$, pFDR = 0.042, uncorrected $p = 0.0053$), DMN and CN ($F = 4.28$, pFDR = 0.043, uncorrected $p = 0.005$) (Figure 5B; Table 4).

Results of the interaction effects at the ROI level

The outlook of the 12 components is shown in Supplementary Figure S3. Patients with PSA had higher frequencies (Figure 5D) and lower variability (Figure 5E) of circuit 3, which connects the occipital, limbic, and somatosensory systems, with the strongest connections between the triangle inferior frontal and lingual gyri ($F = 5.57$, pFDR = 0.026, uncorrected $p = 0.001$), supramarginal and posterior cingulum gyri ($F = 5.42$, pFDR = 0.03, uncorrected $p = 0.001$), and middle cingulum and postcentral gyri ($F = 5.27$, pFDR = 0.036, uncorrected $p = 0.001$) (Figure 5F; Table 4). The frequency of factor 3 was directly anticorrelated with the verbal order score (uncorrected $p = 0.031$) (Figure 5C), and the FC values between the triangle inferior frontal and lingual gyri were directly anticorrelated with the noun transcribing score (uncorrected $p = 0.026$), verb transcribing score (uncorrected $p = 0.022$), command describing score (uncorrected $p = 0.011$), action description score (uncorrected $p = 0.005$), and dictating noun score (uncorrected $p = 0.026$) (Figures 5G–K).

Discussion

This study aimed to calculate the differences in EA stimulus-dependent changes in brain connectivity patterns between

10.3389/fneur.2022.956931

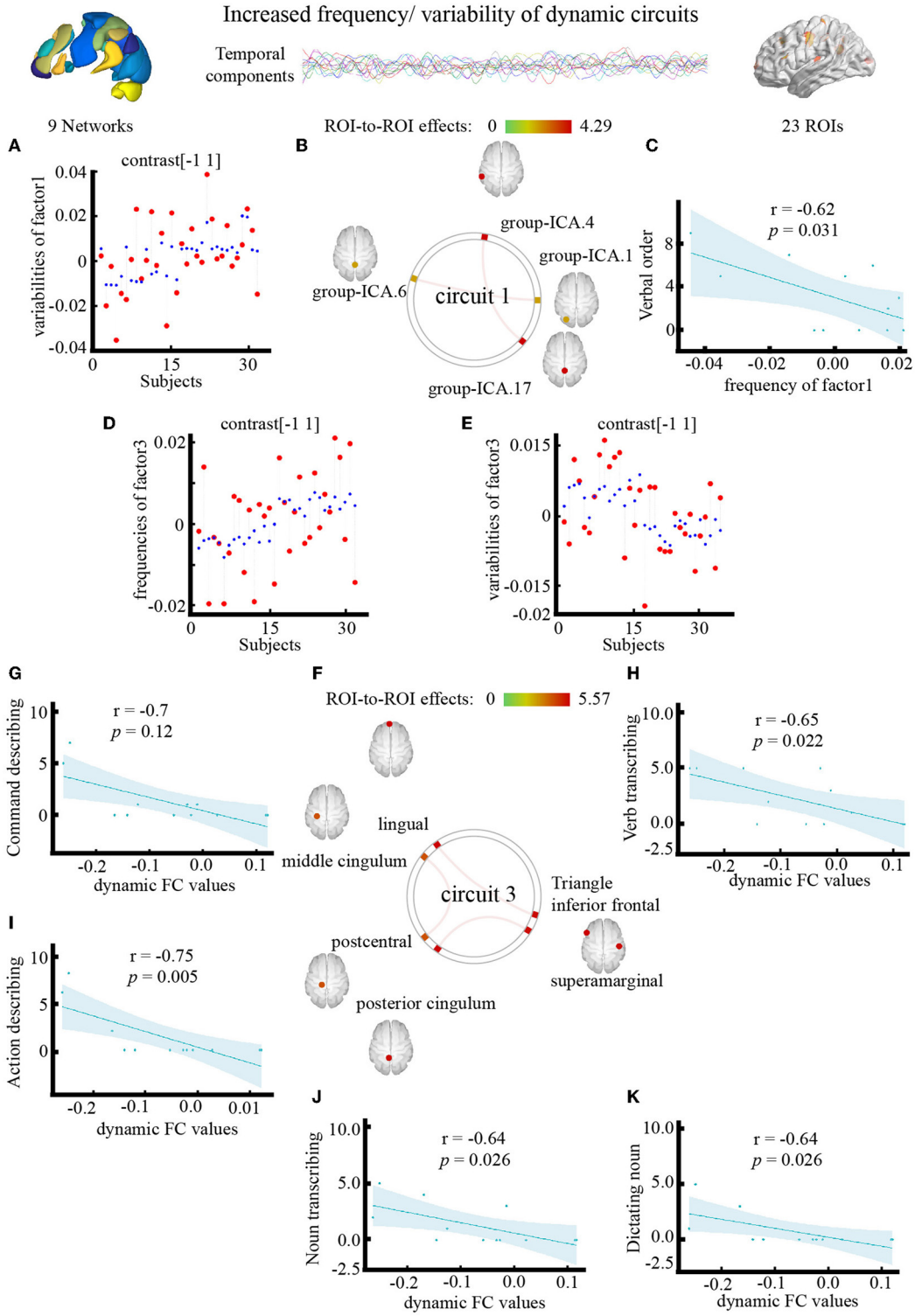

FIGURE 5
Effect of electroacupuncture (EA) stimulation on dynamic independent component analysis. **(A)** Changes in temporal properties varies of circuit1. **(B)** Spatial map of circuit1 for the contrast of condition main effect. **(C)** Correlation between frequency of circuit1 and clinical parameter (CRRCAE score). **(D,E)** Changes in temporal properties varies of circuit3. **(F)** Spatial map of circuit3 for the contrast of condition main effect. **(G–K)** Correlation between clinical parameter (CRRCAE score) and dynamic FC values of triangle inferior frontal and lingual. CRRCAE, Chinese Rehabilitation Research Center for Chinese Standard Aphasia Examination.

TABLE 4 PSA-related differences in dynamic functional connectivity during EA stimulation.

Components	Temporal properties	*F*	*p*-FDR	Spatial properties				*F*	*p*-FDR
				Regions	Side	Regions	Side		
ROI level									
Circuit3	Frequency	2.28	0.030	Lingual	R	Triangle inferior frontal gyri	L	5.57	0.026
				SMG	R	Posterior cingulum gyri	L	5.42	0.031
Circuit3	Variability	−2.23	0.034	PostCG	L	Middle cingulum gyri	L	5.27	0.036
Network level									
Circuit1	Variability	2.34	0.026	DMN		CN		4.28	0.043
				LN		CN		4.29	0.042

Edu, years of education; EA, electroacupuncture; LN, language network; CN, cerebellar network; SN, salience network; ROI, region of interest; SMG, supramarginal gyri; PostCG, postcentral gyri; PSA, post stroke aphasia; HC, healthy control; DMN, default mode network; positive false discovery rate, p-FDR; MNI, montreal neurological institute; R, right; L, left.

patients with PSA and healthy individuals. The interaction between EA stimulation and disease was examined using static ICA, gPPI and Dyn-ICA, with age, sex, and Edu as covariates, similar to a previous study's methods (45). By using static ICA and dynamic ICA approaches, we discovered commonalities with previous studies of acupuncture neuroimaging mechanisms for PSA, as well as some prominent points/networks generated from newer methodologies. The present study is the first to identify a PSA-related neuroimaging mechanism of EA stimulation at HT5 and GB39 both at the ROI and the network level. Our research showed that EA stimulation dramatically changed the nodes of the regions/networks involved in the LN, SN, CN, occipital cortex, somatosensory regions, and cerebral limbic system. Our previous research on the effects of EA on PSA was expanded by these results.

Static ICA

Recently, it has been acknowledged that stroke pathology often affects large-scale functional network structures rather than lesions (46). Based on previous studies, the therapeutic effects of acupuncture extend to the entire brain area and even to the brain network (23). Such influences cannot be calculated using a univariate approach (47) but can be solved using an ICA approach. First, ICA can find functionally independent, potentially spatially overlapping functional networks without the need for prior information of the task paradigm (48). Second, it enables researchers to assess the effects of EA on wider functional networks in patients with PSA. Third, mean activity values within networks as well as frequency and variability distributions could be computed, and the impacts of EA on different portions of a particular network in individual patients contributed to an overall change in score, making this technique more resilient to the impact of varying structural lesions. In the present study, the mean activity levels of left AG and left PostCG in the SN were higher in patients with PSA than in HCs, and the temporal distributions showed significantly higher SN variability, same as the previous study (7). There is abundant evidence in the literature that self-generated speech activates the SN, and the SN had been provided to have a directly correlated with residual language performance in patients with PSA (49). The AG is a region associated with phonological deficits (50). The fact that only individuals with motor aphasia were included may help to explain this. Thus, our findings suggest that EA causes the SN network to transmit more information in motor aphasia.

Static FC analysis

Studies on resting-state connections in healthy persons assume that positive connectivity represents integration and coordination between different brain regions, whereas negative connectivity represents separated or conflicting systems (51). First, we computed the effect of the stimulation condition against the rest of the baseline conditions in each group. Second, we calculated the interactions between the groups and conditions. Our sample's modifications were primarily connected to the somatosensory, language, and occipital cortices. These regions were previously shown to be associated with verb learning and visual word processing (52), and the integration of the visual and sensorimotor systems sustains action naming (53). Our results showed that a crucial neuronal signature underlying EA stimulation processing in PSA may be a change in communication across key regions involved in vision and naming.

Dyn-ICA analysis

These theories assume that FC is "static," while mounting data support the idea that FC is dynamic rather than static (54).

Dyn-ICA can examine time-varying and dynamic extensions of component analysis, which can be accomplished by using a classic component analysis within a sliding window setting (55), and isolate the signal from the noise and boost the sensitivity to identify individual differences (56). Previous studies have used Dyn-ICA to observe the pathological characteristics of diseases (43), and we are the first to use Dyn-ICA to study the mechanism of the effect of acupuncture. Similarly, our studies have clearly shown that Dyn-ICA increases sensitivity to variations between individuals or conditions (56). We used Dyn-ICA to incorporate temporal information, such as frequency and variability, while maintaining the spatial identification of traditional FC at the ROI and network level and arrived at two primary conclusions. First, at the ROI level, PSA-related dynamic connection showed a higher frequency of occipital cortex-limbic system-sensorimotor system connections, and their variability decreased across different dynamic factors. The structure of the FC map showed enhanced connectivity among the occipital, limbic, and sensorimotor system cortices. The higher FC values between the triangle inferior frontal and lingual gyri in the dynamic condition main effect correlated with worse transcribing, describing, and dictating scores. The same results can be found in a previous static analysis of the effect of acupuncture with sham acupuncture as a control (26), but not in a dynamic framework, to the best of our knowledge. Second, perhaps more importantly, at the network level, our results showed that PSA-related dynamic connections between the CN, DMN, and LN are more frequent during EA stimulation than rest at baseline. We found that EA at HT5 and GB39 changes the synchronization between the cerebellum and cerebrum, which is consistent with findings of a previous study (57). The DMN is a collection of areas that are more active at rest than when performing a task (58). These regions are believed to play a role in internal or low-level attentional mechanisms (59). Considerable evidence has demonstrated the essential involvement of the CN in a variety of language functions (60), and CN maps to cerebral association networks have already been reported to correlate with cognitive function (61). Our findings suggest that an aspect of the PSA treatment effect of EA stimulation may be a time-dependent connection between these networks of language function correlations.

Limitations of the present study

This study has some limitations. First, the lesioned voxels can affect fMRI preprocessing and results. However, to the best of our knowledge, there is no accepted standard procedure for the treatment of stroke lesions. We did not mask the lesion, considering that manual mask procuring is time-consuming and subjective (62). The quality of the segmentation and normalization does not seem to be affected in this study, and by adopting the ICA method, some effects of stroke lesions may be offset (56). However, we must admit that there is still more to be done in the future to address this problem. Second, pain and dysfunction in daily life caused by the disease can lead to emotions such as anxiety and depression (63), which can also affect the results of fMRI. Therefore, these factors should be included as covariates in future studies. Third, only patients with motor aphasia were included in this study. Future research is necessary to examine the effects of EA in more types of aphasia.

Conclusions

In conclusion, EA at HT5 and GB39 may improve language function by modulating FC stability among the LN, SN, CN, occipital, somatosensory, and cerebral limbic system regions.

Data availability statement

The raw data supporting the conclusions of this article will be made available by the authors, without undue reservation.

Ethics statement

The studies involving human participants were reviewed and approved by the Medical Research Ethics Committee of Dongzhimen Hospital (ECPJ-BDY-2015-04) and all subjects gave written consent to participate. The patients/participants provided their written informed consent to participate in this study.

Author contributions

YG and JC designed the study. TL, ZT, CL, XL, XH, and JX gathered and managed data. HZ and BZ provided guidance on experimental design and data analysis. MX was responsible for the manuscript's conception, methods, and writing. JC, QK, GK, and SL revised the manuscript. All authors contributed to the article and approved the submitted version.

Funding

This work was supported by Dongzhimen Hospital (hospital/grants), and grants were supported by Special Project of International Cooperation of Traditional Chinese Medicine of State Administration of Traditional Chinese Medicine (project no. 0610-2140NF020630), Special Public Welfare Industry and Scientific Research from the State Administration

of Traditional Chinese Medicine (project no. 201407001-9), and National Natural Science Foundation of China (project no. 81973790).

Acknowledgments

We are appreciative of the participants' steadfast dedication and enthusiasm for our research.

Conflict of interest

The authors declare that the research was conducted in the absence of any commercial or financial relationships that could be construed as a potential conflict of interest.

Publisher's note

Supplementary material

The Supplementary Material for this article can be found online at: https://www.frontiersin.org/articles/10.3389/fneur.2022.956931/full#supplementary-material

References

1. Thiel A, Zumbansen A. The pathophysiology of post-stroke aphasia: a network approach. *Restor Neurol Neurosci.* (2016) 34:507–18. doi: 10.3233/RNN-150632

2. Sheppard SM, Sebastian R. Diagnosing and managing post-stroke aphasia. *Expert Rev Neurother.* (2021) 21:221–34. doi: 10.1080/14737175.2020.1855976

3. Zhu D, Chang J, Freeman S, Tan Z, Xiao J, Gao Y, et al. Changes of functional connectivity in the left frontoparietal network following aphasic stroke. *Front Behav Neurosci.* (2014) 8:167. doi: 10.3389/fnbeh.2014.00167

4. Barbieri E, Mack J, Chiappetta B, Europa E, Thompson CK. Recovery of offline and online sentence processing in aphasia: language and domain-general network neuroplasticity. *Cortex.* (2019) 120:394–418. doi: 10.1016/j.cortex.2019.06.015

5. Klingbeil J, Wawrzyniak M, Stockert A, Saur D. Resting-state functional connectivity: an emerging method for the study of language networks in post-stroke aphasia. *Brain Cogn.* (2019) 131:22–33. doi: 10.1016/j.bandc.2017.08.005

6. Wang C, Qin W, Zhang J, Tian T, Li Y, Meng L, et al. Altered functional organization within and between resting-state networks in chronic subcortical infarction. *J Cereb Blood Flow Metab.* (2014) 34:597–605. doi: 10.1038/jcbfm.2013.238

7. Zhang C, Xia Y, Feng T, Yu K, Zhang H, Sami MU, et al. Disrupted functional connectivity within and between resting-state networks in the subacute stage of post-stroke aphasia. *Front Neurosci.* (2021) 15:746264. doi: 10.3389/fnins.2021.746264

8. Yang M, Li J, Yao D, Chen H. Disrupted intrinsic local synchronization in poststroke aphasia. *Medicine.* (2016) 95:e3101. doi: 10.1097/MD.0000000000003101

9. Liang FR, Wu X. [The developmental status and prospect of the science of acupuncture and moxibustion abroad]. *Zhongguo Zhen Jiu.* (2006) 26:79–82 (Chinese).

10. Hao JJ, Mittelman M. Acupuncture: past, present, and future. *Global Adv Health Med.* (2014) 3:6–8. doi: 10.7453/gahmj.2014.042

11. Wen J, Chen X, Yang Y, Liu J, Li E, Liu J, et al. Acupuncture medical therapy and its underlying mechanisms: a systematic review. *Am J Chin Med.* (2021) 49:1–23. doi: 10.1142/S0192415X21500014

12. Xiao LY, Wang XR, Yang Y, Yang JW, Cao Y, Ma SM, et al. Applications of acupuncture therapy in modulating plasticity of central nervous system. *Neuromodulation.* (2018) 21:762–76. doi: 10.1111/ner.12724

13. Zhang B, Han Y, Huang X, Liu Z, Li S, Chang J, et al. Acupuncture is effective in improving functional communication in post-stroke aphasia: a systematic review and meta-analysis of randomized controlled trials. *Wien Klin Wochenschr.* (2019) 131:221–32. doi: 10.1007/s00508-019-1478-5

14. Li G, Jack CR Jr., Yang ES. An fMRI study of somatosensory-implicated acupuncture points in stable somatosensory stroke patients. *J Magn Reson Imaging.* (2006) 24:1018–24. doi: 10.1002/jmri.20702

15. Li G, Yang ES. An fMRI study of acupuncture-induced brain activation of aphasia stroke patients. *Compl Ther Med.* (2011) 19 Suppl 1:S49–59. doi: 10.1016/j.ctim.2010.11.004

16. Chavez LM, Huang SS, MacDonald I, Lin JG, Lee YC, Chen YH. Mechanisms of acupuncture therapy in ischemic stroke rehabilitation: A literature review of basic studies. *Int J Mol Sci.* (2017) 18:2270. doi: 10.3390/ijms18112270

17. Jiang Y, Wang H, Liu Z, Dong Y, Dong Y, Xiang X, et al. Manipulation of and sustained effects on the human brain induced by different modalities of acupuncture: an fMRI study. *PLoS ONE.* (2013) 8:e66815. doi: 10.1371/journal.pone.0066815

18. Sun L, Chen YY, Fang JL, Hong Y, Wang Y, Xu K, et al. [Correlation between blood oxygen level dependent fMRI signal and GABA content in anterior cingulate cortex after acupuncture of Hegu (LI4)]. *Zhen Ci Yan Jiu.* (2019) 44:878–83 (Chinese). doi: 10.13702/j.1000-0607.190597

19. Jin L, Sun J, Xu Z, Yang X, Liu P, Qin W. Intersubject synchronisation analysis of brain activity associated with the instant effects of acupuncture: an fMRI study. *Acupunct Med.* (2018) 36:14–20. doi: 10.1136/acupmed-2016-011327

20. Zhang W, Lang S, Zheng Y, Qin X, Chen H, You Y, et al. The effects of transcranial direct current stimulation versus electroacupuncture on working memory in healthy subjects. *J Altern Compl Med.* (2019) 25:637–42. doi: 10.1089/acm.2018.0532

21. Liu S, Li M, Tang W, Wang G, Lv Y. An fMRI study of the effects on normal language areas when acupuncturing the Tongli (HT(5)) and Xuanzhong (GB(39)) acupoints. *J Int Med Res.* (2017) 45:1961–75. doi: 10.1177/0300060517720344

22. Li LL, Liu XW, Wu F, Tong DC, Ye LP, Tao HX, et al. Electroacupuncture stimulation of language-implicated acupoint Tongli (HT 5) in healthy subjects: an fMRI evaluation study. *Chin J Integr Med.* (2018) 24:822–9. doi: 10.1007/s11655-017-2924-8

23. Xiao J, Zhang H, Chang JL, Zhou L, Tan ZJ, Zhong HZ, et al. Effects of electro-acupuncture at Tongli (HT 5) and Xuanzhong (GB 39) acupoints from functional magnetic resonance imaging evidence. *Chin J Integr Med.* (2016) 22:846–54. doi: 10.1007/s11655-015-1971-2

24. Zhang J, Song L, Xu L, Fan Y, Wang T, Tian W, et al. Knowledge domain and emerging trends in ferroptosis research: a bibliometric and knowledge-map analysis. *Front Oncol.* (2021) 11:686726. doi: 10.3389/fonc.2021.686726

25. Han X, Jin H, Li K, Ning Y, Jiang L, Chen P, et al. Acupuncture modulates disrupted whole-brain network after ischemic stroke: evidence based on graph theory analysis. *Neural Plast.* (2020) 2020:8838498. doi: 10.1155/2020/8838498

26. Cai RL, Shen GM, Wang H, Guan YY. Brain functional connectivity network studies of acupuncture: a systematic review on resting-state fMRI. *J Integr Med.* (2018) 16:26–33. doi: 10.1016/j.joim.2017.12.002

27. Fan R, Gao Y, Zhang H, Xin X, Sang F, Tan Z, et al. Lesion distribution and early changes of right hemisphere in Chinese patients with post-stroke

aphasia. *Front Aging Neurosci.* (2021) 13:632217. doi: 10.3389/fnagi.2021.632217

28. Chang J, Zhang H, Tan Z, Xiao J, Li S, Gao Y. Effect of electroacupuncture in patients with post-stroke motor aphasia : Neurolinguistic and neuroimaging characteristics. *Wien Klin Wochenschr.* (2017) 129:102–9. doi: 10.1007/s00508-016-1070-1

29. Maeda Y, Kim H, Kettner N, Kim J, Cina S, Malatesta C, et al. Rewiring the primary somatosensory cortex in carpal tunnel syndrome with acupuncture. *Brain.* (2017) 140:914–27. doi: 10.1093/brain/awx015

30. Gao Y, Lin Z, Tao J, Yang S, Chen R, Jiang C, et al. Evidence of timing effects on acupuncture: a functional magnetic resonance imaging study. *Exp Ther Med.* (2015) 9:59–64. doi: 10.3892/etm.2014.2056

31. Song XW, Dong ZY, Long XY Li SF, Zuo XN, Zhu CZ, et al. REST: a toolkit for resting-state functional magnetic resonance imaging data processing. *PLoS ONE.* (2011) 6:e25031. doi: 10.1371/journal.pone.0025031

32. Whitfield-Gabrieli S, Nieto-Castanon A. Conn: a functional connectivity toolbox for correlated and anticorrelated brain networks. *Brain Connect.* (2012) 2:125–41. doi: 10.1089/brain.2012.0073

33. Calhoun VD, Adali T, Pearlson GD, Pekar JJ, A. method for making group inferences from functional MRI data using independent component analysis. *Hum Brain Mapp.* (2001) 14:140–51. doi: 10.1002/hbm.1048

34. Vettore M, De Marco M, Pallucca C, Bendini M, Gallucci M, Venneri A. White-matter hyperintensity load and differences in resting-state network connectivity based on mild cognitive impairment subtype. *Front Aging Neurosci.* (2021) 13:737359. doi: 10.3389/fnagi.2021.737359

35. Tordjman M, Madelin G, Gupta PK, Cordova C, Kurz SC, Orringer D, et al. Functional connectivity of the default mode, dorsal attention and fronto-parietal executive control networks in glial tumor patients. *J Neurooncol.* (2021) 152:347–55. doi: 10.1007/s11060-021-03706-w

36. Ferré P, Jarret J, Brambati S, Bellec P, Joanette Y. Functional connectivity of successful picture-naming: age-specific organization and the effect of engaging in stimulating activities. *Front Aging Neurosci.* (2020) 12:535770. doi: 10.3389/fnagi.2020.535770

37. Alakörkkö T, Saarimäki H, Glerean E, Saramäki J, Korhonen O. Effects of spatial smoothing on functional brain networks. *Eur J Neurosci.* (2017) 46:2471–80. doi: 10.1111/ejn.13717

38. Mclaren DG, Ries ML, Xu G, Johnson SC, A. generalized form of context-dependent psychophysiological interactions (gPPI): a comparison to standard approaches. *Neuroimage.* (2012) 61:1277–86. doi: 10.1016/j.neuroimage.2012.03.068

39. Lee Masson H, Op De Beeck H, Boets B. Reduced task-dependent modulation of functional network architecture for positive versus negative affective touch processing in autism spectrum disorders. *Neuroimage.* (2020) 219:117009. doi: 10.1016/j.neuroimage.2020.117009

40. Ghahremani M, Yoo J, Chung SJ, Yoo K, Ye JC, Jeong YJ. Alteration in the local and global functional connectivity of resting state networks in Parkinson's disease. *J Mov Disord.* (2018) 11:13. doi: 10.14802/jmd.17061

41. Calhoun VD, Miller R, Pearlson G, Adali T. The chronnectome: time-varying connectivity networks as the next frontier in fMRI data discovery. *Neuron.* (2014) 84:262–74. doi: 10.1016/j.neuron.2014.10.015

42. Grami F, De Marco G, Bodranghien F, Manto M, Habas CJ. Cerebellar transcranial direct current stimulation reconfigures brain networks involved in motor execution and mental imagery. *Cerebellum.* (2022) 21:665–80. doi: 10.1007/s12311-021-01322-y

43. Aracil-Bolaños I, Martínez-Horta S, González-De-Echávarri JM, Sampedro F, Pérez-Pérez J, Horta-Barba A, et al. Structure and dynamics of large-scale cognitive networks in Huntington's Disease. *Mov Disord.* (2022) 37:343–53. doi: 10.1002/mds.28839

44. Guerithault N, McClure SM, Ojinnaka CO, Braden BB, Bruening M. Resting-state functional connectivity differences in college students with and without food insecurity. *Nutrients.* (2022) 14:2064. doi: 10.3390/nu14102064

45. Laforce R Jr., Tosun D, Ghosh P, Lehmann M, Madison CM, Weiner MW, et al. Parallel ICA of FDG-PET and PiB-PET in three conditions with underlying Alzheimer's pathology. *NeuroImage Clin.* (2014) 4:508–16. doi: 10.1016/j.nicl.2014.03.005

46. Salvalaggio A, De Filippo De Grazia M, Zorzi M, Thiebaut De Schotten M, Corbetta M. Post-stroke deficit prediction from lesion and indirect structural and functional disconnection. *Brain.* (2020) 143:2173–88. doi: 10.1093/brain/awaa156

47. Darkow R, Martin A, Würtz A, Flöel A, Meinzer M. Transcranial direct current stimulation effects on neural processing in post-stroke aphasia. *Hum Brain Mapp.* (2017) 38:1518–31. doi: 10.1002/hbm.23469

48. Smith SM, Miller KL, Moeller S, Xu J, Auerbach EJ, Woolrich MW, et al. Temporally-independent functional modes of spontaneous brain activity. *Proc Natl Acad Sci USA.* (2012) 109:3131–6. doi: 10.1073/pnas.1121329109

49. Brownsett SL, Warren JE, Geranmayeh F, Woodhead Z, Leech R, Wise RJ. Cognitive control and its impact on recovery from aphasic stroke. *Brain.* (2014) 137:242–54. doi: 10.1093/brain/awt289

50. Na Y, Jung J, Tench CR, Auer DP, Pyun SB. Language systems from lesion-symptom mapping in aphasia: a meta-analysis of voxel-based lesion mapping studies. *NeuroImage Clin.* (2022) 35:103038. doi: 10.1016/j.nicl.2022.103038

51. Fair DA, Dosenbach NU, Church JA, Cohen AL, Brahmbhatt S, Miezin FM, et al. Development of distinct control networks through segregation and integration. *Proc Natl Acad Sci USA.* (2007) 104:13507–12. doi: 10.1073/pnas.0705843104

52. Fiori V, Kunz L, Kuhnke P, Marangolo P, Hartwigsen G. Transcranial direct current stimulation (tDCS) facilitates verb learning by altering effective connectivity in the healthy brain. *Neuroimage.* (2018) 181:550–9. doi: 10.1016/j.neuroimage.2018.07.040

53. Durand E, Masson-Trottier M, Sontheimer A, Ansaldo AI. Increased links between language and motor areas: a proof-of-concept study on resting-state functional connectivity following personalized observation, execution and mental imagery therapy in chronic aphasia. *Brain Cogn.* (2021) 148:105659. doi: 10.1016/j.bandc.2020.105659

54. Fu Z, Iraji A, Sui J, Calhoun VD. Whole-brain functional network connectivity abnormalities in affective and non-affective early phase psychosis. *Front Neurosci.* (2021) 15:682110. doi: 10.3389/fnins.2021.682110

55. Leonardi N, Richiardi J, Gschwind M, Simioni S, Annoni JM, Schluep M, et al. Principal components of functional connectivity: a new approach to study dynamic brain connectivity during rest. *Neuroimage.* (2013) 83:937–50. doi: 10.1016/j.neuroimage.2013.07.019

56. Zhang H, Tao Y, Xu H, Zou S, Deng F, Huang L, et al. Associations between childhood chronic stress and dynamic functional connectivity in drug-naïve, first-episode adolescent MDD. *J Affect Disord.* (2022) 299:85–92. doi: 10.1016/j.jad.2021.11.050

57. Chen J, Wang J, Huang Y, Lai X, Tang C, Yang J, et al. Modulatory effect of acupuncture at Waiguan (TE5) on the functional connectivity of the central nervous system of patients with ischemic stroke in the left basal ganglia. *PLoS ONE.* (2014) 9:e96777. doi: 10.1371/journal.pone.0096777

58. Van De Ven V, Esposito F, Christoffels IK. Neural network of speech monitoring overlaps with overt speech production and comprehension networks: a sequential spatial and temporal ICA study. *Neuroimage.* (2009) 47:1982–91. doi: 10.1016/j.neuroimage.2009.05.057

59. Buckner R, Andrews-Hanna J, Schacter DJ. The brain's default network: anatomy, function, and relevance to disease. *Ann N Y Acad Sci.* (2008) 1124:1–38. doi: 10.1196/annals.1440.011

60. Zheng K, Chen M, Shen Y, Xu X, Gao F, Huang G, et al. Cerebellar continuous theta burst stimulation for aphasia rehabilitation: study protocol for a randomized controlled trial. *Front Aging Neurosci.* (2022) 14:909733. doi: 10.3389/fnagi.2022.909733

61. Buckner RL. The cerebellum and cognitive function: 25 years of insight from anatomy and neuroimaging. *Neuron.* (2013) 80:807–15. doi: 10.1016/j.neuron.2013.10.044

62. Brihmat N, Boulanouar K, Darmana R, Biganzoli A, Gasq D, Castel-Lacanal E, et al. Controlling for lesions, kinematics and physiological noise: impact on fMRI results of spastic post-stroke patients. *MethodsX.* (2020) 7:101056. doi: 10.1016/j.mex.2020.101056

63. Pompon RH, Fassbinder W, Mcneil MR, Yoo H, Kim HS, Zimmerman RM, et al. Associations among depression, demographic variables, and language impairments in chronic post-stroke aphasia. *J Commun Disord.* (2022) 100:106266. doi: 10.1016/j.jcomdis.2022.106266

Frontiers in Neurology

Explores neurological illness to improve patient care

The third most-cited clinical neurology journal explores the diagnosis, causes, treatment, and public health aspects of neurological illnesses. Its ultimate aim is to inform improvements in patient care.

Discover the latest Research Topics

See more →

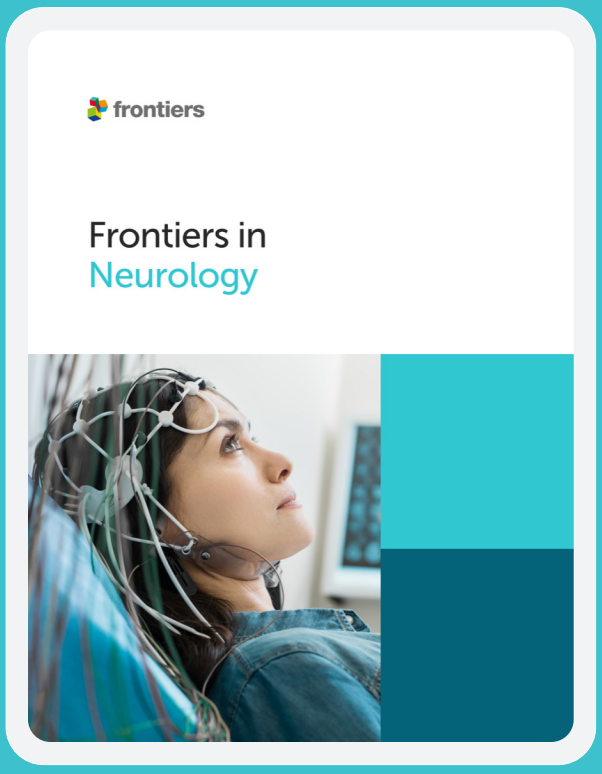

Frontiers

Avenue du Tribunal-Fédéral 34
1005 Lausanne, Switzerland
frontiersin.org

Contact us

+41 (0)21 510 17 00
frontiersin.org/about/contact